THE JOURNAL
OF
CHEMICAL PHYSICS

VOLUME 33, NUMBER 6 DECEMBER, 1960

Electron Spin Resonance of an Irradiated Single Crystal of *N*-Acetylglycine*

ICHIRO MIYAGAWA,† YUKIO KURITA,‡ AND WALTER GORDY

Department of Physics, Duke University, Durham, North Carolina

(Received June 13, 1960)

Electron spin resonance absorption of an irradiated single crystal of *N*-acetylglycine was observed at room temperature at 9 kMc and 12 kMc. From the analysis of the anisotropy in the spectroscopic splitting factor and in the nuclear hyperfine interaction constant, a chemical structure

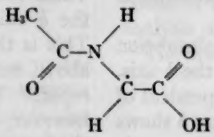

is deduced for the free radical. The C—H bond is in the NCC plane and approximately along the bisector of the NCC angle. The unpaired electron spin density is essentially in a π orbital, about 72% of which is the p orbital of the CH carbon directed perpendicular to the NCC plane.

INTRODUCTION

N-ACETYLGLYCINE is one of the simplest compounds with a peptide bond. When irradiated in powder, the electron spin resonance absorption shows a doublet[1] which is of approximately the same spacing as the doublets of proteins.[2] The study of the single crystal of the compound therefore will provide some knowledge useful for interpretation of radiation damage in proteins. In the earlier paper from this laboratory which contained results on several dipeptides in the powder form,[1] including acetylglycine and glycylglycine, the form of the free radical confirmed by the present study was proposed, and mention was made of these single crystal studies in progress to test it.

EXPERIMENTAL METHOD

The measurements of electron spin resonance were made at 9 kMc and 23 kMc with the same spectrometer employed as in previous reports.[3,4] The second derivative of the actual absorption curve was displayed against magnetic field. The crystal was grown from aqueous solution at room temperature by slow evaporation. Irradiation was accomplished with a kilocurie cobalt-60 gamma-ray source, with dosages ranging from 1 to 5 million r. The crystal was irradiated and the resonance observed at room temperature.

ANALYSIS OF RESULTS

The crystal structure of *N*-acetylglycine was completely analyzed by Carpenter and Donohue.[5] Figure 1 shows its monoclinic crystalline form and crystallographic axes. The symmetry of the crystal is C_{2h}^5—$P2_1/c$. There are four molecules in the unit cell. These are grouped into pairs, with the two molecules of each pair related by a center of symmetry. Two molecules which belong to the different pairs are related by a twofold screw axis parallel to the b axis.

If the assumption is made that the free radicals formed by the irradiation have their magnetic axes fixed in space, the four molecules in a unit cell should

* This research was supported by the U. S. Air Force through the Air Force Office of Scientific Research and Development Command and by the Office of Ordnance Research, Department of the Army.

† Present address: The Institute for Solid-State Physics, The University of Tokyo, Tokyo, Japan.

‡ Fellow of the Visiting Research Scientist Program, National Academy of Sciences.

[1] G. McCormick and W. Gordy, J. Phys. Chem. **62**, 783 (1958).

[2] W. Gordy and H. Shields, Radiation Research **9**, 611 (1958).

[3] I. Miyagawa and W. Gordy, J. Chem. Phys. **30**, 1590 (1959).

[4] I. Miyagawa and W. Gordy, J. Chem. Phys. **32**, 255 (1960).

[5] G. B. Carpenter and J. Donohue, J. Am. Chem. Soc. **72**, 2315 (1950).

Copyright © 1960 by the American Institute of Physics

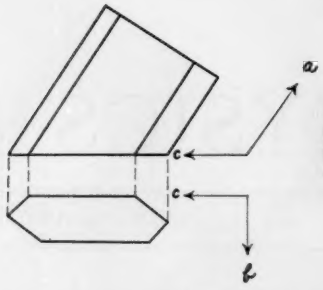

FIG. 1. Crystalline form and crystallographic axes of *N*-acetylglycine.

give rise to free radicals of four different orientations. However, because of centers of symmetry two of the four orientations are magnetically equivalent to the other two; therefore, only two distinct absorption patterns are expected. This is found to be true. When the magnetic field is parallel to, or perpendicular to, the *b* axis, all the four orientations are found to be magnetically equivalent, giving only one absorption pattern.

Figure 2 shows a typical pattern of the absorption when the magnetic field is perpendicular to the *b* axis. The pattern is a simple doublet which is independent of the microwave frequency in its spacing. Figure 3 shows a typical pattern of the absorption for the magnetic field in an arbitrary direction. This is a spectrum of four lines with equal intensity which will be designated as *a*, *b*, *c*, and *d* in order of increasing magnetic field. The separation between *a* and *d*, and also that between *b* and *c*, is independent of the microwave frequency. However, *a* and *b* shift linearly with microwave frequency relatively to *c* or *d*. The absorption pattern is therefore of two overlapping doublets with different nuclear hyperfine coupling constants and different spectroscopic splitting factors. Figure 4 shows the measured positions of these doublets in the *bc* plane. The principal elements of the nuclear hyperfine coupling constant (A) and those of the spectroscopic splitting

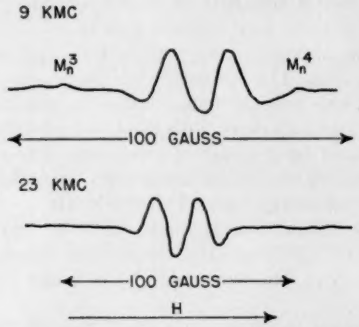

FIG. 2. Electron spin resonance curves for a gamma-irradiated single crystal of *N*-acetylglycine at 9kMc and 23 kMc for the imposed magnetic field at $+90°$ from the *c* axis in the *ca* plane. The small pips indicated by Mn^3 and Mn^4 are M^{++} hyperfine components, of 67 gauss spacing, used as scale markers.

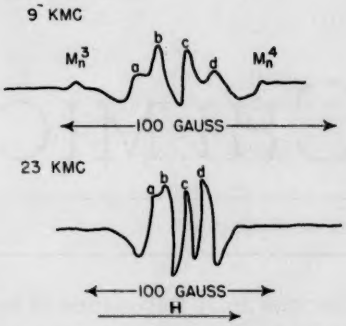

FIG. 3. Absorption curves similar to Fig. 2 but for the imposed magnetic field at $+45°$ from the *b* axis in the *bc* plane. The small pips indicated by Mn^3 and Mn^4 are M^{++} hyperfine components, of 67 gauss spacing, used as scale markers.

factor (g) are given in Table I. The two sets of (A) in the table correspond to the two doublets in Fig. 3. These two sets are related by the C_2 symmetry along the *b* axis in agreement with the crystal symmetry. This is the same for (g). The basic formulas for the above analysis were already described in a previous report.[3] The sign of the (A) was not determined; however, all the three components were found to have the same sign. If one of the components has a different sign from the others, the doublet spacing must be zero in a certain direction. This vanishing of the doublet splitting was not observed. The value of (A) in the table shows that the second order effect observed in alanine crystals[4] must be observed also in this crystal

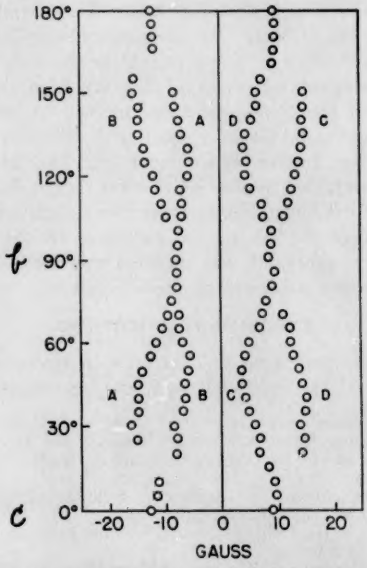

FIG. 4. Observed positions of two doublets of the electron resonance at 9 kMc of gamma-irradiated *N*-acetylglycine related to the resonance of DPPH. The static magnetic field is in the *cb* plane.

at the employed frequencies. The large linewidth of the absorption would, however, prevent observation of this effect. The linewidth is about 15 gauss, or about twice as broad as that of dimethylglyoxime[3] or that of alanine.[4]

ORBITAL OF THE UNPAIRED ELECTRON

The *N*-acetylglycine molecule is planar in the crystal, and the molecular plane is approximately parallel to the *bc* plane.[5] As shown previously,[3] the spectroscopic splitting factor of a free radical is minimum along the symmetry axis of the orbital of the unpaired electron. Table I shows that the direction of the minimum g is perpendicular to the *bc* plane, or to the molecular plane, for both sets of the (g) within the experimental error. It is concluded therefore that the unpaired electron is essentially a π electron. Later, it will be shown that it has about 72% of its density on the CH carbon. Thus the spin density is largely in a p orbital of the C which has its direction perpendicular to the molecular plane.

ORIGIN OF THE DOUBLET

The origin of the doublet is undoubtedly a proton which is the only nucleus with spin $\frac{1}{2}$ of *N*-acetylglycine, $CH_3CONHCH_2COOH$; however, this molecule has four species of chemically different hydrogens as shown in the above chemical formula. Deuterium-exchanged *N*-acetylglycine, $CH_3CONDCH_2COOD$, gave an identical doublet with that of *N*-acetylglycine in powder within the experimental error. If the unpaired electron interacts with a proton of the NH group or that of the COOH group, the deuterium exchanged *N*-acetylglycine must give a triplet. Therefore the origin of the doublet is a hydrogen either of the methyl group or of the CH_2 group. Another deuterium-exchanged compound, $CD_3CONHCH_2COOH$, or $CH_3CONHCD_2COOH$, which provides the final assignment for the origin of the doublet, was not observed in the present experiment. However, when the proton of a methyl group contributes to hyperfine structure, a quartet or a more complex pattern is usually observed rather than a doublet. It is therefore highly probable that the origin of the doublet is one of the protons in the CH_2 group of the parent molecule.

STRUCTURE OF THE FREE RADICAL

From the preceding considerations, the chemical structure[1]

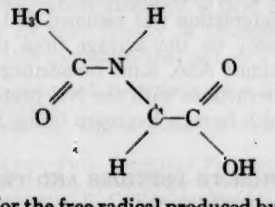

is indicated for the free radical produced by γ irradiation of acetylglycine. This radical is produced from the parent molecule by the destruction of one of the C—H bonds in the CH_2 group. Its structure is confirmed by analysis of the hyperfine structure given below.

TABLE I. The magnitudes of the principal elements of the nuclear hyperfine coupling constant (A) and the spectroscopic splitting factor (g). This is for one of the two sets. The other set is related to this by the C_2 symmetry along the *b* axis.

	(A) and (g)	Direction[a]
A_1	27±2 gauss	+55° from the *b* axis in the *bc* plane
A_2	17±2 gauss	Perpendicular to the *bc* plane
A_3	10±2 gauss	+145° from the *b* axis in the *bc* plane
g_1	2.0027±0.0004	Perpendicular to the *bc* plane
g_2	2.0032±0.0004	Parallel to the *b* axis
g_3	2.0042±0.0004	Parallel to the *c* axis

[a] The error is within ±10°. The signs of A_1, A_2, and A_3 are not obtained from the measurement, but they are all of the same sign and are probably negative.

The nuclear hyperfine interaction constant (A) of the

fragment consists of an isotropic Fermi term (A_f) and an anisotropic dipole-dipole interaction term (A_μ), as described in preceding papers.[3,4] The value of (A_f) is obtained from the observed elements by $(A_1+A_2+A_3)/3$ to be 18 gauss for the present free radical. The anistropic interaction for a

fragment has been estimated by McConnell and Strathdee[6] as the dipole-dipole coupling between a p electron on the carbon atom and the proton nucleus. Their calculated values of the principal elements of this anisotropic coupling are 15.4, −1.6, and −13.8 gauss along the C—H bond, along the density axis of the p orbital, and perpendicular to those two, respectively, in decreasing order. The magnitude of (A_f) is, however, 23–25 gauss when the electron density is completely concentrated on the carbon, as in the CH_3 radical.[7] Thus the observed magnitude of (A_f), 18 gauss, indicates that the electron spin density on the CH carbon is here reduced to 72% of its full value. We accordingly reduce these anisotropic values by 28%—to 11, −1.1, and −10 gauss, respectively. From previous

[6] H. M. McConnell and J. Strathdee, Molecular Phys. **2**, 129 (1959).

[7] W. Gordy and C. G. McCormick, J. Am. Chem. Soc. **78**, 3243 (1956); B. Smaller and M. S. Matheson, J. Chem. Phys. **28**, 1169 (1958).

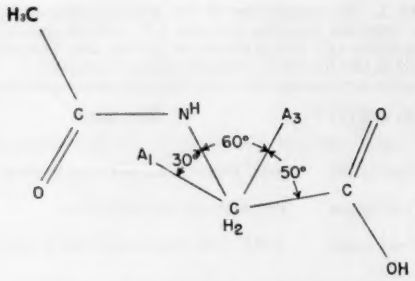

FIG. 5. Diagram of *N*-acetylglycine showing the directions of the principal elements of the nuclear coupling, A_1 and A_3, in the molecular plane. The element A_2, not shown, is perpendicular to this plane.

work on the

fragment in irradiated alanine,[4] for which (A_f) and (A_μ) are opposite in sign, and from theoretical considerations,[8] we are justified in taking the sign of (A_f) to be negative. Thus when H is parallel to the CH bond axis the anisotropic component in the coupling is of opposite sign to the Fermi coupling. Adding a value of -18 gauss for (A_f) to the above anisotropic components yields -7 gauss for the coupling value with the magnetic field parallel to the CH bond, -19 gauss with it parallel to the p orbital and perpendicular to the CH bond, and -28 gauss with it perpendicular to both the p orbital and the CH bond. In magnitude these compare reasonably well with the observed magnitudes of the principal values: $A_3=10$ gauss, $A_2=17$ gauss, and $A_1=27$ gauss, with A_3 along the CH bond and A_2 perpendicular to the plane of the molecule. The diagram of Fig. 5 shows the directions of the prinicpal magnetic axes, A_1 and A_3, in the plane of the molecule. A_2, not shown, is perpendicular to this plane for one assignment. If the assignment is reversed, the directions of A_1 and A_3 do not agree with those obtained theoretically.

From these results we conclude that the free radical in irradiated acetylglycine is formed by the loss of one hydrogen from the CH_2 group, followed by a reorientation of the remaining CH bond into the plane of the molecule. Since A_3, which is along the CH bond of the free radical, is 60° from the CN bond of the parent molecule, there is evidently an opening up of the NCC bond from 110° to about 120° when the free radical is formed. This change in angle would accompany the switching of the CH bond to the molecular plane. One would actually expect the NCC angle in the free radical to be slightly larger than 120° and slightly larger than the NCH angle because of the probable effects of the contributing structure II,

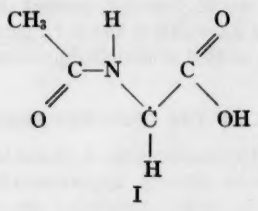

I

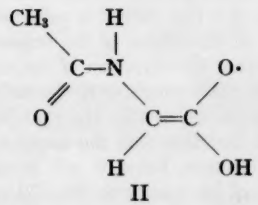

II

Although structure I most nearly represents the ground state of the free radical, contributions from structure II are probably responsible for most of the reduction of the spin density on the CH to 72% of the value expected for structure I alone. Our measurements of the principal values of A_μ are not sufficiently accurate, however, to detect this deviation of A_3 (or the CH bond) from the bisection of the NCC bond in the radical. The direction of A_2, perpendicular to the molecular plane, is consistent with the minimum value of g also in this direction. Both indicate that the electron spin density is concentrated in an orbital which is perpendicular to the molecular plane. This conclusion is also consistent with the assumption of delocalized, π bonding as indicated by contributions from structure II.

LINEWIDTH

The unpaired electron which was concluded to be a π electron is expected to interact to a slight extent with the lone pair electrons of the nitrogen atom. Though the nitrogen hyperfine structure was not observed, this may be the origin of the broadening of the absorption line. The axis of the lone-pair electron, which is probably a sp^3 electron, may be nearly parallel to that of the π electron, but not exactly. This is in agreement with the small contribution of the nitrogen interaction. If the difference between the linewidth in this molecule and that in alanine is assumed to originate exclusively from the nitrogen interaction, the spin density on the nitrogen atom is estimated as 0.06. The contribution of the nitrogen interaction was assumed as 130 gauss for unit spin density on the average from the result in dimethylglyoxime.[3] Also, some broadening may result from slight interactions with the NH proton and with the proton which forms a hydrogen bridge to the C=O oxygen.

APPLICATION TO PEPTIDES AND PROTEINS

(Glycyl)$_n$glycine ($n=1$, 2, and 3) and several proteins such as albumin have been reported to show doublets similar to that of *N*-acetyl-glycine in powder.[1,2]

[8] H. M. McConnell and D. B. Chesnut, J. Chem. Phys. **28**, 107 (1958), where many references to previous work are given.

It was also proved by deuterium exchange[9] that the origins of the doublets are not from the hydrogens of $-N^+H_3$, $=NH$, or $-COOH$ groups. It is highly probable that those doublets of the three peptides originate from a radical similar to that of *N*-acetylglycine, viz.,

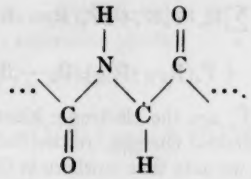

This radical structure is also expected to be produced in the proteins, if a C—R bond of their polypeptide chains.

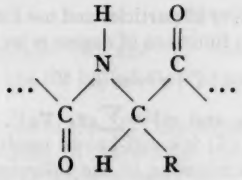

is broken by irradiation. The anisotropy observed in the nuclear couplings of stranded silk[2] is expected for this radical structure.

[9] W. Gordy and I. Miyagawa, Bull. Am. Phys. Soc. **5**, 227 (1960).

THE JOURNAL OF CHEMICAL PHYSICS VOLUME 33, NUMBER 6 DECEMBER, 1960

Forces in Molecules. I. Application of the Virial Theorem*

WILLIAM L. CLINTON†

Chemistry Department, Brookhaven National Laboratory, Upton, New York

(Received February 10, 1960)

It is shown that the virial theorem can be used to derive a force constant expression that sheds new light on the process of molecular binding. In connection with the latter the quantum-mechanical virial theorem is derived in such a way as to be useful in discussing molecular applications in which the Born-Oppenheimer approximation is applied.

I. INTRODUCTION

IN the field of molecular quantum mechanics the subject of adiabatic energy derivatives has recently received rather detailed treatment.[1] The present work attempts to further develop this subject. In so doing a new expression for the second-order energy derivative (force constant in molecular jargon) has been developed. This new expression is useful in discussing molecular binding.

In the process of this research it was found convenient to introduce[2] the quantum-mechanical virial theorem in such a way that there is a relationship for the kinetic energy of each individual particle. This method is useful in discussing the effect of the Born-Oppenheimer approximation on the virial theorem. The treatment is given in parts II and III.

In the remainder of the paper molecular binding is discussed. Particular attention is paid to the extent to which the electron density is changed in a nuclear vibration. It is concluded that not only can this change not be ignored but, on the contrary, it is the only thing that gives rise to a nonvanishing force constant.

II. QUANTUM-MECHANICAL VIRIAL THEOREM

Consider the following derivation of the virial theorem. Let $\mathbf{r}_K$ and $\mathbf{p}_K$ denote the coordinate and momenta of the Kth particle. We have then for the nth eigenstate

$$\langle n \mid [\mathbf{r}_K \cdot \mathbf{p}_K, H] \mid n \rangle = 0, \tag{1}$$

where H is the total Hamiltonian of the system. Equation (1) follows from the fact that for any time-independent Hamiltonian the diagonal element of its commutator with any operator is zero.

Equation (1) is simplified by using the following commutator identities,

$$[\mathbf{r}_K \cdot \mathbf{p}_K, H] = [\mathbf{r}_K, H] \cdot \mathbf{p}_K + \mathbf{r}_K \cdot [\mathbf{p}_K, H] \tag{2a}$$

$$[\mathbf{r}_K, H] = (i\hbar/m_K)\,\mathbf{p}_K \tag{2b}$$

$$[\mathbf{p}_K, H] = -i\hbar \nabla_K V, \tag{2c}$$

where V is the total potential energy operator of the system. Equation (1) now becomes

$$m_K^{-1} \langle n \mid \mathbf{p}_K \cdot \mathbf{p}_K \mid n \rangle - \langle n \mid \mathbf{r}_K \cdot \nabla_K V \mid n \rangle = 0. \tag{3}$$

* Research performed under the auspices of the U.S. Atomic Energy Commission.

† Present address: National Bureau of Standards, Washington 25, D. C.

[1] W. B. Brown, Proc. Cambridge Phil. Soc. **54**, 251 (1958); P. O. Lowdin, J. Mol. Spectroscopy **3**, 46 (1959).

[2] See, for example, E. C. Kemble, *Fundamental Principles of Quantum Mechanics* (McGraw-Hill Book Company, Inc., New York, 1937), p. 516.

Or in terms of the kinetic energy, T_K, of the Kth particle

$$2\langle n \mid T_K \mid n\rangle = \langle n \mid \mathbf{r}_K \cdot \nabla_K V \mid n\rangle. \quad (4)$$

If we now sum over all particles and use Euler's theorem for homogeneous functions of degree m we have

$$2\langle n \mid T \mid n\rangle = m\langle n \mid V \mid n\rangle, \quad (5)$$

where $T \equiv \sum T_K$ and $mV \equiv \sum_K \mathbf{r}_K \cdot \nabla_K V$.

Although Eq. (5) is a well-known result,[3] the present derivation is illuminating in the following sense. Not only is (5) true but so also is Eq. (4). That is, a virial theorem holds for every particle just as in the classical case. This latter result is not brought out in the standard derivation.[4] It will be seen in the next section that it allows the molecular virial theorem to be presented in a more satisfactory manner.

III. MOLECULAR CASE

We now want to consider the virial theorem for a general molecule. Denoting the nuclear coordinates by $(\mathbf{R}_1, \cdots \mathbf{R}_\nu)$ and electronic coordinates by $(\mathbf{r}_1, \cdots \mathbf{r}_n)$ we may write

$$2\sum_\alpha \langle T(\mathbf{R}_\alpha)\rangle + 2\sum_i \langle T(\mathbf{r}_i)\rangle = -\langle V(\mathbf{R}_1, \cdots \mathbf{R}_\nu, \quad \mathbf{r}_1, \cdots \mathbf{r}_n)\rangle, \quad (6)$$

where the bracket means,

$$\langle f\rangle \equiv \int \cdots \int \psi^*(\mathbf{R}, \mathbf{r}) f \psi(\mathbf{R}, \mathbf{r}) d\mathbf{R}_1 \cdots d\mathbf{R}_\nu d\mathbf{r}_1 \cdots d\mathbf{r}_n.$$

But from Eq. (4) we also have the separate particle condition

$$2\langle T(\mathbf{R}_\alpha)\rangle = \langle \mathbf{R}_\alpha \cdot \nabla_\alpha V\rangle. \quad (7)$$

Now, since the averaging in (7) is over all space no further results can be obtained unless some assumption is made about $\psi(\mathbf{R}_1 \cdots \mathbf{R}_\nu, \ \mathbf{r}_1 \cdots \mathbf{r}_n)$. We therefore assume that the nuclear and electronic motions are separable such that in the zeroth order

$$\psi(\mathbf{R}_1 \cdots \mathbf{R}_\nu, \quad \mathbf{r}_1 \cdots \mathbf{r}_n) = \phi_N(\mathbf{R}_1 \cdots \mathbf{R}_\nu)\phi_e(\mathbf{r}_1 \cdots \mathbf{r}_n, \mathbf{R}_1 \cdots \mathbf{R}_\nu). \quad (8)$$

In this case we can integrate over electronic coordinates so that (7) becomes

$$2\langle T(\mathbf{R}_\alpha)\rangle = \int \cdots \int \mid \phi_N \mid^2 \mathbf{R}_\alpha \cdot \nabla_\alpha W_e d\mathbf{R}_1 \cdots d\mathbf{R}_\nu, \quad (9)$$

where we have used the Hellmann-Feynman[5] theorem obtaining

$$\int \cdots \int \phi_e^* \nabla_\alpha V \phi_e d\mathbf{r}_1 \cdots d\mathbf{r}_n = \nabla_\alpha W_e, \quad (10)$$

where $W_e(\mathbf{R}_1 \cdots \mathbf{R}_\nu)$ is the normal Born-Oppenheimer molecular energy.[6]

We can now integrate over electronic coordinates in Eq. (6) and substitute for every $T(\mathbf{R}_\alpha)$ term using (9). Thus

$$\int \cdots \int \mid \phi_N \mid^2 \{\sum_\alpha \mathbf{R}_\alpha \cdot \nabla_\alpha W_e + 2\bar{T}_e(\mathbf{R}_1 \cdots \mathbf{R}_\nu) + \bar{V}_e(\mathbf{R}_1 \cdots \mathbf{R}_\nu)\} d\mathbf{R}_1 \cdots d\mathbf{R}_\nu = 0, \quad (11)$$

where $\bar{T}_e$ and $\bar{V}_e$ are the electronic kinetic and total electrostatic potential energies, respectively.

At this point we note that nowhere in the derivation of (11) was it necessary to assume that the nuclear kinetic energy is zero. The only approximation was the use of the zeroth-order separable wave function.

From Eq. (11) it is possible to arrive at the standard expression for the molecular virial theorem in two different ways.

A. We may require that the quantity in brackets vanish for all $\mathbf{R}$, yielding

$$\sum_{\alpha,j} X_{\alpha j}(\partial W/\partial X_{\alpha j}) + 2\bar{T}_e = -\bar{V}_e, \quad (12)$$

where j sums over the cartesian coordinates of the αth nucleus. Equation (12) is certainly a solution of (11).

B. Assume the nuclei are localized essentially at the points $(\mathbf{R}_1', \cdots \mathbf{R}_\nu')$. Mathematically this is equivalent to choosing $\mid \phi_N \mid^2$ to be a three ν-dimensional delta function, for by definition of the delta function we have

$$\int \cdots \int f(\mathbf{R}_1 \cdots \mathbf{R}_\nu)\delta(\mathbf{R}_1 - \mathbf{R}_1', \cdots) d\mathbf{R}_1 \cdots d\mathbf{R}_\nu = f(\mathbf{R}_1' \cdots \mathbf{R}_\nu'). \quad (13)$$

But $\mathbf{R}'$ is arbitrary so that (12) holds for all $\mathbf{R}$'s. This assumption is also equivalent to the classical choice of the nuclear kinetic energy zero.

The following conclusions can therefore be drawn. First, the nuclear kinetic energy of the αth nucleus in the separable case is given by $\frac{1}{2}\langle \mathbf{R}_\alpha \cdot \nabla_\alpha W_e\rangle$. Second, one knows, from Eq. (11), exactly what assumptions must be made in deriving (12)—the standard statement of the molecular virial theorem. Although in the case of assumption (A) no knowledge as to its validity is available, since there is no reason for example to believe that the integrand in (11) is everywhere positive. If the latter were true of course Eq. (12) would follow. In view of this it seems that assumption B is the correct choice.[7]

---

[3] J. C. Slater, J. Chem. Phys. **1**, 687 (1933).

[4] See, for example, H. Eyring, J. Walter, and G. E. Kimball, *Quantum Chemistry* (John Wiley & Sons, Inc., New York, 1944), p. 355.

[5] See, for example, R. P. Feynman, Phys. Rev. **56**, 340 (1939).

[6] In order that W_e have the significance of a nuclear potential energy one must invoke the full Born-Oppenheimer approximation which contains some assumptions not necessary in the derivation of Eq. (11).

[7] This seems to be the most reasonable choice since it is only in the limit as the nuclear masses become infinite that the exact wave function goes into the separable one, and surely as the nuclear masses become infinite $\mid \phi_n \mid^2$ goes into a delta function. This can be easily seen, for example, in the case of the harmonic oscillator.

IV. APPLICATION TO FORCE CONSTANTS

In a diatomic molecule $A-B$ with the origin of coordinates such that $\mathbf{R}_A \equiv (0,0,0)$ and $\mathbf{R}_B \equiv (X_B, 0, 0)$ we let $X_B = R$ so that (12) becomes

$$R(\partial W_e/\partial R)+2W_e=\bar{V}_e, \tag{14}$$

where we have used the fact that $W_e=\bar{T}_e+\bar{V}_e$. Differentiating this expression yields

$$(\partial^2 W_e/\partial R^2)+(2/R)(\partial W_e/\partial R)$$

$$=(1/R)\int\frac{\partial}{\partial R}(|\phi_e|^2)V d\mathbf{r}_1\cdots d\mathbf{r}_n \tag{15}$$

since

$$\partial W_e/\partial R=\int|\phi_e|^2\partial V/\partial R d\tau$$

from the Hellmann-Feynman theorem. Now it is clear from Eq. (15) that if one assumes that $|\phi_e|^2$ is independent of R an unbound molecular state results [i.e., the solution of (15) when the right-hand side is zero is simply $a+b/R$ since (15) is then simply the Laplace equation for a spherical potential].

The fact that the amount of electronic charge following the nuclei must be large has also been pointed out by Brown.[1] However, the foregoing equation makes it much more apparent that the assumption of a static electronic charge distribution cannot yield reasonable results. Although no one would argue that ϕ_e is independent of R, it may seem reasonable to assume that the change in ϕ_e gives rise to a relatively small contribution to the force constant. *However Eq. (14) states simply that the change in ϕ_e is the only thing that gives rise to a nonvanishing force constant!*

V. DISCUSSION OF MOLECULAR MODELS

In 1950 Platt[8] achieved some remarkable results in his theoretical calculation of force constants of the diatomic hydrides M—H. His results, however, were based on an assumption that violates the theorem of part IV of this paper. In the following we will try to justify this apparently incompatible situation.

A brief resume of Platt's method will now be given using a slightly different method. The assumptions made were as follows

(a) The total electron density is spherically symmetrical about the atom M of nuclear charge Z_M.

(b) The total electron density is independent of R, the internuclear separation.

(c) The total electron density is given by the density of the united atom of charge Z_M+1.

With assumption (a) we can immediately write down the force on the proton in the hydride M—H as

$$\partial W/\partial R=-Z_M/R_{MH}^2+[Q(R_{MH})/R_{MH}^2], \tag{16}$$

where $Q(R_{MH})$ is the total electronic charge in a sphere about M of radius R_{MH}. The equilibrium condition is $Z_M=Q(R_{MH}^0)$ so that the force constant is

$$\partial^2 W/\partial R_{MH}^2|_0=(1/R_{MH}^2)(dQ/dR_{MH})|_0$$

$$=4\pi\rho(Z_M+1)|_0, \tag{17}$$

where assumptions (b) and (c) have been invoked and $\rho(Z_M+1)$ is the united atom density evaluated at $r=R_{MH}$.

The derivation of Eq. (17) cannot be correct since as previously stated it implicitly violates the virial theorem. This violation is embodied in the equilibrium condition since, according to Eqs. (14) and (15), setting $\partial W/\partial R$ equal to zero is equivalent [in view of assumption (b)] to setting $\partial^2 W/\partial R^2=0$. Unfortunately this result is not apparent from the Hellmann-Feynman theorem alone.

The preceding arguments leave unanswered the question of how Platt achieved such good agreement with experiment. Since his method involved no empirical parameters it is necessary to answer such a question. We attempt to do this as follows. Let the exact electron density as measured from nucleus M be

$$\rho(\mathbf{r}_M, R)=\rho_{uA}(\mathbf{r}_M)+\Delta(\mathbf{r}_M, R), \tag{18}$$

where $\rho_{uA}(\mathbf{r}_M)$ is the exact united atom density. We now consider the force on nucleus B (the proton in the hydride example). If $\rho_{uA}(\mathbf{r}_M)$ is derived from a nondegenerate electronic state, this is

$$\partial W/\partial R=[Z_B(Q-Z_M)/R^2]$$

$$+Z_B\int\Delta(\mathbf{r}_M, R)(X_B/r_B^3)d\tau, \tag{19}$$

where Q has the same meaning as in Eq. (15). The second term in (19) is just the force on nucleus B due to the correction density $\Delta(\mathbf{r}_M, R)$. The force constant is obtained by differentiating (19). Thus

$$\partial^2 W/\partial R^2=(Z_B/R^2)(dQ/dR)-[2Z_B(Q-Z_M)/R^3]$$

$$+Z_B(\partial/\partial R)\left\{\int\Delta(\mathbf{r}_M, R)(X_B/r_B^3)d\tau\right\}. \tag{20}$$

Letting

$$\int\Delta(\mathbf{r}_M, R)(X_B/r_B^3)d\tau\equiv F_A,$$

and using the equilibrium condition, we have

$$\partial^2 W/\partial R^2|_0=\{4\pi\rho_{uA}+(2Z_B/R)F_A+Z_B(\partial F_A/\partial R)\}|_0. \tag{21}$$

Now, since the first term is exactly the Platt formula, it is only necessary to show that the last two terms cancel in some approximation.

It is apparent that if F_A were a simple inverse-square force involving λ units of charge, the previously men-

[8] J. R. Platt, J. Chem. Phys. 18, 932 (1950).

tioned canceling would occur. That is

$$F_A=\lambda/R^2; \quad \{2(Z_B/R)F_A+Z_B(\partial F_A/\partial R)\}\,|_0=0 \quad (22)$$

independent of the sign of F_A. Moreover this will not involve all of the correction density since any amount of spherical (or otherwise symmetrically disposed) charge about the proton will have no effect on F_A. Thus, accepting Platt's results as sufficiently close to experiment to be correct, one can argue that the effective correction density is so disposed relative to the proton so as to appear like a point charge.[9] The latter, incidentally, does not preclude the possibility that Δ has over-all multipolar character. On the contrary the integral of Δ over all space must, by definition, vanish.

Finally, it may be noted that a formula analogous to Eq. (17) can be derived if one assumes a density of the form $\rho_M+\rho_H$ where the latter are spherical functions about M and H, respectively. This "double-sphere" model, although it yields the proper ordering of the force constants in hydrides and also avoids to some extent the virial violation, lacks in other respects (the most obvious of which is that it does not give the correct numerical results). The reason for the deficiencies in this model is that it does not give the variation in ρ its proper place in the force constant formula since that part of ρ (i.e., ρ_H) that results in $\partial\rho/\partial R\neq 0$ is not even involved in the final expression for $\partial^2W/\partial R^2$.

VI. KINETIC ENERGY THEORY OF MOLECULAR BINDING

The theorem of Sec. IV can be cast into a further useful form by using the kinetic instead of the potential energy formulation of the virial. We may write then

$$\partial^2W_e/\partial R^2\,|_0=-(1/R_0)\,(\partial\bar{T}_e/\partial R)\,|_0, \quad (23)$$

where $\bar{T}_e$ is the electronic kinetic energy. We therefore have the following stability requirement: *at the equilibrium internuclear separation the electronic kinetic energy must be increasing with decreasing R to insure a positive force constant.* This formulation makes it quite clear that any attempt to explain molecular stability on the basis of a reduction of kinetic energy is doomed to failure.[10] One can, however, use the kinetic energy formulation to obtain some other qualitative ideas about molecular binding. For example, one may assume a shape for the molecule and calculate the force constant on the basis of the "particle in a box" model. The simplest such calculation would proceed as follows. If the electrons, on the average, are contained in a sphere of radius $a(R)$, then $\langle T\rangle\propto a^{-2}$ so that

$$K=(\lambda/R_0a^3)\,(\partial a/\partial R)\,|_{R_0}, \quad (24)$$

where λ is a proportionality constant. Near the equilibrium position it is reasonable to assume $a(R)\propto R$ so that K becomes

$$K=(\lambda'/R_0^4). \quad (25)$$

We note that the form of Eq. (25) is the same as one used by Birge and Mecke[11] for force constant correlation.

VII. CONCLUSIONS

We conclude at this point by noting that the virial theorem allows a force constant formula to be derived that puts certain limitations on molecular models. Although it may be intuitively attractive to ignore the change in the electronic wave function as the nuclei move, it seems to make no physical sense to adopt such a procedure. However, from a computational point of view, at least for diatomic hydrides, it yields good results. But this does not necessarily shed any light on the process of molecular binding, since less severe assumptions allow one to derive essentially the same formula.

VIII. ACKNOWLEDGMENTS

The author would like to record his indebtedness to Professor R. A. Marcus of Brooklyn Polytechnic Institute for many helpful and suggestive discussions. Appreciation is also due Dr. W. C. Hamilton, Dr. R. F. Schneider, Dr. M. Wolfsberg, and Dr. E. H. Kerner of this Laboratory.

[9] The position of this point charge is also somewhat arbitrary. That is, if the distance of Δ from the proton is R' where R' is proportional to R Eq. (22) is still satisfied.

[10] G. Hall has also pointed out this inconsistency and is quoted by Lowdin in footnote 1. See also W. Lichten, J. Chem. Phys. **22**, 1278 (1954).

[11] R. T. Birge, Phys. Rev. **25**, 240 (1925); R. Meche, Z. Physik **32**, 823 (1925).

THE JOURNAL OF CHEMICAL PHYSICS VOLUME 33, NUMBER 6 DECEMBER, 1960

Molecular Size Distribution and Gelation of Irradiated Copolymers

MITIO INOKUTI

Department of Applied Physics, Faculty of Engineering, University of Tokyo, Tokyo, Japan

(Received January 18, 1960)

A theory is developed about the molecular size distribution in a system of copolymers which are composed of two different kinds of monomer units and undergo random crosslinking when exposed to high-energy radiations. The radiation-induced change in the molecular size distribution is described by an integro-differential equation, which we solve exactly by means of Laplace transform for an arbitrary initial distribution to obtain the number-average as well as the weight-average degree of polymerization as a function of radiation dose. Further, the gel point, or the dose required for incipient gelation, is given as a function of concentrations of the monomer units constituting the copolymeric system. The present theory, which also involves the problem of crosslinking in a mixture of two kinds of polymers as a special case, leads to a condition for gelation of such a mixture due to irradiation when crosslinking competes with main-chain scission. This condition proves to be completely independent of the initial distribution.

INTRODUCTION

As is well known, polymers become crosslinked and/or degraded when subjected to high-energy radiations. The molecular size distribution in a polymeric substance is then continually altered so that changes in various average degrees of polymerization and solubility are brought about. In particular, an insoluble gel or a macroscopically large molecular network is formed at a certain dose as far as crosslinking predominates over degradation.[1]

Concerning the variation of the molecular size distribution due to random crosslinking and main-chain scission, several theories have been worked out by Flory,[2] Stockmayer,[3] Charlesby,[4,5] Saito,[6] and others.[7,8]

In these years, several experimental data about irradiation of copolymers and of mixtures of different kinds of polymers have been reported.[1,9–13] However, theoretical treatments have been restricted to ordinary polymers composed of a single kind of monomer unit only. In this paper, we will develop a theory of the molecular size distribution and gelation of irradiated copolymers composed of two different kinds of monomer units. The present formalism is a generalization of Saito's theory,[6,7] which has proved to be not only very fruitful but also capable of extension to complicated cases.[14] Our treatment will also involve the problem of crosslinking of a mixture of two kinds of polymers as a special case.

THE BASIC EQUATION

Let us consider a system of copolymers composed of two kinds of monomer units. We will hereafter refer to each of the two kinds as the first and the second, respectively. Let N_i $(i=1, 2)$ be the total number of the monomer units of the ith kind in the whole system, then the number concentration ν_i $(i=1, 2)$ is written as

$$\nu_i=N_i/N, \qquad N=N_1+N_2, \tag{1}$$

where we must have

$$\nu_1+\nu_2=1. \tag{2}$$

We suppose that exposure to high-energy radiation introduces the following three types of crosslinks, i.e.,

(i) (1–1) link, meaning a crosslink between a pair of monomer units of the first kind,

(ii) (1–2) link, meaning a crosslink between a monomer unit of the first kind and one of the second kind,

(iii) (2–2) link, meaning a crosslink between a pair of monomer units of the second kind.

Now we are interested in the description of the change in the molecular size distribution caused by irradiation. For this purpose, we define the molecular size distribution function $n(p_1, p_2, R)dp_1dp_2$ as the number of copolymers composed of $p_1\sim p_1+dp_1$ monomer units of the first kind and $p_2\sim p_2+dp_2$ monomer units of the second kind when the system has been irradiated up to

[1] Cf., e.g., F. A. Bovey, *The Effects of Ionizing Radiation on Natural and Synthetic High Polymers* (Interscience Publishers, Inc., New York, 1958), Polymer Reviews, Vol. 1.

[2] P. J. Flory, J. Am. Chem. Soc. **63**, 3083, 3091, 3096 (1941); J. Phys. Chem. **46**, 132 (1942); J. Am. Chem. Soc. **69**, 30 (1947).

[3] W. H. Stockmayer, J. Chem. Phys. **11**, 45 (1943); **12**, 125 (1944).

[4] A. Charlesby, J. Polymer Sci. **11**, 513 (1953).

[5] A. Charlesby, Proc. Roy. Soc. (London) **A222**, 542 (1954); **A224**, 120 (1954); **A231**, 521 (1955); **A241**, 495 (1957).

[6] O. Saito, J. Phys. Soc. Japan **13**, 198, 1451, 1465 (1958).

[7] M. Inokuti, J. Phys. Soc. Japan **14**, 79; M. Inokuti and K. Katsuura, *ibid.* **14**, 1379 (1959).

[8] V. S. Nanda and R. K. Pathria, J. Chem. Phys. **30**, 27, 31, 35, 1322 (1959).

[9] E. J. Lawton, A. M. Bueche, and J. S. Balwit, Nature **172**, 76 (1953).

[10] P. Alexander and A. Charlesby, Proc. Roy. Soc. (London) **A230**, 136 (1955).

[11] R. Bauman and J. Glantz, J. Polymer Sci. **24**, 397 (1957).

[12] J. A. Parker, F. F. Bentley, E. A. Peterson, and D. Hale, *The Effects of Gamma Radiation on Acrylonitrile-Butadiene Copolymers*, *WADC-TR-58-78* (Wright Air Development Center, Ohio, 1958).

[13] W. Burlant, D. Green, and C. Taylor, J. Appl. Polymer Sci. **1**, 296 (1959).

[14] O. Saito, J. Phys. Soc. Japan **14**, 792, 798 (1959).

radiation dose R. Here we regard with Saito[6] the number of monomer units as a continuous, rather than discrete, variable in order to facilitate mathematical treatments. This is permissible as long as we deal with high polymers with large degree of polymerization.

Further we assume with Charlesby,[4,5] Saito,[6] and others[2,3] that crosslinking takes place at random so that we can define the probability of crosslinking. Thus we denote by c_{ij} $(i=1, 2; j=1, 2)$ the probability of the occurrence of an $(i-j)$ link per unit dose per each of the monomer units taking part in the $(i-j)$ link.

Now we will derive an equation that describes the change in $n(p_1, p_2, R)$ due to irradiation. We will neglect cyclization or a crosslinking within a molecule. In view of Saito's result,[6] the effect of cyclization generally introduces only a negligible correction. The rate of change in $n(p_1, p_2, R)$, or $\partial n(p_1, p_2, R)/\partial R$, consists of various contributions that we will enumerate in the following.

For the sake of brevity, we will refer to a copolymer composed of p_1 monomer units of the first kind and p_2 monomer units of the second kind as a copolymer (p_1, p_2). When a monomer unit of the first kind within a copolymer (p_1, p_2) undergoes (1-1) links, then $n(p_1, p_2, R)$ decreases by the amount $2c_{11}\nu_1 p_1 n(p_1, p_2, R)$ per unit dose, according to the definition of c_{11}. Note that the factor 2 comes from both of the partners of the (1-1) link. The contribution of (2-2) links to the decrease of $n(p_1, p_2, R)$ per unit dose is evidently given by the analogous term $2c_{22}\nu_2 p_2 n(p_1, p_2, R)$. The contribution of (1-2) links to the decrease of $n(p_1, p_2, R)$ consists of two terms corresponding to the two possibilities that either a monomer unit of the first kind or that of the second kind within the copolymer (p_1, p_2) takes part in the (1-2) link. Thus it is given by $2c_{12}(\nu_1 p_2+\nu_2 p_1)n(p_1, p_2, R)$.

Next we examine the increase of $n(p_1, p_2, R)$. When a copolymer (q_1, q_2) and a copolymer (p_1-q_1, p_2-q_2) form a crosslink together, we have a copolymer (p_1, p_2), where $0\leq q_1\leq p_1$, $0\leq q_2\leq p_2$. It is easy to see that the (1-1) link contributes to the increase of $n(p_1, p_2, R)$

$$(c_{11}/N)\int_0^{p_1}dq_1\int_0^{p_2}dq_2 q_1(p_1-q_1)n(q_1, q_2, R)\,n(p_1-q_1, p_2-q_2, R),$$

and the (2-2) link

$$(c_{22}/N)\int_0^{p_1}dq_1\int_0^{p_2}dq_2 q_2(p_2-q_2)n(q_1, q_2, R)\,n(p_1-q_1, p_2-q_2, R).$$

The contribution of the (1-2) link is made up of two terms, each of which represents whether the monomer unit of the first kind taking part in the (1-2) link has belonged to either the copolymer (q_1, q_2) or the copolymer (p_1-q_1, p_2-q_2). Thus we have

$$(c_{12}/N)\int_0^{p_1}dq_1\int_0^{p_2}dq_2\{q_1(p_2-q_2)+(p_1-q_1)q_2\}\,n(q_1, q_2, R)n(p_1-q_1, p_2-q_2, R)$$
$$=(2c_{12}/N)\int_0^{p_1}dq_1\int_0^{p_2}dq_2 q_1(p_2-q_2)n(q_1, q_2, R)\,n(p_1-q_1, p_2-q_2, R)$$

as the contribution of the (1-2) link to the increase of $n(p_1, p_2, R)$.

Collecting all the terms, we obtain the following equation:

$$\partial n(p_1, p_2, R)/\partial R$$
$$=-\{2c_{11}\nu_1 p_1+2c_{22}\nu_2 p_2+2c_{12}(\nu_2 p_1+\nu_1 p_2)\}n(p_1, p_2, R)$$
$$+N^{-1}\int_0^{p_1}dq_1\int_0^{p_2}dq_2$$
$$\times\{c_{11}q_1(p_1-q_1)+c_{22}q_2(p_2-q_2)+2c_{12}q_1(p_2-q_2)\}$$
$$\times n(q_1, q_2, R)n(p_1-q_1, p_2-q_2, R). \quad (3)$$

For convenience we will hereafter work with the normalized distribution function

$$m(p_1, p_2, R)=n(p_1, p_2, R)/N. \quad (4)$$

Then the basic equation is rewritten as

$$\partial m(p_1, p_2, R)/\partial R$$
$$+\{2c_{11}\nu_1 p_1+2c_{22}\nu_2 p_2+2c_{12}(\nu_2 p_1+\nu_1 p_2)\}m(p_1, p_2, R)$$
$$=\int_0^{p_1}dq_1\int_0^{p_2}dq_2\{c_{11}q_1(p_1-q_1)+c_{22}q_2(p_2-q_2)$$
$$+2c_{12}q_1(p_2-q_2)\}m(q_1, q_2, R)m(p_1-q_1, p_2-q_2, R). \quad (5)$$

Once the initial distribution is specified, we can determine $m(p_1, p_2, R)$ for an arbitrary dose R by solving (5). The solution will be discussed later.

Here we will give a few remarks on the interpretation of the crosslinking probabilities c_{11}, c_{12}, c_{22}. In this paper they will be regarded as constants. Under some circumstances they may be functions of concentrations ν_1 and ν_2, depending on the specific mechanism of crosslinking reactions. But, as far as our formalism is concerned, it is evident that nothing would be affected even if c_{11}, c_{12}, and c_{22} depended on ν_1 and ν_2. It should be also noted that we have assigned a definite probability of crosslinking to every monomer unit. This means that we implicitly assume that the formation of a crosslink is independent of the configuration of monomer units within a copolymer. This assumption, if we understand it too literally, cannot always be reasonable, because steric hindrance and other configuration-dependent effects sometimes favor and sometimes dis-

favor the formation of a crosslink. Consequently, we must interpret c_{11}, c_{12}, and c_{22} as statistical quantities referring to the probabilities on the average.

CONSERVATION OF TOTAL NUMBER OF MONOMER UNITS AND NUMBER-AVERAGE DEGREE OF POLYMERIZATION

Before solving (5), we make some preliminary observations. First, we define $f^{(k,l)}(R)$ by

$$f^{(k,l)}(R)=\int_0^\infty dp_1\int_0^\infty dp_2 p_1^k p_2^l m(p_1, p_2, R). \tag{6}$$

Performing the operation

$$\int_0^\infty dp_1\int_0^\infty dp_2 p_1^k p_2^l$$

on both sides of (5), we obtain the following equation:

$$\begin{aligned}df^{(k,l)}/dR&+2c_{11}\nu_1 f^{(k+1,l)}+2c_{22}\nu_2 f^{(k,l+1)}\\&+2c_{12}(\nu_2 f^{(k+1,l)}+\nu_1 f^{(k,l+1)})\\&=\sum_{r=0}^{k}\sum_{s=0}^{l}{}_kC_r\,{}_lC_s\{c_{11}f^{((r+1,s)}f^{(k-r+1,l-s)}\\&+c_{22}f^{(r,s+1)}f^{(k-r,l-s+1)}+2c_{12}f^{(r+1,s)}f^{(k-r,l-s+1)}\}.\end{aligned} \tag{7}$$

Putting $k=1$, $l=0$, and $k=0$, $l=1$, we have

$$\begin{aligned}df^{(1,0)}/dR&=2(c_{11}f^{(2,0)}+c_{12}f^{(1,1)})(f^{(1,0)}-\nu_1)\\&\quad+2(c_{12}f^{(2,0)}+c_{22}f^{(1,1)})(f^{(0,1)}-\nu_2),\\df^{(0,1)}/dR&=2(c_{11}f^{(1,1)}+c_{12}f^{(0,2)})(f^{(1,0)}-\nu_1)\\&\quad+2(c_{12}f^{(1,1)}+c_{22}f^{(0,2)})(f^{(0,1)}-\nu_2).\end{aligned} \tag{8}$$

Now, by the definition of $m(p_1, p_2, 0)$, $f^{(1,0)}(0)$, and $f^{(0,1)}(0)$ must be the concentrations of the monomer units of the first kind and of the second kind, respectively,

$$f^{(1,0)}(0)=\nu_1, \qquad f^{(0,1)}(0)=\nu_2. \tag{9}$$

Then it is easy to see that, by (8) and (9),

$$f^{(1,0)}(R)=\nu_1, \qquad f^{(0,1)}(R)=\nu_2 \tag{10}$$

for any R, as far as the quantities on the right-hand sides of the Eqs. (8) are analytic functions of R. Thus we have shown that the total number of each kind of monomer unit conserves. This confirms the self-consistency of our formalism.

For $k=l=0$, (7) is written as

$$df^{(0,0)}/dR=-c_{11}\nu_1^2-2c_{12}\nu_1\nu_2-c_{22}\nu_2^2, \tag{11}$$

where use has been made of (10). Therefore,

$$f^{(0,0)}(R)=f^{(0,0)}(0)-(c_{11}\nu_1^2+2c_{12}\nu_1\nu_2+c_{22}\nu_2^2)R. \tag{12}$$

Then the number-average degree of polymerization $P_n(R)$ at dose R is given as

$$\begin{aligned}P_n(R)&=\frac{\int_0^\infty dp_1\int_0^\infty dp_2(p_1+p_2)m(p_1, p_2, R)}{\int_0^\infty dp_1\int_0^\infty dp_2 m(p_1, p_2, R)}\\&=[f^{(0,0)}(R)]^{-1}\\&=\frac{P_n(0)}{1-(c_{11}\nu_1^2-2c_{12}\nu_1\nu_2+c_{22}\nu_2^2)P_n(0)R},\end{aligned} \tag{13}$$

where $P_n(0)$ is the number-average degree of polymerization prior to irradiation.

It is difficult to calculate the weight-average degree of polymerization $P_w(R)$ at dose R

$$\begin{aligned}P_w(R)&=\frac{\int_0^\infty dp_1\int_0^\infty dp_2(p_1+p_2)^2 m(p_1, p_2, R)}{\int_0^\infty dp_1\int_0^\infty dp_2(p_1+p_2)m(p_1, p_2, R)}\\&=f^{(2,0)}(R)+2f^{(1,1)}(R)+f^{(0,2)}(R)\end{aligned} \tag{14}$$

by means of (7). To derive an expression for it, we had better resort to another method that will be given later.

LAPLACE TRANSFORM

We define the Laplace transform $F(x_1, x_2, R)$ of $m(p_1, p_2, R)$ by

$$\begin{aligned}&F(x_1, x_2, R)\\&=\int_0^\infty dp_1\int_0^\infty dp_2 m(p_1, p_2, R)\exp(-p_1x_1-p_2x_2).\end{aligned} \tag{15}$$

Carrying out the operation

$$\int_0^\infty dp_1\int_0^\infty dp_2\exp(-p_1x_1-p_2x_2)$$

on both sides of (5), and interchanging orders of integrations, we obtain the following partial differential equation for $F(x_1, x_2, R)$,

$$\begin{aligned}\partial F/\partial R&=2(\nu_1c_{11}+\nu_2c_{12})(\partial F/\partial x_1)\\&\quad+2(\nu_1c_{12}+\nu_2c_{22})(\partial F/\partial x_2)+c_{11}(\partial F/\partial x_1)^2\\&\quad+2c_{12}(\partial F/\partial x_1)(\partial F/\partial x_2)+c_{22}(\partial F/\partial x_2)^2.\end{aligned} \tag{16}$$

Now we have to impose on $F(x_1, x_2, R)$ the initial condition

$$\begin{aligned}F(x_1, x_2, 0)=G(x_1, x_2)&\equiv\int_0^\infty dp_1\int_0^\infty dp_2 m(p_1, p_2, 0)\\&\quad\times\exp(-p_1x_1-p_2x_2),\end{aligned} \tag{17}$$

where the function $G(x_1, x_2)$ is the Laplace transform of the initial distribution $m(p_1, p_2, 0)$.

Then the required solution of (16) is given by

$$F=G(s_1, s_2)-R\{c_{11}(\partial G/\partial s_1)^2+2c_{12}(\partial G/\partial s_1)(\partial G/\partial s_2)+c_{22}(\partial G/\partial s_2)^2\}, \quad (18)$$

$$x_1-s_1+2R[c_{11}(\partial G/\partial s_1)+c_{12}(\partial G/\partial s_2)+\nu_1 c_{11}+\nu_2 c_{12}]=0, \quad (19)$$

$$x_2-s_2+2R[c_{12}(\partial G/\partial s_1)+c_{22}(\partial G/\partial s_2)+\nu_1 c_{12}+\nu_2 c_{22}]=0, \quad (20)$$

where s_1 and s_2 are parameters. If we eliminate s_1 and s_2 from (18), (19), and (20), we obtain F as a function of x_1, x_2, and R. The derivation of this result is given in Appendix. The distribution function $m(p_1, p_2, R)$ itself can be evaluated by the inverse Laplace transform formula[15]

$$m(p_1, p_2, R)=[(2\pi i)^2]^{-1}\int_{-i\infty+\tau_1}^{i\infty+\tau_1}dx_1\int_{-i\infty+\tau_2}^{i\infty+\tau_2}dx_2 F(x_1, x_2, R)\times\exp(+p_1x_1+p_2x_2) \qquad (\tau_1>0, \tau_2>0). \quad (21)$$

The quantity $f^{(k,l)}(R)$, defined by (6), is expressed in terms of $F(x_1, x_2, R)$ as

$$f^{(k,l)}(R)=[(-\partial/\partial x_1)^k(-\partial/\partial x_2)^l F(x_1, x_2, R)]_{x_1=x_2=0}. \quad (22)$$

Differentiating (18), (19), and (20) with respect to x_1, we find

$$\partial F/\partial x_1=(\partial G/\partial s_1)(\partial s_1/\partial x_1)+(\partial G/\partial s_2)(\partial s_2/\partial x_1) -2R\{c_{11}(\partial G/\partial s_1)(\partial/\partial x_1)(\partial G/\partial s_1) +c_{12}(\partial G/\partial s_2)(\partial/\partial x_1)(\partial G/\partial s_1) +c_{12}(\partial G/\partial s_1)(\partial/\partial x_1)(\partial G/\partial s_2) +c_{22}(\partial G/\partial s_2)(\partial/\partial x_1)(\partial G/\partial s_2)\}, \quad (23)$$

$$1-(\partial s_1/\partial x_1)+2R\{c_{11}(\partial/\partial x_1)(\partial G/\partial s_1)+c_{12}(\partial/\partial x_1)(\partial G/\partial s_2)\}=0, \quad (24)$$

$$-(\partial s_2/\partial x_1)+2R\{c_{12}(\partial/\partial x_1)(\partial G/\partial s_1)+c_{22}(\partial/\partial x_1)(\partial G/\partial s_2)\}=0. \quad (25)$$

Combining (23), (24), and (25), we have

$$\partial F/\partial x_1=\partial G/\partial s_1. \quad (26a)$$

Similarly, we also have

$$\partial F/\partial x_2=\partial G/\partial s_2. \quad (26b)$$

[15] P. M. Morse and H. Feshbach, *Methods of Theoretical Physics* (McGraw-Hill Book Company, Inc., New York, 1953), Vol. 1, p. 468.

Putting $x_1=x_2=0$ in (26) and taking note of (10) and (22),

$$[\partial G/\partial s_1]_{x_1=x_2=0}=[\partial F/\partial x_1]_{x_1=x_2=0}=-f^{(1,0)}(R)=-\nu_1,$$
$$[\partial G/\partial s_2]_{x_1=x_2=0}=[\partial F/\partial x_2]_{x_1=x_2=0}=-f^{(0,1)}(R)=-\nu_2. \quad (27)$$

Then we put $x_1=x_2=0$ in (19) and (20) and employ (27) to find that

$$s_1=s_2=0 \quad \text{when } x_1=x_2=0. \quad (28)$$

It should be noted that a previous result (11) can be easily derived by putting $x_1=x_2=0$ in (18).

WEIGHT-AVERAGE DEGREE OF POLYMERIZATION AND GELATION

To evaluate the weight-average degree of polymerization $P_w(R)$, defined by (13), we first calculate $f^{(2,0)}(R)$. By (22), (27) and (28), we find

$$f^{(2,0)}(R)=[\partial^2F/\partial x_1^2]_{x_1=x_2=0}=[(\partial/\partial x_1)(\partial G/\partial s_1)]_{x_1=x_2=0}$$
$$=[(\partial^2G/\partial s_1^2)(\partial s_1/\partial x_1)+(\partial^2G/\partial s_2\partial s_1)(\partial s_2/\partial x_1)]_{x_1=x_2=0}.$$

For simplicity, we introduce the following abbreviations,

$$A_1\equiv f^{(2,0)}(0), \qquad A_2\equiv f^{(0,2)}(0), \qquad B\equiv f^{(1,1)}(0), \quad (29)$$

$$\alpha_1\equiv[\partial s_1/\partial x_1]_{x_1=x_2=0}, \qquad \alpha_2\equiv[\partial s_2/\partial x_1]_{x_1=x_2=0}. \quad (30)$$

Then,

$$f^{(2,0)}(R)=A_1\alpha_1+B\alpha_2. \quad (31)$$

Putting $x_1=x_2=0$ in (24), we have

$$1-\alpha_1+2R\{c_{11}(A_1\alpha_1+B\alpha_2)+c_{12}(B\alpha_1+A_2\alpha_2)\}=0, \quad (32)$$

$$-\alpha_2+2R\{c_{12}(A_1\alpha_1+B\alpha_2)+c_{22}(B\alpha_1+A_2\alpha_2)\}=0. \quad (33)$$

By (32) and (33), α_1 and α_2 are determined as

$$\alpha_1=\{1-2R(Bc_{12}+A_2c_{22})\}/\Delta, \quad (34)$$

$$\alpha_2=2R(A_1c_{12}+Bc_{22})/\Delta, \quad (35)$$

where

$$\Delta\equiv 1-2R(A_1c_{11}+2Bc_{12}+A_2c_{22})+4R^2(A_1A_2-B^2)(c_{11}c_{22}-c_{12}^2). \quad (36)$$

Substitution of (34) and (35) into (31) then yields

$$f^{(2,0)}(R)=\{A_1-2R(A_1A_2-B^2)c_{22}\}/\Delta. \quad (37)$$

Quite similarly, $f^{(0,2)}(R)$ is given as

$$f^{(0,2)}(R)=\{A_2-2R(A_1A_2-B^2)c_{11}\}/\Delta. \quad (38)$$

Further, we calculate $f^{(1,1)}(R)$ in an analogous way,

$$f^{(1,1)}(R)=[\partial^2F/\partial x_1\partial x_2]_{x_1=x_2=0}=[(\partial/\partial x_1)(\partial G/\partial x_2)]_{x_1=x_2=0}$$
$$=B\alpha_1+A_2\alpha_2$$
$$=\{B+2R(A_1A_2-B^2)c_{12}\}/\Delta. \quad (39)$$

Consequently, substituting (37), (38), and (39)

into (14), we arrive at the following expression for $P_w(R)$,

$$P_w(R)=\{A_1+2B+A_2-2R(A_1A_2-B^2)\times(c_{11}-2c_{12}+c_{12})\}/\Delta. \quad (40)$$

Now we will examine the behavior of $P_w(R)$ as a function of R. We are interested particularly in the value of R where a gel is formed incipiently. This value of R, which we call the gel point [5,6] and denote by R_g, is mathematically defined by

$$\lim_{R\to R_g-0}P_w(R)=+\infty. \quad (41)$$

For subsequent discussion it is necessary to note a lemma that

$$f^{(2,0)}(R)f^{(0,2)}(R)\geq\{f^{(1,1)}(R)\}^2 \quad (42)$$

for any R and any initial distribution. This is proved in the following way. Consider a non-negative quantity

$$\int_0^\infty dp_1\int_0^\infty dp_2(tp_1+p_2)^2m(p_1,p_2,R)\geq 0,$$

where t is any real number. This expression can be written as

$$t^2f^{(2,0)}(R)+2tf^{(1,1)}(R)+f^{(0,2)}(R)\geq 0.$$

Since t is an arbitrary real number, it follows that the inequality (42) must hold. Especially for $R=0$, (42) leads to

$$A_1A_2\geq B^2.$$

If we rewrite (40) as

$$\frac{P_w(R)}{P_w(0)}=\frac{1-\rho_0R}{(1-\rho_1R)(1-\rho_2R)},\qquad P_w(0)\equiv A_1+2B+A_2, \quad (43)$$

then ρ_0, ρ_1, and ρ_2 are given by

$$\rho_0=2(A_1A_2-B^2)(c_{11}-2c_{12}+c_{22})/(A_1+2B+A_2), \quad (44)$$

$$\left.\begin{matrix}\rho_1\\ \rho_2\end{matrix}\right\}=A_1c_{11}+2Bc_{12}+A_2c_{22}\pm D^{\frac{1}{2}}\qquad(\rho_1\geq\rho_2), \quad (45)$$

$$D=(A_1c_{11}+2Bc_{12}+A_2c_{22})^2-4(A_1A_2-B^2)(c_{11}c_{22}-c_{12}^2)$$
$$=A_1A_2\{2c_{12}+(B/A_1A_2)(A_1c_{11}+A_2c_{22})\}^2$$
$$+[(A_1A_2-B^2)/A_1A_2](A_1c_{11}-A_2c_{22})^2. \quad (46)$$

With the aid of the lemma (42), we see that $D\geq 0$ so that ρ_1 and ρ_2 must be real. Then we consider the expression $(\rho_0-\rho_1)(\rho_0-\rho_2)$. We can reduce it after some calculation to the following form,

$$(\rho_0-\rho_1)(\rho_0-\rho_2)=-4(A_1A_2-B^2)(A_1+2B+A_2)^{-2}$$
$$\times[\{(A_1-A_2)c_{12}+(A_1+B)c_{11}-(B+A_2)c_{22}\}^2$$
$$+2(A_1+B)(B+A_2)c_{11}c_{22}].$$

Again, with the aid of the lemma (42), we see that this expression is nonpositive, i.e.,

$$\rho_1\geq\rho_0\geq\rho_2. \quad (47)$$

Thus we arrive at the following conclusion: When R starts increasing from zero, $P_w(R)$ increases monotonously and diverges to infinity at $R=R_g$, where R_g is given by

$$1/R_g=\rho_1=A_1c_{11}+2Bc_{12}+A_2c_{22}+(D)^{\frac{1}{2}}. \quad (48)$$

Besides, $P_w(R)$ behaves like $1/(R-R_g)$ near $R=R_g$ for any values of c_{11}, c_{12} and c_{22} as well as for any initial distribution.

It should be noted that our formalism with its consequences is a generalization of Saito's theory[6] in the sense that the former reduces to the latter in an appropriate limit, e.g., $c_{11}=c$, $c_{12}=0$, $c_{22}=0$, $\nu_1=1$, and $\nu_2=0$.

EXAMPLES

(1) Mixture of two samples of polymers, in each of which the distribution is uniform. Consider two samples of polymers of different kinds. In each of the samples the distribution is assumed to be uniform and the degree of polymerization is denoted by $u_i(i=1,2)$; the mixture is specified by the following distribution function,

$$m(p_1,p_2,0)=\frac{2}{u_1u_2}\left\{\frac{\nu_1}{u_1}\delta\left(\frac{p_1}{u_1}-1\right)\delta\left(\frac{p_2}{u_2}\right)+\frac{\nu_2}{u_2}\delta\left(\frac{p_1}{u_1}\right)\delta\left(\frac{p_2}{u_2}-1\right)\right\}, \quad (49)$$

where $\delta(x)$ is the Dirac delta function.[16] For this initial distribution, we find that

$$f^{(k,l)}(0)=u_1^ku_2^l\{(\nu_1/u_1)\delta_{l0}+(\nu_2/u_2)\delta_{k0}\}, \quad (50)$$

where δ_{ij} is the Kronecker symbol. The function (49), satisfies the normalization condition (9). By (45), (46) and (50), the gel point turns out to be

$$1/R_g=\nu_1c_{11}u_1+\nu_2c_{22}u_2$$
$$+[(\nu_1c_{11}u_1-\nu_2c_{22}u_2)^2+4\nu_1\nu_2c_{12}^2u_1u_2]^{\frac{1}{2}}. \quad (51)$$

(2) Mixture of two samples of polymers, in each of which the distribution is Poisson-like. Consider again two samples of different kinds of polymers. In each of the samples, the distribution is now assumed to be Poisson-like and the number-average degree of polymerization is denoted by u_i $(i=1,2)$. The mixture is specified by[16]

$$m(p_1,p_2,0)=\frac{2}{u_1u_2}\left\{\frac{\nu_1}{u_1}\exp\left(-\frac{p_1}{u_1}\right)\delta\left(\frac{p_2}{u_2}\right)+\frac{\nu^2}{u_2}\delta\left(\frac{p_1}{u_1}\right)\times\exp\left(-\frac{p_2}{u_2}\right)\right\}, \quad (52)$$

[16] The factor 2 on the right-hand side of (49) is accounted for by the fact that

$$\int_0^\infty\delta(x)dx=\tfrac{1}{2}\int_{-\infty}^\infty\delta(x)dx=\tfrac{1}{2}$$

because $\delta(x)$ is an even function.

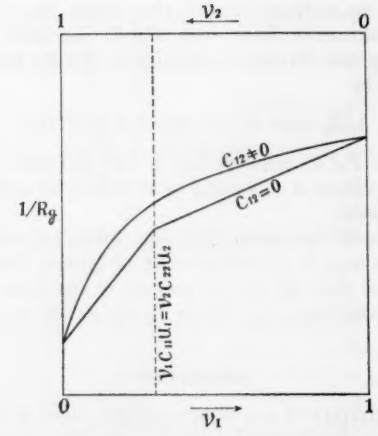

FIG. 1. The behavior of $1/R_g$ for a mixture of two kinds of polymers (schematic).

which is normalized as (9). Then we have

$$f^{(k,l)}(0) = u_1^k u_2^l \{(\nu_1/u_1)\Gamma(k+1)\delta_{l0} + (\nu_2/u_2)\Gamma(l+1)\delta_{k0}\}, \quad (53)$$

so that the gel point is given by

$$1/R_g = 2\{\nu_1 c_{11} u_1 + \nu_2 c_{22} u_2 + [(\nu_1 c_{11} u_1 - \nu_2 c_{22} u_2)^2 + 4\nu_1\nu_2 c_{12}^2 u_1 u_2]^{\frac{1}{2}}\}. \quad (54)$$

This result is similar to (51). In Fig. 1 the behavior of $1/R_g$ as a function of ν_1 or ν_2 is schematically shown. If $c_{12}=0$, the curve consists of two straight lines intersecting at $\nu_1 c_1 u_{11} = \nu_2 c_2 u_{22}$. This fact may be used to determine through experimental data whether a crosslink between different kinds of monomer units occurs or not.

(3) System of copolymers where the distribution is uniform. Let us consider a system of copolymers where the molecular size distribution is uniform. Namely, every copolymer in the system is assumed to be composed of $\nu_1 u$ monomer units of the first kind and $\nu_2 u$ monomer units of the second kind. Such a situation is represented by the initial distribution

$$m(p_1, p_2, 0) = u^{-1}\delta(p_1 - \nu_1 u)\,\delta(p_2 - \nu_2 u) \quad (55)$$

normalized as (9). Then

$$f^{(k,l)}(0) = \nu_1^k \nu_2^l u^{k+l-1}. \quad (56)$$

Therefore, the gel point is given by

$$1/R_g = 2u(c_{11}\nu_1^2 + 2c_{12}\nu_1\nu_2 + c_{22}\nu_2^2). \quad (57)$$

In this case $1/R_g$ behaves as shown in Fig. 2. The curve is a portion of a parabola and is convex upwards or downwards according as $c_{11}+c_{22}-2c_{12}$ is positive or negative. This result may be also useful for analysis of experimental data.

(4) System of copolymers where the distribution is Poisson-like. As the last example, we discuss the initial distribution

$$m(p_1, p_2, 0) = (\nu_1\nu_2 u^3)^{-1} \exp[-(p_1/\nu_1 u) - (p_2/\nu_2 u)], \quad (58)$$

which is normalized as (9). This function represents a system of copolymers where the distribution is Poisson-like. In this case,

$$f^{(k,l)}(0) = \nu_1^k \nu_2^l u^{k+l-1}\Gamma(k+1)\Gamma(l+1), \quad (59)$$

and the gel point is given by the following function, whose behavior is rather complicated,

$$1/R_g = u\{2(c_{11}\nu_1^2 + 2c_{12}\nu_1\nu_2 + c_{22}\nu_2^2) + [(c_{11}\nu_1^2 + 4c_{12}\nu_1\nu_2 + c_{22}\nu_2^2)^2 + 3(\nu_1^2 c_{11} - \nu_2^2 c_{22})^2]^{\frac{1}{2}}\}. \quad (60)$$

GELATION OF A MIXTURE WHEN CROSSLINKING COMPETES WITH SCISSION

So far we have dealt with the case where only crosslinking results from irradiation. In this section we will extend our discussion to a more complicated case where crosslinking competes with main-chain scission. It is naturally expected that there should be a certain condition for gelation in this case. For, if scission predominates over crosslinking to a certain extent, it is evident that a gel can never be formed. As for an ordinary polymeric system (composed of a single kind of monomer unit only), Saito[6] derived that gelation occurs as a consequence of random crosslinking and main-chain scission if, and only if, $r/c<4$ regardless of the initial molecular size distribution where c and r refer to the probability per monomer unit per unit dose of crosslinking and of scission, respectively.

In what follows, we will discuss the gelation of a *mixture of two samples of polymers of different kinds.*

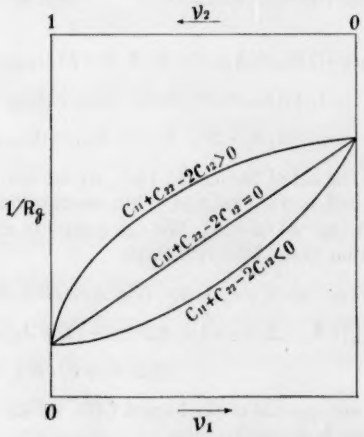

FIG. 2. The behavior of $1/R_g$ for a system of copolymers where the distribution is uniform (schematic).

This mixture is given by[16]

$$m(p_1, p_2, 0) = 2\{\nu_1 m_1(p_1)\delta(p_2) + \nu_2 m_2(p_2)\delta(p_1)\}, \quad (61)$$

where $m_i(p)$ $(i=1, 2)$ stands for the initial distribution in each of the samples of polymers prior to mixing and should satisfy

$$\int_0^\infty p m_i(p)dp = 1 \quad (62)$$

in order that the normalization (9) may hold.

In accordance with previous theories,[5,6] we consider first the change in the molecular size distribution due to main-chain scission only and then that due to crosslinking only, because the order of successive crosslinking and scission is irrelevant as far as molecular size distribution is concerned.[6] Neglecting the so-called "indirect effect,"[17] a polymer of the first kind undergoes main-chain scission with a definite probability independent of the presence of polymers of the second kind and *vice versa* so that we can apply the result of Saito[6] and Charlesby[5] to each kind of the polymers separately. Thus, if we denote by r_i $(i=1, 2)$ the probability of scission of polymers of the ith kind per monomer unit per unit dose, the effect of scission up to dose R is incorporated by replacing the initial distribution (61) by[18]

$$m^*(p_1, p_2) = 2\{\nu_1 m_1^*(p_1)\delta(p_2) + \nu_2 m_2^*(p_2)\delta(p_1)\}, \quad (63)$$

where

$$m_i^*(p) = \left\{m_i(p) + 2\tau_i\int_p^\infty dq m_i(q) + \tau_i^2\int_p^\infty dq\int_q^\infty dq' m_i(q')\right\} \times \exp\{-\tau_i p\} \quad (i=1, 2), \quad (64)$$

and

$$\tau_i = r_i R. \quad (i=1, 2). \quad (65)$$

Next we consider the effect of crosslinking. Then the molecular size distribution changes according to the basic Eq. (5), starting with the *virtual* initial condition (63). Here it should be understood that we must regard τ_i merely as a parameter involved in the initial condition (63) when we solve (5) and it is after the establishment of the solution that we replace τ_i by $r_i R$ according to (65). Regarding $m^*(p_1, p_2)$ as the virtual initial condition and applying our formalism in the preceding sections, we find the weight-average degree of polymerization $P_w(R)$ is given by

$$P_w(R) = A_1 + A_2 - 2RA_1A_2(c_{11} - 2c_{12} + c_{22})/\Delta(R), \quad (66)$$

$$\Delta(R) = 1 - 2R(A_1c_{11} + A_2c_{22}) + 4R^2A_1A_2(c_{11}c_{22} - c_{12}^2), \quad (67)$$

where we have made use of the fact that

$$B = f^{(1,1)}(0) = \int_0^\infty dp_1\int_0^\infty dp_2 p_1 p_2 m^*(p_1, p_2) = 0,$$

and A_1 and A_2 are expressed as

$$A_1 = f^{(2,0)}(0) = \int_0^\infty dp_1\int_0^\infty dp_2 p_1^2 m^*(p_1, p_2) = \nu_1\int_0^\infty m_1^*(p)p^2dp,$$

$$A_2 = f^{(0,2)}(0) = \int_0^\infty dp_1\int_0^\infty dp_2 p_2^2 m^*(p_1, p_2) = \nu_2\int_0^\infty m_2^*(p)p^2dp. \quad (68)$$

According to the definition (41), the gel point is determined as the smallest positive root of the equation

$$\Delta(R) = 0. \quad (69)$$

Hence, the condition for gelation is equivalent to that for the existence of a positive root of (69). Otherwise, $P_w(R)$ is finite for any positive R, or gelation never occurs.

To investigate the just-mentioned condition, it is convenient to define

$$h_i(R) \equiv r_i R A_i/2\nu_i = \int_0^\infty [m_i(p)/r_i R]\{\exp(-r_i pR) - 1 + r_i pR\}dp \quad (i=1, 2), \quad (70)$$

where the last expression can be derived by substituting (64) into (68) and interchanging orders of repeated integrations. Since the integrand in (70) is positive for any positive R, $h_i(R)$ is always positive. The derivative

$$h_i'(R) = \int_0^\infty [m_i(p)/r_i R^2]\{1 - \exp(-r_i pR) - r_i pR\exp(-r_i pR)\}dp$$

is also shown to be positive for any positive R, so that $h_i(R)$ is a monotonously increasing function. Further it is easy to show that

$$h_i(R) = r_i w_i R/2 + O(R^2) \quad \text{for small } R, \quad (71)$$

$$h_i(R) = 1 - 1/r_i u_i R + O(R^{-2}) \quad \text{for large } R, \quad (72)$$

where u_i and w_i stand for the number- and the weight-average degree of polymerization of the polymers of the

[17] P. Alexander and A. Charlesby, J. Polymer Sci. **23**, 355 (1957).

[18] Although it was Saito[6] who first derived the Eq. (64), Charlesby [reference 5, **A224**, 120 (1954)] had already given a formula which is just the Mellin transform of (64) and hence has the same meaning.

ith kind prior to mixing, respectively, i.e.,

$$1/u_i \equiv \int_0^\infty m_i(p)\,dp,$$

$$w_i \equiv \int_0^\infty m_i(p)\,p^2 dp.$$

Using (70), we write (67) as

$$\Delta(R) = 1 - \{\theta_{11}h_1(R) + \theta_{22}h_2(R)\} + (\theta_1\theta_2 - \theta_{12}^2)h_1(R)h_2(R), \quad (73)$$

where we have introduced, for simplicity, the abbreviations

$$\theta_{ii} \equiv 4\nu_i c_{ii}/r_i \quad (i=1,2), \qquad \theta_{12} \equiv 4c_{12}(\nu_1\nu_2/r_1r_2)^{\frac{1}{2}}. \quad (74)$$

Now let us look for the condition that the Eq. (69) has a positive root. For this purpose, we first note that

$$\Delta(\infty) \equiv \lim_{R\to+\infty}\Delta(R) = (1-\theta_{11})(1-\theta_{22}) - \theta_{12}^2. \quad (75)$$

If $\Delta(\infty)<0$, there must be a positive root of (68) because $\Delta(0)=1>0$, as far as $\Delta(R)$ is a continuous function.

If $\Delta(\infty)>0$, we distinguish two cases, namely,

case (i) $\quad \theta_{11}>1$ and $\theta_{22}>1$,

case (ii) $\quad \theta_{11}<1$ and $\theta_{22}<1$.

In case (i) we consider a function

$$\Delta_1(R) \equiv \{1-\theta_{11}h_1(R)\}\{1-\theta_{22}h_2(R)\}, \quad (76)$$

which evidently satisfies

$$\Delta_1(R) \geq \Delta(R). \quad (77)$$

Since $h_i(R)$ behaves as shown in Fig. 3 and assumes every value between zero and unity, the equation $\Delta_1(R)=0$ must have a positive root. Hence, by (77), the Eq. (69) must have a positive root, too. In case (ii), we differentiate $\Delta(R)$ to obtain

$$d\Delta/dR = -\theta_{11}h_1'(R)\{1-\theta_{22}h_2(R)\} - \theta_{22}h_2'(R)\{1-\theta_{11}h_1(R)\} - \theta_{12}^2\{h_1'(R)h_2(R) + h_1(R)h_2'(R)\} < 0,$$

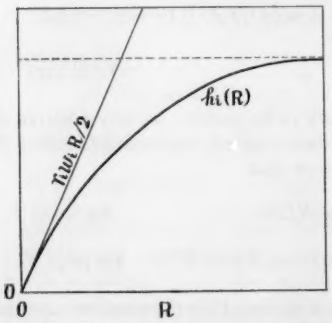

FIG. 3. The behavior of the function $h_i(R)$ (schematic).

where we have made use of the property of $h_i(R)$ that

$$1 \geq h_i(R) \geq 0 \quad \text{and} \quad h_i'(R) > 0.$$

Thus we see that $\Delta(R)$ is a monotonously decreasing function and therefore $1=\Delta(0)>\Delta(R)>\Delta(\infty)>0$, or the Eq. (69) cannot have a positive root.

Consequently, we arrive at the following conclusion: If, and only, if

$$\theta_{11}<1, \qquad \theta_{22}<1 \quad (78)$$

and

$$(1-\theta_{11})(1-\theta_{22}) > \theta_{12}^2 \quad (79)$$

hold, gelation does not occur. Note that this condition is completely independent of the functional form of $m_i(p)$, or of the initial distribution of each kind of polymer prior to mixing. When $\theta_{11}>1$ or $\theta_{22}>1$, gelation is possible for any value of c_{12}; this is a generalization of Saito's result already-mentioned. Particularly interesting is the fact that, even if $\theta_{11}<1$ and $\theta_{22}<1$, gelation is still possible as far as c_{12} is large enough to satisfy $(1-\theta_{11})(1-\theta_{22})<\theta_{12}^2$.

A few words should be necessary to explain a restriction of our treatment in this section. We have discussed only *a mixture* of two different kinds of polymers and not *a system of copolymers*. The reason for this restriction is that there is an essential difficulty in the problem of scission of copolymers. The function $m(p_1, p_2, 0)$, which does not involve any specification of configuration of two kinds of monomer units within a copolymer, is quite insufficient for the description of a system of copolymers which undergoes main-chain scission. This fact may be easily understood through the following argument. Consider a copolymer composed of p_1 monomer units of the first kind and p_2 monomer units of the second kind. Suppose a scission takes place at a bond between a pair of monomer units of the first kind within the copolymer. What do we obtain as the result of the scission? The answer is indefinite as long as we do not specify both the configuration of the two kinds of monomer units and the position where the scission in question is to take place. This situation is so complicated that we have not yet succeeded in establishing a proper mathematical formulation of the problem.

SUMMARY

We have established an integro-differential equation describing the changes in molecular size distribution in a copolymeric system due to radiation-induced random crosslinking. This equation has been solved exactly by means of Laplace transform for an arbitrary initial distribution to give the number-average as well as the weight-average degree of polymerization as a function of radiation dose.

The gel point is given as a function of concentrations of the two kinds of monomer units constituting the copolymers in the system. Assuming suitable initial distribution and comparing the calculated gel points

for various concentrations with experiment, we shall be able to estimate the values of c_{11}, c_{12}, and c_{22}, which will be readily converted to the so-called G values of crosslinking.

Another interesting result is the condition for gelation of a mixture of two kinds of polymers when not only crosslinking, but also main-chain scission, takes place. The fact that this condition does not depend on the shape of the initial distribution is of great significance from experimental viewpoint, because the initial distribution is rather difficult to control in practice.

ACKNOWLEDGMENTS

The author is very grateful to Professor A. Amemiya, University of Tokyo, for helpful discussions throughout the work and to Professor A. Harasima, International Christian University, for kind critical review of the manuscript. He also acknowledges valuable comments and interests of Professor O. Saito, Chuo University, Dr. T. Watanabe, Japan Atomic Energy Research Institute, and K. Katsuura, University of Tokyo.

APPENDIX. SOLUTION OF EQ. (16)

The general solution of the partial differential equation (16) is given by[19]

$$F=a_1x_1+a_2x_2+b(a_1,\,a_2)\,R+c(a_1,\,a_2), \tag{A1}$$

$$b(a_1,\,a_2)=c_{11}a_1^2+2c_{12}a_1a_2+c_{22}a_2^2 +2(\nu_1c_{11}+\nu_2c_{12})\,a_1+2(\nu_1c_{12}+\nu_2c_{22})\,a_2, \tag{A2}$$

$$x_1+(\partial b/\partial a_1)\,R+(\partial c/\partial a_1)=0, \tag{A3}$$

$$x_2+(\partial b/\partial a_2)\,R+(\partial c/\partial a_2)=0, \tag{A4}$$

where $c(a_1,\,a_2)$ is an as yet arbitrary function, and a_1 and a_2 are parameters to be eliminated. The required solution is obtained when we adjust the functional form of $c(a_1,\,a_2)$ so that the initial condition (17) is satisfied. Thus, $c(a_1,\,a_2)$ should be determined by

$$G(s_1,\,s_2)=a_1s_1+a_2s_2+c(a_1,\,a_2), \tag{A5}$$

$$s_1+(\partial c/\partial a_1)=0, \tag{A6}$$

$$s_2+(\partial c/\partial a_2)=0, \tag{A7}$$

where we have written s_1 and s_2 instead of x_1 and x_2 in order to make clear that they are merely parameters. It should be understood that we shall obtain $c(a_1,\,a_2)$ if we eliminate s_1 and s_2 from (A5), (A6), and (A7).

Differentiating (A5) and taking Eqs. (A6) and (A7), into consideration, we find that

$$\partial G/\partial s_1=a_1+s_1(\partial a_1/\partial s_1)+s_2(\partial a_2/\partial s_1)+(\partial c/\partial a_1)(\partial a_1/\partial s_1) +(\partial c/\partial a_2)(\partial a_2/\partial s_1)$$

$$=a_1+[s_1+(\partial c/\partial a_1)](\partial a_1/\partial s_1) +[s_2+(\partial c/\partial a_2](\partial a_2/\partial s_1)=a_1. \tag{A8}$$

Similarly,

$$\partial G/\partial s_2=a_2. \tag{A9}$$

Substitution of (A8) and (A9) into (A5) yields

$$c(a_1,\,a_2)=G(s_1,\,s_2)-s_1(\partial G/\partial s_1)-s_2(\partial G/\partial s_2). \tag{A10}$$

Then (A1), (A3), and (A4) are rewritten with the aid of (A10) as

$$F=G(s_1,\,s_2)+(x_1-s_1)\,(\partial G/\partial s_1)+(x_2-s_2)\,(\partial G/\partial s_2), \tag{A11}$$

$$x_1-s_1+R(\partial/\partial a_1)b[(\partial G/\partial s_1),\,(\partial G/\partial s_2)]=0, \tag{A12}$$

$$x_2-s_2+R(\partial/\partial a_2)b[(\partial G/\partial s_1),\,(\partial G/\partial s_2)]=0, \tag{A13}$$

where

$$(\partial/\partial a_i)b[(\partial G/\partial s_1),\,(\partial G/\partial s_2)] \qquad (i=1,\,2)$$

means the value of $\partial b/\partial a_i$ at $a_1=\partial G/\partial s_1$ and $a_2=\partial G/\partial s_2$.

We can further rewrite (A11) using (A12) and (A13) as

$$F=G(s_1,\,s_2) -R\{(\partial G/\partial s_1)\,(\partial/\partial a_1)b[(\partial G/\partial s_1),\,(\partial G/\partial s_2)] +(\partial G/\partial s_2)\,(\partial/\partial a_2)b[(\partial G/\partial s_1),\,(\partial G/\partial s_2)] -b[(\partial G/\partial s_1),\,(\partial G/\partial s_2)]\}. \tag{A14}$$

Since

$$a_1(\partial b/\partial a_1)+a_2(\partial b/\partial a_2)-b(a_1,\,a_2) =c_{11}a_1^2+2c_{12}a_1a_2+c_{22}a_2^2$$

according to the definition (A2) of $b(a_1,\,a_2)$, (A14) reduces to

$$F=G(s_1,\,s_2)-R\{c_{11}(\partial G/\partial s_1)^2+2c_{12}(\partial G/\partial s_1)\,(\partial G/\partial s_2) +c_{22}(\partial G/\partial s_2)^2\}. \tag{A15}$$

Further, (A12) and (A13) are also rewritten, with the aid of (A2), as

$$x_1-s_1+2R(c_{11}(\partial G/\partial s_1)+c_{12}(\partial G/\partial s_2) +\nu_1c_{11}+\nu_2c_{12})=0, \tag{A16}$$

$$x_2-s_2+2R(c_{12}(\partial G/\partial s_1)+c_{22}(\partial G/\partial s_2) +\nu_1c_{12}+\nu_2c_{22}]=0. \tag{A17}$$

The last three equations, which are identical to (18), (19), and (20), constitute a parametric representation of $F(x_1,\,x_2,\,R)$.

[19] A. R. Forsyth, *A Treatise on Differential Equations* (MacMillan and Company, Ltd., London, England, 1921), 5th ed., p. 407.

Infrared Absorption Spectrum of $NdCl_3$†

F. VARSANYI AND G. H. DIEKE

The Johns Hopkins University, Baltimore, Maryland

(Received June 23, 1960)

The infrared absorption spectrum of $NdCl_3$ is obtained under high resolution which show the transitions from the ground state to $^4I_{13/2}$ and $^4I_{15/2}$ the latter of which was hitherto unknown. The crystals were 5% and 50% $NdCl_3$ in $LaCl_3$ and the higher Nd concentration shows a decided frequency shift of the lines.

THE spectrum of $NdCl_3$ has been extensively studied[1,2] in absorption and fluorescence and most of the low and medium energy levels identified. However no fluorescence could be found to the $^4I_{15/2}$ level the highest component of the ground multiplet which remained therefore unknown. The absorption $^4I_{9/2} \rightarrow {}^4I_{15/2}$ should lie in the infrared.

Conditions for obtaining the infrared absorption spectrum of anhydrous salts are more favorable than for those salts where absorption of the crystal water can interfere. Use was made of a high-resolution infrared spectrometer[3] with a cooled PbS cell. For wavelength measurements a neon spectrum was superimposed on the crystal spectra. The polarization data were obtained by using about 60 microscope cover glasses of 0.1 mm thickness at Brewster's angle. The effectiveness of this polarizer was about 95% and the transmission up to 2.5 μ was about 85–90% and declined gradually beyond that. All measurements were made at liquid He temperature. In order to obtain the weaker lines a crystal with 50% Nd in $LaCl_3$ was used which was grown by A. Piksis in this laboratory according the procedure described by Hutchison and Wong.[4] Sixteen absorption lines were found in the 1.7 μ and 2.5 μ region where the transitions to the $^4I_{13/2}$ and $^4I_{13/2}$ Stark levels are expected. The latter are known from the fluorescence spectrum.[1,2] The agreement between the values of the levels obtained from infrared absorption and fluorescence was considerably less than expected from the accuracy of the wavelength measurements.

CONCENTRATION EFFECTS

Comparison with the spectrum of a crystal with 5% Nd concentration showed that there are systematic shifts at the higher concentrations which are approximately constant within the $^4I_{15/2}$ and $^4I_{13/2}$ groups but different in the two groups. This is illustrated in Fig. 1 and Fig. 2 which show these shifts clearly. Measurements show that the levels of the $^4I_{13/2}$ group are shifted up in energy compared to the ground state by about 2.2 cm^{-1} whereas those for $^4I_{15/2}$ are shifted down about 0.5 cm^{-1}. The values for the $^4I_{13/2}$ levels are summarized in Table I. The line X_2 seems to be weak as it was not observed in the 5% crystal and was masked

TABLE I. Energy levels of $^4I_{13/2}$.

Level	50% Nd	5% Nd	Polarization	From fluorescence[2]	μ
X_1	3931.59 cm^{-1}	3931.23	$\sigma\pi$	3931.84	$\frac{1}{2}$
X_2	3979.4 3976.4 3973.6		$\sigma\pi$	3974.88	$\frac{3}{2}$
X_3	4001.36	3999.16	$\sigma\pi$	3998.89	$\frac{1}{2}$
X_4				4012.92	$\frac{5}{2}$
X_5	4034.13	4031.93	$\sigma\pi$	4031.86	$\frac{1}{2}$
X_6	4044.82	4042.32	σ	4042.08	$\frac{3}{2}$
X_7				4083	$\frac{1}{2}$

TABLE II. Energy levels of $^4I_{15/2}$.

Level	5% Nd	$\Delta\nu$ obs.	Polarization	μ[b]	$\Delta\nu$ calc[5]
W_1	5869.3 cm^{-1}	0.0	$\sigma\pi$	$\frac{1}{2}$	3
W_2	5942.4±0.1	73.1	$\sigma\pi$	$\frac{1}{2}$	75
W_3	5992.2±0.1	122.9	σ	$\frac{3}{2}$	130
W_4				$\frac{5}{2}$	188
W_5	6079.5[a]±1.0	210.2	$\sigma\pi$	$\frac{1}{2}$	205
s	6123.2[a]±1.0	253.9	$\sigma\pi$	$\frac{1}{2}$	
W_6	6154.2[a]±1.0	284.9	σ	$\frac{3}{2}$	275
W_7	Not observed			$\frac{3}{2}$	319
W_8				$\frac{5}{2}$	385

[a] Observed only in the 50% Nd crystal. The frequency observed there was increased by 0.5 cm^{-1} which was the average shift found for the lines $W_1W_3W_5$.

[b] The μ values for the observed lines are those derived from the polarization. With the exception of the line marked s they agree with the values predicted by Judd.[5]

† Work carried out with the support of the U. S. Atomic Energy Commission.

[1] E. Carlson and G. H. Dieke, J. Chem. Phys. **29**, 229 (1958).

[2] E. Carlson, Johns Hopkins Spectroscopic Report Number 18 (1960).

[3] Wm. G. Fastie, H. M. Crosswhite, and P. Gloersen, J. Opt. Soc. Am. **48**, 106 (1958).

[4] C. A. Hutchison and E. Wong, J. Chem. Phys. **29**, 754 (1958).

by 3 satellites which did not show the proper polarization in the 50% crystal. The other values at low concentrations agree satisfactorily with those obtained from the fluorescence spectrum.

THE $^4I_{15/2}$ LEVELS

Table II shows the data obtained for the $^4I_{15/2}$ levels. The normal state of the Nd^{+++} ion in $NdCl_3$ has the crystal quantum number $\mu''=\frac{5}{2}$ which with electric dipole selection rules allows transitions to $\mu'=\frac{1}{2}$ with $\sigma\pi$ polarization, to $\mu'=\frac{3}{2}$ with σ polarization, and forbids transitions to $\mu'=\frac{5}{2}$. This is in agreement with the observations. As seen in Fig. 3 the polarization indicates very clearly the character of each line so crystal quantum numbers can be assigned to them unambiguously. The whole pattern including the μ values as deduced from the polarization data seems to be in rather good agreement with the calculations of Judd[5]

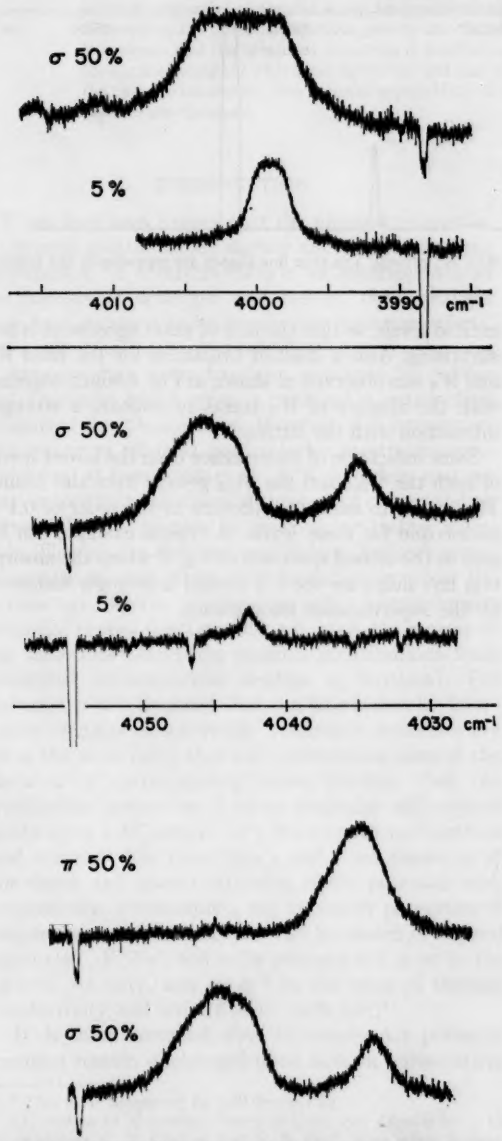

FIG. 1. Representative lines of the $^4I_{15/2}$ group showing concentration and polarization effects. Emission lines are neon in higher orders.

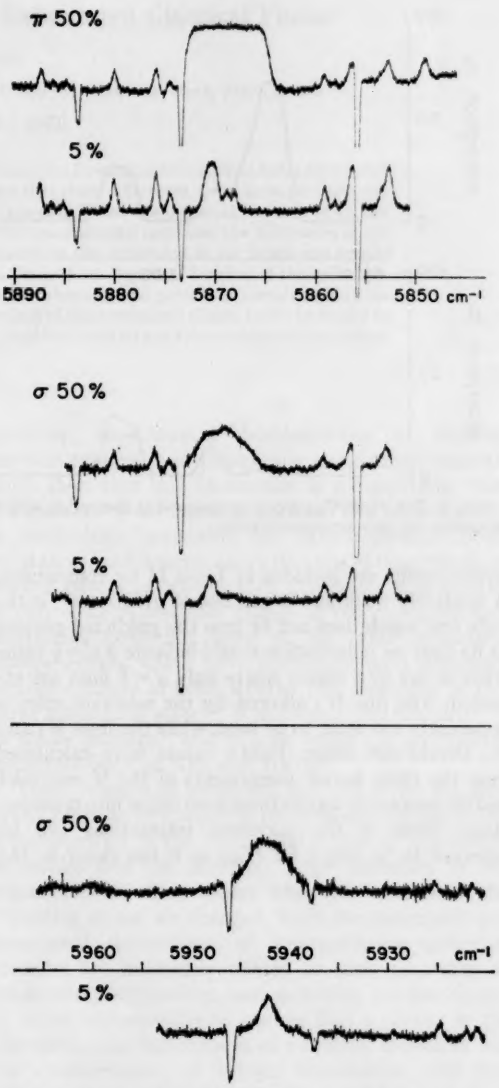

FIG. 2. Representative lines of the $^4I_{15/2}$ group with water vapor absorption and higher order neon emission spectra superimposed.

[5] B. R. Judd, Proc. Roy. Soc. (London) **251**, 134 (1959) (also private communication concerning the $^4I_{15/2}$ levels).

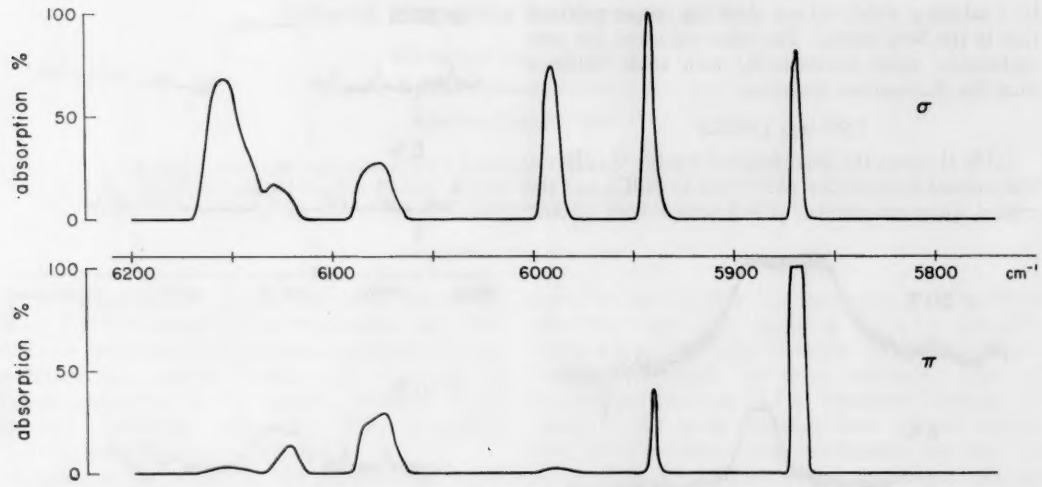

FIG. 3. The whole $^4I_{15/2}$ group as observed in absorption with the 50% Nd crystal. The true line shapes are reproduced but relative intensities are only semiquantitative.

whose results are included in Table II for comparison. A relatively weak and broad line at 6122.7 cm^{-1} is the only one which does not fit into the predicted pattern as its clear $\sigma\pi$ polarization would indicate a $\mu'=\frac{1}{2}$ value while it lies in a region where only $\mu'=\frac{3}{2}$ lines are expected. The line W_7 allowed by the selection rules is apparently too weak to be seen, while the lines W_4 and W_8 should not occur. Judd's values were calculated from the three lowest components of the ^4I multiplet and all reasonable interactions were taken into consideration. Some of the uncertain interactions can be expected to be larger for $^4I_{15/2}$ as it lies closer to the excited levels, so that the lack of exact agreement is not surprising. Also a marked broadness for the lines W_5 and W_6 was observed as shown in Fig. 3 which together with the absence of W_7 seems to indicate a stronger interaction with the lattice.

Some indication of fluorescence from the lowest levels of both the $^4I_{13/2}$ and the $^4I_{15/2}$ groups were also found. This seems to indicate a lifetime in the order of 0.1–1 millisecond for these levels. A typical example can be seen in the second spectrum of Fig. 2 where the absorption line shape for the 5% crystal is strongly distorted by the superimposed fluorescence.

THE JOURNAL OF CHEMICAL PHYSICS VOLUME 33, NUMBER 6 DECEMBER, 1960

Physical Properties of Isotopically Substituted Classical Fluids*

W. A. STEELE

Department of Chemistry, The Pennsylvania State University, University Park, Pennsylvania

(Received June 13, 1960)

The observed differences in physical properties between isotopically substituted classical fluids are treated in terms of the theorem of corresponding states. It is shown that these differences are at least partially due to changes in the intermolecular potential energies of interaction. When the potential function of an isotopically substituted molecule is conformal with that of the unsubstituted molecule, the differences in the physical properties of the fluids can be quantitatively related to the differences in the depth and spatial extension of the potential functions, and to the changes in the internal degrees of freedom of the molecules. It is shown that the measured properties of perdeutero benzene-benzene and perdeutero cyclohexane-cyclohexane are consistent with these equations, and that the values of the parameters chosen to fit the theory to the data are reasonable. The limits of applicability of this treatment and its possible extension to less simple systems are discussed.

INTRODUCTION

IT has long been known that the physical properties of most substances are slightly altered upon isotopic substitution. In a certain class of substances, such as the isotopes of hydrogen and helium, these changes have been ascribed to intermolecular quantum effects, and a quantum-mechanical modification of the theorem of corresponding states has been presented by deBoer and Lunbeck[1] which gives a reasonably satisfactory account of this phenomenon. However, this intermolecular quantum effect is negligible for most substances which boil at temperatures of 150°K or higher, and one may expect that the classical theorem of corresponding states will be applicable to these higher boiling materials. This implies that the equilibrium thermodynamic properties of such fluids will depend only upon the parameters which characterize the intermolecular potential energy function and not upon the masses of the molecules (excepting possible contributions from quantized intramolecular degrees of freedom). For instance, if it is assumed that the intermolecular interaction energies of spherically symmetric molecules are all of the same form, then the conventional form of the theorem of corresponding states predicts that the equilibrium properties of these molecules will depend solely upon ϵ/kT and $V/N\sigma^3$, the reduced temperature and volume.[2] The quantities ϵ and σ are measures of the depth and spatial extension of the potential well, respectively. Furthermore, the transport properties of simple point center molecules can be shown to depend upon ϵ/kT, $V/N\sigma^3$, and to be proportional to $m^{\frac{1}{2}}$ in the case of viscosity, and to $m^{-\frac{1}{2}}$ in the cases of thermal conductivity and self-diffusion coefficient.[3]

It is often assumed that intermolecular potential energies remain unchanged upon isotopic substitution. However, experimental determinations of various physical properties of isotopically substituted classical fluids show that this assumption is incompatible with the theorem of corresponding states. This phenomenon is particularly noticeable for deuterium-substituted substances, and it seems likely that one of the secondary isotope effects associated with deuterium substitution is that of an appreciable change in the intermolecular interaction potential. Some of the other secondary isotope effects which have previously been discussed include changes in bond lengths (for molecules in the same vibrational state)[4]; in molecular polarizability[5–7]; in dipole moment[8]; and in bond angle (in asymmetric molecules such as NH_3 and H_2O).[8,9]

These changes in molecular size and shape are generally taken to be a result of the combined effects of the anharmonicity of the vibrational modes of polyatomic molecules and the relatively large alteration in the eigenstates of these modes when the masses of the vibrating atoms are changed. Since the magnitude and functional dependence of intermolecular potential energies are intimately related to such quantities as molecular polarizability, and molecular size and shape, it is not unreasonable to assume that a change in the intermolecular interactions of vibrating molecules will be a consequence of isotopic substitution, and that these changes will be largest when the other secondary isotope effects are largest, i.e., upon deuterium substitution. Furthermore, it is clear that intermolecular

* This work supported by API Project 42.

[1] J. deBoer in *Molecular Theory of Gases and Liquids* by J. O. Hirschfelder, C. F. Curtiss, and R. B. Bird (John Wiley & Sons, Inc., New York, 1954), Chap. 6.

[2] Footnote reference 1, p. 235 ff.

[3] Footnote reference 1, p. 613 ff.

[4] G. Herzberg, *Infrared and Raman Spectra of Polyatomic Molecules* (D. Van Nostrand Company, Inc., Princeton, New Jersey, 1945), p. 456.

[5] R. W. Terhune and C. W. Peters, J. Mol. Spectroscopy **3**, 138 (1959).

[6] O. E. Frivold, O. Hassel, and E. Hetland, Physik. Z. **40**, 29 (1939); O. E. Frivold, O. Hassel, and S. Rustad, *ibid.* **38**, 191 (1937).

[7] R. T. Davis and R. W. Schiessler, J. Am. Chem. Soc. **75**, 2763 (1953); J. A. Dixon and R. W. Schiessler, *ibid.* **76**, 2197 (1954).

[8] J. M. A. deBruyne and C. P. Smyth, J. Am. Chem. Soc. **57**, 1203 (1935).

[9] E. A. Halevi, Trans. Faraday Soc. **54**, 1441 (1958); R. P. Bell and I. E. Coop, Trans. Faraday Soc. **34**, 1209 (1938).

potential functions for polyatomic molecules which are to be used in practical calculations of macroscopic properties must be defined to be those associated with the vibrating molecules.

In general, three or more parameters are required to specify the magnitude and functional dependence of the intermolecular interaction between two rigid, nonspherical molecules.[10] Any or all of these parameters may change upon isotopic substitution. In this work, it will be assumed that the magnitude and spatial extension of the potential function are appreciably altered when a deuterium atom is substituted for hydrogen, but that the form of the potential energy remains unchanged. In this case, the changes in physical properties of fluids made up of such molecules may be quantitatively related to the changes in the intermolecular potential. When these changes are small, the relationships can be obtained by carrying out a Taylor series expansion of the reduced expression for the property of interest. It can be shown that changes in the internal degrees of freedom upon isotopic substitution also make appreciable contributions to some physical properties. These changes can often be estimated from spectral data, and will be explicitly included in this work wherever possible.

At present, only a few comprehensive studies of the physical properties of classical isotopically substituted liquids have been published. Furthermore, it is unlikely that the theory presented here will be applicable to such well-known systems as water or ammonia, because of the requirement that the potential curves of the isotopic modifications of a molecule remain conformal with one another. Since it is believed that the bond angles change in going from H_2O to D_2O, and from NH_3 to ND_3, it is obvious that the occurrence of conformal potential functions in such systems is extremely unlikely.

However, extensive data have been published on two pairs of molecules which might be expected to conform to the restrictions of the treatment presented here, these systems are per-deutero cyclohexane-cyclohexane, and per-deutero benzene-benzene.[7,11,12] The theoretical expressions for the differences in vapor pressure, liquid molar volume, and liquid viscosity of isotopically substituted molecules which are given in this paper are compared with the experimental results for these systems. It is shown that there is good agreement between experiment and theory, and that the values chosen for the adjustable parameters used in the theory are reasonable. Some discussion is given of the effect of nonconformal behavior upon the observed changes in physical properties, and a brief qualitative analysis of some of the results on polar liquids is presented.

[10] J. S. Rowlinson, *Liquids and Liquid Mixtures* (Academic Press, Inc., New York, 1959), Chaps. 7 and 8.

[11] J. A. Dixon and R. W. Schiessler, J. Phys. Chem. **57**, 966 (1953).

[12] J. A. Dixon and R. W. Schiessler, J. Phys. Chem. **58**, 430 (1953).

THEORETICAL

The vapor pressure difference between a pair of isotopically substituted classical liquids depends upon the difference in the molar Gibbs free energy G between the two liquids, and is most easily computed from the equation

$$G_{\text{liq}}-G_{\text{gas}}=0=(G_{\text{liq}})_{\text{conf}}-RT\ln p+\ln(q_{\text{liq}}/q_{\text{gas}}), \quad (1)$$

where q denotes the internal molecular partition function, and $(G_{\text{liq}})_{\text{conf}}$ is the configurational Gibbs free energy of the liquid (a configurational property is generally defined to be a quantity which depends solely upon the potential energy of the molecules, the temperature and the volume[10]). If the vapor pressure of a liquid made up of heavy molecules (subscript H) is compared with that of a liquid made up of light molecules (subscript L), the result is (at temperature T)

$$RT\ln p_H/p_L=[(G_{\text{liq}})_H-(G_{\text{liq}})_L]_{\text{conf}}+\ln[(q_{\text{liq}})_L(q_{\text{gas}})_H/(q_{\text{liq}})_H(q_{\text{gas}})_L]. \quad (2)$$

A quantitative expression for the difference in configurational Gibbs free energy can be given in terms of the differences in intermolecular potential energy curves if it is assumed that the potential functions of the light and heavy molecules are conformal with one another, and that only pair interactions contribute significantly to the total potential energies of the fluids. The fractional changes in the depth scale ϵ and the spatial extension scale σ of the potential curve are defined as δ and γ, respectively,

$$\delta=(\epsilon_H-\epsilon_L)/\epsilon_L \quad (3)$$

$$\gamma=(\sigma_H-\sigma_L)/\sigma_L. \quad (4)$$

If δ and γ are small, the Taylor series expansion for the differences in configurational Gibbs free energy between two liquids at equal T and p which has been given in connection with the theory of conformal solutions[13,14] can be used here. In the notation of the present work, the result is

$$RT\ln p_H/p_L=\delta(E_{\text{liq}}')_L+3\gamma[RT-(PV_{\text{liq}})_L]+\ln[(q_{\text{liq}})_L(q_{\text{gas}})_H/(q_{\text{liq}})_H(q_{\text{gas}})_L]+\text{higher terms in }\delta^2,\gamma^2,\delta\gamma,\text{ etc.}, \quad (5)$$

where $(E'_{\text{liq}})_L$ is the molar configurational energy of the liquid L, and is equal to $-\Delta H+RT-(PV_{\text{liq}})$ for an ideal vapor phase, where ΔH is the heat of vaporization of L at temperature T.

The internal partition function for a molecule with no internal rotations is just the vibrational partition function of the molecule. Since the spacing of the vibrational levels in most molecules is large compared to kT

[13] H. C. Longuet-Higgins, Proc. Roy. Soc. (London) **A205**, 247 (1951).

[14] W. B. Brown, Proc. Roy. Soc. (London) **A240**, 561 (1957).

at liquid temperatures, it will often be possible to write

$$\ln[(q_{liq})_L(q_{gas})_H/(q_{liq})_H(q_{gas})_L]$$
$$=(E_{liq}{}^0)_H-(E_{liq}{}^0)_L-(E_{gas}{}^0)_H$$
$$+(E_{gas}{}^0)_L)=\Delta^2E^0, \quad (6)$$

where E^0 is the zero-point vibrational energy of the molecule.

When small terms are dropped, the final equation for the vapor pressure ratio of two classical conformal liquids can be given as

$$\ln p_H/p_L=-(1/RT)(\delta\Delta H_L+\Delta^2E^0)+3\gamma-\delta. \quad (7)$$

The differences in the molar volumes of classical polyatomic conformal liquids can be computed from a suitable modification of the statistical-mechanical equations of Buff *et al.*[15,16] for the number density of a monatomic fluid at a given absolute activity. However, the result obtained for polyatomic systems with pairwise interactions is identical to that given by the corresponding states calculation of the theory of conformal solutions.[13,14] At low pressures, the fractional change in molar volume due to changes in ϵ and σ is

$$(V_H-V_L)/V_L=3\gamma-\delta\beta_LT, \quad (8)$$

where β_L is the isothermal compressibility of liquid L.

Expressions for the differences in the transport properties of isotopically substituted fluids can also be obtained by means of a corresponding states treatment. When the dimensionless expressions for the transport properties of simple fluids are expanded in a Taylor series, the changes in the viscosity η, the thermal conductivity λ, and the diffusion coefficient D for given changes in ϵ and σ are written

$$(\eta_H/\eta_L)(m_L/m_H)^{\frac{1}{2}}-1=\tfrac{1}{2}\delta-2\gamma$$
$$+p(\delta-3\gamma)(-\partial\ln\eta_L/\partial p)_T$$
$$+\delta T(-\partial\ln\eta_L/\partial T)_p+\cdots \quad (9)$$

$$(\lambda_H/\lambda_L)(m_H/m_L)^{\frac{1}{2}}-1=\tfrac{1}{2}\delta+2\gamma$$
$$+p(\delta-3\gamma)(-\partial\ln\lambda_L/\partial p)_T$$
$$+\delta T(-\partial\ln\lambda_L/\partial T)_p+\cdots \quad (10)$$

$$(D_H/D_L)(m_H/m_L)^{\frac{1}{2}}-1=\tfrac{1}{2}\delta+\gamma$$
$$+p(\delta-3\gamma)(-\partial\ln D_L/\partial p)_T$$
$$+\delta T(-\partial\ln D_L/\partial T)_p+\cdots. \quad (11)$$

These equations are rigorously correct for monatomic fluids. In polyatomic systems, momentum and energy can be transferred by exchange of rotational momentum and energy, and by inelastic collisions in which the internal degrees of freedom take part in the process.[17] To date, the magnitude of these effects has been only roughly estimated. The neglect of such effects in Eqs. (9)–(11) may result in appreciable errors when conformal molecules with different moments of inertia or differences in their internal degrees of freedom are considered.

Liquid transport properties are generally measured on liquids in equilibrium with their vapors. If the vapor pressures of the liquids at the temperature of measurement are not too large, the pressure terms in Eqs. (9)–(11) can be dropped. In particular, the equation for the viscosity change can be simplified to

$$(\eta_H/\eta_L)(m_L/m_H)^{\frac{1}{2}}-1=\tfrac{1}{2}\delta-2\gamma+\delta T(-\partial\ln\eta_L/\partial T)_P. \quad (12)$$

Many more expressions for the differences in the physical properties of conformal polyatomic fluids can be written down. The relationships previously given for the fractional changes of the thermodynamic variables of a monatomic substance at a phase transition point[10] also apply to polyatomic fluids if it is assumed that the changes in internal degrees of freedom at a transition point are negligible compared to the changes in the configurational properties (spectral data indicate that this is an adequate assumption for nonpolar molecules at the triple point, but little is known about variations in molecular degrees of freedom near the critical point). The equation for the difference in transition temperature is of particular interest, since many determinations of the changes in this parameter upon isotopic substitution have been reported. In systems which are classical and conformal, the fractional change in transition temperature is equal to δ.

COMPARISON WITH EXPERIMENT

The published data on the perdeutero cyclohexane-cyclohexane system include vapor pressures, molar volumes, and liquid viscosities at temperatures from 20°–80°C.[11,12] If this system conforms to the assumptions of the present theoretical treatment, then it should be possible to fit these data to Eqs. (7), (8), and (12) by adjusting the values of the three parameters δ, γ, and Δ^2E^0. A reasonably good fit between experiment and theory was obtained by using the following values for the parameters,

$$\delta=-2.0\times10^{-3}, \qquad \gamma=-1.0\times10^{-3},$$
$$\Delta^2E^0=-34 \text{ cal/mole}.$$

Experimental values for the heat of vaporization,[12,18] thermal expansion,[11] and $(-\partial\ln\eta/\partial T)_p$[11] of cyclohexane are

$$\Delta H=11\,300-11T \text{ cal/mole}, \qquad \beta=1.26\times10^{-3}(°C)^{-1},$$
$$(-\partial\ln\eta/\partial T)_p=1.72\times10^{-2}(°C)^{-1},$$

[15] F. P. Buff and R. Brout, J. Chem. Phys. **23**, 458 (1955).
[16] F. P. Buff and F. M. Schindler, J. Chem. Phys. **29**, 1075 (1959).
[17] Footnote reference 1, p. 496 ff.
[18] C. K. Ingold, C. G. Raisin, C. L. Wilson, and C. R. Bailey, J. Chem. Soc. **1936**, 915.

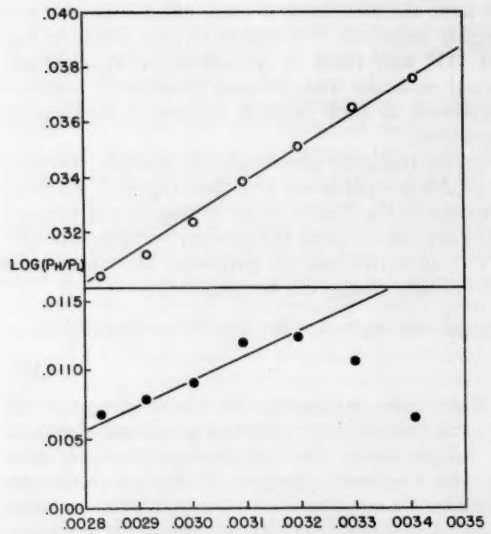

FIG. 1. The logarithms of the experimental vapor pressure differences between perdeutero-benzene and benzene, and perdeuterocyclohexane and cyclohexane are shown as filled and open circles, respectively. $\text{Log}_{10}p_H/p_L$ is plotted versus $1/T$ (H and L denote heavy and light molecules). The lines are calculated from Eq. (7) using the values given in the text for the adjustable parameters. Note the difference between the $\log p_H/p_L$ scales in the upper and lower parts of the figure.

over the range $T=20$–80°C. The experimental vapor pressure differences are shown in Fig. 1; the line in this figure is calculated from Eq. (7). In Table I, the differences in molar volumes and viscosities calculated from Eqs. (8) and (12) are compared with the experimental results. The differences between theory and experiment are of the same order of magnitude as the experimental errors.

It is possible to make a similar analysis of the vapor pressure, liquid viscosity and molar volume of the perdeutero benzene-benzene system.[11,12,18] The earlier vapor pressure measurements on these compounds reported by Ingold *et al.*[18] do not agree with those of Schiessler *et al.* However, since a considerable number of physical property measurements were carried out on the C_6D_6 sample prepared by Schiessler *et al.* it is most consistent to use their pressure data in this analysis. The values chosen for the adjustable parameters were

$$\delta=4.0\times10^{-3},\quad \gamma=-1.3\times10^{-3},\quad \Delta^2E^0=-51 \text{ cal/mole}.$$

TABLE I.

T (°K)	$[(V_H-V_L)/V_L]\times10^3$ Exptl.	Theory	$[(\eta_H/\eta_L)(m_L/m_H)^{\frac{1}{2}}-1]\times10^3$ Exptl.	Theory
293	−2.5	−2.3	−6	−9
313	−2.0	−2.2	−8	−10
333	−1.6	−2.1	−10	−11

Experimental results for benzene show that[11,12,19]

$$\Delta H=10\,500-9T \text{ cal/mole},\quad \beta=1.25\times10^{-3}(°\text{C})^{-1},$$
$$(-\partial \ln\eta/\partial T)_p=1.45\times10^{-2}(°\text{C})^{-1}.$$

The experimental and theoretical vapor pressures are shown in Fig. 1, and the liquid viscosities and molar volumes are shown in Table II. Also shown in Table II is the experimental change in melting point measured by Ingold *et al.*[18] compared with the theoretical prediction of the present analysis. It can be seen that the agreement between experiment and theory is not as complete as in the cyclohexane system. In particular, the experimental vapor pressures show quite a large deviation from the theoretical values at temperatures near the melting point of benzene.

It is of interest to attempt to ascertain whether or not the values of γ, δ and Δ^2E° are in reasonable agreement with independent estimates. Information concerning the sign and order of magnitude of γ and Δ^2E° can be obtained from infrared spectra. It is well known that C—D bond lengths are shorter than C—H, and the

TABLE II.[a]

T (°K)	$[(V_H-V_L)/V_L]\times10^3$ Exptl.	Theory	$[(\eta_H/\eta_L)(m_L/m_H)^{\frac{1}{2}}-1]\times10^3$ Exptl.	Theory
293	−2.5	−2.5	27	22
313	−2.7	−2.4	24	23
333	−2.5	−2.3	23	24

[a] $T_H-T_L=1.3$°C observed; 1.1°C calculated.

analysis of the rotational spectra of perdeutero methane indicates that this decrease amounts to about 0.004 A for molecules in their vibrational ground states.[5] Since the position of the repulsive portion of the intermolecular interaction potential of nonpolar molecules depends strongly upon the positions of the peripheral atoms in the molecule, one might expect that a negative γ of the order of magnitude of 10^{-3} would be most consistent with a decrease of 0.004 A in the C—H bond length upon deuteration. Furthermore, the vibrational spectra of liquid and gaseous hydrocarbons indicates that[20] $\nu_{\text{gas}}-\nu_{\text{liq}}\simeq8$ cm^{-1} for CH stretching, and $\simeq4$ cm^{-1} for CH bending. The sum of these changes for the three vibrational modes of one H atom attached to a rigid frame amounts to a total increase in vibrational zero point energy of 23 cal/mole upon vaporization. Assuming that $\nu_{CD}=0.7\nu_{CH}$, it is seen that Δ^2E° is negative and amounts to approximately 7 cal/mole per deuterium substituted for hydrogen. This crude estimate of the expected value of Δ^2E° is in reasonable order of magnitude agreement with the chosen values of −2.8 cal/mole

[19] J. G. Aston and S. V. R. Mastrangelo in *Physical Chemistry of Hydrocarbons*, edited by A. Farkas (Academic Press, Inc., New York, 1952), p. 99 ff.

[20] L. J. Bellamy, *The Infrared Spectra of Complex Molecules* (John Wiley & Sons, Inc., New York, 1958), 2nd ed.

per deuterium in the cyclohexane system and −8.5 cal/mole per deuterium in the benzene system.

The ultraviolet spectra of the benzenes were first reported in the paper of Ingold *et al.*,[18] and it was pointed out that $\nu_{C_6D_6}-\nu_{C_6H_6}/\nu_{C_6H_6}=0.005$ for the first three (closely spaced) vibrational-electronic transitions in these molecules. The relative oscillator strengths of the benzenes were also discussed and it was concluded that this quantity is most likely invariant with isotopic substitution, since it depends only upon the electronic wave functions. Davis and Schiessler[7] measured the refractive indices of the liquid benzenes and cyclohexanes as a function of frequency. Information about oscillator strengths and transition energies can be obtained from these data by the use of the simple quantum mechanical version of the Drude equation[21]

$$(n^2-1)/(n^2+2)=(e^2/3\pi m)\{Af/[(\nu^0)^2-\nu^2]\}, \quad (13)$$

where n is the refractive index, f is an average oscillator strength for the transition with energy $h\nu^0$, A is the number of molecules per cm³, and ν is the frequency of the light. When the data are fitted to Eq. (13), the results show that the oscillator strengths do not change appreciably with isotopic substitution for either the benzenes or the cyclohexanes, and that $\nu_H{}^0-\nu_L{}^0/\nu_L{}^0=0.006$ for the benzenes, in good agreement with Ingold's results, and 0.0025 for the cyclohexanes.

In its simple form, London's treatment predicts that the dispersion energy of a pair of structureless molecules ϕ is proportional to $\alpha^2\nu^0$, where α is the polarizability at zero frequency.[21] Furthermore, the simple quantum-mechanical equation for the static polarizability shows that α is proportional to f/ν^{02}. When these relationships are combined, an equation for the fractional change in dispersion energy upon isotopic substitution can be written down,

$$(\phi_H-\phi_L)/\phi_L=[(f_H-f_L)/f_L]-3[(\nu_H{}^0-\nu_L{}^0)/\nu_L{}^0]$$
$$=-0.018 \text{ for the benzenes}$$
$$=-0.008 \text{ for the cyclohexanes.}$$

Because of the lack of detailed information concerning the shape of the intermolecular potential energy curves, it is quite difficult to correlate these changes in dispersion energy with the δ values. As can be seen from Fig. 2, δ depends on the fractional changes in both σ and ϕ. In the systems considered here, there is a partial cancellation of the two effects, thus making the estimated value of δ small, but otherwise unknown.

DISCUSSION

The fact that the vibrational energy of a molecule depends upon the state of aggregation of the system is well known. Some time ago, the relationship between this phenomenon and the change in heat of vaporization of a substance upon isotopic substitution was discussed

[21] Footnote reference 1, Chaps. 12 and 13.

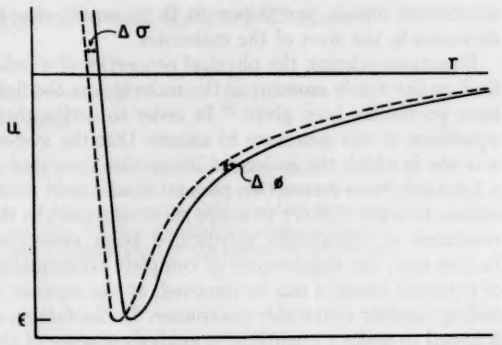

FIG. 2. A schematic diagram of the intermolecular potential energy u of a pair of isotopically substituted molecules plotted as a function of intermolecular distance. The full line is the potential energy curve of the reference substance. The dotted line shows the potential energy function of a pair of molecules which has simultaneously undergone a decrease in molecular size ($\Delta\sigma$) and a decrease in dispersion energy ($\Delta\phi$). It is seen that the effects of these two changes upon the depth of the well are in the opposite direction to each other, and will partially cancel one another. (Note that the two potential curves shown are only approximately conformal.)

by Urey.[22] It might be possible to equate the entire observed change in heat of vaporization in the systems discussed here to the change in vibrational zero point energy upon vaporization. However, it is difficult to explain the appearance of a temperature-independent term in the vapor pressure difference equation in this way, nor is it easy to account for the changes in molar volumes and liquid viscosities. Furthermore, measurements of the changes in triple point, critical temperature, and heat of fusion for a number of polar substances show that the values of these properties are all affected by deuterium substitution.[23] In many of the previous discussions of these phenomena, it has been assumed that these changes were due to the quantization of the molecular motions in the liquid and solid.[18,24] For instance, the decrease in molar volume in going from H_2O to D_2O has been ascribed to a decrease in the amplitude of the oscillatory motion of the D_2O molecule in the liquid.[25,26] This implies that molecular motions are quantized in these fluids, since the amplitude of a classical oscillator with kinetic energy kT does not depend upon its mass and thus, the molar volume of a classical fluid will not depend upon the masses of the molecules in the fluid. It seems unlikely that intermolecular quantum effects can be appreciable in many of the systems studied to date. In the present treatment, decreases in molar volumes in classical, isotopically

[22] H. Urey, J. Chem. Soc. **1947,** 562.
[23] H. Kopper, Z. physik. Chem. (Leipzig) **A175,** 469 (1936); K. Clusius, Z. Electrochem. **44,** 21 (1938).
[24] K. F. Herzfeld and E. Teller, Phys. Rev. **54,** 912 (1938); I. Kirshenbaum, J. Chem. Phys. **10,** 717 (1942); K. Shäfer, Z. Electrochem. **52,** 245 (1948).
[25] E. Whalley, *Proceedings of the Conference on Thermdynamic and Transport Properties of Fluids, London, July, 1957,* p. 15.
[26] J. D. Bernal and G. Tamm, Nature **135,** 229 (1933).

substituted liquids, are shown to be primarily due to decreases in the sizes of the molecules.

Equations relating the physical properties of a polar fluid to the dipole moment of the molecules in the fluid have previously been given.[10] In order to derive these equations, it was necessary to assume that the system was one in which the molecular interaction consisted of a Lennard-Jones interaction plus an ideal dipole interaction. It is not difficult to adapt these equations to the treatment of isotopically substituted polar molecules. In this way, the requirement of complete conformality of potential energies can be removed, at the expense of adding another adjustable parameter. In the future, it is hoped to make a quantitative analysis of some of the data on polar molecules in terms of this extended form of the theory.

Since the present approach to the interpretation of the properties of isotopically substituted molecules involves a relatively large number of adjustable parameters, it is clear that extensive data are required if one wishes to apply this theory quantitatively. Unfortunately, few extensive studies of this type have been reported. Nevertheless, it is possible to make some qualitative generalizations from the published results. In particular, the triple points and critical temperatures of a large number of simple deuterium-substituted compounds are found to be roughly 0.5% less than those of the hydrogen-containing substances[23,25] (the variations from this value are greatest for the triple point differences of highly polar molecules. This is not unexpected, since the deviations from conformal behavior may become large for asymmetrically substituted molecules, and such deviations will have the greatest effect on the properties of a substance at low temperatures and high densities). One may thus conclude that the magnitude of the intermolecular interaction energies of simple deuterium substituted compounds is generally of the order of 0.5% less than that of the hydrogen-containing compounds.

The agreement between experiment and theory for the cyclohexane system is reasonably good, and the values of the parameters chosen to fit the data are in agreement with independent estimates. It would thus appear that the intermolecular potential functions of C_6D_{12} and C_6H_{12} are conformal to a good degree of accuracy. This is to be expected, since the hydrogen atoms are distributed fairly evenly over the periphery of the C_6H_{12} molecule. Bellemans[27] has also given an analysis of the vapor pressure and molar volume differences in the cylohexane system. Although this treatment was quite similar to the present work in that the changes in the parameters of the potential function were computed by application of the theorem of corresponding states, the contributions of the changes in intramolecular degrees of freedom to the vapor pressure ratios were not explicitly taken into account, since the values of δ and γ obtained were three to five times as large as those used in this analysis. A different set of δ and γ values was used to fit each property considered, but neither set gives an adequate prediction of the liquid viscosity change.

One might expect that the potential function in benzene would not be completely conformal with that of perdeutero benzene, since the hydrogen atoms in benzene are all in the same plane, thus implying asymmetric substitution. The deviation between the theoretical and experimental vapor pressure ratios of the benzenes at temperatures near the melting point may be due to this effect. However, it should be noted that the measured differences in vapor pressure are quite small in this temperature region and are thus quite sensitive to experimental error or sample impurity. Indeed, the measured differences in physical properties upon isotopic substitution are quite small in general (less than 1% of the total). The interpretation of much of the data now in the literature is considerably complicated by the fact that relatively small quantum effects (either rotational or translational)[27] or small deviations from conformal behavior may have a large effect on the observed changes in physical property. For instance, it is possible that the quantization of the rotation of molecules such as CH_4 or HCl in the liquid is appreciable compared to the deuterated molecules. If this is so, it might account for the anomalous values of the configurational heats of vaporization differences in these systems.[23,28]

---

[27] A. Bellemans, Nuovo cimento Suppl. (10) **9**, 1, 181 (1958).
[28] A. Frank and K. Clusius, Z. physik. Chem. (Leipzig) **B42**, 395 (1939); A. Kruis, Z. Naturforsch. **3a**, 596 (1948); G. T. Armstrong, F. G. Brickwedde, and R. B. Scott, J. Research Natl. Bur. Standards **55**, 39 (1955).

Pressure Effects in Nickel Dimethylglyoxime and Related Chelates*

J. C. ZAHNER AND H. G. DRICKAMER

Department of Chemistry and Chemical Engineering, University of Illinois, Urbana, Illinois

(Received June 7, 1960)

The effect of pressure on the absorption peak characteristic of the solid phase of certain metal chelates has been measured for $Ni(DMG)_2$, $Pd(DMG)_2$, $Pt(DMG)_2$, Ni nioxime, Pd nioxime, Ni benzoxime, and Ni heptoxime. The peak shifts strongly red with pressure. At high pressure the shift levels off for nickel, tends to reverse for palladium and reverses strongly for platinum. There is considerable pressure broadening. These and other related observations are consistent with the assignment of the transition as from the A_{1g} (or A_{1g} and E_g) ground state to the A_{2u} (p_z) excited state.

THE effect of pressure has been measured on the absorption peak which occurs only in the solid phase of nickel dimethylglyoxime and related compounds. The high-pressure optical techniques have been described elsewhere.[1–3] The nickel dimethylglyoxime, $Ni(DMG)_2$ was obtained from G. Cook of the Chemistry Department, University of Illinois. The rest of the nickel and palladium compounds were obtained from D. W. Barnum of the Shell Development company. The platinum dimethylglyoxime was prepared from an aqueous solution of potassium tetrachloroplatinate (II) and an alcoholic solution of dimethylglyoxime.[4] The results are discussed under three headings below.

METAL DIMETHYLGLYOXIMES

The structure of solid $Ni(DMG)_2$ has been determined by Godychi and Rundle.[5] The planar molecules shown in Fig. 1 stack one above the other with a rotation of 90° for alternate layers. The nickel ions line up to form a chain having a nickel-nickel distance of 3.25 A. The structure is common to all solids discussed in this paper.

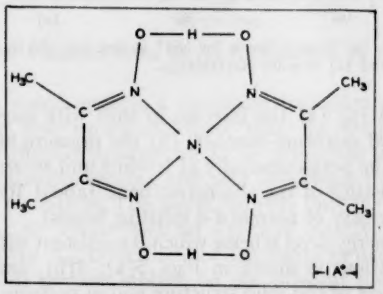

FIG. 1. Nickel dimethylglyoxime (schematic).

In the solid phase a rather sharp absorption peak occurs near 19 000 cm^{-1} which does not have an obvious counterpart in solution.[6] The peak is dichroic with the perpendicular component of higher intensity and displaced to the red.[6,7] In these studies the $Ni(DMG)_2$ or related compound was dispersed in 1–2% concentration in a salt pellet. This concentration produces a peak which can be studied readily in the high pressure optical apparatus. At this dilution the absorption coefficient α at the peak maximum is of the order of 40 cm^{-1}.

The effect of pressure on the location of the absorption maximum was studied for nickel (II), palladium (II), and platinum (II) dimethylglyoxime. The shift in peak frequency of $Ni(DMG)_2$ is shown in Fig. 2, together with the experimental points. In general, the

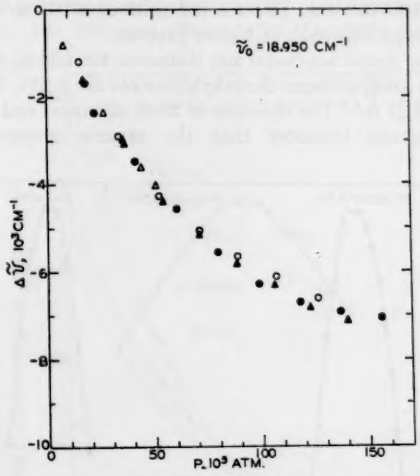

FIG. 2. Frequency shift of $Ni(DMG)_2$ ν_m vs pressure—showing experimental points.

* This work was supported in part by U. S. Atomic Energy Commission.

[1] R. A. Fitch, T. E. Slykhouse, and H. G. Drickamer, J. Opt. Soc. Am. **47**, 1015 (1957).

[2] T. E. Slykhouse and H. G. Drickamer, J. Phys. Chem. Solids **7**, 207 (1958).

[3] T. E. Slykhouse and H. G. Drickamer, J. Phys. Chem. Solids **7**, 210 (1958).

[4] S. Yamada and R. Tsuchida, Bull. Chem. Soc. Japan **27**, 156 (1954).

[5] L. E. Godychi and R. E. Rundle, Acta Cryst. **6**, 487 (1953).

[6] C. V. Banks and D. W. Barnum, J. Am. Chem. Soc. **80**, 4767 (1958).

[7] S. Yamada and R. Tsuchida, J. Am. Chem. Soc. **75**, 6351 (1953).

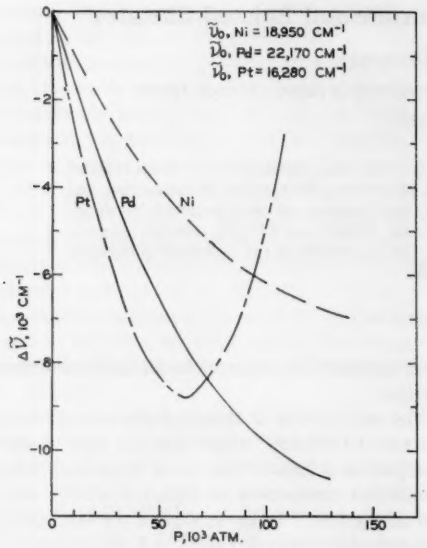

FIG. 3. Frequency shifts for $Ni(DMG)_2$, $Pd(DMG)_2$ and $Pt(DMG)_2\nu_m$ vs pressure.

reproducibility was as shown in Fig. 2 for all compounds. Figure 3 compares the shift of the peak frequency with pressure for the three compounds. The most important effects noted are: (1) the very large initial red shift (in 100 000 atm 6100 cm^{-1} for nickel and 9800 cm^{-1} for palladium), (2) the leveling of the nickel and palladium curves at about 120–150 000 atm, (3) the reversal in the shift for platinum at about 63 000 atm (after a red shift of 8700 cm^{-1} and the large blue shift at higher pressure.

The metal ion-metal ion distances for nickel, palladium and platinum dimethylglyoxime are 3.233, 3.253, and 3.25 A.[6,8] The closeness of these distances and their magnitude indicates that the organic groups are responsible for the spacing of the metal ions and probably for the compressibility of the lattices. Then Fig. 3 indicates the effect of the principal quantum number on the energy levels for a similar perturbation.

It was also found that pressure broadened the absorption peak. The broadening became more pronounced in going from $Ni(DMG)_2$ to $Pd(DMG)_2$ to $Pt(DMG)_2$. Figure 4 shows the broadening for $Pt(DMG)_2$.

We believe that the following observations from the data are significant: (1) the red shift with pressure for an absorption peak associated with transition metal ions rather than the blue shift associated with increased *d-d* splitting, (2) the very large magnitude of the shift, (3) the reversal of the direction of the shift in $Pt(DMG)_2$, (4) the increase in shift with increase in principal quantum number, (5) the pressure broadening of the peaks especially at leveling and reversal, (6) the intensity of the absorption band (about 100 times the intensity of normal *d-d* splitting bands).

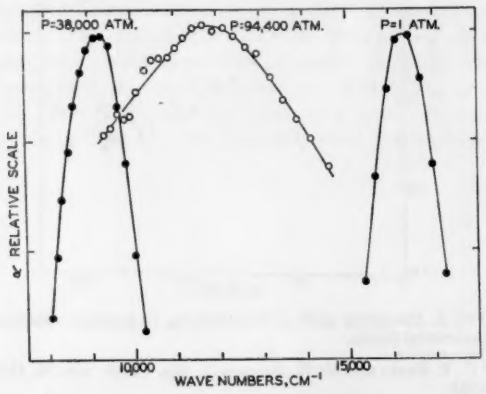

FIG. 4. Pressure broadening of $Pt(DMG)_2$ peak.

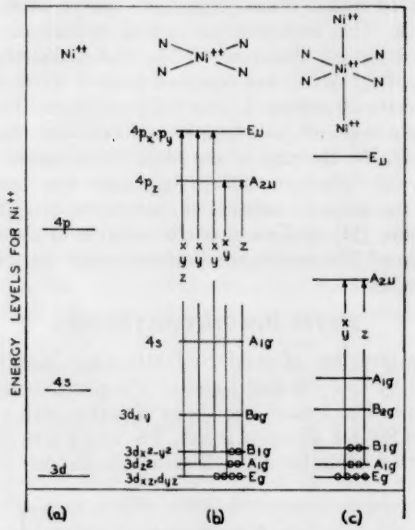

FIG. 5. (a) Energy levels for Ni^{++} in free ion; (b) in D_4: symmetry; and (c) in solid $Ni(DMG)_2$.

An energy-level scheme which is consistent with these observations is shown in Figs. 5(a), 5(b), and 5(c). The effect of the solid structure and of pressure on the levels of the metal ion are inferred. The eight electrons are paired in the metal ion levels since the compound is diamagnetic.[9] Although the nitrogens are not exactly located for D_{4h} symmetry for Ni^{++}, it is reasonable to approximate the field of the ligands as such. The metallic wave function assignments associated with the orbitals identified by symmetry conditions indicate the metallic component of the total wave function and do not preclude the possibility of bonding or of hybridiza-

[8] A. G. Sharpe and D. B. Wakefield, J. Chem. Soc. **1957**, 281.

[9] K. Sone, Bull. Chem. Soc. Japan **25**, 1 (1952).

tion. The polarizations for one electron (electric dipole) allowed transitions are also indicated. Similar diagrams would hold for $Pd(DMG)_2$ and $Pt(DMG)_2$ with increase in the principal quantum number.

Figure 5(a) shows the levels for the free ion. In Fig. 5(b) relative spacings of the energy levels are indicated for a Ni^{++} ion in D_{4h} symmetry as well as all transitions allowed in this symmetry. This would correspond to the molecule in solution. In Fig. 5(c) the effect of the lattice structure is shown, i.e., a positively charged metal ion is added above and below the plane of the molecule. The energy of the E_g state is used as a base. A larger effect is predicted for orbitals localized in the z direction and for those with higher principal quantum number. The optical transitions

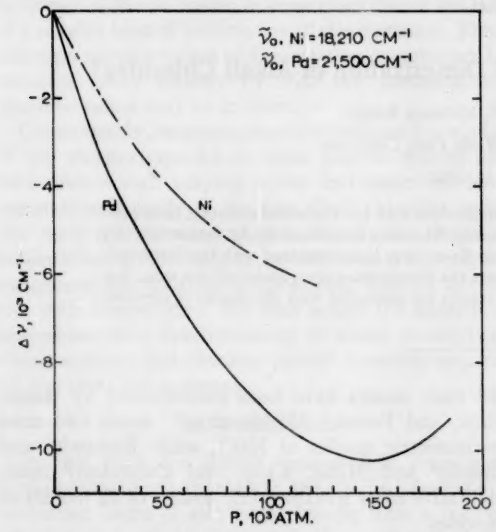

FIG. 6. Frequency shifts for Ni, Pd nioxime ν_m vs pressure.

which would undergo a significant frequency shift are shown. One would anticipate that the predominant initial effect of pressure would be to increase the effect of the positive charges, and thus to decrease the energy of the transitions. This would continue until the $A_{2u}(P_z)$ orbital no longer sees an effective positive charge. When the A_{2u} orbital on one ion starts to overlap the occupied electron orbitals on the adjacent metal ions, it (the A_{2u} orbital) starts to increase in energy; this effect increases with increasing pressure. The preceding description appears to be convincingly demonstrated by $Pt(DMG)_2$. Whether the ground state of the peak is A_{1g} or the A_{1g} and E_g orbitals, is not certain, nor, do we feel, relevant.

The pressure broadening could be the "natural" broadening as the electrons become more and more part of a one-dimensional metallic lattice, rather than the result of splitting the A_{1g} and E_g ground states. The assignment of the transition from the A_{1g} (or A_{1g} and

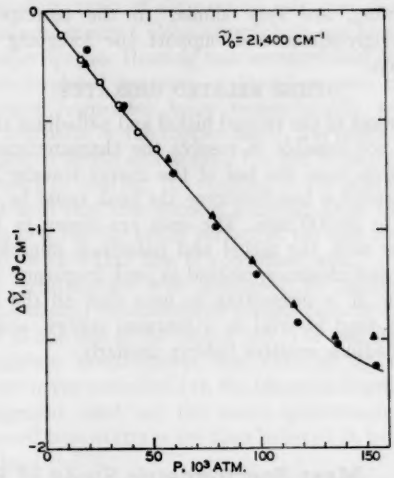

FIG. 7. Peak frequency comparisons for Ni and Pd chelates.

E_g) ground state to the A_{2u} orbital is consistent with the six observations listed. It is also supported by the facts that it is not readily identified in solution spectra and that dichroism exists with the appropriate relative energies.

METAL NIOXIMES

The shift of the peak frequency with pressure has also been determined for nickel and palladium 1,2 cyclohexane dionedioxime (nioxime) for the peak characteristic of solids (see Fig. 6). The Ni–Ni and Pd–Pd distances are 3.237 and 3.250 A.[5] There is the large initial red shift, which for Pd nioxime reverses at about 150 000 atm. The results, including pressure

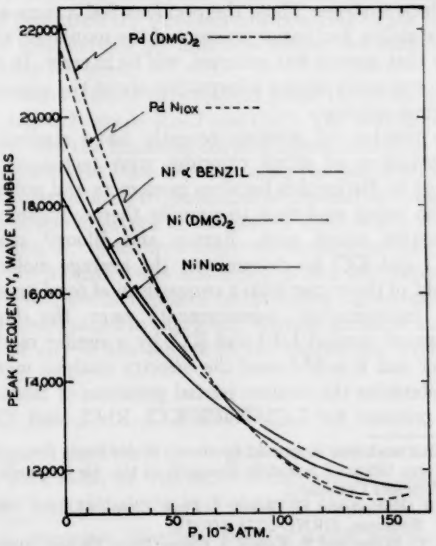

FIG. 8. Frequency shift of Ni heptoxime ν_m vs pressure.

broadening, are very similar to the corresponding dimethylglyoximes and support the foregoing interpretation.

OTHER RELATED CHELATES

For most of the related nickel and palladium analogs it was not possible to resolve the characteristic solid absorption from the tail of the charge transfer bond.

For nickel α benzildioxime the peak could be determined to 60 000 atm. The data are shown in Fig. 7 together with the nickel and palladium dimethylglyoximes and nioximes, plotted as peak frequency versus pressure. It is interesting to note that all the nickel chelates tend to level at a common energy, and that the palladium chelates behave similarly.

Pressure experiments were also made with nickel 1,2 cycloheptane dionedioxime (heptoxime). The results are shown in Fig. 8. The shift is only 20–25% of that of the other nickel chelates. This may be due to a markedly smaller compressibility for the heptoxime due to steric effects of the organic groups.

ACKNOWLEDGMENTS

The authors would like to thank Glen Cook of these laboratories for the $Ni(DMG)_2$, and D. W. Barnum of Shell Development for the remaining nickel and palladium compounds. J. C. Zahner would like to acknowledge assistance from a National Science Foundation Fellowship.

Mass Spectrometric Study of Heats of Dimerization of Alkali Chlorides*

THOMAS A. MILNE AND H. MICHAEL KLEIN

Stanford Research Institute, Menlo Park, California

(Received May 16, 1960)

The heats of sublimation of the important species in equilibrium with the five alkali chlorides have been determined using the Bendix time-of-flight mass spectrometer. The mass spectrometrically determined differences between the heats of sublimation of monomer and dimer have been combined with the best available value for the monomer heat of sublimation to calculate the dimerization energies for all five salts. For LiCl a trimerization energy was also determined. These results are compared with the results of previous studies.

INTRODUCTION

IN recent years the recognition that polymer molecules are an important constituent in the vapor in equilibrium with the alkali halides has renewed interest in these systems. Thus, the previous deductions about the stability and vapor pressure of the monomer, where only that species was assumed, will be in error. In addition, one seeks similar information about the important polymer species.

A number of workers recently have studied the vaporization of alkali chlorides with techniques designed to distinguish between monomers and polymers in the vapor and thus to provide thermodynamic information about each. Barton and Bloom[1] studied NaCl and KCl by determining the average molecular weight of the vapor from a comparison of total pressure and transpiration measurements over the liquid; Beusman[2] studied LiCl and KCl by a similar method. Miller and Kusch[3,4] used the velocity analysis method to determine the relative partial pressures of monomer and polymer for LiCl, NaCl, KCl, RbCl, and CsCl; and their results have been reinterpreted by Bauer, Diner, and Porter.[5] Akishin *et al.*[6,7] made two mass spectrometric studies of NaCl, while Berkowitz and Chupka[8] and Milne, Klein, and Cubicciotti[9] made qualitative mass spectrometric studies of all five alkali chlorides.

The molecular weight method of determining the fraction of polymer depends upon the assumption that there are only two species present—in this case, monomer and dimer. Other work[4] has shown that this is not true for LiCl and in this instance the molecular weight data yield no unambiguous thermodynamic information about individual species. Also, the method would be subject to large error in systems such as RbCl and CsCl where only small amounts of dimer are present. The velocity analysis method also lacks sensitivity in systems containing small amounts of polymer, although more than two species can be sorted out. The mass spectrometric method is particularly suitable for

* This work was supported by the U. S. Air Force through the Air Force Office of Scientific Research of the Air Research and Development Command.

[1] J. L. Barton and H. Bloom, J. Phys. Chem. **63**, 1785 (1959).
[2] C. Beusman, ORNL-2323 (1957).
[3] R. C. Miller and P. Kusch, J. Chem. Phys. **25**, 860 (1956).
[4] R. C. Miller and P. Kusch, **27**, 981 (1957).
[5] S. H. Bauer, R. M. Diner, and R. F. Porter, J. Chem. Phys. **29**, 991 (1958).
[6] L. N. Gorokhov, U. S. Khodev, and P. A. Akishin, Zhur. Neorg. Khim. **3**, 2597 (1958).
[7] P. A. Akishin, L. N. Gorokhov, and L. N. Sidorov, Zhur. Fiz. Khim. **33**, 2822 (1959).
[8] J. Berkowitz and W. A. Chupka, J. Chem. Phys. **29**, 653 (1958).
[9] T. A. Milne, H. M. Klein, and D. Cubicciotti, J. Chem. Phys. **28**, 718 (1958).

studying systems with more than two species and for studying minor species directly.

In all of these approaches the data can be interpreted by the second-law or slope method, or by the third-law method. In the latter it is necessary to determine the ratio of the monomer species to the various polymer species. In the case of the mass spectrometric work this involves relating ion intensity ratios to partial pressure ratios.

To obtain information about the stability of the dimer requires an estimate of the entropy of dimerization together with a knowledge of the stability of the monomer. At present the entropy of dimerization can only be estimated—mainly because of a lack of knowledge of the vibrational frequencies of the dimer—and is subject to large uncertainty. The stability of the monomer is also uncertain in some cases due to the lack of a reliable heat of sublimation of the monomer. Thus, although relative values of dimerization energies can be obtained fairly reliably by third-law methods, the absolute values may be in error.

Consequently, in attempting to extend our knowledge of the thermodynamics of these gaseous species and their trends with varying cation and anion, we have undertaken a study of the five alkali chlorides, using the mass spectrometer to give directly the heats of sublimation of the various species from a second-law analysis of the variation in the appropriate ion intensities with temperature. We thus accept the hazards of second-law heat determinations to avoid assumptions about entropy and absolute partial pressures required by the third-law approach.

EXPERIMENTAL

In this work the Bendix time-of-flight mass spectrometer was used to analyze the species present in a molecular beam of salt vapor issuing from a conventional Knudsen cell. As a general description of this spectrometer has been given by Wiley and McLaren,[10] we will discuss only features and behavior pertinent to our particular experiment.

The spectrometer is designed so that it can accept a collimated molecular beam from below the ionization chamber, the collimation being such that little or none of the molecular beam strikes any part of the interior of the ionization chamber. In our experiments a resistance-heated, pure copper Knudsen cell was placed inside a water-cooled can which in turn was attached to a flanged entrance port just below the ionization chamber. The Knudsen cells used were similar in construction to those of Miller and Kusch[3]: 1-in. cubes, containing a $\frac{1}{2}$-in. diam hole drilled to a depth of $\frac{3}{4}$ in. This hole was covered directly by two 1-in. x $\frac{1}{2}$-in. x $\frac{1}{8}$-in. copper blades, tapered to a knife edge. Runs were made with slit widths of about 0.005 in. Recent work on the kinetics of evaporation of alkali halides indicates that the resultant ratio of slit area to salt area should be adequate to ensure a close approach to equilibrium for the major species. Heating was accomplished by using ceramic-insulated tungsten or tantalum wire inserted into eight horizontal holes symmetrically arranged along two sides of the copper block. Tantalum shields were placed above and around the cell to improve the uniformity of heating. No clogging of the slits was observed with this arrangement although after the completion of a run the under surface of the slits often was covered with a thin film of condensed salt.

The temperature was measured by means of a chromel-alumel thermocouple peened directly into the center of one side of the copper cell. The validity of the temperature measurement was checked by running cooling curves with NaCl in the identical experimental arrangement used for the mass spectrometer runs. Measured temperatures are thus believed to be reliable to at least $\pm 5°K$.

A magnetically operated shutter was used to interrupt the molecular beam of salt and thus to distinguish between ions formed from residual gas molecules and those formed from the molecular beam. The continuous, collimated molecular beam of salt vapor which passed directly through the ionization chamber of the time-of-flight mass spectrometer from below was then ionized by a pulsed beam of electrons of known energy. The bunches of positive ions were drawn out of the ionization chamber, accelerated through 3000 v, and then allowed to drift in a field-free tube about 1 *m* long to allow separation of masses according to their velocities. The ions of different masses arrived at the input of an electron multiplier of special design,[11] at different times and the output of the multiplier was amplified and displayed on an oscilloscope. For quantitative studies a dual pulse counter and gate arrangement permitted the simultaneous counting of the number of ions arriving per unit time at any two masses, up to about 600 amu.

The salts studied were reagent grade LiCl, NaCl, and KCl and C.P. grade RbCl and CsCl. The samples were loaded into the Knudsen cell and slowly heated in high vacuum to near their melting point. No ions other than those attributable to molecules of the salt in question were observed except in the case of RbCl where an appreciable K^+ peak was observed throughout the run. The K^+ intensity was about 5% of the Rb^+ intensity and would not be expected to invalidate the second-law heats determined in this work. No indications of a reaction of any of the salts with the copper cell were observed.

RESULTS

Several experiments were performed with each of the five pure salts, as well as with different salt pairs. In Table I are listed the ions observed from each of the

[10] W. C. Wiley and I. H. McLaren, Rev. Sci. Instr. **26**, 1150 (1955).

[11] D. Harrington, Cincinnati Division, Bendix Aviation Corporation (private communication).

TABLE I. Ions observed in the mass spectra of the alkali chlorides and their relative intensities.[a]

Salt	M^+	MX^+	M_2X^+	$M_3X_2^+$
LiCl	...[b]	27	100	4
NaCl	110	80	100	...[b]
KCl	570	...[b]	100	
RbCl	600	37	100	
CsCl	980	...[b]	100	

[a] 20 ev ionizing electron energies. Total pressures approx. 10^{-6} atm.
[b] Observed with sufficient intensity for quantitative measurement but not recorded during this slope study.

pure salts and their approximate proportions. These results were obtained at an ionizing electron energy of 20 ev and at settings of the mass spectrometer parameters which tended to minimize any mass discrimination effects. Rather serious mass discrimination occurred with our mass spectrometer for masses in the range 2 to 7 due to some unexplained circumstance connected with our particular instrument. Thus we noted that our observed ratios of Li^+/Li_2Cl^+ were about one-fiftieth of the value obtained by Berkowitz and Chupka[8] and by the Bendix research division on its research spectrometer.[11] As a result of this lack of sensitivity at very low masses we were unable to study the temperature dependence of Li^+, as will be discussed later.

For the salts and species reported in Table I, the results agree satisfactorily with those obtained by Berkowitz and Chupka[8] at 75 ev and at similar temperatures. The relation of the observed ions to their neutral parents has been discussed in detail for these and similar salts by others.[8,12] The conclusion is that the species $M_3Cl_2^+$ and M_2Cl^+ undoubtedly come from $M_3Cl_3(g)$ and $M_2Cl_2(g)$, respectively, MCl^+ may originate partly from polymer in addition to monomer, and M^+ arises principally from the monomer. LiCl may provide an exception to this generalization. There is evidence in the work of Friedman[13] and the recent work of Schoonmaker and Porter[14] that an appreciable amount of Li^+ may arise from dissociative ionization of Li_2Cl_2. With this exception we have chosen the temperature dependence of M^+, M_2X^+, and $M_3X_2^+$ for slope determinations of the heats of sublimation of monomer, dimer, and trimer, respectively.

Approximate appearance potentials were obtained for the major ions from each salt and were consistent with the above assumptions as to molecular precursors. The possibility that ion-molecule reactions in the ionization chamber could be responsible for an appreciable fraction of the complex ions has also been discussed previously[8] and has definitely been eliminated in the present studies by the results of experiments described elseswhere.[15]

The principal experimental effort was put into the determination of the temperature dependence of the intensity of the ions attributed to the monomer and dimer of the pure salts. It can be shown[13] that the partial pressure of a species in the Knudsen cell is proportional to I^+T where I^+ is the intensity of an ion formed from the species and T is the absolute temperature. Consequently, the quantity I^+T was determined for as wide a temperature range over the solid as possible. This kind of experiment requires a constant sensitivity of the mass spectrometer over a period of hours. The Bendix machine was fairly stable during the course of the 8–9 hours required in our experiments, as evidenced by the agreement between measurements taken at the same temperatures during the course of the runs. Under the best conditions, however, there still seemed to be more or less random short-term variations of the order of $\pm 10\%$ in the sensitivity of the machine at any given mass. This variation is believed to be responsible for the scatter in results observed in different experiments and required taking considerable data for each salt. The source of this fluctuating sensitivity was not determined. It should be noted that the fluctuation in the ratio of intensities of two peaks was much less than $\pm 10\%$ since all masses were affected simultaneously in approximately the same way.

Table II summarizes the results obtained from such runs for the five alkali chlorides. In Fig. 1 are shown

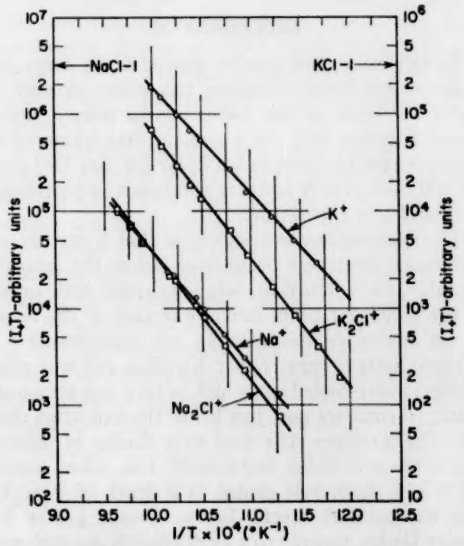

FIG. 1. Temperature variation of ion intensities in typical Knudsen experiments using the Bendix time-of-flight mass spectrometer.

[12] R. F. Porter and R. C. Schoonmaker, J. Chem. Phys. **29**, 1070 (1958).
[13] L. Friedman, J. Chem. Phys. **23**, 477 (1955).
[14] R. C. Schoonmaker and R. F. Porter, J. Phys. Chem. **64**, 457 (1960).
[15] T. A. Milne, J. Chem. Phys. **32**, 1275 (1960).

TABLE II. Mass spectrometrically determined heats of sublimation of major species from the alkali chlorides.

Salt	Run No.	Temp. range °K	Second law heat of sublimation: Monomer (M^+) kcal/mole	Dimer (M_2Cl^+) kcal/mole	Trimer ($M_2Cl_2^+$) kcal/mole	ΔH_{subl} (dim) − ΔH_{subl} (mon) kcal/mole
LiCl	1	737–878	(42.5)[a]	49.6		
	4	736–871	54.2 (MX^+)	49.5		
	3	714–877		51.4	57.5	
	4	708–878		50.3	57.6	
	5	724–871	53.8 (MX^+)	50.1		
	6	718–875	51.8 (MX^+)	51.9		
	av	approx. 800°K	53.3	50.5	57.6	
NaCl	1	886–1038	53.8	60.4		
	2	827–988	51.0	59.3		
	3	843–994	51.0	58.3		
	av	approx. 930°K	51.9	59.3		7.4
KCl	1	842–1001	50.0	60.8		
	2	774–999	48.9	57.2		
	3	814–1016	50.0	57.7		
	4	822–953	52.5	63.7		
	av	approx. 900°K	50.4	59.9		9.5
RbCl	1	835–950	45.6	55.9		
	2	782–950	47.3	56.6		
	3	827–949	48.8	59.4		
	4	796–970	45.6	54.2		
	av	approx. 880°K	46.8	56.5		9.7
CsCl	1	686–903	40.0[b]	48.8[b]		
	2	793–906	44.5	49.1		
	3	764–886	42.3	48.4		
	4	738–906	42.6	49.4		
	5	744–914	43.5	49.2		
	6	804–900	40.8	(43.7)[a]		
	7	784–901	40.8	47.3		
	av	approx 818°K	41.8	48.7		6.9

[a] Not averaged.
[b] Average of two runs—given double weight.

the plots, for NaCl–1 and KCl–1, of the kind of data obtained, together with the least-squares lines from which the heats were determined.

In addition to these temperature-dependent experiments on pure salts, determinations of the relative intensities of various ions were made for the approximately equimolar mixtures NaCl–KCl, KCl–RbCl, and RbCl–CsCl. Besides the species characteristic of each salt, the ion $MNCl^+$ was observed in each case with an intensity greater than either M_2Cl^+ or N_2Cl^+. These relative intensities can be used to calculate approximately the differences in dimerization energies of the two salts, as well as the heat of formation of the mixed dimer molecule from the two pure dimers, and they served as rough qualitative checks on the second-law derived heats of the pure salts. The assumptions involved have been discussed previously.[16] The results of such measurements on the three mixtures at two electron energies are given in Table III.

[16] R. C. Schoonmaker and R. F. Porter, J. Chem. Phys. **30**, 283 (1959).

ANALYSIS OF DATA

Because no previous studies of this type have been made with the Bendix time-of-flight spectrometer it appeared that the most reliable data could be obtained by using the mass spectrometric data to determine the difference between the heats of sublimation of dimer and monomer. This difference was then added to the heat of sublimation of the monomer as determined by third-law methods from other data with an appropriate correction for the fraction of polymers in the vapor to give the heat of sublimation of the dimer. Then from these heats of sublimation the heat of dimerization could be calculated. This procedure is satisfactory only for LiCl, NaCl, and KCl since reliable third-law heats for the monomer of the other two salts are not available. For RbCl and CsCl a second-law monomer heat had to be used.

LiCl

For this salt there existed until quite recently only estimated heat capacity data for the solid. However,

TABLE III. Relative ion intensities observed in the mass spectra of equimolar salt pairs and derived thermodynamic results.

Salt pair NCl–MCl	Temp. °K	Electron energy ev	Number of observations	$K_1=[(M^+ + MCl^+)/(N^+ + NCl^+)]^2 \times (N_2Cl^+/M_2Cl^+)$ Range of values	$\Delta F°(M_2Cl_2) - \Delta F°(N_2Cl_2)$ (dimerization) kcal mole	$\Delta H_M - \Delta H_N$ (dimerization) kcal/mole	$K_2=(MNCl^+)^2/M_2Cl^+N_2Cl^+$
NaCl–KCl	946	20	4	8.3–12.0	4.5±0.5		5.4–5.6
		50	1	20	5.6		5.0
	986	20	2	8.8–13.2	4.7±0.5	5.8	5.2
					av 5.1		
KCl–RbCl	978	20	1	2.49	1.8		3.4
		50	1	2.19	1.5		3.5
	1006	20	1	2.79	2.1		2.8
		50	1	2.15	1.5	1.7	3.2
					av 1.7		
RbCl–CsCl	917	20	1	4.53	2.8		3.16
		50	1	5.69	3.2		3.01
	942	20	1	4.99	2.9	3.7	2.56
		50	1	6.03	2.4		2.54
					av 2.8		

Douglas, Harman, and Dever[17] and Rodigina *et al.*[18] have reported heat capacity data for both the liquid and solid salt. These two sets of heat capacities lead to substantially the same results so that only the former was used. A value of $S_{298}°$ for LiCl(s) of 14.17 gbs/mole (1 gbs=1 gibbs=1 cal/deg K)[19] has also recently become available from the work of Giauque and Shirley.[20] The thermodynamic functions for LiCl(g) were calculated assuming a rigid rotator[21] with r_e= 2.027 A and a harmonic oscillator[22] with ω_e=662 cm^{-1}. To calculate the third-law heat of sublimation of LiCl(g) one requires only the partial pressure of monomer in equilibrium with the solid. Knudsen measurements on solid LiCl have been carried out by Niwa[23] and by Nesmeyanov and Sazonov[24] with results that differ by about 30%, the latter being higher. The results of Nesmeyanov and Sazonov were chosen for the following calculations.

In a Knudsen experiment using a detection system which counts a dimer molecule as two monomers, a trimer as three, etc., P_{mon}', calculated on the assumption of monomer only, is related to the true pressure of monomer by

$$P_{mon}=P_{mon}'/(1+2a_2+3a_3+\cdots),$$

where a_2, a_3, $\cdots$, are the ratios of dimer, trimer, $\cdots$, to monomer in the molecular beam effusing from the Knudsen cell. These values are given directly for all the chlorides except CsCl from the velocity analysis data of Miller and Kusch.[4] At T=870°K they report for LiCl a_2=2.62 and a_3=0.15 which requires dividing the reported Knudsen pressures by 6.69 to obtain the true monomer pressure and increases the third-law heat of sublimation by 3.3 kcal/mole. The resulting third-law heat of sublimation of monomer at 800°K, the average temperature of our mass spectrometric studies, is 50.3 kcal/mole.

Unfortunately, in our mass spectroscopic work we were not able to quantitatively study a species that could be identified as coming from the monomer only. The species $LiCl^+$ as well as Li^+ very likely has some contribution from dissociative ionization of the dimer as was found for LiI.[13] The second-law heats obtained for $LiCl^+$, Li_2Cl^+, and $LiCl_2^+$ from our work are 53.3, 50.5, and 57.6 kcal/mole, respectively, with the data being quite badly scattered for $LiCl^+$. The last two values will be taken as the heats of sublimation of dimer and trimer, respectively, with the third-law value of 50.3 kcal/mole chosen for the monomer. These results yield a heat of dimerization at 800°K of −50.1 kcal/mole and a heat for dimer plus monomer going to trimer of −43.2 kcal/mole.

In Fig. 2 are plotted the extrapolated partial pressures of the three species, based on Miller and Kusch's ratios applied to the Knudsen data of Nesmeyanov and Sazonov and using the mass spectrometrically determined heats for dimer and trimer, the third-law heat of sublimation of monomer, a heat of fusion of

[17] T. B. Douglas, A. W. Harman, and J. L. Dever, unpublished data reported in Natl. Bur. Standards Rept. 6484 (July, 1959).
[18] E. N. Rodigina, K. Z. Gomelskii, and V. F. Luginina, Zhur. Neorg. Khim. **4**, 442 (1959).
[19] W. F. Giauque, E. W. Hornung, J. E. Kunzler, and T. R. Rubin, J. Am. Chem. Soc. **82**, 62 (1960).
[20] L. Brewer (private communication of results of Giauque and Shirley).
[21] L. Pauling, Proc. Natl. Acad. Sci. India, **A25** (1956).
[22] W. Klemperer and S. A. Rice, J. Chem. Phys. **26**, 6181 (1957).
[23] K. Niwa, J. Chem. Soc. Japan **59**, 637 (1938).
[24] An. N. Nesmeyanov and L. A. Sazonov, Zhur. Neorg. Khim. **4**, 98 (1959).

4.71 kcal/mole from recent calorimetric studies,[18,25] and the liquid heat capacity data of Douglas *et al.*[17] In all the extrapolations above the melting point, fully excited heat capacities for the gases can be assumed without significant error. It is seen that the pressure of the monomer rapidly increases relative to dimer and trimer above the melting point and, in fact, equals the partial pressure of dimer at about 1400°K.

The extrapolated boiling point from the data in Fig. 2 is about 1750°K, substantially higher than the values of 1610–1653 reported by Ruff and Mugdan,[26] Maier,[27] Beusman,[2] and von Wartenburg and Schultz[28] from total pressure measurements over the liquid. The monomer heat of sublimation would have to be increased by about 3 kcal/mole to bring the boiling point into agreement with the liquid studies. Smaller increases in both the monomer and dimer heats would achieve the same effect.

With the heats of sublimation of monomer and trimer equal to or greater than that of the dimer, then the second-law heats from Niwa's data and that of Nesmeyanov and Sazonov ought to be equal to or slightly greater than the dimer heat of sublimation since the vapor is mostly dimer over the solid. The over-all slope heats of 46.7 and 46.8 kcal/mole, respectively, reported by them are thus in disagreement with our mass spectrometric results and are unaccountably low.

It is interesting to compare the proportions of monomer and dimer and their temperature dependence over the liquid with the molecular weight studies of Beusman.[2] From a comparison of total pressure by the Rodebush method[29] and results of transpiration experiments Beusman deduced that the molecular weight of the vapor was about 71.0 with little temperature variation from 1229°–1013°K. From our extrapolated results in Fig. 1 the molecular weight varies from 69 to 71 over this temperature range—in very good agreement with Beusman—although our extrapolated total pressures are about half as great as his. The over-all slope heats determined over the liquid by the previously mentioned workers range from about 37–40 kcal/mole at 1300°K. The slope determined graphically from our extrapolated total pressures in this temperature range is 37 kcal/mole.

In summary, there is disagreement between our results and the second-law heats measured over the solid. There is also disagreement between the extrapolated pressures from our heats plus corrected Knudsen pressures over the solid and the total pressures measured over the liquid by several workers. There is agreement with the molecular weights determined by Beusman and with the second-law heats over the liquid. Increasing all our heats of sublimation by about a kilocalorie each would lead to a general consistency of all the data cited above, except the second-law heats over the solid.

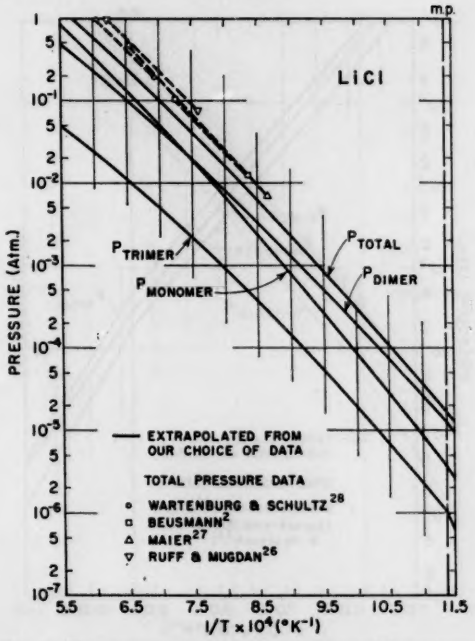

FIG. 2. The temperature variation of the partial pressures of the important species in equilibrium with LiCl.

The heats of dimerization and trimerization will be compared with other values following the discussion of the other salts.

NaCl

For NaCl(s) the entropy data and heat capacity data up to the melting point have been accurately measured and are reported by Kelley.[30] The thermodynamic functions for NaCl(g) have been calculated by Klemperer and Rice.[31] In addition a number of workers have measured the apparent total pressure over the solid, with results which agree closely. To determine the heat of sublimation of monomer we have taken the Knudsen pressure data of Zimm and Mayer,[32] which differ negligibly from those of Nesmeyanov and Sazonov[33] and Niwa,[23] and corrected them for dimer according to the data of Miller and Kusch.[4]

The resulting third-law value of the heat of sublimation at 930°K is 52.1 kcal/mole, with the effect of the correction for dimer such as to increase the heat of sublimation by only 0.8 kcal/mole. The uncorrected second-law heat of sublimation from Zimm and

[26] A. S. Dworkin and M. A. Bredig, J. Phys. Chem. **64**, 269 (1960).
[26] O. Ruff and S. Mugdan, Z. anorg. Chem. **117**, 147 (1921).
[27] C. G. Maier, Bureau of Mines Tech. Paper No. 360 (1925).
[28] H. von Wartenberg and H. Schultz, Z. Elektrochem. **27**, 568 (1921).
[29] W. H. Rodebush and A. L. Dixon, Phys. Rev. **26**, 851 (1925).
[30] K. K. Kelley, Bureau of Mines Bulls. 477 and 584.
[31] S. A. Rice and W. Klemperer, J. Chem. Phys. **27**, 643 (1957).
[32] B. H. Zimm and J. E. Mayer, J. Chem. Phys. **12**, 362 (1944).
[33] An. N. Nesmeyanov and L. A. Sazonov, Zhur. Neorg. Khim. **2**, 946 (1957).

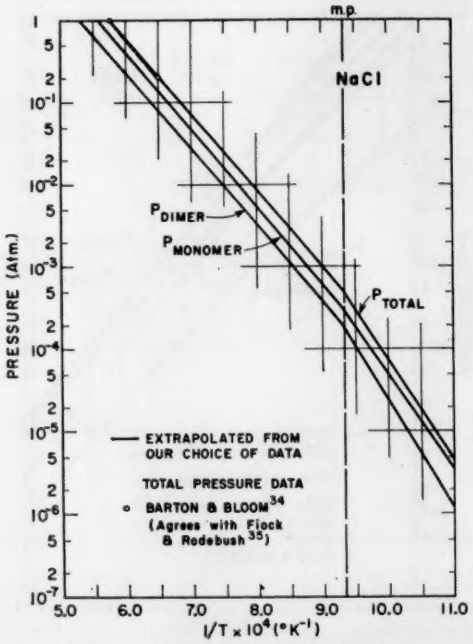

FIG. 3. The temperature variation of the partial pressures of the important species in equilibrium with NaCl.

Mayer's work is $\Delta H_{936}^{sub1} = 52.3$ kcal/mole, insignificantly higher than the third-law value although in the direction to be expected since the heat of sublimation of the dimer is greater than that of the monomer. The mass spectrometric value at 930°K is, from Table II, equal to 51.9 kcal/mole. This agreement is very satisfactory and indicates that the methods and assumptions made in this study are valid.

Although the values of the heats of sublimation of monomer and dimer determined in this study are uncertain by ±1–2 kcal/mole, the uncertainty in the difference between these two quantities is no greater than this since, in general, high or low values were obtained simultaneously for both the monomer and dimer, indicating some nonrandom, instrumental source of error in both heats. Thus from Table II one takes ΔH_{sub1} (dim) $-\Delta H_{sub1}$ (mon) $= 7.4 \pm 1.0$ kcal/mole and combines this with the third-law value above for the monomer to obtain a heat of sublimation of the dimer of 59.5 kcal/mole and ΔH (dimerization) $= -44.7$ kcal/mole. In Fig. 3 we have extrapolated the vapor pressures of monomer and dimer, obtained from Miller and Kusch's ratios and Zimm and Mayer's Knudsen pressure data, to the liquid region based on the heats for monomer and dimer given above and a heat fusion of 6.70 kcal/mole taken from Bredig and Dworkin,[25] and liquid heat capacities taken from Kelley.[30]

The extrapolated boiling point is 1726°K, in excellent agreement with the value 1734°K obtained from the total pressure results of Barton and Bloom[34] and Fiock and Rodebush,[35] considering the long extrapolation involved. One can compare these extrapolated results with the molecular weight studies of Barton and Bloom.[1] They found 54.9% monomer and 48.7% dimer in the vapor at 1362°K with the ratio of monomer to dimer increasing slowly with temperature, in qualitative agreement with our extrapolated results.

KCl

For this salt also, there are adequate data on the solid and gas from the same sources as for NaCl to permit a reliable third-law derivation of the monomer heat of sublimation. Using the Knudsen data of Zimm and Mayer,[32] which are again in substantial agreement with those of Nesmeyanov and Sazonov,[36] and Niwa,[23] and correcting for dimer as above from the data of Miller and Kusch,[4] one obtains a third-law heat of sublimation of monomer of 51.0 kcal/mole at 900°K, with the correction for dimer affecting the heat in this case by only 0.3 kcal/mole. Our mass spectroscopic value is 50.4 kcal/mole, again in very satisfactory agreement. The uncorrected second-law value of Zimm and Mayer is 51.7 kcal/mole. Based on 51.0 for the monomer and a measured difference between the heat

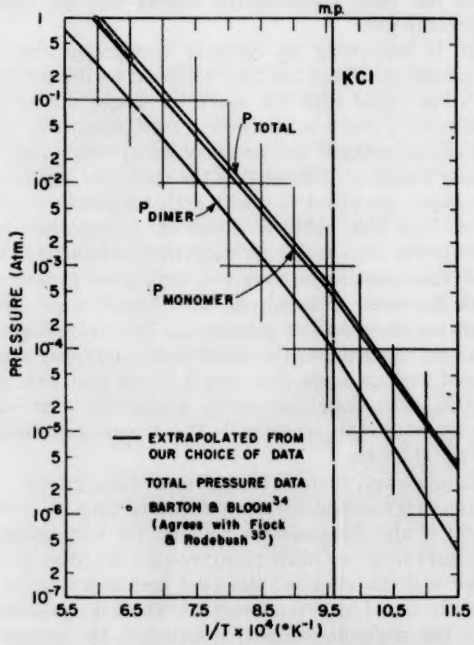

FIG. 4. The temperature variation of the partial pressures of the important species in equilibrium with KCl.

[34] J. L. Barton and H. Bloom, J. Phys. Chem. **60**, 1413 (1956).
[35] E. F. Fiock and W. H. Rodebush, J. Am. Chem. Soc. **48**, 2522 (1926).
[36] An. N. Nesmeyanov and L. A. Sazonov, Zhur. Neorg. Khim. **2**, 1183 (1957).

of sublimation of dimer and monomer of 9.5±1.5, the heat of sublimation of dimer equals 60.5 kcal/mole and ΔH (dimerization) = −41.5 kcal/mole. We have presented in Fig. 4 the pressures for monomer and dimer extrapolated to the liquid region, using a heat of fusion of 6.3 kcal/mole as reported by Dworkin and Bredig.[25] The boiling point so obtained is 1653°K, in reasonable agreement with the value of 1686°K from the total pressure measurements of Barton and Bloom[34] and Fiock and Rodebush.[35]

For this salt at 1360°K, Barton and Bloom[1] report 71% monomer and 29% dimer with no discernible temperature trend in the relative proportions, again consistent with our results. Beusman[2] has also studied the molecular weight of KCl by comparing vapor pressure results between Rodebush and transpiration experiments and finds about 75% monomer and 25% dimer at 1300°K with little temperature dependence of this ratio over the liquid.

RbCl

In the case of RbCl(s) no reliable third-law heat of sublimation of the monomer can be obtained from existing data. The reason is that only estimated $S_{298}°$ and C_p data are available for the solid.[30] Consequently, we have decided to use our heats from slopes for both monomer and dimer rather than literature second-law heats corrected for dimer. The resulting value for the monomer from Table II is 46.8 kcal/mole at 880°K. Second-law determinations over the solid, from the data of Niwa,[23] Nesmeyanov and Sazonov,[33] Treadwell and Werner,[37] and Mayer and Wintner[38] give values of 47.5, 45.2, 46.7, and 49.3 kcal/mole, respectively. From our measured difference between the heats of sublimation of dimer and monomer of 9.7±1 kcal/mole we obtain for the heat of sublimation of dimer, 56.5 kcal/mole and for ΔH (dimerization), −37.1 kcal/mole.

In Fig. 5 the pressures of monomer and dimer obtained from Miller and Kusch's ratios and the data of Mayer and Wintner, which are intermediate between the data of Niwa and of Nesemeyanov and Sazonov, are extrapolated to the liquid range using our mass spectrometric heats of monomer and dimer, the heat of fusion of RbCl of 5.67 kcal/mole recently reported by Dworkin and Bredig,[25] and an estimated liquid heat capacity. The resultant boiling point is 1655°K compared to values of 1656°K and 1661°K reported by von Wartenberg and Schultz[28] to Ruff and Mugdan[26] from measurements of total pressure over the liquid, indicating excellent consistency of our choice of heats and absolute pressures over the solid. For this salt the percentage of dimer appears to increase significantly with temperature even above the melting point; it reaches a value of about 25% near the boiling point.

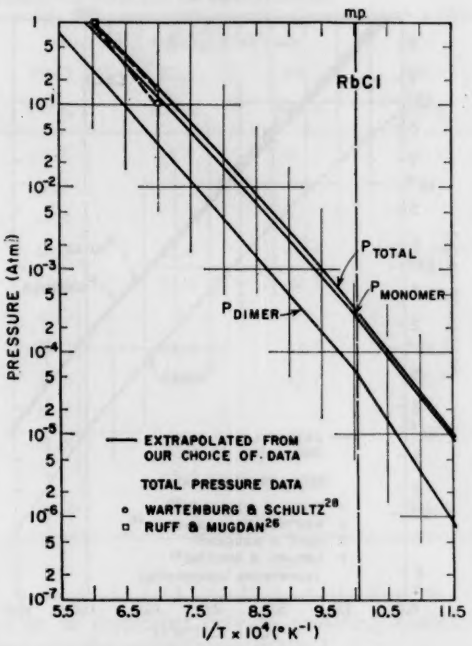

FIG. 5. The temperature variation of the partial pressures of the important species in equilibrium with RbCl.

CsCl

Although the heat capacity of the solid and liquid from 300°C–900°C has recently been experimentally determined,[39] only estimated values for $S_{298}°$ are available for the crystal. This, together with the fact that there is a disagreement by a factor of four among the vapor pressure results over the solid, makes the third-law heat of sublimation uncertain.

The monomer and dimer heats measured in this work are, at 815°K, 41.8 and 48.7 kcal/mole, respectively. This heat of sublimation of monomer is in serious disagreement with gross second-law values measured by other workers. Thus Niwa,[23] Treadwell and Werner,[37] and Cogin and Kimball[40] obtain values of 44.4, 45.7, and 46.7 kcal/mole, respectively, at this temperature from measurements over the solid while measurements over the liquid[26,28,35,41] lead also to values around 45–47 kcal/mole for the solid.

In addition, if we take the above heats together with a heat of fusion of 4.84 kcal/mole[25] and the pressure measurements over the solid of Cogin and Kimball, which are the highest, corrected for dimer on the

[37] W. D. Treadwell and W. Werner, Helv. Chim. Acta. **36**, 1436 (1953).
[38] J. E. Mayer and I. H. Wintner, J. Chem. Phys. **6**, 301 (1938).
[39] C. E. Kaylor, G. E. Walden, and D. F. Smith, J. Phys. Chem. **64**, 276 (1960).
[40] G. E. Cogin and G. E. Kimball, J. Chem. Phys. **16**, 1035 (1948).
[41] W. Kangro and H. W. Wieking, Z. Physik. Chem. **A183**, 199 (1938).

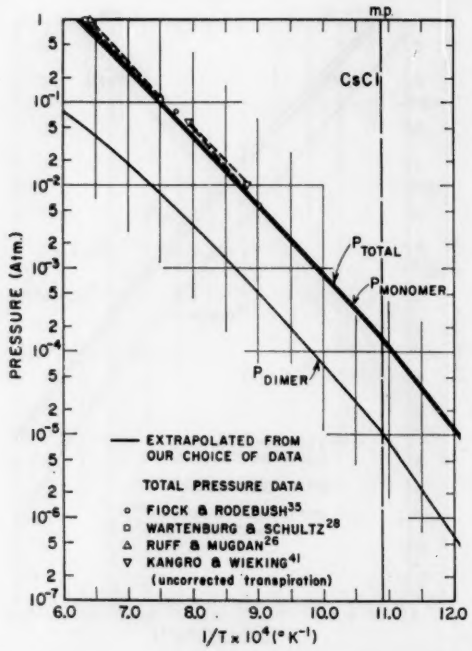

FIG. 6. The temperature variation of the partial pressures of the important species in equilibrium with CsCl.

basis of an estimated $a_2=0.35$ (see the following), then the extrapolated boiling point falls considerably above the values determined from total pressure measurements over the liquid. An increase in the mass spectrometric heats of 2–3 kcal/mole would be required to give agreement with liquid total pressures. If a lower value of the pressures over the solid were used, then still larger heats of sublimation would be required.

Although the gross second-law heats would be slightly greater than the true monomer heats it appears that the heats measured in this work are 3 to 5 kcal too low, even though there was nothing in the experimental work to cause undue suspicion with this salt. Pending further experimental vapor pressure studies and the availability of entropy data for the solid, we will deduce the heat of dimerization assuming a monomer heat of sublimation at 815°K of 45.8 kcal/mole, based on the average second-law heat from previous studies of apparent monomer pressures over the solid. On the assumption that the difference between the heat of sublimation of monomer and dimer measured in our work is reliable, this choice yields a heat of sublimation of dimer of 52.7 kcal/mole and ΔH(dimerization) = −38.9 kcal/mole. In Fig. 6 we plotted the extrapolated pressures based on the above heats and the intermediate solid data of Treadwell and Werner. The boiling point so obtained is in substantial agreement with the total pressure measurements over the liquid.

DISCUSSION

In Table IV are collected the values of the heat of dimerization determined in this work and by others. The first row contains the results obtained from our mass spectrometrically determined heats of sublimation as described previously. The second row gives the result of Akishin *et al*.[6] in which they combined a mass spectrometrically determined heat of sublimation of dimer (from Na_2Cl^+) of 55.3 kcal/mole with a value for the monomer of 51.3 kcal/mole, determined from the temperature dependence of $NaCl^+$ with corrections for the contribution to $NaCl^+$ from dissociative ionization of the dimer. In the third row is the result of another mass spectrometric study of NaCl by Akishin *et al*.,[7] which involved the use of a two-chamber effusion cell in which the gaseous equilibrium could be shifted by maintaining the two chambers at different temperatures. In addition to the heat of dimerization, they determined the relative proportions of monomer, dimer, and trimer. At 1002°K they report the proportions of monomer, dimer, and trimer as 1.00/0.34/0.01, compared to our extrapolated values of 1.00/0.50 from Fig. 3.

The fourth row gives the values obtained by Bauer, Diner, and Porter[5] from the experimental ΔF° values of Miller and Kusch[4] and calculated entropies of dimerization. The value in parentheses for CsCl was calculated by us using an entropy consistent with the assumptions of Bauer, Diner, and Porter and estimating the value of a_2 for CsCl by a comparison of Miller and Kusch's a_2 for RbCl with the ratios of $(M^+ + MCl^+)$ to M_2Cl^+ for both RbCl and CsCl determined by Berkowitz and Chupka.[8] The spread in values arises from the disagreement by a factor of four among the determinations of the pressure over the solid.

The fifth row contains the directly determined values of Miller and Kusch[4] and Eisentadt, Rao and Rothburg[42] from temperature dependence studies of the dimerization equilibrium. In the sixth row are values calculated according to a very simple ionic model proposed by Pauling.[21] The seventh row lists the values calculated by Berkowitz[43] using an ionic model, including specific polarization terms, similar to the one used by O'Konski and Higuchi[44] for NaCl (eighth row). Approximate zero point energy and heat capacity corrections have been added to all these calculated values. The ninth and tenth rows contain the values deduced from temperature dependence studies of the dimerization equilibria as determined from molecular weight measurements of Barton and Bloom[1] and Beusman,[2] respectively.

From Table IV it is seen that the trends from LiCl to

[42] M. Eisenstadt, V. S. Rao, and G. M. Rothburg, J. Chem. Phys. **30**, 604 (1959).
[43] J. Berkowitz, J. Chem. Phys. **29**, 1386 (1958).
[44] C. T. O'Konski and W. I. Higuchi, J. Chem. Phys. **23**, 1175 (1955).

TABLE IV. A comparison of different values for the dimerization heats of the alkali chlorides.

	$-\Delta H(2MX=M_2X_2)$ kcal/mole				
	LiCl	NaCl	KCl	RbCl	CsCl
	800°K	930°K	900°K	880°K	815°K
(1) This work	50.1	44.7	41.5	37.1	38.9
(2) Gorokhov, Khodev, and Akishin		47.2			
(3) Akishin, Gorokhov, and Sidorov		47.5			
(4) Bauer, Diner, and Porter	52.7	48.0	43.6	41.5	(37.0–39.0)[b]
(5) Miller and Kusch	52.9	46.4	47.6	49.7	...
(5a) Eisenstadt, Rao, and Rothburg		49.7			
(6) Milne and Cubicciotti	53.1	51.2	45.6	43.5	40.5
(7) Berkowitz	34.4	35.6	33.7	32.7	34.1
(8) O'Konski and Higuchi		41.1			
(9) Barton and Bloom		51.8	41.7		
(10) Beusman			43.9		
(11) Mixed experiments, this work		44.7[a]	38.9	37.2	33.5

[a] Chosen to agree with our mass spectrometric value.
[b] Calculated from estimated σ_i.

CsCl shown by our results are in qualitative agreement with the calculated results of Bauer, Diner, and Porter, as well as of Milne and Cubicciotti,[46] although they are several kcal lower than these values. Also these trends would seem to favor a lower value for CsCl than that shown in row 1. It appears from this comparison and also from a comparison of the binding energy of monomers, that the simple Pauling model predicts binding energies that are substantially too large. The results of the calculations by Berkowitz seem to be too low with too little variation from LiCl to CsCl although this model with the proper choice of parameters would be expected to give a much better result than the Pauling model.

In the last row of Table IV we have listed the results derived from the crude-mixture experiments reported in Table II. We have computed the differences in heats of dimerization by using the differences in entropy of dimerization calculated by Milne and Cubicciotti[45] plus the free energy differences from Table II. Taking the value for NaCl to be 44.7 kcal/mole gives the results shown. Here again the trend is to decreasing ΔH_{dim} from NaCl through CsCl although these results are to be considered only as providing qualitative checks on the values chosen in row 1.

Referring to the last column of Table III, it is seen that the equilibrium constant for the reaction $M_2Cl_2+N_2Cl_2\rightarrow 2MNCl_2$ is not far from 4 in each case, the value to be expected if $\Delta H=0$ for the reaction.

For LiCl, the only salt for which the temperature dependence of the trimer could be measured, a value of ΔH for the reaction $M_3X_3(g)\rightarrow M_2X_2(g)+MX(g)$ of 43.2 kcal/mole at 800°K was obtained. Miller and Kusch[4] report $\Delta H_{870}=35.8$ kcal/mole from their velocity analysis studies while Milne and Cubicciotti[46] calculated a value at 0°K of 55 kcal/mole with no correction for zero point energies. Once again the calculations based on the simple Pauling model, with no specific polarization terms included, appears to give results that are considerably too high.

ACKNOWLEDGMENTS

The authors are indebted to Dr. D. Cubicciotti for many helpful discussions during the course of this work and to Professor Leo Brewer for communicating to us some thermodynamic data for the alkali chlorides.

[46] T. A. Milne and D. Cubicciotti, J. Chem. Phys. **29**, 846 (1958).

[46] T. A. Milne and D. Cubicciotti, J. Chem. Phys. **30**, 1625 (1959).

Potential Energy Curves for CO*

IRWIN TOBIAS, ROBERT J. FALLON, AND JOSEPH T. VANDERSLICE

Institute for Molecular Physics, University of Maryland, College Park, Maryland

(Received June 13, 1960)

Potential energy curves for the $X\,^1\Sigma^+$, $a\,^3\Pi_r$, $a'\,^3\Sigma^+$, $d\,^3\Delta$, $e\,^3\Sigma^-$, $A\,^1\Pi$, and $B\,^1\Sigma^+$ electronic states of the CO molecule have been calculated by the Rydberg-Klein-Rees method. The curve for the $A\,^1\Pi$ state will have to bend sharply in the range between 1.9 and 2.1 A or it will have to pass through a maximum to reach the proper dissociation limit.

INTRODUCTION

THE development and application of various methods for obtaining accurate representations of the potential energy of a diatomic molecule as a function of the internuclear distance has long been an important field of activity.[1] Such curves are significant in their own right as fundamental molecular properties with which results of quantum-mechanical calculations can be compared. Also, any quantitative description of the many phenomena arising from atomic or molecular collisions will ultimately require a detailed knowledge of the interaction energies between the species involved.

Recently, the Rydberg-Klein-Rees (RKR) method[2] has been used to obtain reliable potential curves for the electronic states of a number of different diatomic molecules.[3] The curves so obtained for NO[3b] and O_2[3e] have been useful in formulating possible explanations for the quenching of $Hg(^3P_1)$ by NO[4] and O_2[5] and for the appearance of the Schumann-Runge bands in flames containing O_2.[6]

Since reliable curves are sometimes quite helpful in any discussion of the mechanisms of chemical reactions, it was felt that a systematic study of the potential curves for various diatomic molecules would be worthwhile. For the moment, we are restricting ourselves to those diatomic species which appear to be present in flames in the hope that a knowledge of the accurate potential curves may lead to a better understanding of the chemistry involved. The present paper deals with CO. The RKR method has been used to obtain potential curves for the $X\,^1\Sigma^+$, $a\,^3\Pi_r$, $a'\,^3\Sigma^+$, $d\,^3\Delta$, $e\,^3\Sigma^-$, $A\,^1\Pi$, and $B\,^1\Sigma^+$ electronic states.[7]

TABLE I. Potential energy of the $X\,^1\Sigma^+$ state of CO.[a]

v	V (cm^{-1})	r_{max} (A)	r_{min} (A)	V (ev)
0	1082	1.179	1.084	0.1341
1	3225	1.220	1.054	0.3998
2	5342	1.250	1.035	0.6623
3	7432	1.276	1.020	0.9214
4	9496	1.300	1.007	1.1773
5	11533	1.322	0.997	1.4298
6	13544	1.343	0.987	1.6792
7	15530	1.363	0.979	1.9254
8	17488	1.382	0.971	2.1681
9	19425	1.401	0.964	2.4083
10	21332	1.420	0.958	2.6447
11	23215	1.438	0.952	2.8782
12	25073	1.456	0.946	3.1085
13	26904	1.474	0.941	3.3355
14	28708	1.491	0.936	3.5591
15	30487	1.509	0.932	3.7797
16	32240	1.526	0.927	3.9970
17	33967	1.544	0.923	4.2111
18	35665	1.561	0.919	4.4216
19	37342	1.579	0.915	4.6295
20	38996	1.596	0.911	4.8346
21	40623	1.614	0.908	5.0363
22	42207	1.631	0.905	5.2327
23	43778	1.649	0.901	5.4275

[a] Experimental data from footnote references 9 and 11–13.

METHOD AND RESULTS

The RKR method is a WKB procedure for obtaining the classical turning points of the motion directly from the measured vibrational and rotational energy levels of the molecule.[2] The curves so obtained are thus based directly on the experimental data and therefore should be quite reliable. The method has been amply described in recent articles so the procedure will not be repeated here.[3,8] The method is rapid and appears to be accurate. Data were obtained from Herzberg and Rao,[9] Schmid and Gerö,[10,11] Rao,[12] Pearse and

* This research was supported in part by the National Aeronautics and Space Administration.

[1] G. Herzberg, *Spectra of Diatomic Molecules* (D. Van Nostrand Company, Inc., Princeton, New Jersey, 1950), pp. 101–103.

[2] (a) R. Rydberg, Z. Physik **73,** 376 (1931); (b) O. Klein, *ibid.* **76,** 226 (1932); (c) A. L. G. Rees, Proc. Phys. Soc. (London) **A59,** 998 (1947); (d) J. T. Vanderslice, E. A. Mason, W. G. Maisch, and E. R. Lippincott, J. Mol. Spectroscopy **3,** 17 (1959).

[3] (a) J. T. Vanderslice, E. A. Mason, and E. R. Lippincott, J. Chem. Phys. **30,** 129 (1959); (b) J. T. Vanderslice, E. A. Mason, and W. G. Maisch, *ibid.* **31,** 738 (1959); (c) J. T. Vanderslice, E. A. Mason, and W. G. Maisch, *ibid.* **32,** 515 (1960); (d) R. J. Fallon, J. T. Vanderslice, and E. A. Mason, *ibid.* **32,** 698 (1960); (e) R. D. Verma, *ibid.* **32,** 738 (1960).

[4] R. J. Fallon, J. T. Vanderslice, and E. A. Mason, J. Phys. Chem. **63,** 2082 (1959).

[5] R. J. Fallon, J. T. Vanderslice, and E. A. Mason, J. Phys. Chem. **64,** 505 (1960).

[6] R. J. Fallon, I. Tobias, J. T. Vanderslice, and W. G. Maisch, Can. J. Chem. **38,** 743 (1960).

[7] R. S. Mulliken [Can. J. Chem. **36,** 10 (1958)] has pointed out that the state previously labeled $^3\Pi_i$ is more than likely a $^3\Delta$.

[8] F. Gilmore (Rand Corporation, Santa Monica, California) has corrected the basic working equations given in these earlier papers. The numerical results are not significantly affected. See errata published in J. Mol. Spectroscopy **5,** 83 (1960) and J. Chem. Phys. **33,** 614 (1960).

[9] G. Herzberg and K. N. Rao, J. Chem. Phys. **17,** 1099 (1949).

[10] R. Schmid and L. Gerö, Z. Physik **93,** 656 (1935).

[11] R. Schmid and L. Gerö, Z. Physik **101,** 343 (1936).

[12] K. N. Rao, Astrophys. J. **110,** 304 (1949).

TABLE II. Potential energy of the $a\,^3\Pi_r$ state of CO.[a]

v	V (cm^{-1})	r_{max} (A)	r_{min} (A)	V (ev)	$V+T_e$[b] (ev)
0	866	1.263	1.156	0.1074	6.1431
1	2581	1.310	1.124	0.3200	6.3557
2	4260	1.344	1.103	0.5281	6.5638
3	5925	1.375	1.087	0.7346	6.7703
4	7550	1.403	1.074	0.9360	6.9717
5	9150	1.429	1.063	1.1344	7.1701

[a] Experimental data from footnote references 15, 17, and 18.
[b] T_e is the difference in energy between the bottom of the state in question and the bottom of the $X\,^1\Sigma^+$ state.

TABLE III. Potential energy of the $a'\,^3\Sigma^+$ state of CO.[a]

v	V (cm^{-1})	r_{max} (A)	r_{min} (A)	V (ev)	$V+T_e$ (ev)
0	613	1.423	1.296	0.0759	6.9967
1	1821	1.479	1.257	0.2258	7.1466
2	3009	1.521	1.232	0.3730	7.2938
3	4175	1.558	1.214	0.5176	7.4384
4	5321	1.591	1.198	0.6597	7.5805
5	6447	1.622	1.185	0.7992	7.7200
6	7552	1.652	1.174	0.9363	7.8571
7	8638	1.681	1.164	1.0709	7.9917
8	9704	1.710	1.154	1.2031	8.1239
9	10751	1.737	1.146	1.3329	8.2537
10	11779	1.765	1.139	1.4603	8.3811
11	12788	1.792	1.132	1.5854	8.5062
12	13778	1.819	1.125	1.7082	8.6290
13	14750	1.846	1.119	1.8287	8.7494
14	15703	1.872	1.113	1.9468	8.8676
15	16638	1.899	1.108	2.0627	8.9835
16	17554	1.926	1.103	2.1762	9.0970
17	18451	1.953	1.099	2.2853	9.2083
18	19330	1.981	1.094	2.3965	9.3173
19	20191	2.008	1.090	2.5032	9.4240
20	21033	2.036	1.086	2.6076	9.5283
21	21856	2.064	1.082	2.7096	9.6304
22	22660	2.093	1.078	2.8093	9.7301
23	23445	2.122	1.075	2.9067	9.8274

[a] Experimental data from footnote reference 14.

TABLE IV. Potential energy of the $d\,^3\Delta$ state of CO.[a]

v	V (cm^{-1})	r_{max} (A)	r_{min} (A)	V (ev)	$V+T_e$ (ev)
0	567	1.448	1.316	0.0703	7.7989
1	1684	1.506	1.277	0.2088	7.9374
2	2792	1.550	1.252	0.3461	8.0747
3	3881	1.589	1.233	0.4812	8.2098
4	4949	1.624	1.217	0.6136	8.3422
5	5998	1.657	1.204	0.7436	8.4722
6	7027	1.688	1.193	0.8712	8.5998
7	8040	1.719	1.183	0.9968	8.7254
8	9035	1.749	1.174	1.1201	8.8487
9	10011	1.778	1.165	1.2411	8.9697
10	10969	1.807	1.158	1.3599	9.0885
11	11899	1.837	1.151	1.4752	9.2038
12	12799	1.868	1.143	1.5868	9.3154
13	13643	1.898	1.137	1.6914	9.4200
14	14506	1.928	1.130	1.7984	9.5270
15	15336	1.959	1.124	1.9013	9.6299
16	16130	1.991	1.119	1.9998	9.7284
17	16911	2.022	1.113	2.0966	9.8252
18	17662	2.054	1.107	2.1897	9.9183
19	18388	2.087	1.102	2.2797	10.0083
20	19094	2.122	1.097	2.3672	10.0958

[a] Experimental data from footnote references 15 and 16.

TABLE V. Potential energy of the $A\,^1\Pi$ state of CO.[a]

v	V (cm^{-1})	r_{max} (A)	r_{min} (A)	V (ev)	$V+T_e$ (ev)
0	753	1.296	1.182	0.0934	8.1627
1	2229	1.348	1.148	0.2763	8.3456
2	3677	1.387	1.126	0.4559	8.5252
3	5084	1.422	1.110	0.6303	8.6996
4	6462	1.454	1.096	0.8011	8.8704
5	7803	1.484	1.085	0.9674	9.0367
6	9110	1.513	1.075	1.1294	9.1987
7	10394	1.542	1.066	1.2886	9.3579
8	11632	1.571	1.058	1.4421	9.5114
9	12835	1.599	1.050	1.5912	9.6605
10	13998	1.628	1.044	1.7354	9.8047
11	15134	1.656	1.038	1.8763	9.9456
12	16239	1.685	1.032	2.0133	10.0826
13	17309	1.714	1.026	2.1459	10.2152
14	18347	1.744	1.021	2.2746	10.3439
15	19342	1.774	1.017	2.3980	10.4673
16	20305	1.805	1.012	2.5174	10.5867
17	21232	1.836	1.007	2.6323	10.7016
18	22113	1.867	1.003	2.7420	10.8113

[a] Experimental data from footnote references 11 and 15.

Gaydon,[13] Herzberg and Hugo,[14] Tanaka, Jursa, and Le Blanc,[15] Gerö,[16] Budò,[17] and Beer.[18] The results are shown in Tables I–VII and the curves are shown in Fig. 1.

In an earlier paper,[2d] it was mentioned that, since the RKR method was a WKB procedure, it would be wise to have some check on the magnitude of the higher order terms arising from the WKB method. The only real check was to compare the RKR results with those obtained by the Dunham method,[19] since this procedure

TABLE VI. Potential energy of the $e\,^3\Sigma^-$ state of CO.[a]

v	V (cm^{-1})	r_{max} (A)	r_{min} (A)	V (ev)	$V+T_e$ (ev)
0	545	1.467	1.332	0.0675	8.1659
1	1619	1.527	1.292	0.2008	8.2992
2	2675	1.572	1.266	0.3317	8.4301
3	3712	1.611	1.246	0.4602	8.5586
4	4730	1.647	1.230	0.5864	8.6847
5	5728	1.681	1.217	0.7102	8.8086
6	6708	1.713	1.205	0.8316	8.9300
7	7669	1.745	1.194	0.9507	9.0491
8	8611	1.776	1.185	1.0675	9.1659
9	9534	1.806	1.176	1.1819	9.2803
10	10438	1.836	1.169	1.2940	9.3924
11	11323	1.866	1.161	1.4038	9.5022
12	12190	1.895	1.154	1.5113	9.6096
13	13038	1.924	1.147	1.6164	9.7148
14	13867	1.953	1.140	1.7192	9.8176
15	14678	1.982	1.134	1.8197	9.9181
16	15470	2.012	1.128	1.9179	10.0163
17	16243	2.042	1.124	2.0138	10.1122

[a] Experimental data from footnote reference 14.

[13] R. W. B. Pearse and A. J. Gaydon, *Identification of Molecular Spectra* (Chapman and Hall, Ltd., London, 1950).
[14] G. Herzberg and T. J. Hugo, Can. J. Phys. **33**, 757 (1955).
[15] Y. Tanaka, A. S. Jursa, and F. Le Blanc, J. Chem. Phys. **26**, 862 (1957).
[16] L. Gerö, Ann. Physik **35**, 597 (1939).
[17] A. Budò, Z. Physik **98**, 437 (1936).
[18] B. S. Beer, Z. Physik **107**, 73 (1937).
[19] J. L. Dunham, Phys. Rev. **41**, 713, 721 (1932).

TABLE VII. Potential energy of the $B\,^1\Sigma^+$ state of CO.[a]

v	V (cm^{-1})	r_{max} (A)	r_{min} (A)	V (ev)	$V+T_e$ (ev)
0	1065	1.172	1.075	0.1320	10.9110
1	3139	1.215	1.046	0.3892	11.1681
2	5139	1.249	1.027	0.6371	11.4161

[a] Experimental data from footnote references 10 and 15.

is known to be accurate near the minimum. Good agreement was obtained. Recently, Jarmain[20,21] has been able to show that the two procedures are equivalent to a first approximation over part of the range of energy. He has expressed the classical turning points of the motion as given by the Rydberg-Klein-Rees procedure in terms of a series expansion involving the vibrational quantum number v. He was able to show that this expansion is the same one that is obtained by inversion of Dunham's series. He then suggests that this series expansion be used to obtain reliable potential curves rapidly. Jarmain has published results on the $X\,^1\Sigma g^+$ state of N_2 and on the $X\,^2\Pi_i$ state of OH for levels whose energy is roughly half the dissociation energy. His results agree well with our previously published results[2a] for N_2 and with our unpublished results on OH.[22]

We have not used this method but have preferred to use the original formulation of Rees,[2e,2d,8] which is itself rapid. Our reason for doing so is that Jarmain's representation cannot be used outside the range of energy levels from which the spectroscopic constants were derived.[20,21] Also, as v gets larger, the results depend more strongly on $\omega_e z_e$, one of the least reliably known spectroscopic constants, and hence one might expect his procedure to yield results which are not too reliable at the higher v values. Finally, for cases where $\omega_e z_e$ is large, convergence cannot be depended upon.[20,21]

DISCUSSION

Potential energy curves for the $X\,^1\Sigma^+$, $a\,^3\Pi_r$, $a'\,^3\Sigma^+$, $d\,^3\Delta$, $e\,^3\Sigma^-$, $A\,^1\Pi$, and $B\,^1\Sigma^+$ states of CO have been calculated by the RKR method. Of the curves obtained, only that of the $A\,^1\Pi$ state deserves special mention at the moment. Available evidence[15] indicates

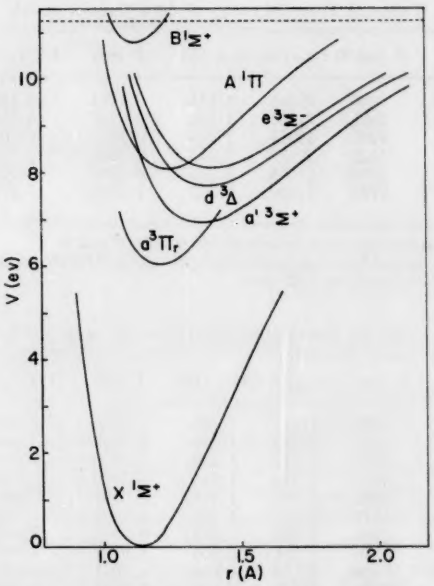

FIG. 1. Potential curves for the different electronic states of CO.

that a molecule in this state dissociates to $C(^3P)$ and $O(^3P)$ corresponding to a dissociation energy D_0 of 11.11 ev. As Fig. 1 shows, the $A\,^1\Pi$ curve is approaching this limit (dotted line) much more rapidly than those of the three other states, $e\,^3\Sigma^-$, $d\,^3\Delta$, and $a'\,^3\Sigma^+$, which are dissociating to the same limit. This indicates that the curve will either bend over sharply in the region between 1.9 and 2.1 A or it will show a slight maximum. Mulliken[23] has pointed out that this latter behavior should be more prevalent than is commonly thought. Further experimental and theoretical evidence on this point would be valuable.

Finally, relatively little theoretical work has been done on CO[24–26] and it will be of interest to see how the extensive calculations now in progress on CO[27,28] will check with the results reported here.

[20] W. R. Jarmain, J. Chem. Phys. **31,** 1137 (1959).
[21] W. R. Jarmain, Can. J. Phys. **38,** 217 (1960).
[22] R. J. Fallon, I. Tobias, and J. T. Vanderslice (to be published).
[23] R. S. Mulliken, J. Phys. Chem. **41,** 5 (1937).
[24] W. Moffitt, Proc. Roy. Soc. (London) **A196,** 510, 524 (1949).
[25] R. C. Sahni, Trans. Faraday Soc. **49,** 1246 (1953).
[26] H. Brion and C. Moser, J. Chem. Phys. **32,** 1194 (1960).
[27] P. Merryman, C. M. Moser, and R. K. Nesbet, J. Chem. Phys. **32,** 631 (1960).
[28] R. K. Nesbet (private communication).

THE JOURNAL OF CHEMICAL PHYSICS VOLUME 33, NUMBER 6 DECEMBER, 1960

Halogen Bond Character in the Alkyl Halides*

B. P. DAILEY

Department of Chemistry, Columbia University, New York, New York

(Received May 16, 1960)

The quantity $(I+s^2)$, the sum of the ionicity and s hybridization, has been calculated from nuclear quadrupole coupling data for 24 alkyl halides. The ionicity has been estimated independently from calculated values of ϵ_z, the effective charge on the halogen. The average derived values of s^2, the amount of s character in the hybrid halogen bonding orbital, are 13.6% for carbon-chlorine bonds, 8.6% for carbon-bromine bonds, and 1.8% for carbon-iodine bonds.

VALUES of the nuclear quadrupole coupling constant are now available for a fairly sizeable series of alkyl halides. Qualitative trends in these data have been discussed previously, but it is the purpose of this communication to present a new and more detailed analysis. While gas-phase measurements are available for a few of the simpler molecules, most of the results were obtained by analysis of the direct quadrupole spectra of solids. The increased ionicity exhibited by the halogen bonds in solids is a function of the detailed crystal structure but for this closely related series of compounds seems to be at least roughly constant. The average ratio of the gas-phase quadrupole coupling constant to the value in the solid state, for those molecules in this group for which both measurements are available, is 1.083. In Table I the gas-phase values of eQq taken from reference d have been obtained by multiplying the solid-state value by this number.

In previous work[1-3] the use of the equation,

$$q_{zz}=(1-s^2+d^2-I-II)q_{at},$$

for the analysis of quadrupole coupling data has been discussed. Focusing attention on the halogen bond in the alkyl derivative, A-X, the use of a wave function of the following form is implied,

$$\chi=(\chi_X+i\chi_A)/(1+i^2+2iS)^{\frac{1}{2}}$$

$$S=\int \chi_X\chi_A d\tau.$$

I is the ionicity of the halogen bonding orbital where

$$I=(1-i^2)/(1+i^2).$$

The halogen bonding orbital is assumed to have the form

$$\chi_X=(1-s^2-d^2)^{\frac{1}{2}}\chi_{p_zX}+s\chi_{sX}+d\chi_{d_{z^2}X},$$

where s^2 and d^2 are the amounts of s and d hybridization. II is a factor, related to the amount of double-bond character, defined by

$II=$[electron density in p_x (or p_y) state of the free X atom—electron density of p_x (or p_y) state of the bound X atom].

Since in several of the molecules for which gas-phase data are available it has been shown that II is negligible, it is assumed in the following discussion that this is true for all of the alkyl derivatives included in this study. The quadrupole coupling data can be used only to evaluate s^2-d^2 and not the two quantities separately. However, it is reasonable to assume that d^2 is considerably smaller than s^2. Using appropriate values of q atomic, the quantity $I+s^2-d^2$ was calculated for each halogen bonding orbital and entered in Table I.

The molecular dipole moment data has been discussed by Eyring *et al.*[4,5] using a semiempirical approach. Their calculated effective charges, based on a set of bond polarizabilities, on the dipole moments of the methyl halides, plus a few other arbitrary parameters, reproduce the dipole moments of the whole series of alkyl halides in a very satisfactory fashion. Using their parameters, the effective charge on the halogen atom was calculated for each alkyl halide and is given in Table I. This negative charge is balanced by positive effective charges distributed over the carbon and hydrogen atoms in the alkyl radical. The ionicity of the halogen bonding orbital, I, was obtained by dividing ϵ_z by the value of the electronic charge. The quantity s^2-d^2 was obtained as the difference of $I+s^2-d^2$ and I.

In an earlier paper[2] the following rule had been proposed for predicting the amount of hybridization in a halogen bonding orbital. If the halogen atom is bonded to an atom (or radical) having an electronegativity smaller than its own by 0.25 unit, then there will be

* Supported by grants from the National Science Foundation, the Alfred P. Sloan Foundation, and by the Office of Scientific Research, Air Research and Development Command, U. S. Air Force.

[1] C. H. Townes and B. P. Dailey, J. Chem. Phys. **17**, 782–796 (1949).

[2] B. P. Dailey and C. H. Townes, J. Chem. Phys. **23**, 118–123 (1955).

[3] T. P. Das and E. L. Hahn, *Nuclear Quadrupole Resonance Spectroscopy* (Academic Press, Inc., New York, 1958).

[4] R. P. Smith, T. Ree, J. L. Magee, and H. Eyring, J. Am. Chem. Soc. **73**, 2263 (1951).

[5] R. P. Smith and E. M. Mortensen, J. Am. Chem. Soc. **78**, 3932 (1956).

TABLE I. Calculated s character in halogen bonding orbitals.

	eQq solid	Ref.	eQq gas	$I+s^2-d^2$ %	ϵ_z	I %	s^2-d^2%	r (gas/solid)
CH_3Cl	−68.06	a	−74.74[d]	31.9	−0.99	20.8	+11.1	1.098
CH_2Cl_2	−72.47	a	−78.4[d]	28.5	−0.70	14.6	+13.9	1.082
$CHCl_3$	−76.54	a	−82.9	24.4	−0.52	10.8	+13.6	
CCl_4	−81.18	a	−87.9	19.9	−0.39	8.1	+11.8	
C_2H_5Cl	−65.95	a	−70.07[d]	36.1	−1.03	21.4	+14.7	1.062
$(CH_3)_2CHCl$	−63.88	a	−69.2	36.9	−1.06	22.0	+14.9	
C_3H_7Cl	−65.94	a	−71.4	34.9	−1.03	21.4	+13.5	
$(CH_3)_3CCl$	−62.14	b	−67.3	38.7	−1.10	22.0	+15.8	
CH_2ClCH_2Cl	−68.72	a	−74.4	32.2	−0.95	19.8	+12.4	
$(CH_3)_2CCl_2$	−69.76	a	−75.6	31.1	−0.80	16.7	+14.4	
CH_3CCl_3	−75.88	a	−82.2	25.1	−0.57	11.9	+13.2	
							av +13.6	
CH_3Br^{81}	441.96	a	482.4[d]	25.0	−0.87	18.1	+6.9	1.092
CH_2Br_2	470.40	a	509.4	20.8	−0.59	12.3	+8.5	
$CHBr_3$	502.11	c	543.8	15.4	−0.42	8.8	+6.6	
C_2H_5Br	415.58	a	450.9[d]	29.9	−0.92	19.2	+10.7	1.085
C_3H_7Br	420.56	a	455.5	29.2	−0.92	19.2	+10.0	
CH_2BrCH_2Br	435.80	a	472.0	26.6	−0.84	17.5	+9.1	
							av +8.6	
CH_3I^{127}	1767.3	c	1931.5[d]	15.8	−0.74	15.4	+0.4	1.093
CH_2I_2	1912.6	c	2073.3	9.6	−0.47	9.8	−0.2	
$CHI_3 \cdot 3S_8$	2048	a	2220	3.2	−0.32	6.7	−3.5	
CI_4	2160	a	2341	0.0	−0.24	5.0	−5.0	
C_2H_5I	1649.2	c	1771[d]	22.8	−0.76	15.8	+7.0	1.074
$(CH_3)_2CHI$	1573	c	1705	25.6	−0.83	17.3	+8.3	
C_3H_7I	1673.1	c	1813.6	21.9	−0.79	16.5	+5.4	
							av +1.8	

[a] H. O. Hooper and P. J. Bray (to be published).
[b] R. Livingston, J. Chem. Phys. **20**, 1170 (1952).
[c] H. Zeldes and R. Livingston, J. Chem. Phys. **21**, 1418 (1953).
[d] C. H. Townes and A. L. Schawlow, *Microwave Spectroscopy* (McGraw-Hill Book Company, Inc., New York, 1955).

15% s hybridization at the halogen atom. Otherwise the s hybridization is zero. The d hybridization is assumed to be less than 5%. Gordy,[6] on the other hand, had described the halogen bonding orbital as containing only p character.

The following qualitative considerations led to the above rule. Bond angle and quadrupole coupling data for many compounds of oxygen, sulfur, nitrogen, and arsenic, indicate about 20% s character in their bonding orbitals. The s character for a halogen bonding orbital should be smaller than this figure, but greater than zero. Consideration of promotional energy would indicate that bonds with considerable ionicity would have larger amounts of s character and that d character would be minimized. The halogen electronegativities are such that one would expect on the basis of the above rule a maximum of 15% for s^2-d^2 in chlorine and bromine bonding orbitals and values near zero for iodine bonding orbitals in the alkyl halides. The last column in Table I indicates that these predictions are surprisingly well borne out by the results of these calculations. On the average, s^2-d^2 is less for bromine

[6] W. Gordy, *Microwave Spectroscopy* (John Wiley & Sons, Inc., New York, 1953).

orbitals than for chlorine and least for the case of iodine.

Several of the values of s^2-d^2 for iodine compounds are negative. Taken at face value this would indicate more d than s hybridization. This may, however, simply represent the relatively large error in this method of determining the degree of hybridization

It is interesting to note that the pattern of electronic charge distribution indicated by the dipole moments is remarkably consistent with that indicated by the halogen quadrupole coupling data. This is especially noteworthy since the dipole moments depend on the entire charge distribution throughout the molecule, while the quadrupole coupling data depend primarily on the charge distribution in the immediate neighborhood of the halogen nuclei.

THE JOURNAL OF CHEMICAL PHYSICS VOLUME 33, NUMBER 6 DECEMBER, 1960

Trimethylene Oxide. I. Microwave Spectrum, Dipole Moment, and Double Minimum Vibration*

SUNNEY I. CHAN,† JOHN ZINN,‡ JOSE FERNANDEZ,§ AND WILLIAM D. GWINN

Department of Chemistry, University of California, Berkeley, California

(Received June 27, 1960)

The microwave spectra of four isotopic species of trimethylene oxide have been investigated. Analysis of the spectra indicates that the four-membered ring is essentially planar. From the intensity measurements of the rotational transitions and their vibrational satellites, it was concluded that the energy levels in the ring-puckering vibration are single levels. The Stark effect also provided independent evidence that the ring is not highly puckered. The dipole moment of the molecule was found to lie solely on the C—O molecular axis. A value of 1.93±0.01 Debye was obtained. The existence of a small barrier in the potential function, however, was established by a detailed analysis of the observed vibration-rotation interaction. Quantitative considerations have led to an accurate determination of the barrier height and the general shape of the potential function. The barrier restricting the ring-puckering motion has been found to be 35±5 cm^{-1}. The ground vibrational level is 8±4 cm^{-1} above the top of the barrier.

INTRODUCTION

OUR interest in trimethylene oxide,

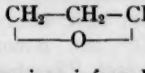

stems from the previous infrared and Raman spectroscopic studies on cyclobutane.[1] These studies indicated that cyclobutane in the lower vibrational levels has a puckered ring.

In four-membered rings, the classical ring strain would tend to make the ring planar while the preferred staggered positions of the hydrogens on adjacent methylene groups would tend to pucker the ring.[2,3] The actual planarity of these rings will therefore be dependent upon the relative magnitudes of these opposing forces. This question of ring planarity for any particular case is probably best resolved by an investigation into the nature of the potential function which governs the ring-puckering vibration.

Various facets of the microwave spectrum may lead to important information on the nature of this potential function. For example, the detailed structure of the molecule, the component of the dipole moment perpendicular to the average plane of the ring, the determination of the statistical weights involved by measuring the relative intensities of certain microwave transitions; all these have been shown to lead to some fairly definite conclusions as to the planarity of four- and five-membered rings.[4–6] In four-membered rings the frequency of the ring-bending vibration is sufficiently low so that many excited vibrational levels in this mode are appreciably populated at room temperatures. Here more definite information may be obtained from a study of the variation of the effective moments of inertia with the vibrational levels of the ring-puckering mode.[7] This is, in essence, a determination of the mean

* This research was supported by grants from the Alfred P. Sloan Foundation and the California Research Corporation.

† Kaiser Aluminum and Chemical Corporation Fellow, 1958–59; National Science Foundation Cooperative Fellow, 1959–60.

‡ Present Address: Los Alamos Scientific Laboratory, Los Alamos, New Mexico.

§ Present Address: Universidad de Oriente, Santiago de Cuba, Cuba.

[1] G. W. Rathjens, N. K. Freeman, W. D. Gwinn, and K. S. Pitzer, J. Am. Chem. Soc. **75**, 5634 (1953).

[2] J. Fernandez, R. J. Myers, and W. D. Gwinn, J. Chem. Phys. **23**, 758 (1955).

[3] W. D. Gwinn, Discussions Faraday Soc. **19**, 43 (1955).

[4] W. S. Wilcox and J. H. Goldstein, J. Chem. Phys. **20**, 1656 (1952).

[5] W. S. Wilcox, K. C. Brannock, W. De More, and J. H. Goldstein, J. Chem. Phys. **21**, 563 (1953).

[6] N. Kwak, J. H. Goldstein, and J. W. Simmons, J. Chem. Phys. **25**, 1203 (1956).

[7] W. D. Gwinn, J. Zinn, and J. Fernandez, Bull. Am. Phys. Soc. **4**, 153 (1959).

distances from the planar configuration for various vibrational states.

This paper represents the application of all of these methods to the determination of the nature of the potential function for the ring-puckering mode of trimethylene oxide. Additional and important information has been afforded by the recently published far infrared spectrum of the molecule.[8,9]

EXPERIMENTAL

Trimethylene oxide was prepared by dropping γ-chloropropyl acetate onto a molten mixture of NaOH and KOH, as originally described by Derick and Bissell[10] and later modified by Searles.[11] The gases evolved were condensed in a cold trap and purified according to Noller's procedure,[12] which is to treat the crude product with bromine to eliminate unsaturated compounds, dry with anhydrous sodium sulfate, and distill. The boiling point, 48.5°C, the refractive index, $n_D^{25}=1.3898$, and its infrared spectrum, were in good agreement with those reported in the literature.

β-monodeuterated trimethylene oxide was prepared in the following manner. Methyl monodeutero-β-chloropropionate was obtained by the addition of DCl to methyl acrylate. The deuterium atom was found to be exclusively located at the α position of β-chloropropionic acid. Reduction of this methyl α-monodeutero-β-chloropropionate with $LiAlH_4$ yielded the monodeuterated chlorohydrin, which was then acetylated with acetyl chloride. The γ-chloropropyl acetate so obtained was cyclized with alkali and purified as in the case of the normal species, yielding approximately 50% monodeuterated product.

To prepare 1,1,3,3-tetradeutero trimethylene oxide, diethyl malonate was reduced with $LiAlD_4$ to the symmetric tetradeutero trimethylene glycol. The crude glycol was then converted to the chlorohydrin by reaction with HCl gas at 150–170°C. Cyclization of the tetradeuterated chlorohydrin with alkali gave the desired product.

The synthesis of trimethylene oxide-O^{18} started with the preparation of acetic acid-O^{18}, which was obtained by dropping acetyl chloride onto 50 mg of 82% enriched H_2O^{18}. The acetic acid-O^{18} was converted to sodium acetate-O^{18} by adding a 1.2N methanolic sodium methoxide solution until the mixture was neutral to bromothymol blue. Addition of a stoichiometric amount of γ-chloropropyl p-toluene sulfonate to the methanolic solution yielded the γ-chloropropyl acetate-O^{18} after 18 hours of reflux at 80–100°C. This γ-chloropropyl acetate-O^{18} was then treated with alkali as before. This synthesis necessarily brought about a 50% dilution of O^{18}. The microwave spectrum indicated that the product was close to the theoretical 41% enrichment.

With the exception of the normal compound, all the isotopic species were further purified with vapor-phase chromatography before running their microwave spectra.

The microwave spectrometer used was a typical Stark effect type employing 5-kc Stark modulation.

SPECTRA

The microwave spectra of trimethylene oxide, trimethylene oxide-O^{18}, and β-monodeuterated trimethylene oxide were found to consist of rotational transitions arising from the component of the dipole moment along the axis of least moment of inertia (a-type selection rules). Substitution of four deuterium atoms in the alpha positions causes the dipole moment to lie along the axis of intermediate moment of inertia so that the 1,1,3,3-tetradeutero trimethylene oxide follows b-type selections rules.

The microwave spectrum of each isotopic species has been investigated from 16–42 kMc. Since the quantity $(A+C)/2$ is of the order of 8–10 kMc for each of the isotopic species, Q-branch transitions up to $J=60$ still have intensities comparable to those of low J lines. The spectrum for each species is thus reasonably dense. It is further complicated by satellite lines, the corresponding rotational transitions from low-lying excited vibrational levels. In the case of normal trimethylene oxide, it has been possible to assign rotational constants for each of five vibration states (including the lowest). In 1,1,3,3-tetradeutero trimethylene oxide, four vibrational states have been assigned, and in trimethylene oxide-O^{18} and β-monodeuterated trimethylene oxide, two each. The observed lines for the four isotopic species are tabulated in Table I. The rotational constants determined from these assigned transitions are listed in Table II.

VIBRATIONAL SATELLITES

In trimethylene oxide, the lowest vibrational frequency is most certainly to be an out-of-plane bending motion of the four-membered ring. On the basis of the previous work on cyclobutane, this frequency was expected to be about 100 cm^{-1}. The next lowest vibrational frequency is mot likely to be above 500 cm^{-1}. Since this ring-puckering frequency is so low, a large number of the excited vibrational levels would be appreciably populated at room temperature. Rotational constants are in general different in each of these vibrational states due to "vibration-rotation" interaction, and as a result, satellite lines are observed. All of the observed satellite lines appeared to lie in a series and we have, as a result, considered them as arising from excited states of the ring-puckering vibration.

[8] A. Danti, W. J. Lafferty, and R. C. Lord, J. Chem. Phys. **33**, 294 (1960).
[9] S. I. Chan, J. Zinn, and W. D. Gwinn, J. Chem. Phys. **33**, 295 (1960).
[10] C. G. Derick and D. W. Bissell, J. Am. Chem. Soc. **38**, 2478 (1916).
[11] S. Searles, J. Am. Chem. Soc. **73**, 125 (1951).
[12] C. R. Noller, Org. Synthesis **29**, 92 (1949).

TABLE I. Assigned transitions of trimethylene oxide.[a]

Transition	Ground state	1st excited	2nd excited	3rd excited	4th excited
		Normal trimethylene oxide (*a*-type)			
0_{00}–1_{01}	18 465.0	18 498			
1_{01}–2_{02}	32 223.3	32 358.6	32 405±2	32 471.3	32 521.6
1_{11}–2_{12}	31 926.0	32 043.4	32 086.0±0.2	32 138.9	32 182±2
1_{10}–2_{11}	41 932.7	41 950.5	41 945.7	41 940.5	
3_{12}–3_{21}	16 490.2	16 443.8	16 417.5		
4_{22}–4_{31}	17 268.2	17 283.2	17 281.6	17 278.1	
5_{23}–5_{32}	18 346.5	18 452.1	18 490.0		
6_{33}–6_{42}	26 081	25 928			
7_{43}–7_{52}	26 333	26 215	26 152.0		
7_{53}–7_{62}	24 592	24 240			
8_{53}–8_{72}	26 725	26 665	26 630.1	26 587.1	
8_{63}–8_{82}	23 890	23 460			
9_{63}–9_{82}	27 302.9	27 332.3	27 337.0	27 345.0	27 341.8
9_{73}–9_{92}	22 976				
10_{73}–10_{92}	28 125.0	28 279.0	28 342.4	28 421.2	28 485.0
11_{83}–$11_{10,2}$	29 252.6		29 717.5	29 893.2	30 040.8
		1,1,3,3-Tetradeutero trimethylene oxide (*b*-type)			
1_{01}–2_{12}	29 493.5	28 582.65	28 614.75	28 654.5±0.5	
1_{10}–2_{21}	39 592.57	39 592.6	38 579.7	38 565.8	
2_{12}–3_{03}	38 735.5	38 915.7±0.3			
3_{13}–3_{22}		20 610.72			
4_{04}–4_{13}	28 806.9	26 623.1		26 426±2	
4_{14}–4_{23}	27 758.8			27 327±2	
4_{22}–4_{31}	22 291.15	22 097.3			
4_{32}–4_{41}	22 740.19				
4_{31}–4_{40}	18 674.62				
5_{14}–5_{23}	24 960.27	24 812.0			
5_{24}–5_{33}	28 065.3	27 847.3	27 741.2	27 613±2	
5_{23}–5_{42}	24 889.50		24 531.6		
5_{42}–5_{51}			27 450±2	27 263±2	
6_{24}–6_{33}	22 306.55				
6_{34}–6_{43}	29 080.7	28 836.27	28 716.5±0.5	28 573±2	
6_{43}–6_{52}	28 624.7±0.5			27 993±2	
8_{35}–8_{44}	28 818.6				
8_{35}–8_{62}	24 785.55				
10_{64}–10_{73}	27 293.4	26 885±5			
12_{75}–12_{84}	28 778±2				
		Trimethylene oxide-O^{18} (*a*-type)			
1_{01}–2_{02}	31 605.4	31 730±3			
1_{11}–2_{12}	30 871.35	30 985.7			
6_{34}–6_{33}	34 624.3				
6_{33}–6_{42}	27 656.0	27 582.45			
7_{43}–7_{62}	29 751±5	29 783.0			
8_{53}–8_{64}	32 440.75	32 002.9			
8_{53}–8_{72}	32 973.15				
9_{64}–9_{63}		29 910.5			
		β-monodeutero trimethylene oxide (*a*-type)			
0_{00}–1_{01}	17 248.3	17 281.33			
1_{01}–2_{02}	31 067.9	31 187.2			
1_{11}–2_{12}	30 181.8	30 290.5			
1_{10}–2_{11}	38 811.4	38 834.73			
3_{03}–3_{22}	24 336.87				
3_{13}–3_{12}	23 488.5				
3_{12}–3_{21}	18 635.55	18 621.8			
4_{04}–4_{23}	33 646.22	33 398.61			
4_{14}–4_{13}	33 522.45	33 267.02			
4_{13}–4_{22}	24 872.5	24 730.0			
5_{14}–5_{23}	33 610.18	33 367.40			
5_{24}–5_{23}	33 123.27				
6_{24}–6_{43}	33 695.12	33 462.65			
7_{34}–7_{53}	34 082.82	33 884.65			
8_{44}–8_{63}	35 051.33	34 926.2			

[a] Frequencies are in Mc, and unless otherwise specified are good to ±0.1 Mc when quoted to that accuracy.

TABLE II. Rotational constants (Mc).

Rotational constant	Ground state	1st excited	2nd excited	3rd excited	4th excited
			Normal trimethylene oxide		
A	12 045.2	12 058.0	12 058.9	12 060.2	12 058.0
B	11 734.0	11 726.0	11 718.8	11 710.0	11 698.7
C	6 730.7	6 772.6	6 789.1	6 809.6	6 827.6
			1,1,3,3-Tetradeutero trimethylene oxide		
A	10 910.53	10 899.39	10 890.54	10 880.5	
B	8 976.55	8 991.74	8 996.45	9 002.0	
C	5 860.99	5 894.41	5 908.07	5 924.3	
			Trimethylene oxide-O^{18}		
A	12 044.6	12 054.8			
B	11 207.5	11 201.3			
C	6 554.6	6 594.8			
			β-monodeutero trimethylene oxide		
A	11 839.53	11 852.0			
B	10 781.54	10 776.7			
C	6 466.75	6 504.6			

If the C–C–C–O ring of trimethylene oxide were planar, then there would necessarily be a minimum potential energy for that configuration in which the ring atoms were coplanar. The vibrational energy levels would be single levels of roughly equal spacing. The vibrational wave functions will be alternately symmetric and antisymmetric. As the ring tends to become puckered as a consequence of a hump in the potential function at the planar configuration, the vibrational levels will tend to approach each other in pairs. Each pair will contain a symmetric and an antisymmetric level. Now, if the ring were more or less permanently bent, then the potential function would have a high barrier for the planar configuration. The pairs of energy levels will become more nearly degenerate, until in the limit of an infinite barrier, they will coincide and there will be one vibrational satellite for each pair of levels.

The relative intensities of a rotational transition and its vibrational satellites will depend upon the nuclear statistical weights associated with the vibrational and rotational levels concerned. By the application of well-known group theoretical methods, it is possible to determine that the nuclear-spin statistical weights are in the ratio of 9 to 7. The appropriate weight factor depends upon the particular vibrational and rotational energy level. For planar and not too puckered trimethylene oxide, it is found that the intensities of rotational transitions from the ground and excited vibrational states would be in the ratio of 7:9 $\exp -E_1/kT$: 7 $\exp -E_2/kT$ for $A-B_a$ rotational transitions and 9: 7 $\exp -E_1/kT$: 9 $\exp -E_2/kT$ for B_b-B_c rotational transitions, where E_1 and E_2 are the energy levels for the first two excited vibrational levels relative to the ground state. If the molecule were highly puckered so that satellites from successive pairs of vibrational levels were not resolvable, then the statistical weights would appear to be (7+9):(7+9) or 1:1, and the relative intensities of the main line and its observed satellites will be given by 1: $\exp -E_1/kT$: $\exp -E_2/kT$.

Since the permanently bent or highly puckered structure and the planar or near planar structure appear to give rise to different sets of statistical weights, it is in principle possible through the use of intensity measurements to decide between the case in which the barrier is very high and that in which the barrier is zero or not quite so high. (The range in the latter is, however, somewhat indefinite.)

In trimethylene oxide, intensities of several sets of lines were measured to sufficient accuracy to conclude that the statistical weights are necessary. In Table III, we have summarized the results of these intensity measurements. The interpretation of the relative intensities with and without the use of the statistical weights is shown. The data are sufficiently good to determine that the splitting between the ground and first excited states is 60 ± 20 cm^{-1}, and that between the first and second excited states, 110 ± 20 cm^{-1}. Temperature variation of the relative intensities of one of the sets of lines seems to confirm our conclusion. The results of the latter measurements are independent of the statistical weights.

Evidence is thus presented indicating that the vibrational energy levels in the ring-puckering vibration of trimethylene oxide are single levels. Trimethylene oxide is therefore not permanently bent. The ring is then either planar or near planar.

TABLE III. Energy splittings from microwave intensity measurements.

Transition	Symmetry	No statistical weights used		Statistical weights used	
		E_1-E_0 cm^{-1}	E_2-E_1 cm^{-1}	E_1-E_0 cm^{-1}	E_2-E_1 cm^{-1}
$1_{11}-2_{12}$	B_b-B_c	105	...	55	...
$1_{10}-2_{11}$	B_b-B_c	100	80	45	130
$3_{12}-3_{21}$	B_b-B_c	125	50	75	105
$4_{22}-4_{41}$	$A-B_a$	0	170	50	120
$9_{82}-9_{63}$	$A-B_a$	15	140	65	90
				Mean 60±20	110±20
$9_{82}-9_{63}$	(from temperature dependence)[a]			70±30	100±40

[a] Does not involve statistical weights.

STARK EFFECT

The Stark effect in the microwave spectrum is strongly influenced by the height of the barrier in the ring-puckering potential function and a study of this effect provides additional evidence as to the planarity of the trimethylene oxide ring.

If the barrier is high so that the splitting between the first two inversion levels is small, for example, less than 100 Mc, the molecule may be considered to be permanently bent. The dipole moment will then have a component in the out-of-plane direction. This c dipole may be small so that c-type transitions would be too weak to be observed. However, the Stark splittings of the a-type transitions would be very sensitive to this permanent c dipole, since trimethylene oxide is close to an oblate symmetric top, and therefore in an electric field the c dipole connects levels which are nearly degenerate. Careful measurements of the ratio of the Stark splittings of the $M=0$ and the $M=1$ Stark components of the $1_{01}-2_{02}$ line set an upper limit of 2×10^{-3} Debye for the c component of the dipole moment. From these splittings, a value of 1.93 ± 0.01 Debye is obtained for the a component of the dipole moment when the c-type interactions are neglected. Since $\mu_b=0$ from symmetry, and $\mu_c\cong0$, the dipole moment of the molecule then lies solely along the C–O molecular axis and is equal to 1.93 ± 0.01 Debye. Using the component of the dipole along the a axis and the geometry of the molecule, it is possible to estimate an upper limit of only about 0°40′ for the dihedral angle between the C–O–C and the C–C–C planes of the puckered molecule. Such a high barrier separating two minima only 0°40′ apart would be physically unreasonable, and need not be considered as a possibility.

The pronounced effect of a permanent c dipole on the Stark effect of the a-type transitions is convincingly illustrated by the observed Stark effect in the spectrum of β-monodeutero trimethylene oxide. Here the replacement of a hydrogen by a deuterium in the β-carbon position tilts the inertia axes so that they are no longer coincident with the molecular axes. This angle of tilt is $\cong0°40'$ so that μ_c is $\cong0.02$ Debye. This small perturbation nevertheless has a drastic influence on the Stark effect. Certain a-type transitions have their origin in levels which are involved in near degeneracies. These nearly degenerate levels are coupled by the interaction of the permanent c dipole with the electric field. The coupling of these nearly degenerate levels gives rise to some strange Stark effects. The Stark splittings of the $3_{12}-3_{13}$, $3_{22}-3_{03}$, $4_{13}-4_{14}$, and $4_{23}-4_{04}$, for instance, are first order or nearly first order in the electric field. The magnitudes of these splittings are furthermore much larger by many powers of ten than would be expected when the a-type interactions were considered alone. This near first-order Stark effect becomes particularly interesting when the interaction of the c dipole with the electric field gets to be of the same order of magnitude as the splitting of the near degenerate levels. Whereas in the absence of an electric field, an a-type transition from some given level to only one of the levels of the near-degenerate pair was allowed, in the presence of a moderate field, there is sufficient "mixing" between this degenerate pair so that transitions are allowed to Stark levels of both members of the pair. This phenomenon results in "mirror" lines similar to those reported by Hughes, Good, and Coles for methyl alcohol.[13,14]

Thus the Stark effect also rules out the possibility of a very high barrier between the two puckered forms. For lower barriers, one must worry about inversion doubling, a phenomenon which is also present in the high-barrier case, but nevertheless could be ignored. As the barrier is lowered, the inversion levels split but the interaction between them still has an important influence on the Stark effect. The nature of this interaction will be clearly understood by considering the symmetry of the inversion-rotational wave functions.

The transformation properties of the vibrational-rotational-nuclear spin wave functions of trimethylene oxide are deduced from the representations of the product group $P_6\times C_{2v}\times D_2$.[15] However, since we are only interested in the ring-puckering vibration, we may

[13] R. H. Hughes, W. E. Good, and D. K. Coles, Phys. Rev. **84**, 418 (1951).

[14] E. V. Ivash and D. M. Dennison, J. Chem. Phys. **21**, 1804 (1953).

[15] P_6 is the sixth-order permutation group.

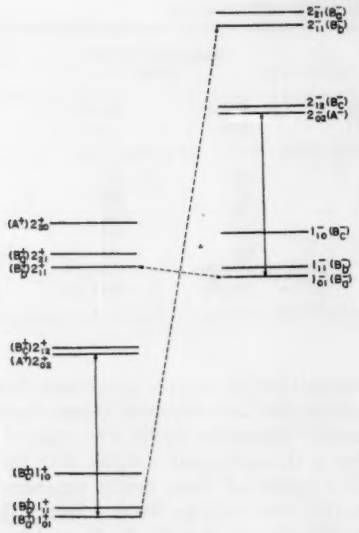

FIG. 1. An example of possible strong and asymmetric c-type interactions in the Stark effect of the $1_{01}-2_{02}$ transition. Here the separation between the first two inversion levels is about 47 kMc.

for convenience consider only the subgroups $D_2\times\sigma_{v'}$, where $\sigma_{v'}$, unlike the usual reflection operator σ_v which reflects the molecule through the plane of the ring, simply reverses the vibrational coordinate of the ring puckering motion without interchanging the hydrogen nuclei at the β-carbon position. $\sigma_{v'}$ as defined here would be the usual σ_v combined with the operation (3, 4) of P_6 which interchanges the two β-hydrogens of trimethylene oxide. In this subgroup, we may label the representations as A, B_a, B_b, and B_c according to the usual nomenclature for the symmetry of the over-all rotational wave functions (D_2)[16] and add a + or − superscript to indicate their symmetry with respect to $\sigma_{v'}$. With the irreducible representations so classified, it is easy to show that the permanent dipoles[17] along the a, b, and c axes transform according to the representation B_a^+, B_b^+, and B_c^+, respectively, and a transition dipole between the inversion levels according to representation B_c^-.

The above subgroup is desirable because of the ease of applying similar language for normal trimethylene oxide to the β-monodeuterated molecule, even though the latter does not possess C_{2v} symmetry. In β-monodeutero trimethylene oxide, the dipole along the c axis is produced by the tilting of the inertia axes. This c dipole in our language would be symmetric with respect to the operation $\sigma_{v'}$, and thus belong to the representation B_c^+. It therefore connects rotational levels all of which belong to either the symmetric or antisymmetric inversion levels. The anomalous Stark effects described above for the β-monodeutero compound are the results of near degeneracies in the rotational sublevels within a given inversion state.

The c dipole formed as a result of the puckered ring is however very different. It belongs to the representation B_c^- and therefore connects rotational sublevels of symmetric inversion states with those of antisymmetric states. If normal trimethylene oxide were very puckered, the first two inversion levels would be degenerate and similar anomalous Stark interactions as in β-monodeutero trimethylene oxide should have been observed. These effects would, as a matter of fact, be more pronounced in the normal species since it is much closer to an oblate symmetric top than the β-monodeuterated molecule. The absence of these effects in normal trimethylene oxide is therefore taken as evidence that if a barrier exists, it is low.

As the barrier is lowered, the degeneracies would be broken and the Stark effect would not always be so sensitive to the c dipole. When the splitting between the first pair of inversion levels is much less than 2 cm^{-1}, the transition dipole (B_c^-) connecting rotational sublevels of adjacent near-degenerate inversion states will give rise to Stark interactions, but the interactions will be appreciable only when the levels involved in the transitions are nearly degenerate with connected rotational sublevels in the other inversion state. Such a situation is illustrated in Fig. 1 for the $1_{01}-2_{02}$ transition. One notices that when such near degeneracies do occur, the interactions will usually not be symmetrical for the two overlapping a-type transitions. The effect may be much more pronounced for the rotational transition from either the symmetric or antisymmetric inversion level, thus causing the Stark effect of this transition to be very different in magnitude than in

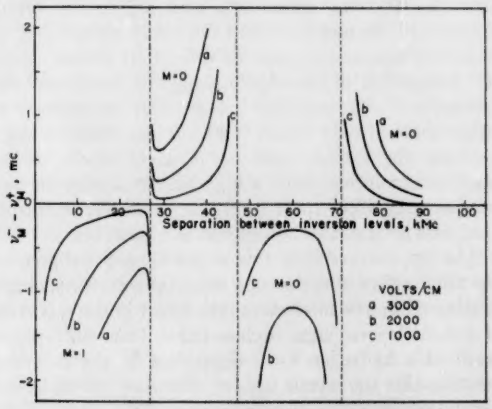

FIG. 2. Possible splittings between the Stark components arising from the $1_{01}^+-2_{02}^+$ and $1_{01}^--2_{02}^-$ transitions when the separations between the first two inversion levels is 0 to 3.0 cm^{-1}.

[16] G. W. King, R. M. Hainer, and P. C. Cross, J. Chem. Phys. **11**, 27 (1943).

[17] Of course, all the so-called permanent dipoles become transition dipoles when the possibilities of reflecting the entire molecule through various other planes and centers of inversion are considered.

that arising from the other inversion level. The net result is that the Stark components may split. The amount of splitting depends of course on the differences in the magnitudes of these c-type interactions for the four levels concerned. In the limit of complete degeneracy for one of the levels, the Stark effect of one of the transitions would approach first order. Detailed calculations have been made on the magnitudes of these interactions in the Stark effects of the two 1_{01}–2_{02} transitions. The results are shown in Fig. 2, where the splitting between the Stark components arising from the symmetric and antisymmetric levels are plotted vs the separation between the first two inversion levels for Stark fields of 1000, 2000, and 3000 v/cm. A transition c dipole of 0.2 Debye has been assumed in the calculations. This corresponds to the situation where the four-membered ring is bent by about 12°. For this particular transition, the c-type interactions are sufficiently strong so that their domains of influence extend over regions covering approximately 20 kMc. Since the resolution of our spectrometer is better than 0.3 Mc, our calculations would seem to indicate that it is possible to observe splittings in the Stark components of this transition at sufficiently high fields when the separation between the inversion states is less than 75 kMc or 2.5 cm^{-1}. No splitting of the Stark components was ever observed even at high fields of 2000-3000 v/cm. From these considerations, we may thus set a lower limit of approximately 2.5 cm^{-1} for the separation between the first two inversion levels.

If the splitting of the ground and first inversion levels were much greater than 2.5 cm^{-1}, their interaction would not produce a measurable effect on the Stark effect of the 1_{01}–2_{02} transition. However, at this point, splitting of satellite lines due to vibration-rotation interaction should have been observed, at least in those from the upper states. The satellite lines show no such splitting. We thus arrive at the independent conclusion that the vibrational satellites observed in the microwave spectra arise from nondegenerate vibrational levels. Trimethylene oxide is therefore planar or near planar.

VIBRATION-ROTATION INTERACTION

The relative intensities, together with the Stark effect of the rotational transitions and their respective vibrational satellites, both point toward a planar or near planar structure for trimethylene oxide. The evidence is strong that trimethylene oxide does not have a highly puckered structure and that the phenomenon known as inversion doubling does not occur. There still remains, however, the problem of distinguishing between a truly planar molecule and a "slightly bent" one. We shall now attempt to decide between the latter two cases through a study of vibration-rotation interaction.

The instantaneous principal moments of inertia of the molecule may be represented by an expansion in the instantaneous vibrational normal coordinates. For example,

$$I_{gg}=I_{gg}^{0}+\sum_{k}^{3N-6}a_{k}^{gg}Q_{k}+\sum_{j,k}^{3N-6}a_{jk}^{gg}Q_{j}Q_{k}+\sum_{j,k,l}^{3N-6}a_{jkl}^{gg}Q_{j}Q_{k}Q_{l}+\sum_{k}^{3N-6}a_{jklm}^{gg}Q_{j}Q_{k}Q_{l}Q_{m}+\cdots.$$

Here I_{gg} is an instantaneous principal moment of inertia; I_{gg}^{0} is the corresponding moment of inertia for the rigid molecule; that is, when all the atoms in the molecule are at their respective equilibrium positions, Q_k is the instantaneous value of the kth vibrational normal coordinate. The above expansion may be obtained by setting up the instantaneous inertia tensor in the principal axis coordinate system of the rigid molecule and applying perturbation theory to the off-diagonal elements.

The instantaneous, reciprocal, principal moments of inertia may likewise be expanded in terms of the vibrational normal coordinates. The time averages of these reciprocal moments of inertia may be obtained when one replaces the instantaneous values of powers of the vibrational normal coordinates by their quantum mechanical expectation values. These time averages of the reciprocal moments of inertia are, however, not quite equivalent to the effective rotational constants due to coriolis interaction. This effect gives rise to additional terms similar to the ones mentioned above and also to cross terms containing powers of the vibrational normal coordinates and powers of their conjugated momenta. They are terms of the type $Q_j^{n}Q_k^{n}$, $Q_j^{n}(P_k/h)^{m}$ where $j\neq k$, and $n\geq m$. Coriolis interaction terms of the latter type are expected to be small compared to the other vibration-rotation interaction terms in the absence of near-vibrational degeneracies,[18] and will therefore be neglected in our discussion. Terms of the type $Q_j^{n}Q_k^{n}$ will be included, however.[19]

In trimethylene oxide where we only have data for the ring-puckering vibration, the treatment of the vibration-rotation interaction can be greatly simplified. Because we are concerned only with molecules in the ground states of all the normal modes except the ring-bending mode, it is possible for us to include all the terms involving these other modes either into the rigid rotor term or into the coefficients of the expansion, provided we make the assumption that the kinetic and potential energies associated with the ring-puckering vibration are separable from the rest of the Hamil-

[18] E. B. Wilson, Jr., and J. B. Howard, J. Chem. Phys. 4, 260 (1936).

[19] Centrifugal distortion will not be considered here since these effects are usually taken care of in the evaluation of effective rotation constants.

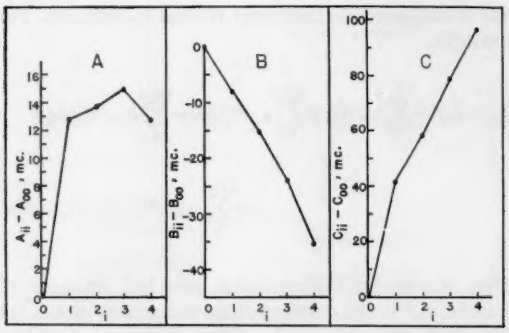

FIG. 3. Experimental rotational constants vs vibrational level for normal trimethylene oxide.

tonian. With this assumption we may then write

$$(B_{gg})_{ii} = [B_{gg}^0 + \sum_k{}' b_k^{gg}(Q_k)_{00} + \sum_{j,k} b_{jk}^{gg}(Q_jQ_k)_{00} + \cdots]$$
$$+ [b_1^{gg} + \sum_j{}' b_{1j}^{gg}(Q_j)_{00} + \sum_{j,k}{}' b_{jk1}^{gg}(Q_jQ_k)_{00} + \cdots](Q_1)_{ii}$$
$$+ [b_{11}^{gg} + \sum_j{}' b_{j11}^{gg}(Q_j)_{00} + \cdots](Q_1^2)_{ii} + \cdots$$
$$= \mathfrak{B}_{gg}^0 + \beta_1^{gg}(Q_1)_{ii} + \beta_2^{gg}(Q_1^2)_{ii} + \cdots,$$

where Σ' designates a summation over all the normal modes except the ring-bending vibration. The normal coordinate for the ring-puckering vibration is denoted by Q_1. The subscript ii denotes a particular vibrational state of the ring-bending mode.

Symmetry considerations further indicate that the potential function governing this ring-bending vibration is symmetric with respect to the normal coordinate. Odd power terms in this normal coordinate in the aforementioned expansions therefore vanish.

In order to interpret the experimentally observed vibration-rotation interaction, we must now determine (1) the expectation values of Q_1^2 and Q_1^4, etc., and (2) the coefficients in the rotational constant expansions, that is, the β^{gg}'s. In Fig. 3, the measured rotational constants of normal trimethylene oxide in their various vibrational states are plotted vs the vibrational "quantum number." The peculiar zigzag shape of these plots will be shown in the following section to be evidence that the vibration is of a double-minimum nature.

DOUBLE-MINIMUM POTENTIAL FUNCTIONS

The expectation values of powers of the normal coordinate depend upon the nature of the potential function governing the mode of vibration in question. This potential function can be obtained, in principle, if the nature of all the interactions in the molecule is quantitatively understood, and if the exact details of the vibration are known. This is seldom the case. However, one can approximate the potential function by a physically realistic expression containing parameters which can be varied. For a given potential function, the expectation values of powers of the normal coordinate may be evaluated and these may in turn be used to compute the rotational constants if the β^{gg}'s are known. Certain other experimentally observable quantities may also be calculated using the potential function. The parameters in the potential function may thus be adjusted until the best agreement is obtained for all the available experimentally observed quantities, including the vibration-rotation interaction.

We here assume that we may write the Hamiltonian for this ring-bending vibration in the following simple form

$$H = (P_1^2/2) + V(Q_1),$$

where $V(Q_1)$ is the potential energy associated with the ring-puckering motion. The familiar harmonic potential, $V(Q_1) = aQ_1^2$, is probably the simplest and most reasonable function to start with. If this potential function, however, proves to be inadequate, it may be modified in a certain number of ways. For instance, we may steepen the potential well by the addition of a quartic term and/or higher-order terms. The introduction of a central barrier also constitutes another possibility. In order to be able to take into account all these possibilities, we have taken the potential function to be of the following form

$$V(Q_1) = aQ_1^2 + bQ_1^4 + c\exp(-dQ_1^2).$$

In other words, we have taken the general potential function to be a simple harmonic oscillator function perturbed by a quartic term and a Gaussian term. This choice was dictated by two criteria, the first of these being that it gives a physically reasonable potential function. Second, with the potential energy in this mathematical form, the evaluation of matrix elements for the Hamiltonian becomes mathematically simple.

For ease in machine computation, we have rewritten the potential energy in the following form

$$V(Q_1) = h\nu_0[(\gamma Q_1^2/2) + \lambda\gamma^2 Q_1^4 + \alpha\exp(-\beta\gamma Q_1^2)];$$

ν_0, λ, α, and β are empirical parameters, ν_0 is the fundamental frequency of vibration for the unperturbed harmonic oscillator, and γ takes on the usual definition $4\pi^2\nu_0/h$.[20]

A 20- $\times$20-Hamiltonian matrix was set up using the first 20 harmonic-oscillator wave functions as the basis functions. Matrix elements for the unperturbed Hamiltonian and the quartic term are well known and readily available.[21] Matrix elements for the Gaussian term were evaluated using the generating function for the Hermite polynomials in the standard way.[22] These turned out to be polynomials in β.

[20] E. B. Wilson, Jr., J. C. Decius, and P. C. Cross, *Molecular Vibrations* (McGraw-Hill Book Company, Inc., New York, 1955), see p. 290.
[21] See footnote reference 20, pp. 289–291.
[22] L. I. Schiff, *Quantum Mechanics* (McGraw-Hill Book Company, Inc., New York, 1955), p. 64.

The entire problem was set up on an electronic computer (IBM 701). The calculations included the evaluation of the Hamiltonian matrix elements for selected values of the parameters in the Hamiltonian operator, the diagonalization of the Hamiltonian matrix to give the energy levels, and the transformation of the Q_1^2 and Q_1^4 matrices in the harmonic-oscillator wave function representation to yield the expectation values of Q_1^2 and Q_1^4. Since we were also interested in infrared intensities, the Q_1 matrix was also transformed.

Although Q_1^4 terms will eventually be included, let us suppose for the moment that the above rotational constant expansions converge reasonably rapidly so that we may ignore terms beyond the Q_1^2 term. We note then that the variation in rotational constants with vibrational level is directly proportional to the corresponding variation in $(Q_1^2)_{ii}$.

In Figs. 4 and 5, we have plotted $2\gamma(Q_1^2)_{ii}$ vs the vibrational level for a variety of potential functions. For a harmonic oscillator, the expectation value of Q_1^2 is a linear function of the vibrational quantum number. This is represented by the diagonal straight line. Upon the addition of a quartic term, the curve assumes negative curvature and bends downward. In the potential function employed for this plot, the quartic contribution to the total potential energy is roughly twice that of the quadratic term[23] when Q_1= 1.5 amu$^{\frac{1}{2}}$ A and ν_0=100 cm^{-1}. For sake of comparison, we have also plotted the expectation values of Q_1^2 for the case of an infinite square well. The position of this curve relative to the others is arbitrary. In this ultimate limiting case, the curve bends over rapidly to give a plateau. Such a quartic term in the potential function may explain the general curvature in the experimental plots, particularly in the case of rotational constant A. But in all the cases, the calculated variations are smooth, and therefore such potential functions cannot be used to explain the peculiar zigzagging details of the experimental curves.

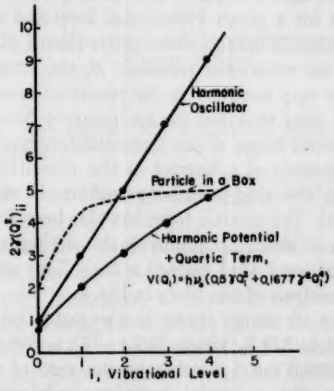

FIG. 4. Variations in the expectation values of Q_1^2 for several typical potential functions.

[23] This corresponds to a vibrational displacement of about 0.15 when an effective reduced mass of 97.2 amu is assumed for the ring-puckering vibration.

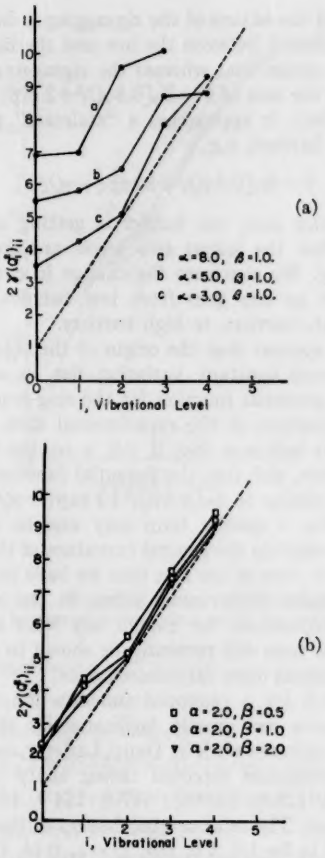

FIG. 5(a), (b). Variations in the expectation values of Q_1^2 for several double-minimum potential functions.

This zigzagging variation in the rotational constants can be explained by the introduction of a central barrier into the potential function. Since wave functions for the odd vibrational levels contain nodes at the planar configuration, the barrier gives rise to a much larger perturbation for the even levels than for the odd ones. These ideas have been borne out in detailed calculations.

In Fig. 5, we have plotted $2\gamma(Q_1^2)_{ii}$ for a number of such double-minimum potential functions. Each of these corresponds to a different barrier height. The zigzagging feature is reproduced beyond doubt. The addition of a hump to the harmonic oscillator potential results in quite a remarkable increase in the value of $(Q_1^2)_{ii}$ for levels below and slightly above the top of the barrier. At very high vibrational levels, where the perturbation becomes negligible, $(Q_1^2)_{ii}$ approaches the value for a harmonic oscillator. The

degree and the nature of the zigzagging is furthermore grossly different between the low and the high barrier cases. We notice that whereas the zigzagging is rather smooth in the case of $V=h\nu_0[0.5\gamma Q_1^2+2\exp(-\beta\gamma Q_1^2)]$ (low barrier), it approaches a "staircase" pattern at very high barriers, e.g.,

$$V=h\nu_0[0.5\gamma Q_1^2+8\exp(-\gamma Q_1^2)].$$

In the latter case, the barrier is getting sufficiently high so that the lowest two levels are approaching degeneracy. We also note the change in curvature of the curves as one goes from low barriers, through intermediate barriers, to high barriers.

It thus appears that the origin of the zigzagging in the rotational constant variation lies in a double-minimum potential function for the ring-bending motion. Comparison of the experimental data with the above plots indicates that if this is so, the barrier is probably low, and that the potential function may be somewhat similar to $h\nu_0[0.5\gamma Q_1^2+2\exp(-\gamma Q_1^2)]$. It is possible that a quartic term may also be necessary in order to explain the general curvature of the curves. However, in view of the fact that we have not, at this point, included higher-order terms in the rotational constant expansions, we cannot say with certainty. The quartic term will presently be shown to be necessary to interpret some far-infrared data.

Our search for a potential function for the ring-bending mode was greatly facilitated by the results of some far-infrared work by Danti, Lafferty, and Lord.[24] These investigators reported strong sharp bands at 89.8, 118.3, 128.9, (139.0), 147.6, 154.9, 161.8 cm^{-1} for the vapor. The relative absorbances of these bands were found to be 1.0, 1.0, 0.9, (···), 0.44, 0.35, and 0.30, respectively. Beside a broad weak band in the region 250 cm^{-1} to 300 cm^{-1}, no additional vapor absorption was detected below 600 cm^{-1}. Weak bands, however, were also reported at about 390 and 410 cm^{-1} for the liquid.

There is little doubt that these bands arise from the puckering of the four-membered ring. From our intensity measurements of the vibrational satellites in the microwave spectrum, we have already obtained splittings of 60 ± 20 cm^{-1}, and 110 ± 20 cm^{-1} for the fundamental and the 1st hot band, respectively. These separations appear to be in good agreement with the 89.8 and 118.4 bands reported by the infrared investigators. The remaining strong bands are most likely the 2nd, 3rd, 4th, 5th, and 6th "hot bands." We can infer this from the reported intensity pattern. The diverging energy level pattern also represents strong evidence for a steeper well than that of the harmonic oscillator.

In order to confirm our interpretation, a serious attempt was therefore made to find a potential function that will fit the above far-infrared data. If we are successful, we shall use this potential function to calculate the expectation values of Q_1^2 and Q_1^4. To determine whether the potential function, which fits the infrared data, will yield the desired set of expectation values for Q_1^2 and Q_1^4, we will at the present resort to a semiempirical approach. This would not have been necessary if the coefficients in the rotational constant expansions had already been accurately determined. However, these coefficients are still unknowns at this stage, and furthermore, they can only be approximated very crudely at best.

In this approach, we chose to carry the rotational constant expansions up to the Q_1^4 term. Using the values of $(Q_1^2)_{ii}$, $(Q_1^4)_{ii}$ as calculated from the potential function, the coefficients in the expansions for A, B, and C were determined by numerically fitting the experimental rotational constants for three vibrational levels. With these calculated coefficients, the expansions can then be used to evaluate the rotational constants for the remaining levels. The applicability of the potential function is judged by the agreement for these remaining levels. Figure 6 gives the results of this treatment to the three rotational constants for several potential functions. The experimental data was fitted using the values for the ground state, first excited state, and the 4th excited state.

The potential function that has been found to best fit the far-infrared data and the rotational constant variation is given by $V(Q_1)=h\nu_0[0.5\gamma Q_1^2+0.08384\gamma^2 Q_1^4+1.4\exp(-\gamma Q_1^2)]$, $\nu_0=93.00$ cm^{-1}. This potential function together with the first few energy levels are illustrated in Fig. 7. The corresponding unperturbed harmonic oscillator potential well is also included to depict the magnitudes of the quartic and Gaussian perturbations.

That this potential function gives a nearly perfect fit to the vibration-rotation interaction can be seen in Fig. 6. The agreement between the calculated rotational constants for a given vibrational level and the experimental values is in most cases better than 1 Mc. Except, perhaps, for rotational constant B, the fitting can be seen to be very sensitive to the potential function. This approach thus provides for an accurate determination of the general shape of the potential function.

The presence of a barrier in the potential function restricting the ring-puckering motion is now firmly established. The quartic term has also been found to be necessary in order to improve the fitting at the 4th vibrational level (3rd excited state). This can be seen from an analysis of the plots in Fig. 6.

The first 10 energy levels in this potential well are: 141.3, 211.4, 329.8, 456.4, 595.1, 742.1, 896.8, 1058.0, 1225.9, 1398.0 cm^{-1} relative to the zero of energy as defined by the potential function (minimum of the parabola). The corresponding infrared-active frequencies are listed in Table IV. Except for the fundamental, the agreement is really quite remarkable.

The relative absorbances of the fundamental and the

[24] See footnote reference 8.

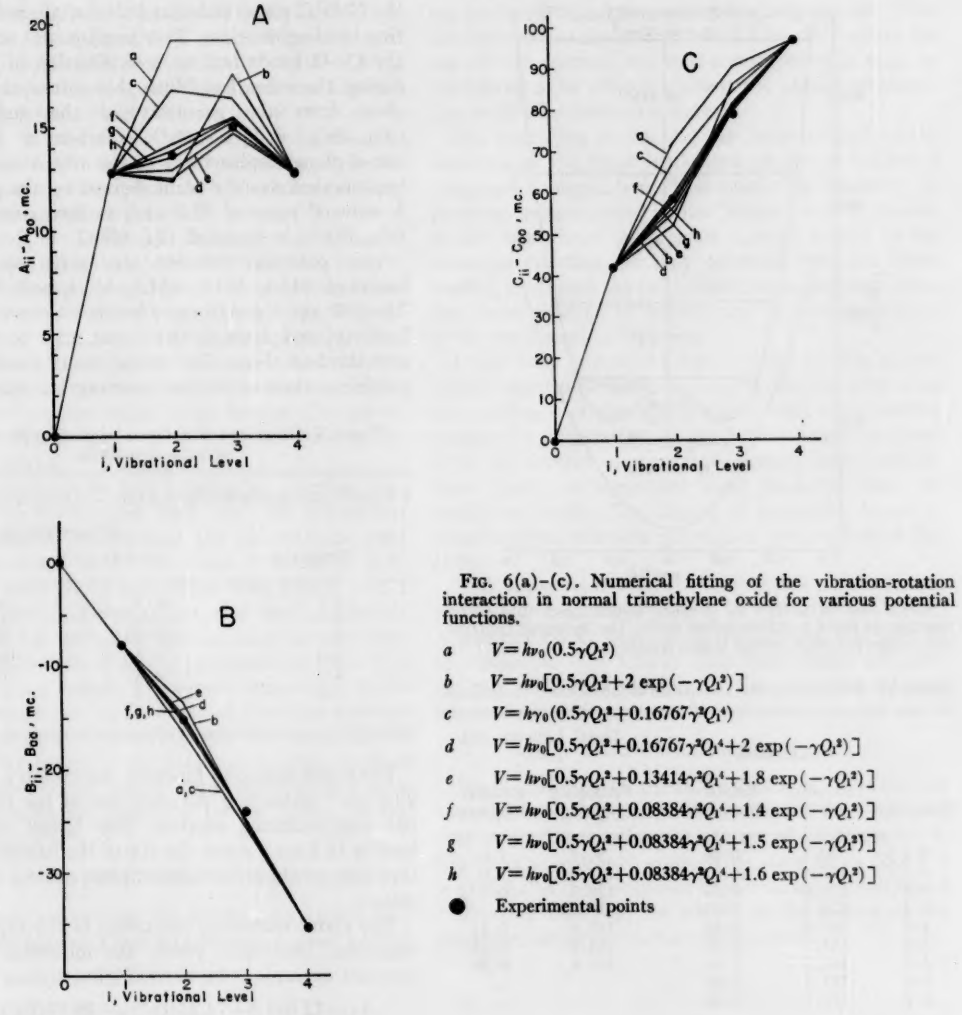

FIG. 6(a)-(c). Numerical fitting of the vibration-rotation interaction in normal trimethylene oxide for various potential functions.

a $V = h\nu_0(0.5\gamma Q_1^2)$

b $V = h\nu_0[0.5\gamma Q_1^2 + 2\exp(-\gamma Q_1^2)]$

c $V = h\gamma_0(0.5\gamma Q_1^2 + 0.16767\gamma^2 Q_1^4)$

d $V = h\nu_0[0.5\gamma Q_1^2 + 0.16767\gamma^2 Q_1^4 + 2\exp(-\gamma Q_1^2)]$

e $V = h\nu_0[0.5\gamma Q_1^2 + 0.13414\gamma^2 Q_1^4 + 1.8\exp(-\gamma Q_1^2)]$

f $V = h\nu_0[0.5\gamma Q_1^2 + 0.08384\gamma^2 Q_1^4 + 1.4\exp(-\gamma Q_1^2)]$

g $V = h\nu_0[0.5\gamma Q_1^2 + 0.08384\gamma^2 Q_1^4 + 1.5\exp(-\gamma Q_1^2)]$

h $V = h\nu_0[0.5\gamma Q_1^2 + 0.08384\gamma^2 Q_1^4 + 1.6\exp(-\gamma Q_1^2)]$

● Experimental points

successive "hot bands" are evaluated using the well-known expression[25]

$$(8\pi^3/3hc)(N_{v'}-N_{v''})\nu_{v'v''}\sum_g |\mu_{v'v''g}|^2.$$

Since the first few levels in this potential function are appreciably populated, induced emission was found to be relatively important and could not be ignored. As a matter of fact, the intensity of the 0−1 transition is calculated to be weaker than the 1–2 transition because of the large fraction of molecules in the first excited vibrational level. For the $i \rightarrow i+1$ vibrational transitions, the dipole matrix elements are given by $(\partial\mu_c/\partial Q_1)_0(Q_1)_{i,i+1}$. Since these are *c*-type transitions, they should give rise to sharp *Q* branches in the far infrared spectrum. The results of the intensity calculations are tabulated in Table IV. The 118.4 band has been used to normalize the intensities.

First overtone bands, $i \rightarrow i+2$, are predicted at 188.5, 245.0, 265.3, 285.7, 301.7, and 315.9 cm^{-1}. The transition dipole moment matrix elements for these transitions are given by $(\partial^2\mu_a/\partial Q_1^2)_0(Q_1^2)_{i,i+2}$. These first overtone bands are *a*-type bands, and as pointed out by Danti, Lafferty, and Lord, should give rise to bands without sharp *Q* branches. In this case, they would appear as a set of broad overlapping bands. Calculations show that integrated intensities of the first overtone bands are roughly down by a factor of 50 compared to the aforementioned *c*-type bands. The first and second dipole derivatives are evaluated assuming that the dipole moment of the molecule lies solely in

[25] See footnote reference 20, p. 163.

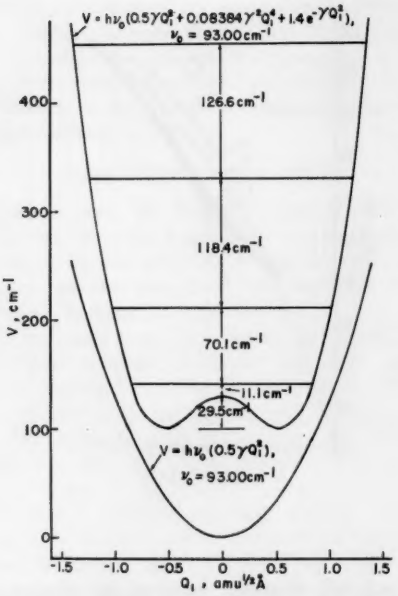

FIG. 7. Lower portion of double-minimum potential energy function as fitted to trimethylene oxide. The harmonic contribution to the potential energy is also shown.

TABLE IV. Frequencies and intensities of far-infrared transitions.

Transition	Calculated[a] Frequency cm⁻¹	Calculated[a] Relative absorbance	Danti, Lafferty, and Lord[b] Frequency cm⁻¹	Danti, Lafferty, and Lord[b] Relative absorbance
0–1	70.1	0.46	89.8	1.0
1–2	118.4	(1.0)	118.3	1.0
2–3	126.6	0.89	128.9	0.9
3–4	138.7	0.69	(139.0)	...
4–5	147.0	0.46	147.6	0.44
5–6	154.7	0.28	154.9	0.35
6–7	161.2	0.16	161.8	0.30
7–8	167.9	0.08	...	...
8–9	172.1	0.04	...	...
1st overtone bands				
0–2	188.5	≈0.009		
1–3	245.0	≈0.017		
2–4	265.3	≈0.017		
3–5	285.7	≈0.015	Broad weak absorption from 250 to 300 cm⁻¹	
4–6	301.7	≈0.011		
5–7	315.9	≈0.007		
2nd overtone bands				
0–3	315.1	0.048		
1–4	383.7	0.021	390(liquid)	weak
2–5	412.3	0.014	410(liquid)	weak
3–6	440.4	0.008		
4–7	462.9	0.005		

[a] $V = h\nu_0[0.5\gamma Q_1^2 + 0.08384\,\gamma^2 Q_1^4 + 1.4\,\exp(-\gamma Q_1^2)]$, $\nu_0 = 93.00\ \text{cm}^{-1}$.
[b] See footnote reference 8 of text.

the C–O–C plane and that it is not altered during the ring-bending motion. This implies no stretching of the C—O bonds and no redistribution of the charges during the vibration. With this assumption, one can show from the geometry of the molecule that $|(\partial\mu_c/\partial z)_0| = |\frac{1}{2}(\partial^2\mu_a/\partial z^2)_0|$, where z (A) is the out-of-plane displacement of the ring atoms from the hypothetical average plane defined by the planar ring. A reduced mass of 97.2 amu is then used to obtain $(\partial^2\mu_a/\partial Q_1^2)_0$ in terms of $(\partial\mu_c/\partial Q_1)_0$.

This potential function also gives 2nd overtone bands at 315.1, 383.7, 412.3, 440.4, and 462.9 cm⁻¹. The 390 and the 410 cm⁻¹ bands observed by Danti, Lafferty, and Lord in the liquid may be the second and third of these. The intensities of these are comparable to those of the first overtone transitions.

TABLE V. Calculated vibrational frequencies for two other potential functions.

$V = h\nu_0[0.5\gamma Q_1^2 + 0.08384\gamma^2 Q_1^4 + \alpha\exp(-\gamma Q_1^2)]$, $\nu_0 = 93.00\ \text{cm}^{-1}$.

Transition	Frequency, cm⁻¹ $\alpha = 1.5$	Frequency, cm⁻¹ $\alpha = 1.6$
0–1	67.5	64.9
1–2	118.6	118.8
2–3	125.9	125.2
3–4	138.4	138.2
4–5	146.8	146.6
5–6	154.5	154.4
6–7	161.2	161.1

From this potential function, we obtain a barrier of 29.5 cm⁻¹ restricting the inversion of the molecule in the ring-puckering motion. The lowest vibrational level is 11.1 cm⁻¹ above the top of the barrier. We may therefore conclude that trimethylene oxide is essentially planar.

The above numerical treatment of the experimental rotational constants yields the following rotational constant expansions for normal trimethylene oxide:

$$A_{ii} = 12\,031.8 + 74.83(Q_1^2)_{ii} - 29.79(Q_1^4)_{ii}\ \text{Mc}$$

$$B_{ii} = 11\,739.6 - 15.66(Q_1^2)_{ii} - 14.08(Q_1^4)_{ii}\ \text{Mc}$$

$$C_{ii} = 6\,692.4 + 182.3(Q_1^2)_{ii} - 31.65(Q_1^4)_{ii}\ \text{Mc}.$$

The units of Q_1^2 are amu A². These expansions are all taken up to the $(Q_1^4)_{ii}$ term. The contributions of the Q_1^4 term are actually rather large in each case, so that one might worry about the rapidity of the convergence of the above series. However, a sixth-order term has not been included in the expansions since better agreement with the experimental data is not necessary. Furthermore, a separate plot of the Q_1^2 and Q_1^4 contributions indicates that the zigzagging variation appears to have been solely contributed by the Q_1^2 term in the expansions. The Q_1^4 variation is smooth. Our evidence for the existence of the barrier in the potential function is therefore independent of the introduction of the Q_1^4 and higher-order terms in the rotational constant expansions.

It is possible to fit the vibration-rotation interaction better with the potential functions $V(Q_1)=h\nu_0[0.5Q_1^2+0.08384\gamma^2Q_1^4+1.5\exp(-\gamma Q_1^2)]$, $\nu_0=93.00$ cm^{-1} and $V(Q_1)=h\nu_0[0.5Q_1^2+0.08384\gamma^2Q_1^4+1.6\exp(-\gamma Q_1^2)]$, $\nu_0=93.00$ cm^{-1}. These potential functions contain slightly higher barriers of 34.7 cm^{-1}, and 40.1 cm^{-1}, respectively. In the former potential function, the ground vibrational level is 7.7 cm^{-1} above the top of the barrier, and in the latter, 4.3 cm^{-1}. The corresponding energy level separations for these potential functions are tabulated in Table V. Our selected potential function, $V(Q_1)=h\nu_0[0.5\gamma Q_1^2+0.08384\gamma^2Q_1^4+1.4\exp-\gamma Q_1^2)$, $\nu_0=93.00$ cm^{-1}, probably fits the far-infrared data better. However, the lower fundamentals obtained with these latter potential functions are probably consistent with our microwave intensity measurements. Due to these uncertainties, we have selected a value of 35 ± 5 cm^{-1} for the height of the barrier. The lowest vibrational level is taken to be 8 ± 4 cm^{-1} above the top of the barrier.

In our endeavors to find a potential function that would fit the far-infrared data and the microwave vibration-rotation interaction, the calculations were carried out over a fairly wide range of values of α, β, and λ. For example, α was varied from 0 to 8, and λ from 0 to 1.6767. Three values of β were employed, namely 0.5, 1.0, and 2.0. The calculations were not explicitly dependent upon the parameter ν_0, since it is merely a scaling factor. The results were found to be relatively insensitive to the value of β chosen, particularly for calculations involving very low barriers. The actual barrier height in the potential function appears to be the more crucial factor; λ was found to be a very sensitive parameter, especially in the fitting of the higher energy levels.

CONCLUSION

It has been shown that the trimethylene oxide ring is essentially planar. There is, however, a small barrier of 35 ± 5 cm^{-1} separating the two minima corresponding to the two slightly puckered configurations. Since the lowest vibrational level is still 8 ± 4 cm^{-1} above the top of this barrier, the four-membered ring may be considered to be vibrating about the planar configuration in all the vibrational states.

The puckering of the ring can be attributed to the tendency of the three methylene groups to achieve a staggered configuration. This puckering tendency is, however, being opposed by the "strain" already present in the ring. Since there exists a small barrier in the potential function, we may conclude that the forces tending to stagger the methylene groups slightly exceed the forces tending to oppose any further diminution of the bond angles of the ring.

It has been postulated that cyclobutane has a nonplanar ring,[1] and the nonplanarity should arise from the tendency of the methylene groups to achieve a staggered configuration. If the barrier height increases with the number of methylene groups, then cyclobutane should be somewhat more puckered than trimethylene oxide. The degree of puckering found in trimethylene oxide now serves as a confirmation of this result.

This paper represents the first of two papers on our completed microwave studies of trimethylene oxide. A separate paper devoted to the detailed structure of the molecule will follow. This next paper will also contain additional details on the vibration-rotation interaction problem.

ACKNOWLEDGMENTS

We would like to thank Professor R. C. Lord for several interesting discussions during the final stages of this work. The continuous interest of Professor R. J. Myers is also deeply appreciated. One of us (S.I.C.) is grateful to the Computer Center at the University of California, Berkeley, for advice on the coding of the programs employed in our computations.

THE JOURNAL OF CHEMICAL PHYSICS VOLUME 33, NUMBER 6 DECEMBER, 1960

Small Angle X-ray Scattering Study of Sodium Montmorillonite Clay Suspensions*

ROBERT HIGHT, JR.
Department of Physics, University of Missouri, Columbia, Missouri
WILLIAM T. HIGDON
Shell Development Company, Houston, Texas
AND
PAUL W. SCHMIDT
Department of Physics, University of Missouri, Columbia, Missouri

(Received June 16, 1960)

Suspensions of montmorillonite clay with concentrations of ½ and 2% have been investigated by small angle x-ray scattering, with two different centrifuge fractions being studied for each concentration. At a given concentration the scattering was observed to be the same for both centrifuge fractions. The scattered intensity was always proportional to the concentration. These results are what would be expected from dilute suspensions of thin platelets of identical thickness but different surface areas. When corrections for the finite height of the collimating slits are applied to the scattering curves, good agreement with the theoretical curves for thin platelets is obtained. From the deviation between the experimental and the theoretical curves at the largest observed scattering angles, the thickness of the platelets was calculated to be 9 A. An independent determination of the thickness can be made from a measurement of the zero angle scattered intensity from some material for which the ratio of the scattered intensity to the scattering from a single electron can be calculated. Two heavy gases, SF_6 and $C_2Cl_2F_4$ (Freon 114), were used for this purpose. The feasibility of using Ludox colloidal silica as a third standard was investigated. Within experimental accuracy, the thickness values calculated from these data agree with the values obtained from the shape of the scattering curves. Both values agree with the thickness determined from the light scattering experiments of M. B. M'Ewen and M. I. Pratt [Trans. Faraday Soc. **53**, 535 (1957)]. Since the scattering curve for the clay is proportional to the inverse square of the angle at the smallest observed angles, the large dimensions of the particle must be at least 500 A.

INTRODUCTION

THE determination of the physical structure of montmorillonite clay has been the object of a number of investigations. Electro-optical birefringence studies[1] provide an approximate value for the major particle dimensions for very dilute suspensions. Electron-microscope studies[2] of dilute suspensions have indicated that the particles exist in thin sheets when in a water suspension. This result is in agreement with crystal structure studies.[3] Melrose[4] has measured the light scattering from montmorillonite clay suspensions. He determined the thickness of the platelet particle indirectly from measurements of the molecular weight and the large particle dimension. A disadvantage to this method is that a geometrical model must be assumed. For a model, Melrose used a cylindrical disk of uniform thickness and a diameter large compared to the crystallographic unit cell thickness. M'Ewen and Pratt[5] employed a different light scattering method to determine the mass per unit area of the platelets.

The purpose of the present small angle x-ray scattering investigation is to make an independent determination of the size of the clay particles. As is shown in the next section, small angle scattering, unlike other techniques, gives a direct measurement of the platelet thickness.

THEORY

In this section we shall review some of the concepts used in the analysis of small angle x-ray scattering curves from platelet particles.

In general the scattering curve for platelets will consist of three regions, each of which is characterized by a particular slope on the plot of the logarithm of the intensity I vs the logarithm of the scattering angle ϕ. First, there will be a region where, for dilute suspensions of thin platelets of uniform electron density σ per unit area, the scattered intensity will be given by[6]

$$I(h)=2\pi cV(\sigma/d)h^{-2}I_e\sigma, \tag{1}$$

where $h=4\pi(\lambda)^{-1}\sin\phi/2$, λ is the x-ray wavelength, V is the irradiated sample volume, c is the concentration in grams per unit volume, d is the mass per unit area of the platelet, and I_e is the scattered intensity from a single electron for the particular experimental apparatus used. This region will occur when $hD\gg1$ and $hH\ll1$, where D is the large dimension of the platelet and H is the thickness of the platelet. In this region the scattering curve is proportional to the inverse second power of the scattering angle. In the second region, which is found at angles so large that hH is at least of the order of 1, the intensity is proportional to h^{-4} instead of h^{-2}. In the third region, for which $hD\ll1$,

* Work supported by Shell Development Company.

[1] A. Kahn and D. R. Lewis, J. Phys. Chem. **58**, 801 (1954).
[2] B. T. Shaw, J. Phys. Colloid Chem. **46**, 1032 (1942).
[3] C. E. Marshall, *The Colloid Chemistry of the Silicate Materials* (Academic Press, Inc., New York, 1949), Chap. 7.
[4] J. C. Melrose, Ph.D. thesis, Stanford University (1954).
[5] M. B. M'Ewen and M. I. Pratt, Trans. Faraday Soc. **53**, 535 (1957).
[6] P. W. Schmidt and R. Hight, Jr., J. Appl. Phys. **30**, 866 (1959).

there is a different angular dependence of the scattering. Ordinarily, in this region the scattering will decrease less rapidly than h^{-2}.

In Eq. (1) it has been assumed that the particles are in vacuum. When the platelets are in a solvent, the right-hand side of this equation must be multiplied by $(1-\sigma_0/\sigma)^2=(1-n_s\rho_s/n\rho)^2$, where σ_0 is the number of electrons per unit area in a volume of solvent of the same thickness as that of the platelet, ρ and ρ_s are the mass per unit volume for the platelet and the solvent, respectively, and n and n_s are the number of electrons per gram for the platelet and solvent.[7]

The experimental curves can be analyzed by comparing their shape with theoretical scattering curves determined by assuming a particular particle shape. The location of the angular regions where the slope of the scattering curve changes can be used to determine the platelet dimensions. The place where the transition from inverse second to inverse fourth power scattering occurs depends only on the thickness[8] and occurs at an angle for which $1/h$ is approximately equal to the thickness. The location of the transition from inverse second to a power less than inverse second is determined by the platelet diameter. If no deviation from the inverse second power is observed at the smallest angles for which experimental values can be measured, then only lower limit to the particle diameter can be obtained. These transitions can be located more precisely if one assumes a particle shape. For example, one can use the scattering curves for monodisperse[6] and polydisperse[8] ellipsoids of revolution and monodisperse right circular cylinders.[9]

Another method of determining the thickness of platelets is to measure the absolute magnitude of the intensity of the small angle x-ray scattering from a solution of known concentration. In Eq. (1) the ratio (σ/d) will ordinarily be a characteristic of the material of which the particle is composed. Thus, if we can determine I_e, we can calculate σ, which is proportional to the platelet thickness.

The zero-angle scattered intensity from a gas can be expressed as[7,10]

$$I_g=N_gV_gF_g^2I_e, \tag{2}$$

where V_g is the irradiated sample volume, N_g is the number of gas molecules per unit volume, and F_g is the x-ray structure factor. In the small-angle region, F_g can be taken equal to the number of electrons in the gas molecules. From the equation of state for the gas, N_g can be found. Determination of I_g thus permits the calculation of I_e for the experimental apparatus.

In addition to using other gases, one can check the value of I_e experimentally by another type of scatterer. The scattering at relatively large angles from a dilute solution of monodisperse spherical particles can be written as[11]

$$I(h)=2\pi(n\rho-n_s\rho_s)^2Sh^{-4}I_e, \tag{3}$$

where S is the total surface area and the other symbols are the same as defined previously. For a given particle, S can be determined by independent means (e.g., B.E.T. nitrogen adsorption). One can then compute I_e.

EXPERIMENTAL METHODS

The clay used in this study, Wyoming bentonite, is an occurrence of the clay mineral, montmorillonite, in almost a pure form. The formula weight from chemical analyses[12] is

$$(Al_{1.54}Fe_{0.16}Mg_{0.33})(Al_{0.09}Si_{3.91})O_{10}(OH)_2(Na_{0.20}\tfrac{1}{2}Ca_{0.02}).$$

Unit cell dimensions calculated from x-ray diffraction analyses vary somewhat from the structure of pyrophyllite, depending on the amount of aluminum substitution in the tetrahedral layer and iron and magnesium substitution in the octahedral layer. Using Brindley's[13] relation and the analyses given above, the b_0 dimension of the unit cell is calculated to be 8.924 A compared with the pyrophyllite b_0 of 8.90 A. Again according to Brindley[14] a_0 dimensions may be calculated from b_0 as $a_0=b_0/\sqrt{3}$ which gives an a_0 value of 5.152 A for the montmorillonite used here. These calculated values may be compared with the experimental values $a_0=$ 5.16 A and $b_0=8.93$ A reported in Grim.[15] Brindley[16] quotes Mering's value for dry Na-montmorillonite $d(001)$ spacing, the c dimension, as 9.6 kX for dry clay. This value, which is essentially 9.6 A, has been obtained for the basal spacing of the dry Na Wyoming bentonite used in this study. From the unit cell dimensions of 5.15 A by 8.92 A by 9.6 A and the two formula weights per unit cell a crystallographic density of 2.784 g/cm³ is computed.

The Na^+ Wyoming bentonite samples were prepared from a handpicked sample of the Clayspur, Wyoming, occurrence of the mineral. Two-percent suspensions of the clay were prepared from the raw material by stirring in distilled water. Conductivity water was used throughout in the preparation of the suspensions. The coarse particles were allowed to sediment overnight and the supernantant suspension of fine particles was passed through a Na^+ saturated Dowex 50 ion-exchange column until the clay was completely in the Na^+ form.

[7] Louis Katz, Ph.D. thesis, University of Wisconsin, 1959.
[8] P. W. Schmidt, Acta Cryst. 11, 674 (1958).
[9] A. Guinier, *et al.*, *Small Angle Scattering of X-Rays* (John Wiley & Sons, Inc., New York, 1955), p. 21 and p. 28.
[10] A. G. Tweet, Phys. Rev. 93, 15 (1954).
[11] Reference 9, p. 17.
[12] A.P.I. Research Project 49, Reference Clay Minerals, Preliminary Report No. 7, *Analytical Data on Reference Clay Materials* (July, 1950), p. 53.
[13] G. W. Brindley, editor, *X-Ray Identification and Crystal Structures of Clay Minerals* (Mineralogical Society, London, 1951), p. 104.
[14] Reference 13, p. 16.
[15] R. E. Grim, *Clay Mineralogy* (McGraw-Hill Book Company, Inc., New York, 1953), p. 128.
[16] Reference 13, p. 128.

TABLE I. Centrifuge data for the clay samples.

Sample designation	Equivalent spherical particle size	Spinco centrifuging conditions: rpm, No. 20 rotor	Spinco centrifuging conditions: time, min.
R_1+R_2	>810 A−2μ	6000	10
R_3	400–810 A	10 000	15
R_4	230–400 A	15 000	20
R_5	70–230 A	20 000	120

The dilute Na^+ form suspension was concentrated to a paste (>10% clay) by centrifugation which served as a base stock for particle size fractionation. Dilute suspensions of the paste were fractionated according to equivalent spherical particle size by successive centrifugation of the same sample under increasingly severe centrifuging conditions. In each step the sediment was retained as the labeled sample and the suspension phase centrifuged again at higher rpm and for a longer time to obtain the next particle size fraction.

Table I gives the centrifuge data for the samples The upper limit of equivalent spherical particle size under the centrifuging conditions employed means that no particles larger than this should be found in the sample. The lower limit, on the other hand, does not mean that no particle smaller than this size is found in the sample. Instead, the lower limit for one fraction is merely the upper limit for the next smaller size fraction. The actual distribution function is highly peaked at the given lower limit.

The resuspensions of the sediments obtained in the fractionation process were found to be salt free by conductance measurements. The sediments were diluted to obtain the desired concentration in percent by weight of clay dried overnight at 110°C. Concentration determinations of the samples, made up to contain 2.000, 1.000, and 0.500 percent by weight, for three different fractions, nine samples in all, averaged 0.022% less clay than desired with an average deviation of ±0.003%.

The x-ray apparatus used to obtain the scattering curves has been described elsewhere.[17]

The sample holders for the montmorillonite clay and the Ludox colloidal silica (spherical particles) were made of sheet aluminum, with a $\frac{3}{16}$-in. by $1\frac{1}{4}$-in. area cut out to provide room for the suspension The holders were covered with Saran Wrap windows. The solutions were introduced into the sample area by use of a syringe inserted through a small hole in the top of the holder. After filling was completed, the syringe was removed, and the hole was sealed with Apiezon wax. The sample holder was held in place in the path of the x-ray beam by means of a brass fitting which slipped on a 1-in. shaft positioned directly over the center of rotation of the collimating slits. The thickness of the sample holders varied from about 0.5 mm to 1 mm. A special brass fitting was machined for use as the gas sample holder, for which the sample area itself was $\frac{1}{4}$ in. thick, with all other dimensions the same as in the other sample holders. Outlets fitted with needle valves were provided at the bottom and the top of the holder. The gases used were obtainable in such quantities that the sample holder could be thoroughly flushed at every filling.

To obtain scattering curves over the entire small angle region it is necessary to make composite curves. Measurements at the smaller angles were taken with 0.011-in. slit widths, while those at the larger angles were obtained with 0.032-in. slits. The composite curves for the clay extend from 0.002 to about 0.045 rad, with an overlap extending from 0.006 to 0.017 rad. The composite curves for the Ludox extend from 0.002 to 0.040 rad, with an overlap from 0.008 to 0.015 rad. The gas scattering curves were obtained only for the 0.032-in. slits. All of the scattering curves were reproduced at least once for each sample considered.

The experimentally measured intensity for each sample was corrected for the absorption of the sample and for the background radiation. The transmission was measured experimentally in all cases and compared to the theoretical value when the latter could be computed. In most cases the difference was only a few percent. For the solutions it was found that most of the absorption was due to the solvent, which was water. The calculated and measured values for the gas transmission were in good agreement. As all sample holder windows were of the same material, and since the measured transmission of the window material was repeatable within experimental accuracy, the absorption due to the windows was not included in either the absolute scattered intensity determination or the analysis of the scattering curves from their shape.

The equations cited in the theory assume the incident radiation to be perfectly collimated by pinholes of negligible aperture. Because of intensity requirements it is necessary to use collimating slits of finite extent, thus introducing a "smearing" out of the measured intensity. These smearing effects must be eliminated if quantitative information is to be obtained from the scattering curves. Numerical methods have been developed[18] which allow this correction to be made in a routine manner, either with an electronic computer or a desk calculator. For a given slit system the correction depends on the shape of the scattering curve and the scattering angle. For the system used in these investigations, the correction is such that a constant intensity is not affected by the slit height; hence, the gas data were not "unsmeared." Both the clay and the Ludox curves were corrected for slit height effects. The use of finite slit widths also introduces some error in the scattering curves. In this work no correction was made

[17] H. D. Bale and P. W. Schmidt, J. Phys. Chem. **62**, 1179 (1958).

[18] P. W. Schmidt and R. Hight, Jr., Acta Cryst. (to be published).

for this effect since the error is generally less than the statistical error.

Another effect which can introduce errors is that of interparticle interference. This effect is most noticeable at the smaller angles and for monodisperse systems.[19] The fact that the scattering curves for the clay suspensions were proportional to the concentration indicated that interparticle interference was negligible in the angular region examined. The scattering curves from the Ludox colloidal silica indicated that interparticle interference was present for concentrations greater than about 3%. The correction was found by diluting the Ludox with known amounts of distilled water until further dilution had no effect on the shape of the scattering curve at the smallest observed scattering angles. It was then assumed that this shape was the shape one would find for the more concentrated solutions in the absence of interparticle interference.

There is also the possibility that the clay particles may tend to orient themselves in some preferred direction in the thin sample holders. To investigate this effect, four measurements of the scattering from the same sample were made, one with the sample holder in its normal position perpendicular to the x-ray beam, and three others with the sample rotated approximately 10° from the normal position, in each of three mutually perpendicular planes. As no difference in either the shape or the intensity was observed, the orientation effect on the scattering curve was considered negligible.

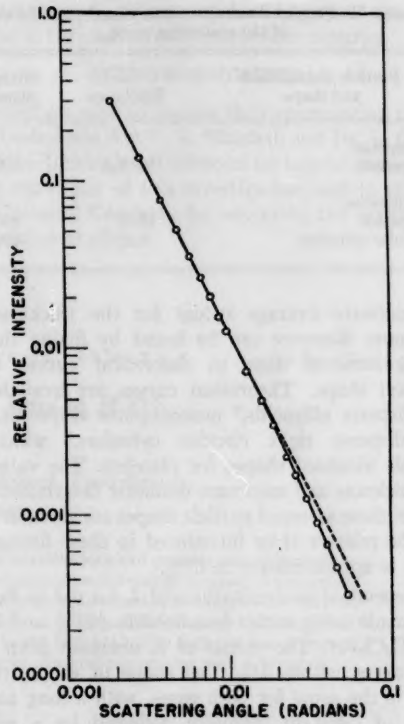

FIG. 1. Scattering from 2% Na^+ Wyoming Bentonite, R_5 centrifuge fraction. Dotted line is an inverse-square curve. Open circles represent the slit-height-corrected experimental curve.

RESULTS AND DISCUSSION

The R_3 and R_5 centrifuge fractions were studied, each at concentrations of 0.5% and 2%. Within experimental error, both centrifuge fractions gave identical scattering patterns at a given concentration, and the scattering was found to be proportional to the concentration. Figure 1 shows the scattering curve for the 2% R_5 sample. As the scattering from the other three samples was essentially equivalent, only one curve is shown.

The fact that the scattered intensity is proportional to the concentration means that in the angular range in which measurements were made, interactions between particles do not affect the scattering curve, and consequently, the theory of scattering from dilute solutions can legitimately be applied in analyzing the data.

The result that the scattering is the same for different centrifuge fractions at first seems somewhat paradoxical, since one ordinarily thinks that the centrifuge separates particles of different sizes, and that different sizes of particles give different scattering patterns. The observed curves, however, are actually what one would expect for thin platelets of identical thickness. As Eq. (1) shows, in the angular region where the intensity is proportional to h^{-2}, at a given concentration the scattered intensity is determined only by the platelet thickness and is independent of the large dimensions of the platelet. Also, the location of the angular region where the transition from inverse second to inverse fourth power scattering occurs is unaffected by the large dimensions of the particles. The scattering data therefore indicate that the clay particles have roughly the same thickness, with the different centrifuge fractions containing particles which differ only in their large dimensions.

In the preparations we have studied, the shape of the scattering curve is the same for all concentrations, and so there is no scattering evidence that the average platelet thickness changes with concentration.

If the thickness of a platelet particle is to be found from the shape of the scattering curve, the plot of the logarithm of the unsmeared intensity I vs the logarithm of the scattering angle ϕ must have a relatively long region in which the slope is equal to -2, followed by a region where the slope is steeper than -2. For the determination of the large dimension of the platelet, there should be an angular region, at relatively small angles, where the intensity decreases less rapidly than with the inverse square of the angle. As such a region does not occur in Fig. 1, we can determine only an approximate lower limit to the platelet diameter.

[19] Reference 9, p. 70.

TABLE II. Platelet dimensions determined from the shape of the scattering curve.

Particle distribution and shape	Thickness	Minimum diameter
Polydisperse:		
Ellipsoids	12.0 A	800 A
Monodisperse:		
Ellipsoids	10.8	500
Circular cylinders	8.3	400

Approximate average values for the thickness and minimum diameter can be found by fitting the slit-height-corrected data to theoretical curves of an assumed shape. Theoretical curves are available for polydisperse ellipsoids,[8] monodisperse ellipsoids,[6] and monodisperse right circular cylinders,[9] which are possible idealized shapes for platelets. The values for the thickness and minimum diameter determined from each of these assumed particle shapes are given in Table II. The relative error introduced in these fitting processes is approximately $\pm 10\%$.

Independent determinations of I_e for use in Eq. (1) were made using sulfur hexafluoride (SF_6) and Freon 114 ($C_2Cl_2F_4$). The values of I_e obtained from these gases agree within 4%. The shape of the scattering curve is the same for both gases, with a long angular region of constant intensity, followed by a gradual decrease in intensity for angles greater than about 0.06 rad. The region of constant intensity makes the extrapolation to the zero angle intensity a relatively easy matter. The scattering curve for SF_6 had the same shape as the curve obtained by Katz[7] for the same gas. Since there are several sources of error, which give a total error of about $\pm 10\%$, the close agreement between the values of I_e would seem to be fortuitous.

I_e was also determined by measuring the scattering from Ludox colloidal silica. The scattering curves obtained from these studies agree with the results obtained by Bragg.[20] The value of I_e found from the Ludox data agrees within 20% with the results from the gas scattering. This agreement is considered within experimental accuracy, since the value for the total surface area S of the Ludox is difficult to determine and easily could be in error by 20%. The Ludox data can be considered as a check on the order of magnitude of I_e, but not on its exact value.

The ratio (σ/d) is the number of electrons per gram of the platelet, and depends only on the chemical composition of the clay. Substitution of this ratio and I_e in Eq. (1) gives a value for σ, the number of electrons per square angstrom. When (1) is corrected for the fact that the particles are in water and not in vacuum, σ is found to be 7.6×10^{16} electrons/A^2. From the values of σ, (σ/d), and the density ρ of the platelet, the platelet thickness is found to be 9.0 A. From σ one can also determine the pass per unit area of the unit cell. The result of this calculation is 15.3 mass units/A^2. This latter value agrees with the value of 15.6 determined in the light scattering experiments of M'Ewen and Pratt.[5]

Although fitting the experimental scattering curves to theoretical scattering curves offers no experimental difficulties, there is the disadvantage that a reasonable model must be chosen to approximate the shape of the actual scatterer. The results given in Table II should be considered as essentially equivalent. The polydisperse ellipsoid model gives the most questionable results, since there is a certain amount of arbitrariness in choosing an average radius[8] in the calculation of the theoretical curves. Because of this, no significance should be placed on the difference between the values obtained for the polydisperse model and the monodisperse models. The results from the monodisperse models should be considered as practically equivalent, since the volume computed for each model is nearly the same.

In the determination of the platelet thickness from the absolute scattered intensity, no assumption about the shape of the platelet is made except that it has a uniform electron density and is thin. The measurement of I_e experimentally, however, requires careful work. Heavy gases can be used for this determination, but they are relatively weak scatterers. The low intensity problem can be avoided by using some high-scattering spherical system such as Ludox; however, the calculations are more complex and require knowledge of the total surface area S which is itself hard to determine. Despite the low scattering, the gas scattering gives the most reliable results.

Since the thickness determined by each of the methods above is essentially an average value, we have no direct evidence that the platelets are of uniform thickness. However, the thickness of the crystallographic unit cell c dimension is 9.6 A, hence one would not expect to find particles any thinner than this value. Also, if there were particles thicker than one unit cell, they would be expected to be integral multiples of the c dimension. Such particles, if present in large numbers, would affect the scattering curves appreciably. Since the average value for the thickness, determined by small angle scattering, is approximately equal to the unit cell c dimension, a large fraction of the platelets must be one unit cell thick.

If, instead of being independent platelets one unit cell layer thick, the clay particles consisted of two or more crystallographic layers bound rigidly together, with 8 to 10 A water between the layers, an entirely different scattering pattern would be observed. When the particles consist of several layers, the transition from inverse square to inverse fourth power scattering would occur at a smaller angle than for single-layer particles,

[20] R. H. Bragg, Armour Research Foundation, private communication.

because in the former case the particles are thicker. Also, the effective value of σ, the number of electrons per unit area of the platelet, used in (1) would be greater for a multilayer particle than for a particle consisting of a single layer. As an experimental test of these ideas, the scattering was measured from a sample of calcium montmorillonite, for which the particles are considered to be several unit cell layers thick. As would be expected, the resulting scattering curve indicated that the clay particles in the calcium montmorillonite had an average thickness considerably greater than the particles in the sodium montmorillonite samples.

ACKNOWLEDGMENTS

The authors wish to express their appreciation to Dr. K. B. Deshpande, Dr. C. E. Marshall and Dr. B. Goodman of the University of Missouri for helpful discussions during the course of this investigation, and to the Du Pont Chemical Company for supplying the samples of Ludox colloidal silica.

THE JOURNAL OF CHEMICAL PHYSICS VOLUME 33, NUMBER 6 DECEMBER, 1960

Excitation and Negative Ions in H_2O†

G. J. SCHULZ

Westinghouse Research Laboratories, Pittsburgh, Pennsylvania

(Received April 4, 1960)

By combining the trapped-electron method with the study of negative ions and positive ions, it is possible to obtain data which can be used for construction of an approximate potential energy diagram of molecules. The experimental methods used are described and the H_2O molecule is discussed. The negative ion current peaks at 6.5±0.1 and 8.8±0.1 ev. Kinetic energy measurements on the negative ions show that the latter peak is associated with the same state at infinite separation as the first peak. The inelastic loss processes are essentially in agreement with optical absorption experiments. An inelastic process with a threshold at about 3.4 ev is observed.

THE energy loss suffered by electrons passing through a molecular gas is studied by the trapped-electron method and the negative ion formation by conventional techniques. The experimental procedure of the trapped-electron method and the results obtained by this technique for atomic gases (helium and mercury) as well as a simple molecular gas (hydrogen) are described in a previous publication.[1] As an example of these combined techniques, the results for the H_2O molecule are presented. The reader is referred to footnote 1 for a description of the experimental details; a brief review of the pertinent considerations is given in the following section.

I. REVIEW OF THE TRAPPED-ELECTRON METHOD

The aim of the trapped-electron method is the separation of those electrons in a beam which have suffered an energy loss (by inelastic collisions with an atom or a molecule) and subsequent collection of these electrons on a separate collector. Figure 1 shows a schematic diagram of the tube and the amplifying and recording system. The tube is almost identical to that described in footnote 1 while the recording system is in many respects an improvement over previously described methods and will be described in the next section. An electron beam from the thoriated iridium filament F is aligned by a magnetic field B and traverses the electron gun (only the retarding plate P_2 is shown in Fig. 1) and the collision chamber and is collected on the electron collector E. The electron gun employs the retarding potential difference method[2] so that the effect of a nearly monoenergetic slice of electrons can be measured. The cylindrical grid G is surrounded by the cylindrical collector M. When measuring trapped electrons, the potential on M is 22 v positive with respect to G, of which 0.3 v penetrates to the axis of the tube. Thus, the well depth (potential difference between the axis of the tube and the grid) is 0.3 v. This value is determined by measuring the shift of the electron retarding curve when a negative potential of 22 v is applied between M and G.[3]

Electrons in the beam which have made an inelastic collision and whose residual energy is between zero and 0.3 ev are trapped in the potential well and are collected at the collector M. The current reaching M is called the "trapped-electron current" (also referred to as "current

† This work has been supported in part by the Office of Naval Research.

[1] G. J. Schulz, Phys. Rev. **112**, 150 (1958).

[2] R. E. Fox, W. M. Hickam, D. J. Grove, and T. Kjeldaas, Rev. Sci. Instr. **26**, 1101 (1955). See also footnote reference 1. The total width of the electron energy distribution, using freshly gold plated electrodes is of the order of 0.1 ev. However, the width slowly broadens as the electrodes are exposed to H_2O. After about 50 hr of operation in H_2O, the width deteriorates to about 0.5 ev.

[3] G. J. Schulz, Phys. Rev. **116**, 1141 (1959).

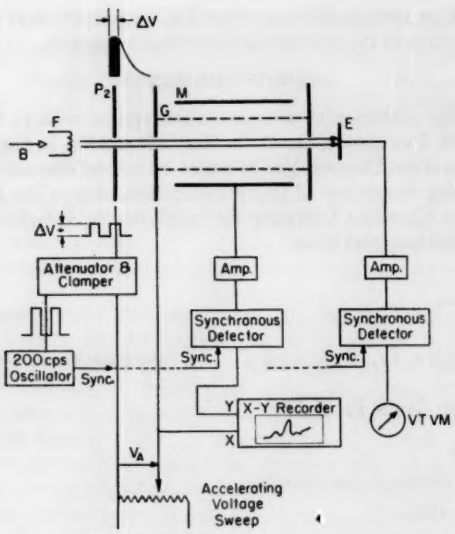

FIG. 1. Schematic diagram of tube with associated circuit.

of slow electrons" in footnote 1). The energy scale is calibrated by retarding the electron beam between the retarding plate P_2 and the collision chamber (the potential difference between P_2 and the collision chamber is V_A in Fig. 1), and collecting the unretarded fraction of the beam current on the electron collector which is kept several volts positive with respect to the collision chamber. From a plot of the electron current vs V_A, one obtains the distribution of electrons entering the collision chamber.[4] The width of this distribution is of the order of 0.1 ev.[2] The energy scale thus established usually agrees with a known positive ion onset to an accuracy better than 0.1 v. (See Fig. 8.)

There are four types of processes which lead to a current arriving at the collector M:

(1) Trapping of electrons due to the excitation of electronic states of the molecule.

(2) Trapping of electrons due to the excitation of vibrational states. This process can occur via an intermediate temporary negative-ion state[3] which decays into a vibrationally excited state of the molecule plus an electron. This process has been previously observed for N_2,[3] CO,[3] and N_2O,[5] and it is characterized by a large cross section in an energy range far above the threshold for vibrational excitation of the first vibrational level. The threshold behavior of vibrational excitation has not yet been detected by the trapped-electron method.

(3) Formation of negative ions which reach the collector in addition to the trapped-electron current. It is possible to measure the negative ion current separately by decreasing the potential between M and G to zero (or $\sim$2 v) such that no trapping occurs and the negative ions reach the collector separately. This procedure has to be applied to the interpretation of the results in the electronegative gases.

(4) Trapping of electrons due to elastic scattering at or near zero accelerating voltage. This effect can be explained by considering that the electrons, after an elastic collision, have essentially an isotropic angular distribution. Thus, at low energies, most of the elastically scattered electrons have a component of velocity in the axial direction which is not sufficient to escape from the trap. Near zero accelerating voltage, it takes a very improbable subsequent collision to direct the velocity in exactly the axial direction so that the electron can escape. At higher energies, the escape cone becomes larger and the trapped-electron current due to elastic scattering disappears. Thus, the curves of trapped-electron current vs accelerating voltage are plotted starting at about 1 ev, so as to exclude the elastically scattered contribution.

II. INSTRUMENTATION FOR RECORDING OF TRAPPED-ELECTRON DATA

In some gases, it is difficult to keep the filament emission steady for prolonged times and, therefore, a system was devised to record data faster than is possible conventionally when using the retarding potential difference method. The retarding potential difference method requires that the potential of the retarding plate (P_2 in Fig. 1) be changed by about 0.1 v, and that the difference between the two currents arriving at M be read. This difference in current results from a slice of electrons in the voltage interval, ΔV, as indicated schematically on the left upper part of Fig. 1. A square wave at a frequency of about 200 cps and amplitude, 0.05–0.1 v, is applied through a clamper to plate P_2. The current at M (trapped-electron current or negative or positive ion current) and at E (electron beam current) is amplified[6] and synchronously detected. The synchronous detectors are synchronized to the 200-cps signal. The accelerating voltage V_A is swept by a motor driven helipot which also supplies the x sweep of the x-y recorder. The y signal is supplied by the output of the synchronous detector from M. Thus, it is possible to record a trapped-electron curve from 0 to 20 v in about 30 sec. A photoreproduction of a typical trace is shown in Fig. 2. It represents the negative-ion formation in water vapor. Other data are presented as line drawings, with the noise averaged. The data of electron beam current vs accelerating voltage can also be exhibited on the x-y recorder by using the output of the synchronous

[4] For processes in which all the electrons in the distribution are involved, the peak of the electron distribution is usually taken as a reference for the electron energy scale. For processes which depend only on the high-energy portion of the electron distribution (as is the case for a threshold process), the high-energy cutoff of the distribution is taken as the reference.

[5] G. J. Schulz (to be published).

[6] The design of the low-noise preamplifier is identical to that used by D. S. Burch and S. Smith, at the National Bureau of Standards (private communication).

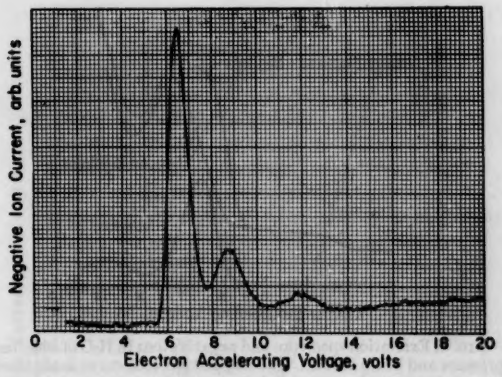

FIG. 2. Negative ions in H_2O. The curve is a reproduction of the trace on the $x-y$ recorder. The peaks of H^- occur at 6.5 ± 0.1 and 8.8 ± 0.1. The peak at 12.0 ev is believed to be the O^- ion. Add 0.02 v to the accelerating voltage to obtain the electron energy.

detector from E for the y sweep. The latter connection is used for plotting electron retarding curves.

III. NEGATIVE IONS

It is known that negative ions are produced in H_2O by electron impact. Lozier[7] reported peaks in negative ion current at 6.6 and 8.8 ev. Mann, Hustrulid, and Tate[8] studied the production of negative ions from H_2O in a mass spectrometer and found H^- peaks at 7.1 ± 0.5 ev and 8.9 ± 0.5 ev, and O^- peaks coinciding with the second peak of H^-, and also O^- peaks in the 10–12 ev range. The relative abundance of H^- and O^- at 8.9 ev cannot be determined from a mass spectrometer experiment because the kinetic energy of the H^- and O^- at 8.9 ev is different, leading to discrimination against high-energy ions in a mass spectrometer.[9] The present experiment indicates that it is predominantly H^- that contributes to the peak at 8.9 ev. Buchelnikova,[10] using essentially monoenergetic electrons, found the peaks at 6.4 ev and 8.6 ev. The present experiment (see Fig. 2) shows peaks at 6.5 ± 0.1 and 8.8 ev in excellent agreement with previous work. The third rather broad peak in Fig. 2 occurs at 12.0 ev, and can be interpreted as production of O^- from H_2O. The present experiment shows that the O^- yield at 12 ev is much smaller than the maximum H^- yield.

The kinetic energy of the negative ions is measured by retarding the ions between the grid and the collector, keeping the electron energy fixed. Figure 3 shows two typical ion-retarding curves taken at electron energies of 7.0 and 8.8 ev, respectively. The former is typical of the shape of the retarding curves in the energy range of the first peak of Fig. 2, the latter for the energy range of the second peak. The kinetic energy is obtained by linear extrapolation to the "zero" of the curve and is indicated by the arrows. The 7.0-ev curve is typical of curves obtained with the present tube for simple dissociative attachment, when the angular distribution of ions is isotropic, thus giving a straight line retarding plot. The 8.8-ev curve is surprising since we would have expected that the second peak of Fig. 2 resulted from a process, such as $H_2O+e\rightarrow H^-+OH^*$, where the OH radical is left in an excited state. This process results in low-energy ions (approximately 0.30 ev at an electron energy of 8.8 ev if the first electronic level of OH is excited). In view of the large ion kinetic energy at 8.8 ev, this cannot be the predominant process. However, the shape of the 8.8-ev curve (with a hump at 0.8 v) makes it probable that low-energy ions are actually contributing to the retarding curve below a retarding voltage of 0.8 v. These low-energy ions could result from the reaction, $H_2O+e\rightarrow H^-+OH^*$, or from a reaction leading to O^-.

Another method for obtaining the kinetic energy of the negative ions is the study of the "appearance potential" of the negative-ion current with the ion retarding potential as a parameter.[11] The "onset" of the curve of negative-ion current vs electron energy is affected by the fastest electrons in the distribution. This is taken into account by determining the energy of the appearance from the high-energy tail of the electron distribution.[12]

Further insight into the processes involved can be gained from an examination of Fig. 4. There the kinetic energy is plotted against electron energy. The open points are obtained from ion-retarding curves similar to those shown in Fig. 3. The closed points are obtained

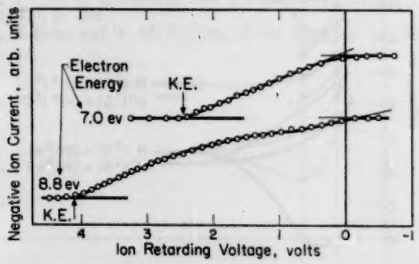

FIG. 3. Two typical ion-retarding curves. The zero of the two curves is displaced. The maximum kinetic energy of the ions is indicated by the arrows. The top curve is typical of simple dissociative attachment. The structure of the bottom curve indicates that ions with various amounts of kinetic energy are present.

[7] W. W. Lozier, Phys. Rev. **36**, 1417 (1930).

[8] M. M. Mann, A. Hustrulid, and J. T. Tate, Phys. Rev. **58**, 340 (1940).

[9] C. E. Berry, Phys. Rev. **78**, 597 (1950). The kinetic energy of H^- ions at an electron energy of 8.9 ev is 4.2 ev; whereas the kinetic energy of the O^- ion at 8.9 ev is of the order of 0.2 ev assuming the process $H_2O+e\rightarrow 2H+O^-$ postulated in footnote reference 8. Because of the high kinetic energy of the H^- ions, the production of H^- is strongly underestimated in a mass spectrometer.

[10] I. S. Buchelnikova, Zhur. Eksptl. i Teoret. Fiz. **35**, 1119 (1958), translation, Soviet Phys. JETP **35**, 783 (1959).

[11] W. W. Lozier, Phys. Rev. **46**, 268 (1934).

[12] When determining the energy at which a peak of a curve occurs, the energy scale is usually obtained from the peak of the electron distribution.

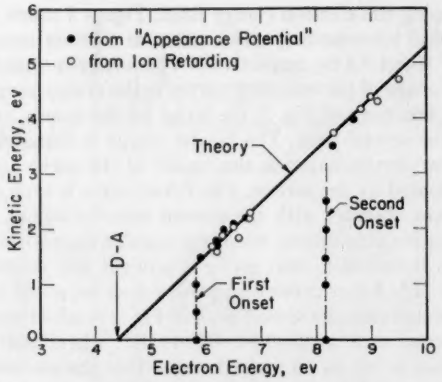

FIG. 4. Kinetic energy vs electron energy of H^- ions from H_2O. The open circles are obtained from the curves of Fig. 3 and similar curves not shown. The closed circles are obtained from the shift in the appearance potential of the negative ion current. The line marked "theory" is drawn with the theoretical slope (17/18) intersecting the axis at the accepted value of $D-A$ (4.4 ev).

from the appearance potential at a particular ion-retarding potential. The line marked "theory" is plotted assuming the reaction $H_2O+e \rightarrow H^-+OH$. The slope on a plot of kinetic energy vs electron energy appropriate to this reaction is 17/18, and the intercept is equal to D−A, the difference between the dissociation energy and the affinity equal to $5.11-0.74=4.4$ ev. All points are on this single line, indicating that the products of the negative ion formation are the same at infinite internuclear separation, regardless of electron energy, and that the same species of negative ions is produced in the whole range of electron energies. It is believed, however, that above an electron energy of approximately 8 ev there exist, in addition, low-energy negative ions. Figure 5 shows how these observations can be catalogued on the basis of a potential energy diagram. The two repulsive curves leading to $H^-(^1S)+OH(^2\pi)$ at infinite separation may differ from each other in the symmetry of the intermediate state as discussed by Laidler[13] and by Schuler.[14] The remaining features of Fig. 5 are discussed in the next section.

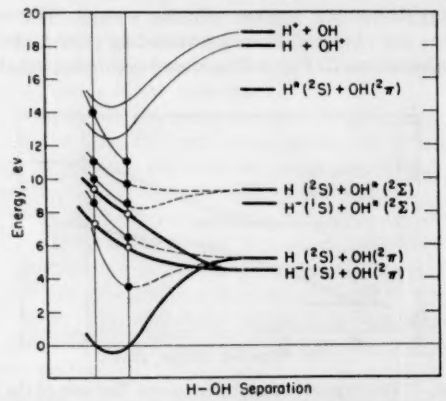

FIG. 5. Hypothetical energy level diagram of H_2O. The intercepts of the potential curves with the Franck-Condon region are obtained from the data of Fig. 2 for negative-ion formation (open circles) and the data of Fig. 7 for excitation (solid points). The shape of the potential curves, as well as the designations at infinite separation, are hypothetical. The diagram is presented only as a convenient way to catalog the results of the present experiment.

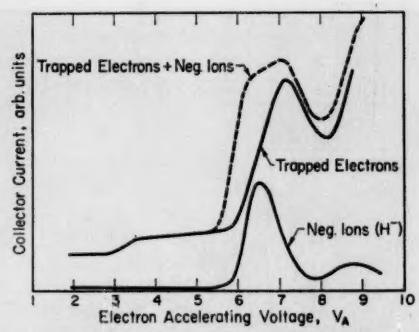

FIG. 6. Excitation spectrum and negative ions in H_2O at identical pressure and beam current. The trapped electron curve is obtained by substracting the negative ion current from the experimental curve (dashed) as described in the text. The ordinates of the two curves are displaced for clarity.

IV. EXCITATION

Figure 6 shows experimental results for the trapped-electron current and negative ion current vs electron accelerating voltage. The top curve (partially dashed) is obtained with a well depth of 0.3 v, and thus includes both the trapped electrons and negative ions. The bottom curve is obtained with practically zero well depth, and thus includes only negative ions.[15] Since the two curves are taken at identical pressures and electron beam currents, one can subtract the bottom curve from the top curve after shifting the top curve by 0.3 v to the right. This shift results from the fact that the well

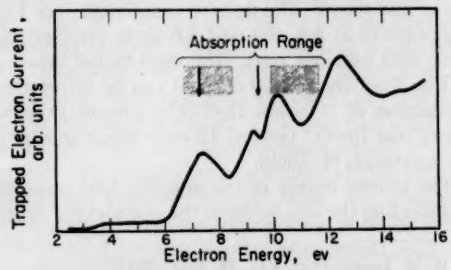

FIG. 7. Excitation spectrum of H_2O up to 15 ev.

[13] K. J. Laidler, J. Chem. Phys. **22**, 1740 (1954).
[14] K. E. Schuler, J. Chem. Phys. **21**, 624 (1953).
[15] The negative ion current arriving at the collector is independent of the drawout voltage in the range 0 to 10 v. At higher voltages, the trapped-electron current adds to the negative ion current and makes an independent determination of the negative ions impossible. It is assumed that the negative ion current remains independent of drawout potential beyond 10 v.

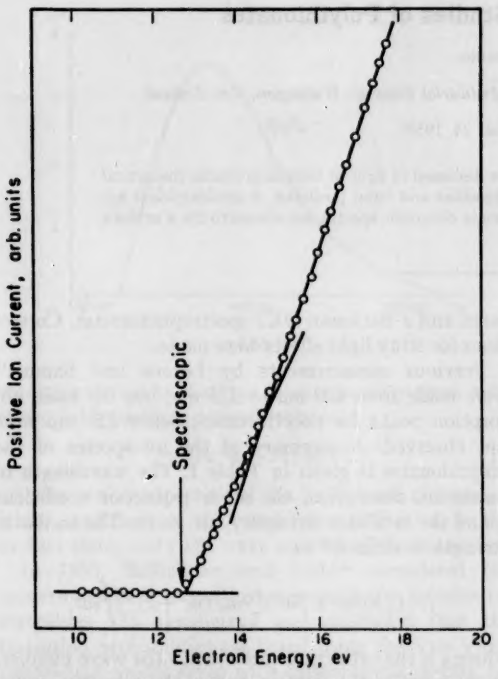

FIG. 8. Formation of positive ions in H_2O near threshold. The spectroscopic value of the onset is 12.61 ev. The break in the curve occurs at 1.9±0.3 ev above the threshold.

accelerates the beam electrons by an additional 0.3 ev. After this subtraction, the true trapped-electron curve is obtained. This curve gives the energy at which the potential curve of the respective electronically excited state traverses the Franck-Condon region.[16] The trapped-electron curve is extended to higher energies in Fig. 7. The rise of the trapped electron-electron curve at 3.4 ev is reproducible and indicates the onset of an energy-loss process which has not been observed previously. The data of Fig. 7 can be correlated with optical absorption data in the vacuum ultraviolet. Watanabe and Zelikoff[17] find absorption peaks at 7.3 ev and 9.5 ev (indicated by the arrows in Fig. 7) and further absorption in the energy range 9.9–11.8 ev (shaded area in Fig. 7). By comparison, the trapped-electron peaks occur at 7.3 ev, 9.2 ev, 10.1 ev, and 12.4 ev. However, the 9.2-ev value could be in error because the position of this peak may be influenced by the neighboring process. It is possible to use the data obtained by the trapped-electron method for construction a Franck-Condon diagram purely from experimental data. Such an attempt is shown in Fig. 5 following the suggestion of Laidler[13] that the energy be plotted against H–OH internuclear separation. The shape of the curves is hypothetical as are the designations at infinite separation.

Figure 8 shows the threshold behavior of the positive ion current from its onset to about 5 ev above onset. The positive ion produced is probably H_2O^+. The energy scale is established from electron retarding. The onset of the curve (12.7 ±0.1 ev) is in good agreement with the spectroscopic value (12.61 ev).[18] It seems that the curve can be approximated by two linear segments with a break occurring at 1.9 ±0.3 ev above onset in excellent agreement with Price and Sugden,[19] who also found a break in the positive ion curve 1.9 ev above onset. The two positive-ion states of Fig. 5 are drawn to conform to this observation.

V. ACKNOWLEDGMENTS

The author wishes to thank the members of the atomic physics group of the Westinghouse Research Laboratories for many helpful discussions. Especially, thanks are due to A. V. Phelps. The author is indebted to W. Uhlig and H. Garstka for help in the design and construction of the tube, and to J. Kearney for technical assistance.

[16] H. D. Hagstrum and J. T. Tate, Phys. Rev. **59**, 354 (1941).

[17] K. Watanabe and M. Zelikoff, J. Opt. Soc. Am. **43**, 753 (1953).

[18] F. H. Field and J. L. Franklin, *Electron Impact Phenomena and the Properties of Gaseous Ions* (Academic Press, Inc., New York, 1957), p. 280.

[19] W. C. Price and T. M. Sugden, Trans. Faraday Soc. **44**, 108 (1948).

Ultraviolet and Structural Studies of Polythionates

R. M. GOLDING

Dominion Laboratory, Department of Scientific and Industrial Research, Wellington, New Zealand

(Received September 24, 1959)

The ultraviolet spectral results of the polythionates are discussed in light of various available theoretical approaches in evaluating inorganic complex spectral intensities and band positions. A semiempirical approach shows that the oscillator strengths of the polythionate electronic spectra are related to the π orbitals of the sulfur chain.

SINCE Blomstrand[1] and Mendeleyeff[2] first postulated the structure of the polythionates as straight-chain sulfur atoms, much work has been done in an attempt to confirm these structures. Recent x-ray crystallographic results of potassium barium hexathionate[3] show that the sulfur atoms are in unbranched and nonplanar chains. Results of chemical investigations such as of reactivity[4] and exchange reactions[5] have supported the sulfur-chain postulate and include evidence for two SO_3^- units.

Physical measurements such as x-ray emission,[6] Raman,[7] infrared, uv and x-ray diffraction[8] have been made, but the interpretation of the results and correlation with the polythionate structures is difficult. Interpretation of uv spectra of the polythionates given in this paper supports the sulfur-chain structures.

The polythionates were prepared as outlined in *Handbuch der Praparative Anorganischen Chemie*[9] and analyzed by the methods developed by Kurtenacker.[10]

EXPERIMENTAL

The uv spectra of the polythionates were measured with a Beckman DU with the photo-multiplier attachment and a Beckman DK2 spectrophotometer. Corrections for stray light effects were made.

TABLE I.

Compound	λ max	log ϵ max	f
$S_2O_6^{2-}$	no spectrum		
$S_3O_6^{2-}$	$\approx$195 mμ		0.0011
$S_4O_6^{2-}$	216.0 (Fig. 1)	3.85	0.115
$S_5O_6^{2-}$	214.0 (Fig. 2)	3.92	0.130
$S_6O_6^{2-}$	217.0 (Fig. 3)	4.19	0.200

Previous measurements by Lorenz and Samuel[11] were made from 400 mμ to 225 mμ, but the main absorption peaks for polythionates, below 225 mμ were not observed. A summary of the uv spectra of the polythionates is given in Table I. The wavelength of maximum absorption, the molar extinction coefficient ϵ, and the oscillator strength f, are given. The oscillator strength is defined[12] as

$$f=(2303m/\pi\,\mathrm{Ne}^2)[9n_0/(n_0^2+2)^2]\int\epsilon d\bar{\nu},$$

where ϵ is the extinction coefficient, $\bar{\nu}$ the wave number, m the mass of the electron and n_0 the refractive index of the medium in which the absorbing molecules are dissolved. For water solutions,

$$f=3.64\times10^{-9}\int\epsilon d\bar{\nu}.$$

DISCUSSION

From the spectral results of the polythionates the oscillator strengths increase to 10^{-1} from $S_2O_6^{2-}$ to $S_6O_6^{2-}$, whereas the wavelength maxima are in the same region. Figures 1–3 give the spectra for tetra-, penta-, and hexathionate. As a starting point in the discussion, the polythionates shall be considered as straight-chain sulfur atoms with a thionate group at both ends of the chain. Wolfsberg and Helmholz[13] calculated, using a semiempirical approach, the electronic spectra of XO_4 type compounds of symmetry T_d, namely MnO_4^-, CrO_4^{2-} and ClO_4^-. Later[14] they considered similar compounds of C_{3v} and C_{2v} symmetry using the same approach. Briefly, this considered only $3d$, $4s$, and $4p$ atomic orbitals of the oxygen atoms in constructing the molecular orbitals using the LCAO molecular orbital method. The transition probability was calculated using the approximation that it was the coefficient of the oxygen π orbital in the first excited l_2 orbital. The

[1] C. W. Blomstrand, Chemie Jetzyeit, 157 (1869); Ber. German Chem. Soc. **3**, 957 (1870).
[2] D. I. Mendeleyeff, J. Russ. Phys-Chem. Soc. **2**, 276 (1870); **3**, 871 (1871); Ber. German Chem. Soc. **3**, 870 (1970).
[3] O. Foss, A. Hordvik, and K. Palmork, Acta Chem. Scand. **12**, 1339 (1958).
[4] O. Foss, Kgl. Norske Videnskab. Selskabs, Skrifter **2** (1945).
[5] J. A. Christiansen and W. Drost-Hansen, Nature **164**, 759 (1949).
[6] M. Goehring, FIAT Rev. Ger. Sci., Inorganic Chemistry I **1946**, 132.
[7] M. Eucken and J. Wagner, Acta Phys. Austriaca **I**, 339 (1948).
[8] This laboratory (unpublished).
[9] F. Feher in *Handbuch der Praparative Anorganischen Chemie*, edited by G. Braver (Stuttgart, 1951–54).
[10] A. Kurtenacker, *Analytische Chemie der Sauerstoffsauren des Schmefels*, edited by W. Bottger (Enke, Stuttgart, 1938), Vol. 38.
[11] L. Lorenz and R. Samuel. Z. Phys. Chem. **B14**, 218 (1932).
[12] N. Q. Ohako, J. Chem. Phys. **2**, 645 (1934).
[13] M. Wolfsberg and L. Helmholz, J. Chem. Phys. **20**, 837 (1952).
[14] L. Helmholz, H. Brennan, and M. Wolfsberg, J. Chem. Phys. **23**, 857 (1955).

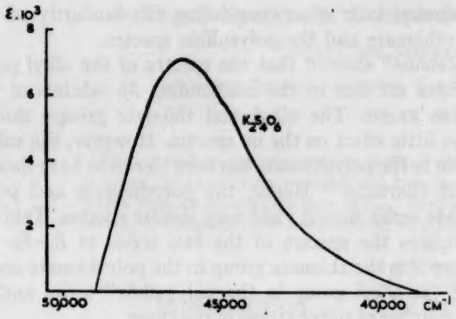

FIG. 1.

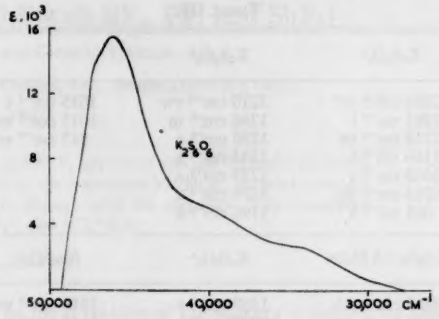

FIG. 3.

oscillator strengths of all the three symmetry cases were evaluated from their derived formula

$$f=(8\pi^2mc\bar{\nu}/3h)3d^2k^2, \qquad (1)$$

where d is the projection of the S—O bond distance, k is the coefficient of the π-orbital contribution in the excited state, and $\bar{\nu}$ the wave number of the transition.

In 1958, Ballhausen and Liehr[15] considered the modern available theoretical approaches for tetrahedral complexes (T_d symmetry) and concluded that the transition probabilities predicted using the Van Vleck ligand-field model agree with experimental results for labile complex ions. However, introduction of ligand π molecular orbitals must be considered for staple complex ions. For the transition

$$t_1(\pi)\rightarrow t_2(\sigma,\pi); \quad f(^1A_1\rightarrow{}^1T_2)=2g^2C^2\cdot 8\pi^2mc\bar{\nu}/3h, \quad (2)$$

where g is the "full σ-bond covalency" for the $t_2(\sigma,\pi)$ and C the ligand coupling constant. The latter approach is considered the more correct theoretical treatment of tetrahedral complexes. Since the methods available to calculate the energy levels require a number of approximations in the wave functions and the integrals, a more detailed study at present is not warranted. However, the method and discussions employed by Wolfsberg *et al.* show that SO_4^{2-} ion is analogous to the ClO_4^- ion and will have one main absorption band in the ultraviolet region. Consider one of the oxygen atoms replaced by a sulfur atom giving a symmetry of C_{3v}. By changing the symmetry from T_d to C_{3v} the irreducible representations are changed as shown in Table II, where U breaks into AE but the final analysis is the same.

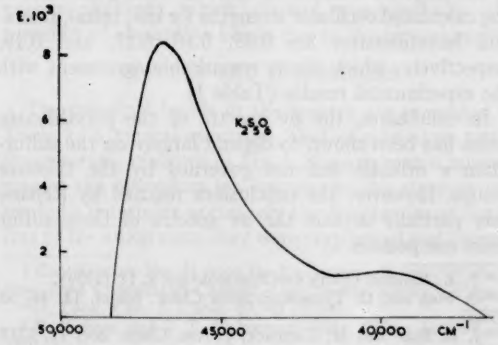

FIG. 2.

[15] C. J. Ballhausen and A. D. Liehr, J. Mol. Spectroscopy **2**, 342 (1958).

Therefore, we would expect similar diagrams for SO_4^{2-} and $S_2O_3^{2-}$ and this is observed in the spectra (one main band in the ultraviolet). Consider the series of molecules $^-O_3S-S_n-SO_3^-$, where $n=1-4$. Each thionate group may be considered as independent and hence the type of molecule could be reduced to $X-SO_3^-$, where X is a "modified" sulphur group, and once again the energy diagram will be similar to SO_4^{2-} although the character of X will effect the position of the single band in the ultraviolet. This is observed; and to gain an insight of the S—O bond in the thionate group consider the infrared data for the polythionate series (Table III).

All the polythionates give a basic infrared spectrum; a series of strong peaks near 1230 cm^{-1}, 1030 cm^{-1}, and a medium band near 645 cm^{-1}. The peaks at 3363 cm^{-1} and 1634 cm^{-1} are due to the water molecule as in $K_2S_5O_6$ 1.5 H_2O.

To assign the vibrational frequencies to the main bands of the polythionate spectra, the structure will be considered as $O_3S-S_n-SO_3$, where $n=1$–4. A symmetrical top molecule of the form SO_3 will have six frequencies but ν_2 and ν_4 are doubly degenerate hence four frequencies will be observed.

The symmetrical top group $S-SO_3$ will have a couple of additional frequencies ν_5 and ν_6 due to the additional S atom, but the assignment of ν_1, ν_2, ν_3, and ν_4 will be the same for the SO_3 molecule.

TABLE II.

Symmetry	Compound	Bonds MO's	Bonds AO's	Bonds
T_d	SO_4^{2-}	a.u.	sp^3, sd^3, fp^3	ETU
C_{3v}	$S-SO_3^{2-}$	A^3E	sp^3, sp^2d, dp^2	ABE^3

TABLE III.

$K_2S_2O_6$[a]	$K_2S_4O_6$[a]	
2205 cm^{-1} m[b]	2210 cm^{-1} vw	1035 cm^{-1} s
1291 cm^{-1} i	1266 cm^{-1} m	1015 cm^{-1} vs
1213 cm^{-1} vs	1256 cm^{-1} s	645 cm^{-1} m
1166 cm^{-1} i	1243 cm^{-1} s	
1045 cm^{-1} s	1223 cm^{-1} s	
1014 cm^{-1} vs	1208 cm^{-1} s	
661 cm^{-1} s	1196 cm^{-1} s	
$K_2S_3O_6$ 1.5 H_2O[a]	$K_2S_6O_6$[a]	Na_2SO_3[c]
3363 cm^{-1} mb	1259 cm^{-1} s	1215 cm^{-1} vw
1634 cm^{-1} wb	1239 cm^{-1} s	1135 cm^{-1} w
1233 cm^{-1} s	1215 cm^{-1} vs	965 cm^{-1} vs; b
1216 cm^{-1} vs	1038 cm^{-1} s	634 cm^{-1} w
1032 cm^{-1} s	1026 cm^{-1} i	
1019 cm^{-1} vs	647 cm s	
637 cm^{-1} m		

[a] There was no difference between the spectra in paraffin mulls and KBr disks.
[b] V—very; w—weak; m—medium; s—strong; b—broad; i—inflexion.
[c] F. A. Miller and C. H. Wilkins, Anal. Chem. **24**, 1253 (1952).

The additional sulfur atom in $S-SO_3$ will have a small effect on ν_1 to ν_4. If a linear symmetrical molecule $O_3S-S_n-SO_3$ is considered, the frequencies ν_1 to ν_4 will be as previously described except that their degeneracies have doubled. This fact will enable some of the frequencies of the polythionates to be assigned by considering the SO_3^{2-} spectrum and its assignment.

The assignment of the SO_3 spectrum has been determined[16] as shown in Table IV, hence the assignment of the frequencies and the type of vibrations of SO_3^{2-} is given as an SO_3 analogy. From the above argument the SO_3^{2-} and the polythionate spectra may be assigned.

It can be seen that for the thionate group the S—O bond force constant remains the same for all the polythionates. Hence the S—O bond in the thionate group remains unaltered as the sulfur atoms are increased and the σ and π bonding character of the S—O bond is therefore assumed constant.

Therefore, the thionate-ligand-coupling-constant C, [Eq. (2)] and π orbital contribution, k, [Eq. (1)] will remain unaltered as the sulfur atoms are increased. Since the dithionate has no detectable spectrum, the ligand-coupling-constant must be very small. Wolfsberg *et al.* show that k is small for the sulfate molecule. Hence the ultraviolet spectra of the polythionates must not be due directly to the thionate group. This will be confirmed later after considering the similarity of the polythionate and the polysulfide spectra.

TABLE IV.

Compound	Frequencies ν_1	ν_2	ν_3	ν_4
SO_3[16]	1069 cm^{-1}	652 cm^{-1}	1330 cm^{-1}	532 cm^{-1}
SO_3^{2-}	965 cm^{-1}	634 cm^{-1}	1235 cm^{-1}	≈500 cm^{-1}
polythionates	1025 cm^{-1}	645 cm^{-1}	1225 cm^{-1}	≈500 cm^{-1}

[16] H. Gerding and L. Lecomte, Physica **6**, 737 (1939).

Rebane[17] showed that the spectra of the alkyl polysulfides are due to the nonbonding $3p$ orbitals of the sulfur atoms. The alkyl and thionate groups should have little effect on the uv spectra. However, the sulfur chain in the polythionate has been shown to have double bond character.[18] Hence, the polythionate and polysulfide series should yield very similar spectra. Table V compares the spectra of the two series as $R-S_N-R$ where R is the thionate group in the polythionate series and the alkyl group in the polysulfide[19] series and N the number of sulfur atoms in the chain.

The short wavelength peaks of the polysulfides agree quite well with the polythionate peaks and although the longer peaks are not detectable in the polythionate series, there is a broad tail with plateaus as indicated. However, the main band for both series is the one with short wavelength peaks.

TABLE V.

N	polythionate		Alkyl polysulfide[b]	
1	51 200 (3.20)[a]		50 000 (3.10)	
2	46 300 (3.85)		50 000 (3.50)	39 700 (2.63)
3	46 700 (3.92)	40,000 (3.14)	46 900 (3.87)	39 800 (3.22)
4	46 100 (4.19)	35 000 (3.46)	47 900 (4.19)	33 300 (3.39)

[a] (log ϵ is given in brackets).
[b] See footnote reference 19.

The theoretical approach developed by Rebane gives the general wavelength trend towards the longer wavelength as the number of sulfur atoms are increased in the chain. However, the spectra are only partially explained.

Considering the sulfur chain as a conjugated system analagous to conjugated carbon chains (cf. the carotenoids) the oscillator strength is given[20] as $f=(64/3\pi^2)[N^2(N+1)^2/(2N+1)^3]$ cos 37. The calculated oscillator strength for tetrathionate is 0.40 which is too large by a factor of four. However, the ratio of the calculated oscillator strengths for tri-, tetra-, penta- and hexathionates are 0.05, 0.10, 0.17, and 0.19, respectively, which shows remarkable agreement with the experimental results (Table I).

In conclusion, the uv spectra of the polythionate series has been shown to depend largely on the sulfur-chain π orbitals and not governed by the thionate groups. However, the conclusions reached by Rebane only partially explain the uv spectra of these sulfur chain compounds.

[17] T. K. Rebane, Optics and Spectroscopy **6**, 11 (1959).
[18] O. Foss and O. Tjomsland, Acta Chem. Scand. **12**, 44, 52 (1958).
[19] J. E. Baer and M. Carmack, J. Am. Chem. Soc. **71**, 1215 (1949).
[20] W. Kauzmann, *Quantum Chemistry, An Introduction* (Academic Press, Inc., New York, 1957).

Infrared Spectra of Complexes of NO_2F with BF_3, PF_5 and SbF_5†

DENYS COOK, STEPHEN J. KUHN, AND GEORGE A. OLAH

Exploratory Research Laboratory, Dow Chemical of Canada, Ltd., Sarnia, Ontario, Canada

(Received May 13, 1960)

The infrared spectra of complexes of NO_2F with BF_3, PF_5, and SbF_5 have been studied. In each case bands at about 2360 cm^{-1} were recorded and have been attributed to the nitronium ion NO_2^+. Bands consistent with a complex anion of the form MF_{n+1}^- have been observed, though with less accuracy. It is considered correct to designate these complexes as $NO_2^+BF_4^-$, $NO_2^+PF_6^-$, and $NO_2^+SbF_6^-$.

INTRODUCTION

THE use of infrared spectroscopic methods to determine the presence, and to a certain extent the structure, of active species in complex compounds is becoming more prevalent. The acetylium ion in the complexes $CH_3COCl:AlCl_3$[1] and $CH_3COF:BF_3$[2], the nitronium ion in HNO_3 solutions, particularly in the presence of H_2SO_4,[3] are but a few examples. The present paper deals with such an investigation of the salts derived from nitryl fluoride and boron trifluoride, phosphorus pentafluoride, and antimony pentafluoride.

Attention has already been drawn to the remarkable nitrating properties of nitronium salts, such as nitronium tetrafluoroborate.[4] It was postulated in this work that the species in these salts responsible for nitration was the nitronium ion NO_2^+. Our purpose at the present time is to show that this postulate is correct and that $NO_2F \cdot BF_3$, $NO_2F \cdot PF_5$, and $NO_2F \cdot SbF_5$ consist of the ionic species NO_2^+ and a complex anion probably of the type MF_{n+1}^-.

Among previous work on the infrared absorption spectrum of the nitronium ion, the results of Teranishi and Decius stand out.[5] Their investigation of the solid nitrogen pentoxide (N_2O_5) showed many bands which could be nicely attributed to the nitronium and nitrate ions. The range of their work enabled calculations of the force constants to be made. Marcus and Fresco[3] also published a full account of their work on the infrared spectrum of pure nitric acid, and its solution in various solvents which showed unequivocally the presence of absorption bands due to the nitronium ion.

RESULTS AND DISCUSSIONS

The principal bands in the spectra are presented in Table I. A typical spectrum, that of nitronium tetrafluoroborate, is shown in Fig. 1. Since our main interest was in the nitronium ion frequencies, no attempt was made to determine accurately the frequencies of bands due to the anion since they were very broad and intense.

The main feature of the spectra is the strong absorption at ~2360 cm^{-1}, which is present in all three salts. This is undoubtedly the asymmetric stretching vibration of the nitronium ion. Teranishi and Decius have this band at 2375 and 2319 cm^{-1}, the doublet being due to the two nitrogen isotopes. Marcus and Fresco reported a single sharp band at 2360 cm^{-1}. This small range in frequency (with the exception of the band due to the N^{15} isotope) as observed in three investigations is noteworthy, since the nitronium ion is in a widely different environment in each case. Teranishi and Decius studied solid N_2O_5 at 87°K; Marcus and Fresco worked with liquid HNO_3 solutions at room temperature; solids at room temperature were used in the present work.

TABLE I. Principal bands in the spectra.[a]

	$NO_2^+BF_4^-$	$NO_2^+PF_6^-$	$NO_2^+SbF_6^-$
$\nu_1+\nu_3(NO_2^+)$	3735 w		3717 w
$\nu_3(NO_2^+)$	2358 vs	2364 s, b	2358 vs
			1630 w
	1307 w		
$\nu_3(MF_{n+1}^-)$	~1035 vs, b	~855 vs, b	~667 vs, b

[a] s=strong; w=weak; v=very; b=broad.

The bending mode ν_2 at 538 cm^{-1}, as determined by Teranishi and Decius, cannot be observed on a spectrometer using sodium chloride optics. The only other vibration of the cation is the symmetrical stretching mode, permitted by Raman selection rules, at 1400 cm^{-1}.[6] This is, of course, absent from the infrared spectrum, but the combination tone of this band and ν_3 (1400+2360=3760 cm^{-1}) suggested by Marcus and Fresco, seems to be present in some of the spectra.

As far as the other bands in the spectrum are concerned, the main ones, and by far the strongest, are due to the anion. For BF_4^-, the strong band at 1035 cm^{-1} is undoubtedly the triply degenerate ν_3 (f_2), which has frequently been observed. For PF_6^- and SbF_6^- the bands at 855 and 667 cm^{-1}, respectively, are probably best assigned to ν_3 (f_1) of a more or less regular octahedron. The frequencies, due to the strength and breadth of the bands are not accurately known. They

† Contribution No. 24 from the Exploratory Research Laboratory, Dow Chemical of Canada, Ltd., Sarnia, Ontario, Canada.

[1] D. Cook, Can. J. Chem. **37**, 48 (1959).

[2] B. P. Susz and J. J. Wuhrmann, Helv. Chim. Acta **40**, 722 (1957).

[3] R. A. Marcus and J. M. Fresco, J. Chem. Phys. **27**, 564 (1957).

[4] G. A. Olah, S. J. Kuhn, and A. Mlinko, J. Chem. Soc. **1956**, 4257.

[5] R. Teranishi and J. C. Decius, J. Chem. Phys. **22**, 896 (1954).

[6] C. K. Ingold, D. J. Millen, and H. G. Poole, J. Chem. Soc. **1950**, 2576.

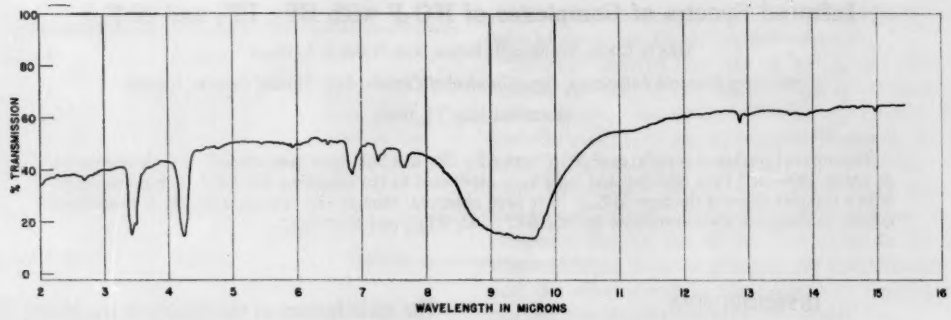

FIG. 1. Infrared spectrum of nitronium tetrafluoroborate (Nujol mull).

are, however, very different from the corresponding band in the original fluoride as shown in Table II.

The evidence presented shows almost conclusively that the salts of nitryl fluoride with BF_3, PF_5, and SbF_5 contain the nitronium cation and a complex symmetrical anion. There remains the possibility that the 2360 cm^{-1} band could belong to the nitrosonium ion. This ion, in $NO^+AlCl_4^-$, absorbs at about 2340 cm^{-1}.[7] However, the very vigorous reaction of the nitronium salts with benzene, (see experimental section) and the high yields of nitrobenzene produced, with no solid material remaining prove conclusively that no nitrosonium salts were present.

EXPERIMENTAL

The Spectra

A Perkin-Elmer model 221 spectrophotometer equipped with sodium chloride optics was used to record the spectra. Emulsions of the solids in mineral oil (Nujol) and a fluorinated hydrocarbon (fluorolube, S30, Minnesota Mining and Manufacturing Company) were pressed between silver chloride plates, all operations being carried out in a dry box, as the compounds were extremely sensitive to moisture. No etching of the silver chloride plates was observed, in marked contrast to that obtained when sodium chloride plates were used. Even barium fluoride plates were slightly etched.

TABLE II. Infrared bands in gaseous fluoride MF_n and in solid ion MF_{n+1}^-

BF_3[a]	PF_5[d]	SbF_5[e]
480 (ν_4, e')	534 (E')	678 (ν_6, E' or ν_2, A_1')
691 (ν_2, a_2'')	576 (A_2'')	708 (ν_4, A_2'')
888 (ν_1, a')	948 (A_2'')	724 (ν_5, E' or ν_1, A_1')
1446 (ν_3, e')	1025 (E')	758 (ν_3, A_2'')
BF_4^-	PF_6^-	SbF_6^-
1035[b]	855[b]	667[b]
1056[c]		

[a] G. Herzberg, *Molecular Spectra and Molecular Structure. II. Infrared and Raman Spectra of Polyatomic Molecules* (D. Van Nostrand Company, Inc., New York, 1945), p. 299.
[b] This work.
[c] Footnote 2.
[d] H. S. Gutowsky and A. D. Liehr, J. Chem. Phys. **20**, 1652 (1952).
[e] L. K. Akers, Ph.D. thesis, Vanderbilt University (1955).

Preparation of the Compounds

We placed 120 ml Freon 113 (trifluorotrichloroethane) in a 500-ml fused silica flask, attached to a vacuum line. Then 6.5 g (0.1 mole) nitryl fluoride and 6.8 g (0.1 mole) boron trifluoride were passed into the reaction vessel, while maintaining the temperature with external cooling at 0°C. A white crystalline precipitate was formed. Solvent and any excess of the reagent were removed by pumping off the system at room temperature. Thereafter, the salt was further dried in vacuo at 50°C for 1 hr. The snow-white solid salt is stable in the absence of moisture. BF_4NO_2 calc.: F 57.1, N 10.5%; F 57.0, N 10.6%. The yield was nearly quantitative.

NO_2SbF_6 and NO_2PF_6 were prepared in a similar way from NO_2F and PF_5 or SbF_5. The complexes could also be prepared from N_2O_5, HF, and BF_3 (PF_5, SbF_5) according to Schmeisser and Elischer[8] and Olah, Kuhn, and Mlinko.[4] However, in this case, extreme care must be taken to maintain N_2O_5 in this form (preferably in an oxidizing atmosphere like ozone), otherwise, decomposition could contaminate the product with nitrosonium salts.

The nitronium salts so prepared, when reacted with benzene and toluene,[4] gave 84 to 94% yield of nitrobenzene or nitrotoluene and some dinitrated products. The nitronium salts were used up quantitatively in these nitration experiments with no solid, unchanged salt remaining. This eliminates the presence of any nitrosonium salt, because in control experiments the corresponding nitrosonium salts were found to be completely unreactive with benzene and toluene.

Note added in proof: Since our manuscript was submitted we noticed a paper by R. W. Sprague, A. B.

[7] H. Gerding and H. Houtgraaf, Rec. trav. chim. **72**, 21 (1953).

[8] M. Schmeisser and S. Elischer, Z. Naturforsch. **7b**, 583 (1952).

Garrett, and H. H. Sisler, J. Am. Chem. Soc. **82,** 59 (1960) on nitronium salts. We must conclude that many of the bands in the recorded spectra are due to reaction products of the nitronium salts with the material of the optical windows, for example, sodium chloride. We have observed similar bands ourselves with NaCl plates, which was the only reason for the subsequent use of inert and transparent silver chloride plates.

ACKNOWLEDGMENT

We are indebted to Dr. R. P. Ruh of The Dow Chemical Company, Midland, Michigan, for the nitryl fluoride used in this work.

THE JOURNAL OF CHEMICAL PHYSICS VOLUME 33, NUMBER 6 DECEMBER, 1960

Generation of Free Carriers in Photoconducting Anthracene. I.

W. MOORE,
University of North Carolina, Chapel Hill, North Carolina
AND
M. SILVER,
Office of Ordnance Research, United States Army, Durham, North Carolina

(Received April 7, 1960)

The source of free carriers in photoconducting anthracene was determined from an investigation of the spatial distribution of trapped electrons. Free carriers are generated in the bulk in addition to electrons being injected into the anthracene at the negative electrode. The bulk generated carriers cannot come from an intrinsic process which simultaneously yields a free electron and a free hole. A tentative extrinsic model for the generation of free carriers is proposed in which electrons are injected at the negative electrode, free holes and trapped electrons are generated by the incident radiation in the bulk at impurities or other defects, and free holes are generated by the incident radiation at the positive illuminated electrode. On the basis of these results, one concludes that anthracene is an extrinsic rather than an intrinsic photoconductor.

INTRODUCTION

ALTHOUGH photoconductivity in anthracene has been investigated since 1906,[1–4] the processes involved are still not understood. The mechanism by which free carriers are generated has been particularly troublesome. Several possibilities have been suggested which involve the intrinsic behavior of the anthracene.[5,6] None of these are satisfactory. For example, Lyons calculates an activation energy which is approximately double the measured value. Rosenberg assumes that electrons can be thermally excited to the triplet level which is approximately 1.8 ev above the ground state. The Boltzmann factor at room temperature is about 10^{-30} making this transition highly improbable.

Recently Kallman and Pope[7] showed that holes are injected into the anthracene from a positive electrolytic electrode and that this constitutes the major source of free positive carriers. On the basis of their results the question arises, are any carriers generated in the bulk, or are all the carriers generated at the surface by injection or perhaps by the dissociation of excitons? Also, since holes are injected into the anthracene by an acceptor electrode (iodine-iodide solutions), are electrons injected by metal electrodes?

Information regarding the source of free carriers may be gleaned from an investigation of the persistent internal polarization effect.[8] This effect has been shown to be primarily a result of a distribution of trapped electrons in the bulk of the anthracene.[9] Since the electrons have a finite range, one can determine the source of the electrons from a knowledge of where they are trapped.

This paper is a report on an investigation of the persistent internal polarization produced in a sandwich cell of anthracene after it has been irradiated through the positive, semitransparent, metal electrode with light that is highly absorbed in the anthracene. It will be shown that carriers are generated in the bulk in addition to electrons being injected into the anthracene at the negative metal electrode. It will also be shown that the bulk generated carriers do not come from an intrinsic process which yields simultaneously a free electron and a free hole. A tentative extrinsic model for the generation of free carriers is proposed in which electrons are injected at the negative electrode, free holes and trapped

[1] A. Pochettino, Acad. Lincei Redoconti **15** (1), 355 (1906).
[2] M. Volmer, Ann. Physik **40,** 775 (1913).
[3] A. G. Chynoweth and W. G. Schneider, J. Chem. Phys. **22,** 1021 (1954).
[4] D. M. J. Compton, W. G. Schneider, and T. C. Waddington, J. Chem. Phys. **27,** 160 (1957).
[5] L. E. Lyons, J. Chem. Soc. **1957,** 5001.
[6] B. Rosenberg, J. Chem. Phys. **29,** 1108 (1958).
[7] H. Kallmann and M. Pope, J. Chem. Phys. **32,** 300 (1960).
[8] H. Kallmann and B. Rosenberg, Phys. Rev. **97,** 1596 (1955).
[9] M. Silver, Ph.D. thesis, New York University, February, 1959.

electrons are generated by the incident radiation in the bulk at impurities or other defects, and free holes are generated by the incident radiation at the positive illuminated electrode.

On the basis of these results, one concludes that anthracene is an extrinsic rather than an intrinsic photoconductor.[10]

THEORY OF THE MEASUREMENTS AND EXPERIMENTAL DETAILS

The persistent internal polarization effect in anthracene is primarily due to a spatial distribution of deeply trapped electrons. These distributions are a direct consequence of the passage of a photocurrent through the bulk of the material. The trapped electrons persist for a long time ($>10^6$ sec)[8] and therefore measurements can be made long after the photocurrent has ceased.

The total number of electrons trapped and the center of charge of their distribution are determined from measurements of the image charge induced on the electrodes after they are shorted together or from direct measurements of the internal field near the electrodes.

Given a distribution of trapped electrons between two grounded parallel-plane electrodes, from Gauss' law the fields at the electrodes are not changed if one replaces this distribution by a thin layer of charge equal to the total charge in the original distribution and placed at the center of charge of the original distribution. With this simplification, one can show that the total number of trapped electrons and the center of charge of their distribution are determined from the measurements to be described.

The charge and field distributions of a thin layer are shown in Fig. 1. The total charge trapped is designated by Q_t. The distance to the center of charge from the electrode that was positive during polarization is designated by D_1 and the thickness of the sample is designated by D_0. From simple electrostatics, Q_t is equal to the sum of the image charges on the two electrodes, A and B.[¶] (The designations A and B are arbitrary except that electrode A will always mean the electrode that was positive during polarization.) The ratio $D_1/(D_0-D_1)$ is equal to the image charge on electrode B divided by the image charge on electrode A.

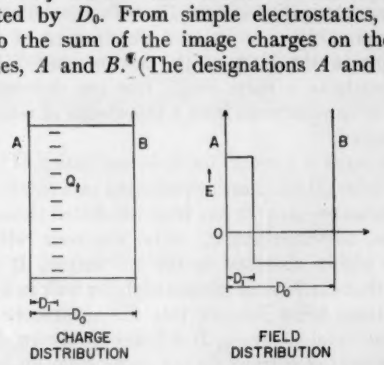

FIG. 1. Charge and field distributions for a thin layer of electrons located a distance D_1 from electrode A.

[10] The terminology "extrinsic" and "intrinsic" used in this paper is the same as that used by the semiconductor physicist, i.e., an intrinsic process is one which essentially involves only a band-to-band transition and the conductivity is not affected by impurities. An extrinsic process involves the generation of carriers because of the presence of impurities or other defects.

The image charge on electrode A, Q_{iA}, is determined by discharging the trapped electrons by irradiating the sample through electrode B with light that is highly absorbed in the anthracene and measuring the total displaced charge. The total displaced charge, Q_B, is

$$Q_B=Q_t[(D_0-D_1)/D_0]=Q_{iA}. \quad (1)$$

The image charge on electrode B, Q_{iB}, is determined by discharging the space charge with radiation transmitted through electrode A and measuring Q_A, the total displaced charge; Q_A is

$$Q_A=Q_t(D_1/D_0)=Q_{iB}. \quad (2)$$

This latter measurement, although convenient, is not too accurate for many of the distributions investigated because the field near electrode A generally varies very rapidly with distance, and consequently not all the generated positive carriers move away from electrode A.

As an alternate to Q_A measurements, the field at electrode B is measured directly by a null method.[9] This is accomplished by using a bucking voltage and a weak intensity pulse of highly absorbed radiation transmitted through electrode B. The field at electrode B is $-V'/D_0$ where V' is the bucking voltage needed to yield no current pulse during a light pulse. The image charge on electrode B is

$$Q_{iB}=CV', \quad (3)$$

where C is the geometric capacitance of the sample. These V' measurements were made with an accuracy of better than 5%.

Two additional measurements are useful in determining the source of free carriers: a measurement of Q_p^+, the total charge passed through the sample during polarization, and Q_p^-, the charge passed through the sample when it is irradiated through the negative electrode for the same time needed to obtain Q_p^+. These measurements are made by using a charged capacitor in parallel with the sample as a voltage source and measuring its voltage before and after irradiation.

The apparatus for making Q and V' measurements is shown in Fig. 2.

All the experiments to be discussed were made on 60-μ thick anthracene crystals. These samples were grown from the melt between two semitransparent Inconel-coated Vycor electrodes. Scintillation grade anthracene was used and no further purification was attempted. The spectral dependence of the steady-state photocurrent agreed with the results of Kommandeur[11] indicating acceptable purity.

[11] J. Kommandeur and W. G. Schneider, J. Chem. Phys. 28, 592 (1958).

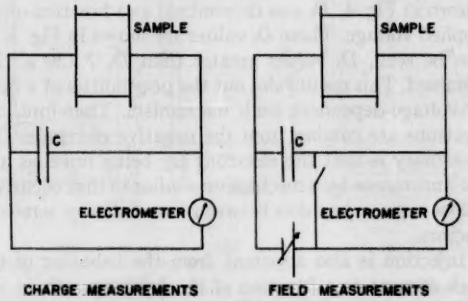

FIG. 2. Apparatus for making charge displacement and internal field measurements.

BULK GENERATED CARRIERS

The conclusion that free carriers are generated in the bulk was arrived at on the basis of the results obtained on the dependence of D_1 on the wavelength of the polarizing radiation transmitted through the positive electrode.

Following the analysis of Brown and Van Heyingen,[12] D_1 is calculated as follows. If $n(x)dx$ electrons are generated between $x+dx$ and x, the number per unit length of these trapped in the interval between $x'+dx'$ and x' is

$$dn_t(x') = [n(x)dx/w] \exp[-(x-x')/w], \quad (4)$$

where x and x' are distances measured from the positive electrode, x is greater than x', w is the range of the electrons, and $n_t(x')$ is the density of electrons trapped at x'. The density of electrons trapped at x' is

$$n_t(x') = \int_{x=x'}^{x=D_0} [n(x)/w] \exp[-(x-x')/w]dx. \quad (5)$$

For carriers generated only by excitation by the incident radiation

$$n(x)dx = (n_b/x_0) \exp(-x/x_0)dx, \quad (6)$$

where x_0 is the absorption depth of the incident radiation. The center of charge of the distribution is

$$D_1 = \int_0^{D_0} x' n_t(x')dx' \Big/ \int_0^{D_0} n_t(x')dx' \simeq x_0, \quad (7)$$

assuming $\exp(-D_0/x_0) \ll 1$.

It will be shown that electrons are injected into the anthracene at the negative electrode in addition to being generated in the bulk. If one assumes, as will be done later, that the range of the bulk-generated electrons is zero, the value of D_1 including the effect of the injected electrons is

$$D_1 = \frac{n_b x_0 + n_i\{D_0 - w[1 - \exp(-D_0/w)]\}}{n_b + n_i[1 - \exp(-D_0/w)]}, \quad (8)$$

where n_b is the number of bulk-generated electrons, n_i is the number of injected electrons, and w now is the range of the injected electrons.

This basic theory which assumed only that trapping is a monomolecular process and that the crystal is homogeneous, predicts that when carriers are generated in the bulk, D_1 will be a function of x_0.

The dependence of D_1 on the wavelength of the polarizing radiation transmitted through the positive electrode is shown in Fig. 3. A high-pressure mercury lamp and a Leiss double monochromator were used to obtain a monochromatic unpolarized beam of light. The bandwidth of the incident radiation was 25 A. Sixty volts were applied during polarization. The D_1 values were obtained from measurements of Q_A and Q_B. The Craig-Hobbins[13] data on absorption depth of the incident radiation in anthracene are also plotted in Fig. 3 for comparison. As can be seen, D_1 varies according to the absorption depth indicating that at least some of the carriers are generated in the bulk by the incident radiation.

It should be noted that the magnitude of D_1 is larger than x_0 while its variation with wavelength is smaller than the variation of x_0. It is not likely that carriers generated in the bulk by the reabsorbed fluorescence could account for this behavior because, as Kommandeur[11] has shown, radiation in the fluorescent band is not a very efficient generator of free carriers.

SURFACE GENERATED CARRIERS

In this section the experimental evidence is presented from which it was concluded that electrons are injected into the anthracene at the negative electrode. These results are primarily concerned with the behavior of the distribution of trapped electrons as a function of applied voltage.

The range of the electrons increases linearly with field strength provided that the electrons' drift velocity is small compared with their thermal velocity.[12] Since the

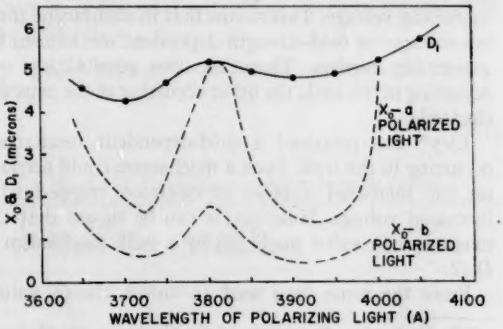

FIG. 3. Comparison of D_1 and absorption depths as a function of wavelength of the incident radiation.

[12] R. S. Van Heyningen and F. C. Brown, Phys. Rev. **111**, 462 (1958).

[13] D. P. Craig and P. C. Hobbins, J. Chem. Soc. **1955**, 2302.

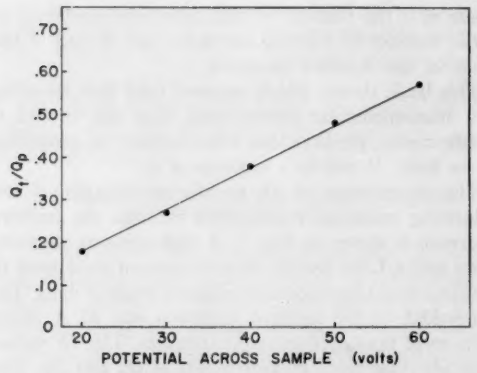

FIG. 4. Total charge trapped as a function of applied voltage.

mobility of the electrons in anthracene is of the order of 1 cm^2/v-sec,[14] this condition is satisfied.

A consequence of an increase in the range is that the number of electrons trapped will decrease for a given number of electrons generated. However, it was found that the number of trapped electrons increases with increasing applied voltage. This means that the number of electrons generated increases with increasing applied voltage. These results are shown in Fig. 4 and were obtained as follows. At each applied voltage, highly absorbed radiation (3650 A) was transmitted through the positive electrode for a time necessary to pass approximately 4×10^{-9} coul/cm^2 through the sample. Since the photocurrent increases with increasing voltage, the sample was irradiated for a shorter time when larger voltages were applied than when smaller voltages were applied. The total amount of charge trapped was determined from measurements of Q_B and the internal field at electrode B.

Since the sample was irradiated for a shorter time when larger voltages were applied than when smaller voltages were applied, fewer electrons were generated in the bulk by the incident radiation. In spite of this, the total number of trapped electrons increases with increasing voltage. This means that in anthracene there is a voltage- or field-strength-dependent mechanism for generating carriers. There are two possibilities: one occurring in the bulk, the other occurring at the negative electrode.

Eley[15] has proposed a field-dependent mechanism occurring in the bulk. Such a mechanism could account for the increased number of electrons trapped with increased voltage. However, it can be shown that the maximum D_1 value predicted by a bulk mechanism is $D_0/2$.

From the same data used to obtain the Q_t values shown in Fig. 4, D_1 was determined as a function of the applied voltage. These D_1 values are shown in Fig. 5. As can be seen, D_1 values greater than $D_0/2$ (30 μ) are obtained. This result rules out the possibilities of a field- or voltage-dependent bulk mechanism. Therefore, the electrons are coming from the negative electrode. One possibility is that the electrons are being injected into the anthracene by a mechanism similar to that occurring across a $p-n$ junction between two ordinary semiconductors.

Injection is also apparent from the behavior of the dark current as a function of the field strength at the negative electrode. An electric field can be produced across the bulk of the anthracene by (a) applying an external voltage in addition to the polarization field, (b) using only the field due to the polarization; and (c) applying an external voltage of opposite polarity to (a) in addition to the polarization field. The dark current was measured for each of these three field conditions. The three field conditions used are shown in Fig. 6. The sample was polarized for a time sufficient to make the polarization field in the D_0-D_1 region approximately half the originally applied electric field. Only under condition (a) will the field at the negative electrode allow electron injection. Further, the field in the D_0-D_1 region is three times larger under condition (c) than under condition (a).

The dark currents for these three field conditions as a function of the originally applied voltage, V_0, (see Fig. 6) are given in Table I. When electron injection is allowed, condition (a), the dark current was found to be as much as four orders of magnitude larger than when injection is not allowed, conditions (b) and (c).

Injection across a $p-n$ junction depends exponentially on the applied voltage. If this is the process that is taking place at the negative electrode, the steady state photocurrent would be limited by this injection and the current should also be an exponential function of applied voltage unless the field strength is large

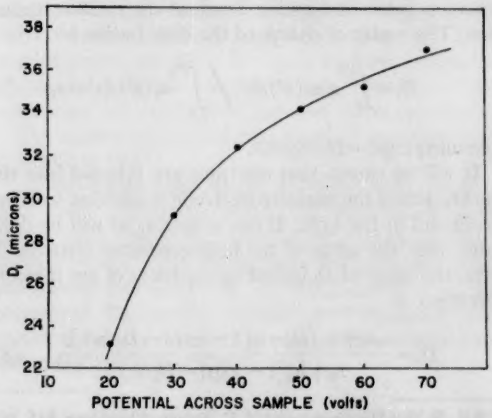

FIG. 5. Dependence of D_1 on applied voltage.

[14] R. G. Kepler, *Proceedings of the Conference on Electronic Conductivity in Organic Solids* (Interscience Publishers, Inc., New York, 1960).

[15] D. D. Eley and M. R. Willis, *Proceedings of the Conference on Electronic Conductivity in Organic Solids* (Interscience Publishers, Inc., New York, 1960).

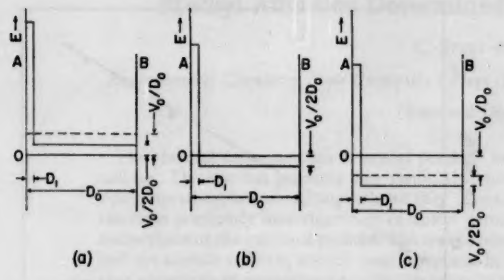

FIG. 6. Internal field produced across the bulk of the sample by (a) applying an external voltage V_0 in addition to the polarization field; (b) using only the polarization field; and (c) applying an external voltage $-V_0$ in addition to the polarization field.

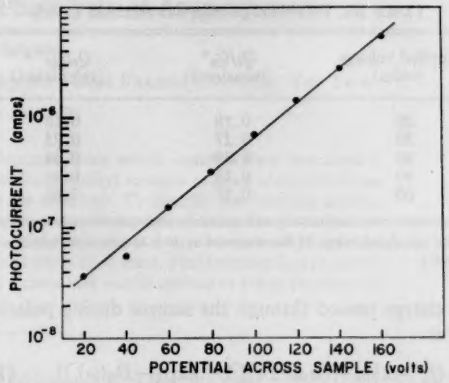

FIG. 7. Steady-state photoconduction current vs applied voltage.

enough to cause saturation. Such an exponential behavior was found and these results are shown in Fig. 7. The photocurrents were produced by irradiating the samples through the positive electrode with highly absorbed radiation. These currents were measured 20 min after the start of irradiation in order to ensure steady-state current flow.

DISCUSSION OF RESULTS

From the measurements of the dependence of the distribution of trapped electrons on the wavelength of the incident polarizing radiation and on the applied voltage, it is concluded that carriers are generated in the bulk by excitation by the incident radiation in addition to free electrons being injected into the anthracene at the negative electrode. This conclusion is based somewhat on the assumption that no positive carriers are trapped in the bulk of the material. There may, however, be a layer of trapped holes located very close to the negative electrode. The existence of such a layer would not effect these conclusions because this layer would be at most one or two microns from the negative electrode.[9] Thus, even if the total charge in this positive layer was equal to the total negative charge trapped in the bulk, which is highly unlikely,[9] the D_1 values would be decreased by only 1 or 2 μ.

The injection process may be similar to that occurring across a $p-n$ junction between two inorganic semiconductors. The voltage dependence of the steady-state photocurrent indicates that this may be so; however, this result by itself is not conclusive because other possible mechanisms can also cause an exponential behavior of the photocurrent.

The bulk-generated carriers cannot arise from an intrinsic process or any process that yields simultaneously a free electron and a free hole. This conclusion is arrived at from the following considerations: Assume that the bulk generation process is intrinsic. The bulk generated electrons will have the same range as the injected electrons. On integrating Eq. (5) where

$$n(x)=(n_b/x_0)\exp(-x/x_0)$$
$$+n_i \text{ electrons injected at } x=D_0, \quad (9)$$

one obtains for N_t, the total number of trapped electrons

$$N_t=n_b x_0/(x_0+w)+n_i[1-\exp(-D_0/w)], \quad (10)$$

where n_b is the total number of electrons generated in the bulk. D_1 is

$$D_1=\frac{[n_b x_0^2/(x_0+w)]+n_i\{D_0-w[1-\exp(-D_0/w)]\}}{N_t}. \quad (11)$$

TABLE I. Dark current for various internal field conditions.[a]

Applied voltage (volts)	Current for condition (a) (amp)	Current for condition (b) (amp)	Current for condition (c) (amp)
20	3×10^{-11}	0.6×10^{-11}	1×10^{-11}
40	3×10^{-10}	1×10^{-11}	2×10^{-11}
60	2×10^{-9}	0.8×10^{-11}	4×10^{-11}
80	9×10^{-9}	1×10^{-11}	3×10^{-11}
100	4×10^{-8}	1×10^{-11}	5×10^{-11}
120	1×10^{-7}	0.8×10^{-11}	5×10^{-11}
140	3×10^{-7}	1×10^{-11}	7×10^{-11}
160	6×10^{-7}	0.8×10^{-11}	11×10^{-11}

[a] The measured value of D_1 at all voltages was approximately 2 μ.

TABLE II. Total charge trapped: intrinsic model.

Applied voltage (volts)	$Q_t/Q_p{}^+$ (measured)	$Q_t/Q_p{}^+$ [a] (calculated)
20	0.18	0.18
30	0.27	0.17
40	0.39	0.18
50	0.48	0.20
60	0.57	0.27

[a] The calculated range of the electrons at 20 v is approximately 8 μ.

TABLE III. Total charge trapped: extrinsic model.

Applied voltage (volts)	Q_t/Q_p^+ (measured)	Q_t/Q_p^+ [a] (calculated)
20	0.18	0.18
30	0.27	0.25
40	0.39	0.34
50	0.48	0.46
60	0.57	0.66

[a] The calculated range of the electrons at 20 v is approximately 8 μ and $n_b/n_s \approx 0.1$.

The charge passed through the sample during polarization is

$$Q_p^+ = e\{n_b + (n_i w/D_0)[1 - \exp(-D_0/w)]\}. \quad (12)$$

Since w is a linear function of field strength, from the measured values of D_1, Q_t/Q_p^+ was calculated as a function of voltage assuming x_0 to be approximately 1 μ. These calculated values along with the measured values are given in Table II. As can be seen, the calculated values are too small (except at 20 v where the calculated value was made to fit the experimental data). Thus, an intrinsic model cannot account for these results.

Consider an extrinsic process where holes are generated at the positive electrode, holes and trapped electrons are simultaneously generated in the bulk, and where electrons are injected into the anthracene at the negative electrode. Such an extrinsic process for hole generation may be the dissociation of excitons at the positive illuminated electrode giving a free hole and the dissociation of exitons at impurities or other defects giving a free hole and a trapped electron. These may be either one or two photon processes.

The calculated values of N_t, D_1, and Q_p^+ are

$$N_t = n_b + n_i[1 - \exp(-D_0/w)], \quad (13)$$

$$D_1 = \frac{n_b x_0 + n_i\{D_0 - w[1 - \exp(-D_0/w)]\}}{N_t}, \quad (14)$$

and

$$Q_p^+ = e\{n_s + n_b + n_i(w/D_0)[1 - \exp(-D_0/w)]\}, \quad (15)$$

where n_b is the number of carriers generated in the bulk, n_s is the number of holes generated at the positive electrode, n_i is the number of injected electrons, and w is the range of the injected electrons. There are four unknowns: n_s, n_b, n_i, and w. Another measurement is needed to obtain these quantities unambiguously. The measurement made was Q_p^-, the amount of charge passed through the sample when it is irradiated through the negative electrode for the same time required to obtain Q_p^+. This is not too satisfactory a measurement because the electric field at the negative electrode, or the voltage across the junction where injection occurs, is probably different during opposite electrode illumination from that during negative electrode illumination. However, this measurement is probably not too bad at 20 v because the injection at 20 v is small. A more reliable experiment is being investigated in order to check this extrinsic model more carefully.

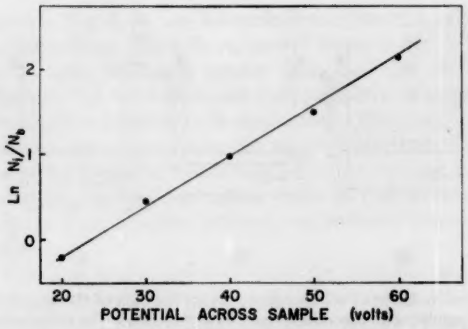

FIG. 8. Log of the number of injected electrons per bulk generated carrier vs applied voltage.

Q_p^- is

$$Q_p^- = e\{n_b(x_0/D_0) + n_i(w/D_0)[1 - \exp(-D_0/w)]\}. \quad (16)$$

The ratio Q_p^+/Q_p^- was measured and found to be 75 at 20 v.

Q_t/Q_p^+ was calculated as a function of the applied voltage assuming $x_0 \ll D_0$. These calculated values are given in Table III. As can be seen there is fairly good agreement between the calculated and measured values.

The log of the number of injected electrons per bulk generated carrier was also calculated. The results of this calculation are shown in Fig. 8. As can be seen the injection is an exponential function of the applied voltage. This is in agreement with the dependence of the photocurrent on the applied voltage (Fig. 7).

To summarize, free carriers are generated in the bulk in addition to free electrons being injected into the anthracene at the negative electrode. The bulk generated carriers do not arise from an intrinsic process which simultaneously yields a free electron and a free hole. Therefore, one concludes, on the basis of these results, that anthracene is an extrinsic rather than an intrinsic photoconductor.

ACKNOWLEDGMENTS

The authors would like to express their appreciation to Dr. H. Kallmann and Dr. M. Pope of New York University for their helpful discussions.

THE JOURNAL OF CHEMICAL PHYSICS VOLUME 33, NUMBER 6 DECEMBER, 1960

Methyl Affinities Determined by Photolysis of Azomethane*

C. STEEL AND M. SZWARC

Department of Chemistry, State University College of Forestry at Syracuse University, Syracuse, New York

(Received December 14, 1959)

The thermal decomposition of acetyl peroxide forms acetate radicals which decarboxylate into methyl radicals. The reaction products may result, therefore, either from methyl radicals or from acetate radicals which decarboxylate simultaneously as they interact with the substrate. To identify the reacting species, reactions previously investigated in an acetyl peroxide system were reinvestigated using the photolysis of azomethane as the source of radicals. The results prove that at least in hydrocarbon solvents methyl radicals, and not acetate radicals, are the reacting species in the acetyl peroxide system. Furthermore, it was shown that photolysis of azomethane in solution provides us with a clean and simple system to study reactions of methyl radicals.

REACTIVITIES of various classes of substrates toward methyl radicals have been extensively studied in this laboratory.[1] These investigations were concerned mainly with the addition reaction (a),

$$CH_3 + \text{substrate} \rightarrow CH_3 \cdot \text{substrate} \cdot, \qquad (a)$$

and to a lesser extent with the hydrogen abstraction reaction (b),

$$CH_3 + \text{substrate} \rightarrow CH_4 + \text{substrate radical}. \qquad (b)$$

In all these studies methyl radicals were generated by the thermal decomposition of acetyl peroxide. This compound decomposes unimolecularly, the rupture of the O—O bond being the primary and rate determining step in the decomposition[2,3]

$$(CH_3 \cdot COO)_2 \rightarrow 2CH_3 \cdot COO. \qquad (c)$$

The fate of the acetate radicals produced in reaction (c) is the subject of some controversy. In earlier publications from this laboratory[3] it was claimed that acetate radicals are unstable and decompose instantaneously into carbon dioxide and methyl radicals so that the latter radicals undergo the subsequent addition and abstraction reactions. The labile nature of acetate radicals is indicated by the thermochemical data,[4] since their decarboxylation was found to be *exothermic* to an extent of 17 kcal/mole. In a later publication,[5] a detailed discussion of this decarboxylation process led to the conclusion that this reaction requires a small activation energy, perhaps not more than 1–2 kcal/mole, but even then the acetate radical would have only a fleeting existence of the order of 10^{-10} or 10^{-11} sec.

On the other hand, some investigators, notably Urry,[6] expressed the opinion that acetate radicals are sufficiently stable to react, and that the observed addition and abstraction reactions are due to these entities which decarboxylate in the course of these processes. Such reactions, of course, yield the same products as would be expected from the reactions of methyl radicals, and therefore one cannot solve the problem of the identity of the reacting species by mere chemical analysis. [Urry's work was rejected and extended by Herk and Szwarc, J. Am. Chem. Soc. **82**, 3558 (1960). Their results contradict those of Urry.]

We have, therefore, reinvestigated quantitatively some addition and abstraction reactions, using an alternative source of methyl radicals. Photolysis of azomethane was chosen for this purpose since this reaction seems to be free of complicating factors which vitiate the photolysis of acetone if the latter reaction proceeds in solution at low temperatures. The respective rate constants of the addition and abstraction reactions were then determined and found to be identical with those observed in the system in which acetyl peroxide was used as radical source. Thus, one has to conclude that in the systems studied in this laboratory the reactions caused by the decomposition of acetyl peroxide are due to methyl radicals and not to acetate radicals.

EXPERIMENTAL

Materials

The following procedure was used in the preparation of azomethane. *Sym*-dimethylhydrazine dihydrochloride (Aldrich Chemical Company) was dissolved in an excess of sodium hydroxide to yield the free base. This solution was added slowly and with constant stirring to a suspension of mercuric oxide[7] (a rapid addition can lead to an explosion). The azomethane was distilled

* This work was supported by the Office of Ordnance Research of U. S. Army.

[1] (a) M. Szwarc and J. H. Binks, *Theoretical Organic Chemistry* (Butterworths Scientific Publications, Ltd., London, 1959), p. 262; (b) M. Szwarc, J. Polymer Sci. **16**, 367 (1955), and (c) M. Szwarc, J. Phys. Chem. **61**, 40 (1957).

[2] A. Rembaum and M. Szwarc, J. Am. Chem. Soc. **76**, 5975 (1954).

[3] M. Levy, M. Steinberg, and M. Szwarc, J. Am. Chem. Soc. **76**, 5978, 5981 (1954).

[4] I. Jaffe, E. I. Prosen, and M. Szwarc, J. Chem. Phys. **27**, 416 (1957).

[5] M. Szwarc and L. Herk, J. Chem. Phys. **29**, 438 (1958).

[6] W. H. Urry, abstract of a paper read in Org. Symposium, Denver (1950).

[7] Renaud and Leitch, Can. J. Chem. **32**, 545 (1954).

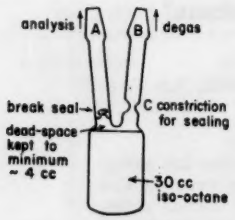

FIG. 1. Reaction vessel.

off on a water bath and collected in a solid carbon dioxide trap (yield 60–70%). The gas was dried with P_2O_5 and then with KOH, degassed, and stored at liquid nitrogen temperature. Its purity was confirmed by gas chromatography.

Philips Petroleum Company spectrograde iso-octane was distilled under vacuum, passed through an 8-ft silica gel column (Fisher 28–200 mesh) to remove the last traces of olefinic compounds, and stored over sodium wire. The purity of the iso-octane was checked on a Cary-Recording spectrophotometer.

Matheson C. P. propene (99.0% min) and butene-1 (99.0% min) were purified by bulb-to-bulb distillation before use.

Procedure

About 30 cc of iso-octane was frozen, degassed and thawed 5 times in the reaction vessel shown in Fig. 1. Thereafter known amounts of degassed azomethane and the investigated gas (propene or butene-1) were condensed into the reaction vessel by cooling the latter with liquid nitrogen. The reaction vessel was then sealed off at the constriction *C*, placed in a thermostated water bath, allowed to equilibrate with the bath and then irradiated with ultraviolet light using a General Electric A-H6 mercury-arc lamp. After 5 min of irradiation approximately 10% of the azomethane had been photolysed and at this stage the reaction was stopped.

The reaction vessel was then attached to the analysis apparatus and the products pumped into a calibrated storage flask using a Hg-diffusion pump and Toepler pump working in series. The gases were passed through a trap held at −78°, where most of the iso-octane was condensed, then through two more traps held at −190° where the remaining iso-octane and all the undecomposed azomethane and ethane were frozen out. After it had been ascertained that all the methane and nitrogen were collected in the storage vessel, their pressure was determined, and then a sample of the mixture withdrawn for analysis on the mass spectrometer. The ratio $[CH_4]/[N_2]$ was determined from the equation $[CH_4]/[N_2]=(h_{15}/h_{28})f$ where h_{15} and h_{28} are the relative heights for masses 15 and 28, respectively.[8] The scaling factor f was found by calibrating the instrument with known CH_4:N_2 mixtures. The mass spectrometric method is especially convenient since it allows for ready detection of impurities. For example, if air was present in the sample this was shown by its contribution to the mass 32 peak over and above the normal background.

The shape of the reaction vessel was such that a negligible volume was left for vapor. Thus, the amount of olefin present in the vapor phase was very small compared with that dissolved in the iso-octane, and consequently it could be neglected in calculating the concentrations. This point was checked further by using the reaction vessel described by Gazith and Szwarc,[9] the results (runs 11–18) being the same as those obtained with the newly designed reaction vessel.

TABLE I. Photolysis of azomethane carried out to completion.

T°C	Conc of CH_3NNCH_3 in moles/liter	CH_4/N_2[a]	C_2H_6/N_2[a]	$(CH_4+2C_2H_6)/N_2$[a]
~52	$1.8.10^{-3}$	0.576	0.722	2.02
~52	$1.8.10^{-3}$	0.558	0.708	1.97
~100	$1.7.10^{-3}$	0.72	0.66	2.04

[a] Composition of the mixtures determined mass spectrometrically.

TABLE II. Decomposition of acetyl peroxide at 65°C in iso-octane [Peroxide] = 2.10^{-3} *M*.

[Azomethane] moles/cc·10^5	$[CH_4]$ mm Hg in collecting vessel
0.0	1.84
0.0	1.84
3.0	1.84
3.0	1.84

Results

Photolysis of azomethane in iso-octane solution gave three gaseous products: CH_4, C_2H_6, and N_2. A 2.10^{-3}-*M* solution of the azo-compound was used in the experiments described in this paper, and the material balance, given in Table I, shows that under these experimental conditions the two hydrocarbons account for *all* the

TABLE III. Methyl affinity of azomethane (Conc of the peroxide 0.01 *M*; T=65°C).

Azomethane moles·10^2	Iso-octane moles·10^2	CH_4	N_2	CO_2	C_2H_6[a]	Methyl affinity[b]
		all in units cc cm Hg				
0	5.54	19.81	0	23.6	0.43	...
0.303	5.54	17.09	4.88	37.5	7.6	15
0.526	5.54	14.85	3.74	37.4	3 3	12

[a] Determination of ethane represents the upper limit since azo-methane contributes to the mass-peak 30.

[b] Methyl affinity was calculated on the basis of CH_4/CO_2 using the equation Methyl affinity = {[S]/[Az]}·{$[CH_4/CO_2]_{blank}-[CH_4/CO_2]$}/$[CH_4/CO_2]$.

[8] The masses 16 and 15 are nearly equally abundant in the mass-spectrum of methane. We have chosen the mass 15 for our determination since the mass 16 has a contribution from O_2 if a trace of the latter is present in the investigated mixture.

[9] M. Gazith and M. Szwarc, J. Am. Chem. Soc. 79, 3339 (1957).

methyl radicals formed in the photolysis. This means that no addition of methyl radicals to azomethane does take place at these concentrations; nor does a recombination of methyl radicals with iso-octyl radicals take place. For further verification of the first point a solution of acetyl peroxide was decomposed thermally in presence and in absence of azomethane (conc. 3.10^{-3} M). Identical amounts of methane were found (see Table II), demonstrating again the absence of reaction between methyl radicals and azomethane.

The methyl affinity of azomethane is indeed too low to permit any measurable addition of methyl radicals at concentrations of the zero compound ranging from 10^{-2}–10^{-3} M. An approximate estimate of this methyl affinity was obtained by applying the usual technique (see Table III). The peroxide seems to induce some decomposition of azomethane (notice the presence of some nitrogen in the products), and consequently the experimental results are somewhat uncertain. However, the correct value of the methyl affinity of azomethane certainly cannot differ by more than a factor of 2 from the experimental findings.[10]

In the photolysis experiments described here the rate of formation of methyl radicals was about 6.10^{-5} millimoles/cc min, i.e., comparable to the rate observed in the decomposition of 6.10^{-2} M solution of acetyl peroxide at 65°C.[3] It was demonstrated[3] that under these conditions the ethane formed, results from a cage reaction and not from a bimolecular recombination of methyl radicals, and this conclusion applies of course, to the present results. Nevertheless, to avoid any doubts about the origin of the ethane formed in the photolysis the CH_4/N_2 ratio was measured in experiments carried out under identical conditions but with greatly different concentrations of azomethane. Table IV summarizes the findings and shows that bimolecular recombination is not observed.

Consequently, the method previously developed for the determination of methyl affinities[1b,1c] is also applicable to the present system. We redetermined, therefore, the methyl affinities of propene and 1-butene using photolysis of azomethane as a source of methyl radicals. The necessary data are collected in Tables V and VI. The rate constants k_1 and k_2 refer to reactions (1) and (2),

$$CH_3 + \text{iso-octane} \rightarrow CH_4 + \text{iso-octyl radical} \quad (1)$$

$$CH_3 + \text{olefin} \rightarrow CH_3\cdot\text{olefin}\cdot, \quad (2)$$

[10] Addition of methyl radicals to azomethane was observed in gas-phase photolysis by M. Burton, T. W. Davies, and H. A. Taylor, J. Am. Chem. Soc. **59**, 1038 (1937) and by F. E. Blacet and A. Taurog, J. Am. Chem. Soc. **61**, 3024 (1939). Recent work of M. H. Jones and E. W. R. Steacie, J. Chem. Phys. **21**, 1018 (1953) documents further this reaction and the product of addition $(CH_3)_2\cdot N\cdot N(CH_3)_2$ was observed by them mass spectrographically. These observations do not invalidate our conclusion, because presence of a solvent and the low concentration of the azo-compound prevent the addition.

TABLE IV. Photolysis of azomethane at 50°C.[a]

Concentration azomethane mole/l	CH_4/N_2
$2.1.10^{-4}$	0.535, 0.540
$2.1.10^{-3}$	0.534, 0.540
$2.1.10^{-2}$	0.523, 0.525

[a] Two experiments were done at each concentration.

TABLE V. Methyl affinity of propene (azomethane $\approx 0.0045 \cdot 10^{-2}$ moles).

Run	Temperature, °C	Propene moles·10^2	Iso-octane moles·10^2	$[CH_4]/[N_2]$	k_2/k_1
11	95.3	0.487	18.46	0.427	24.5
12	95.3	0.484	18.46	0.436	23.4
13	95.3	0.484	18.46	0.453	21.1
14	95.3	...	18.46	0.701	...
15	95.3	...	18.46	0.706	...
17	95.3	0.829	19.69	0.348	24.2
19	95.3	...	20.60	0.660(?)	...
20	95.3	0.244	19.38	0.543	23.8
21	95.3	0.820	16.00	0.310	24.6
22	95.3	...	16.00	0.702	...
23	50.0	...	16.61	0.541	...
25	50.0	...	16.61	0.540	...
27	50.0	0.168	17.54	0.434	25.2
28	50.0	0.338	17.54	0.362	25.7
28a	50.0	0.686	17.54	0.274	25.0
29	70.9	0.364	17.54	0.395	24.8
30	70.9	...	17.54	0.599	...
31	70.9	...	18.46	0.595	...
32	70.9	0.367	18.46	0.413	22.4

TABLE VI. Methyl affinity of butene-1. (Azomethane: $\approx 0.0045 \times 10^{-2}$ moles. Temperature: 70.9°C).

Run	Butene-1 moles·10^2	Iso-octane moles·10^2	$[CH_4]/[N_2]$	(k_2/k_1)expt
33	0.468	17.13	0.390	21.1
34	0.121	16.65	0.515	26.7
35	0	17.28	0.619	...
36	0.366	16.65	0.432	19.3
37	0.733	17.28	0.338	19.3
38	0	17.85	0.610	..
39	1.514	17.85	0.263	15.8
40	0.444	16.61	0.395	20.8
41	1.011	16.61	0.300	17.3

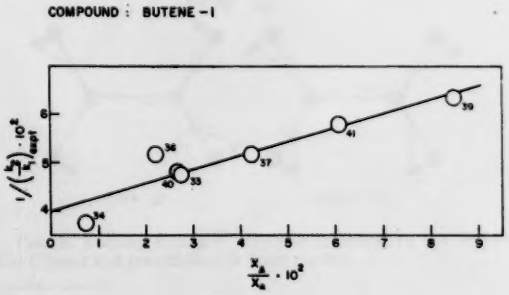

FIG. 2. Compound: butene-1.

TABLE VII.

Substrate	T°C	Acetyl peroxide system k_2/k_1	Acetyl peroxide system k_3/k_2	Photolysis of azomethane k_2/k_1	Photolysis of azomethane k_3/k_2
Propene	50.0	25.2[a]	...	25.3±1[b]	...
Propene	70.9	23.7[a]	...	23.6±1	...
Propene	95.3	22.6[a]	...	23.6±1[b]	...
Butene-1	70.9	26.3[a]	0.25	25±1.5	0.28

[a] These values are obtained through intrapolation or extrapolation, using the respective Arrhenius line. The respective activation energies are uncertain within ±0.6 kcal/mole, and this may account for the apparent discrepancy at 95°C.

[b] These experiments were repeated by M. Feld and M. Szwarc, J. Am. Chem, Soc. **82**, 3791 (1960). The following values were reported: at 50°C $k_2/k_1=25.7$, at 95°C $k_2/k_1=19.7$.

their ratio (k_2/k_1) representing the respective methyl affinities. The reaction with 1-butene involves also the abstraction of an α-hydrogen, i.e., reaction (3), as well as the addition to the C=C double bond,

$$CH_3+CH_2{:}CH\cdot CH_2\cdot CH_3\rightarrow CH_4+CH_2{:}CH\cdot CH\cdot CH_3. \quad (3)$$

Therefore, the calculated $(k_2/k_1)_{exp}$ vary with the mole fraction of butene-1 in the reacting mixture, and the correct values of k_2/k_1 and k_3/k_2 are obtained by plotting $(k_2/k_1)_{exp}^{-1}$ vs [butene-1]/[iso-octane]. Such a plot gives a straight line,[11] its intercept gives k_1/k_2 and its slope is equal to k_3/k_2. The line obtained for butene-1 at 70.9°C is shown in Fig. 2, and leads to the constants $k_2/k_1=25\pm1.5$ and $k_3/k_2=0.28$.

The agreement between these values and those found by Buckley and Szwarc[11] (see Table VII) is most gratifying. It confirms the validity of the method and it proves that the observed radical addition and abstraction reactions caused by the decomposition of acetyl peroxide result from methyl radicals and not from acetate radicals. This point was reconfirmed by recent work of Feld and Szwarc[12] who redetermined methyl affinities of ethylene, propylene, isobutene, styrene, α-methyl styrene, butadiene, and isoprene over a wide range of temperatures and showed consistency with previous determinations.

ACKNOWLEDGMENT

We wish to thank M. Feld for his help in performing some of these experiments.

[11] R. P. Buckley and M. Szwarc, Proc. Roy. Soc. (London) **A240**, 396 (1957).

[12] M. Feld and M. Szwarc, J. Am. Chem. Soc. **82**, 3791 (1960).

Transferability of Urey-Bradley Force Constants. V. Bromoethylenes

JAMES R. SCHERER AND JOHN OVEREND

Chemical Physics Research Laboratory, The Dow Chemical Company, Midland, Michigan

(Received June 23, 1960)

Urey-Bradley force constants (UBFC's), calculated by a least-squares method, were obtained for ethylene, vinyl bromide, vinylidene bromide, *trans*-dibromoethylene, *cis*-dibromoethylene, tribromoethylene, and tetra bromoethylene. Even with complete isotopic data it was found impossible to determine all the force constants for an individual bromoethylene; moreover, from the viewpoint of giving stability to the calculation, values have been supplied by transfer from other molecules within this series and these force constants have been constrained in the least-squares refinement. By inspection of the correlation matrix, the uncertainties in the various force constants were, in many cases, found to be intimately related, and, it was usually found unnecessary to constrain both force constants of an indeterminate pair; in this manner we have kept the number of transferred force constants to a minimum. A comparison of the remaining UBFC's shows that they are moderately transferable. Although the flexible bond parameter S_{HH} was found to be significant (but not transferable) in those molecules containing hydrogen atoms *trans* to one another, i.e., ethylene, vinyl bromide, and *trans*-dibromoethylene, its value in *cis*-dibromoethylene was small and made no significant contribution in explaining the observed frequencies. A potential function which includes a quadratic cross term between *trans*-hydrogen bending coordinates was found to be adequate throughout the series and moderately transferable.

INTRODUCTION

IT is obvious that the number of determinable force constants in a potential function cannot exceed the number of available data. However, it has often been felt that a general quadratic potential function could be completely determined, given an excess of observed vibrational frequencies or other spectroscopic parameters. It is a sobering experience to learn that, for a molecule such as vinyl bromide, it is impossible to fix with certainty the F_{CBr} repulsive constant in a simplified Urey-Bradley force field (UBFF) containing only 12 parameters, despite the fact that there are available eight isotopes or 72 planar vibrational frequencies.

Since, for a single molecule, the UBFF may contain force constants which are highly uncertain, values must first be supplied for these, either by *a priori* calculation or by direct transfer from other molecules where they are known with greater certainty, before the remainder of the Urey-Bradley force constants (UBFC) may be fixed. With increasing molecular size, the lack of isotopic data, and the disappearance of symmetry, the problem of calculating force constants becomes impossible if we cannot remove the effectively indeterminate ones from the general refinement. Consequently, the utility of a potential function for larger molecules depends strongly on its over-all transferability.

Since almost complete vibrational assignments have been made for the isotopic bromoethylenes we have undertaken a systematic study of the transferability of the UBFF within this series. In this work UBFC's have been supplied by direct transfer only when their uncertainties are comparable to their magnitudes. Using a minimum number of these transferred force constants we have found the remaining UBFC's moderately transferable throughout the bromoethylene series. Slight but significant differences appear between similar UBFC's in these molecules and those are discussed in detail in the following.

A complicating feature of this study is the fact that a simple UBFF, with only *gem* nonbonded repulsions, cannot simultaneously reproduce the B_{1g} and B_{2u} rocking modes of ethylene. Shimanouchi[1] has shown that, a UBFF which gives a reasonable fit to the B_{1g} rocking frequency, leads to a calculated B_{2u} rocking frequency approx. 20% higher than the observed one at 810 cm^{-1}. Accordingly he has proposed a modification of the UBFF which takes up this discrepancy in a parameter

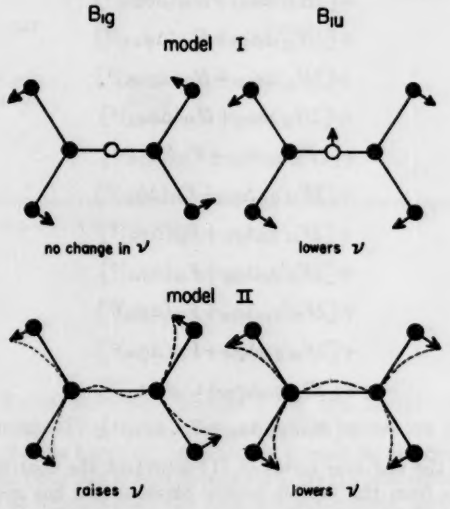

FIG. 1. Rocking modes of ethylene according to the flexible C=C bond and general flexible bond models.

[1] T. Shimanouchi, J. Chem. Phys. **26**, 594 (1957).

α, which is inversely related to the flexibility of the C=C bond (H_{CC}). Briefly, the kinematic requirements of this model (I) are the introduction of a weightless atom at the center of the C=C bond and an additional bending force constant H_{CC} associated with the planar deviation of this atom from the line connecting the two carbon atoms. The effect of this modification may be qualitatively appreciated from Fig. 1. It is important to note that in this model only the C=C bond is assumed to be flexible. Shimanouchi[1] has also proposed a second model (II) in which he included both the flexibility of all bonds and the concept of orbital following. From Fig. 1 it may be seen that this model accounts for the higher energy of the B_{1g} rocking mode and the lower energy of the B_{2u} rocking mode. The complete potential function for model II may be written[2] (in the notation of Fig. 2) as

$$2V = 2V_{UBFF} + 2S_{36}\Delta\phi_{312}\Delta\phi_{126} + 2S_{45}\Delta\phi_{412}\Delta\phi_{125} - 2S_{35}\Delta\phi_{312}\Delta\phi_{521} - 2S_{46}\Delta\phi_{412}\Delta\phi_{621}, \quad (1)$$

where

$$\begin{aligned} 2V_{UBFF} = {} & [2K_{12}'r_{12}\Delta r_{12} + K_{12}(\Delta r_{12})^2] \\ & + [2K_{13}'r_{13}\Delta r_{13} + K_{13}(\Delta r_{13})^2] \\ & + [2K_{14}'r_{14}\Delta r_{14} + K_{14}(\Delta r_{14})^2] \\ & + [2K_{25}'r_{25}\Delta r_{25} + K_{25}(\Delta r_{25})^2] \\ & + [2K_{26}'r_{26}\Delta r_{26} + K_{26}(\Delta r_{26})^2] \\ & + [2H_{34}'\Delta\phi_{314} + H_{34}(\Delta\phi_{314})^2] \\ & + [2H_{56}'\Delta\phi_{526} + H_{56}(\Delta\phi_{526})^2] \\ & + [2H_{32}'\Delta\phi_{312} + H_{32}(\Delta\phi_{312})^2] \\ & + [2H_{42}'\Delta\phi_{412} + H_{42}(\Delta\phi_{412})^2] \\ & + [2H_{51}'\Delta\phi_{521} + H_{51}(\Delta\phi_{521})^2] \\ & + [2H_{61}\Delta\phi_{621} + H_{61}(\Delta\phi_{621})^2] \\ & + [2F_{32}'q_{32}\Delta q_{32} + F_{32}(\Delta q_{32})^2] \\ & + [2F_{42}'q_{42}\Delta q_{42} + F_{42}(\Delta q_{42})^2] \\ & + [2F_{51}'q_{51}\Delta q_{51} + F_{51}(\Delta q_{51})^2] \\ & + [2F_{61}'q_{61}\Delta q_{61} + F_{61}(\Delta q_{61})^2] \\ & + [2F_{34}'q_{34}\Delta q_{34} + F_{34}(\Delta q_{34})^2] \\ & + [2F_{56}'q_{56}\Delta q_{56} + F_{56}(\Delta q_{56})^2] \\ & + [2C_{35}'q_{35}\Delta q_{35} + C_{35}(\Delta q_{35})^2] \\ & + [2C_{46}'q_{46}\Delta q_{46} + C_{46}(\Delta q_{46})^2], \quad (2) \end{aligned}$$

and the last four terms of (1) represent the contributions from the flexible bonds. Shimanouchi has given

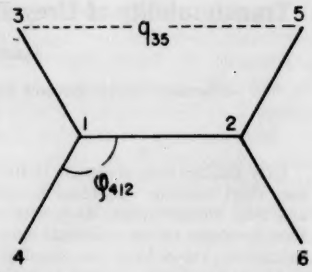

FIG. 2. Numbering of atoms in the general ethylene.

explicit expressions for the S_{ij} force constants in terms of individual bond flexibilities and it may be seen from Eq. (28) of footnote reference 1 that the expressions for S_{ij} are equivalent if atoms i and j have identical connecting bonds, irrespective of their cis or trans configurations. Hence for ethylene $S_{36}=S_{35}=S_{45}=S_{46}=S_{HH}$. Upon transforming this potential function to a symmetry $\mathfrak{F}$ matrix, the diagonal B_{1g} rocking constant is raised by $2S_{HH}$ and the corresponding B_{2u} element is lowered by $2S_{HH}$. The bromoethylenes require three flexibility parameters: S_{HH}, S_{HBr}, S_{BrBr}, and one might expect them to be roughly transferable throughout the series.

In the course of this work we have tried a third modification which we shall call the trans-interaction model (III). We intend to show that the vibrational frequencies of the complete series of bromoethylenes may be explained if a cross term between the trans CH bending coordinates is added to the potential energy whenever hydrogen atoms are trans to one another in a H–C–C–H system. The potential function for ethylene then takes the form

$$2V = 2V_{UBFF} + 2T(\Delta\phi_{312}\Delta\phi_{621} + \Delta\phi_{412}\Delta\phi_{521}), \quad (3)$$

where V_{UBFF} is defined in (2).

We shall discuss this model and the flexible bond model in a later section.

EXPERIMENTAL

The force constants and calculated frequencies were obtained by a least-squares adjustment process[3] which was terminated when corrections to all the force constants became less than | 0.0014 | md/A. Unless otherwise indicated all observed frequencies were given a weight of $1/\lambda_{obs}$[4] and all force constants except those transfered were refined simultaneously. The automatic input phase of POCO II[4] was used to construct the **G** and **Z** matrices for each molecule from the Cartesian coordinates and a code defining the internal coordinates. All input information, **F**, **G**, **Z** and £ matrices, potential-energy distribution (PED) matrices, Cartesian displacements, calculated-frequency dispersions, and correlation matrices, and the UBFC dispersion and

[2] In papers I, II, and III of this series the bending coordinates were scaled by multiplying by an arbitrary bond length r_0. It should therefore be noted that the bending force constants in those papers must be multiplied by r_0^2 for comparison with the present values.

[3] J. Overend and J. R. Scherer, J. Chem. Phys. **32**, 1289 (1960).

[4] J. R. Scherer and J. Overend, J. Chem. Phys. **32**, 1720 (1960).

TABLE I. Best estimates $\bar{\phi}_i$ of the force constants for the bromoethylenes assuming the flexible bond model. The dispersions $\sigma\{\bar{\phi}_i\}$ are given below each force constant.[a] Early in this study the refined magnitude of F_{HH} in ethylene was found to be 0.023 with a dispersion of 0.027 md/A. A similar result was found for vinylidene bromide and we have consequently set F_{HH} to zero and removed it from following refinements. For physical reasons we have also ignored C_{HH}.

	C_2H_4	C_2H_3Br	CH_2CBr_2	*trans*-$C_2H_2Br_2$	*cis*-$C_2H_2Br_2$	C_2Br_3H	C_2Br_4
K_{CC}	7.460 0.11	7.420 0.084	7.514 0.19	7.220 0.15	7.577 0.079	7.238 0.11	7.060 0.16
K_{CH}	4.807 0.030	4.878 0.043	4.927 0.069	4.897 0.025	4.845 0.025	4.847 0.035	
K_{CBr}		2.613 0.13	2.146 0.13	2.349 0.10	2.188 0.011	2.416 0.21	2.275 0.12
H_{CH}	0.319 0.023	0.262 0.042	0.301 0.070	0.187 0.061	0.270 0.022	0.209 0.060	
H_{CBr}		0.217 0.10	0.256 0.11	0.285 0.070	0.252 0.067	0.084 0.074	0.084 0.045
H_{BrBr}			0.235 0.095			0.236[f] ...	0.166 0.29
H_{HBr}		0.313 0.060		0.312 0.080	0.259[h] ...	0.277 0.082	
H_{HH}	0.413 0.008	0.401 0.016	0.387 0.014				
F_{CH}	0.495 0.049	0.427 0.073	0.374 0.12	0.427[h] ...	0.365[h] ...	0.427[e] ...	
F_{CBr}		0.618[e] ...	0.564 0.18	0.618[e] ...	0.867 0.069	0.638 0.14	0.618 0.14
F_{BrBr}			0.500[e]			0.744 0.20	0.500 0.17
F_{HBr}		0.272 0.060		0.272[e] ...	0.344 0.049	0.272[e] ...	
C_{BrBr}					0.100 0.035	0.187 0.067	0.228 0.065
C_{HBr}		0.053 0.033	0.049 0.10	0.047[f] ...		0.047[f] ...	
S_{HH}	0.048[b] 0.003	0.023[b] 0.008		0.089[b] 0.029	−0.017[d] 0.013		
S_{HBr}		0.056 0.030	0.001[d] 0.042	d,g			
S_{BrBr}							d,g

[a] Stretching and repulsive constants are in units of md/A. All bending constants are in units of 10^{-11} erg/(rad)^2.
[b] Necessary for good frequency fit.
[c] Transferred from C_2Br_4.
[d] Not needed for good frequency fit.
[e] Transferred from C_2H_3Br.
[f] Transferred from CH_2CBr_2 with S_{HBr} set to zero.
[g] Assumed zero.
[h] Transferred from the refinement of C_2H_3Br shown in Table II.

correlation matrices for all isotopes of the molecules in this series were dumped from the computer and are filed for convenient reference. Since we shall present only information pertinent to the ensuing discussion, viz., the UBFC's, observed and calculated frequencies, and PED's, there is no need to define here the internal coordinates used in the solution of the secular equations. We have in all cases constructed orthonormal symmetry coordinates and removed the angular redundancies.

Force constants calculated on the flexible bond model (II) and the trans-interaction model are given in Tables I and II, respectively. It must be emphasized that both sets of force constants $\bar{\phi}_i$ are the best estimates of ϕ_i which satisfy the least-squares criteria, and that the sole differences are in the model used, and in some cases, the type of UBFC transferred. The dispersions $\sigma\{\bar{\phi}_i\}$ of the best estimates are given below each force constant. In subsequent tables the best estimate of the

TABLE II. Best estimates $\tilde{\phi}_i$ of the force constants for the bromoethylenes assuming *trans*-H interaction. The dispersions are given below each force constant.[a]

	C_2H_4	C_2H_3Br	CH_2CBr_2	*trans*-$C_2H_2Br_2$	*cis*-$C_2H_2Br_2$	C_2Br_3H	C_2Br_4
K_{CC}	7.108 0.12	7.361 0.074	7.511 0.087	7.254 0.13	7.594 0.079	7.267 0.091	7.060 0.16
K_{CH}	4.834 0.024	4.909 0.035	4.926 0.042	4.906 0.035	4.826 0.022	4.840 0.041	
K_{CBr}		2.478 0.084	2.144 0.065	2.287 0.12	2.147 0.085	2.294 0.20	2.275 0.12
H_{CH}	0.335 0.018	0.332 0.025	0.302 0.032	0.238 0.031	0.247 0.015	0.216 0.029	
H_{CBr}		0.199 0.079	0.258 0.051	0.266 0.061	0.199 0.053	0.107 0.054	0.084 0.045
H_{BrBr}			0.236 0.092			0.236[d] ...	0.166 0.29
H_{HBr}		0.259 0.038		0.259[c] ...	0.259[c] ...	0.259[c] ...	
H_{HH}	0.440 0.008	0.395 0.011	0.387 0.014				
F_{CH}	0.450 0.037	0.365 0.059	0.376 0.074	0.365[c] ...	0.365[c] ...	0.365[c] ...	
F_{CBr}		0.618[b] ...	0.568 0.062	0.618[b] ...	0.897 0.064	0.669 0.12	0.618 0.14
F_{BrBr}			0.500[b] ...			0.725 0.16	0.500 0.17
F_{HBr}		0.303 0.047		0.334 0.063	0.393 0.035	0.370 0.068	
C_{BrBr}					0.107 0.035	0.173 0.055	0.228 0.065
C_{HBr}		0.039 0.025	0.047 0.022	0.043 0.040		0.041[d] ...	
T	0.087 0.006	0.057 0.011		0.089 0.017			

[a] See footnote to Table I.
[b] Transferred from C_2Br_4.
[c] Transferred from C_2H_3Br.
[d] Transferred from CH_2CBr_2.

TABLE III. Correlation matrix for vinylidene bromide.

K_{CC}	K_{CBr}	K_{CH}	H_{CBr}	H_{BrBr}	H_{CH}	H_{HH}	F_{CBr}	F_{BrBr}	F_{CH}	C_{HBr}
1	0.87	−0.57	−0.80	−0.91	−0.33	0.51	0.80	0.91	0.55	−0.56
	1	−0.68	−0.80	−0.95	−0.46	0.71	0.88	0.96	0.68	−0.77
		1	0.60	0.71	0.85	−0.38	−0.71	−0.71	−0.97	0.65
			1	0.85	0.29	−0.38	−0.86	−0.85	−0.59	0.54
				1	0.45	−0.67	−0.93	−0.999	−0.71	0.77
					1	−0.22	−0.40	−0.45	−0.89	0.37
						1	0.66	0.67	0.36	−0.79
	Sym.						1	0.93	0.71	−0.85
								1	0.70	−0.76
									1	−0.64
										1

frequency ν_i and its deviation from the observed frequency are denoted $\tilde{\nu}_i$ and $e=(\tilde{\nu}_{obs}-\tilde{\nu}_i)$. All PED matrix elements have been rounded to the nearest percent.

In preliminary studies each molecule was treated as a separate problem and an attempt was made to adjust all the force constants in the potential function to fit the available frequencies of each isotope. However, we

TABLE IV. Observed and calculated frequencies of ethylene. I, flexible bond model. II, Trans interaction model. All frequencies are in cm^{-1}.

	C_2H_4					C_2D_4				
		I		II			I		II	
	ν_{obs}	$\bar{\nu}_i$	e_i	$\bar{\nu}_i$	e_i	ν_{obs}	$\bar{\nu}_i$	e_i	$\bar{\nu}_i$	e_i
A_{1g}	3019.3	3003	16	3004	15	2251	2204	47	2205	46
	1623.3	1627	−4	1650	−27	1515	1525	−10	1507	−8
	1342.4	1322	20	1333	9	981	962	19	995	−14
B_{1g}	3075	3099	−24	3100	−25	2304	2130	−6	2313	−9
	1236	1240	−4	1229	7	1006	1010	−4	1000	6
B_{2u}	3105.5	3113	−8	3112	−7	2345	2315	30	2315	30
	810.3	810	0	815	−5	584	583	1	586	−2
B_{3u}	2989.5	3025	−36	3023	−34	2200.2	2198	2	2195	5
	1443.5	1466	−23	1448	−5	1077.9	1080	−2	1067	11

	C_2H_3D					C_2D_3H				
		I		II			I		II	
	ν_{obs}	$\bar{\nu}_i$	e_i	$\bar{\nu}_i$	e_i	ν_{obs}	$\bar{\nu}_i$	e_i	$\bar{\nu}_i$	e_i
	3103	3106	−3	3107	−4	3045	3063	18	3063	18
	3063	3063	0	3063	0	2280	2313	−33	2314	−34
	3002	3013	−11	3012	−10	2232	2255	−23	2255	−23
	2274	2255	19	2255	19	2222	2201	21	2200	22
	1605	1604	1	1617	−12	1546	1550	−4	1541	5
	1404	1413	−9	1394	10	1289.5	1287	2	1282	7
	1291	1279	12	1287	4	1046.9	1046	1	1042	5
	1129	1127	2	1126	3	995	988	7	1002	−7
	730	719	11	723	7	609.7	617	−7	621	−11

	CH_2CD_2					CHDCHD *trans*				
		I		II			I		II	
	ν_{obs}	$\bar{\nu}_i$	e_i	$\bar{\nu}_i$	e_i	ν_{obs}	$\bar{\nu}_i$	e_i	$\bar{\nu}_i$	e_i
A_1	3019	3014	5	3013	6	3035	3054	−19	3055	−20
	2231	2201	30	2200	31	2276	2255	21	2258	17
	1585	1590	−5	1598	−13	1567	1570	−3	1568	−1
	1384	1386	−2	1370	14	1282	1276	6	1286	−4
	1032	1015	17	1032	0	1001	1001	0	1007	−6
B_1	3095	3106	−11	3106	−11	3065	3072	−7	3070	−5
	2335	2313	22	2314	21	2271	2254	27	2253	28
	1150	1150	0	1140	10	1300	1310	−10	1295	5
	660	673	−13	676	−16	678	661	17	664	14

	CHDCHD *cis*					CHDCHD *cis* (continued)				
		I		II			I		II	
	ν_{obs}	$\bar{\nu}_i$	e_i	$\bar{\nu}_i$	e_i	ν_{obs}	$\bar{\nu}_i$	e_i	$\bar{\nu}_i$	e_i
A_1	3058	3062	−4	3062	−4	3056	3064	−8	3063	−7
	2300	2254	46	2255	45	2254	2255	−1	2255	−1
	1567	1572	−5	1569	−2	1344	1349	−5	1334	10
	1215	1196	19	1222	−7	1041	1050	−9	1040	1
	646	650	−4	656	−10					
B_1										

quickly found that such a procedure was undesirable since it lead to grossly uncertain force constants and a high instability in the refinement process. Indeed in the worst cases, the presence of a few highly uncertain force constants raised the uncertainties of other UBFC's to levels of 100% and greater. This leakage of instability arises from correlations between the various UBFC's. An estimate of the extent of this leakage may be obtained from the correlation matrix[5] which shows which force constants are sensitive to changes in other force constants. This matrix is symmetric and has unit entries along the diagonal; the off-diagonal elements which may have values between ± 1 are the correlation

[5] N. Arley and K. R. Buch, *Introduction to the Theory of Probability and Statistics* (John Wiley & Sons, Inc., New York, 1950) Chaps. 5 and 6.

TABLE V. Potential energy distributions for C_2H_4. I, flexible bond model; II, trans interaction model.

		I						II					
	ν_{obs}	K_{CC}	K_{CH}	H_{CH}	H_{HH}	F_{CH}	S_{HH}	K_{CC}	K_{CH}	H_{CH}	H_{HH}	F_{CH}	T
A_{1g}	3019.3	1	93	...	...	5	...	1	94	...	...	4	...
	1623.3	59	1	10	25	5	...	43	1	13	35	4	4
	1342.3	24	1	14	36	24	...	41	...	9	24	23	2
B_{1g}	3075	...	95	...	...	5	...	...	95	...	...	4	...
	1236	...	...	50	...	34	15	...	...	53	...	32	14
B_{2u}	3105.5	...	94	...	...	6	...	...	94	...	...	6	...
	810.3	...	2	72	...	47	−22	...	1	75	...	43	−20
B_{3u}	2989.5	...	92	...	...	8	...	...	93	...	...	7	...
	1443.5	...	2	23	60	14	...	...	2	25	66	13	−6

coefficients. A positive correlation coefficient between two force constants implies that a small increase in one force constant will cause the other to increase and vice versa.

Previously[4] we have shown that it is impossible to determine simultaneously, with much certainty, the F_{BrBr} and H_{BrBr} force constants of vinylidene bromide. From the correlation matrix in Table III it may be seen that the uncertainties in these two force constants are highly correlated so that in a subsequent refinement where only one of these two UBFC's has been transferred and held fixed, the other one is determined within pleasingly narrow limits. Moreover the high correlation coefficients of K_{CC}, K_{CBr}, and F_{CBr} with H_{BrBr} and F_{BrBr} indicate that the uncertainties of these may be, and indeed are, reduced by such a transfer. It is important to note that transferring some other UBFC such as H_{HH} or H_{CH} will not relieve the uncertainties in H_{BrBr} and F_{BrBr} since the respective correlation coefficients are small. Tables I and II show the results of transferring F_{BrBr} from C_2Br_4 and it may be noted the uncertainties in all the remaining UBFC's are lower than in footnote reference 4.

It has been our experience that large uncertainties result if one tries to determine simultaneously all the force constants of the di- and tribromoethylenes. Consequently we have supplied values for some of the force constants, taking them from other molecules in this series where the form of the normal coordinates allows their evaluation with greater certainty. However the problem of which force constants to supply and constrain is more complicated in these cases because the correlations are much more complex. In making our choice, we have been guided by the correlation matrix, and have tried to restrict the number of force constants transferred to the minimum necessary to eliminate the gross uncertainties; our final results are summarized in Tables I and II.

The geometry adopted for the bromine-substituted members of the series was $r_{CBr}=1.90$ A, $r_{CC}=1.31$ A, $<CCBr=123°$ and except for ethylene and the hydrogen parameters adopted were $r_{CH}=1.07$ A, $<CCH=121.5°$. Allen and Plyler[6] have obtained accurate geometry for ethylene and we have used their values. The frequency data and the results are described for each molecule in the following:

Ethylene

Curtis[7] has already evaluated UBFC's for ethylene as part of an extensive comparison of various potential functions for that molecule. However, since he did not use the Allen-Plyler geometry, we have repeated his work for the UBFF with the flexible-bond parameter S_{HH}, but have found that these modifications to the

TABLE VI. Observed and calculated frequencies of tetrabromoethylene.

	ν_{obs}	$\bar{\nu}_i$	e_i
A_{1g}	1535	1535	0
	265	275	−10
	144	142	2
B_{1g}	880	882	−2
	208	196	12
B_{2u}	766	760	6
	119	120	−1
B_{3u}	635	641	−6
	188	181	7

TABLE VII. Potential energy distributions for C_2Br_4.

	ν_{obs}	K_{CC}	K_{CBr}	H_{CBr}	H_{BrBr}	F_{CBr}	F_{BrBr}	C_{BrBr}
A_{1g}	1535	85	8	...	1	5	1	...
	265	2	58	...	...	17	20	4
	144	...	...	2	10	14	37	37
B_{1g}	880	...	63	10	...	22	...	6
	208	...	28	6	...	65	...	...
B_{2u}	766	...	87	...	...	12	1	2
	119	...	1	5	...	24	...	71
B_{3u}	635	...	57	1	4	32	6	−1
	188	...	10	3	11	8	66	2

[6] H. C. Allen, Jr. and E. K. Plyler, J. Am. Chem. Soc. **80**, 2673 (1958).
[7] E. C. Curtis, dissertation, University of Minnesota, 1959.

TABLE VIII. Observed and calculated frequencies of vinylidene bromide (consistent with Table II).

	CH_2CBr_2			CD_2CBr_2			$CHDCBr_2$		
	ν_{obs}	$\bar{\nu}_i$	e_i	ν_{obs}	$\bar{\nu}_i$	e_i	ν_{obs}	$\bar{\nu}_i$	e_i
A_1	3023	3027	−4	2230	2213	17	3061	3077	−16
	1593	1600	−7	1545	1540	5	2282	2266	16
	1379	1372	7	1019	1020	−1	1563	1565	−2
	467	468	−1	453	452	1	1258	1261	−3
	184	184	0	183	183	0	949	949	0
							655	654	1
B_1	3108	3121	−13	2339	2325	14	458	460	−2
	1065	1068	−3	932	929	3	300	300	0
	696	702	−6	624	618	6	184	183	1
	322	319	3	283	285	−2			

TABLE IX. Potential energy distribution for CH_2CBr_2 (consistent with Table II).

	ν_{obs}	K_{CC}	K_{CBr}	K_{CH}	H_{CBr}	H_{CH}	H_{BrBr}	H_{HH}	F_{CBr}	F_{CH}	F_{BrBr}	C_{HBr}
A_1	3023	1	...	94	...	...	...	...	...	4	...	...
	1593	66	2	1	...	7	...	18	2	2	...	...
	1379	19	2	1	...	16	...	42	...	15	...	3
	467	1	53	...	2	...	4	...	30	...	6	3
	184	...	9	...	8	...	14	...	6	...	60	2
B_1	3108	...	...	96	...	...	...	...	...	4	...	...
	1065	...	11	...	5	50	...	...	3	26	...	4
	696	...	69	...	8	8	...	...	5	4	−1	5
	322	...	10	...	24	...	...	...	55	...	...	11

geometry result in only slight differences in the force constants. We used the assignment of Crawford, Lancaster, and Inskeep[8] and the UBFC's in Tables I and II were obtained by fitting selected frequencies of Table VI in footnote reference 8. The observed and calculated frequencies for the flexible-bond and trans-interaction models are given in Table IV and the corresponding PED's are given in Table V.

Tetrabromoethylene

Mann, Fano, Meal, and Shimanouchi[9] have calculated a set of UBFC's which reproduce the observed frequencies of this molecule quite well. Because we have chosen to fit the observed frequencies on equal merit and not on a percentage basis[4] our weighting function and hence the resulting force constants differ slightly from theirs: the deviations are not, however, outside the dispersions $\sigma\{\bar{\phi}_i\}$ obtained here. The observed and calculated frequencies are given in Table VI and the PED is given in Table VII.

Vinylidene Bromide

Preliminary work on the UBFF of this molecule has already been reported.[4] However, the present results differ slightly as we have now transfered a force constant from C_2Br_4. The assignment used in the refinement was that of DeHemptinne, Velghe, and Van Riet[10] and the observed and calculated frequencies and PED matrix for CH_2CBr_2 are given in Tables VIII and IX, respectively.

Vinyl Bromide

Charette and DeHemptinne[11] have measured the vibrational spectra of eight isotopes of vinyl bromide but they were unable to assign any of the planar fundamentals of the cis and trans mixtures of C_2H_2DBr and C_2D_2HBr. We have found that our calculations with the UBFF allow us to make an assignment from their spectral data. The zeroth-order calculations (ν_{calc}°) for these four cis and trans molecules are shown in Table X. Since all the force constants adopted in this calculation were transferred from related molecules, many of the calculated frequencies are systematically larger or smaller than the observed ones; viz, all the calculated CBr bending modes (~320 cm^{-1}) were low by ~10 cm^{-1} and all the CBr stretching frequencies (~580 cm^{-1} were low by ~20 cm^{-1}. If allowance is made for this absolute error, we find that many of the bands observed by Charette and DeHemptinne, can be assigned to their respective molecules. By including these newly assigned frequencies and those for the remaining four molecules in a general refinement, a second set of calculated frequencies was obtained, and,

[8] B. L. Crawford, J. E. Lancaster, and R. G. Inskeep, J. Chem. Phys. **21**, 678 (1953).

[9] D. E. Mann, L. Fano, J. H. Meal, and T. Shimanouchi, J. Chem. Phys. **27**, 51 (1957).

[10] M. DeHemptinne, C. Velghe, and R. Van Riet, Bull. classe sci. acad. roy. Belg. **30**, 40 (1944).

[11] J. Charette and M. DeHemptinne, Bull. classe sci. acad. roy. Belg. **38**, 934 (1952).

TABLE X. Zeroth-order calculation, first refinement, and assignments for *cis*- and *trans*-C_2H_2DBr and C_2D_2HBr.

			1st refinement			
	ν_{calc}[a]	1st assignment	wt	$\bar{\nu}_i$	e_i	2nd assignment
	3074	3089	a	3098	−9	3089
	3065	?	0	3074		?
	2258	?	0	2263		?
	1569	1574.5	a	1570	4	1574.5
trans-C_2H_2DBr	1254	1268	a	1274	−6	1268
	1158	?	0	1224		?
	866	?	0	892		886
	558	578	a	577	−1	578
	326	336	a	334	2	336
	3074	3089	a	3097	−8	3089
	3066	?	0	3074		?
	2255	?	0	2265		?
	1572	1574.5	a	1569	5	1574.5
cis-C_2H_2DBr	1279	1297	a	1303	−6	1297
	1124	?	0	1156		1188
	865		0	909		899
	582	599	a	599	0	599
	311	319	a	322	−3	319
	3065	3052	a	3075	−23	3052
	2275	?	0	2282		?
	2254	?	0	2263		?
	1544	1549	a	1556	−7	1549
cis-C_2D_2HBr	1230	1249	a	1256	−7	1249
	958	?	0	1030		1017
	776	784	a	780	4	780
	547	565	a	562	3	562
	323	332	a	332	0	332
	3066	3052	a	3074	−22	3052
	2277	?	0	2283		?
	2248	?	0	2264		?
	1544	1549	a	1553	−4	1549
trans-C_2D_2HBr	1250	1265	a	1260	5	1265
	898	?	0	972		983.5
	812	?	0	821		805
	565	585	a	577	8	585
	309	317	a	320	−3	317

[a] Weight matrix element $= 1/\lambda_{obs}$.

from this set (Table X) additional bands were assigned. The small frequency separation between the calculated C=C stretching vibrations in the cis and trans mixtures suggests that the assumption that $\nu_{C=C}$ is the same in both cis and trans isomers is not seriously in error. The calculated frequencies on the basis of this last assignment are given in Table XI and the PED for C_2H_2Br is given in Table XII.

Cis-Dibromoethylene

The assignments[12–15] of the frequencies of this molecule are listed in Table XIII with the calculated frequencies, the PED for $C_2H_2Br_2$ is given in Table XIV.

Trans-Dibromoethylene

The assignments[12–15] which have been made for this molecule are not in complete agreement, the difficulty being that no one has observed the infrared allowed B_u fundamental ν_{12}. DeCroes *et al.* adopted a value of 220 cm^{-1} for this fundamental in $C_2H_2Br_2$, whereas Dowling *et al.* assigned it a value of 192 cm^{-1} from combination-band data. DeCroes *et al.* observed a weak line in the Raman spectrum of CHBrCDBr at 197 cm^{-1}, which they assigned to the heretofore unobserved trans bromine out-of-plane deformation ν_7, but we prefer to assign this line to ν_{12} of CHBrCDBr. However, a far-infrared measurement on all three isotopes of this molecule must be made before this question can be finally settled. Fortunately the differences between the two assignments do not detract seriously from the information which may be obtained from the planar hydrogen deformations. The calculated frequencies are given in Table XV and the PED for $C_2H_2Br_2$ is given in Table XVI.

[12] J. Charette, dissertation, University of Louvain, Belgium, 1954.
[13] J. M. Dowling, P. G. Puranik, and A. G. Meister, J. Chem. Phys. **26**, 233 (1957).
[14] M. DeCroes, M. Perlinghi, and R. Van Riet, Bull. classe sci. acad. roy. Belg. **42**, 379 (1956).
[15] J. C. Evans, H. J. Bernstein, Can. J. Chem. **33**, 1171 (1955).

TABLE XI. Observed and calculated frequencies for vinyl bromide. I, flexible bond model; II, trans interaction model.

$CHBrCH_2$					$CDBrCH_2$				
	I		II			I		II	
ν_{obs}	$\bar{\nu}_i$	e_i	$\bar{\nu}_i$	e_i	ν_{obs}	$\bar{\nu}_i$	e_i	$\bar{\nu}_i$	e_i
3113	3116	−3	3115	−2	3110	3115	−5	3114	−4
3086	3100	−14	3102	−16	3020	3023	−3	3020	0
3027	3022	5	3020	7	2308	2282	26	2283	25
1604	1599	5	1610	−6	1588	1589	−1	1597	−9
1373	1386	−13	1375	−2	1374	1371	3	1363	11
1256	1241	15	1252	4	1091	1093	−2	1102	−11
1006	1004	1	1007	−1	841	845	−4	850	−9
613	614	−1	614	−1	595	592	3	590	5
348	348	0	347	1	345	346	−1	345	0

trans-CHBrCHD					*cis*-CHBrCDH				
	I		II			I		II	
ν_{obs}	$\bar{\nu}_i$	e_i	$\bar{\nu}_i$	e_i	ν_{obs}	$\bar{\nu}_i$	e_i	$\bar{\nu}_i$	e_i
3089	3103	−16	3104	−15	3089	3101	−12	3103	−14
3057[a]	3070	−13	3069	−12	3057[a]	3072	−15	3070	−13
2289[a]	2262	27	2263	26	2274.5[a]	2261.1	13.4	2261.1	13.4
1574.5	1569.8	4.7	1571.5	3	1574.5	1569.3	5.2	1569.3	5.2
1268	1269	−1	1260	8	1297	1308	5	1303	−6
1244[a]	1240	4	1248	−4	1188	1161	27	1181	7
886	887	−1	881	5	899	900	−1	888	11
578	573	5	577	1	599	602	−3	602	−3
336	335	1	335	1	319	320	−1	321	−2

cis-CDBrCDH					*trans*-CDBrCHD				
	I		II			I		II	
ν_{obs}	$\bar{\nu}_i$	e_i	$\bar{\nu}_i$	e_i	ν_{obs}	$\bar{\nu}_i$	e_i	$\bar{\nu}_i$	e_i
3052	3072	−20	3070	−18	3052	3072	−20	3070	−18
2291[a]	2282	9	2284	7	2282.5[a]	2281.5	−1	2283.7	−1.2
2264.5[a]	2261.5	3	2262.3	2.2	2243.5[a]	2260.8	−17.3	2260.2	16.7
1549	1556	−7	1556	−7	1549	1554	−5	1552	−3
1249	1257	−8	1256	−7	1265	1260	5	1265	0
1017	1031	−14	1029	−12	983.5	972.5	11	981.2	2.3
784	777	7	778	6	805	815	−10	808	−3
565	562	3	565	0	585	585	0	584	1
332	332	0	333	−1	317	318	−1	319	−2

$CHBrCD_2$					$CDBrCD_2$				
	I		II			I		II	
ν_{obs}	$\bar{\nu}_i$	e_i	$\bar{\nu}_i$	e_i	ν_{obs}	$\bar{\nu}_i$	e_i	$\bar{\nu}_i$	e_i
3080	3101	−21	3103	−23	2351	2320	31	2320	31
2337	2320	17	2320	17	2317	2281	36	2283	34
2234	2208	26	2208	26	2226.5	2207.7	18.8	2208.0	18.5
1548	1549	−1	1544	8	1524	1532	−8	1525	−1
1239	1243	−4	1240	−1	1030	1049	−19	1041	−11
1018	1003	15	1013	5	984	964	20	975	9
860	866	−6	852	8	775.5	769.6	5.9	763.7	11.8
567.5	556.5	1	570.0	2.5	560	557	3	559	1
309	310	−1	313	−4	306	308	−2	311	−5

[a] Given zero weight in the present refinement.

TABLE XII. Potential energy distribution for C_2H_3Br (consistent with Table II).

ν_{obs}	K_{CC}	K_{CBr}	K_{CH}	H_{CBr}	H_{CH}	H_{HBr}	H_{HH}	F_{CBr}	F_{CH}	F_{HBr}	C_{HBr}	T
3113	...	...	95	...	...	...	...	...	4	...	...	...
3086	...	...	93	...	...	...	...	...	4	2	...	...
3027	1	...	94	...	...	...	...	...	4	...	...	...
1604	59	2	1	...	11	2	19	1	3	1	...	1
1373	14	2	1	...	22	4	40	...	14	2	1	−2
1256	12	1	...	...	34	13	1	1	23	9	1	4
1006	...	2	...	1	55	8	...	1	26	8	2	−3
613	...	69	...	3	6	1	...	6	3	11	1	...
348	...	4	...	17	7	6	...	50	3	3	9	−1

TABLE XIII. Observed and calculated frequencies for *cis*-dibromoethylene (consistent with Table II).

	CHBrCHBr			CDBrCDBr			CHBrCDBr		
	ν_{obs}	$\bar{\nu}_i$	e_i	ν_{obs}	$\bar{\nu}_i$	e_i	ν_{obs}	$\bar{\nu}_i$	e_i
A_1	3080	3091	−11	2301	2281	20	3078	3091	−13
	1589	1588	1	1552	1557	−5	2302	2275	27
	1150	1150	0	823	819	4	1575	1573	2
	589	586	3	574	573	1	1227	1224	3
	114	114	0	114	114	0	924	912	12
							707	707	0
B_1	3073	3091	18	2281	2269	12	576	579	−3
	1264	1270	−6	1003	1010	−7	459	462	−3
	758	753	5	675	682	−7	114	114	0
	469	472	−3	459	454	5			

TABLE XIV. Potential energy distribution for the *cis*-$C_2H_2Br_2$ (consistent with Table II).

	ν_{obs}	K_{CC}	K_{CH}	K_{CBr}	H_{CBr}	H_{CH}	H_{HBr}	F_{CBr}	F_{CH}	F_{HBr}	C_{BrBr}
A_1	3080	...	92	...	...	...	...	...	4	3	...
	1589	80	...	4	...	3	5	3	3	2	...
	1150	5	...	...	...	24	24	...	20	26	...
	589	...	...	69	...	1	...	18	1	8	1
	114	...	...	...	12	5	3	37	3	3	35
B_1	3073	...	92	...	...	...	...	...	4	3	...
	1264	...	...	4	...	31	25	...	20	19	...
	758	...	...	37	13	2	6	17	1	21	1
	469	...	...	32	6	2	2	56	2	1	...

TABLE XV. Observed and calculated frequencies for *trans*-dibromoethylene (consistent with Table II).

	CHBrCHBr			CDBrCDBr			CHBrCDBr		
	ν_{obs}	$\bar{\nu}_i$	e_i	ν_{obs}	$\bar{\nu}_i$	e_i	ν_{obs}	$\bar{\nu}_i$	e_i
A_g	3089	3101	−12	2322	2287	35	3083	3106	−23
	1579	1574	5	1528	1539	−11	2316	2285	31
	1247	1252	−5	972	973	−1	1561	1557	4
	745	748	−3	671	671	0	1215	1208	7
	217	217	0	217	216	1	929	924	5
							717	716	1
B_u	3094	3112	−18	2293	2282	11	668	659	9
	1162	1157	5	863	875	−12	217	217	0
	687	687	0	650	654	−4	197	200	−3
	?	205	...	?	196	...			

TABLE XVI. Potential energy distribution for *trans*-$C_2H_2Br_2$ (consistent with Table II) (value in brackets is a calculated frequency).

	ν_{obs}	K_{CC}	K_{CH}	K_{CBr}	H_{CBr}	H_{CH}	H_{HBr}	F_{CBr}	F_{CH}	F_{HBr}	C_{HBr}	T
A_g	3089	...	93	...	...	...	...	...	3	3	...	...
	1579	72	...	6	...	6	7	2	2	3	...	2
	1247	14	...	...	1	22	14	1	23	11	4	8
	745	...	...	37	18	2	8	12	1	20	2	1
	217	1	...	36	9	1	3	45	1	1	3	...
B_u	3094	...	92	...	...	...	...	...	5	3	...	...
	1162	...	...	1	...	28	32	1	18	24	5	−10
	687	...	...	74	...	...	...	17	...	8	1	...
	(205)	...	...	3	26	8	4	35	5	6	15	−3

Tribromoethylene

The assignments[15,16] of this molecule are straightforward and are listed with the calculated frequencies in Table XVII the PED for C_2HBr_3 is given in Table XVIII.

DISCUSSION

It is our intent in the following to discuss two points: the first is the problem of the transferability of UBFC's and the second is that of bond flexibility. The latter discussion of bond flexibility will in no way alter our conclusions about the transferability of the UBFF since it may be seen through comparison of Tables I and II that both sets of UBFC's, excluding the flexibility parameters, are moderately transferable.

Transferability

One way to demonstrate the transferability of a force-field is to assume that all similar force constants in related molecules are identical and to carry out a simultaneous refinement of all molecules. However, this procedure is open to the criticism that small, but possibly significant differences between the force constants are ignored. A second way of demonstrating transferability is to show that the best estimates of similar force constants in different molecules, obtained by a general solution of all force constants for each molecule, are the same within reasonable limits. In this work we have followed the latter course and have sought an independent solution for each molecule. However, as we have seen even for a relatively small molecule it is usually impossible to determine all the force constants and hence we have transferred, within this series, a minimum number of those UBFC's which were highly uncertain, while at the same time maintaining a satisfactory fit to the observed frequencies (see Fig. 3). The best estimates of the remaining UBFC's were then compared from the viewpoint of their transferability. Comments regarding the transfer of the UBFC's in Tables I and II are discussed molecule by molecule in the following. All stretching and repulsive UBFC's, K, F, and C, are in units of md/A and the bending UBFC's, H and S are in units of 10^{-11} erg/(rad)^2.

TABLE XVII. Observed and calculated frequencies of tribromoethylene (consistent with Table II).

C_2HBr_3			C_2DBr_3		
ν_{obs}	$\bar{\nu}_i$	e_i	ν_{obs}	$\bar{\nu}_i$	e_i
3080	3092	−12	2290	2273	17
1557	1561	−4	1550	1546	4
1210	1214	−4	953	947	6
832	826	6	775	793	−18
704	702	2	678	668	10
504	505	−1	493	492	1
238	242	−4	238	242	−4
184	179	5	182	179	5
115	115	0	115	115	0

[16] J. R. Scherer, J. C. Evans, and J. Overend, J. Chem. Phys. 33, 314 (1960).

Ethylene

The dispersions and the best estimates of the UBFC's in Tables I and II show that ethylene is the only molecule in the series which admits a reasonably certain solution without transfering force constants.

Tetrabromoethylene

It is interesting to note that even though this molecule has a high degree of symmetry and a small number of UBFC's the force constant H_{BrBr} is not particularly

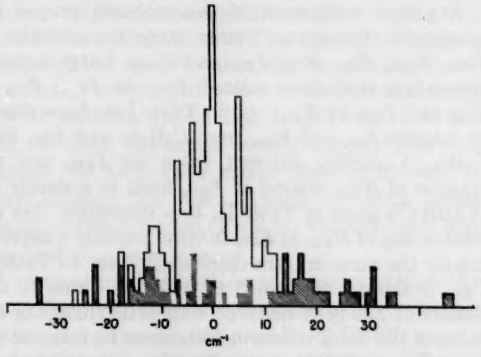

FIG. 3. Distribution of errors e_i for all the bromoethylenes, consistent with Table II. The mean error is +1 cm^{-1} and the standard deviation is ±12 cm^{-1}.

TABLE XVIII. Potential energy distributions for C_2Br_3H (consistent with Table II).

ν_{obs}	K_{CC}	K_{CBr}	K_{CH}	H_{CBr}	H_{CH}	H_{BrBr}	H_{HBr}	F_{CBr}	F_{CH}	F_{BrBr}	F_{HBr}	C_{BrBr}	C_{HBr}
3080	...	...	92	...	...	...	...	...	4	...	3	...	...
1557	81	6	...	...	...	...	3	4	1	1	1	...	...
1210	3	3	...	...	24	...	24	1	20	...	20	...	5
832	...	64	...	9	...	...	3	17	...	−1	5	2	1
704	...	69	...	1	...	1	...	18	...	1	9	...	...
504	1	46	...	3	2	3	...	35	2	5	1	...	1
238	...	30	...	3	1	2	1	31	...	29	...	1	...
184	...	10	...	4	...	9	...	29	...	40	...	2	3
115	...	1	...	8	1	...	2	32	1	...	2	48	3

well defined. Unfortunately, it is not possible to determine a better value for this force constant from the other molecules in this series, despite the fact that isotopic frequency data are available.

Vinylidene Bromide

In the preceding it was shown that the H_{BrBr} and F_{BrBr} force constants are strongly correlated and that they cannot be determined simultaneously. We have therefore transferred F_{BrBr}, in preference to H_{BrBr}, from C_2Br_4 where it is known with more certainty. As expected, the remaining force constants compare well with our previous work[4] and the PED in Table XII is also comparable with the exception of the 194 cm^{-1} mode.

Vinyl Bromide

In preliminary work on this molecule, the refined values of F_{CBr} and H_{CBr} were found to be 0.973 and −0.005 with dispersions of 0.45 and 0.26, respectively. Because of a moderate (negative) correlation coefficient between these two force constants we have only transferred F_{CBr} from C_2Br_4. In a refinement not shown here, a value of 0.258 for H_{CBr} transferred from vinylidene bromide gave a value of 0.556 for F_{CBr} with a dispersion of 0.13 md/A.

Trans-Dibromoethylene

A general refinement of this molecule proved impracticable because of rather large uncertainties in F_{CBr}, K_{CBr}, F_{CH}, H_{CH}, F_{HBr} and H_{HBr}. Large negative correlation coefficients related K_{CBr} to F_{CBr}, F_{CH} to H_{CH} and F_{HBr} to H_{HBr} and in Table I we have chosen to transfer F_{CH} and F_{HBr} from C_2H_3Br and F_{CBr} from C_2Br_4. A slightly different value for F_{CH}, and the transfer of H_{HBr} instead of F_{HBr} leads to a similar set of UBFC's given in Table II. It is interesting that the relationship of H_{HBr} to F_{HBr} in vinyl bromide is approximately the same in trans dibromoethylene. In Table I, C_{HBr} is shown constrained to 0.047: in Table II this constraint has been removed with little change in the value of this force constant. Note must be taken of the low value (∼0.24) of the H_{CH} force constant. It is equally probable that a satisfactory fit to the observed frequencies could be obtained by transferring H_{CH} from vinylidene bromide but this would drop F_{CH} lower than its value in vinyl bromide.

Cis-Dibromoethylene

The difficulties found for *cis*-$C_2H_2Br_2$ were as serious as those found for *trans*-$C_2H_2Br_2$: F_{CH} was found to be uncertain and only moderately correlated (negative) with H_{CH} and we have consequently transferred it from C_2H_3Br. F_{CBr} converged to a larger value (0.89) than in C_2Br_4, and, H_{CBr} seems reasonably compatible with previous values determined from CH_2CBr_2 and C_2H_3Br: a mean value for the series is centered around 0.2×10^{-11} erg/(rad)^2. C_{BrBr} was the best determined force constant in this molecule and despite the instability of early refinements, it converged to the value 0.1 md/A with low uncertainty. Again the H_{HBr} constant was highly correlated (negative) with the F_{HBr} constant.

Tribromoethylene

In this molecule, the choice of which force constants to transfer was particularly difficult. Our first approach was to transfer a sufficient number of force constants to determine the remaining ones with reasonable precision. In this way we were able to obtain a set of UBFC's which allowed us to reproduce the observed frequencies within 4 cm^{-1}. This extremely good fit was obtained by allowing both H_{HBr} and F_{HBr} to vary in the refinement. The values thus obtained for H_{HBr} and F_{HBr} were 0.068±0.073 and 0.522±0.089, respectively. Now in the rest of this series, with model III, we have used a single value of H_{HBr}=0.259 determined from vinyl bromide and through a desire to introduce as much uniformity as possible into the force constants, we have constrained H_{HBr} to this value and have obtained a set of force constants which fit the frequencies within the expected limits of the UBFF. In the case of model II we chose to transfer F_{HBr}, and with a slightly different transferred value of F_{CH}, obtained an equally satisfactory set of force constants. It is interesting that in both Tables I and II F_{BrBr} is higher than in C_2Br_4, which suggests that a more suitable compromise value for this force constant might be ∼0.6 md/A. As in *cis*-dibromoethylene the C_{BrBr} force constant was determined with considerable precision.

Résumé

In general, these results indicate that the UBFF is a moderately transferable force field. Tables I and II show that the H_{HH} constant is well determined and only slightly different in the three cases studied. Values of H_{CH} are also very similar but when the carbon atom of a CH bond is also joined to a bromime atom, H_{CH} seems to decrease slightly reaching a low value of ~0.2 in tribromoethylene. This decrease might have shown itself in vinyl bromide had we not chosen to assume that all H_{CH} bending constants are the same; however, it was felt that the degree of uncertainty introduced by this more general model did not warrant its use. This apparent drop in the H_{CH} constant may not be real since in the three molecules where it has a low value, it was necessary to fix either F_{CH} or H_{CH}. Indeed, if we had chosen to transfer the value of H_{CH} instead of F_{CH} the correlation coefficients indicate that the value of F_{CH} would have decreased in the series. As pointed out in the preceding the H_{HBr} and F_{HBr} constants are reasonably constant throughout the series; if there is a slight trend, it is such that F_{HBr} increases and H_{HBr} decreases with increased halogen substitution. The value of C_{BrBr} is well determined in the di- tri-, and tetrabromoethylenes. Moreover the low correlation with the other force constants suggests that the trend observed for this constant is significant.

Bond Flexibility

Shimanouchi[1] has shown the importance of both the C=C flexible-bond model and general flexible-bond model in explaining the rocking frequencies of ethylene. However Mann *et al.*, in their studies of the per-halo ethylenes, found that the flexible C=C bond parameter α converged to a small value and they excluded it from their calculations. In view of the otherwise similar properties of the C=C bond, it is disturbing that it should have such a different flexibility in C_2Br_4 than in C_2H_4.

Model II avoids this difficulty since it incorporates the flexibility of the CH and CBr bonds and hence we would not necessarily expect S_{HH} to be the same as S_{BrBr}. Since the converged value of S_{BrBr} in C_2Br_4 was small ($\bar{S}_{BrBr}=-0.046$), uncertain ($\sigma\{\bar{S}_{BrBr}\}=0.076$), and did not improve the fit to any of the observed fundamentals by more than 2 cm^{-1}, we have assumed S_{BrBr} to be zero for the whole series. We also see from Table I the value of S_{HBr} obtained from CH_2Br_2 and C_2H_3Br is small and uncertain, and again it was found that the frequency fit was not significantly improved by its inclusion. In general Table I shows that the flexibility parameter S_{HH} is only important for C_2H_4, C_2H_3Br, and *trans*-$C_2H_2Br_2$. On the basis of model II the flexibility term S_{HH} also appears in *cis*-dibromoethylene, but, in this case it appears as the coefficient to the interaction term between the *cis*-CCH angles. If then, the S_{HH} term is significant in *trans*-dibromoethylene we would expect it to be equally important in *cis*-dibromoethylene. Such is, in fact, not the case for in Table I we see that the refined magnitude of this constant in *cis*-dibromoethylene is small and not comparable with the *trans*-dibromoethylene value. We therefore conclude that an interaction term appears to be needed between *trans*-CCH angle deformations and the reason for the partial success of model II stems from the incorporation of these trans-interaction terms.

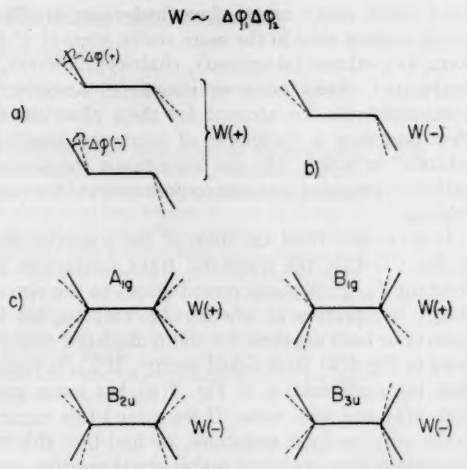

FIG. 4. Contribution to the potential energy W, when the product of the trans angle bending coordinates is positive or negative and the interaction constant T_{ij} is positive. (a) High-energy forms ($W+$). (b) Low-energy form ($W-$). (c) Application of (a) and (b) to ethylene.

The relative importance of the S_{HH} terms in *cis*- and *trans*-$C_2H_2Br_2$ has led us to try a third model, referred to earlier as the trans-interaction model (III), in which we supplement the UBFF with quadratic cross terms between trans CCH angle bending coordinates. Tables II and IV show that this interaction term is significant and that it does as well as the flexible bond model in explaining the frequency data for ethylene. From the ethylene PED's for models II and III in Table V we see that the contributions of T are parallel to those of S_{HH} except for small terms in the A_{1g} and B_{3u} classes. The signs of these contributions to the potential energy may be understood from Fig. 4. In Table II we note that the trans interaction is also important in vinyl bromide but to a lesser extent than in ethylene. In *trans*-$C_2H_2Br_2$, S_{HH} and T have the same refined magnitudes since models II and III are equivalent when S_{HBr} and S_{BrBr} are zero.

Unfortunately, we have found it easier to show that a trans bending interaction constant removes the most serious objections to an unmodified UBFF, than to explain the origin of such a term. Stewart and Eyring[17]

[17] G. H. Stewart and H. Eyring, J. Chem. Ed. **35**, 550 (1958).

have noted many cases where molecular equilibrium configurations exist in the more stable *trans*-H–C–C–H form, i.e., ethane (staggered), chair-cyclohexanes, and conjugated chains such as butadiene, acrolein, and crotonaldehyde. To account for these observed cases they postulate a "principle of minimum bending of orbitals" in which "the electrons prefer the straighter pathways provided by trans conformation of four-center orbitals."

It is obvious from the form of the potential energy in Eq. (3) that the quadratic trans interaction force constant T_{ij} gives equal contributions to the potential energy irrespective of whether $\Delta\phi_i$ and $\Delta\phi_j$ are both positive or both negative, i.e., both displaced configurations in Fig 4(a) have equal energy. If T_{ij} is positive, then the configuration in Fig. 4(b) has lower energy than 4(a) and vice versa. If we extend this argument to the ethylene-type molecules, we find that this trans interaction force constant makes equal positive contributions to the A_{1g} and B_{1g} symmetry force constants and equal negative contributions to the B_{2u} and B_{3u} ones.

However, when we try to reconcile this force constant with the Eyring-Stewart concept we immediately run into difficulties. Even though the "degree-of-bending" of an orbital is a somewhat transcendental quantity, we feel intuitively that, if there is any substance in the principle of minimum bending, the configurations in Fig. 4(a) should have different energies, one higher and one lower than that of Fig. 4(b). An even potential function can never give such an energy distribution, and therefore we should expect the Eyring-Stewart effect to appear in cubic or possibly higher odd terms in the potential energy. There is always a danger that the trans-interaction term might be the result of forcing a quadratic potential function to fit the observed frequencies, and that harmonic-frequency data would not require such a term. Unfortunately, the presently available anharmonicity corrections for ethylene[8] were derived by an approximate method and cannot be expected to settle this question. A detailed study of the overtone and combination bands of ethylene, with a view to establishing precise values for the zeroth-order frequencies, would be particularly helpful and we shall defer further discussion of this effect until such additional data become available.

The fact that inclusion of the quadratic trans-interaction cross term makes for a fairly consistent transferability picture in this series of bromoethylenes has encouraged us to try similar terms in the UBFF of ethane and propane. Preliminary results, which will be reported in another paper, indicate that here again T_{ij} is a significant parameter.

ACKNOWLEDGMENTS

We should like to express our gratitude to Dr. N. Wright and Dr. W. J. Potts for their continued encouragement in this work.

THE JOURNAL OF CHEMICAL PHYSICS VOLUME 33, NUMBER 6 DECEMBER, 1960

Dynamical Jahn-Teller Effect in Hydrocarbon Radicals*

W. D. HOBEY† AND A. D. MCLACHLAN‡

Gates and Crellin Laboratories of Chemistry,§ California Institute of Technology, Pasadena, California

(Received May 9, 1960)

The first part of this paper shows how the ordinary Born-Oppenheimer approximation for separating nuclear and electronic motion can be adapted to a degenerate electronic state. To set up equations of motion for the dynamical Jahn-Teller effect in their simplest form we use vibrational amplitudes associated with special linear combinations of the degenerate electronic wave functions, chosen to vary as slowly as possible with nuclear displacements. We also discuss briefly the symmetry-forbidden electronic transitions allowed by a Jahn-Teller distortion. In the second we make molecular orbital calculations of the energies and distorted shapes of some aromatic hydrocarbon molecules. The differences in energy between the distorted and symmetrical shapes (in kcal/mole) are cyclobutadiene 11.43; cyclopentadienyl 1.414, cycloheptatrienyl 0.859; benzene negative ion 1.077; triphenylene and coronene negative ions 0.385 and 0.299. In the last three each shape of minimum energy is separated from two equivalent ones by a small potential barrier, respectively, 0.000, 0.001, and 0.002. The ground state of each radical is doubly degenerate, and it can oscillate about a continuous series of distorted shapes. In the excited ${}^1E_{1u}{}^+$ and ${}^3E_{1u}{}^+$ states of benzene the distortions are much smaller, and the CC bonds probably bend rather than stretch.

INTRODUCTION

IN the last few years there has been great interest in the properties of the stable, radical ions formed by many aromatic hydrocarbons in solution,[1–4] and in the information[5,6] about their electronic structure which has been provided by electron-resonance experiments.[7] Of special interest are the negative radical ions of benzene, coronene, and triphenylene studied by Weissman, Tuttle, and de Boer.[7] The molecular orbital theory predicts that all three of these highly symmetrical radicals are in a spatially degenerate electronic ground state,[7] so that according to Jahn and Teller's theorem[8–10] they will tend to distort into one of several more stable nondegenerate configurations of lower symmetry. Also, unless the zero-point energies of the molecular vibrations which remove the electronic degeneracy are much smaller than the energy the molecule can gain by distorting, the motions of nuclei and electrons are closely coupled together—there is a dynamical Jahn-Teller effect.[11,12] The molecule is then still in a degenerate state and passes regularly through a series of distorted shapes with different electronic wave functions. Three types of observation suggest that this kind of motion does take place in the radicals prepared by Weissman. First, the ring-proton hyperfine-splitting constants of all three ions have the full molecular symmetry, implying that the unpaired electron distributions of the different distorted forms interchange at a rate much higher than a typical hyperfine frequency (approx. 10^7 cps). Then Townsend and Weissman[13] have found that the hyperfine linewidths are much larger than in comparable nondegenerate ions (such as naphthalene negative ion). McConnell and McLachlan[14] proposed an explanation of this. Surrounding solvent molecules force the radical from one distorted configuration to another, so that the unpaired electron density fluctuates and has a time-dependent isotropic hyperfine interaction with each ring hydrogen atom. Line broadening occurs when this interaction has a strong Fourier component in the neighborhood of zero frequency. Finally, Hoijtink's experimental and theoretical work[15] on the electronic spectra of coronene and triphenylene negative ions has revealed intense "forbidden" transitions which could occur in a distorted configuration.

Several authors[11,12,16,17] have studied the theory of the coupled nuclear and electronic motion which results from given distortion energies ΔE and vibrational frequencies ω and have found three different ranges of behavior. The important quantities are the ratio $\Delta E/\hbar\omega$ and the sizes of the energy barriers between different distorted shapes. It would be interesting to know which type of behavior can be expected from the hydrocarbon negative ions. The energies of the

* Supported in part by the U. S. Public Health Service, the National Science Foundation, and the Office of Ordnance Research, U. S. Army.

† Du Pont Postgraduate Teaching Assistant 1959–1960.

‡ Harkness Fellow of the Commonwealth Fund 1959–1961.

§ Contribution No. 2575.

[1] E. de Boer and S. I. Weissman, J. Chem. Phys. **26**, 963 (1957).

[2] G. J. Hoijtink and W. P. Weijland, Rec. trav. chim. pays-bas, **76**, 836 (1957).

[3] W. P. Weijland, Ph.D. thesis, Free University of Amsterdam (1958).

[4] P. Balk, Ph.D. thesis, Free University of Amsterdam (1957).

[5] H. M. McConnell, Ann. Rev. Phys. Chem. **8**, 105 (1957).

[6] A. D. McLachlan, Mol. Phys. **2**, 271 (1959).

[7] S. I. Weissman, T. R. Tuttle, and E. de Boer, J. Phys. Chem. **61**, 26 (1957); S. I. Weissman and E. de Boer, J. Am. Chem. Soc. **80**, 4549 (1958).

[8] H. A. Jahn and E. Teller, Proc. Roy. Soc. (London) **A161**, 220 (1937); H. A. Jahn, *ibid.* **A164**, 117 (1937).

[9] U. Öpik and M. H. L. Pryce, Proc. Roy. Soc. (London) **A238**, 425 (1957).

[10] W. L. Clinton and B. Rice, J. Chem. Phys. **30**, 542 (1959).

[11] H. C. Longuet-Higgins, U. Öpik, M. H. L. Pryce, and R. A. Sack, Proc. Roy. Soc. (London) **A244**, 1 (1958).

[12] W. Moffitt and A. D. Liehr, Phys. Rev. **106**, 1195 (1957).

[13] M. G. Townsend and S. I. Weissman, J. Chem. Phys. **32**, 309 (1960).

[14] H. M. McConnell and A. D. McLachlan (to be published).

[15] G. J. Hoijtink, Mol. Phys. **2**, 85 (1959).

[16] W. Moffitt and W. R. Thorson, in *Calcul des fonctions d'onde moleculaire* (Rec. mem. centre Nationale de la Recherche Scientifique, November, 1958).

[17] W. Moffitt and W. R. Thorson, Phys. Rev. **108**, 1251 (1957).

distorted configurations of cyclopentadienyl and the benzene negative ion have already been estimated by Liehr,[18] using simple, molecular-orbital theory with allowance for the σ-bond compression energy. In this paper we present similar calculations for triphenylene and coronene, using slightly different assumptions about the relation between the length and energy of the double bonds. In benzene negative ion and cyclopentadienyl we have improved a little upon Liehr's work by allowing all the Hückel orbitals to vary during the distortion. Before we discuss these energies, however, a gap in the theory must be filled. Previous authors[11,12] have used simplified ideal models to treat the pynamical problem, from which it is not clear whether the ordinary Born-Oppenheimer electronic wave functions and nuclear potential energy surfaces have any significance for the coupled motion where the Born-Oppenheimer approximation breaks down. That they are significant, and that the potential energy surfaces do determine the coupled motion, is shown in the next two sections.

THE BORN-OPPENHEIMER APPROXIMATION

Because of the small masses and high velocities of the electrons compared with the nuclei in a molecule, it is usually an excellent approximation to treat their motions separately by the Born-Oppenheimer approximation.[19] To discuss degenerate electronic states properly we first present a summary of the elementary theory as restated by Born,[20] who avoids the cumbersome power series expansions of the original method. In the equations that follow q stands for the electron coordinates, Q for the nuclear ones, while $-\partial^2/\partial q^2$ and $-\partial^2/\partial Q^2$ represent the respective kinetic energies,

$$\partial^2/\partial q^2=\sum_j(\hbar^2/2m)(\partial^2/\partial q_j^2),$$

$$\partial^2/\partial Q^2=\sum_k(\hbar^2/2M_k)(\partial^2/\partial Q_k^2).$$

If $U(q, Q)$ is the potential energy of the electrons in the field of the nuclei and one another, and $V(Q)$ is the mutual potential energy of the nuclei alone, the total Hamiltonian of the molecule has the form

$$H=-(\partial^2/\partial q^2)+U(q, Q)+V(Q)-(\partial^2/\partial Q^2). \quad (1)$$

The complete wave function $\Psi_{nj}(q, Q)$ is taken to be a product of an electronic part $\psi_n(q, Q)$, representing the nth electronic state when the nuclei are fixed at Q, and a normalized vibrational part $\chi_{nj}(Q)$ representing the jth vibrational level of the electronic state n; $\psi_n(q, Q)$ is normalized at each nuclear position Q.

$$\Psi_{nj}(q, Q)=\psi_n(q, Q)\chi_{nj}(Q), \quad (2)$$

$$\int\psi_n^*(q, Q)\psi_n(q, Q)dq=1 \quad \text{for all } Q. \quad (3)$$

We choose ψ_n to satisfy the Schrödinger equation

$$[-(\partial^2/\partial q^2)+U(q, Q)]\psi_n(q, Q)=E_n(Q)\psi_n(q, Q) \quad (4)$$

for the electrons in the field of nuclei fixed at Q, so that $E_n(Q)$ is the electronic energy in this configuration. Having found $E_n(Q)$, one uses it as a potential energy for the nuclear motion, and solves a second Schrödinger equation

$$[-(\partial^2/\partial Q^2)+V(Q)+E_n(Q)]\chi_{nj}(Q)=W_{nj}'\chi_{nj}(Q) \quad (5)$$

to find the vibrational wave function. In the elementary treatment it is supposed that the solutions of Eqs. (4) and (5) separate the motions of electrons and nuclei as much as possible. Unfortunately with these wave functions the exact Hamiltonian H still has nonvanishing matrix elements between different vibrational levels i, j of the same electronic state n, and the average value of H for the function $\Psi_{nj}(q, Q)$ is not equal to W_{nj}'. Instead,

$$\langle\Psi_{ni}\mid H\mid\Psi_{nj}\rangle=\int\chi_{ni}^*(Q)\langle n\mid-\partial^2/\partial Q^2\mid n\rangle\chi_{nj}(Q)dQ, \quad (6)$$

and

$$\langle\Psi_{ni}\mid H\mid\Psi_{ni}\rangle$$

$$=W_{ni}'+\int\chi_{ni}^*(Q)\langle n\mid-\partial^2/\partial Q^2\mid n\rangle\chi_{ni}(Q)dQ, \quad (7)$$

where

$$\langle m\mid-\partial^2/\partial Q^2\mid n\rangle=-\int\psi_m^*(q, Q)(\partial^2/\partial Q^2)\psi_n(q, Q)dq. \quad (8)$$

Symbols like $\langle m\mid T\mid n\rangle$ will be used similarly for the matrix elements of an operator T between two electronic wave functions at a fixed nuclear configuration. [In Eqs. (6) and (7) we suppose that ψ is always real, so that $\langle n\mid\partial/\partial Q\mid n\rangle=0$.] The unwanted term $\langle n\mid-\partial^2/\partial Q^2\mid n\rangle$ can be completely eliminated by including it in the nuclear potential energy which determines $\chi_{nj}(Q)$. Equation (5) then becomes

$$[-(\partial^2/\partial Q^2)+V(Q)+E_n(Q)+\langle n\mid-\partial^2/\partial Q^2\mid n\rangle]\chi_{nj}(Q)$$

$$=W_{nj}\chi_{nj}(Q) \quad (5')$$

and the new energy matrix constructed from the solutions of (4) and (5′) has elements

$$\langle\Psi_{ni}\mid H\mid\Psi_{ni}\rangle=W_{ni}; \quad \langle\Psi_{ni}\mid H\mid\Psi_{nj}\rangle=0 \quad (\text{for } i\neq j); \quad (9)$$

[18] A. D. Liehr, Z. physik. Chem. **9**, 338 (1956).
[19] M. Born and R. J. Oppenheimer, Ann. Physik **84**, 457 (1927).
[20] M. Born, Festschrift Gött. Nachr. Math. Phys. Kl. 1 (1951).

and

$$\langle \Psi_{mi} \mid H \mid \Psi_{nj} \rangle = \int \chi_{mi}^*(Q) [\langle m \mid -\partial^2/\partial Q^2 \mid n \rangle - 2\langle m \mid \partial/\partial Q \mid n \rangle (\partial/\partial Q)] \chi_{nj}(Q) dQ, \quad (10)$$

where $\langle m \mid \partial/\partial Q \mid n \rangle (\partial/\partial Q)$ stands for

$$\sum_j (\hbar^2/2M_j) \langle m \mid \partial/\partial Q_j \mid n \rangle (\partial/\partial Q_j).$$

The Born-Oppenheimer approximation only succeeds because the electronic parts $\langle m \mid -\partial^2/\partial Q^2 \mid n \rangle$ and $\langle m \mid \partial/\partial Q \mid n \rangle$ of the off-diagonal matrix elements are small compared with electronic excitation energies when ψ_m and ψ_n vary only slowly with nuclear displacements. If these matrix elements are treated as a small perturbation, the unperturbed energy W_{ni} is correct in the first order and the largest correction is a second-order one. From the Schrödinger equation (4) it follows that

$$\langle m \mid \partial/\partial Q \mid n \rangle = [E_n(Q) - E_m(Q)]^{-1} \langle m \mid \partial U(q, Q)/\partial Q \mid n \rangle, \quad (11)$$

and it is always true that

$$\langle m \mid \partial^2/\partial Q^2 \mid n \rangle = \sum_k \langle m \mid \partial/\partial Q \mid k \rangle \langle k \mid \partial/\partial Q \mid n \rangle + (\partial/\partial Q) \langle m \mid \partial/\partial Q \mid n \rangle, \quad (12)$$

so that in a molecule which is degenerate or has low-lying electronic-excited states, the neglected terms can become very large as the energies approach one another. At the same time the approach of the levels makes them combine more easily under a perturbation, and the Born-Oppenheimer method fails completely.

DEGENERATE ELECTRONIC STATES

To form the exact wave function of a molecule one must add up products of an electronic and a vibrational part. Let $\psi_r(q, Q)$ be an *arbitrary complete set* of orthogonal electronic wave functions defined at each nuclear configuration Q. Then the exact wave function will be of the form

$$\Psi(q, Q) = \sum_r \psi_r(q, Q) \chi_r(Q), \quad (13)$$

in which $\chi_r(Q)$ is a partial vibrational amplitude associated with each electronic state. The Schrödinger equation $H\Psi(q, Q) = W\Psi(q, Q)$ now becomes

$$\sum_s \{\chi_s \cdot \mathcal{E}\psi_s + \psi_s \cdot [-(\partial^2/\partial Q^2) + V(Q)]\chi_s - 2\mathcal{C}\psi_s(\partial/\partial Q)\chi_s - W\psi_s\chi_s\} = 0, \quad (14)$$

where

$$\left.\begin{aligned} \mathcal{E} &= -(\partial^2/\partial q^2) + U(q, Q) - (\partial^2/\partial Q^2), \\ \mathcal{C}\psi_s(q, Q) &= (\partial/\partial Q)\psi_s(q, Q). \end{aligned}\right\} \quad (15)$$

Multiplication of (14) on the left by $\psi_r^*(q, Q)$ and integration with respect to q gives a series of coupled differential equations for the χ's involving the electronic matrix elements of $\mathcal{E}$ and $\mathcal{C}$;

$$[-(\partial^2/\partial Q^2) + V(Q) + \mathcal{E}_{rr}(Q) - W]\chi_r(Q) + \sum_s{}' [\mathcal{E}_{rs}(Q) - 2\mathcal{C}_{rs}(Q)(\partial/\partial Q)]\chi_s(Q) = 0. \quad (16)$$

Our next aim is to make the coupling terms $\mathcal{E}_{rs}$ and $\mathcal{C}_{rs}$ in a degenerate state as small as possible by a good choice of the electronic wave functions ψ_r. If ψ_r are a *fixed* basic set independent of Q, $\mathcal{C}_{rs} = 0$ and $\mathcal{E}$ is equivalent to the electronic energy operator $-\partial^2/\partial q^2 + U(q, Q)$. Clearly $\mathcal{E}_{rs}(Q)$ can then only be made to vanish at one configuration $Q = 0$, say, and may otherwise be large. On the other hand if $\psi_r(q, Q)$ are the ordinary solutions of (4), $\mathcal{E}_{rs}(Q) = \langle r \mid -\partial^2/\partial Q^2 \mid s \rangle$ so that $\mathcal{E}_{rs}$ and $\mathcal{C}_{rs}$ can both become very large between two components of the degenerate level. However, since they are still negligible for all other pairs of electronic states, one can neglect in the expansion (13) all the electronic wave functions except $\psi_1(q, Q) \cdots \psi_g(q, Q)$, the solutions of Eq. (4) which become degenerate in the symmetrical configuration $Q = 0$. The coupling terms of (16) will be made as small as possible by choosing special variable linear combinations of $\psi_1 \cdots \psi_g$ as a basic set.

We take

$$\Psi(q, Q) = \sum_{\mu=1}^{g} \phi_\mu(q, Q) \chi_\mu(Q); \quad (17)$$

with

$$\phi_\mu(q, Q) = \sum_{r=1}^{g} a_{\mu r}(Q) \psi_r(q, Q), \quad (18)$$

and the coefficients $a_{\mu r}(Q)$ chosen so that

$$\int \phi_\lambda^*(q, Q)(\partial/\partial Q)\phi_\mu(q, Q) dq = 0 \quad (\text{for all } \lambda, \mu, Q). \quad (19)$$

This can be done by solving the first-order differential equations

$$(\partial a_{\mu r}/\partial Q) + \sum_s a_{\mu s} \langle r \mid \partial/\partial Q \mid s \rangle = 0, \quad (20)$$

which fix $\phi_\mu(q, Q)$ once the orthonormal set $\phi_\mu(q, 0)$ has been chosen. The choice of $\phi_\mu(q, 0)$ is arbitrary and has no physical significance, since any new combination

$$\phi'_\lambda(q, Q) = \sum_\mu b_{\lambda\mu} \phi_\mu(q, Q), \quad (21)$$

derived by an orthogonal transformation still satisfies (19). The condition (19) ensures that $\mathcal{C}_{\lambda\mu} = \langle \phi_\lambda \mid \partial/\partial Q \mid \phi_\mu \rangle = 0$, and the term $\langle \lambda \mid -\partial^2/\partial Q^2 \mid \mu \rangle$ in $\mathcal{E}_{\lambda\mu}$ is small too, since the expansion (12) now only contains the negligible contributions from higher electronic states. It is consistent with the spirit of the Born-Oppenheimer method to omit these contributions from

the coupled equations (16), and obtain

$$[-(\partial^2/\partial Q^2)+v_{\lambda\lambda}(Q)+V(Q)-W]\chi_\lambda(Q) + \sum_\mu{}' v_{\lambda\mu}(Q)\chi_\mu(Q)=0, \quad (22)$$

in which the coupling terms are pure electronic energies,

$$v_{\lambda\mu}(Q)=\langle\lambda\,|\,-(\partial^2/\partial q^2)+U(q,Q)\,|\,\mu\rangle. \quad (23)$$

Equation (22), which has been the starting point of previous theoretical work,[11,12] expresses the coupling of nuclear and electronic motions in its simplest form. For any degenerate level which is well separated from all other electronic states, the terms neglected in Eq. (22) are as small as those neglected in the ordinary Born-Oppenheimer theory for nondegenerate states. Since the eigenvalues of the matrix $\|v_{\lambda\mu}(Q)\|$ are the ordinary electronic energies $E_n(Q)$, the electronic wave functions $\psi_n(q,Q)$ and their distortion energies play a fundamental part in the coupled motion. When the coupling is small compared with vibrational energies the wave functions $\phi(q,Q)$ represent quasi-stationary states of electronic motion in the vibrating nuclear framework, whose high-frequency components can follow the vibrations adiabatically, while the low-frequency ones are unable to. On the other hand, if the electronic degeneracy is effectively removed by a large distortion the motion is mainly confined to the lowest sheet $E_0(Q)$ of the electronic energy surface, and the Born-Oppenheimer approximation is again useful.

THEORETICAL ASSUMPTIONS

To find the equilibrium bond lengths and energies of a conjugated molecule in a spatially degenerate electronic state, we shall use an elegant theoretical method described by Longuet-Higgins and Salem[21] in a paper on the alternation of bond lengths in long polyene molecules. They assume that the total energy W is the sum of two parts, one arising from the σ bonds and the other from the π electrons,

$$W=F+E. \quad (24)$$

The σ-electron energy is assumed to be the sum of independent contributions from the CC bonds;

$$F=\sum_i f(r_i), \quad (25)$$

but the π-electron energy is calculated by the LCAO molecular orbital theory, and is a function of the resonance integrals $\beta_i=\beta(r_i)$ and bond orders $p_i=p_i(\beta_1,\beta_2,\cdots)$ of the bonds,

$$E=2\sum_i p_i\beta_i. \quad (26)$$

When an entire molecule is in static equilibrium $\partial W/\partial r_i=0$ for each bond, which implies that

$$f_i'+2p_i\beta_i'+\sum_j 2\beta_j(\partial p_j/\partial\beta_i)\beta_i'=0. \quad (27)$$

Now the π-electron energy remains unchanged for small variations of the wave function (and hence of p_j) so that the third term of Eq. (27) vanishes, or

$$f_i'+2p_i\beta_i'=0. \quad (28)$$

As Longuet-Higgins and Salem realized, Eq. (28) implies a fixed relation between the order and the length of a bond *in static equilibrium* since $f(r)$ and $\beta(r)$ are unique functions of r. This relation exists independently of any special assumptions about the form of $f(r)$ or $\beta(r)$, and holds also in the Pariser, Parr, and Pople self-consistent molecular orbital theory.[22,23]

The form of the unique relation is found empirically. In many molecules the formula

$$P(r)=6.667(1.500-r), \quad (r \text{ in A}) \quad (29)$$

holds for $P(r)$, the order of an sp^2 CC bond in equilibrium, and we shall assume throughout our calculations that this relation holds exactly. $P(r)$ and $\beta(r)$ completely determine the variation of $f(r)$, since

$$f'(r)+2P(r)\beta'(r)\equiv 0. \quad (30)$$

An assumption about the form of $\beta(r)$ is necessary. Longuet-Higgins and Salem adopted the exponential form

$$\beta(r)=\beta_0\exp[-(r-1.40\text{ A})/a], \quad (31)$$

with $a=0.3106$ A and $\beta_0=-25.56$ kcal/mole. These values were deduced from the observed force constants for the totally symmetric and totally antisymmetric CC stretching vibrations of benzene. Every numerical quantity used in the theory is therefore derived from experimental data. The above simple assumptions ignore the effect of CC bending vibrations and out-of-plane motions, but the conjugation energy of a planar molecule probably depends far more strongly on the CC bond lengths than on the angles.

An alternative set of assumptions about the σ- and π-electron energies is due to Lennard-Jones,[24] and was used by Liehr[18] in his work. Let s and d stand for the lengths of a single and a double bond. Lennard-Jones assumes that

$$f(r)=\tfrac{1}{2}k_1(r-s)^2+\text{const},$$
$$2\beta(r)=\tfrac{1}{2}k_2(r-d)^2-\tfrac{1}{2}k_1(r-s)^2+\text{const}, \quad (32)$$

where k_1 and k_2 are the observed force constants of a single bond in ethane and a double one in ethylene. The theories of Lennard-Jones and Longuet-Higgins lead to rather different conclusions about the energies

[21] H. C. Longuet-Higgins and L. Salem, Proc. Roy. Soc. (London) **A251**, 172 (1959).

[22] R. Pariser and R. G. Parr, J. Chem. Phys. **21**, 466, 767 (1953).

[23] J. A. Pople, Trans. Faraday Soc. **49**, 1375 (1953).

[24] J. E. Lennard-Jones, Proc. Roy. Soc. (London) **A158**, 280 (1937).

of distorted configurations and the potential barriers between them, because $\beta''(r)$ is positive in the former and negative in the latter approximation. The available evidence strongly favors Longuet-Higgins' assumptions; apart from the unreasonable assumption that $\beta(r)$ and $f(r)$ have a parabolic form in the entire range $r=1.35$–1.54 A, the relation between bond order and bond length derived from (28) and (32) does not fit[25] the known bond lengths of benzene and graphite as well as Eq. (29). Furthermore differentiation of Eq. (28) shows that the force constants of ethylene and of the totally symmetric CC vibration of benzene are both given by

$$w''=-2p'(r)\beta'(r) \tag{33}$$

evaluated at $r=1.35$ and 1.40 A, respectively. Thus if we accept the empirical bond-order bond-length curve (29) in which $p'(r)=P'$ is constant, the negative sign of β'' follows immediately from the greater force constant of ethylene. Indeed Longuet-Higgins' form of $\beta(r)$ reproduces both force constants fairly well. It also leads to a σ bond energy function

$$f(r)=-2P'\beta_0[r-1.50\text{ A}+a]\exp[-(r-1.40\text{ A})/a], \tag{34}$$

which is qualitatively similar to the observed potential functions of many diatomic molecules.[26] The chief doubt about his assumptions is whether β varies sufficiently rapidly with r; for the energy of a bond in static equilibrium is

$$w(r)=-2\beta_0 aP'\exp[-(r-1.40\text{ A})/a], \tag{35}$$

which leads to only 47 kcal/mole difference between a double and single sp^2 bond. The observed difference between normal double and single (sp^3) bonds is (145.8–82.6) =63.2 kcal/mole.[27]

BOND ORDERS AND RESONANCE INTEGRALS

In the undistorted configuration each of the highly symmetrical radicals that concern us has an n-fold rotation axis of symmetry. The degenerate electronic wave functions Ψ^+ and Ψ^- are of symmetry e'', and may be chosen so that a rotation C_n through $2\pi/n$ about the axis multiplies each by a numerical factor ω or ω^{-1},

$$C_n\Psi^+=\omega\Psi^+, \qquad C_n\Psi^-=\omega^{-1}\Psi^-. \tag{36}$$

Symmetry restricts ω to the values $\exp(2\pi ik/n)$, with $k=0, 1, \cdots(n-1)$. When the wave function is a linear combination

$$\Psi=a^+\Psi^++a^-\Psi^-, \tag{37}$$

the electron density $\Psi^*\Psi$ contains terms which acquire factors of ω^{2m} and ω^{-2m} under a rotation $(C_n)^m$ through $2\pi m/n$. This implies a special relation between the orders of equivalent bonds which are interconverted by a rotation. Suppose we label each different family of equivalent bonds by a letter j, and give the n bonds in each family numbers m running from 0 to $n-1$ round the molecule: then in the state Ψ, p_{mj} has parts which vary as $\exp(\pm 4\pi ikm/n)$. In any distorted configuration the degenerate level breaks up into two states with real wave functions, and it is convenient to express Ψ in the new form

$$\Psi=\Psi'\cos\theta-\Psi''\sin\theta, \tag{38}$$

where Ψ' and Ψ'' are the real and imaginary parts of Ψ^+. As the radicals have symmetries D_{nh} we can choose Ψ' and Ψ'' to be those states in which the orbitals ψ' and ψ'' of the unpaired electron are, respectively, symmetric and antisymmetric across a vertical σ_v reflection plane. The mth bond order p_m in a family is now given by an equation

$$p_m=\bar{p}+\mathcal{P}\cos[(4\pi mk/n)+2\theta+\xi], \quad (\mathcal{P}>0), \tag{39}$$

in which $\bar{p}$, $\mathcal{P}$, and ξ are different for each family; $\bar{p}$ is the average of p_m' and p_m'' for Ψ' and Ψ'' (independent of m), while $\mathcal{P}$ and ξ depend on the LCAO coefficients c_λ', c_μ'' of the unpaired electron orbitals ψ' and ψ''. Let the first bond ($m=0$) of the family join atoms 1 and 2, and define

$$S=\tfrac{1}{2}(c_1'c_2'-c_2''c_2''); \qquad T=\tfrac{1}{2}(c_1'c_2''+c_1''c_2'). \tag{40}$$

Then

$$\mathcal{P}^2=S^2+T^2, \quad \text{and} \quad \tan\xi=T/S. \tag{41}$$

It is clear that the only distortions which can remove the degeneracy are ones in which β_m has a portion which varies like $\exp(\pm 4\pi imk/n)$. In the neighborhood of the undistorted length $\bar{r}$ (corresponding to $\bar{p}$) the resonance integral is approximately

$$\beta(r)=\bar{\beta}+(r-\bar{r})\beta'+\tfrac{1}{2}(r-\bar{r})^2\beta'', \tag{42}$$

neglecting terms in $(r-\bar{r})^3$.

Suppose now that we make a distortion in which the extension R_m of bond m is

$$R_m=\mathcal{R}\cos[(2\pi wm/n)-\phi], \quad (\mathcal{R}>0) \tag{43}$$

and calculate the resonance integral

$$\beta_m=(\bar{\beta}+\tfrac{1}{4}\mathcal{R}^2\beta'')+\mathcal{R}\beta'\cos[(2\pi wm/n)-\phi] +\tfrac{1}{4}\mathcal{R}^2\beta''\cos[(-4\pi wm/n)+2\phi]. \tag{44}$$

The part which is linear in $\mathcal{R}$ removes the electronic degeneracy only if $w=2k$ *mod* n, and the quadratic part if $2w+2k=0$ *mod* n. Both may do so simultaneously in the ions of benzene, triphenylene, and coronene, where $6k=0$ *mod* n; but not in cyclobutadiene or cyclopentadienyl. We shall restrict ourselves to distortions whose

[25] C. A. Coulson, Proc. Roy. Soc. (London) **A169**, 413 (1939).
[26] G. Herzberg, *Spectra of Diatomic Molecules* (D. van Nostrand Company, Inc., Princeton, New Jersey, 1950), p. 147.
[27] T. L. Cottrell, *The Strengths of Chemical Bonds* (Butterworths Scientific Publications, Ltd., London, 1958), 2nd ed., p. 272.

interactions with the degenerate states are linear in $\mathcal{R}$, that is, with $w=2k$. For the first three molecules such a distortion leads to resonance integrals of the form

$$\beta_m=(\bar{\beta}+\tfrac{1}{4}\mathcal{R}^2\beta'')+\mathcal{R}\beta'\{\cos[(4\pi km/n)-\phi]+\tfrac{1}{4}\mathcal{R}(\beta''/\beta')\cos[(4\pi km/n)+2\phi]\}. \quad (45)$$

In the others the linear and quadratic parts vary differently with m, and only the linear one affects the total energy.

THE DISTORTION ENERGY

When any conjugated molecule distorts, each Hückel orbital changes too, and the energy contains second-order perturbation terms from excited electronic states. As a first approximation we shall neglect these changes, and take the wave function to be a linear combination (38) of the two degenerate states in the undistorted configuration. The π-electron energy is a function of θ and the resonance integrals;

$$E(\theta)=2\sum_i p_i(\theta)\beta_i(r_i). \quad (46)$$

In a given electronic state [fixed values of θ and $p_i(\theta)$] the lowest energy shape is fixed by the conditions

$$(\partial W/\partial r_i)_\theta=0, \quad (47)$$

or

$$f'(r_i)+2p_i(\theta)\beta'(r_i)=0, \quad (48)$$

and the unique relation (29) between bond order and bond length must hold. Thus the distortion is governed completely by the difference between the actual bond order p and the value $\bar{p}=P(\bar{r})$ appropriate to the undistorted length $\bar{r}$. According to (30) there is a force of

$$-(\partial w/\partial r)_p=2[P(r)-p]\beta'(r) \quad (49)$$

tending to stretch a bond which is not in equilibrium, and the bond extends until $P(r)$ is equal to p. The linear form of $P(r)$ leads to a remarkable conclusion. The equilibrium extension of each bond in the molecule is exactly proportional to its deviation from the average order $\bar{p}_i$;

$$R_i=(p_i-\bar{p}_i)/P'=-0.150(p_i-\bar{p}_i), \quad (50)$$

and its distortion energy is found to be

$$w_i-\bar{w}_i=2(p_i-\bar{p}_i)\beta(\bar{r}_i)+[\beta'(\bar{r}_i)/P'](p_i-\bar{p}_i)^2+[\beta''(\bar{r}_i)/3(P')^2](p_i-\bar{p}_i)^3 \quad (51)$$

up to terms in $(p-\bar{p})^3$. To derive Eq. (51) one expands the energy in powers of R_i up to R_i^3, substitutes from (50), and eliminates $f''(\bar{r}_i)$ and $f'''(\bar{r}_i)$ by differentiation of Eq. (30),

$$f''+2P\beta''=-2P'\beta'; \qquad f'''+2P\beta'''=-4P'\beta''. \quad (52)$$

In the final result the contribution to the $(p-\bar{p})^3$ term from R^3 cancels two-thirds of the contribution from R^2. This means that if we truncated the expansion of the energy in powers of R at the R^2 term we should overestimate the potential barriers discussed below [Eq. (60)] by a factor of three.

In a symmetrical molecule the equilibrium extension of each bond in a family is found from the general formula (39) for the bond order

$$R_m=\Delta R\cos[(4\pi mk/n)+2\theta+\xi-\pi], \quad (53)$$

where

$$\Delta R=-\mathcal{P}/P'. \quad (54)$$

This is of the same form as (43), provided that $w=2k$ and $(2\theta+\phi+\xi)=\pi$. When the total energy of each family is evaluated, a sharp distinction appears between radicals like cyclopentadienyl or cycloheptatrienyl on the one hand, and those with a 3-fold or 6-fold axis on the other. In the first group the distortion energy $\Delta W=W-\bar{W}$ is independent of θ, and has the value

$$\Delta W=\tfrac{1}{2}n\mathcal{P}^2\beta'/P', \quad (55)$$

while in the second it depends on the angle 6θ,

$$\Delta W=-n\mathcal{P}^2A(\bar{r})[1+B\mathcal{P}\cos(6\theta+3\xi)]. \quad (56)$$

The minimum energy for each family occurs when $(6\theta+3\xi)=0$, and the values of A and B are

$$A(r)=-\beta'(r)/2P'=6.174 \text{ kcal/mole} \quad (r=1.40 \text{ A}), \quad (57)$$

$$B=\beta''/6\beta'P'=0.0805. \quad (58)$$

With the simple theory used here the total distortion energy is simply a sum of independent contributions from each family j (this is not true when excited electronic states are considered), and

$$\Delta W=\sum_j \Delta W_j. \quad (59)$$

Our special choice of Ψ' and Ψ'' means that each of these functions corresponds to a distortion of extreme energy, and in both cases the distorted radical has D_{2h} or C_{2v} instead of D_{nh} symmetry. Hence the total distortion energy in the benzene, coronene, and triphenylene negative ions has the form

$$\Delta W=-\Delta E\pm\tfrac{1}{2}\Delta U\cos 6\theta, \qquad \Delta U>0. \quad (60)$$

ΔE, the mean value, is proportional to β', while the potential barrier ΔU between adjacent pairs of stable distorted shapes depends on β'' and is opposite in sign for the Longuet-Higgins and Lennard-Jones approximations. In all of these ions the ratio $\Delta U/\Delta E$ is small; indeed it vanishes exactly in the C_5H_5 and C_7H_7 radicals.

The pairing of electronic states in alternant hydrocarbons[6] should lead to identical distortion energies in the negative and positive ions of benzene, triphenylene, and coronene.

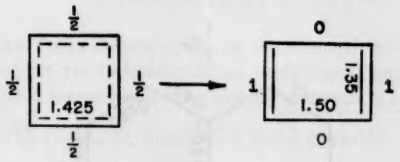

FIG. 1. Cyclobutadiene. Bond lengths and bond orders.

INDIVIDUAL MOLECULES

Cyclobutadiene

At present there is no certainty that C_4H_4 exists at all in a planar form. However if it does have an undistorted planar configuration with the four carbon atoms arranged at the corners of a square the highest-filled molecular orbital is doubly degenerate. As a result there are four low-lying electronic states of almost equal energy; one triplet and three singlets. Simple MO theory makes all four degenerate, and one might therefore expect a triplet ground state, since this has a lower electron-repulsion energy. However the singlet state may be lower yet if the molecule distorts into a rectangular shape with two double and two single bonds, and thereby gains energy, (Fig. 1). Liehr[18] estimated this energy at 20.9 kcal/mole, but according to our assumptions the square shape with bond orders of 1/2 and bond lengths of 1.425 A is only 11.43 kcal/mole above the rectangular one. Admittedly the CC bond energy may vary rather differently with length when the C—C—C angle is 90° instead of 120°, but the small distortion energy we find makes it likely that the lowest state of planar cyclobutadiene is a triplet with the square shape. The relative stability of planar or bent shapes appears then not to be connected with the Jahn-Teller distortion.

C_5H_5 and C_7H_7

Cyclopentadienyl is of symmetry D_{5h}, and its unpaired electron occupies an orbital with "angular momentum" $k=\pm 1$. The average bond order $\bar{p}$ is 0.585, corresponding to an undistorted length of 1.412 A, and $\mathcal{P}=1/5$. There is a continuous series of distorted shapes of equal energy. In a typical one the mth CC bond is stretched to a length

$$r_m=\bar{r}+\Delta R\cos[(4\pi m/5)-\phi] \qquad (61)$$

and the bond order is

$$p_m=\bar{p}-1/5\cos[(4\pi m/5)-\phi]. \qquad (62)$$

From Eqs. (54) and (55) we deduce that $\Delta R=0.030$ A and $\Delta E=1.188$ kcal/mole or 416 cm^{-1}. This is probably about half a vibrational quantum $\hbar\omega$ of the CC stretching vibration which removes the degeneracy. Liehr[18] found a very similar value ($\Delta E=1.602$ kcal/mole).

We next treated the π orbitals of the distorted molecule by first-order perturbation theory to find a more accurate estimate of the energies and magnitudes of the distortions. When the shape is described by Eq. (61) with $\Delta R=0.030$ A, the revised energy is $\Delta E=1.414$ kcal/mole (495 cm^{-1}) and is still independent of ϕ. Also the bond orders are modified, and equilibrium is only reached after a larger distortion, approximately given by $\Delta R=0.037$ A in (61). For this radical at any rate, the simpler, first calculation gives a useful estimate of the energy.

Cycloheptatrienyl behaves very similarly. $\bar{p}=0.610$, $\mathcal{P}=1/7$, and $\bar{r}=1.408$ A. Hence $\Delta R=0.021$ A and the energy is smaller, with $\Delta E=0.859$ kcal/mole for each of a continuous series of distortions of the type

$$R_m=\Delta R\cos[(8\pi m/7)-\phi]. \qquad (63)$$

Benzene Negative Ion

Symmetry requires that the states of extreme energy are those in which the unpaired electron's orbital is either symmetric or antisymmetric to reflection in a σ_v plane through two opposite carbon atoms. We find that the symmetric one is lowest, with $\Delta E=0.985$ kcal/mole (345 cm^{-1}), and the potential barrier ΔU is only 0.029 kcal/mole (9 cm^{-1}) using the theory above. The amplitude ΔR of the distortion is 0.0250 A. Lennard-Jones's assumptions put the antisymmetric state lowest,[18] because $\beta''>0$, and gave $\Delta E=1.336$, $\Delta U=0.139$.

If the Hückel orbitals are allowed to vary during the distortion the bond orders change to a different extent in the symmetric and antisymmetric states, and the energy difference between them becomes so small that it is impossible to tell which is lowest. An approximate perturbation calculation similar to that for C_5H_5 gave, respectively, $\Delta R=0.0272$, 0.0280 A, and $\Delta W=-1.077$ kcal/mole (377 cm^{-1}) for both states; a surprising coincidence. It is unlikely that ΔU vanishes exactly, but the precise value derived from our assumptions is almost certainly less than 0.05 kcal/mole (17 cm^{-1}).

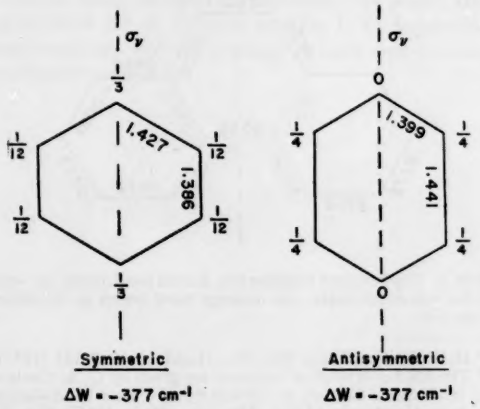

FIG. 2. Benzene negative ion. Distorted bond lengths and spin densities.

Figure 2 shows the spin densities and bond lengths in the resulting D_{2h} shapes of maximum and minimum energy.

To treat the vibronic levels of the ion precisely one has to divide the energy ΔE between the four E_{2g} normal vibrations,[28] of which the two most important are probably the CC stretching (1595 cm^{-1} in C_6H_6) and CC bending (606 cm^{-1}) modes. However the division is made the ratio $2\Delta E/\hbar\omega$ for either mode (which corresponds to the parameter k^2 of Longuet-Higgins *et al.*)[11] lies between 0 and 1.25, so that the lowest vibronic state is doubly degenerate with a total "angular momentum" of $\pm\hbar$, and the ion can interchange freely between all its distorted shapes. The small potential barrier ΔU merely splits the first excited level into a close doublet, and leaves the lowest one degenerate.

Triphenylene and Coronene Negative Ions

In both these large ions the distortion energies are much smaller than in benzene. Since the CC stretching vibrations will have frequencies similar to benzene the nuclear and electronic motions are more weakly coupled. There is virtually no barrier between the various distorted shapes. In triphenylene the symmetric state is lowest with $\Delta E=0.385$, $\Delta U=0.001$ kcal/mole, while the antisymmetric one is lowest in coronene. Here $\Delta E=0.299$ and $\Delta U=0.002$ kcal/mole. Figures 3 and 4 show the average bond orders $\bar{p}$ and the deviations $(p'-\bar{p})$ in the symmetric state of each ion.[29] $(p''-\bar{p})$ is equal but opposite in the antisymmetric state.

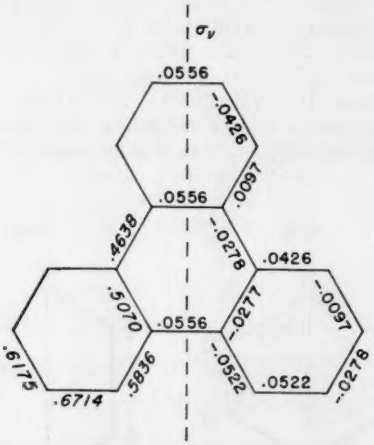

FIG. 3. Triphenylene negative ion. Excess bond orders $(p_i'-\bar{p}_i)$ for the symmetric state, and average bond orders $\bar{p}_i$ (in italics on the left).

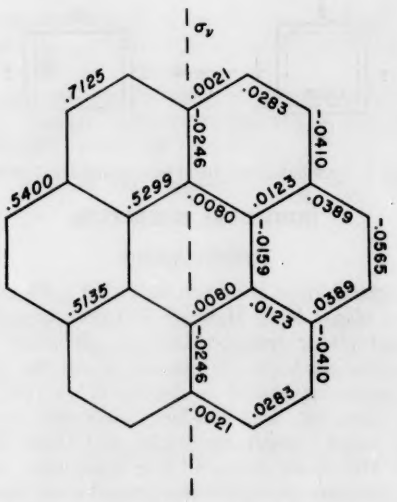

FIG. 4. Coronene negative ion. Excess bond orders $(p_i'-\bar{p}_i)$ for the symmetric state, and average bond orders $\bar{p}_i$ (in italics).

The $^1E_{1u}^+$ and $^3E_{1u}^+$ States of Benzene

Benzene has four low-lying singlet states and four triplets[30] which result from the excitation of an electron out of the highest bonding orbital (ψ_1 or ψ_{-1}) into the lowest antibonding one (ψ_2 or ψ_{-2}). The singlets $^1B_{2u}^-$, $^1B_{1u}^+$, and $^1E_{1u}^+$ have all been observed and have energies, respectively, 4.71, 5.96, and 6.76 ev above the ground state $^1A_{1g}^-$. The lowest triplet is $^3B_{1u}^+$ at 3.59 ev, but the $^3E_{1u}^+$ and $^3B_{2u}^-$ states have not yet been seen. It is interesting that in both the doubly degenerate states the bond orders predicted by molecular orbital theory are uniform and independent of the way the singly excited orbital configurations ($\psi_1\rightarrow\psi_2$) and ($\psi_{-1}\rightarrow\psi_{-2}$) are combined together. Indeed, no *one electron* perturbation of any kind can mix the two degenerate levels. We therefore anticipate that neither the CC stretching vibration at approx. 1595 cm^{-1} nor the bending one at approx. 606 cm^{-1} is very effective in the Jahn-Teller distortion. Furthermore, mixing of the $^1B_{1u}^+$ and $^1E_{1u}^+$ states will not cause the latter state to be distorted although the former may be. It is interesting, though, that CC bending vibrational structure[31] is found in the electronic spectra of some Rydberg $^1E_{1u}$ states of benzene.[32]

FORBIDDEN ELECTRONIC TRANSITIONS

In any particular case the calculation of the intensity of an electronic transition is a complex problem requiring knowledge of the electronic and vibrational wave functions. However it may be of interest to draw some qualitative conclusions about the effect of

[28] D. H. Whiffen, Trans. Roy. Soc. (London) **A248**, 131 (1955).
[29] The Hückel orbitals of coronene are given by C. A. Coulson and R. Daudel, Editors, in *Dictionary of Values of Molecular Constants* (Centre de Chimie Theorique, Paris, 1955), Vol. II. The orbitals of triphenylene in this book are wrong, and correct ones may be had from us on request.
[30] R. Pariser, J. Chem. Phys. **24**, 250 (1956).
[31] A. D. Liehr and W. Moffitt, J. Chem. Phys. **25**, 1074 (1956).
[32] P. J. Wilkinson, Can. J. Phys. **34**, 596 (1956).

the Jahn-Teller deformations on the strength of transitions which are forbidden in an undistorted molecule. Consider a transition from a doubly degenerate state

$$\Psi_{0i}(Q, q) = \phi_A(Q, q)\chi_{Ai}(Q) + \phi_B(Q, q)\chi_{Bi}(Q) \quad (64)$$

in the notation of (17), to a nondegenerate one $\Psi_{nj}(Q, q) = \psi_n(q, Q)\chi_{nj}(Q)$. The intensity is proportional to the square of the transition electronic dipole moment $\langle 0i \mid \mathbf{M} \mid nj \rangle$. For small displacements from the symmetrical configuration $Q=0$ the electronic matrix elements of $\mathbf{M}$ can be approximated by the formulas

$$\left.\begin{aligned} \mathbf{M}_{An}(Q) &= Q(\mathbf{M}_{An}') + \tfrac{1}{2}Q^2(\mathbf{M}_{An}''), \\ \mathbf{M}_{Bn}(Q) &= Q(\mathbf{M}_{Bn}') + \tfrac{1}{2}Q^2(\mathbf{M}_{Bn}''). \end{aligned}\right\} \quad (65)$$

Here $\mathbf{M}_{An}'$ and $\mathbf{M}_{An}''$ stand for the first and second derivatives at $Q=0$ of

$$\langle A \mid \mathbf{M} \mid n \rangle = \int \phi_A^*(Q, q)\mathbf{M}\psi_n(Q, q)\,dq. \quad (66)$$

A first approximation to the transition moment is thus

$$\langle 0i \mid \mathbf{M} \mid nj \rangle = \mathbf{M}_{An}' \int \chi_{Ai}^*(Q) Q \chi_{nj}(Q)\,dQ + \mathbf{M}_{Bn}' \int \chi_{Bi}^*(Q) Q \chi_{nj}(Q)\,dQ. \quad (67)$$

The forbidden intensity therefore depends on the two vibrational matrix elements $Q(Ai \rightarrow nj)$ and $Q(Bi \rightarrow nj)$. For a weak Jahn-Teller effect the excursions of the molecule from $Q=0$ are no larger than the zero-point amplitudes of Q, and the intensities should be of about the same strength as those of symmetry-forbidden transitions in normal molecules (e.g., the ${}^1A_{1g}^- \rightarrow {}^1B_{2u}^-$ transition of benzene).[33] On the other hand if the distortion is large $Q(Ai \rightarrow nj) \approx \Delta R$, and the intensity may be much greater. It appears from our calculations that the situation in the degenerate hydrocarbons is midway between these two extremes, and the forbidden bands observed by Hoijtink[15] are probably due to Jahn-Teller distortions.

[33] J. N. Murrell and J. A. Pople, Proc. Phys. Soc. (London) **A69**, 245 (1956).

DISCUSSION

The important point about all these hydrocarbons is that the distortion energies are less than one quantum of a CC stretching vibration. The vibronic ground state of each is doubly degenerate, and it may oscillate indifferently about any of a series of deformed shapes. The sweeping approximations we use make the precise numbers uncertain. Ideally we should have worked out self-consistent molecular orbitals in an arbitrarily distorted carbon skeleton; yet the perturbation calculations we made for C_5H_5 and $C_6H_6^-$ suggest that a sophisticated theory would lead to very similar conclusions. The Jahn-Teller effect is strongest in the smaller molecules, where the deforming forces are concentrated in a small region. For example in the cyclic polyene radicals $C_{2m+1}H_{2m+1}$ the extension of each bond varies as $1/(2m+1)$, and decreases with size until the special effects associated with bond alternation set in.[21] Out of plane distortions are improbable in aromatic hydrocarbons since the forces which lower the symmetry are due to the π electrons and act only in the molecular plane. If they did occur in the negative ions, for example, the resulting $\sigma-\pi$ interactions would at once alter the ring hydrogen isotropic hyperfine splittings in their electron resonance spectra.

In conclusion it would now be interesting to study the forbidden electronic bands and the selection rules for vibrational transitions in more detail for both coronene and triphenylene ions and the degenerate excited states of simple molecules.

ACKNOWLEDGMENTS

We owe much to Professor Harden M. McConnell for discussing many features of this work. We would also like to thank Dr. A. D. Liehr and Dr. L. C. Snyder for their comments and for sending us their own calculations before publication.

THE JOURNAL OF CHEMICAL PHYSICS VOLUME 33, NUMBER 6 DECEMBER, 1960

Frequency Distribution and the Specific Heat of NaCl at Low Temperatures*

ELIZABETH M. ARASE AND ROBERT D. HATCHER
New York University, Washington Square College, New York

(Received March 31, 1960)

Using the Kellerman model of the NaCl crystal, the eigenfrequencies at 0°K are found from those at room temperature by a first-order perturbation theory, which is developed here. From this the frequency distribution at 0°K is obtained and is compared with the room-temperature frequency spectrum. The specific heat and apparent Debye temperatures below 100°K based on both distributions as well as a linearly weighted average are given.

I. INTRODUCTION

THE frequency distribution of the normal modes of vibration for NaCl at room temperature has previously been investigated by Kellerman[1] and Neuberger,[2] assuming Coulomb forces and first neighbor repulsive forces between the ions. For these computations, the elastic constants and lattice constant at room temperature were used to obtain the coupling coefficients. In the computation of the specific heat at low temperatures however, the force constants should be chosen so as to fit the elastic data at these temperatures. Karo[3] recently found the specific heat at low temperatures based on the frequency distribution at 0°K by machine computation. He used a division of 10 along each wave vector axis in reciprocal lattice space to sample the frequencies. We obtained the frequency distribution for NaCl at 0°K for a division of 12 along each wave vector axis, with approximately one and one half times as many frequencies. Furthermore, a first-order perturbation theory was developed (Sec. III) to find the eigenfrequencies at low temperatures, using the frequencies and eigenvectors at room temperature as our unperturbed set. This was possible, since the eigenfrequencies belonging to the same wave vector change but little with temperature. In our formulation only the repulsive terms in the force constants are perturbed and the perturbed frequencies are expressed simply enough to allow rapid evaluation. In addition, this method may be extended to include second neighbor repulsive forces as a perturbation. The frequency distribution at 0°K was computed and compared with the distribution at room temperature (Sec. IV).

The specific heat based on both frequency distributions is found at low temperatures as well as the apparent Debye temperature (Sec. V). The latter quantity is compared with the experimental data by Morrison and co-workers.[4]

* The research reported in this paper has been sponsored in part by the Electronics Research Directorate of the Air Force Cambridge Research Center, Air Research and Development Command.

[1] E. W. Kellerman, Trans. Roy. Soc. (London) **238**, 513 (1940); Proc. Roy. Soc. (London) **A178**, 17 (1941).

[2] J. Neuberger, Ph.D. thesis, Physics Department, New York University (1958).

[3] A. M. Karo, J. Chem. Phys. **31**, 1489 (1959).

[4] W. T. Berg and J. A. Morrison, Proc. Roy. Soc. (London) **A242**, 467 (1957); T. H. K. Barron, W. T. Berg, and J. A. Morrison, *ibid.* **A242**, 478 (1957).

II. THE KELLERMAN MODEL OF THE NaCl CRYSTAL

From the theory of small vibrations and under the assumption of a plane wave solution, the equations of motion for the ions are in the Kellerman notation

$$\omega^2 U_{kx} - \sum_{k'} \sum_{y} \begin{Bmatrix} kk' \\ xy \end{Bmatrix} U_{k'y} = 0. \tag{1}$$

Here k indicates the basis index and is 1 and 2 for the NaCl crystal, while 1 denotes the lattice index. U_{kx} is one of the six components of the eigenvector labeled by k and $x=x, y, z$ and ω the circular frequency. The bracketed quantities are given by

$$\begin{Bmatrix} kk' \\ xy \end{Bmatrix} = \sum_{l} \zeta_{xy} \begin{pmatrix} l \\ kk' \end{pmatrix} \frac{\cos(2\pi \mathfrak{d} \cdot \mathbf{r}_{k'k^l})}{(m_k m_{k'})^{\frac{1}{2}}} \equiv \frac{-1}{(m_k m_{k'})^{\frac{1}{2}}} \begin{bmatrix} kk' \\ xy \end{bmatrix} \tag{2}$$

where $\mathfrak{d}$ is the wave vector, $\mathbf{r}_{k'k^l}$ is the vector from the kth particle in the lth cell to the kth particle in the basic cell. Kellerman considered the coupling constant

$$\begin{bmatrix} kk' \\ xy \end{bmatrix}$$

as defined by Eq. (2) due to Coulomb forces (indicated by C) and due to first neighbor repulsive forces (indicated by R). After lengthy transformations, the Coulomb coefficients assume the form

$$\begin{bmatrix} kk' \\ xy \end{bmatrix}^C = (e^2/v_a) G \begin{pmatrix} \mathfrak{d} \\ xy \end{pmatrix}. \tag{3}$$

Here

$$G \begin{pmatrix} \mathfrak{d} \\ xy \end{pmatrix}$$

is a dimensionless quantity, $v_a = 2r_0^3$ is the volume of the unit cell, where r_0 is the lattice constant and e is the charge of the electron. The repulsive coefficients are given by

$$\begin{bmatrix} kk \\ xy \end{bmatrix}^R = -(e^2/v_a)(A+2B)\delta_{xy}$$

$$\begin{bmatrix} kk' \\ xy \end{bmatrix}^R = (e^2/v_a)[A \cos\pi q_x + B(\cos\pi q_y + \cos\pi q_z)]\delta_{xy} \tag{4}$$

where

$$\delta_{xy}=1 \quad \text{for } x=y$$
$$=0 \quad \text{for } x\neq y,$$

and

$$A=(12r_0^4/x_0e^2)+\tfrac{4}{3}\alpha$$
$$B=-\tfrac{2}{3}\alpha. \tag{5}$$

Here α is the Madelung constant and x_0 the isothermal compressibility. The q_i are defined as the dimensionless components of the wave vectors such that

$$\mathbf{q}=(2r_0)^{-1}(q_x, q_y, q_z)=(2r_0h)^{-1}(p_x, p_y, p_z) \tag{6}$$

with h as an integer. The cyclic boundary and symmetry conditions restrict the q_x and hence the p_x such that

$$q_x+q_y+q_z\leq 3/2$$
$$1\geq q_x\geq q_y\geq q_z\geq 0 \tag{7}$$

and by choosing a division of wave-vector space with $h=12$, the restrictions on the p_x are

$$12\geq p_x\geq p_y\geq p_z\geq 0 \quad \text{and} \quad p_x+p_y+p_z\leq 18. \tag{8}$$

This division corresponds to a total of 74 wave vectors.

It may be seen from Eq. (3) and following material, that the only constants in the coupling coefficients

$$\begin{bmatrix} kk' \\ xy \end{bmatrix}$$

varying with temperature are the lattice constant r_0 and the isothermal compressibility x_0.

III. THE EIGENFREQUENCIES AT LOW TEMPERATURES BY FIRST-ORDER PERTURBATION THEORY

By direct computation, it was determined that the change in the eigenfrequencies of NaCl for a given wave vector is small for large temperature changes. This is essentially due to the small changes in the elastic constants. Therefore, first-order perturbation theory is used to find the eigenfrequencies at low temperature. Here the eigenvectors and eigenfrequencies at room temperature, which were obtained by machine computation by Neuberger,[2] are considered as the unperturbed set and our new quantities at 0°K as the perturbed set.

We adopt a new notation for the equations of motion given by Eq. (1), such that at room temperature they may be written in the form

$$(\omega_m^0)^2U_{im}^0-\sum_j a_{ij}^0U_{jm}^0=0 \qquad i,j=1, 2\cdots 6. \tag{9}$$

For each eigenfrequency ω_m^0, at room temperature, we have six equations of this type for the six components of the eigenvector U_m^0. The new notation is given in terms of the old one as

old notation (kx)	$1x$	$2x$	$1y$	$2y$	$1z$	$2z$
new notation (i)	1	2	3	4	5	6.

The a_{ij}^0 are hence the coupling coefficients at room temperature and are related to those in the Kellerman notation by

$$a_{ij}^0=(m_km_{k'})^{\frac{1}{2}}\begin{bmatrix} kk' \\ xy \end{bmatrix}. \tag{10}$$

Since all terms a_{ij}^0 have a term of e^2/v_a associated with them, it is convenient to introduce

$$b_{ij}^0=(v_a/e^2)a_{ij}^0 \quad \text{and} \quad \lambda_m^0=(v_a/e^2)(\omega_m^0)^2 \tag{11}$$

so that Eq. (9) is of the form

$$\lambda_m^0U_{im}^0+\sum_j b_{ij}^0U_{jm}^0=0. \tag{12}$$

The transformation given by Eq. (11) ensures that at low temperatures only those coefficients b_{ij} are altered which contain repulsive terms. The perturbed equations at low temperatures are then given by

$$\lambda_m'U_{im}'+\sum_j b_{ij}'U_{jm}'=0, \tag{13}$$

where $\lambda_m'=(v_a'/e^2)(\omega_m')^2$ and ω_m' is the perturbed circular frequency. U_m' is the perturbed eigenvector and v_a' is the new volume.

Since the perturbed values vary but little from the unperturbed ones, we may expand the perturbed eigenvalues, eigenvectors, and coupling coefficients in a series

$$U_m'=U_m^0+BU_m'+B^2U_m^2+\cdots$$
$$\lambda_m'=\lambda_m^0+B\lambda_m^1+B^2\lambda_m^2+\cdots$$
$$b_{ij}'=b_{ij}^0+Bb_{ij}^1. \tag{14}$$

The zero-order terms result again in Eq. (12), while the first-order equation is

$$\lambda_m^1U_{im}^0+\lambda_m^0U_{im}^1=-\sum_j(b_{ij}^0U_{jm}^1+b_{ij}^1U_{jm}^0). \tag{15}$$

In the case where λ_m^0 is nondegenerate, even though some other eigenvalues belonging to the complete set of eigenvectors may be degenerate, we may expand the perturbed eigenvectors in terms of the unperturbed set, such that

$$U_m^1=\sum_k a_k^mU_k^0. \tag{16}$$

Substituting Eq. (16) in Eq. (15), we obtain

$$\lambda_m^1U_{im}^0+\sum_k\lambda_m^0a_k^mU_{ik}^0=-\sum_j b_{ij}^0\sum_k a_k^mU_{jk}^0 - \sum_j b_{ij}^1U_{jm}^0 \tag{17}$$

since in the term

$$\sum_j b_{ij}^0\sum_k a_k^mU_{jk}^0$$

the summation may be interchanged, and since from Eq. (12)

$$\sum_j b_{ij}^0U_{jk}^0=-\lambda_k^0U_{ik}^0$$

we obtain after substitution in Eq. (17) for all the components of the vector U_k^0 the vector equation

$$\lambda_m^1\begin{bmatrix}U_{1m}^0\\U_{2m}^0\\U_{3m}^0\\U_{4m}^0\\U_{5m}^0\\U_{6m}^0\end{bmatrix}+\sum_k\lambda_m^0 a_k^m\begin{bmatrix}U_{1k}^0\\U_{2k}^0\\U_{3k}^0\\U_{4k}^0\\U_{5k}^0\\U_{6k}^0\end{bmatrix}=\sum_k\lambda_k^0 a_k^m\begin{bmatrix}U_{1k}^0\\U_{2k}^0\\U_{3k}^0\\U_{4k}^0\\U_{5k}^0\\U_{6k}^0\end{bmatrix}-\begin{bmatrix}b_{11}^1&b_{12}^1&0&0&0&0\\b_{12}^1&b_{22}^1&0&0&0&0\\0&0&b_{33}^1&b_{34}^1&0&0\\0&0&b_{34}^1&b_{44}^1&0&0\\0&0&0&0&b_{55}^1&b_{56}^1\\0&0&0&0&b_{56}^1&b_{66}^1\end{bmatrix}\begin{bmatrix}U_{1m}^0\\U_{2m}^0\\U_{3m}^0\\U_{4m}^0\\U_{5m}^0\\U_{6m}^0\end{bmatrix}. \tag{18}$$

We multiply Eq. (18) by U_n^0, since the vectors U_n^0 are real, and sum over n, making use of the orthonormality of the unperturbed eigenvectors U_n^0.

Hence

$$\lambda_m^1\delta_{mn}+(\lambda_m^0-\lambda_n^0)a_n^m=-B_{nm}'. \tag{19}$$

If $m=n$ we obtain

$$\lambda_m^1=-B_{mm}'=-\sum_{ij}U_{mi}^0 b_{ij}^1 U_{mj}^0. \tag{20}$$

From Eq. (3) and (4), it may be seen that only the repulsive terms change in this formulation, where A as defined by Eq. (4) changes by ΔA. Hence, the perturbing matrix (b_{ij}^1) is given by

$$(b_{ij}^1)=\Delta A\begin{bmatrix}-\frac{1}{m_1}&\frac{\cos\pi q_x}{(m_1m_2)^{\frac{1}{2}}}&0&0&0&0\\\frac{\cos\pi q_x}{(m_1m_2)^{\frac{1}{2}}}&-\frac{1}{m_2}&0&0&0&0\\0&0&-\frac{1}{m_1}&\frac{\cos\pi q_y}{(m_1m_2)^{\frac{1}{2}}}&0&0\\0&0&\frac{\cos\pi q_y}{(m_1m_2)^{\frac{1}{2}}}&-\frac{1}{m_2}&0&0\\0&0&0&0&-\frac{1}{m_1}&\frac{\cos\pi q_z}{(m_1m_2)^{\frac{1}{2}}}\\0&0&0&0&\frac{\cos\pi q_z}{(m_1m_2)^{\frac{1}{2}}}&-\frac{1}{m_2}\end{bmatrix}. \tag{21}$$

Therefore from Eq. (20) and Eq. (21), making use of the orthonormality of the U_m^0, B_{mm}' is given by

$$B_{mm}'=\Delta A\{(-m_1^{-1}+m_2^{-1})[(U_{m1}^0)^2+(U_{m3}^0)^2+(U_{m5}^0)^2]+[2/(m_1m_2)^{\frac{1}{2}}](U_{m1}^0U_{m2}^0\cos\pi q_x+U_{m3}^0U_{m4}^0\cos\pi q_y+U_{m5}^0U_{m6}^0\cos\pi q_z)\}. \tag{22}$$

Hence from Eq. (11) and Eq. (20) the perturbed circular eigenfrequency is obtained as

$$\omega'=[v_a(v_a')^{-1}(\omega_0)^2-e^2(v_a')^{-1}B_{mm}']^{\frac{1}{2}}. \tag{23}$$

Equations (21), (22), and (23) are valid for degenerate eigenvalues only if B_{nm}' is zero. In this event, the perturbed eigenvalues are again degenerate. For the NaCl crystal the degeneracy is due to the symmetry of the crystal itself. This, of course, is not temperature-dependent in our model, and the degeneracy would not be removed by going to higher order terms in the perturbation series. Hence, the above equations may also be used to find the perturbed frequencies for the degenerate case.

For the computation of the eigenfrequencies, the

following constants were used at 0°K for NaCl:

$$r_0 = 2.7886 \times 10^{-8} \text{ cm}$$

$$\alpha = 1.7476$$

$$m_1 = 38.1724 \times 10^{-24} \text{ g}$$

$$m_2 = 58.8722 \times 10^{-24} \text{ g}$$

$$x_0 = 3.89 \times 10^{-12} \text{ cm}^2/\text{dyne}.$$

A sample set of the circular frequency ω as a function of the wave vector σ is shown in Fig. 1 for 0°K as well as for 300°K. The wave vectors are given in rectangular and inverse lattice space components. For a given wave vector, the 0°K frequencies are larger than the 300°K ones, as is expected. The shape of the curves is not altered appreciably.

The convergence of the perturbation series as given by Eq. (14) was checked. It was found that neglecting second-order terms results in an error of less than 0.1% in the frequency.

IV. THE FREQUENCY DISTRIBUTION AT 0°K AND COMPARISON WITH THE RESULTS AT ROOM TEMPERATURE

The frequencies found in the last section were limited to that fraction of wave-vector space given by Eq. (8). For the complete first Brillouin zone the frequencies belonging to each wave vector are obtained by a suitable weighted sum. We thus have a total of 11 454 frequencies on which to base our frequency distribution. To obtain the latter, the frequency scale was divided

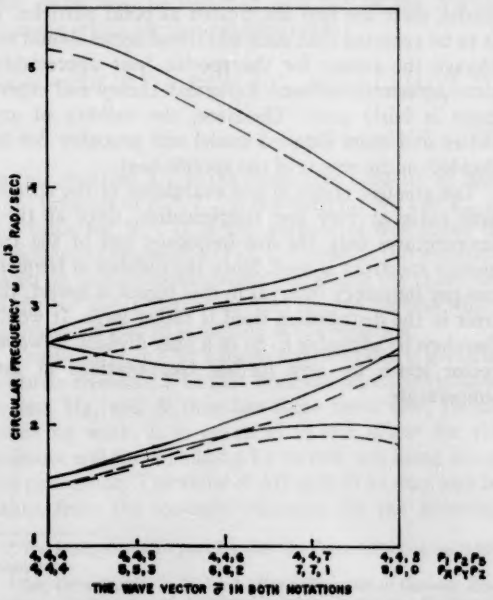

FIG. 1. The circular frequency ω as a function of the wave vector at 0°K (——) and 300°K (-----).

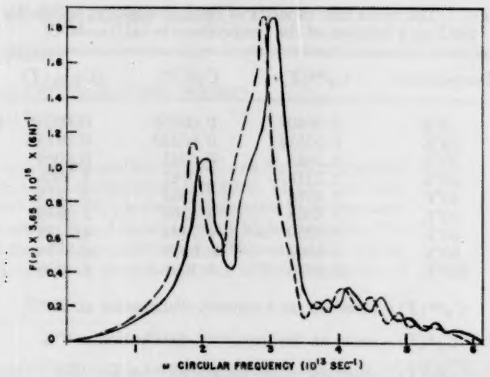

FIG. 2. The frequency distribution for NaCl at 0°K (——) and 300°K (-----).

into intervals $\Delta\omega = 2 \times 10^{12}$ sec^{-1}, and the number of computed values falling into each interval were counted. Four of these step curves were plotted, each shifted with respect to the previous one by 0.5×10^{12} sec^{-1} on the ω scale. In addition, a second set of three step curves of interval 3×10^{12} sec^{-1} was plotted with a shift of 1×10^{12} sec^{-1} on the ω scale. While the latter set of points tends to smooth out the curve more, it was felt to be more accurate in regions of a small number of frequencies per interval and was mostly used in these regions. Neuberger's[2] values for the frequencies at 300°K were recounted by the same method, and both distributions are given in Fig. 2. The normalization factor was obtained from the condition

$$\int_0^{\nu_{\max}} f(\nu)\, d\nu = 6N \tag{24}$$

where N is Avogadro's number, and $f(\nu)$ is the frequency distribution.

The 0°K distribution increases more slowly with frequency than the room temperature one at the low-frequency end. At lower temperature, the two principal maxima are shifted to higher frequencies. The first maximum is broader and lower at low temperature, while the second principal maximum and the fine structure at high frequencies has approximately the same shape as the one at room temperature.

V. HEAT CAPACITIES AND APPARENT DEBYE TEMPERATURES

From the methods of statistical mechanics, the molar heat capacity at constant volume is given by

$$C_V = k \int_0^{\nu_{\max}} \frac{(h\nu/kT)^2 \exp(h\nu/kT)}{[\exp(h\nu/kT) - 1]^2} f(\nu)\, d\nu. \tag{25}$$

From this equation, the molar specific heat at constant volume was found by numerical integration. We used both the 0°K as well as the 300°K frequency distribution at each temperature. The intervals for the numerical

TABLE I. The molar heat capacity of NaCl at constant volume for NaCl as a function of the temperature in cal/(mole°C).

Temperature	$C_V^{300}(T)$	$C_V^{0}(T)$	$\langle C_V\rangle_{Av}(T)$
5°K	0.00407	0.00358	0.00358
10°K	0.03518	0.03149	0.03159
20°K	0.3443	0.3041	0.3065
30°K	1.2218	1.0767	1.1006
40°K	2.4974	2.2503	2.2818
50°K	3.8163	3.5369	3.5819
60°K	5.0750	4.7494	4.8128
80°K	6.9969	6.6928	6.7724
100°K	8.0398	8.3081	8.1276

$C_V^{300}(T)$ – based on the frequency distribution at 300°K

$C_V^{0}(T)$ – based on the frequency distribution at 0°K

$\langle C_V\rangle_{Av}(T)$ – weighted values computed from Eq. (26)

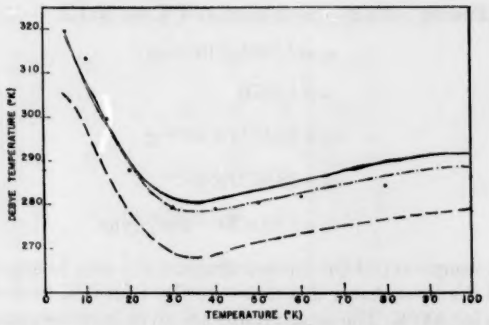

FIG. 3. The apparent Debye temperature as a function of temperature for NaCl. —— based on C_V^{0}, -·-·-· based on $\langle C_V\rangle_{Av}$, ------ based on C_V^{300}, ● experimental values.

integration were chosen as $\Delta\nu=5(2\pi)^{-1}\times10^{11}$ sec^{-1}. The molar specific heat was seen to vary by at most 13%, depending on which frequency distribution was chosen. It seems therefore reasonable to weight these two values of the heat capacity linearly with the temperature interval in the first approximation, such that

$$\langle C_V\rangle_{Av}(T)=C_V^{300}(T)T/(300)+C_V^{0}(T)(300-T)/(300). \quad (26)$$

Here $C_V^{300}(T)$ and $C_V^{0}(T)$ are the molar heat capacities at constant volume at the temperature T, based on the 300°K and 0°K frequency distributions respectively. These specific heats in the range from 5–100°K are given in Table I.

To estimate the deviation from Debye theory, the apparent Debye temperatures corresponding to C_V^{0}, C_V^{300}, and $\langle C_V\rangle_{Av}$ were found and are compared with the experimental[4] values of C_V in Fig. 3. The values of the apparent Debye temperature corresponding to C_V^{0} lie, except at very low temperature, above the experimental points, while the ones corresponding to C_V^{300} are below the measured values. The apparent Debye temperatures due to $\langle C_V\rangle_{Av}$ agree fairly well with the experimental data. The slight disagreement at higher temperatures may be due to the fact that the linear weighting with temperature, as given by Eq. (26), is only a first approximation.

VI. CONCLUSION

As may be seen from the apparent Debye temperature, the Kellerman model gives good agreement between experiment and computation for the above quantities. In principle, of course, to obtain the specific heat at a given temperature, the frequency distribution at this temperature should be used, instead of the averaging process given by Eq. (26). The amount of work necessary for this computation is greatly reduced by the perturbation method which was developed above, for if the eigenvectors and eigenvalues at one temperature are known for a given net of points in wave-vector space, the eigenfrequencies at all other temperatures for the same net may easily be found from Eq. (23). The only quantities that vary with temperature in this formulation are the isothermal compressibility and the lattice constant. This method may also be extended to include other perturbing terms, such as polarization terms. These terms are neglected in the Kellerman model, since the ions are treated as point particles. It is to be expected that such additional terms should not change the results for the specific heat appreciably, since agreement between Kellerman theory and experiment is fairly good. Therefore, the validity of any better and more detailed model will probably not be decided on the results of the specific heat.

The greatest errors in our evaluation of the specific heat enter at very low temperatures, since at these temperatures only the low-frequency end of the frequency spectrum is used. Since the number of frequencies per frequency interval in this region is lowest, the error in the distribution itself is rather large. It would therefore be advisable to go to a finer division in wave-vector space for any further computations at low temperature.

THE JOURNAL OF CHEMICAL PHYSICS VOLUME 33, NUMBER 6 DECEMBER, 1960

Statistical Mechanics of Molecular Ions*

ROBERT N. VARNEY

Washington University, Department of Physics, St. Louis, Missouri

(Received May 19, 1960)

The N_4^+ ion is shown to be able to be in equilibrium against dissociation into N_2^+ and N_2 under specified experimental conditions only if it possesses a considerable degree of vibrational excitation. The A_2^+ ion, lacking the numbers of modes of vibrational freedom possessed by the N_4^+, is therefore unstable under the same conditions. It would become stable in much weaker electric fields and simultaneously higher pressures. Experimentally, the A_2^+ ion is known to exist in contradiction to this prediction, but theoretical and experimental evidence is advanced that it is metastable and subject to dissociation with sufficient numbers of collisions in the gas.

FOR nearly 10 years, the existence of ions composed of pairs of atoms or molecules has been recognized in cases where the pairing does not occur in the neutral state. Thus clear cut identification exists today for He_2^+, Ne_2^+, A_2^+, Kr_2^+, Xe_2^+, N_4^+, $(CO)_2^+$, as well as other combinations such as N_3^+ and H_3^+.[1] Recently, an analysis following thermodynamic lines has been made of the direct association and dissociation of the nitrogen molecule ion,

$$N_4^+ = N_2^+ + N_2.^2 \quad (1)$$

In that work, combined with earlier experimental data, the equilibrium constant K for the reaction was evaluated, a value of the heat of dissociation, ΔH was determined, at least a rough scale for determining ion temperatures from the field strength-to-pressure ratio E/p_0 was found, and a graph was plotted showing $\ln K$ vs $1/T_i$, where T_i is the effective ion temperature. The graph may be regarded as a plot of the Nernst equation which for this reaction reads

$$\ln K = -(\Delta H/RT) + R^{-1}\int\left[\int(C_{p_3}+C_{p_4}-C_{p_1})dT \Big/ T^2\right] \times dT + (\Delta S_0/R). \quad (2)$$

In this equation, C_{p_3} is the molal heat capacity at constant pressure of N_2^+, C_{p_4} is the same for N_2; and C_{p_1} is the value for N_4^+. It is the purpose of this paper to complete the evaluation of all the terms in this equation based on various assumptions concerning the character of the N_4^+ ion in particular, and thus to disclose which assumptions lead to satisfying of the equation.

The value of $\ln K$ at various temperatures is given in footnote reference 2. In that work the pressure was used in mm Hg, and K thus has those units also. In the following work, it is practical to use d/cm² for the pressure and for K; adding 7.1 to $\ln K$ will bring about the conversion. The value of ΔH as 0.50 ev may also be taken from the footnote reference. In the following calculations, a temperature for the ions of 1000°K has been used. This corresponds closely to a value of E/p_0 of 55 v/(cm×mm Hg) and to a typical mid-point of the graph of footnote reference 2. At this temperature, the value of $\ln K$ is 7.1.

The integral term of Eq. (2) will next be treated on the assumption that the various heat capacities are constants. The term then takes the form

$$(\Sigma C_{p_i}/R)\ln T. \quad (3)$$

The approximation involved is likely to be no worse than the error in $\ln K$ which may be near to ± 1. The C_p's each have the form

$$C_p = C_{p_{\text{trans}}} + C_{p_{\text{rot}}} + C_{p_{\text{vib}}}. \quad (4)$$

The values of $C_{p_{\text{trans}}}$ for all constituents are 5 cal/mole °K. The values of $C_{p_{\text{rot}}}$ are 2 cal/mole °K if the molecules are linear. The values of $C_{p_{\text{vib}}}$ are 2 cal/mole °K for each degree of vibrational freedom that is fully excited.

The term $\Delta S_0/R$ in Eq. (2) also has translational, rotational, and vibrational parts which may be calculated by statistical mechanical methods.[3] The entropy constant S_0 for each constituent has the form

$$S_0 = Ri + C_p + C_p \ln k, \quad (5)$$

where i is the chemical constant which may in turn be broken up into

$$i = i_{\text{trans}} + i_{\text{rot}} + i_{\text{vib}}. \quad (6)$$

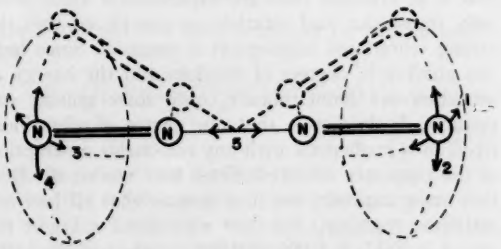

FIG. 1. Vibrations of the linear N_4^+ molecule ion.

* Work supported in part by the Air Force Office of Scientific Research.

[1] See, for example, L. B. Loeb, *Basic Processes of Gaseous Electronics* (University of California Press, Berkeley, California, 1955), Chap. 1.

[2] R. N. Varney, J. Chem. Phys. **31**, 1314 (1959).

[3] See, for example, L. D. Landau and E. M. Lifshitz, *Statistical Physics* (Pergamon Press, New York; English translation 1958), Chap. 4 ff.

TABLE I. Trial substitutions in the Nernst equation.

Type of motion	$-(\Delta H/RT)$	$(\Sigma C_p/R)\ln T$	$(\Delta S_0/R)$	Exptl $\ln K=7.1$ / Theoret. $\ln K$
Translation only	−5.8	−71.5	+105.4	+28.1
Trans+2 deg Rot.	−5.8	−100.1	+138.5	+32.6
Trans+3 deg Rot.[a]	−5.8	−86.2	+120.3	+28.3
Trans+2 rot+5 vib with $\hbar\omega=0.002$ ev	−5.8	+43.0	−28.5	+8.7
Trans+3 rot[a]+4 vib with $\hbar\omega=0.001$ ev	−5.8	+28.6	−15.7	+7.1

[a] Only the N_4^+ molecule ion can have the third degree of rotational freedom.

The respective values are

$$i_{\text{trans}}=\tfrac{3}{2}\ln(m/2\pi\hbar^2) \quad (7)$$

$$i_{\text{rot}}=\ln(I/\hbar^2) \text{ for symmetric, linear molecules} \quad (8)$$

$$i_{\text{vib}}=\ln(1/\hbar\omega) \text{ provided } \hbar\omega\ll kT. \quad (9)$$

The following considerations are then applicable:

(1) The translational terms in both Eqs. (3) and (5) must be used for all constituents of reaction (1).

(2) A two-dimensional rotation is certainly applicable to each constituent. The N_2^+ and the N_2 cannot have more. The N_4^+ is suspected of having the structure N═N—N═N and hence at most two degrees of rotational freedom.

(3) The N_2^+ and N_2 molecules are well known and do not exhibit vibrations at all below the 1000 to 2000°K temperature range.

(4) The linear N_4^+ structure has 7 degrees of vibrational freedom. Of these, the two involving the double electron bonds are suspected of not being excited as they resemble the nonexcited vibrations in N_2^+. The normal modes of vibration may be roughly pictured as shown in Fig. 1. Those labeled 1, 2, 3, and 4 are likely to have relatively low frequency. The fifth vibration is that along the single electron bond which is presumed to break at 0.50 ev, if dissociation occurs, Whether this vibration is excited is difficult to predict.

Table I shows the result of making these substitutions.

It is clear from Table I that the calculated value of $\ln K$ is so different from the experimental value when only translation and rotation are considered that the strong vibrational supplement is essential. Since both the number of degrees of freedom and the energy of vibration are indeterminate, only some guesses are possible. It does seem that one degree of vibrational freedom is inadequate with any reasonable assumption of the frequency involved. Since four modes of vibration are symmetric, one may assume that all four are activated together. The low vibrational energies assigned in Table I, 0.001 to 0.002 ev, are perhaps valid as the experimental data of Kovar, Varney, and Beaty[4] suggest that the vibrations are still active at a temperature of 77°K.

The picture of the N_4^+ molecule ion in a high state of vibrational excitation is compatible with the belief that the association of N_2^+ and N_2 occurs in single, binary collisions. Such an association is impossible unless a mechanism for dissipating the binding energy exists.

It now becomes of interest to calculate the equilibrium constant for the reaction

$$A_2^+=A^+ + A. \quad (10)$$

The molecule ion is wellknown in ion drift velocity work (see footnote reference 1) and has been identified mass spectroscopically.[5] It is believed to be formed at pressures in the 1-cm range by the Hornbeck-Molnar process, the association of an excited and a normal atom with ejection of the extra electron. Direct studies of reaction (10) do not exist.

Statistical computations for Eq. (10) are simpler than for nitrogen as the right side contains only atomic terms subject only to translational motions. The left side can have at most two degrees of rotational freedom and one degree of vibration. If one may judge from the vibrational frequency of the He_2^+ ion, which is known, the vibration in argon is not excited because of requiring too great energy. The value of $\ln K$ calculated is then 18.7. For this value, the heat of dissociation has been taken to be 0.7 ev from footnote reference 5. A temperature of 1000°K has been chosen as it was for nitrogen.

The calculated value of $\ln K$ indicates that the equilibrium of Eq. (10) is nearly completely on the right side, i.e., the A_2^+ is dissociated. Association would first be favored at temperatures of the order of 400°K. Since it is ion temperature that is involved, the lower temperature would in fact call for a lower value of E/p_0. Using the E/p_0 vs T scale for nitrogen from footnote reference 2, and with a lab temperature of 300°K, the value of E/p_0 favoring association would be below 8 v/(cm×mm Hg). Finally, the temperature

[4] F. R. Kovar, R. N. Varney, and E. C. Beaty, Phys. Rev. **107**, 1490 (1957).

[5] J. A. Hornbeck and J. P. Molnar, Phys. Rev. **84**, 621 (1951).

scale of E/p_0 for argon may *not* be the same as for nitrogen, and if one may guess from the behavior of electrons in the two gases, the argon ions may still be "too hot" at E/p_0 of 8 to permit association.

In the meantime, there is the experimental observation that in drift velocity experiments, both the atomic and the molecular ions are seen concurrently in the range of E/p_0 from 8 to 50.[1] The molecular ion was shown to be formed by the Hornbeck-Molnar process. Prior to the present work, it has not been clear whether the A^+ or the A_2^+ was the less intrinsically stable ion. The prediction now, based on the calculated equilibrium constant, is that the A_2^+ should dissociate. It is apparently necessary to assume that the molecule ion is in a sort of metastable condition. Since it does not have all the modes of vibration that the N_4^+ ion has, it is likely that the argon molecule ion can only be jarred out of its metastable condition and dissociated by a secondary process like a three-body collision.

There is further evidence to support this picture. Beaty[6] studying argon at pressures in the range of 2 to 4 cm Hg, finds the drift velocity of A_2^+ closing toward the value for A^+, i.e., in the light of the preceding discussion, dissociating. Biondi and Chanin[7] working below 10 mm Hg pressure, find the drift velocity of A_2^+ retaining a markedly different value from that for A^+. The suggestion here is that the results of Biondi and Chanin are more nearly correct on the grounds that their lower pressures forestall dissociation of the molecule ions.

It will be of interest to explore the drift velocities of ions in argon at a higher pressure, 10 to 20 cm Hg, at values of E/p_0 ranging from 1 to 20 v/(cm×mm Hg) to see if association and dissociation in flight will appear as for the case of nitrogen. Such experiments are in progress in the author's laboratory.

[6] E. Beaty, Phys. Rev. **104**, 17 (1956).
[7] M. A. Biondi and L. M. Chanin, Phys. Rev. **94**, 910 (1954).

Helium Atom Wave Functions from Slater Orbitals of Nonintegral Principal Quantum Number*

LAWRENCE C. SNYDER† ‡

Department of Chemistry, Carnegie Institute of Technology, Pittsburgh, Pennsylvania

(Received June 14, 1960)

Slater orbitals of nonintegral principal quantum number have been used to construct a He ground-state wave function of the form

$$\Psi = c_1(ns, n's) + c_2(n''p)^2 + c_3(n'''d)^2 + c_4(n''''f)^2.$$

The variation method has been employed to determine the five orbital exponents, the five principal quantum numbers n, and the four linear coefficients. The minimized energy is 0.0058 a.u. above the nonrelativistic limit of −2.9037 a.u. computed by Pekeris. This may be compared with a difference of 0.0063 a.u. obtained by Taylor and Parr upon minimizing the energy of the same wave function constrained to have integral principal quantum numbers.

I. INTRODUCTION

THE choice of a convenient basis set of orbitals is a fundamental problem in the construction of wave functions for atoms and molecules. Recently Parr and Joy[1,2] suggested the use of Slater orbitals of nonintegral and principal quantum number and applied them to the hydrogen molecule. Saturno and Parr have used them in single determinant wave functions for atoms[3] and the methane molecule.[4] Reported in the following is the result of repeating with orbitals of variable principal quantum number, the configuration interaction treatment of the He wave function made by Taylor and Parr.[5]

II. METHOD

The Slater orbitals used here may be written compactly

$$(n, l, m)^\zeta = (2\zeta)^{n+\frac{1}{2}}[(2n)!]^{-\frac{1}{2}} r^{n-1} \exp(-\zeta r)\, Y_{l,m}(\theta, \phi), \tag{1}$$

where the parameter ζ is called the "orbital exponent" and the parameter n is called the "principal quantum number." The (spin free) wave function for the helium atom is taken to have the form

$$\psi = c_1(ns, n's) + c_2(n''p)^2 + c_3(n'''d)^2 + c_4(n''''f)^2, \tag{2}$$

* Based on part of a thesis submitted by the author in partial fulfillment of the requirements for the degree of Doctor of Philosophy, Carnegie Institute of Technology, 1959.

† National Science Foundation Predoctoral Fellow, 1953–1954, 1956–1958.

‡ Present address: Bell Telephone Laboratories, Murray Hill, New Jersey.

[1] R. G. Parr and H. W. Joy, J. Chem. Phys. **26**, 424 (1957).
[2] H. W. Joy and R. G. Parr, J. Chem. Phys. **28**, 448 (1958).
[3] A. F. Saturno and R. G. Parr, J. Chem. Phys. **29**, 490 (1958).
[4] A. F. Saturno and R. G. Parr, J. Chem. Phys. **33**, 22 (1960).
[5] G. R. Taylor and R. G. Parr, Proc. Natl.Acad. Sci. U.S. **38**, 154 (1952).

TABLE I. Helium wave functions and energy.

Config.	Coef.	Integral n[a]	Nonintegral n[b]
$(ns, n's)$	C_1	0.99810800	0.99808054
$(n''p)^2$	C_2	−0.06022944	−0.06057875
$(n'''d)^2$	C_3	−0.01159017	−0.01213619
$(n''''f)^2$	C_4	−0.00430410	−0.00426518
E(au)		−2.8974216	−2.8979483
$E-E_{exp}$[c]		0.0063027	0.0057760

[a] The parameter values used minimized the energy for Taylor and Parr (footnote 5): $n=1$, $\zeta=1.19$; $n'=1$, $\zeta'=2.18365$; $n''=2$, $\zeta''=2.4752$; $n'''=3$, $\zeta'''=3.7683333$; $n''''=4$, $\zeta''''=4.76$.

[b] With variation of the n, the listed parameter values minimize E: $n=1.0169724$, $\zeta=1.2238977$; $n'=0.98011602$, $\zeta'=2.1389558$; $n''=2.2466527$, $\zeta''=2.7650670$; $n'''=3.5391383$, $\zeta'''=4.2246558$; $n''''=4.4046323$, $\zeta''''=5.2710910$.

[c] $E_{exp}=-2.90372431$ a.u., nonrelativistic limit computed by Pekeris (footnote 6).

where

$$(ns, n's) \equiv N_s\{((n,0,0)\zeta(1)\cdot(n',0,0)\zeta'(2)) + ((n',0,0)\zeta'(1)\cdot(n,0,0)(2))\},$$

$$(n''p)^2 \equiv N_p\{((n'',1,+1)\zeta''(1)\cdot(n'',1,+1)\zeta''(2)) + ((n'',1,0)\zeta''(1)\cdot(n'',1,0)\zeta''(2)) + ((n'',1,-1)\zeta''(1)\cdot(n'',1,-1)\zeta''(2))\}$$

with analogous expressions for $(n'''d)^2$ and $(n''''f)^2$. Here N_s and N_p are normalization factors. Formulas for integrals and matrix elements required in computations are detailed in the literature.[2]

TABLE II. Hamiltonian matrix elements for helium wave functions.[a,b]

i^j	1	2	3	4
1	−2.8756603 −2.8758796	+0.31693386 +0.31951994	+0.18343074 +0.17817644	+0.11741894 +0.11901848
2		+2.2494461 +2.2555538	+0.44585270 +0.45334547	+0.27270249 +0.28416101
3			+10.391021 9.3076072	+0.51458635[c] +0.52573343
4				+19.123426[c] +19.410701

[a] In the pairs of matrix elements, the upper is for the integral n and the lower for the nonintegral n computation of Table I.

[b] The overlap matrix is the unit matrix.

[c] These matrix elements correct a minor error by Taylor and Parr (footnote 5).

TABLE III. Effect of introducing angularly dependent configurations.

Angular type	Suggested exact energy increment[a]	Increment integral n	Increment nonintegral n
S[b,c]	−0.02149	−0.01952	−0.01982
$S+P$	−0.00228	−0.00183	−0.00184
$S+P+D$	−0.00055	−0.00041	−0.00041
$S+P+D+F$			

[a] Computed from Table III of footnote 8.

[b] Suggested exact S limit is −2.87900 a.u. (footnote 8).

[c] Energies for integral and nonintegral n may be computed from matrix elements in Table II.

Taylor and Parr found the linear coefficients and orbital exponents which minimize the energy E of (2), subject to the condition that the usual integral n values be used. In this study, the energy of (2) has been minimized with respect to these parameters plus the principal quantum numbers n.

III. RESULTS

The results found are summarized in Tables I and II. The thoroughness of the energy minimization for the nonintegral n computation is indicated by the ratio of kinetic to total energy, which is −0.99960461.

IV. DISCUSSION

The variation of n may be seen to remove only about 8% of the difference between the best energy computed with integer n and the nonrelativistic limit computed by Pekeris.[6] This may be contrasted with the observation[3] that the energy of a single determinant wave function $(1s)^2$ is more significantly improved with the best n of $(ns)^2$ for atoms isoelectronic with He. The variation of orbital principal quantum numbers appears to be most profitable with a single determinant wave function.

Based on their calculations and on those of Nesbet,[7] Shull, and Löwdin[8] have estimated the limiting contribution of angular types (s^2, p^2, d^2, f^2, etc.) to an expansion of the true He wave function. In Table III are given the energy increments obtained upon adding the angular types in the present computations. In both the integral and nonintegral n computations, a large fraction of the suggested exact increment limit was recovered by the single angular term added.

[6] C. L. Pekeris, Phys. Rev. **112**, 1649 (1958).

[7] R. K. Nesbet and R. E. Watson, Phys. Rev. **110**, 1073 (1958).

[8] H. Shull and P. O. Löwdin, J. Chem. Phys. **30**, 617 (1959).

THE JOURNAL OF CHEMICAL PHYSICS VOLUME 33, NUMBER 6 DECEMBER, 1960

Dielectric Study of Some Liquid Alkyl Nitrites*

R. F. GRANT† AND D. W. DAVIDSON
Division of Applied Chemistry, National Research Council, Ottawa, Canada
AND
PETER GRAY
School of Chemistry, The University, Leeds, England

(Received May 23, 1960)

The dielectric constants of liquid methyl, *n*-propyl and isopropyl nitrite have been measured over an extensive range of temperature and the results used to estimate the relative abundances of the *trans* and *cis* isomers. It is concluded that the *trans* form predominates in all three liquids, in contradiction, in the case of the propyl nitrites, to the conclusions from recent NMR studies. It is suggested that the assignments to the appropriate NMR peaks should be reversed for the higher alkyl nitrites. Dielectric relaxation in *n*-propyl nitrite was found to be of the asymmetrical Cole-Davidson type.

THE doubling of several infrared bands of the alkyl nitrites has been ascribed to the existence of *cis* and *trans* isomers arising from an appreciable potential energy barrier to rotation about the O—N bond.[1,2] A similar explanation has been given for the appearance at low temperatures of two peaks associated with the protons α to the nitrite group in the nuclear magnetic resonance (NMR) spectra of liquid nitrites.[3–6] These studies and a thermodynamic investigation[7] suggest high values (~10 kcal/mole) for the energy barriers to rotation and low values (0 to 500 cal/mole) for the energies of isomerization.

There are however some unsatisfactory features in the existing information relating to isomeric abundances. The infrared evidence, for both the vapor[1] and the liquid[2] state, suggests a predominance of the *trans* form in all the nitrites that have been investigated, except for methyl nitrite in which the abundance ratio is of the order of unity at room temperature. The NMR results, on the other hand, have been taken to show that, while the *trans* form predominates in methyl nitrite at low temperatures, the *cis* form is the more abundant in the higher nitrites. One interpretation[3] of the differences between the infrared and NMR results for the higher nitrites requires that the ratio of the infrared extinction coefficients for the *trans* and *cis* forms assumes large and variable values. In view of the rather arbitrary nature of the original infrared and NMR assignments, it was decided to investigate isomerism in the liquid nitrites by an independent method.

Since the *trans* form of an alkyl nitrite molecule has a much higher dipole moment than the *cis* form,[8] the *trans*:*cis* abundance ratio should be related to the dielectric constant of the liquid. We have measured the dielectric constants of methyl, *n*-propyl, and isopropyl nitrites over a considerable temperature range and used the dipole moments derived from the Onsager equation to estimate the isomeric abundances. The dielectric dispersion of *n*-propyl nitrite, which remains liquid at low temperatures, has also been studied.

EXPERIMENTAL METHODS

Methyl nitrite was prepared by the addition of sulfuric acid to sodium nitrite in aqueous methanol solution, followed by distillations over calcium chloride and potassium hydroxide. The infrared spectrum agreed with that of Tarte.[1] *n*-Propyl and isopropyl nitrite were prepared by the method of Chretien and Longi,[9] followed by drying over anhydrous sodium sulfate and fractionation in a Todd still. *n*-Propyl nitrite: bp_{760} 47.6°, n_D^{25} 1.3570; isopropyl nitrite: bp_{771} 40.5°, n_D^{25} 1.3483.

Dielectric constant and loss measurements were made at frequencies up to 500 kc/sec using a three-terminal stainless steel cell and instrumentation previously described.[10] The cell was originally filled with methyl nitrite by injecting the sample into the cooled cell, but the conductance was considerably diminished by modifying the lid of the containing can to permit the sample to be directly distilled into the cell under reduced pressure. This filling procedure was used for all three nitrites.

Dielectric constants of dilute solutions of the propyl nitrites in cyclohexane were measured at 10 kc/sec and 22°C with a Balsbaugh cell of 37 pfarad capacitance. From these values and the refractive indices of the same solutions, the dipole moments of the propyl nitrites in solution were calculated.

* Issued as NRC Publication No. 5929.
† NRC Postdoctorate Fellow, 1959–61.
[1] P. Tarte, J. Chem. Phys. **20**, 1570 (1952).
[2] R. N. Haszeldine and B. J. H. Mattinson, J. Chem. Soc. **1955**, 4172.
[3] W. D. Phillips, C. E. Looney, and C. P. Spaeth, J. Mol. Spectroscopy **1**, 35 (1957).
[4] L. H. Piette, J. A. Ray, and R. A. Ogg, Jr., J. Chem. Phys. **26**, 1341 (1957).
[5] L. H. Piette and W. A. Anderson, J. Chem. Phys. **30**, 899 (1959).
[6] P. Gray and L. W. Reeves, J. Chem. Phys. **32**, 1878 (1960).
[7] P. Gray and M. W. J. Pratt, J. Chem. Soc. **1958**, 3403.
[8] T. Chiba, Bull. Chem. Soc. Japan **28**, 505 (1955).
[9] A. Chretien and Y. Longi, Compt. rend. **220**, 746 (1945).
[10] D. W. Davidson, Can. J. Chem. **35**, 458 (1957).

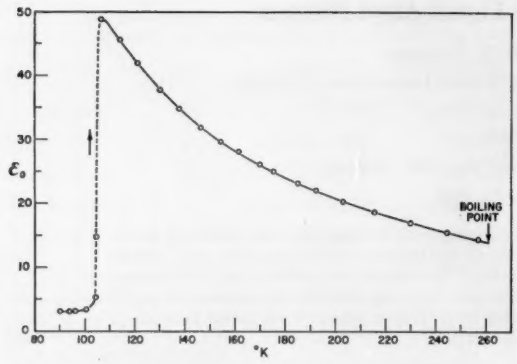

FIG. 1. Static dielectric constant of methyl nitrite.

Densities were determined over a considerable temperature range by the Mohr-Westphal method. The densities obtained were sufficiently accurate for use in the Onsager equation.

RESULTS

The temperature dependence of the static dielectric constant for the three nitrites investigated is shown in Figs. 1 and 2.

Methyl Nitrite

The dielectric constant may be described by

$$\epsilon_0 = -5.47 + 4658/(T - 22.5_0),$$

which represents the results of measurements at 16 temperatures between 110 and 260°K with an average deviation of ±0.3%. There was no dependence of dielectric constant on measuring frequency up to frequencies of at least 500 kc/sec at any temperature.

Samples distilled directly into the cell had dc conductivities ranging from 5×10^{-8} at the freezing point to

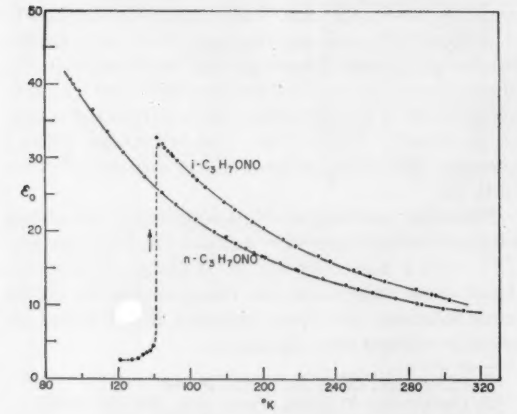

FIG. 2. Static dielectric constants of *n*-propyl and isopropyl nitrites.

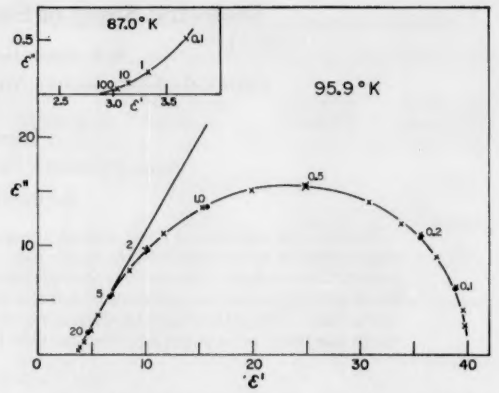

FIG. 3. Complex dielectric constant plot of *n*-propyl nitrite. Numbers are frequencies in kc/sec, × experimental points, ● points calculated from $\epsilon(i\omega) = 3.49 + 36.55(1+i\omega\tau_0)^{-0.705}$, in which $\tau_0 = 3.93\times10^{-4}$ sec.

10^{-6} ohm^{-1} cm^{-1} at the boiling point. These are final values, reached after the samples had been sitting in the cell for about a day. One sample showed a decrease in conductance on heating from 200 to 235°K which perhaps arose from the evolution of a volatile, conducting impurity.

Within the experimental accuracy, the density (g/cm^3) over the liquid temperature range was found to be representable by $d(t°C) = 0.993 - 2.92\times10^{-4}t$. The refractive index, measured with an Abbé refractometer at −20°C, was 1.3315±0.0003.[11]

n-Propyl Nitrite

The results at 26 temperatures between 120°K and the boiling point are given by

$$\epsilon_0 = -3.97 + 3916/(T - 10.0_0),$$

with an average deviation of less than ±0.3%. At lower temperatures the static dielectric constant assumes smaller values than predicted by the equation above, being 36.3 at 105.9°K and 40.7 at 94.1°K, for example.

This nitrite did not freeze even after several days at temperatures below 100°K. The dc conductivity increased monotonically from 10^{-10} ohm^{-1} cm^{-1} at 107.5°K

TABLE I. Dispersion parameters for *n*-propyl nitrite.

T°K	ϵ_0	ϵ_1	β	τ_0(sec)
94.1	40.7	3.62	0.71	1.62×10^{-3}
95.9	40.0	3.49	0.705	3.9×10^{-4}
99.0	39.0	3.54	0.70	4.6×10^{-5}
105.9	36.3	3.50	0.70	7.1×10^{-7}
113.8	33.5		0.70[a]	4.1×10^{-8}
122.7	30.7		0.70[a]	7.1×10^{-9}

[a] Assumed.

[11] We are indebted to J. J. Samolewicz for use of a low-temperature room in the Division of Mechanical Engineering.

to 6×10^{-7} at 298°K. The temperature dependence corresponded to an "activation energy" for conductance varying from 6 kcal/mole at 120°K to 2 kcal/mole at room temperature.

The dielectric dispersion and absorption effects observed at low temperatures are characteristic of the Cole-Davidson type[12] of relaxation behavior, as shown by the plot in Fig. 3. Typical relaxation parameters are given in Table I. The variation of the "cutoff" relaxation time τ_0 with temperature is shown in Fig. 4. The activation energy given formally by the slope varies from 14.2 kcal/mole at temperatures below 100°K to 5.7 kcal/mole near 120°K, where it is therefore about the same as that for conductance. As with other examples of this asymmetric type of dispersion behavior,[12,13] there is a small secondary dispersion region at high frequencies (illustrated in the inset of Fig. 3) which is not described by the Cole-Davidson equation.

The density is given by $d(t°C)=0.9118-1.25_9\times10^{-3}t$ between -120°C and room temperature.

Isopropyl Nitrite

Between 140 and 295°K the equation

$$\epsilon_0=-8.33+5785/T$$

fits the data at 24 temperatures with an average deviation of $\pm0.3\%$. The melting point is about 141°K but the liquid may be supercooled a few degrees.

As for methyl nitrite, there was an anomalous temperature dependence of dc conductance. The conductance increased with decreasing temperature between about 244 and 185°K followed by a regular decrease. The result was a conductivity ($\sim2\times10^{-7}$ ohm^{-1} cm^{-1}) at the melting point which was almost as high as that at room temperature.

As was the case in methyl nitrite, there is evidence of some absorption conductance in the vicinity of the freezing point but this is obscured by the large dc conductance.

Between the freezing point and room temperature the density is given by $d(t°C)=0.887_0-1.26_6\times10^{-3}t$.

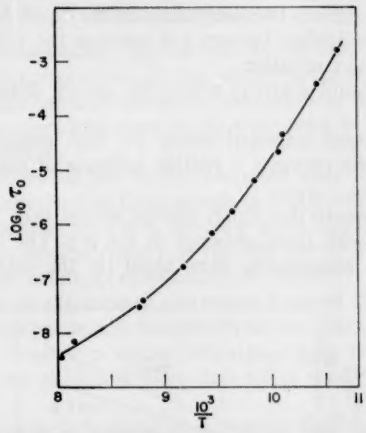

FIG. 4. Variation of relaxation time τ_0 of *n*-propyl nitrite with temperature. $\beta=0.70$ is assumed for lowest five points.

[12] D. W. Davidson and R. H. Cole, J. Chem. Phys. **19**, 1484 (1951).
[13] D. J. Denney, J. Chem. Phys. **27**, 259 (1957).

TABLE II. nsagerO moments in μ_0 in debyes.

	T°K	ϵ_0	μ_0
Methyl nitrite	260	14.14	2.20
	230	16.98	2.27
	200	20.77	2.33
	170	26.11	2.41
	140	34.17	2.50
	110	47.76	2.61
n-Propyl nitrite	310	9.08	2.39
	250	12.35	2.39
	190	17.79	2.38
	150	24.00	2.37
	110	34.92	2.37
Isopropyl nitrite	300	10.95	2.64
	260	13.92	2.68
	220	17.97	2.71
	180	23.81	2.72
	150	30.24	2.73

Onsager Moments

The Onsager equation has been used to calculate the "effective" dipole moments of the nitrite molecules from the dielectric constants, densities and refractive indices. The latter were measured at one temperature for each nitrite and the Lorenz-Lorentz equation used to estimate their values at other temperatures. The results are shown for several temperatures in Table II.

Solution Moments

The dipole moments of *n*-propyl and isopropyl nitrite were obtained in cyclohexane solution at 22°C according to the method of Guggenheim.[14] The values obtained were 2.28 (identical with the result of Cowley and Partington[15] for benzene solution) and 2.49 debye, respectively.

DISCUSSION

Calculation of Isomer Abundances

Our calculation of isomeric composition assumes that the Onsager dipole moment μ_0 as given by

$$\mu_0^2=[9kTM(\epsilon_0-n_D^2)(2\epsilon_0+n_D^2)]/[4\pi Nd\epsilon_0(n_D^2+2)^2],$$

adequately represents the dipole moment of a gaseous mixture of the same isomeric composition as the liquid, and that it may therefore be related to the dipole mo-

[14] E. A. Guggenheim, Trans. Faraday Soc. **47**, 573 (1951).
[15] E. G. Cowley and J. R. Partington, J. Chem. Soc. **1933**, 1252.

TABLE III. Mole fraction (x) of *trans* form. Case 1: μ_{trans}= 2.70 debye, μ_{cis}=0.74 debye. Case 2: μ_{trans}=2.79 debye, μ_{cis}= 0.88 debye.

	T°K	x(case 1)	x(case 2)
Methyl nitrite	260	.64	.58
	230	.68	.62
	200	.72	.66
	170	.78	.72
	140	.85	.78
	110	.93	.86
n-Propyl nitrite	310	.77	.71
	250	.76	.70
	190	.76	.70
	150	.75	.69
	110	.75	.69
Isopropyl nitrite	300	.96	.89
	260	.99	.92
	220	1.01	.94
	180	1.02	.95
	150	1.02	.95

ments of the individual isomeric molecules in the vapor by

$$\mu_0^2 = x\mu_{trans}^2 + (1-x)\mu_{cis}^2,$$

where x is the mole fraction of *trans* form. Support for the validity of the Onsager equation in the present case is provided by nitromethane, for which the temperature-independent Onsager moment of 3.7 debye is in good agreement[16] with the gas moment of 3.6 debye. Two assignments of moments to the *trans* and *cis* isomers have been made, based on the dipole moment of *t*-butyl nitrite (2.70 debye in the gas) obtained by Chiba.[8] For this nitrite Tarte's infrared spectrum[1] shows almost exclusively *trans* form. For the first case, we have taken μ_{trans}=2.70 debye and computed the corresponding *cis* moment from tetrahedral angles[17] and the following bond moments: m_{R-O}1.10,[8] m_{N-O}0.50,[18] and $m_{N=O}$1.73 debye. The last of these bond moments was obtained from the assumed *trans* moment and the other two bond moments. The second choice of isomer moments was suggested by the observation of Tarte[1] that the ratio of optical densities D_{cis}:D_{trans} for the N=O stretching vibrations of *t*-butyl nitrite in the vapor is about 0.03. We have assumed that the ratio of extinction coefficients k_{trans}:k_{cis} is not likely to be greater than 2.5 and therefore that this nitrite is not likely to be less than 93% *trans* form. The "maximum" individual dipole moments are therefore those given by

$$(2.70)^2 = 0.93\mu_{trans}^2 + 0.07\mu_{cis}^2,$$

in conjunction with the C—O and N—O bond moments mentioned previously, and are given as case 2 in Table III. Under these assumptions, the isomer abundances in Table III may be taken as extremes.

[16] C. J. F. Böttcher, *Theory of Electric Polarization* (Elsevier Publishing Company, Inc., New York, 1952), p. 324.
[17] F. Rogowski, Ber. deut. chem. Ges. **B75**, 244 (1942).
[18] J. W. Smith, *Electric Dipole Moments* (Butterworths Scientific Publications, Ltd., London, 1955), p. 92.

For methyl nitrite a fall in temperature from −13°C to −163°C is accompanied by a steady increase in the abundance of the more polar *trans* form from a mole fraction of approx. 0.60 to approx. 0.90. This trend establishes the greater stability of the *trans* form in the liquid.

In liquid *n*-propyl nitrite there is no appreciable change in the isomeric composition (x=approx. 0.73) over a temperature range of some 200°. Isopropyl nitrite, which consists almost exclusively of *trans* form at all temperatures in the liquid, appears to show a trend toward increasing *trans* abundance with decreasing temperature. The moments of both propyl nitrites in cyclohexane solution correspond to smaller *trans* abundances than do those of the undiluted liquids, the *trans* mole fraction being 0.69 (case 1) and 0.63 (case 2) for *n*-propyl nitrite in solution and 0.84 and 0.77, respectively, for isopropyl nitrite.

Energy Differences between *cis* and *trans* Forms

The temperature dependence of the relative abundance of the two isomers enables their energy difference to be determined: $E = E_{cis} - E_{trans} = Rd\ln K/d(1/T)$, for $K = x/(1-x)$.

For liquid methyl nitrite an approximate isomerization energy may be deduced from the plots of Fig. 5, which correspond to the two assignments of dipole moments to the isomers. The isomerization energy derived from the slope in case 1 changes from about 600 cal/mole near the boiling point to about 900 cal/mole near the freezing point. The isomerization energy corresponding to Case 2 is 570 cal/mole and is practically independent of temperature. On the basis of these results the molar energy difference between the isomers may be taken as 700±200 cal and is probably somewhat dependent on temperature. The estimate of error recognizes the uncertainty in the dipole moments of the individual isomers but assumes the validity of the Onsager equation.

For liquid *n*-propyl nitrite the energy difference is zero.

For liquid isopropyl nitrite the high proportion of *trans* form prevents a reliable estimate of the energy difference.

The results for liquid methyl nitrite may be contrasted with those obtained in the gas. The original[1] infrared assignments were based on the assumption

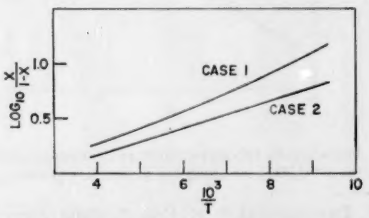

FIG. 5. Variation of *trans*:*cis* abundance ratio in methyl nitrite with temperature.

TABLE IV. Mole fraction (x) by NMR and fractional optical density (f) for $\nu_{N=O}$, attributed to *trans* form.

	NMR (liquid state)			Infrared		
Nitrite	T°K	x	Method	T°K	f	State
Methyl	294	0.5	Mean frequency[a]	296	0.50	Gas[b]
	221	0.73	Intensities[c]			
	213	0.78	Intensities[a]			
	198	0.77	Intensities[d]			
n-Propyl	293	0.36	Mean frequency[e]	296	0.76	Liquid[e]
	198	0.33	Intensities[d]	296	0.75	Gas[b]
	173	0.33	Intensities[e]	296	0.75	Gas[b]
Isopropyl	293	0.88	Mean frequency[e]	296	0.90	Liquid[e]
	198	0.06	Intensities[d]	296	0.85	Gas[b]
	173	0.88	Intensities[e]			

[a] Piette, Ray and Ogg, footnote reference 4.
[b] P. Tarte, footnote reference 1.
[c] Peter Gray and L. W. Reeves, footnote reference 6.
[d] L. H. Piette and W. A. Anderson, footnote reference 5.
[e] Phillips, Looney, and Spaeth, footnote reference 3.

that the stable form is *cis* and Chiba[8] obtained $\Delta E_{gas} = -350$ cal/mole. The greater stability of the *trans* form in the liquid reflects the greater contribution to the cohesive energy to its higher dipole moment. According to an approximate relation[19] derived from the Onsager treatment, the difference in free energies of solution of the *cis* and *trans* forms should increase with the difference in the squares of their dipole moments and with the dielectric constant of the medium.

For the propyl nitrites it is worth noting that the abundance of *trans* form does diminish as the solvent medium is changed from polar nitrite to nonpolar cyclohexane, although both in this solvent and in the vapor phase,[8] the *trans* form predominates.

Comparison with Other Results and Revision of NMR Assignments

Notwithstanding the sensitivity of the derived isomeric composition to the values assumed for the individual isomeric moments, the values in Table III indicate a predominance of the *trans* form in all three liquid nitrites.

These results are to be compared with the abundances obtained by three groups of NMR workers and with the fraction which the *trans* band contributes to the total optical density of the two N=O stretching vibration bands, as summarized in Table IV.

There is satisfactory agreement between the NMR and dielectric results for methyl nitrite. Extrapolation of the dielectric x values indicates a mole fraction of *trans* form of slightly more than 0.5 at room temperature.

It is evident, however, that a *trans* mole fraction of 0.69 to 0.75 as indicated by the dielectric results for *n*-propyl nitrite is not consistent with the NMR values. For isopropyl nitrite there is qualitative agreement between the dielectric values and those of Phillips, Looney, and Spaeth[3] but not with those of Piette and Anderson.[5]

It thus appears probable that there is a difference between methyl nitrite and the higher nitrites in the relative positions (with respect to the strength of magnetic field) of the NMR peaks of the α protons of the *trans* and *cis* forms. A reversal of the assignments of these peaks in the higher alkyl nitrites (except for the isopropyl nitrite assignment of Phillips, Looney, and Spaeth[3] which is already reversed) would remove the inconsistencies between the NMR and dielectric results. It would have the further advantage of making the ratios of the extinction coefficients of the $\nu_{N=O}$ bands (and other bands) of the *trans* and *cis* isomers of the order of unity; these assume variable values between 1 and 6 for the original NMR assignments.[3] The revised ratios of extinction coefficients for the nitrites investigated by Phillips *et al.* are listed in Table V.

The correctness of the original vibrational assignments, on the other hand, is supported by the general correlation that exists between the magnitude of the vapor phase dipole moment[8] and the relative intensity of the vibrational bands attributed to the *trans* isomer.[1] Moreover, the three vibrations of the O—N=O group resemble those of nitrous acid[20] in that the frequencies of $\delta_{O-N=O}$ and ν_{O-N} are higher in the *cis* form and that

TABLE V. Ratios of extinction coefficients of $\nu_{N=O}$ bands.

Nitrite	k_{trans}/k_{cis}
N-Propyl	1.75
n-Butyl	1.03
Isopropyl	~1.18
Isobutyl	1.25
Isoamyl	1.28

[19] Reference 16, p. 154.

[20] L. H. Jones, R. M. Badger and G. Moore, J. Chem. Phys. **19**, 1599 (1951).

of $\nu_{N=O}$ higher in the *trans* form. In nitrous acid the bands arising from the two isomers have been definitely assigned on the basis of the rotational structure.[19]

ACKNOWLEDGMENT

We are indebted to Dr. H. J. Bernstein for an encouraging discussion.

THE JOURNAL OF CHEMICAL PHYSICS VOLUME 33, NUMBER 6 DECEMBER, 1960

Velocity Analysis of Molecular Beams Generated from NaOH Vapors*

V. S. RAO AND RICHARD C. SCHOONMAKER

Columbia Radiation Laboratory, Department of Physics, Columbia University, New York

(Received May 12, 1960)

A molecular beam velocity analysis technique has been employed to determine the molecular composition of vapors in equilibrium with liquid sodium hydroxide in the temperature range 887–996°K. The experimental results are nonreproducible to an extent which far exceeds the expected experimental uncertainties. It is inferred that this anomalous behavior is characteristic of the NaOH system and several possible explanations for the discrepancies are discussed.

INTRODUCTION

SEVERAL recent mass spectrometric,[1–3] effusion,[4] transpiration,[5] and infrared spectral[6] studies have been concerned with the vaporization of sodium hydroxide. The mass spectrometric studies have established the importance of monomeric and polymeric species in the temperature range 573–1050°K. However, several questions of significance remain unanswered or doubtfully answered in the studies which have been reported. The partial pressures of monomeric and dimeric species in the vapors in equilibrium with a pure condensed phase have not been determined. The heats of vaporization of these species remain uncertain.[2] There has been some question, which is relevant to the interpretation of the mass spectra, concerning the importance of Na(g) formed in the vaporization process through decomposition of the hydroxide or interaction with the container, impurities, etc. The present investigation was undertaken with the anticipation of resolving these difficulties and of making it possible to supplement the existing thermochemical data with values which have not been previously reported (partial pressures and entropies of the vapor species, etc.).

EXPERIMENTAL

The experimental technique involves the use of a molecular beam velocity selector to determine the molecular composition of NaOH vapors in a Knudsen-type oven. Details of the apparatus and experimental procedure are similar to those previously discussed by Miller and Kusch.[7,8] Modifications to the MK apparatus include installation of inhomogeneous field beam deflecting magnets at each end of the rotor, increased diffusion pump capacity, and alteration of the rotor by removal of a section of approximately 5 cm length near the detector end. Ovens were of the single chamber design and were machined from silver. Orifices were 0.005 cm×0.318 cm in cross section and slits were 0.005 cm thick. Electrolytically produced pellets of sodium hydroxide were employed with a major impurity of 0.5% Na_2CO_3. The curve fitting necessary to find relative abundances of the various gaseous polymers from the experimental velocity distribution curve[8] was accomplished at the IBM Watson Laboratory with the IBM 650 computer.

RESULTS

Approximately 250 runs worthy of analysis were recorded in the temperature range 887–996°K. During the first 225 of these runs, 6 different silver ovens were used with pure NaOH as condensed phase. In several

* Work supported in part under a joint service contract with the U. S. Army Signal Corps, the Office of Naval Research, and the Air Force Office of Scientific Research, and also in part under a contract with the U. S. Air Force monitored by the Air Force Office of Scientific Research of the Air Research and Development Command and in part under a contract with the Office of Naval Research.

[1] R. C. Schoonmaker and R. F. Porter, J. Chem. Phys. **28**, 454 (1958).

[2] R. C. Schoonmaker and R. F. Porter, J. Chem. Phys. **31**, 830 (1959).

[3] R. C. Schoonmaker and R. F. Porter, J. Phys. Chem. **64**, 457 (1960).

[4] (a) L. H. Spinar, S. P. Randall, and J. L. Margrave, 132nd American Chemical Society Meeting, (September, 1957); (b) F. T. Greene, G. E. Leroi, S. P. Randall, J. R. Soulen, L. H. Spinar, and J. L. Margrave, *Proceedings of the Symposium on Propellant Thermodynamics, American Rocket Society, Columbus, Ohio, July*, **1959** (to be published).

[5] E. Kay and N. W. Gregory, J. Am. Chem. Soc. **80**, 5648 (1958).

[6] L. H. Spinar and J. L. Margrave, Spectrochim. Acta **12**, 44 (1958).

[7] R. C. Miller and P. Kusch, Phys. Rev. **99**, 1314 (1955).

[8] R. C. Miller and P. Kusch, J. Chem. Phys. **25**, 860 (1956).

runs where beam deflecting magnets were utilized, the total beam intensity was independent of the magnetic field gradient. Thus, confirmation was obtained for the inference from mass spectrometric studies[2,3] that Na(g) is negligible in the vaporization of NaOH from silver ovens in the temperature range under investigation. Several other oven materials were employed in the mass spectrometric investigations and in all cases Na(g) was detected as an effusing species. Thus, of the metallic materials studied, silver appears to be the only container which is substantially inert to attack by NaOH at high temperatures. Apparently MgO[4] and possibly other ceramic containers would be chemically inert to NaOH. In general a series of 5–10 consecutive runs was made at each temperature and increments of

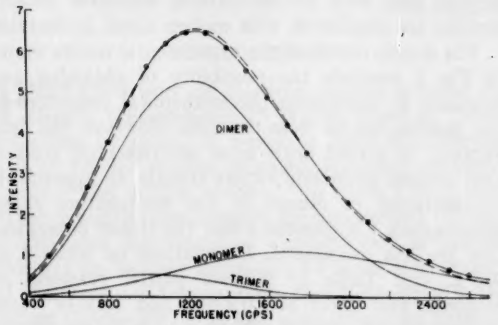

FIG. 1. Typical least squares fit of theoretical velocity distribution to measured intensity at the detector at an oven temperature of 897°K. Upper solid curve is best fit assuming monomers, dimers, and trimers in the effusing beam with $a_2=2.42$ and $a_3=0.168$ where a_n is the ratio of the concentration of n-mer to that of monomer in the composite beam. Broken curve is best fit assuming only monomers and dimers. Central velocity of transmitted beam, $v_0=50.15f$.

approximately 10° occurred between such groups of runs throughout the range of interest. In many cases a series at a given temperature was repeated over intervals of several days to determine the reproducibility of the data. In almost all instances, excellent fits of the experimental data to theoretically derived velocity distributions[5] could be obtained for a given run by assuming the presence of monomers, dimers and trimers in the equilibrium vapors. One such fit at 897°K is shown in Fig. 1. Within a series of consecutive runs the relative concentrations of the species were generally in good agreement. However, when it was attempted to reproduce a series of runs after having taken data at other temperatures or after changing ovens the discrepancy often far exceeded the expected uncertainty. Results for 4 series, each consisting of 5 to 7 runs, at 936°K are summarized in Table I. Within each series of runs the largest and smallest values of a_2 differed by less than 15%, where a_n represents the ratio of the concentration of n-mer to that of the monomer in the molecular beam. The large, nonreproducible effect at 936°K was typical

TABLE I. Reproducibility of a_2 and a_3 at 936°K.[a]

Series no.	a_2	a_3	Oven no.
1	1.98	0.139	1
2	1.23	0.081	1
3	2.59	0.101	2
4	1.55	0.116	6

[a] $a_n=(C_n/n^{\frac{1}{2}}C_1)$; C_n=concentration of gaseous n-mer in the oven. a_2 and a_3 are averaged values obtained from 5–7 runs in each series.

of the results obtained at other temperatures as shown in Fig. 2 where each point represents the average of 5 to 10 consecutive runs. Comparison of the reproducibility of data in this investigation with that previously obtained in velocity analyses of alkali halide beams[6–10] suggests that the effect is characteristic of the hydroxide system rather than a manifestation of systematic and undetermined errors in the apparatus and technique.

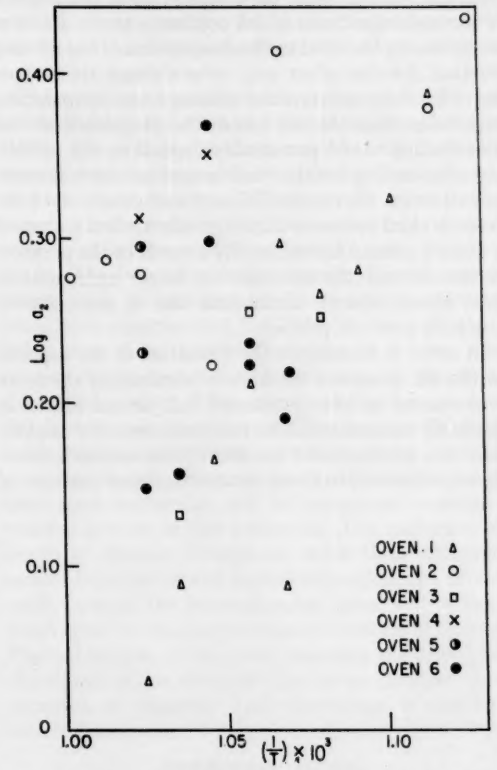

FIG. 2. Temperature dependence of dimer-monomer ratios in molecular beams of NaOH illustrating nonreproducibility of data as a function of experimental conditions.

[9] M. Eisenstadt, G. Rothberg, and P. Kusch, J. Chem. Phys. **29**, 797 (1958).
[10] M. Eisenstadt, V. S. Rao, and G. Rothberg, J. Chem. Phys. **30**, 604 (1959).

DISCUSSION

Observation of the ovens which had been used for several series of runs invariably revealed a surface layer of hydroxide on the external slit faces. In some cases where prolonged heating had occurred a channel of material several mils thick formed around the orifice. There are a number of conceivable ways in which the presence of NaOH on the slit faces may account for the anomalous behavior of this system. The molecular beam which is analyzed under these conditions represents a composite of molecular species effusing from the oven aperture and those formed during vaporization from the slit faces. A low evaporation coefficient of the order of 6×10^{-3} for $Na_2(OH)_2(g)$ has recently been suggested by Spinar *et al.*[4] A coefficient of this magnitude would not materially affect the attainment of saturated equilibrium for the species in our oven because the ratio of orifice cross-sectional area to evaporating surface area was less than 1.6×10^{-4}. If, however, the evaporation coefficient of the monomer were different from that of the dimer the composition of the fraction of the molecular beam which originates at the slit faces would not be identical to the composition of the effusing fraction. Another effect may occur through the scattering of the components of the effusing beam by molecules vaporizing from the slit faces. The magnitude of this contribution would presumably depend on the scattering cross section for the various species which interact as well as on the detailed history and condition of the oven. A third source of difficulty arises when a channel is formed around the orifice. As a result of the presence of the channel the aperture no longer approximates ideal kinetic theory dimensions and a true effusive condition may not prevail.

In order to investigate the formation of the deposits on the slit faces and methods of eliminating them, an oven was set up in an evacuated bell jar and heated to operating temperature. At temperatures only slightly above the melting point (*ca* 400°C) the molten hydroxide was observed to creep around the inner surfaces of the oven and through the orifice to supply a continuous layer of material to the external slit faces. Similar behavior was observed with nickel ovens. It was also noted that molten NaOH will rise to heights in excess of $4\frac{1}{2}$ in. in a silver container. Space limitations in the present apparatus preclude the use of large containers in an attempt to arrest the flow of liquid to the orifice. Several attempts were made to contain the liquid by inserting a pressed layer of finely divided magnesia into the well[1] before loading the sample. While this technique may have diminished the creep rate it did not eliminate the problem. It now appears evident that some less direct method than that utilized here must be employed if velocity analysis is to be used to determine the molecular composition of alkali hydroxide vapors. Furthermore, it is possible that the perplexing problems described here may be encountered whenever effusive studies are conducted with molten alkali hydroxides.

The erratic nature of the experimental results shown in Fig. 2 preclude the possibility of obtaining any precision in calculating thermochemical properties of the gaseous species from the data. However, the data suggest, in accord with mass spectrometric studies, that sodium hydroxide vapors contain an appreciable concentration of dimers in the temperature range investigated. Conclusions about the trimer concentration are less meaningful. Calculations on series I at 936°K (see Table I) indicate partial pressures of monomer and dimer of 1.0×10^{-3} and 2.9×10^{-3} mm Hg, respectively, and should give an indication of the pressures to be expected in the vaporization of NaOH.

The velocity selector employed in this experiment is currently being modified to allow a detailed investigation of molecular beam scattering and its effect upon the distribution of velocities among the beam components.

ACKNOWLEDGMENT

We would like to acknowledge our appreciation to Professor P. Kusch for helpful discussions relating to this work.

THE JOURNAL OF CHEMICAL PHYSICS VOLUME 33, NUMBER 6 DECEMBER, 1960

On the Molecular Nature of the Dielectric Anomalies in Thiourea

CRISPIN CALVO*

RCA Laboratories, Radio Corporation of America, Princeton, New Jersey

(Received April 7, 1960)

Of the four dielectric anomalies in thiourea, three are shown to be correlated with the disordering of the molecules in the crystal. This disordering involves both a relative rotation and a translation of the molecules between potential minima. One of the other anomalies, the high one in temperature, is shown to result from a translation of the molecules within the unit cell. Lattice parameter measurements as a function of temperature confirm that the lowest transition is of first order and show only a change in slope at the highest transition. An electrostatic model based upon the electronic resonance structures of thiourea is used to discuss the binding energy of the molecules in the crystal, the vibration of the molecules, the equilibrium orientation of the molecules in the unit cell, and the spontaneous polarization of the crystal. A simple statistical model based upon two interpenetrating nonidentical sublattices reveals a disordering of the molecules from 0°K to 178°K and yields the first-order transition together with the two ferrielectric regions of temperature.

INTRODUCTION

PREVIOUS work on thiourea crystals includes dielectric measurements,[1-3] crystal structure determinations by means of x-rays at room temperature[4] and at 120°K,[2] nuclear magnetic resonance measurements,[5,6] and infrared studies.[7,8] In Table I the results of the dielectric measurements are summarized. Column T indicates the transition temperatures of normal thiourea for the four anomalies; ΔT is the shift in each of the transition temperatures upon deuteration to the extent of $93\pm2\%$; P is the spontaneous polarization (extrapolated to 0°K for the region below the lowest transition). The first transition has been shown to be of first order and thus involves a volume discontinuity, while the third transition is of unknown order. The crystal is ferroelectric below 169°K and again in a narrow range about 176°K. Between these states and again above 178°K the crystal is nonpolar; neither pyro- nor piezoelectric. Dielectric loss measurements[3] show a broad dipolar resonance absorption corresponding to a potential barrier of 0.11 ev in the lower ferrielectric range and a discontinuity in the loss curve around 177°K.

The room temperature crystal structure consists of two polar sublattices with the polar direction along the b axis[9] arranged antiparallel so as to cancel each other's polarity exactly. The structure below the lowest anomaly has the molecules in the sublattices rotated oppositely about the c axis with respect to each other and results in an incomplete cancellation of the polarity along the b axis. These x-ray studies show that the molecule, save possibly for the hydrogen atoms, is planar and has intermolecular distances too large to support hydrogen bonds.

The nuclear magnetic resonance data of Emsley and Smith[5] indicate the onset of major molecular motion at 210°K. This is shown by the decrease in both the second moment and the linewidth of a powdered sample as a function of temperature. From single crystal data[6] these authors conclude that the motion is a hindered rotation about the twofold axis of the molecule (C—S bond). The lack of hydrogen bonding in thiourea together with the stability of the crystal through the transitions suggests that the dielectric anomalies arise either from distortions of the molecule or from small relative displacements of the molecules. In either case the understanding of the nature of the transitions in this ferroelectric should be simplified because the dipole resides within the molecule and thus can be treated as an isolatable unit. In this paper the shifts in the transitions upon deuteration will be interpreted in terms of relative motion of the molecules. The molecules are shown to disorder through the lower three transitions and to translate at the highest transition. An effort is made to treat the intermolecular forces with a model based upon the charged resonance structures of thiourea. The last section of this paper discusses the disordering of a dipole lattice which is taken as an idealized representation of thiourea. This disordering is correlated with the phenomena occurring in thiourea below 178°K.

MOLECULAR MODEL

The major point left in doubt about the molecular arrangement by the x-ray studies is the positions of the hydrogen atoms. Kuncher and Truter's[4] room temperature x-ray investigation of thiourea yielded no indication of the positions of the hydrogen atoms, while Goldsmith and White[2] concluded from a low-tempera-

* Present address: McMaster University, Ontario, Canada.

[1] A. L. Solomon, Phys. Rev. **104,** 1191 (1956).

[2] G. J. Goldsmith and J. G. White, J. Chem. Phys. **31,** 1175 (1959).

[3] R. Freyman, M. Freyman, L. Blanchard, M. Hagene, J. LeBot, and J. LeBot, Arch. sci. **10,** 34 (1957).

[4] N. R. Kuncher and M. R. Truter, J. Am. Chem. Soc. **517,** 2551 (1958).

[5] J. W. Emsley and J. A. S. Smith, Proc. Chem. Soc. **53, 1958.**

[6] J. W. Emsley and J. A. S. Smith, Arch. sci. **12,** 122 (1959).

[7] J. E. Stewart, J. Chem. Phys. **26,** 248 (1957).

[8] R. D. Waldron, Ph.D. thesis, California Institute of Technology, 1951.

[9] The axial designation is that of R. W. G. Wyckoff and R. B. Corey, Z. Krist. **81,** 386 (1932).

TABLE I. Summary of dielectric data.

T°K	ΔT°C	ΔT_{calc}°C	P_{obs}(μ coul/cm²)	P_{calc}(μ coul/cm²)	Order	State
169	+16	+15.7±0.3	3.6	2.0	1st	Ferrielectric$<T$
170.5	...	...	...	...	...	...
177	+16	+16.4±0.4	2.5×10^{-3}	...	?	Ferrielectric $T\pm2$ °C
202	+11	+10.1±0.2	...	...	?	...

ture crystal structure investigation that the hydrogen atoms were nearly planar with the rest of the molecule.[10] In addition Waldron[8] inferred that the planar arrangement of the hydrogens results from a stiffening of the C—N bond due to the resonance of thiourea (Fig. 1). This torsional oscillation has been assigned a reasonably high frequency of 520 cm^{-1} by Stewart[7] and thus lends support to Waldron's contention. Lastly the planarity is to be expected from analogy with the results for urea.

Emsley and Smith[6] concluded that the N—H distance is 1.06 A and the H—N—H bond angle is 119° from an NMR investigation on a single crystal at 180°K. However, one may suspect that a high value of the N—H distance will be obtained in this case as was obtained in the NMR study of urea.[11] In this latter case NMR yielded a value of 1.04 A for this distance while the neutron diffraction[12] results were 0.99 A. The smaller bond length for urea is more consistent on spectroscopic and molecular orbital theory grounds[13] and these arguments are expected to be valid for thiourea also. In this paper we choose as a model the planar molecule with the bond distances and angles found in the room temperature x-ray investigation of thiourea and the N—H bond distance (0.99 A) and H—N—H angle (122°) found in the neutron diffraction studies for urea. The molecular arrangement is shown in Fig. 2 together with a Cartesian coordinate system attached at the center of mass and with axis **1** directed along the twofold axis (C—S bond) of the molecule, axis **2** parallel to the N—N vector of the molecule which also parallels the c axis of the structure and axis **3** perpendicular to the molecular plane. These molecular axes will be used in discussing the torque on the molecule and the room temperature molecular oscillations.

MODEL FOR THE DIELECTRIC TRANSITIONS

A comparison of the high- and low-temperature structures shows (Fig. 3) that the room-temperature one is obtained from the low-temperature structure by two molecular displacements. These are a rotation of the molecule about an axis parallel to the c axis through the center of mass and a translation of the center of mass within the unit cell. The rotation results in a nonpolar crystal and the translation adds the glide plane relationship between the two sublattices. Apparently these motions do not occur separately, since to reverse the crystal polarity while preserving the unit cell geometry and symmetry during the reversal, the molecules must both translate and rotate. Figure 23 of footnote 2 shows the relationship between the reversed and normal structure.

In general the shifts of transition temperatures by isotopic substitution can be discussed only if the detailed nature of the potential energy surfaces in the crystal are known. However in the case of thiourea by making a few assumptions we can give an interpretation of the anomalies based upon particular kinds of molecular motions. First we will assume that the potential surfaces do not change upon deuteration. Then the similarity in the temperature shifts for the transitions at 169°K and 177°K indicates that these transitions are fundamentally of the same character while the smaller shift of the 202°K transition indicates that it is of an entirely different nature. The second assumption is that the spacing of the energy levels for both the translational and rotational states are so small in comparison to kT that a classical partition function can be used. The Hamiltonian for the ith molecule of the crystal can be expressed as

$$H_i=(P_T{}^2{}_{,i}/M)+(P^2{}_{\theta,i}/I)+(\text{vibrational terms})+(\text{Coriolis terms})+V, \quad (1)$$

where $P_T{}^2$ and $P_\theta{}^2$ are the translational and rotational momentum, M and I the total mass and total moment of inertia, while V is the potential energy. We have assumed rotation about the c axis only. The classical partition function is

$$\text{P.F.}=h^{-3N}\int\cdots\int\exp-[(kT)^{-1}\sum_i H_i]\prod_i dp_i dx_i \quad (2)$$

where the integration is over all coordinates of the molecules. If the potential surfaces are invariant to deuteration, the normal and deuterated crystals will show equivalent transitions when the partition function for the normal and deuterated crystals correspond. Since only rotational and translational motions are

[10] In a recent paper Z. V. Zvonkova and Y. Tashpulatov [Soviet Phys. Cryst. **3**, 553 (1958)], take issue with the results of Kuncher and Truter, and thus also with Goldsmith and White, as to bond lengths and angles in thiourea. However their results are inconsistent not only with the x-ray determination of thiourea but by analogy with the x-ray and neutron diffraction results for urea.

[11] E. R. Andrew and D. Hyndman, Discussions Faraday Soc. **19**, 195, 251 (1955).

[12] J. E. Worshan, Jr., H. A. Levy, and S. W. Peterson, Acta. Cryst. **10**, 319 (1957).

[13] M. Davies and L. Hopkins, Trans. Faraday Soc. **53**, 1563 (1957).

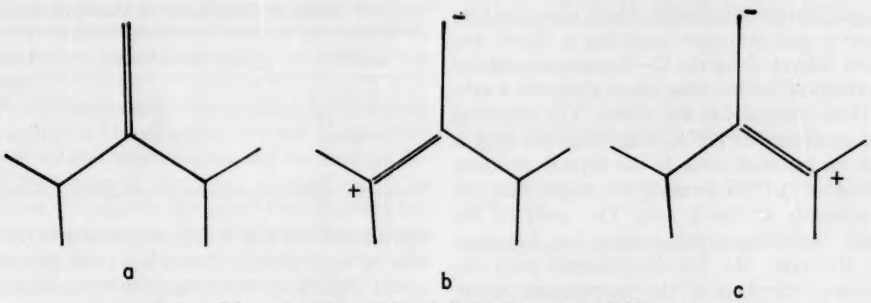

FIG. 1. Schematic representation of the bond character of thiourea.

involved, only the first two terms of the Hamiltonian need be considered. A change in the mass of one of the atoms changes M by ΔM and I by ΔI. The change in temperature ΔT, which places the two partition functions on a corresponding basis $[\text{P.F.}_{\text{normal}}(T) = \text{P.F.}_{\text{deuterated}}(T+\Delta T)]$ will depend upon both ΔM and ΔI in proportion to the relative magnitudes of the translational and rotational kinetic energies. If the kinetic energy of the system is dominated by the translational contribution $(\Delta T/T) = (\Delta M/M)$ or if the rotational energy is dominant, then $(\Delta T/T) = (\Delta I/I)$. These predicted changes in T are $5.0\pm0.1\%$ for the change in mass case and $9.3\pm0.2\%$ for the change in moment of inertia case. These values were calculated using the experimentally determined extent of deuteration and the molecular structure pictured in Fig. 2. The distribution of the deuteriums about the sites available and the change in the position of the center of mass upon deuteration were considered in the computation.

If one assumes that the molecules rotate and translate between potential minima below 180°K and that virtually all the energy is in the rotation of the molecule, one obtains temperature shifts of $+15.7\pm.3$°C at 169°K and $+16.4\pm0.4$°C at 177°K versus measured values of 16°K at both anomalies. If a translation is assumed to occur at 202°K one predicts a temperature shift of 10.1 ± 0.2°C as compared to a measured 11°C.[14]

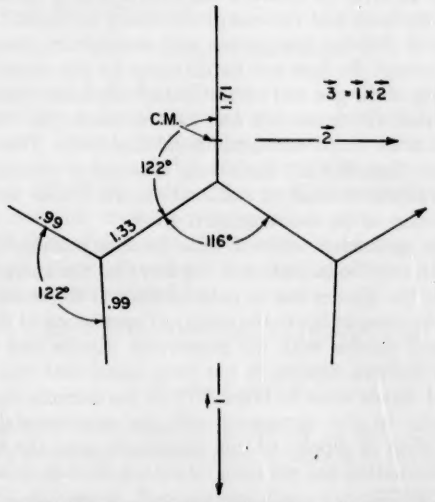

FIG. 2. Molecular model. Bond distances and bond angles are indicated together with the molecular axes **1, 2, 3.**

SPONTANEOUS POLARIZATION

The dipole moment of a thiourea molecule as measured in a dioxane solution by Kumler and Fohlen[15] is 4.86 debyes. The effective dipole moment of a molecule in the crystal will differ from this primarily because the electric field that exists in the crystal will polarize the molecule. This effect is not trivial. If one calculates the

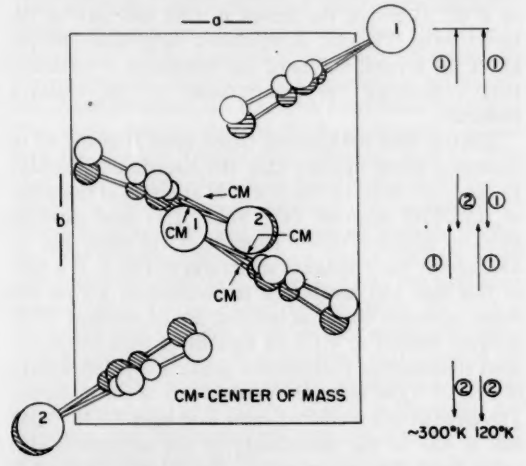

FIG. 3. Thiourea structure projected on to the a, b plane. The full circles correspond to the room-temperature structure and the dashed circles correspond to the low-temperature structure. Molecules labeled 1 are in sublattice 1 and molecules 2 are in sublattice 2. In addition the dipole moment components along b for each molecule is shown for both the room and low temperature structures.

[14] J. G. White has concluded independently from x-ray measurements that this transition corresponds to a translation of the molecules within the unit cell because the symmetry decreases near this point (206°K) without the appearance of a polar state.

[15] W. D. Kumler and G. M. Fohlen, J. Am. Chem. Soc. **64,** 1944 (1942).

expected spontaneous polarization based upon the low-temperature crystal structure assuming a dipole moment of 4.86 debyes along the C—S bond, one obtains 1.6 ± 0.3 μ coul/cm^2 for the component along the b axis. In Fig. 3 these components are shown. The measured value is 3.2 μcoul/cm^2 at 120°K. The estimated error is based upon an assumed error in the crystal structure determination of $\pm1°$ in locating the angle that the molecule subtends at the b axis. The error in the experimental spontaneous polarization has not been estimated. However, the low-temperature x-ray results, because of the form of the temperature factor, indicates that the structure at 120°K is a partially disordered one. A more valid comparison would then be made at 0°K where the extrapolated experimental value is 3.6 μcoul/cm^2. One now must know or estimate the difference in the structure at 0° and 120°K. An estimate was made based upon the disordering model discussed below. There we discussed the relationship of the ordered and disordered positions of a molecule and in addition we can estimate that the structure is about 6% disordered at 120°K. The structure at 120°K then has the angle between the pair of molecules in the same plane effectively contracted by about 1° if this is the plane with the larger dipole component along the b axis or effectively enlarged by about 1° if the molecules of the plane subtend the smaller dipole component along the b axis. The corrected structure leads to a calculated spontaneous polarization of 2.0 μcoul/cm^2 at 0°K. Although the errors in this estimate of the structure at 0°K may be relatively large this does not affect the general nature of the conclusion to be drawn next concerning the polarizability of the thiourea molecule.

Electric field calculations based upon a model to be discussed below indicate that the electric field parallel to the C—S bond on the S and N atoms is of the order of 0.25×10^6 esu/cm^2 (see Table III) and directed so as to induce a dipole moment of the same sign as assigned by the resonance structures of Fig. 1. If a field of this sign and magnitude is assumed to act on the entire molecule then the induced dipole moment (3.89 debyes) needed to yield an agreement with the measured spontaneous polarization predicts a polarizability of 15×10^{-24} cm^3 along the twofold axis of the molecule. The error in this predicted value is at least 5×10^{-24} cm^3 and is due to the uncertainty in the structure. This value is of the proper order; for example, Smythe[16] gives a value of 10.6×10^{-24} cm^3 for the electronic polarizability of C=S. However, a reliable comparison awaits the measurement of the polarizability tensor for the molecule.

NATURE OF THE FORCES

The ground-state configuration of the thiourea molecule has contributions from the ionic resonance structures b and c of Fig. 1. The magnitude of the contribution of each of these forms has been estimated to be about 20% from the measured dipole moment[15] and the C—N bond length by analogy with urea.[17] In fact one can reproduce the measured dipole moment by placing a charge of 0.42 electron at the sulfur site and minus one-half of this on each nitrogen site and ignoring polarization contributions. This representation is the model used in the electrostatic calculations developed next.

TABLE II. Convergence of Madelung energy.

Shell	No. of terms	kcal/mole
0–5 A	4	16.3
5–10	38	2.7
10–15	114	−3.4
		15.6

We inquire whether this simple ionic representation can yield reasonable agreement with some of the measured properties of thiourea. The heat of sublimation of thiourea has been estimated from thermochemical data to be of the order of 15 kcal/mole.[18] A Madelung energy computation was made on the thiourea structure using the room temperature form as the initial state and the infinitely dispersed static molecules as the final state. A charge of 0.42 electron was placed on each sulfur site and -0.21 electron at each nitrogen site. The sum of the charge-weighted reciprocal interatomic distances with the origin at a sulfur atom was carried out to a radial distance of 15 A ignoring the nitrogen charges on the molecule at the origin. This term would correspond to the formation of the infinitely dispersed dipoles from the infinitely dispersed point charges. The value obtained for this energy of sublimation is 15.6 kcal/mole. In order to obtain a calculated heat of sublimation we must add the energy necessary to expand one mole of thiourea gas against one atmosphere pressure and correct the final and initial states for the molecular motion of the gas and crystal lattice vibration. Assuming ideal circumstances one can estimate that these corrections would add a minus 0.3 kcal/mole. Thus we expect that 15.6 ± 1 kcal/mole reasonably represents the calculated heat of sublimation. In Table II an indication of the convergence is given.

The agreement obtained, while ignoring polarizability effects, may be indicative of the fact that the energy to create the dipoles due to polarizability of the molecule may be comparable to the energy of interaction of these induced dipoles with the permanent dipoles and the other induced dipoles. It has been found that this induced dipole must be about 80% of the intrinsic dipole in order to give agreement with the experimental P. The effect of dipoles of this magnitude upon the heat of sublimation has not been estimated since their loca-

[16] C. P. Smythe, *Dielectric Behavior and Structure* (McGraw-Hill Book Company, Inc., New York, 1955), p. 409.

[17] P. Vaughan and J. Donohue, Acta Cryst. **5**, 530 (1952).

[18] S. Sunner, Acta Chem. Scand. **9**, 847 (1955).

tion in the lattice is uncertain. However, if one assumes that they are point dipoles induced at the center of mass, their contribution to the energy of sublimation will be small.

Next we will inquire as to the equilibrium conditions on the molecules in the structure. We will assume that the center of mass is fixed in space and we shall not inquire into the nature of the forces involved except to conclude from Earnshaw's theorem[19] that they are not entirely electrical in origin. For the molecules to be in equilibrium the sum of the torques must be zero. The total torque on our model for the molecule is

$$\mathbf{T}=\mathbf{p}_S\times(Z_S\mathbf{E}_S)+\mathbf{p}_{N1}\times(Z_N\mathbf{E}_{N1})+\mathbf{p}_{N2}\times(Z_N\mathbf{E}_{N2}), \quad (3)$$

where $\mathbf{p}_x$ is the vector distance from the center of mass to atom x, Z_x is the magnitude of the charge on atom x and $\mathbf{E}_x$ is the electric field acting on atom x. Setting $\mathbf{T}=0$ for an arbitrary orientation for the molecules leads to restrictions upon the magnitude of the electric field components at the nitrogen and sulfur position. Only if the mirror plane of the molecule lies in the mirror plane of the structure will some of these restrictions be lifted. The torque can then be expressed as

$$\mathbf{T}=\mathbf{p}_S\times(Z_S\mathbf{E}_S)+Z_N({}_{||}\mathbf{p}_N+{}_{\perp}\mathbf{p}_N)\times({}_{||}\mathbf{E}_N+{}_{\perp}\mathbf{E}_N)$$
$$+Z_N({}_{||}\mathbf{p}_N-{}_{\perp}\mathbf{p}_N)\times({}_{||}\mathbf{E}_N-{}_{\perp}\mathbf{E}_N) \quad (4)$$

by resolving both $\mathbf{p}_x$ and $\mathbf{E}_x$ for the nitrogen atoms into components in and perpendicular to the mirror plane of the crystal lattice. The equality in magnitude of the various components is required by this mirror plane. The expression reduces to

$$\mathbf{T}=\mathbf{p}_S\times(Z_S\mathbf{E}_S)+{}_{||}\mathbf{p}_N\times(2Z_N\mathbf{E}_N). \quad (5)$$

The mirror plane ensures that $\mathbf{E}_S$ will have no component along the c axis. The change in energy, δW, upon a virtual rotation of the molecule about axis i by an angle $\delta\omega_i$ is given by

$$\delta W=T_1\delta\omega_1+T_2\delta\omega_2+T_3\delta\omega_3 \quad (6)$$

where axes **1**, **2**, **3** are chosen as a coordinate system. Since the ${}_{||}\mathbf{p}_x$ lies along axis **1** and the electric fields are in the **1**, **3** plane, the only component of $\mathbf{T}$ which is not required to be zero by the crystal symmetry is T_2. Thus $\delta W=T_2\delta\omega_2$ so that the equilibrium position for the molecule must be with its mirror plane coinciding with that of the lattice but with its position in the mirror plane determined by the condition $\delta W=0$, which can be satisfied by

$$(\mathbf{E}_S\cdot\mathbf{3})/(\mathbf{E}_N\cdot\mathbf{3})=({}_{||}\mathbf{p}_N\cdot\mathbf{3})/(\mathbf{p}_S\cdot\mathbf{3})=0.90$$

or

$$\mathbf{E}_S\cdot\mathbf{3}=\mathbf{E}_N\cdot\mathbf{3}=0.$$

The field component perpendicular to and acting at each end of the molecule must be zero or in the inverse ratio of the moment arms. The values of the various electric field components have been evaluated for both the room-temperature and low-temperature structures and the results are shown in Table III. The model used is the ionic one proposed above with the contribution of the charges external to the molecule considered. In detail the fields are evaluated along axes a and b and then transformed to components along axes **1** and **3**. This procedure subtracts large numbers when determining the component along **3** and thus the error in this component is expected to be larger than that for the component along axis **1**. Convergence within 5% was obtained before one was 20 A away from the origin. The results indicate that the $\mathbf{E}_x\cdot\mathbf{3}$ components are near zero for the low temperature structure and at 20°C that $[(\mathbf{E}_S\cdot\mathbf{3})/(\mathbf{E}_N\cdot\mathbf{3})]=0.82$ rather than 0.90 as predicted in the foregoing. Although the polarizability effects have been ignored they are not entirely negligible. The polarizability will be a tensor with its major axis coinciding with axes **1** and **2**. Again the field component along **2** must cancel in computing the field at the sulfur and nitrogen sites but the component along axes **1** and **3** will not. It is expected that some of the effect of the polarizability can be artificially accounted for by changing the effective charges on the sulfur and nitrogen, and this portion will tend to cancel in evaluating the electric field ratios.

The low-temperature structure was used in the computation of the fields at low temperatures. These values will be in error because of the fact that the structure is partially disordered. In fact, if the disorder is 10%, there will probably be a disordered molecule as second nearest neighbor to an ordered one at an arbitrary origin. Although the disordered position differs by small motions of the atoms, the error introduced in ignoring the disorder (or not using the correct 0°K structure) prevents one from concluding that the torque is zero

TABLE III. Electric field components.

Room-temperature structure	$\mathbf{E}_x\cdot\mathbf{1}$ 10^{-6} (esu/cm²)	$\mathbf{E}_x\cdot\mathbf{2}$ 10^{-6} (esu/cm²)	$\mathbf{E}_x\cdot\mathbf{3}$ 10^{-6} (esu/cm²)
Nearest neighbors to sulfur atom	−0.231	0	+0.044
Nearest neighbors to nitrogen atom	−0.230	+0.230	+0.067
Neighbors up to 25 A from sulfur at origin	−0.248	0	+0.055
Low-temperature structure[a]			
Nearest neighbors to sulfur atom	−0.251	0	−0.014
Nearest neighbors to nitrogen atom	−0.264	...	+0.014

[a] Calculations performed on the disordered structure.

[19] J. A. Stratton, *Electromagnetic Theory* (McGraw-Hill Book Company, Inc., New York, 1941), p. 116.

TABLE IV. Lattice parameter data.

	120°K	290°K
a	5.494±0.005 A	5.520±0.007 A
b	7.516±0.007	7.655±0.007
c	8.519±0.010	8.537±0.007

because the electric fields are zero. This is not expected to invalidate the conclusion that the torque is near zero. For this reason the calculation was not extended until convergence was obtained.

The third application of the ionic model concerns the direction of least resistance to thermally excited oscillatory motion of the molecule. Kuncher and Truter[4] have resolved the molecular motion, as determined by the thermal adjustment of the atomic scattering of the atoms for x-rays, into average root mean square oscillations about axis **1** of 12.5°, axis **2** of 0°, and axis **3** of 5.0°. This result is surprising in the light of the agreement obtained above using **2** as the rotation axis defining the dielectric transformations. In addition these x-ray results are suspect for the following reasons. Motions about axis **3** should be reflected in an expansion of the c axis, but as is shown in Table IV the length of the c axis is virtually the same at 120°K and at room temperature. Secondly the cleavage direction is perpendicular to the b axis and the implied weak bonding across planes perpendicular to the b axis would indicate weak restoring forces to motion about axis **2**. Lastly, motion about both axes **1** and **3** violates the ground-state lattice symmetry of the crystal and therefore one would expect that motion about these axes would be difficult to excite if strong forces are involved between the molecules in the crystal. These "crystal symmetry" forces seem to require hydrogen atoms to occupy positions demanded by the heavy atom symmetry[20] except where strong hydrogen bonds are involved.

A computation of the torque on the molecule for real displacements about each axis was made using the ionic model and the formulas derived in Appendix I. The results are shown in Table V and indicate that for small displacements ($\sin\theta\approx\theta$, $\cos\theta\approx1$) this model predicts major motion about axis **2** and least motion about axis **3**.

LATTICE PARAMETERS AS A FUNCTION OF TEMPERATURE

If the transition at 169°K is of first order at least one of the lattice parameters should be discontinuous across the transition. The a and b lattice parameters are expected to contract while the c lattice parameter is expected to be continuous through 169°K because as the disordering occurs the effective average angle between a pair of molecules in sublattice 1 will decrease thus shortening the b axis and increase in sublattice 2 thus shortening the a axis. This effect will be superposed on the ordinary lattice expansion with temperature and thus will only be seen at the first-order transition which represents a discontinuity in the disordering of the molecules and across which effectively no thermal expansion occurs. Finally there exists no structural basis for expecting an anomaly in the c axis.

TABLE V. Torque components.

$$\mathbf{T}\cdot\mathbf{1}=2Z_NZ_SC_1\Delta p[0.093\sin\theta+0.012(1-\cos\theta)]$$
$$\mathbf{T}\cdot\mathbf{2}=2Z_NZ_SC_0\Delta p[-0.060\sin\theta+0.008(1-\cos\theta)]$$
$$\mathbf{T}\cdot\mathbf{3}=2Z_NZ_SC_0\Delta p[0.123\sin\theta]$$

where θ is the angle through which the molecule is displaced.

[20] M. Atoji and R. E. Rundle, J. Chem. Phys. **29**, 1306 (1958).

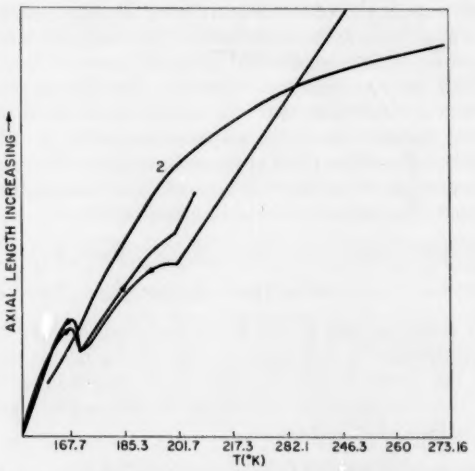

FIG. 4. Lattice parameters vs temperature. Curve 1 indicates changes in the length of the c axis. Both the cooling and heating traces are shown for curve 1.

Lattice parameter changes along the a and c axes as a function of temperature were determined by measuring the change in resistance of a strain gauge attached to a thiourea crystal. Figure 4 shows some typical raw data resulting from these experiments. The converted data are not shown because the discontinuities are seen more clearly in this plot. The c axis changes uniformly in the temperature range considered whereas the a axis shows the expected contraction at 169°K. This discontinuity corresponds to about a 5×10^{-4} A decrease. In addition, a change in slope is detected at 202°K which coincides with the relative translation of the molecules in the sublattices. No anomalies are found in the region of the 177°K transition. Efforts to measure the b-lattice parameter changes resulted in failure because the crystal cleaved under the strain.[21]

[21] J. G. White (private communication) has attempted to measure the b-axis discontinuity by x-rays. He concluded that if a lattice parameter discontinuity does occur it is negative in sign and about 5×10^{-4} A. The dispersion in the data prevented a more positive conclusion.

STATISTICAL MODEL

The conclusion that the transitions at 169°K and 177°K result from the same general mechanism, that is a rotation and translation between potential minima, indicates that the crystal is in fact disordering at finite temperatures below 179°K. The anisotropic thermal vibrations used in evaluating the x-ray structure at 120°K add substance to this expectation. One therefore seeks a tractable model which will reproduce the general nature of the spontaneous polarization versus temperature curve. This curve has a finite monotonically decreasing value at temperatures below 169°K and decreases abruptly at this temperature. Between 170.5°K and 174°K the crystal shows no polarization. Around 176°K the crystal is polar again with a spontaneous polarization of the order of 10^{-3} the value in the first

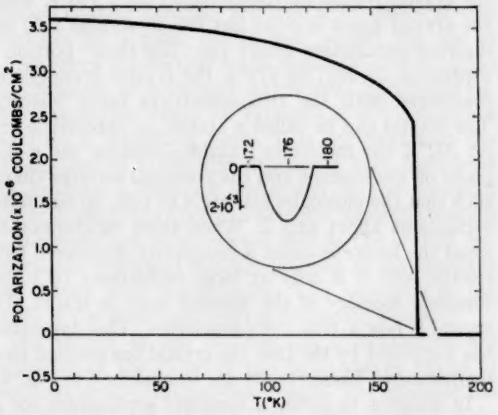

FIG. 5. Experimental spontaneous polarization vs temperature. This figure is a composite of the data of Goldsmith and White.

ferrielectric region but with the polar axis reversed. This polar axis reversal is indicated by the measurements of the pyroelectric coefficient as a function of temperature (see Fig. 11 of reference 2). Figure 5 summarizes this polarization data.

In the case of thiourea the source of the dipole moment is clear and one could contemplate using the force field proposed above to study the disordering of the molecules. That is, the partition function based upon the ionic model is to be evaluated for those states whose torque is zero. This model is difficult to treat and therefore a simpler model will be analyzed. The molecules centered at planes at $z=\frac{1}{4}$ and those planes related by a unit cell translation will be considered as constituting one sublattice while the molecules whose centers of mass are located in planes at $z=\frac{3}{4}$ and those planes related by a unit cell translation will constitute the second sublattice. The pair of molecules in a given unit cell in the same sublattice will be added vectorially to yield a point dipole along the b axis.

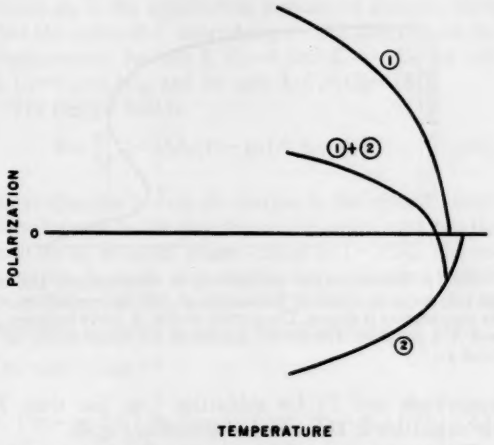

FIG. 6. Polarization vs temperature for special model. Curve 1 is the disorder of sublattice 1 and curve 2 is disorder of sublattice 2 while curve 1+2 represents their sum.

Each sublattice can be treated separately in the manner of Devonshire[22] and the results subtracted if one assumes no interaction between sublattices. Devonshire showed that a system of dipoles restricted so as to be aligned either along or against a given vector will disorder as

$$(P/P_0)=\tanh(P/P_0)(T_0/T) \qquad (7)$$

where P is the spontaneous polarization at temperature T and P_0 is that at 0°K while T_0 is the Curie or maximum-disorder temperature. Such a disordering can lead to two oppositely directed regions of polarization if P_0 for sublattice 1 exceeds P_0 for sublattice 2 in

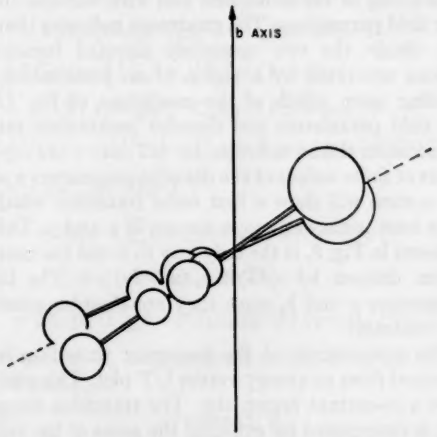

FIG. 7. A comparison of the ordered and disordered orientational position of a thiourea molecule. The full circles is the ordered molecule while the open circles represent the disordered molecule translated so that the center of masses coincide.

[22] A. F. Devonshire, *Advances in Physics* (Taylor and Francis, Ltd., London, 1954), Vol. 3, p. 85.

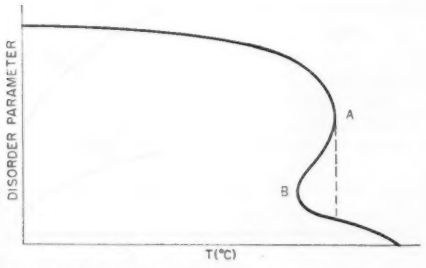

FIG. 8 Disorder-order parameters vs temperature. The expected curve of disorder parameter at $(\partial F/\partial x)=(\partial F/\partial y)=0$ vs temperature is shown. The portion of the A curve between A and B is unstable. The dotted line shows the discontinuity in x (and y).

magnitude and T_0 for sublattice 1 is less than T_0 for sublattice 2. This case is depicted in Fig. 6.

This treatment in addition to ignoring the interaction between sublattices suffers from two other defects *ab initio*. One is that in thiourea the dipoles in each sublattice cannot reverse themselves, but that the disorder of one sublattice proceeds by the molecules rotating so as to change the magnitude of the effective dipole. In one sublattice the effective dipole increases and in the other it decreases. In fact, at 0°K a dipole changes its magnitude upon disordering so as to assume a magnitude identical with that of an ordered dipole of the other sublattice but oppositely directed. The rotational component of the ordered and disordered position of one molecule is seen in Fig. 7. The second defect of the model lies in the fact that the sublattices when completely disordered are identical in appearance.

In Appendix II a long range interaction model is treated with interacting sublattices and the above cited disordering of the molecules, and with variable molecular field parameters. The treatment indicates that one can obtain the two oppositely directed ferrielectric regions separated by a region of no polarization, depending upon which of the conditions of Eq. (A20) the field parameters and disorder parameters satisfy. In addition if the solution to $(dT/dx)=(dT/dy)=0$ exists at finite values of the disorder parameters x and y the system will show a first order transition which results from a discontinuous change in x and y. This, as is shown in Fig. 8, is the only way to avoid the unstable region defined by $(dT/dx), (dT/dy)>0$. The lattice parameters a and b, since they are disorder sensitive, will contract.

The temperature of the first-order transition is determined from an energy versus $1/T$ plot. This plot will show a re-entrant region also. The transition temperature is determined by equating the areas of the regions between the curve U versus $1/T$ and $1/T=$constant. In Fig. 8 the transition is indicated schematically.

DISCUSSION

The results of the experiments on thiourea and their interpretation indicate that the dielectric anomalies result from the relative motion of the molecules and are not due to any change in the substantially planar molecule. The following molecular history on a temperature scale is consistent with the experimental results. At 0°K the crystal consists of two perfectly ordered nonidentical sublattices which give rise to a ferrielectric state whose axis can be reversed by the rotation of all the molecules by angles of the order of 10° about axes parallel to the c axis. As the temperature is increased the molecules in each sublattice disorder. At 169°K a first-order transition occurs and the disorder parameters change discontinuously. The spontaneous polarization also drops abruptly at this point but does not reach zero until 170.5°K is reached. In other words, the crystal remains a ferrielectric between 169 and 170.5°K. Beyond this region the crystal is a partially disordered compensated ferrielectric. The disorder continues with the crystal remaining compensated until 176°K where the crystal again is polar but the crystalline field and disorder parameters satisfy the "less than" portion of expression (A 20). At 179°K the crystal is completely disordered with the two sublattices being identical. The crystal can be called a statistical antiferrielectric. At 202°K the molecules translate creating the n-glide plane on the average and the potential surfaces change such that the molecules can begin to take up significant oscillations about axis **2**. When these oscillations are small the lattice is called a completely disordered ferrielectric and it is only at large oscillations (6°) that complete memory of the disorder state is erased. The crystal is now a true antiferroelectric. This apparently has happened by the time the crystal has reached room temperature. These results are summarized in Fig. 9.

In addition to giving a complete explanation for all the phenomena below 180°K on the basis of one model strongly based upon the crystallography of thiourea, the proposed molecular history has some experimental evidence in its support beyond that cited above. First, the experimental spontaneous polarization does not

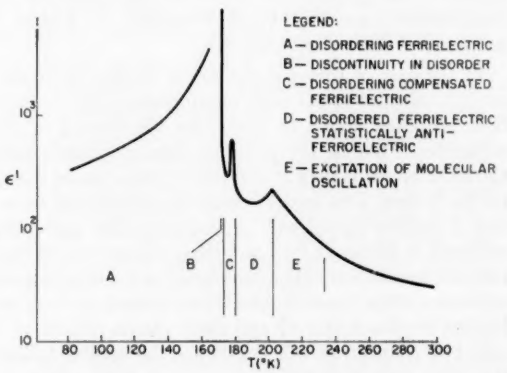

FIG. 9. Summary of the molecular configuration superposed upon the dielectric constants vs temperature curve. The curve is taken from the results of Goldsmith and White.

fall abruptly at 169°K but has a finite slope and becomes zero only after 170.5°K is reached. Thus one must assume that the experiment could not trace accurately the discontinuity at 169°K and the ferrielectric region above it but has averaged the two parts. Second, the pyroelectric coefficient has a finite value beyond 169°K. Third, the dielectric loss (see Fig. 6 of footnote 3) changes discontinuously at the second-order transition (about 177°K) and not at the first-order transition. This supports the fact that the crystal has essentially the same form across the first-order transition as proposed. Lastly, the appearance of a peak in the dielectric constant vs temperature at 170.5°K can be explained within the model proposed.

The question of whether the field parameters can be chosen to satisfy all the conditions imposed by the experimental polarization curve has not been answered. If such parameters were found one would suspect their physical content because, first, the replacement of two molecules by a point dipole and, second, the use of a long-range interaction force certainly oversimplifies the character of molecular interaction. The broad dipolar absorption found by Freyman *et al.*[3] indicates a spectrum of relaxation times. It is not clear that the introduction of a disorder dependent field parameter will produce a sufficient variability in the potential barrier to duplicate Freyman's results. Since the torques on the molecules must remain zero as the crystal disorders, the order and disorder position of the molecule will change with temperature. This probably is the source of the broad spectrum of relaxation times.

The results of the electrostatic computations are suggestive of the value of this point-charge model in obtaining order-of-magnitude results. For example the small field of about 10^3 volts/cm is certainly of the right order of magnitude. The general usefulness of such an approach must await its application to further systems.

ACKNOWLEDGMENTS

The author wishes to acknowledge the aid given by Maxwell M. Hopkins in the experimental portions of this work and Dr. Peter J. Wojtowicz for many helpful discussions.

APPENDIX I

The general expression for the torque on the molecule is

$$\mathbf{T}=Z_S(\mathbf{p}_S\times\mathbf{E}_S)+Z_{N_1}(\mathbf{p}_{N_1}\times\mathbf{E}_{N_1})+Z_{N_2}(\mathbf{p}_{N_2}\times\mathbf{E}_{N_2}), \tag{A1}$$

where the terms in this expression have been defined above. The position of the rigidly displaced molecule is defined in terms of the positions of the sulfur and nitrogen atoms referred to the undisplaced atoms by the expressions

$$\begin{aligned}\mathbf{p}_S&={}_0\mathbf{p}_S+C_0\Delta\mathbf{p}\\ \mathbf{p}_{N_1}&={}_0\mathbf{p}_{N_1}-C_1\Delta\mathbf{p}\\ \mathbf{p}_{N_2}&={}_0\mathbf{p}_{N_2}-C_2\Delta\mathbf{p}\end{aligned} \tag{A2}$$

where ${}_0\mathbf{p}_x$ is the equilibrium position of atom x. Note that the value of C depends upon the direction of the displacement: for axis **1**, $C_0=0$ and $C_1=-C_2$; for axis **2**, $C_1=C_2=1.1C_0$; and for axis **3**, $C_1=C_2=0.8C_0$.

The electric field is

$$\mathbf{E}=\sum_\lambda{}'(-)^\lambda Z_\lambda(\mathbf{r}_\lambda-\mathbf{p}_x)/|\,\mathbf{r}_\lambda-\mathbf{p}_x\,|^3, \tag{A3}$$

where the sum is over all charges in the crystal except those located on the molecule at the origin, and $\mathbf{r}_\lambda$ is the position of an atom whose charge is $(-)^\lambda Z_\lambda$. The assumption is made that neighboring molecules remain fixed during the displacement. The denominator can be expressed in terms of Legendre polynomials by using

$$\begin{aligned}&|\,\mathbf{r}_\lambda-{}_0\mathbf{p}_x-C\Delta\mathbf{p}\,|^{-3}\\ &=|\,\mathbf{r}_\lambda-{}_0\mathbf{p}_x\,|^{-3}\sum_{n=1}^{\infty}\mathbf{p}_n'(\cos\theta)|\,C\Delta\mathbf{p}/(\mathbf{r}_\lambda-{}_0\mathbf{p}_x)\,|^{n-1}\end{aligned} \tag{A4}$$

where P_n' is the derivative of nth Legendre polynomial with respect to $\cos\theta$ where θ is the angle between $\mathbf{r}_\lambda-{}_0\mathbf{p}_x$ and $\Delta\mathbf{p}$. For small displacements, by inserting the conditions of equilibrium, and by using the existence of the mirror plane, one obtains the torque about each axis to linear terms in Δp to be

$$\begin{aligned}\mathbf{T}\cdot\mathbf{1}=&2Z_NC_1\Delta\mathbf{p}\cdot\mathbf{3}\mathbf{E}_N\cdot\mathbf{2}\\ &+2Z_NC_1\sum(-)^\lambda Z_\lambda\mathbf{p}_N\cdot\mathbf{2}\Delta\mathbf{p}\cdot\mathbf{3}\,|\,\mathbf{r}_\lambda-{}_0\mathbf{p}_N\,|^{-3}\\ &-2Z_N\sum(-)^\lambda Z_\lambda\mathbf{p}_N\cdot\mathbf{2}\,|\,\mathbf{r}_\lambda-{}_0\mathbf{p}_N\,|^{-4}C_1\Delta p\\ &\times\cos\theta(\mathbf{r}_\lambda-{}_0\mathbf{p}_N)\cdot\mathbf{3}\end{aligned} \tag{A5}$$

$$\begin{aligned}\mathbf{T}\cdot\mathbf{2}=&Z_S[-C_0\Delta\mathbf{p}\cdot\mathbf{1}\mathbf{E}_s\cdot\mathbf{3}+C_0\Delta\mathbf{p}\cdot\mathbf{3}\mathbf{E}_s\cdot\mathbf{1}]\\ &+Z_S\,{}_0\mathbf{p}_S\cdot\mathbf{1}\{-\sum(-)^\lambda Z_\lambda(\mathbf{r}_\lambda-{}_0\mathbf{p}_S)\cdot\mathbf{3}(\mathbf{r}_\lambda-{}_0\mathbf{p}_s)^{-4}C\Delta p\\ &\times\cos\theta-C_0\Delta\mathbf{p}\cdot\mathbf{3}(\mathbf{r}_\lambda-{}_0\mathbf{p}_S)^{-3}\\ &+2Z_N[C_1\Delta\mathbf{p}\cdot\mathbf{1}\mathbf{E}_N\cdot\mathbf{3}-C_1\Delta\mathbf{p}_S\cdot\mathbf{3}\mathbf{E}_N\cdot\mathbf{1}]\\ &+2Z_N\,{}_0\mathbf{p}_N\cdot\mathbf{1}\{\sum(-)^\lambda Z_\lambda[-(\mathbf{r}_\lambda-{}_0\mathbf{p}_N)\\ &\cdot\mathbf{3}\,|\,\mathbf{r}_\lambda-{}_0\mathbf{p}_N\,|^{-4}C_1\Delta\mathbf{p}\cdot\mathbf{3}\,|\,\mathbf{r}_\lambda-\mathbf{p}_{N0}\,|^{-3}\\ &-C_1\Delta\mathbf{p}\cdot\mathbf{3}\,|\,\mathbf{r}_\lambda-\mathbf{p}_{N0}\,|^{-3}]\}\end{aligned} \tag{A6}$$

$$\begin{aligned}\mathbf{T}\cdot\mathbf{3}=&-Z_SC_0\Delta\mathbf{p}\cdot\mathbf{2}\mathbf{E}_S\cdot\mathbf{1}\\ &+Z_S\mathbf{p}_S\cdot\mathbf{1}\sum(-)^\lambda Z_\lambda C_0\Delta\mathbf{p}\cdot\mathbf{2}\,|\,\mathbf{r}_\lambda-{}_0\mathbf{p}_S\,|^{-3}\\ &+2Z_NC_1\Delta\mathbf{p}\cdot\mathbf{2}\mathbf{E}_N\cdot\mathbf{1}\\ &-2Z_N\mathbf{p}_N\cdot\mathbf{1}\sum(-)^\lambda Z_\lambda C_1\Delta\mathbf{p}\cdot\mathbf{2}\,|\,\mathbf{r}_\lambda-{}_0\mathbf{p}_N\,|^{-3}.\end{aligned} \tag{A7}$$

The value of $\mathbf{E}_x$ is determined at site x for the undisplaced molecule.

APPENDIX II

In this section we will derive the conditions to be imposed upon the value of the molecular field parameters in order to reproduce the general features of the spontaneous polarization vs temperature curve. The model consists of point dipoles formed from a pair of

molecules in a given sublattice within a unit cell. The polarization per unit volume due to the permanent dipoles for each sublattice is given by

$$_{(1)}P_d = N\mu_1 \tfrac{1}{2}(1+x) + N\mu_2 \tfrac{1}{2}(1-x) = N(Ax+B) \quad \text{(A8)}$$

$$_{(2)}P_d = -N\mu_1 \tfrac{1}{2}(1+y) - N\mu_2 \tfrac{1}{2}(1-y) = N(Ay-B), \quad \text{(A9)}$$

where μ_1 and $-\mu_2$ are the values of the dipole moment per pair of molecules in each sublattice at 0°K and μ_2 and $-\mu_1$ are the values of the dipole moment of the respective disordered configurations. N is the number of dipoles per unit volume per sublattice and x and y are the disorder variables which are limited to lie between -1 and $+1$. Subscripts (1) and (2) refer to sublattice 1 and 2, respectively. The constants A and B are half the sum and difference of the dipole moments μ_1 and μ_2. The energy density of the system can be given in terms of the energy of interaction of the permanent dipoles, the energy of interaction of the permanent dipoles with the induced dipoles whose polarization per unit volume is given by $_{(1)}P_e$ and $_{(2)}P_e$, and the energy of interaction of these induced dipoles less the energy expended in their creation. The molecular field parameters of the two sublattices is chosen to be different in the ordered state and allowed to approach the same value as the disorder proceeds. Also the form of the equations must be such that the polarization can be reversed at constant free energy if the sign of both x and y is reversed. In the manner of Devonshire[22] the energy of the system is

$$\begin{aligned} U = &-\tfrac{1}{2}(a+\alpha x)\,{}_{(1)}P_d^2 - \tfrac{1}{2}(a-\alpha y)\,{}_{(2)}P_d^2 \\ &-(b+\beta x)\,{}_{(1)}P_{d(1)}P_e - (b-\beta y)\,{}_{(2)}P_{d(2)}P_e \\ &+\tfrac{1}{2}(C+\gamma x)\,{}_{(1)}P_e^2 + \tfrac{1}{2}(C-\gamma y)\,{}_{(2)}P_e^2 \\ &-{}_{(1,2)}\gamma_{dd(1)}P_{d(2)}P_d - {}_{(1,2)}\gamma_{de(1)}P_{d(2)}P_e \\ &-{}_{(1,2)}\gamma_{de(2)}P_{d(1)}P_e \end{aligned} \quad \text{(A10)}$$

where

$$\begin{aligned} 2a &= {}_{(1)}\gamma_{dd} + {}_{(2)}\gamma_{dd} & 2\alpha &= {}_{(1)}\gamma_{dd} - {}_{(2)}\gamma_{dd} \\ 2b &= {}_{(1)}\gamma_{de} + {}_{(2)}\gamma_{de} & 2\beta &= {}_{(1)}\gamma_{de} - {}_{(2)}\gamma_{de} \\ 2c &= {}_{(1)}\gamma_{ee} + {}_{(2)}\gamma_{ee} & 2\gamma &= {}_{(1)}\gamma_{ee} - {}_{(2)}\gamma_{ee}. \end{aligned}$$

The entropy per unit volume is given by

$$S = \tfrac{1}{2}kN[-(1+x)\ln(1+x) - (1-x)\ln(1-x) - (1+y)\ln(1+y) - (1-y)\ln(1-y) + 2\ln 2]. \quad \text{(A11)}$$

We want to find the temperature variation of the total polarization, $P = {}_{(1)}P_e + {}_{(1)}P_d + {}_{(2)}P_e + {}_{(2)}P_d$, at zero imposed field. The electric field E can be determined from the Helmholtz free energy, F, by $E = (\partial F/\partial P)$ and the extrema in free energy by $(\partial F/\partial x)\,|_y = (\partial F/\partial y)|_x = 0$. The spontaneous polarization can then be determined by setting $E=0$. These differentiations lead to

$$\begin{aligned} &{}_{(1)}P_e \\ &= [(b+\beta x)/(c+\gamma x)]\,{}_{(1)}P_d + [{}_{(1,2)}\gamma_{de}/(c+\gamma x)]\,{}_{(2)}P_d \\ &{}_{(2)}P_e = [(b-\beta y)/(c-\gamma y)]\,{}_{(2)}P_d \\ &\qquad + [{}_{(1,2)}\gamma_{de}/(c-\gamma y)]\,{}_{(1)}P_d \end{aligned} \quad \text{(A12)}$$

and

$$\begin{aligned} x = \tanh(kT)^{-1}\Bigg\{ &{}_{(1)}P_d\left[A\left(a+\alpha x + \frac{(b+\beta x)^2}{c+\gamma x} - \frac{(1,2)\gamma^2_{de}}{c-\gamma y}\right)\right] \\ &+ {}_{(2)}P_d\left[A\left({}_{(1,2)}\gamma_{dd} - {}_{(1,2)}\gamma_{de}\left(\frac{b-\beta y}{c-\gamma y} - \frac{b+\beta x}{c+\gamma x}\right)\right)\right] \\ &+ {}_{(1)}P_{d(2)}P_d\left[\frac{\beta_{(1,2)}\gamma_{de}}{c+\gamma x} - \gamma\frac{b+\beta x}{(c+\gamma x)^2}\,{}_{(1,2)}\gamma_{de}\right]N^{-1} \\ &+ {}_{(1)}P_d^2\left[\tfrac{1}{2}\alpha + \beta\frac{b+\beta x}{c+\gamma x} - \tfrac{1}{2}\gamma\left(\frac{b+\beta x}{c+\gamma x}\right)^2\right]N^{-1} \\ &+ {}_{(2)}P_d^2\tfrac{1}{2}\gamma\frac{(1,2)\gamma^2_{de}}{(c+\gamma x)^2}N^{-1}\Bigg\} \end{aligned} \quad \text{(A13)}$$

$$\begin{aligned} y = \tanh(kT)^{-1}\Bigg\{ &{}_{(2)}P_d\left[A\left(a-\alpha y + \frac{(b-\beta y)^2}{c-\gamma y} - \frac{(1,2)\gamma_{de}}{c+\gamma x}\right)\right] \\ &+ {}_{(1)}P_d\left[A\left({}_{(1,2)}\gamma_{dd} - {}_{(1,2)}\gamma_{de}\left(\frac{b+\beta x}{c+\gamma x} - \frac{b-\beta y}{c-\gamma y}\right)\right)\right] \\ &- {}_{(1)}P_{d(2)}P_d\left[\frac{\beta_{(1,2)}\gamma_{de}}{c-\gamma y} - \gamma\frac{b-\beta y}{(c-\gamma y)^2}\,{}_{(1,2)}\gamma_{de}\right]N^{-1} \\ &- {}_{(2)}P_d^2\left[\tfrac{1}{2}\alpha + \beta\frac{b-\beta y}{c-\gamma y} - \tfrac{1}{2}\gamma\left(\frac{b-\beta y}{c-\gamma y}\right)^2\right]N^{-1} \\ &+ {}_{(1)}P_d^2\tfrac{1}{2}\gamma\frac{(1,2)\gamma_{de}^2}{(c-\gamma y)^2}N^{-1}\Bigg\} \end{aligned} \quad \text{(A14)}$$

where (A12) is used in (A13) and (A14) in order to obtain expressions in terms of $_{(1)}P_d$ and $_{(2)}P_d$. Let the part contained between { } of (A13) be called $I(x, y)$ and the analogous part of (A14) be called $II(x, y)$. We note that $I(x, y) = -II(-y, -x)$. One now expands $I(x, y)$ and $II(x, y)$ in a Taylor series about $x=y=0$ thus obtaining

$$\begin{aligned} x = \tanh(kT)^{-1}\{ &x(\partial I/\partial x)\,|_{x=y=0} + y(\partial I/\partial y)\,|_{x=y=0} \\ &+ \tfrac{1}{2}x^2(\partial^2 I/\partial x^2)\,|_{x=y=0} + xy(\partial^2 I/\partial x\partial y)\,|_{x=y=0} \\ &+ \tfrac{1}{2}y^2(\partial^2 I/\partial y^2)\,|_{x=y=0} + (x^3/3!)(\partial^3 I/\partial x^3)\,|_{x=y=0} + \cdots\} \end{aligned} \quad \text{(A15)}$$

$$\begin{aligned} y = \tanh(kT)^{-1}\{ &y(\partial II/\partial y)\,|_{x=y=0} + x(\partial II/\partial x)\,|_{x=y=0} \\ &+ \tfrac{1}{2}y^2(\partial^2 II/\partial y^2)\,|_{x=y=0} + xy(\partial^2 II/\partial x\partial y)\,|_{x=y=0} \\ &+ \tfrac{1}{2}x^2(\partial^2 II/\partial x^2)\,|_{x=y=0} + (y^3/3!)(\partial^3 II/\partial y^2) + \cdots\}. \end{aligned} \quad \text{(A16)}$$

The terms $I(0, 0)$ and $II(0, 0)$ are set equal to zero to ensure a solution to Eqs. (A15) and (A16) at $x=y=0$ for finite T. The transition or Curie temperature, that is the temperature where the disorder is complete, is found by expanding the transcendental function and keeping the linear terms only. This leads to the simultaneous equations

$$kT_0x=x(\partial I/\partial x)\,|_{x,y=0}+y(\partial I/\partial y)\,|_{x,y=0}$$

$$kT_0y=y(\partial II/\partial y)\,|_{x,y=0}+x(\partial II/\partial x)\,|_{x,y=0} \quad \text{(A17)}$$

and

$$kT_0=(\partial I/\partial x)\,|_{x,y=0}\pm(\partial I/\partial y)\,|_{x,y=0} \quad \text{(A18)}$$

when the relation $I(x, y)=-II(-y, -x)$ is used. Although two transition temperatures are available both sublattices can be shown by Eq. (A17) to require the same solution of Eq. (A18).

We now derive the expression defining an extended region of zero polarization at a finite degree of order. The total polarization is

$$P=\left(\frac{b+\beta x}{c+\gamma x}+\frac{{}_{(1,2)}\gamma_{de}}{c-\gamma y}+1\right){}_{(1)}P_d+\left(\frac{b-\beta y}{c-\gamma y}+\frac{{}_{(1,2)}\gamma_{de}}{c+\gamma x}+1\right){}_{(2)}P_d. \quad \text{(A19)}$$

Thus P will be positive, zero, or negative depending upon the various equivalence conditions of

$$\left(\frac{b+\beta x}{c+\gamma x}+\frac{{}_{(1,2)}\gamma_{de}}{c-\gamma y}+1\right)(A+xB) \gtreqless \left(\frac{b-\beta y}{c-\gamma v}+\frac{{}_{(1,2)}\gamma_{de}}{c+\gamma x}+1\right)(Ay-B). \quad \text{(A20)}$$

All the features of the experimental P versus T curve except the first-order transition can be reproduced if $>$ of (A20) holds from 0 to 170.5°K and $=$ holds between 170.5°K to 174°K and $<$ holds from 174°K to 180°K.

We now examine the conditions for a first-order transition involving a discontinuous change in the disorder parameters from a finite (x, y) pair to a smaller finite pair of (x, y). The expression (A15) and (A16) can be combined to yield

$$\begin{aligned}(x+y)/(1+xy) &= \tanh(T_0/T)\{[(x+y)/T_0][(\partial I/\partial x)+(\partial I/\partial y)] \\ &+T_0^{-1}(\tfrac{1}{2}x^2-\tfrac{1}{2}y^2)[(\partial^2 I/\partial x^2)-(\partial^2 I/\partial y^2)] \\ &+T_0^{-1}[(x^3/3!)+(y^3/3!)][(\partial^2 I/\partial x^2)+(\partial^3 I/\partial y^3)] \\ &+T_0^{-1}[\tfrac{1}{2}(x^2y)+\tfrac{1}{2}(xy^2)][(\partial^3 I/\partial x\partial y^2)+(\partial^3 I/\partial y\partial x^2)] \\ &+\cdots\}. \quad \text{(A21)}\end{aligned}$$

Note that $x+y$ is a monotonic function in T. The coefficients of the disorder variables do permit one to have the disorder decrease with increasing temperature, that is $(\partial T/\partial x)$, $(\partial T/\partial y)>0$ at finite values of x and y. This leads to a first order transition as $(\partial T/\partial x)$, $(\partial T/\partial y)>0$ is a condition of instability (see Fig. 8).

Simpler models, for example, with the molecular field parameters constant and identical between the two sublattices or constant but dissimilar between the two sublattices can not reproduce the change in the sign of the polarity but in the latter case can yield a first-order transition.

THE JOURNAL OF CHEMICAL PHYSICS VOLUME 33, NUMBER 6 DECEMBER, 1960

On the Absorption Spectrum of CF_2 and Its Vibrational Analysis

D. E. MANN AND B. A. THRUSH*

National Bureau of Standards, Washington, D. C.

(Received March 30, 1960)

The flash photolysis of CF_2Br_2 has been used to obtain the absorption spectrum of the CF_2 radical. The principal features of the spectrum are a progression of the upper state bending frequency, and a number of weak bands which are shown to arise from a vibrationally excited lower state. There is no evidence for transitions involving stretching vibrations. The vibrationless origin of the system ($v_1'=0$, $v_2'=0$, $v_1''=0$, $v_2''=0$) is shown to lie at approximately 37 695 cm^{-1}. The deformation frequencies of the lower and upper states are about 660 and 500 cm^{-1}, respectively.

THE CF_2 radical was first identified and investigated by means of its emission spectrum.[1] Passage of a discharge through fluorocarbon vapors gives rise to a system of many-headed bands between 2400 A and 5000 A. Venkateswarlu[1] made a vibrational analysis of the bands in the range 2400–3250 A and concluded that CF_2 is bent. A few of the bands in this region were also seen in absorption in similar discharges by Laird, Andrews, and Barrow[2] and were assigned to a progression of the upper state bending vibration, v_2', with the suggestion, however, that the vibrational numbering given by Venkateswarlu might be in error. As further observations of the absorption spectrum and a more detailed study of the vibrational assignment seemed desirable the investigation of CF_2 by the method of flash photolysis was undertaken. The preliminary results are reported in this paper.

EXPERIMENTAL

The flash photolysis apparatus is of conventional design, and is similar in its essential features to that described by Norrish and Thrush.[3] The photolysis flash was produced by discharging 40μf at 10 kv through a single quartz tube 50 cm long and filled with argon at a pressure of 7 cm Hg. The background was provided by a small spectroscopic flash lamp operated with 2 μf at 10 kv. The duration of the photoflash was about 50 μsec and that of the spectroscopic flash about 25 μsec. In most of the experiments described here a delay of 18 μsec between the former and latter was used. The quartz absorption cell was 27 mm in diam and 50 cm long. The parent substance used for the production of CF_2 spectra was CF_2Br_2. It was obtained commercially from the Matheson Company, East Rutherford, New Jersey. For some experiments it was diluted 1:24 with helium. The total filling pressures for both the diluted and undiluted samples were generally about 5 mm although on occasion pressures as high as 12.5 cm were tried. Renewed samples were flashed successively from 4 to 16 times in order to penetrate the absorption by the parent molecule. All spectra were recorded on Eastman 103a–0 plates with a Hilger medium quartz spectrograph. An iron arc was used for wavelength calibration.

RESULTS

The regular progression first observed in absorption by Laird *et al.*[2] appeared best in our experiments when one part of parent substance was diluted with 24 parts of He at a total pressure of 5 mm, and the spectra from 16 separate flashes were superimposed on the plate. The bands at 2428, 2458, 2488, 2519, 2550, 2583, 2617, and 2652 A appeared distinctly. Except for the band at 2617 A our measurements and those of Laird *et al.*[2] agree as well as can be expected for the dispersion used with those of Venkateswarlu[1] and Durie.[4] We find in agreement with Laird *et al.*[2] that the band found in absorption at 2617 A does not appear to be the same as that measured in the emission spectra at 2617.9 A by Venkateswarlu[1] and 2618.0 A by Durie.[4] The band at 2652 A, given as doubtful by Laird *et al.*[2] is real though weak. These bands form a progression of the upper state bending vibration with the intervals varying from 505 cm^{-1} to about 490 cm^{-1}. It was suggested by Laird *et al.*[2] that the values of v_2' given by Venkateswarlu[1] might have to be raised by 3 if the 2652 A band is genuine. The results reported here show that the 2652 A band does indeed appear in absorption and probably should be assigned as the vibrationless ($v_1'=0$, $v_2'=0$; $v_1''=0$, $v_2''=0$) transition. The possibility that the (0, 0; 0, 0) transition may occur at still longer wavelengths as a band too weak to be seen in these experiments cannot be rigorously excluded though it seems unlikely.

In addition to the bands which form a progression in v_2' and which were seen previously by Laird *et al.*[2] several new bands were found in the flash photolysis absorption spectra. These appeared best when undiluted CF_2Br_2 at a pressure of about 5 mm Hg was photolysed.

* Permanent address: Department of Physical Chemistry, Cambridge University, Cambridge, England.

[1] P. Venkateswarlu, Phys. Rev. **77**, 676 (1950).

[2] R. K. Laird, E. B. Andrews, and R. F. Barrow, Trans. Faraday Soc. **46**, 803 (1950).

[3] R. G. W. Norrish and B. A. Thrush, Quart. Revs. **10**, 149 (1958).

[4] R. A. Durie, Doctoral dissertation, Imperial College, London (1951).

TABLE I. Absorption and corresponding emission bands of CF_2. (1) Present work; (2) Laird *et al.*; (3) Venkateswarlu; (4) Durie.

Absorption					Emission		
λ_{air}(A) (1)	I^a (1)	λ_{air}(A) (2)	ν_{vac}(cm^{-1}) (1) (2)	v_1', v_2'; v_1'', v_2'' (1)	ν_{vac}(cm^{-1}) (3)	ν_{vac}(cm^{-1}) (4)	v_1', v_2'; v_1'', v_2'' (3) (4)
		2345	42630	0, 10; 0, 0			
		2371	42160	0, 9; 0, 0			
		2399.0	41671	0, 8; 0, 0	41667	41671	0, 5; 0, 0
2420.3	9	2428.1	41169	0, 7; 0, 0	41168	41167	0, 4; 0, 0
2457.6	10	2457.6	40678	0, 6; 0, 0	40677	40677	0, 3; 0, 0
2487.8	8	2487.7	40184	0, 5; 0, 0	40184	40184	0, 2; 0, 0
2518.7	6	2518.7	29691	0, 4; 0, 0	39692	39692	0, 1; 0, 0
2550.5	5	2550.6	39196	0, 3; 0, 0	39195	39198	0, 0; 0, 0
2583.3	4	2583.3	38699	0, 2; 0, 0	38695	38699	0, 3; 0, 3
2617.0	3	2617.	38200	0, 1; 0, 0			
2628.8	2		38035	0, 2; 0, 1	38033	38031	0, 0; 1, 0
2651.5	1		37703	0, 0; 0, 0	37691	37699	0, 2; 1, 2
2663.1	2		37539	0, 1; 0, 1	37535	37538	0, 3; 1, 3
2699.1	1		37038	0, 0; 0, 1	37039	37040	0, 2; 1, 3
2711.2	0		36873	0, 1; 0, 2	36872	36876	0, 0; 2, 0
2748.0	0		36379	0, 0; 0, 2	36365	36376	0, 3; 2, 3

[a] Estimated relative intensity.

The new bands occur at 2628, 2663, 2699, 2711, and 2748 A. All correspond well with the CF_2 bands already measured in emission.

The only plausible assignment for the new absorption bands again involves short progressions in v_2' but with the bending vibration singly or doubly excited in the lower state. These progressions also terminate at transitions having the same upper state as the longest wavelength member of the $v_2''=0$ sequence. The assignment suggested for the bands observed in absorption in these experiments is given in Table I. It should be noted that the wavelength measurements are good only to perhaps 0.5 A because of the limited dispersion available. This uncertainty is usually not much larger than the average discrepancy between Venkateswarlu's and Durie's emission measurements.

DISCUSSION

The most interesting result of the present investigation, apart from the reassignment of the system origin, is the absence of bands which involve either lower or upper state stretching vibrations. Of the 57 bands assigned by Venkateswarlu, 44 involved changes in v_1'' and 2 in v_1'. While the upper state stretching frequency was admittedly based on doubtful evidence the assignment included long progressions in the lower state stretching frequency. Venkateswarlu's analysis led him to the conclusion that the deformation frequencies of CF_2 in the lower and upper states are 666.5 and 494.4 cm^{-1}, respectively, and that the lower state stretching frequency is 1162 cm^{-1}. It may be noted, however, that this is equal to the sum of the two deformation frequencies, and that assignments of the type $(0, \alpha; \beta,\gamma)$ can also be explained as $[0, (\alpha-\beta); 0, (\beta+\gamma)]$ where α, β, and γ represent allowed changes in the appropriate quantum numbers, without affecting the position of the band origin. The absence of bands which involve changes in either of the stretching vibrations in the absorption spectrum suggests that the interpretation given by Venkateswarlu and subscribed to by Durie may not be correct. Instead virtually the entire emission spectrum between 2400 and 3250 A can be explained solely in terms of changes in the two bending vibrations. The stretching frequencies remain undetermined. Application of the arguments given by Metropolis[5] to the shading of the K and J rotational structure of the CF_2 bands has already been shown to lead to the conclusion that the apex angle is substantially larger in the upper than in the lower state, and this would lead to the appearance of long progressions in v_2 both in emission and absorption spectra. The present results and interpretation suggest that contrary to the earlier conclusion the bond distance is virtually the same in the two states. This is not incompatible with the theoretical interpretations of the observed electronic spectrum given by Mulliken in Venkateswarlu's paper and by Walsh.[6] While the absence of a progression in v_1' is understandable if the CF distance r' in the upper state is very nearly equal to the distance r'' in the lower state, one or two of the lowest members of the series might still be expected to appear. Their absence suggests that if our analysis of the spectrum is correct r' must indeed be very close to r''.

The absorption measurements are neither precise nor extensive enough to enable a useful vibrational formula to be made for the bending frequencies even in combination with the emission data in view of the numerous discrepancies between Venkateswarlu's and Durie's measurements, which aggravate difficulties caused by $4v_2'$ being almost exactly $3v_2''$. The present work indicates the origin (0, 0; 0, 0) to be at 37 695 cm^{-1}, and

[5] N. Metropolis, Phys. Rev. **60**, 283 (1941).
[6] A. D. Walsh, J. Chem. Soc. **1953**, 2266.

the deformation frequencies of the lower and upper states to be about 660 and 500 cm^{-1}, respectively. Further observations under higher dispersion should lead to improved constants.

ACKNOWLEDGMENT

We acknowledge gratefully the partial support of this research by the Division of Research, U.S. Atomic Energy Commission.

THE JOURNAL OF CHEMICAL PHYSICS VOLUME 33, NUMBER 6 DECEMBER, 1960

Spectrum of Yb^{3+} in Yttrium Gallium Garnet

R. PAPPALARDO AND D. L. WOOD

Bell Telephone Laboratories, Inc., Murray Hill, New Jersey

(Received June 8, 1960)

The optical absorption at various temperatures of an ytterbium-doped yttrium gallium garnet is reported. The effect of a cubic and rhombic crystal field on the splitting of the free-ion levels is calculated. A tentative interpretation of the fine details of the spectrum is given.

INTRODUCTION

CRYSTALS of the garnet structure show a wide variety of magnetic properties and optical absorption spectra. Not only are there many different compositions for the crystal itself, but also many substitutions of foreign ions can be made to further modify the properties of the host lattice.[1-5] This paper reports on the optical absorption of one foreign ion, Yb^{3+}, in a transparent garnet, $Y_3Ga_2(GaO_4)_3$.

There are three different kinds of site in the garnet structure[2-5] classified according to the geometry of coordination of the oxygen atoms around the metal ion. Specifically, there are 4-, 6-, and 8-coordinated sites. Extensive crystallographic studies[2-5] of various garnets have shown that the rare earth impurities will be found always in the 8-coordinated site, replacing Y^{3+}.

The bond lengths for the 8-coordinated sites are long[2-5] and suggest electrostatic rather than covalent bonding, and the analysis of the spectrum of Yb^{3+} will be made on the basis of an electrostatic model of various symmetries for the crystalline field around the rare-earth ion. The free ion Yb^{3+} has the electronic configuration $(Xe)4d^{10}4f^{13}5s^25p^6$, with one electron missing from the complete f shell. If we consider only the levels within the incomplete f shell, there will be just one term possible, ^2F, due to the single hole in the $4f$ shell of the ion. The multiplet components possible will be $^2F_{5/2}$ and $^2F_{7/2}$, their transformation properties being rigorously characterized by $J=\frac{5}{2}$ and $J=\frac{7}{2}$, respectively. Of the two components, $^2F_{7/2}$ will be lower in energy according to Hund's rule. Thus, the free-ion absorption spectrum in theory should be a single line corresponding to the transition $^2F_{7/2}\rightarrow{}^2F_{5/2}$, provided such transitions were possible.

The effect of the crystalline field will be to resolve in part the J degeneracy of the free-ion levels. The number of sublevels arising from $^2F_{7/2}$ (and $^2F_{5/2}$) will depend on the symmetry of the crystalline field,[6] and their separation in energy will depend on the strength of the field.

EXPERIMENTALLY OBSERVED SPECTRUM

The spectra observed at various temperatures for a crystal of yttrium gallium garnet containing 13% Yb_2O_3 by weight (the Yb/Y ratio is 0.24) are shown in Figs. 1, 2, and 3 for the infrared region, where lines appear. The rest of the spectrum is essentially devoid of absorptions except in the uv below 3000 A and in the infrared about 4μ.

The crystal, some 10 mm in diam and 0.28 mm thick, was grown from a flux[1] by J. W. Nielsen of these Laboratories. The spectra were recorded with a Cary model 14 double-beam spectrophotometer under conditions for which the actual resolving power was of the order of 3000.

The cryostat used was constructed of Pyrex glass and the samples were immersed in the coolant. The optical noise caused by bubbling of the nitrogen in the 78°K runs was eliminated by bubbling helium gas through the liquid. A very small flow completely eliminates spontaneous nucleation of bubbles. The bubbling in liquid helium is less objectionable, but can, of course, be eliminated by pumping until the λ point is reached.

[1] J. W. Nielsen and E. F. Dearborn, J. Phys. Chem. Solids **5**, 202 (1958).
[2] G. Menzer, Z. Krist. **69**, 300 (1928).
[3] S. Geller and M. A. Gilleo, J. Phys. Chem. Solids **3**, 30 (1957); M. A. Gilleo and S. Geller, Phys. Rev. **110**, 73 (1958); S. C. Abrahams and S. Geller, Acta Cryst. **11**, 437 (1958).
[4] E. Prince, Acta Cryst. **10**, 787 (1957).
[5] F. Bertaut, F. Forrat, A. Herpin, and P. Meriel, Compt. rend. **224**, 96 (1957).
[6] H. Bethe, Ann. Physik **3**, 133 (1929).

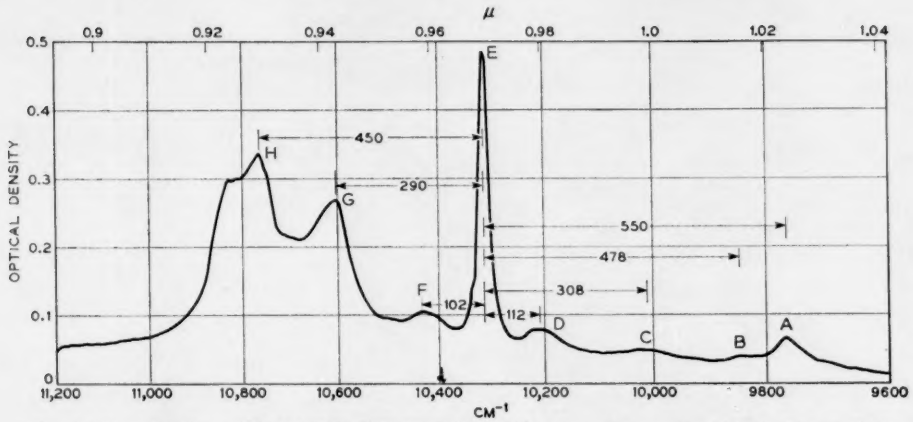

FIG. 1. Absorption lines of YGG+Yb^{3+} (13% Yb_2O_3 in weight) at room temperature. Sample 0.28 mm thick.

At room temperature the spectrum consists of a sharp strong line E at 10 314 cm^{-1} and a series of bands of greater width at both higher and lower frequencies (Fig. 1). The frequencies, line widths, extinction coefficients (for the crystal), and the oscillator strengths are listed for this spectrum in Table I.

At liquid nitrogen temperature, the bands lying lower in frequency than the 10 314 cm^{-1} line are missing, and each of the remaining lines shows some sharpening (Fig. 2). The data for this spectrum are listed in Table II.

The spectrum at 4.2°K shows considerably more detail than those at higher temperatures, and the half-width of the line at 10 314 cm^{-1} is reduced to about 5 cm^{-1} when observed with a spectral slit width of ~2 cm^{-1}. The low-frequency bands are again missing (Fig. 3). The details of this spectrum are listed in Table III.

INTERPRETATION OF THE SPECTRUM

This group of lines, which is observed between 9500 cm^{-1} and 11 000 cm^{-1}, is found in other systems containing the Yb^{3+} ion. A broad absorption has been reported by Hoogschagen[7] for Yb^{3+} aqueous solutions with a main peak at 10 250 cm^{-1} and a smaller one at 10 600 cm^{-1}. Lines have been found at ~10 300 cm^{-1} by Gobrecht[8] in $Yb_2(SO_4)_3 \cdot 8H_2O$ and in the same region by Dieke and Crosswhite[9] in $YbCl_3 \cdot 6H_2O$.

Kasha and Crosby[10] found a single emission line in Yb tris-dibenzoylmethane. Finally, Wickersheim and

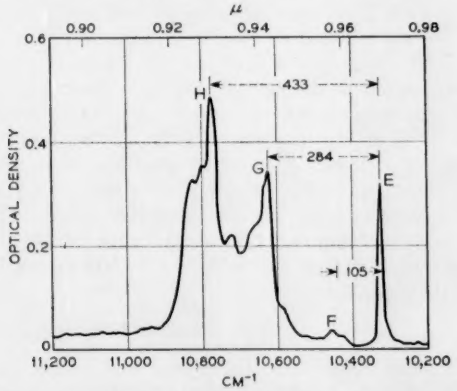

FIG. 2. Absorption lines of YGG+Yb^{3+} at 78°K. Sample 0.28 mm thick.

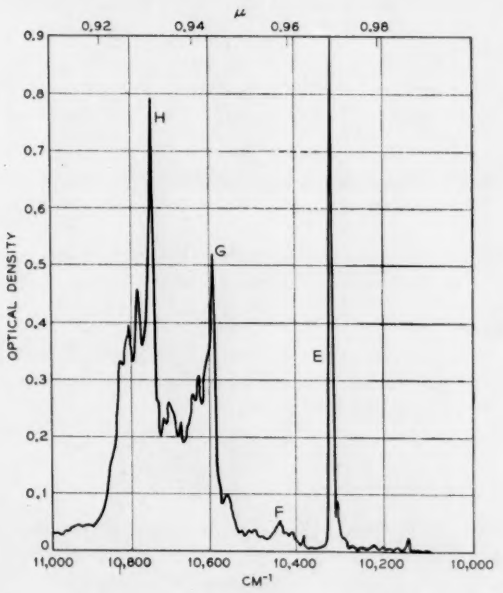

FIG. 3. Absorption lines of YGG+Yb^{3+} at 4.2°K. Sample 0.28 mm thick.

[7] J. Hoogschagen, Physica **11**, 513 (1946).
[8] H. Gobrecht, Z. ges. Naturwiss. **9**, 351 (1937).
[9] G. H. Dieke and H. M. Crosswhite, J. Opt. Soc. Am. **46**, 885 (1956).
[10] G. A. Crosby and M. Kasha, Spectrochim. Acta **10**, 337 (1958).

TABLE I. YGG+Yb^{3+} at room temperature.

Absorpt. peaks	λ (in A)	$\bar{\nu}$ (in cm^{-1})	α_{max} (cm^{-1})	Half-width at $\alpha=\frac{1}{2}\alpha_{max}$ (cm^{-1})	Oscillator strength
A	10 240	9 765	1.8	60	$1.77\ 10^{-7}$
B[a]	10 160	9 842	1.1		
C	9 988	10 012	1.1		
D	9 796	10 208	2.14		
E	9 695	10 314	16.8	25	$6.86\ 10^{-7}$
F[b]	9 595	10 422	2.86		
G	9 430	10 605	9.0	100	$1.47\ 10^{-6}$
H	9 290 9 236	10 764 10 827	10.7 9.65	150	$2.62\ 10^{-6}$

[a] Shoulder.
[b] Doublet structure.

TABLE II. YGG+Yb^{3+} at 78°K.

Absorpt. peaks	λ (in A)	$\bar{\nu}$ (in cm^{-1})	α_{max} (cm^{-1})	Half-width at $\alpha=\frac{1}{2}\alpha_{max}$ (cm^{-1})	Oscillator strength
	9 770[a]	10 235	0.7		
E	9 690	10 320	11.6	14	$2.66\ 10^{-7}$
	9 608	10 408	0.8		
F	9 575	10 443	1.25	60	$9.8\ 10^{-6}$
	9 515	10 510	0.7		
	9 468	10 562			
G	9 430	10 604	12.1	30	$5.9\ 10^{-7}$
	9 405	10 632	8.6		
	9 343	10 703	7.5		
H	9 300	10 753	19.7		
	9 278	10 778	12.5	95	$2.0\ 10^{-6}$
	9 250	10 811	11.8		

[a] Flat.

White[11] have recently reported lines at 10 330 cm^{-1} in ytterbium aluminum garnet and a group of lines between 10 260 cm^{-1} and 10 330 cm^{-1} in ytterbium iron garnet.

The splitting of the ^2F term in Yb^{3+} due to spin-orbit coupling can be obtained using Sommerfeld's formula for the total multiplet separation:[12]

$$\Delta n=\frac{R\alpha_F^2(2L+1)(Z-\sigma)^4}{\nu^3 l(l+1)(2l+1)}, \qquad (1)$$

where R is Rydberg's constant, α_F the fine structure constant, n, l the quantum number of the electrons, and $(Z-\sigma)$ the effective nuclear charge. Gobrecht[8] noted that the observed $\Delta\nu$ in $Yb_2(SO_4)_3\cdot 8H_2O$ would imply $\sigma=35.9$ which is in good agreement with the trend of σ in the rare-earth ions sequence. There can be little doubt that the lines observed arise from the $^2F_{7/2}\rightarrow{}^2F_{5/2}$ transition. The origin of many individual lines in the group, however, needs clarification.

The low-frequency bands in the group, which lie at 9765 cm^{-1}, 9842 cm^{-1}, and 10 012 cm^{-1}, disappear at 78°K and therefore arise from excited levels of the ground state. The rest of the lines, because their spacing is large compared with kT at 78°K, do not arise from excited levels of the ground state and must therefore be due to transitions from the lowest level of the ground state $^2F_{7/2}$ to the $^2F_{5/2}$ states. If this is the case, the maximum number of expected lines should be *three* for crystalline fields of noncubic symmetry, while many more lines are actually observed. Much of the discussion to follow will be concerned with the question of the origin of these additional lines both in the excited and the ground state.

EFFECT OF THE CRYSTAL FIELD

Consider the effect of the crystal field on the rare-earth ion. The 8-coordinated site in yttrium gallium garnet, in which the Yb^{3+} ions are located, is expected

[11] K. A. Wickersheim and R. L. White, Phys. Rev. Letters **4**, 123 (1960).
[12] Quoted by H. Gobrecht in footnote 8.

TABLE III. YGG+Yb^{3+} at 4.2°K.

Absorpt. peaks	λ (in A)	$\bar{\nu}$ (in cm^{-1})	α_{max} (cm^{-1})	Half-width at $\alpha=\frac{1}{2}\alpha_{max}$ (cm^{-1})	Oscillator strength
E	9 704	10 305	3.2	4	$2.2\ 10^{-8}$
	9 693	10 316	40	5	$3.3\ 10^{-7}$
F	9 607	10 409	0.7		
	9 577	10 441	1.43		
	9 515	10 509	1		
	9 497	10 529			
	9 467	10 563	3.2		
	9 448	10 584			
G	9 437	10 597	18.6	15	$4.5\ 10^{-7}$
	9 425	10 610	11.4		
	9 408	10 629	10		
	9 395	10 644			
	9 386	10 654			
	9 380	10 661			
	9 370	10 672	7.1	125	$5.7\ 10^{-7}$
	9 352	10 693	8.2		
	9 344	10 702			
	9 333	10 714	7.5		
	9 320	10 729			
H	9 307	10 744	27	18	$8\ 10^{-7}$
	9 279	10 777	15.5		
	9 259	10 800	13.4	76	$7.5\ 10^{-7}$
	9 240	10 822			
	9 225	10 840			

by analogy with the other garnets to have low symmetry. Although the rare-earth ion is in a nearly cubic field due to the oxygen ligands located at the vertices of a distorted cube,[2-5] there are also noncubic components of the field of magnitude as yet to be determined.

We shall review, therefore, the effect of a cubic field and a rhombic field on the rare-earth ion energy levels and estimate the magnitude of the splitting produced by each. First, for a purely cubic field, we introduce a crystalline potential in the 4*f*-electron coordinates of the form[13]

$$V_{cub}=V_4^0+(V_4^4+V_4^{-4})+V_6^0+(V_6^4+V_6^{-4}) \quad (2)$$

with

$$V_4^0=\tfrac{7}{18}(Ze^2\alpha_s/R^5)[35z^4-30r^2z^2+3r^4]$$
$$=\tfrac{7}{18}(Ze^2\alpha_s/R^5)\,T_4^0 \quad (3)$$

$$V_4^4+V_4^{-4}=\tfrac{35}{18}(Ze^2\alpha_s/R^5)\,(x^4+y^4-6x^2y^2) \quad (4)$$

$$V_6^0=\tfrac{1}{9}(Ze^2\alpha'_s/R^7)[231z^6-315z^4r^2+105z^2r^4-5r^6]$$
$$=\tfrac{1}{9}(Ze^2\alpha'_s/R^7)\,T_6^0=\tfrac{1}{9}(4\pi/13)^{\frac{1}{2}}(Ze^2\alpha'_s/R^7)\,Y_6^0r^6 \quad (5)$$

$$V_6^4+V_6^{-4}=-\tfrac{1}{6}(Ze^2\alpha'_s/R^7)(11z^2-r^2)[(x+iy)^4-(x-iy)^4]$$
$$=-\tfrac{1}{9}(14\pi/13)^{\frac{1}{2}}(Ze^2\alpha'_s/R^7)\,(Y_6^4+Y_6^{-4})r^6 \quad (6)$$

where the crystalline potential is assumed to be due to charges Ze on the nearest neighbors of Yb^{3+}. *R* is their distance from Yb^{3+}, α_s and α_s' are screening factors which take into account the shielding effect of the $5s^2p^6$ electrons. From the consideration of the above formulae, V_l^k will have the same transformation properties as an *l*-dimensional representation of the rotation group. The axial operators T_4^0 and T_6^0 in the above formulas have been introduced by Stevens,[14] so the matrix elements of V_4^0 and V_6^0 are easily obtained using Stevens' formalism. The matrix elements of V_4^{+4} (and V_4^{-4}) are easily obtained from the correlation

$$x^4+y^4-6x^2y^2=\tfrac{1}{2}[(x+iy)^4+(x-iy)^4]$$
$$\rightarrow\tfrac{1}{2}\beta[(J_x+iJ_y)^4+(J_x-iJ_y)^4].$$

On the contrary the matrix elements of V_6^4 (and V_6^{-4}) are more easily obtained from those of V_6^0 using Wigner's coefficients.[15]

For this it is necessary to, (a) split the potential in its spherical harmonic components, (b) evaluate the matrix elements of Y_6^0 using both Stevens' formalism and Wigner's three-vector product formulas, (c) from these using Wigner's coefficients obtain the matrix elements of Y_6^4, and (d) finally, expressing properly the various multiplicative constants, the values of the matrix elements of V_6^4 (and V_6^{-4}) are obtained.

In Appendix I the various matrix elements are tabulated for convenience. Matrix elements connecting $^2F_{7/2}$ and $^2F_{5/2}$ are neglected, because the two levels are widely separated. Using in the potential both fourth-order and sixth-order terms, one obtains the following

[13] W. Low, Phys. Rev. **109**, 265 (1959).

[14] K. H. W. Stevens, Proc. Phys. Soc. (London) **3A**, 209 (1951).

[15] B. L. Van der Waerden, *Gruppentheoretischen Methode in der Quantenmechanik* (Julius Springer, Berlin, Germany, 1932), p. 70.

energy splitting in a cubic potential, after solving the relevant secular equations

$$
{}^2F_{7/2}\begin{cases} -18\mathcal{P}-72\mathcal{R} & (\Gamma_7) \\ 2\mathcal{P}+96\mathcal{R} & (\Gamma_8) \\ 14\mathcal{P}-120\mathcal{R} & (\Gamma_6) \end{cases} \qquad (7)
$$

$$
{}^2F_{5/2}\begin{cases} -4\mathcal{P}' & (\Gamma_7) \\ 2\mathcal{P}' & (\Gamma_8) \end{cases}
$$

with

$$
\mathcal{P}=3D'\left(-\frac{2}{15\times 77}\right)\langle r^4\rangle; \qquad \mathcal{P}'=3D'\left(-\frac{2}{7\times 45}\right)\langle r^4\rangle;
$$

$$
\mathcal{R}=\frac{3D''}{R^2}\left(\frac{4}{13\times 33\times 63}\right)\langle r^6\rangle; \qquad D'=\frac{70}{9}\frac{Ze^2\alpha_s}{R^5};
$$

$$
D''=\frac{70}{9}\frac{Ze^2\alpha'_s}{R^5}
$$

and $\langle r^n\rangle$ the average value of r^n for individual $4f$ electron. The splittings for the cubic field case are shown in Fig. 4. Similar results have been obtained by Ayant and Thomas and by White and Andelin.[16] A remark concerning the proper assignment of the sign is now necessary. The fact that we are using the hole formalism is taken into account by the sign of the numerical factor in round parenthesis in the expressions for $\mathcal{P}$, $\mathcal{P}'$, and $\mathcal{R}$. As for the sign of D', we note that in the present eightfold coordination, the $d\gamma$ orbitals and not the $d\epsilon$ orbitals of a $3d$ electron should be stabiiized. Calculation of the splitting of the $3d$ orbital gives

$$
\langle d\epsilon \mid V_{\text{cub}} \mid d\epsilon\rangle=-\tfrac{4}{7}(Ze^2\alpha/R^5)\langle r^4\rangle
$$

$$
\langle d\gamma \mid V_{\text{cub}} \mid d\gamma\rangle=\tfrac{6}{7}(Ze^2\alpha/R^5)\langle r^4\rangle.
$$

This requires that Z is to indicate both the charge and the *sign* on the nearest neighbor. So we have to assume a negative value of D' in our case.

The Γ_i in (7) are the two-valued representations of the cubic field, and the dimensions of Γ_8 are twice those of Γ_6 and Γ_7. In order to be able to assign the cubic field levels which have been obtained to the various representations Γ_i, it is necessary to have the explicit expression for the wave functions, transforming under cubic group operations according to the various representations of the cubic double group. Such wave functions can be obtained once the appropriate transformation matrix corresponding to each cubic group operation is found.

[16] R. L. White and J. P. Andelin Jr., Phys. Rev. **115,** 1435 (1959); Y. Ayant and J. Thomas, Compt. rend. **250,** 2688 (1960).

One obtains[17]:

$$
\left.\begin{aligned} &{}^2F_{7/2} \\ &\Psi_a{}^{(1)}=\tfrac{1}{2}[\sqrt{3}\Psi_{5/2}-\Psi_{-3/2}] \\ &\Psi_a{}^{(2)}=\tfrac{1}{2}[\sqrt{3}\Psi_{-5/2}-\Psi_{3/2}] \end{aligned}\right\}\Gamma_7
$$

$$
\left.\begin{aligned} &Y_b{}^{(1)}=(\tfrac{7}{12})^{\frac{1}{2}}[\Psi_{7/2}-(5/35^{\frac{1}{2}})\Psi_{-1/2}] \\ &\Psi_b{}^{(2)}=(\tfrac{7}{12})^{\frac{1}{2}}[\Psi_{-7/2}-(5/35^{\frac{1}{2}})\Psi_{1/2}] \\ &\Psi_b{}^{(3)}=\tfrac{1}{2}(\Psi_{5/2}+\sqrt{3}\Psi_{-3/2}) \\ &\Psi_b{}^{(4)}=\tfrac{1}{2}(\Psi_{-5/2}+\sqrt{3}\Psi_{3/2}) \end{aligned}\right\}\Gamma_8 \qquad (8)
$$

$$
\left.\begin{aligned} &\Psi_c{}^{(1)}=(\tfrac{5}{12})^{\frac{1}{2}}[\Psi_{7/2}+(7/35^{\frac{1}{2}})\Psi_{-1/2}] \\ &\Psi_c{}^{(2)}=(\tfrac{5}{12})^{\frac{1}{2}}[\Psi_{-7/2}+(7/35^{\frac{1}{2}})\Psi_{1/2}] \end{aligned}\right\}\Gamma_6
$$

(See also Luttinger and Kittel[18] on Gd^{3+}.)

$$
\left.\begin{aligned} &{}^2F_{5/2} \\ &\Phi_a{}^{(1)}=[1/(6)^{\frac{1}{2}}][\Phi_{5/2}-(5)^{\frac{1}{2}}\Phi_{-3/2}] \\ &\Phi_a{}^{(2)}=[1/(6)^{\frac{1}{2}}][\Phi_{-5/2}-(5)^{\frac{1}{2}}\Phi_{3/2}] \end{aligned}\right\}\Gamma_7
$$

$$
\left.\begin{aligned} &\Phi_b{}^{(1)}=\Phi_{1/2} \\ &\Phi_b{}^{(2)}=\Phi_{-1/2} \\ &\Phi_b{}^{(3)}=[1/(6)^{\frac{1}{2}}][(5)^{\frac{1}{2}}\Phi_{5/2}+\Phi_{-3/2}] \\ &\Phi_b{}^{(4)}=[1/(6)^{\frac{1}{2}}][(5)^{\frac{1}{2}}\Phi_{-5/2}+\Phi_{3/2}] \end{aligned}\right\}\Gamma_8 \qquad (9)
$$

where the Ψ_i are of the type

$$
\Psi_M{}^J \qquad (J=\tfrac{7}{2};\ M=J,\ J-1\cdots -J)
$$

and Φ_i are of the type

$$
\Phi_M{}^J \qquad (J=\tfrac{5}{2};\ M=J,\ J-1\cdots -J).
$$

Using these wave functions, which are an appropriate zero-order set, one can alternatively evaluate directly the energy splitting without solving the secular equation. Using the fourth-order terms, we were thus able to obtain again the same energy splitting of Fig. 2. The same method can easily be applied when in addition sixth-order terms are used. The final splitting will depend on two parameters, essentially $\alpha_s\langle r^4\rangle$ and $\alpha_s'\langle r^6\rangle$. We might here note that only the ground state is affected by $V_6{}^k$. The excited state ${}^2F_{5/2}$ has no matrix elements of $V_6{}^k$ different from zero.

As we have already mentioned, it is known from x-ray and neutron diffraction data[2–5] that the oxygen ions coordinated to the rare-earth ions in the garnets are located at the vertices of a distorted cube. One could

[17] E. Wigner, *Gruppentheorie und ihre Anwendung auf die Quantenmechanik der Atomspektren* (Friedrich Vieweg, 1931), *passim.*

[18] C. Kittel and J. M. Luttinger, Phys. Rev. **73,** 172 (1948).

try to account for this distortion by introducing in the consideration of crystalline field effects, components of rhombic symmetry (D_2). Such, in fact, appears to be the symmetry of the dodecahedral sites in the garnet as found in paramagnetic resonance experiments.[19] Such a low symmetry crystalline potential operating on the individual electron can be expressed as[20]:

$$\begin{aligned}\mathcal{U}_{\text{rhomb}}&=(4\pi/5)^{\frac{1}{2}}\{\mathfrak{A}_2r^2Y_2^0+\mathfrak{A}_4r^4\\&\quad\times[(\tfrac{5}{12})^{\frac{1}{2}}Y_4^0-(\tfrac{7}{24})^{\frac{1}{2}}(Y_4^4+Y_4^{-4})]\\&\quad+\mathfrak{B}_2(r^2/\sqrt{2})(Y_2^2+Y_2^{-2})+\mathfrak{B}_4(r^4/\sqrt{2})(Y_4^2+Y_4^{-2})\}\\&=\tfrac{1}{2}\mathfrak{A}_2(3z^2-r^2)\\&\quad+(3/4)^{\frac{1}{2}}\mathfrak{A}_4(2z^4-x^4-y^4+12x^2y^2-6y^2z^2-6x^2z^2)\\&\quad+\tfrac{1}{2}(3)^{\frac{1}{2}}\mathfrak{B}_2(x^2-y^2)-\tfrac{3}{4}\mathfrak{B}_4(-6x^2z^2+6y^2z^2+x^4-y^4)\\&=\mathcal{U}_2^0+(\mathcal{U}_2^2+\mathcal{U}_2^{-2})+(\mathcal{U}_4^4+\mathcal{U}_4^{-4})+(\mathcal{U}_4^2+\mathcal{U}_4^{-2}).\end{aligned}\tag{10}$$

(Sixth-order terms have been omitted.)

The energy splitting in a rhombic field will in general depend on the value of four unknown parameters $\mathfrak{A}_2$, $\mathfrak{A}_4$, $\mathfrak{B}_2$, $\mathfrak{B}_4$. The relevant matrix elements are tabulated in Appendix II together with the secular determinant, in a rhombic field, of $^2F_{7/2}(\Gamma_i)$ and $^2F_{5/2}(\Gamma_i)$ (Γ_i cubic field levels). An inspection of the secular determinant shows that it is not possible to reduce the number of unknown parameters in the determination of the eigenvalues of the energy, by taking linear combinations of the rhombic field parameters, as done elsewhere.[21]

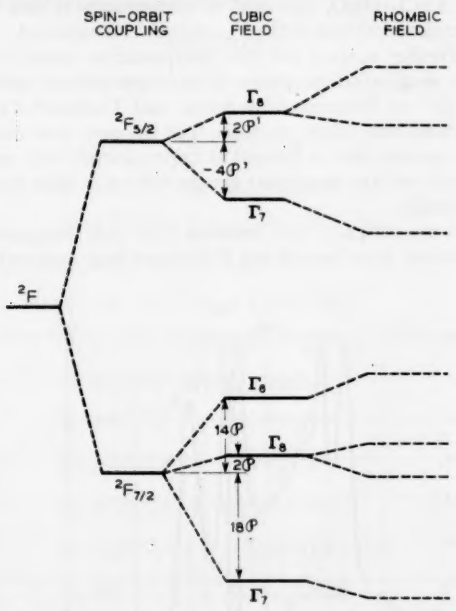

FIG. 4. Energy level scheme for Yb^{3+}. In the cubic field case, we have omitted the sixth-order parameter of Eq. (7). $\mathcal{P}$ and $\mathcal{P}'$ are given in (7). The rhombic field splitting shown is only schematic. The actual splitting depends on the four parameters $\mathfrak{A}_2$, $\mathfrak{A}_4$, $\mathfrak{B}_2$, $\mathfrak{B}_4$ in the secular equations of Appendix IIb.

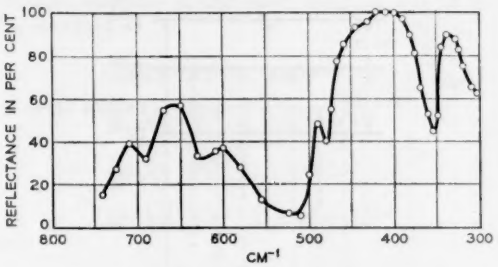

FIG. 5. Reflection spectrum of YGG+Yb^{3+} at 300°K.

DISCUSSION OF THE FINER DETAILS OF THE SPECTRUM

The assignment of the lines in the spectrum to transitions on the energy level diagram of Fig. 4 is not obvious. We have considered several alternatives and the following are two of the more acceptable ones.

A.

The shape and width of line E at low temperatures is quite different from that of the other lines in the spectrum. It is appreciably narrower, stronger, and isolated. It could, therefore, be a single electronic transition with the rest of the lines, then, being sum and difference bands involving lattice vibrations. The lines F, G, and H are sum bands present at low temperatures, while A, B, C, and D are difference bands missing at low temperatures.

Indeed the lattice vibration spectrum shown in Fig. 5, as recorded in reflection in the cesium bromide prism range, allows a fairly detailed assignment to be made on this basis. The vibrations of 490 cm^{-1} and 338 cm^{-1} shown in Fig. 7 may account for lines B, C, G, H. The vibration of frequency near 100 cm^{-1} giving rise to lines D and F is not in the region observed experimentally but is a reasonable value for such vibrations. The other lattice combinations are presumably forbidden or of very weak intensity.

The difficulty with this assignment is that, since only one electronic transition is observed, either the splitting due to the crystal field is less than the width of line E(5 cm^{-1}) or else the transitions connecting the other members of the $^2F_{7/2}$ and $^2F_{5/2}$ manifolds are forbidden. We do not believe that the crystalline field is so small that the splittings it produces are less than 5 cm^{-1}.

The selection rules giving just one transition on the other hand could happen for electric or magnetic dipole

[19] D. Boakes, G. Garton, D. Ryan, and W. P. Wolf, Proc. Phys. Soc. (London) **74**, 663 (1959); J. W. Carson and R. L. White, Appl. Phys. Suppl. **31**, 53S (1960).

[20] S. Koide and M. H. L. Pryce, Phil. Mag. **3**, 607 (1958).

[21] R. Pappalardo, J. Chem. Phys. **31**, 1050 (1959).

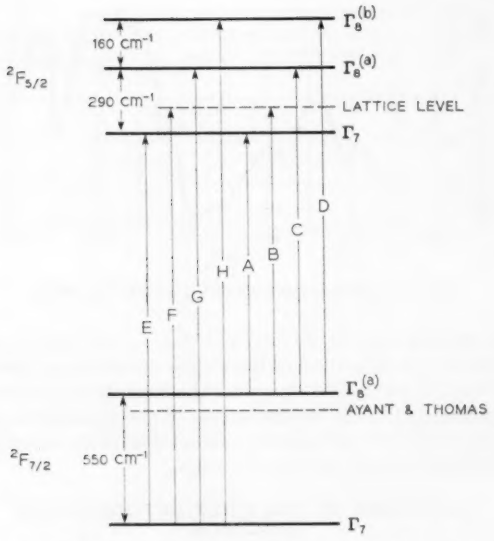

FIG. 6. Assignment of the observed lines to definite transitions. The labels Γ_i refer to the cubic field levels as perturbed by sizable rhombic components of the field. The broken lines represent the first level above the ground state of Yb+YGG according to Ayant and Thomas.[22]

transitions (transformation properties Γ_4) for a field of perfect cubic symmetry, if the ground state had transformation properties Γ_6. Then the product $\Gamma_6\times\Gamma_4=\Gamma_6+\Gamma_8$ does not contain the representation Γ_7 and the matrix elements connecting Γ_6 and Γ_7 are zero from symmetry considerations, alone. But if our over-all assignment is correct for the sign of the constants which determine the order of the ground state sublevels, then the lowest level has Γ_7 symmetry. The product $\Gamma_7\times\Gamma_4$ contains both Γ_7 and Γ_8, so the dipole moment operator connects the ground state to both components of $^2F_{5/2}$ even in a purely cubic field. Furthermore, from what is known about the structure of the crystal, it is unlikely that the field is close to being cubic. We therefore feel that this assignment is difficult to reconcile in detail with the facts.

B.

A more desirable assignment suggests that the three strongest peaks (E, G, H) are due to transitions from the lowest $^2F_{7/2}$ ground level to the three components of the $^2F_{5/2}$ excited state. The room temperature spectrum could then be understood as arising from these transitions plus additional transitions from a $^2F_{7/2}$ level 550 cm^{-1} above the lowest one ($\nu_E-\nu_A$). The relative energy level scheme is shown in Fig. 6. Thus the spectrum consists of two groups of lines (E, G, H) and (A, C, D) separated by 550 cm^{-1}.

A rough estimate of the cubic field splitting of the excited state may be obtained from the relation:

$$|\nu_E-\tfrac{1}{2}(\nu_G-\nu_H)|=360\text{ cm}^{-1}=6\mathcal{D}'.$$

This would lead to a cubic field splitting of the ground state as $\Gamma_7\rightarrow\Gamma_8=328$ cm^{-1} and $\Gamma_7\rightarrow\Gamma_6=524$ cm^{-1}. The 328 cm^{-1} which is to be compared with 550 cm^{-1} observed constitutes a rough agreement, in view of the fact that considerable rhombic components are present in the field ($\nu_H-\nu_G=160$ cm^{-1}), and this estimate is only for cubic components of the field.

The application of the rhombic field calculation previously developed and tabulated in Appendix II is unfortunately impractical, since five parameters are to be fitted with four energy differences.

Even though the quantitative aspects of the splittings cannot be obtained, some support for the assignment can be derived from the spectrum of $YbCl_3\cdot 6H_2O$, where two sets of three lines are also observed. The spectrum is shown in Fig. 7 as we have recorded it at 78°K.

Dieke and Crosswhite[9] have shown that lines A, C, D disappear at 4.2°K, while lines E, G, and H remain. For this spectrum the separation of the two lowest levels would be smaller (132 cm^{-1}), and the splitting of the upper state also less than that for the garnet. In $YbCl_3\cdot 6H_2O$, the field is unsymmetrical and the complete splitting of the $^2F_{5/2}$ manifold is expected.

Further support for this interpretation comes from the magnetization curve of yttrium gallium garnet $+Yb^{3+}$ as interpreted by Ayant and Thomas.[22] These workers have found evidence that the next level above the ground state is located at approximately 480 cm^{-1}, which we take as support for the 550 cm^{-1} value found optically.

Some difficulty still remains with this assignment, however, since lines D and F have not been assigned. It

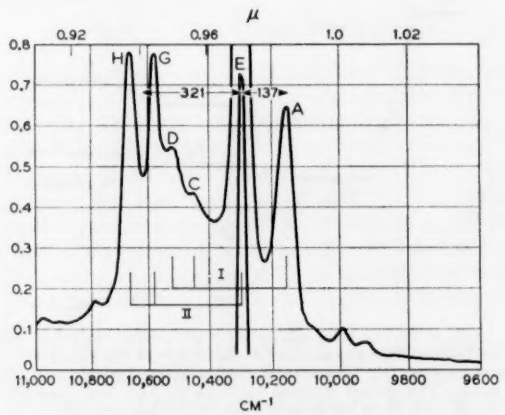

FIG. 7. Absorption lines of $YbCl_3\cdot 6H_2O$ at 78°K. Pattern I disappears at 4.2°K (Dieke and Crosswhite[9]). The most intense line (E) has optical density 1.9. Note the absence of fine structure in the doublet group in contrast with the corresponding G and H lines of the garnet spectrum.

[22] Y. Ayant and J. Thomas, Compt. rend. **248**, 387 (1959).

is not difficult to suggest that these arise from levels associated with lattice vibrations of about 100 cm^{-1} frequency.

The many lines associated with G and H at 4.2°K are not easy to explain this way, however, for if these are due to lattice modes or exchange coupling, why are they not also associated with line E? We have no answer to the assignment of these details. Aside from this, the assignment seems attractive.

CONCLUSION

We have discussed how the levels of Yb^{3+} ion are affected by cubic and rhombic crystal fields. On the basis of these calculations, we conclude that the Yb^{3+} in YGG crystals is located in sites of low symmetry which probably have large rhombic field components. Many of the details of the spectrum can be accounted for on this basis.

ACKNOWLEDGMENTS

The writers wish to thank Dr. J. W. Nielsen for kindly supplying a single crystal of Yb-doped yttrium gallium garnet, Miss S. M. Vincent for the quantitative determination of Yb in the sample by means of x-ray fluorescence, and Miss D. M. Dodd for assistance in the spectrophotometric measurements.

APPENDIX I

Matrix elements of the cubic potential (2) in the $^2F_{7/2}$ manifold.

$$\langle \tfrac{7}{2}, \pm\tfrac{7}{2} \mid V_4^0 \mid \tfrac{7}{2}, \pm\tfrac{7}{2}\rangle = 7\mathcal{P}$$
$$\langle \tfrac{7}{2}, \pm\tfrac{5}{2} \mid V_4^0 \mid \tfrac{7}{2}, \pm\tfrac{5}{2}\rangle = -13\mathcal{P}$$
$$\langle \tfrac{7}{2}, \pm\tfrac{3}{2} \mid V_4^0 \mid \tfrac{7}{2}, \pm\tfrac{3}{2}\rangle = -3\mathcal{P}$$
$$\langle \tfrac{7}{2}, \pm\tfrac{1}{2} \mid V_4^0 \mid \tfrac{7}{2}, \pm\tfrac{1}{2}\rangle = 9\mathcal{P}$$
$$\langle \tfrac{7}{2}, \pm\tfrac{7}{2} \mid V_4^{\pm 4} \mid \tfrac{7}{2}, \mp\tfrac{1}{2}\rangle = \sqrt{35}\mathcal{P}$$
$$\langle \tfrac{7}{2}, \pm\tfrac{5}{2} \mid V_4^{\pm 4} \mid \tfrac{7}{2}, \mp\tfrac{3}{2}\rangle = 5\sqrt{3}\mathcal{P}$$
$$\langle \tfrac{7}{2}, \pm\tfrac{7}{2} \mid V_6^0 \mid \tfrac{7}{2}, \pm\tfrac{7}{2}\rangle = 6\mathcal{R}$$
$$\langle \tfrac{7}{2}, \pm\tfrac{5}{2} \mid V_6^0 \mid \tfrac{7}{2}, \pm\tfrac{5}{2}\rangle = -30\mathcal{R}$$
$$\langle \tfrac{7}{2}, \pm\tfrac{3}{2} \mid V_6^0 \mid \tfrac{7}{2}, \pm\tfrac{3}{2}\rangle = 54\mathcal{R}$$
$$\langle \tfrac{7}{2}, \pm\tfrac{1}{2} \mid V_6^0 \mid \tfrac{7}{2}, \pm\tfrac{1}{2}\rangle = -30\mathcal{R}$$
$$\langle \tfrac{7}{2}, \pm\tfrac{7}{2} \mid V_6^{\pm 4} \mid \tfrac{7}{2}, \mp\tfrac{1}{2}\rangle = -18\sqrt{35}\mathcal{R}$$
$$\langle \tfrac{7}{2}, \pm\tfrac{5}{2} \mid V_6^{\pm 4} \mid \tfrac{7}{2}, \mp\tfrac{3}{2}\rangle = 42\sqrt{3}\mathcal{R}$$

with

$$\mathcal{P} = 3\left(\frac{70}{9}\frac{Ze^2\alpha_s}{R^5}\right)\left(-\frac{2}{15\times 77}\right)\langle r^4\rangle$$

$$\mathcal{R} = 3\left(\frac{70}{9}\frac{Ze^2\alpha'_s}{R^7}\right)\left(\frac{4}{13\times 33\times 63}\right)\langle r^6\rangle.$$

Matrix elements of the cubic potential (2) in the $^2F_{5/2}$ manifold.

$$\langle \tfrac{5}{2}, \pm\tfrac{5}{2} \mid V_4^0 \mid \tfrac{5}{2}, \pm\tfrac{5}{2}\rangle = \mathcal{P}'$$
$$\langle \tfrac{5}{2}, \pm\tfrac{3}{2} \mid V_4^0 \mid \tfrac{5}{2}, \pm\tfrac{3}{2}\rangle = -3\mathcal{P}'$$
$$\langle \tfrac{5}{2}, \pm\tfrac{1}{2} \mid V_4^0 \mid \tfrac{5}{2}, \pm\tfrac{1}{2}\rangle = 2\mathcal{P}'$$
$$\langle \tfrac{5}{2}, \pm\tfrac{5}{2} \mid V_4^{\pm 4} \mid \tfrac{5}{2}, \mp\tfrac{3}{2}\rangle = \sqrt{5}\mathcal{P}'$$

with

$$\mathcal{P}' = 3\left(\frac{70}{9}\frac{Ze^2\alpha_s}{R^5}\right)\left(-\frac{2}{7\times 45}\right)\langle r^4\rangle.$$

Sixth-order terms of the potential do not affect $^2F_{5/2}$.

APPENDIX II

A.

Matrix elements of the rhombic field potential (10) in the $^2F_{7/2}$ manifold.

$$\langle \tfrac{7}{2}, \pm\tfrac{7}{2} \mid U_2^0 \mid \tfrac{7}{2}, \pm\tfrac{7}{2}\rangle = \tfrac{21}{2}\alpha\mathcal{A}_2\langle r^2\rangle$$
$$\langle \tfrac{7}{2}, \pm\tfrac{5}{2} \mid U_2^0 \mid \tfrac{7}{2}, \pm\tfrac{5}{2}\rangle = \tfrac{3}{2}\alpha\mathcal{A}_2\langle r^2\rangle$$
$$\langle \tfrac{7}{2}, \pm\tfrac{3}{2} \mid U_2^0 \mid \tfrac{7}{2}, \pm\tfrac{3}{2}\rangle = -\tfrac{9}{2}\alpha\mathcal{A}_2\langle r^2\rangle$$
$$\langle \tfrac{7}{2}, \pm\tfrac{1}{2} \mid U_2^0 \mid \tfrac{7}{2}, \pm\tfrac{1}{2}\rangle = -\tfrac{15}{2}\alpha\mathcal{A}_2\langle r^2\rangle$$
$$\langle \tfrac{7}{2}, \pm\tfrac{7}{2} \mid U_4^0 \mid \tfrac{7}{2}, \pm\tfrac{7}{2}\rangle = \tfrac{105}{4}\sqrt{3}\beta\mathcal{A}_4\langle r^4\rangle$$
$$\langle \tfrac{7}{2}, \pm\tfrac{5}{2} \mid U_4^0 \mid \tfrac{7}{2}, \pm\tfrac{5}{2}\rangle = -\tfrac{105}{4}\sqrt{3}\beta\mathcal{A}_4\langle r^4\rangle$$
$$\langle \tfrac{7}{2}, \pm\tfrac{3}{2} \mid U_4^0 \mid \tfrac{7}{2}, \pm\tfrac{3}{2}\rangle = -\tfrac{45}{4}\sqrt{3}\beta\mathcal{A}_4\langle r^4\rangle$$
$$\langle \tfrac{7}{2}, \pm\tfrac{1}{2} \mid U_4^0 \mid \tfrac{7}{2}, \pm\tfrac{1}{2}\rangle = \tfrac{135}{4}\sqrt{3}\beta\mathcal{A}_4\langle r^4\rangle$$
$$\langle \tfrac{7}{2}, \pm\tfrac{7}{2} \mid U_2^{\pm 2} \mid \tfrac{7}{2}, \pm\tfrac{3}{2}\rangle = \tfrac{3}{2}\sqrt{7}\alpha\mathcal{B}_2\langle r^2\rangle$$
$$\langle \tfrac{7}{2}, \pm\tfrac{5}{2} \mid U_2^{\pm 2} \mid \tfrac{7}{2}, \pm\tfrac{1}{2}\rangle = \tfrac{3}{2}\sqrt{15}\alpha\mathcal{B}_2\langle r^2\rangle$$
$$\langle \tfrac{7}{2}, \pm\tfrac{3}{2} \mid U_2^{\pm 2} \mid \tfrac{7}{2}, \mp\tfrac{1}{2}\rangle = 3\sqrt{5}\alpha\mathcal{B}_2\langle r^2\rangle$$
$$\langle \tfrac{7}{2}, \pm\tfrac{7}{2} \mid U_4^{\pm 2} \mid \tfrac{7}{2}, \pm\tfrac{3}{2}\rangle = \tfrac{45}{2}\sqrt{21}\beta\mathcal{B}_4\langle r^4\rangle$$
$$\langle \tfrac{7}{2}, \pm\tfrac{5}{2} \mid U_4^{\pm 2} \mid \tfrac{7}{2}, \pm\tfrac{1}{2}\rangle = \tfrac{9}{2}\sqrt{5}\beta\mathcal{B}_4\langle r^4\rangle$$
$$\langle \tfrac{7}{2}, \pm\tfrac{3}{2} \mid U_4^{\pm 2} \mid \tfrac{7}{2}, \mp\tfrac{1}{2}\rangle = -18\sqrt{15}\beta\mathcal{B}_4\langle r^4\rangle$$
$$\langle \tfrac{7}{2}, \pm\tfrac{7}{2} \mid U_4^{\pm 4} \mid \tfrac{7}{2}, \mp\tfrac{1}{2}\rangle = -\tfrac{21}{4}\sqrt{105}\beta\mathcal{A}_4\langle r^4\rangle$$
$$\langle \tfrac{7}{2}, \pm\tfrac{5}{2} \mid U_4^{\pm 4} \mid \tfrac{7}{2}, \mp\tfrac{3}{2}\rangle = -\tfrac{315}{4}\beta\mathcal{A}_4\langle r^4\rangle$$

$$\alpha = \frac{2}{63}; \qquad \beta = -\frac{2}{15\times 77}.$$

Matrix elements of the rhombic field potential (10) in the $^2F_{5/2}$ manifold.

$$\langle \tfrac{5}{2}, \pm\tfrac{5}{2} \mid \mathcal{V}_2^0 \mid \tfrac{5}{2}, \pm\tfrac{5}{2}\rangle = 5\alpha'\mathcal{A}_2\langle r^2\rangle$$
$$\langle \tfrac{5}{2}, \pm\tfrac{3}{2} \mid \mathcal{V}_2^0 \mid \tfrac{5}{2}, \pm\tfrac{3}{2}\rangle = -\alpha'\mathcal{A}_2\langle r^2\rangle$$
$$\langle \tfrac{5}{2}, \pm\tfrac{1}{2} \mid \mathcal{V}_2^0 \mid \tfrac{5}{2}, \pm\tfrac{1}{2}\rangle = -4\alpha'\mathcal{A}_2\langle r^2\rangle$$
$$\langle \tfrac{5}{2}, \pm\tfrac{5}{2} \mid \mathcal{V}_4^0 \mid \tfrac{5}{2}, \pm\tfrac{5}{2}\rangle = \tfrac{15}{4}\sqrt{3}\beta'\mathcal{A}_4\langle r^4\rangle$$
$$\langle \tfrac{5}{2}, \pm\tfrac{3}{2} \mid \mathcal{V}_4^0 \mid \tfrac{5}{2}, \pm\tfrac{3}{2}\rangle = -\tfrac{45}{4}\sqrt{3}\beta'\mathcal{A}_4\langle r^4\rangle$$
$$\langle \tfrac{5}{2}, \pm\tfrac{1}{2} \mid \mathcal{V}_4^0 \mid \tfrac{5}{2}, \pm\tfrac{1}{2}\rangle = \tfrac{15}{2}\sqrt{3}\beta'\mathcal{A}_4\langle r^4\rangle$$
$$\langle \tfrac{5}{2}, \pm\tfrac{5}{2} \mid \mathcal{V}_2^{\pm 2} \mid \tfrac{5}{2}, \pm\tfrac{1}{2}\rangle = (\tfrac{15}{2})^{\frac{1}{2}}\alpha'\mathcal{A}_2\langle r^2\rangle$$
$$\langle \tfrac{5}{2}, \pm\tfrac{3}{2} \mid \mathcal{V}_2^{\pm 2} \mid \tfrac{5}{2}, \mp\tfrac{1}{2}\rangle = 3(\tfrac{3}{2})^{\frac{1}{2}}\alpha'\mathcal{A}_2\langle r^2\rangle$$
$$\langle \tfrac{5}{2}, \pm\tfrac{5}{2} \mid \mathcal{V}_4^{\pm 2} \mid \tfrac{5}{2}, \pm\tfrac{1}{2}\rangle = \tfrac{27}{4}\sqrt{10}\beta'\mathcal{A}_4\langle r^4\rangle$$
$$\langle \tfrac{5}{2}, \pm\tfrac{3}{2} \mid \mathcal{V}_4^{\pm 2} \mid \tfrac{5}{2}, \mp\tfrac{1}{2}\rangle = -\tfrac{45}{4}\sqrt{10}\beta'\mathcal{A}_4\langle r^4\rangle$$
$$\langle \tfrac{5}{2}, \pm\tfrac{5}{2} \mid \mathcal{V}_4^{\pm 4} \mid \tfrac{5}{2}, \mp\tfrac{3}{2}\rangle = -\tfrac{21}{4}\sqrt{15}\beta'\mathcal{A}_4\langle r^4\rangle$$

$$\alpha' = \frac{2}{35}; \qquad \beta' = -\frac{2}{7\times 45}.$$

B.

Secular equation of the cubic field levels of Yb^{3+} in a rhombic potential of the form (10).

$^2F_{7/2}$

Γ_7	$-18\mathcal{P}-w$	$-(8/\sqrt{3}\alpha B_2+45\beta B_4)$	$\tfrac{3}{2}(\sqrt{3}\alpha A_2-45\beta A_4)$	$(\tfrac{105}{4})^{\frac{1}{2}}(\alpha B_2-6\sqrt{3}B_4)$
Γ_8^a		$3\alpha A_2+\sqrt{360}\beta A_4+2\mathcal{P}-w$	$\tfrac{3}{4}(\alpha B_2+50\sqrt{3}\beta B_4)$	$\tfrac{3}{2}\sqrt{35}(\alpha A_2-\sqrt{3}\beta A_4)$
Γ_8^b			$-3\alpha A_2-60\sqrt{3}\beta A_4+2\mathcal{P}-w$	$\tfrac{1}{4}\sqrt{105}(\sqrt{3}\alpha B_2+24\beta B_4)$
Γ_6				$14\mathcal{P}-w$

$^2F_{5/2}$

Γ_8^a	$-4\alpha' A_2+\tfrac{15}{2}\sqrt{3}\beta' A_4+2\mathcal{P}'-w$	$4\alpha' B_2+\tfrac{15}{2}\sqrt{3}\beta' B_4$	$\sqrt{5}(-\alpha' B_2+6\sqrt{3}\beta' B_4)$
Γ_8^b		$4\alpha' A_2-\tfrac{15}{2}\sqrt{3}\beta' A_4+2\mathcal{P}'-w$	$\sqrt{3}(\alpha' A_2+6\sqrt{3}\beta' A_4)$
Γ_7			$-4\mathcal{P}'-w$

with

$$\mathcal{P}' = \tfrac{11}{3}\mathcal{P}; \qquad A_2 = \mathcal{A}_2\langle r^2\rangle; \qquad A_4 = \mathcal{A}_4\langle r^4\rangle; \qquad B_2 = \mathcal{B}_2\langle r^2\rangle; \qquad B_4 = \mathcal{B}_4\langle r^4\rangle$$

$$\alpha = \frac{2}{63}; \qquad \alpha' = -\frac{2}{35}; \qquad \beta = -\frac{2}{15\times 77}; \qquad \beta' = \frac{2}{7\times 45}.$$

THE JOURNAL OF CHEMICAL PHYSICS VOLUME 33, NUMBER 6 DECEMBER, 1960

Infrared Spectra of Crystalline CD_3Cl and CD_3Br†

DAVID A. DOWS

Department of Chemistry, University of Southern California, Los Angeles, California

(Received April 22, 1960)

Infrared spectra have been obtained for deuterated methyl chloride and bromide. The region covered includes all fundamental vibrations, many of which showed splittings similar to those observed for the normal methyl halides. [See D. A. Dows, J. Chem. Phys. **29**, 484 (1958).] Assignments are presented, and librational frequencies in the methyl halides are summarized.

INTRODUCTION

IN a continuation of previous work on the spectra of the crystalline methyl halides,[1,2] the spectra of deuterated methyl chloride and methyl bromide have been studied. The results of this work are of importance to the question of the mechanism(s) of intermolecular coupling between vibrations in these crystals; a subsequent paper will present the results of theoretical treatment of the data now available.

EXPERIMENTAL

The experimental techniques are as previously described,[1] except that a CaF_2 prism has been added to the equipment and provides somewhat more convenient access to the higher frequencies, especially the CH and CD stretching regions. It has been used along with the grating mode of operation of the instrument on the region above about 1200 wave numbers.

Deuterated methyl bromide was obtained from Isotope Specialties Company, Los Angeles. It was not subjected to rigorous purification, and several weaker bands in the spectrum may be due to impurities. CD_3Cl was prepared from the deuterated bromide by passing the sample repeatedly through an asbestos-aluminum chloride-$HgCl_2$ mixture at 100°C in vacuum. The product was purified by vacuum distillation and the purity is estimated at better than 98% from vapor pressure and partial distillation measurements.

Several samples were tested, after sublimation onto the cold window of the cell, by warming them almost to the point where they sublimed from the window. There was evidence of some changes in relative intensities of bands (but not in frequencies) during this warmup-cooldown procedure. This phenomenon was in contradiction to the lack of such effects reported previously; therefore we repeated the experiment with normal methyl chloride as a check. This time we found small changes in intensities for the ν_2 and ν_5 regions. No quantitative intensity measurements were attempted, but the data in Table IV (footnote reference 1) remain qualitatively correct.

Observed spectra are shown in Fig. 1 and frequencies listed in Tables I and II. Gas frequencies are from King, *et al.*[3] An effort was made to measure band splittings accurately. The results are given in parentheses under "assignments."

DISCUSSION

Assignments

Assignments in Tables I and II are analogous to those for the normal methyl halides.[1] The multiplet structures of all bands are consistent with isomorphous crystal structures for the chloride and bromide, with the possible exception of ν_6 of CD_3Cl. The multiplet structures of some bands are not as fully developed as in the cases of the normal isotopic species, probably because the intermolecular forces are not strong enough to cause resolvable splittings, but no multiplet has too many components. Some band shapes require comment. ν_3 of CD_3Cl has only two components, compared with three for CH_3Cl. These two are clearly due to the chlorine isotope effect, and the factor group splitting of CH_3Cl has reduced to a line broadening (observed width of the 675 cm^{-1} line is about 4 cm^{-1}). As an aside, the previous assignment of the CH_3Cl ν_3 multiplet should probably be revised. The two higher components are probably due to Cl^{35} and the lowest to Cl^{37}. This follows from consideration of the most likely number of nearest interacting neighbors of a given kind which may surround a given molecule in the crystal[4]; the most likely Cl^{35} occurence is in triplets while isolated Cl^{37} molecules are the rule. The question of second-order perturbation between the upper two and the lowest frequencies has been considered; taking the splitting of the upper two levels (4.1 cm^{-1}) as a measure of the intermolecular force constant, and taking the unperturbed $Cl^{35}-Cl^{37}$ frequency difference as 5.7 cm^{-1} (from a mixed crystal study), the isotope splitting in the pure crystal is calculated as 6.3 cm^{-1}, in reasonable agreement with the observed difference between the mean of the Cl^{35} components and the Cl^{37} frequency.

† This work was supported by the Office of Ordnance Research, U. S. Army.

[1] D. A. Dows, J. Chem. Phys. **29**, 484 (1958).

[2] D. A. Dows, J. Chem. Phys. **32**, 1342 (1960).

[3] W. T. King, I. M. Mills and B. C. Crawford, Jr., J. Chem. Phys. **27**, 455 (1957).

[4] D. F. Hornig and G. L. Hiebert, J. Chem. Phys. **27**, 752 (1957).

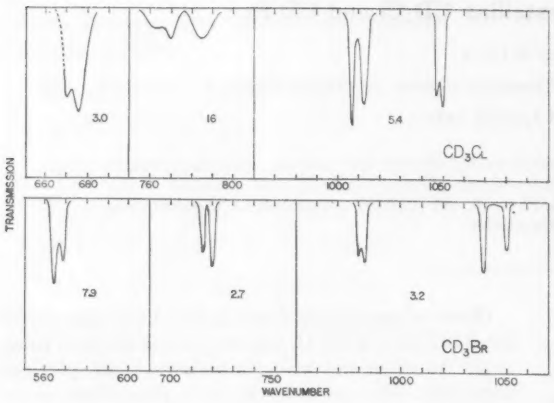

FIG. 1. Infrared absorption spectra of crystalline CD_3Cl and CD_3Br in the fundamental vibrational region. The sample thicknesses (in $\delta\mu$) shown in the figure are accurate in a *relative* sense, but are only very approximate absolutely.

Further notable differences are as follows: ν_5 in CD_3Cl has only two components, with three for CH_3Cl. This is probably due to loss of the factor-group splitting. A 10% mixed crystal of CH_3Cl in CD_3Cl was studied in an effort to assign the ν_5 multiplet with certainty. The ν_3 region showed two lines (as did a solution of CH_3Cl in CH_3I[1]). ν_2 was reduced to a single line at 1343 cm^{-1} (the mean of the components in pure CH_3Cl is 1341 cm^{-1}). In the ν_5 region a single line appeared at 1433 cm^{-1} (somewhat separated from the mean of the CH_3Cl multiplet, 1441 cm^{-1}). This is interpreted as showing that in pure CH_3Cl the 1441 cm^{-1} line is B_1 (out-of-plane), while the 1437 and 1444 cm^{-1} lines are A_1 and B_2 components of ν_5. The latter two lines coalesce in the mixed crystal, falling on top of the B_1 component.

ν_4 was not observed for CD_3Cl, apparently because of weakness and conjunction with strong atmospheric absorption. In the case of CD_3Br the spectrum is closely analogous to that of CH_3Br. The overtones $2\nu_2$ and $2\nu_5$ are not split. ν_4 is not split, and this would probably indicate that the line 3059 in CH_3Br is not really a component of ν_4. The single value 3045.6 cm^{-1} for ν_4 of CH_3Br also gives a gas-solid frequency difference more in line with the other compounds (see Table III).

Table III lists the frequency differences between gas and solid samples. The entries are values of $\nu_{gas}-\nu_{solid}$,

TABLE I. Observed frequencies of CD_3Cl.

ν_{obs}	I	$\Delta\nu_i$	Assignment[a]	ν_{gas}[b]
671.0	s	~3	ν_3(5.3)	695
675.5	vs	4		
761	w			
767.0	w	5	ν_6	775
785	w	14	ν_2+1_1	
1003	w.sh			
1007	s	2.5	ν_2(7.0)	1029
1014	s	2		
1047	s	2.5	ν_5(3.2)	1058
1050	s	2.5		
2016	w	5	$2\nu_2$	
2083	m	4	$2\nu_5$	2103
2147	s	4	ν_1	2161
2183	w	4	ν_1+1_2	

[a] In parentheses are the best values of band splittings, in cm^{-1}.
[b] From footnote reference 3.

TABLE II. Observed frequencies of CD_3Br.

ν_{obs}	I	$\Delta\nu_i$	Assignment[a]	ν_{gas}[b]
563.4	s	3	ν_3(5.1)	578
568.5	s	3		
657	m		...	
667	m		...	
714.6	m	2.5	ν_6(5.7)	712
720.3	m	2.5		
761	m	40	...	
786	m	40	...	
816	w	7	ν_6+1_1	
848	ww	20	...	
927	ww	20	...	
980.0	s	2	ν_2(1.9)	993
981.9	s	2		
1038.6	s	2	ν_5(11.9)	1056.4
1050.5	s	2		
1078	w	20	ν_2+1_1	
1120	w	20	...	
1272	w	5	$\nu_3+\nu_6$	
2070.9	m	4	$2\nu_5$	2090
2139.1	s	2.5	ν_1	2157
2177	w		ν_1+1_2	
2286	m	2.5	ν_4	2293
2330	m		...	

[a] In parentheses are the best values of the band splittings, in cm^{-1}.
[b] From footnote reference 3.

TABLE III. Gas-solid frequency differences in the methyl halides.

	CH_3Cl	CH_3Br	CH_3I	CD_3Cl	CD_3Br	CD_3I
1	11.5	26	34.3	14	18	
2	14.0	10.4	13.3	19	12	
3	33.8	17	2.8	21.5	12	
4	8.1	10.3	24	...	7	
5	13.5	17.1	32	9.5	11.8	14[b]
6	−6.5	−9.4	−11.1	8[b]	−5.5	

[a] If 785 cm^{-1} is a component of ν_6, the value in this table is −1.
[b] From footnote reference 5.

where the latter is the mean of the observed multiplet in the solid spectrum. All data are from this paper or from that cited in footnote reference 1 except the one entry for CD_3I, which was provided by R. M. Hexter.[5] The shifts are all rather small, testifying to the weak forces in the crystals; no explanations will be advanced here concerning the rather nicely displayed trends in frequency shifts.

Librational Frequencies

Librational frequencies are observed as indicated in Tables I and II. Two librations are identified, as with CH_3Cl,[1] presumably one about the B axis (1_1) and one about the A axis (1_2) of the molecule. The values observed for CD_3Br are 98 and 38 cm^{-1}, respectively, while those for CD_3Cl are 111 and 36 cm^{-1}. The 111 cm^{-1} value is questionable, since the band at 785 cm^{-1} may be a component of ν_6 rather than a torsional combination. This is perhaps preferred because of the more reasonable gas-solid frequency shift (Table III). The 785 cm^{-1} band of CD_3Cl has an unusual breadth for a fundamental vibrational absorption in the methyl halides, but there is doubt about its interpretation.

[5] R. M. Hexter, private communication.

TABLE IV. Librational frequencies observed; isotope effect.

Molecule	1_1	1_2	$1_1/1_1^*$	$1_2/1_2^*$
CH_3Cl	120	55	1.08	1.53
CD_3Cl	111	36		
CH_3Br	117	...	1.19	...
CD_3Br	98	38		
Calculated ratios			1.10	1.41

Table IV summarizes the observed librational frequencies and compares the isotope frequency ratios to the theoretical ones for libration about the axes concerned. The assignment of 1_2 as about the A axis is supported by the approximate square-root-of-two ratio of the frequencies, while there is rough agreement also for 1_1. Since these librations are lattice modes, presumably with a considerable spread of frequencies and poorly defined selection rules, no exact agreement with the isotope product rule is expected.

A more detailed consideration of the splittings of bands will be deferred to a subsequent paper where an attempt to calculate them in detail will be presented. It should, however, be mentioned that the observed splittings for both crystals are consistent with the predictions made from the crystal structure of methyl chloride,[1] thus lending a small additional amount of support to the thesis that $CHCl_3$ and $CHBr_3$ have the same crystal structure.

ACKNOWLEDGMENT

I should like to thank J. L. Hollenberg for assistance with some of the measurements.

Critical Opalescence of Polystyrene in Cyclohexane

P. DEBYE, H. COLL, AND D. WOERMANN

Cornell University, Ithaca, New York

(Received May 18, 1960)

Light scattering measurements on the system cyclohexane-polystyrene (molecular weight range 69 000 to 1 000 000) show an angular dissymmetry of critical opalescence in essential agreement with theory. The interaction range between polymer segments as calculated from the data appeared to be considerably smaller than the radius of gyration of the polymer coil. The dependence of critical temperature and concentration on the molecular weight is shown.

THE intensity of light scattered by a binary mixture of critical concentration, at small temperature distances above the critical (consolute) point, depends not only on the average square of the amplitude of the concentration fluctuations, but also on the average square of the gradient of the fluctuations. This concept has recently again been employed in a theoretical treatment.[1] A formula for the intensity of scattered light was derived. It is restated below in a simplified form

$$I = C\frac{T/T_c}{(\Delta T/T_c)+(8\pi^2 l^2/3\lambda^2)\sin^2\theta/2}, \qquad (1)$$

where I is intensity of scattered light; C is constant characteristic for the system; T is temperature, °K; T_c is critical (consolute) temperature, $\Delta T = T - T_c$; λ is wavelength of light in medium; l is interaction range; and θ is angle of scattering.

Implied in (1) is the condition that the incident beam is polarized at right angles to the plane of observation. The parameter l^2 has been defined by

$$l^2 = \frac{l_{11}^2(W_{11}/\omega_1^2)+l_{22}^2(W_{22}/\omega_2^2)-2l_{12}(W_{12}/\omega_1\omega_2)}{W_{11}/\omega_1^2+W_{22}/\omega_2^2-2W_{12}/\omega_1\omega_2},$$

where

$$l_{ij}W_{ij} = \int \epsilon_{ij}(r) r^2 d\tau,$$

$$W_{ij} = \int \epsilon_{ij}(r)\, d\tau.$$

$\epsilon_{ij}(r)$ designates the potential energy between individual molecules, the integration being carried out over the space surrounding the central molecule. The potential energies were assumed to be functions of the distance r only, and need not be known explicitly; ω stands for the volume of the molecules. $(W_{ij}/\omega_i\omega_j)$ are the familiar cohesive energy densities.

Experimental evidence for the validity of (1) has previously been obtained for a system of small molecules.[2]

The purpose of our present study is to establish that the critical opalescence of polymer solutions is quite analogous to the behavior of systems of small molecules in the neighborhood of the consolute point. The interaction range l can be determined from experimental data. It may serve for the characterization of the mutual interaction of polymer molecules in a similar manner as the radius of gyration r characterizes the extension of the single polymer coil in dilute solutions.

Equation (1) in a formal way can also be applied to polymer solutions. With the help of special assumptions it is possible to relate the interaction range l to familiar parameters such as the radius of gyration of the coiled-up molecule. It has been shown[1] that $l \cong r$ if one assumes that the segment density of the polymer coil follows a Gaussian distribution. It is further necessary to make an assumption about the three cohesive energy densities. In Eq. (39′) of reference 1 it was estimated that the factor in front of $R^2/3$, depending on the cohesive energy densities, was approximately equal to one-half. From this it was concluded that l should be of the same order of magnitude as r. The experiments on polystyrene in cyclohexane have shown in the meantime that l is much smaller.

A preliminary report on our findings has recently been published.[3]

MATERIALS

It appeared to be important that the molecular weight range of the polystyrene fractions was narrow enough to give rise to a fairly well defined consolute temperature which could be approached closely without precipitation of the high-molecular-weight components of the fraction. The polystyrene fractions which we used[4] had been prepared by anionic polymerisation of styrene.[5] They are characterized by the data[6] in the first four columns of Table I. Reagent grade cyclohexane was passed through a column of magnesium perchlorate and distilled. The solutions were prepared

[1] P. Debye, J. Chem. Phys. **31**, 680 (1959).

[2] P. Debye, J. Chem. Phys. **31**, (1959), footnote 6, which refers to experiments by B. Zimm. Cf. B. Zimm, J. Phys. Colloid Chem. **54**, 1300 (1950).

[3] P. Debye, H. Coll, and D. Woermann, J. Chem. Phys. **32**, 939 (1960).

[4] Samples were obtained by courtesy of the Dow Chemical Company, Midland, Michigan.

[5] M. Szwarc *et al.*, J. Am. Chem. Soc. **78**, 2656 (1956); **79**, 2026 (1957); M. Szwarc, Nature **178**, 1168, (1956).

[6] H. W. McCormik, Dow Chemical Company (private communication).

TABLE I.

Sample	$\bar{M}_n \times 10^{-3}$	$\bar{M}_w/\bar{M}_n$	Halfwidth,[a] %	T_c, °C[b]	$T_p - T_c$, °C	$(\phi_2)_c$, vol. %	l, A	r, A
A	69	1.16	...	19.2_4	0.69	6.8	23.8	
B	118	1.05	38	21.8_2	0.82	5.6	26.6	
C	147	1.04	30	23.1_9	0.59	5.0	28.4	
D	221	1.08	32	24.9_5	0.53	4.6	30.0	
E	248	1.02	25	25.0_9	0.40	4.3	33.3	
F	522	1.09	...	27.7_9	0.53	2.8	42.1	
G	1000	1.19	...	29.0_0	0.45	2.0	50.1	143 (30°C)
G[c]	(1000)	...	...	28.9_1	0.45	2.0	49.9	133 (30°C) 169 (40°C)

[a] Calculated from molecular weight distribution curves, equal to $(M \times 100)/M_{max}$; M = halfwidth of distribution curve, M_{max} = molecular weight corresponding to peak of distribution curve.

[b] The second decimal place is only significant on our relative temperature scale.

[c] Fractionated sample (see text).

from weighted amounts of polymer and solvent, and the volume fractions calculated by means of the densities 1.08 (polystyrene) and 0.779 (cyclohexane). The concentrations were checked after measurements by weighing a small portion of the solution before and after evaporation of the solvent. Solutions which were used for light scattering were filtered through an "F" (fine pores) glass frit.

We found that solutions of these polystyrene fractions in cyclohexane, after removal of dust by filtration, generally still exhibited appreciable dissymmetries of scattered intensity under conditions such that the influence of critical opalescence was precluded. This residual dissymmetry was much greater than could be accounted for by the size of the polymer molecules, and therefore suggested the presence of an impurity. Because of the greatly increased intensities of scattered light near the consolute point, these impurities made themselves felt only beyond the region of critical opalescence. Yet, we tried to purify the polymer by precipitation. This was done by adding a dilute benzene solution to a large excess of methanol, a procedure which indeed led to a considerable lowering of residual dissymmetries. This method of purification appeared to be fully adequate for our purpose, with the exception of the high-molecular-weight samples, in which case we were also interested in accurate measurements of residual dissymmetries due to the extension of the polymer coil. We shall comment further on this point.

LIGHT SCATTERING APPARATUS

The basic design of the apparatus has been described elsewhere.[7] We modified the equipment to achieve a close control of temperature, and to avoid the use of scattering cells of large diameters because of the high turbidities in the neighborhood of the critical point. Our light scattering cell which consisted of a glass-stoppered Pyrex test tube of 8 mm inside diam, was clamped vertically in a bath of light paraffin oil whose temperature could be controlled within 0.01°C. The oil was contained in a brass tank of 20 cm diam. The tank was equipped with a window in the side wall through which the primary beam entered, and with a semicircular window in the bottom plate through which the scattered light, after reflection at right angles by a metal mirror inside the bath, could pass into the photomultiplier tube underneath. The mirror and the photomultiplier tube could be rotated together around the axis of the scattering cell. The cross section of the primary beam (approx 1×10 mm) was defined by two slits inside the tank in front of the scattering cell. The scattered light had to pass through two narrow slits of 0.5 mm width mounted in front of the mirror and rigidly connected with it, before it was reflected downward into the photomultiplier tube. The primary beam was polarized by means of a Nicol prism. The wavelength of 4360 A (vacuum) was selected by a set of Corning filters which were mounted directly above the photomultiplier housing. The close match of the refractive indices of bath liquid, Pyrex glass, and the polystyrene solutions effectively reduced stray reflections from the scattering cell.

The proper adjustment of the cell was checked by measuring the scattered intensities of "Ludox" and of dilute fluorescein solutions at various angles.

EXPERIMENTAL

In a preliminary experiment we tried to establish the temperature at which phase separation occurred in the polystyrene solutions. Solutions of various concentrations, prepared from a given polymer fraction, were sealed in small glass vials and submerged in a water bath. Lowering of the bath temperature caused an increase of turbidity, until finally district schlieren indicated the point of phase separation, T_p. Generally, T_p changed only little with concentration, and therefore this method was not suitable for finding the critical (consolute) concentration. The latter was obtained from the dissymmetries of scattered intensities, I_{45}/I_{135}, measured as a function of concentration at fixed temperatures of a few tenths of a degree above T_p. Curves

[7] P. Debye and A. M. Bueche, Tech. Rept. **2242**, (1942), Reconstruction Finance Corporation, Office of Rubber Reserve, Polymer Research Branch.

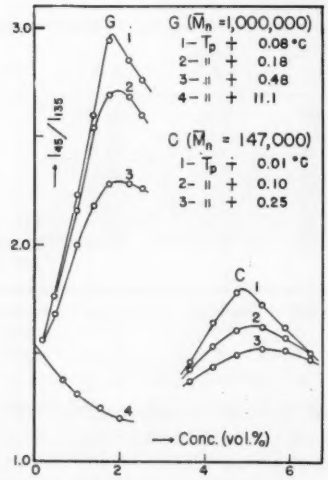

FIG. 1. Plot of dissymmetries (I_{45}/I_{135}) against concentration for two polystyrene samples in cyclohexane at various temperatures above the point of phase separation T_p.

obtained in this manner exhibited distinct maxima which defined the critical concentration (Fig. 1). Next we prepared a solution of that concentration, and measured the intensities of scattered light between the angles of 30 and 135° at various temperatures above T_p, the temperatures being read to 0.01°C on a Beckmann thermometer inserted in the bath. Because of the large variations of intensities, galvanometer readings had to be taken at various amplification levels of the photomultiplier. These levels were well defined, and further, the instrumental variations over the period of one run were small enough to dispense with the necessity of using a standard between the measurements. Finally, blank values obtained with pure cyclohexane were subtracted from the readings.

In the case of sample G, which had the highest molecular weight of the series, we were concerned with eliminating all impurities which could distort our measurements at low concentrations and at temperatures where critical opalescence was no longer effective. Precipitation with methanol as mentioned above was not fully satisfactory. We therefore divided a certain amount of sample G into three portions by fractionations in cyclohexane, retaining the middle fraction for measurements. Because the interaction range l checked with the one obtained for the unfractionated sample, we assumed that fractionation had not changed the average molecular weight perceptibly. On the other hand, the plots of reciprocal intensities against $\sin^2\theta/2$, even at temperatures of 15° above the consolute point, did not show the distinct downward bent at angles below 50° by which the presence of impurities is indicated, and which was typical for the unfractionated samples. Further, the radius of gyration of the polymer coil (at 40°C) was found to be comparable to the results obtained by Notley and Debye.[8] For the necessary measurements at low concentrations we used a large cell (diam 4 cm) in an air bath of 40°C, because measurements with the 8-mm cell were found to be less reliable at very low scattering intensities.

TREATMENT OF DATA

According to Eq. (1) parallel straight lines should be obtained if one plots the reciprocal of the excess intensities of scattered light (for example, in relative units) against $\sin^2\theta/2$. The intensities have to be corrected for the changing volume element of scattering by multiplication with $\sin\theta$. The position of the straight lines in the graph depends on the temperature distance from T_c.[3] Here the assumption is made that the temperature range considered is small enough so that $T/T_c \cong 1$. Slopes (s) and intercepts (i_0) of these plots were calculated by the method of least squares.

Determination of T_c

In accordance with (1) one can write $(i_0) = \text{const}\ (T-T_c)$. Plotting (i_0) against T, one finds T_c from slope and intercept of the resulting straight line. It should be noted that T_c can be expected to coincide with T_p only in the case of an ideally monodisperse polymer.

Determination of l

The slopes (s) have to be converted to their absolute values S. Again, according to (1),

$$S=[(s)/(i_0)](T-T_c).$$

S and l are correlated by

$$l^2=(3\lambda^2/8\pi^2T_c)\,S.$$

Plots of $1/I$ vs $\sin^2\theta/2$ for samples A to E gave parallel straight lines at temperature distances of less than 2 deg from T_p. At higher temperatures the angular dissymmetries became quite small, and probably distorted by small amounts of impurities.

A quick survey of the variations of dissymmetries, z, with temperature is afforded by means of Eq. (1) if one expresses the temperature as a function of $z\ (=I_{45}/I_{135})$, viz.

$$T=T_c+T_cl^2\left[(8\pi^2/3\lambda^2)\,\frac{\sin^2(135/2)-Z\sin^2(45/2)}{Z-1}\right].$$

As illustrated by Fig. 2 one then plots T against the expression in the bracket, which we call f/z). This plot exaggerates small differences at low dissymmetries, and the effect of purification is clearly demonstrated by the branching of the curves with a representing measurements on the original, and b on the reprecipitated polystyrene of molecular weight 147 000. The straight portion of the curve below the point of branching represents

[8] N. T. Notley and P. Debye, J. Polymer Sci. 17, 99 (1955).

the range over which Eq. (1) should be valid. The kink in the curve arises from a sharp increase of dissymmetry due to incipient precipitation at T_p. Finally, the slope of the straight section is porportional to l^2, and the intercept, which is obtained by extrapolation, defines T_c. In the case of linearity between $1/I$ and $\sin^2\theta/2$ this latter treatment of data will give the same results as the one outlined before, but by itself it is insufficient to establish the validity of Eq. (1).

So far we had assumed that no residual dissymmetry, i.e., a dissymmetry due to the extension of the random coil itself, was apparent. This assumption does not hold any longer in the case of a high-molecular-weight sample. It can be shown that this complication can be resolved by introducing the particle scattering factor $P(\theta)$. Hence,

$$I=C(T/T_c)\frac{P(\theta)}{(\Delta T/T_c)+(8\pi^2/3)(l^2/\lambda^2)\sin^2\theta/2}. \quad (2)$$

$P(\theta)$ may be developed as a power series of $\sin\theta/2$, and it can be shown that the first two terms of the series are

$$1-(16\pi^2/3\lambda^2)r^2\sin^2\theta/2,$$

irrespective of the shape of the polymer molecule, r being the radius of gyration. Substitution in (2) and inversion yields

$$I^{-1}=T_c/CT\{[(T-T_c)/T_c]+[(8\pi^2l^2/3\lambda^2)+(T-T_c)/T_c\cdot(16\pi^2r^2/3\lambda^2)]\sin^2\theta/2\}, \quad (3)$$

if one neglects powers higher than $\sin^2\theta/2$. In the case of sample $G(M_n=1\,000\,000)$ the plot $1/I$ against

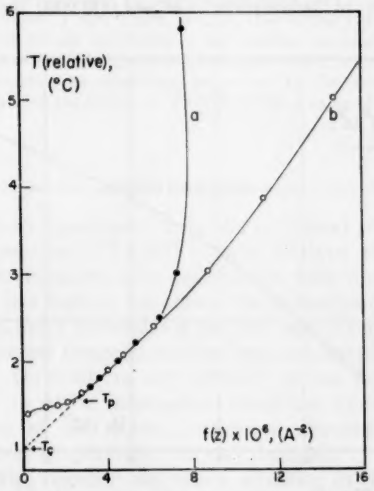

FIG. 2. Plot of relative temperature T against $f(z)$ [see text for definition of $f(z)$]. Polystyrene, $M_n=147\,000$, in cyclohexane. Curve a unpurified, b purified sample. T_p is temperature of phase separation: T_c is consolute temperature.

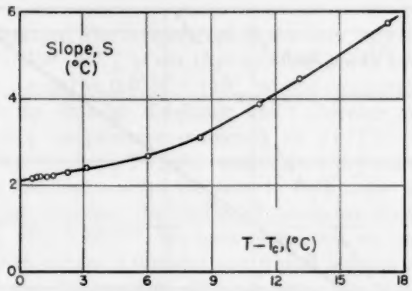

FIG. 3. Plot of absolute slope S against temperature distance from the consolute point, $T-T_c$ (for definition of S see text). Polystyrene, $M_n=1\,000\,000$, in cyclohexane.

$\sin^2\theta/2$ again appears as a straight line within the range of experimental error. Thus, the approximation of $P(\theta)$ appears to be justified. We are then able to evaluate r^2 by plotting the absolute slope S against $T-T_c$ (Fig. 3). Then

$$r^2=[3\lambda^2(S-S_0)/16\pi^2(T-T_c)],$$

S_0 being the intercept of the curve at T_c. The plot is not linear, and r increases with the temperature distance from T_c, viz., $r=133$ A near the consolute point ($T_c=28.9$°C), and $r=169$ A at 40°C. The uncertainty with respect to these values is of the order of 5%. The parameter l^2 follows from S_0, under the assumption that only r varies with temperature while l remains constant. Our experimental data further indicate that the constant C in (2) decreases with increasing temperature. Because of the wider temperature range over which the measurements were taken, we also took into consideration the change of the factor T/T_c.

CONSOLUTE TEMPERATURE AND CONCENTRATION

In the previous section we have shown how T_c, the average consolute temperature of a given polymer fraction, can be estimated from the experimental data. The difference T_p-T_c was found to range between 0.4 and 0.8°C (Table I, column 6). If one interprets T_p as the temperature where the component of highest molecular weight, which is present in the fraction, precipitated these values appear to be reasonable in view of the halfwidths of the molecular weight distribution curves.[9]

Consolute temperatures of the system polystyrene-cyclohexane have previously been determined by Shultz and Flory[10]; their results, however, appear to be generally higher than ours by 2 or 3°C. The difference in the method of determination can only partly explain this disagreement. A redetermination of the molecular weights of a few of our samples from intrinsic viscosities, by using the formula of the other investigators,[10] led to values which were about 10% lower than the ones

[9] A. R. Shultz and P. J. Flory, J. Am. Chem. Soc. **74**, 4760 (1952), cf. Eq. (6).

[10] A. R. Shultz and P. J. Flory, J. Am. Chem. Soc. **74**, 4760 (1952).

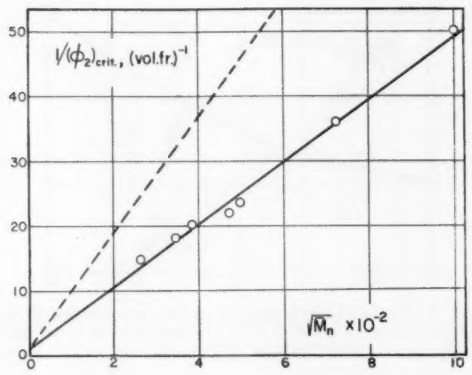

FIG. 4. Plot of reciprocal critical concentration against the square root of molecular weight. Polystyrene in cyclohexane. The broken line represents the result according to the Flory-Huggins theory.

listed in Table I, column 2. However, we believe that a readjustment of molecular weights in this manner is still insufficient to bring the two sets of temperatures to agreement. A plot $1/T_c$ against $[1/(x)^{\frac{1}{2}}+1/2x]$, where x is the number of statistical chain segments,[10] results in a straight line whose reciprocal intercept defines the theta temperature. According to our data the latter is equal to 32.5°C compared with 34° as reported by Shultz and Flory.

With reference to Fig. 1, we note that there is actually some difficulty involved in the determination of the critical concentration $(\phi_2)_c$. Noticeable shifts of the maxima toward lower concentrations with decreasing temperature distances from T_c make our $(\phi_2)_c$ appear somewhat ambiguous. Yet, the plot $1/(\phi_2)_c$ against $(M_n)^{\frac{1}{2}}$ is linear (Fig. 4), in accordance with the theoretical formula $(\phi_2)_c=1/[1+(x)^{\frac{1}{2}}]$ assuming $x=\text{const}\ \bar{M}_n$. The constant calculated from the slope of Fig. 4, however, appears to be only about one-fourth of the theoretical value[10] which is given by $\text{const}=v_p/(M_s\times v_s)$, where v designates the specific volumes, and M_s the molecular weight of the solvent. These theoretical values are illustrated by the broken line in Fig. 4. This means that the experimentally determined critical concentrations are roughly twice as big as the values given by the Flory-Huggins theory. A similar experimental result is also indicated by the phase-separation curves in the publication by Shultz and Flory.

THE INTERACTION RANGE l

Figure 5 shows a plot of l^2 against $\bar{M}_n$ of the polymer fractions. We have pointed out at the beginning that only under very special conditions $l\cong r$. More generally,

$$l^2=[l_{11}^2(W_{11}/\omega_1^2)/(\Delta_1+\Delta_2)]+[2\Delta_2/(\Delta_1+\Delta^2)]r^2, \quad (4)$$

where l_{11} is the range of molecular forces of the solvent molecules,

$$\Delta_1=(W_{11}/\omega_1^2)-(W_{12}/\omega_1\omega_2),$$
$$\Delta_2=(W_{22}/\omega_2^2)-(W_{12}/\omega_1\omega_2)$$

with $(W_{ij}/\omega_i\omega_j)$ as the respective cohesive energy densities of solvent, polymer segments, and mixture. The first term on the right side of (4) takes into account the contribution of the solvent molecules, so that in the general case a plot of l^2 vs r^2 or of l vs $\bar{M}_n$ does not go through the origin. If there is a Gaussian density distribution of polymer segments, r^2 should be proportional to $\bar{M}_n$, and the plot in Fig. 5 should be linear. Although our results suggest nonlinearity, we think that a definite conclusion should be based on a larger number of experimental points. Since we have determined r^2 for sample $G(M_n=1\,000\,000)$, we may calculate the factor in front of r^2 in (4). If we extrapolate l^2 toward $M_n=0$, it appears that the first term in (4) is approximately equal to 350 A^2. Therefore,

$$\Delta_2/(\Delta_1+\Delta_2)=(l^2-350)/2r^2=0.061.$$

To calculate $\Delta_2/(\Delta_1+\Delta_2)$ from cohesive energy densities would in most cases require an exceedingly accurate knowledge of the latter; it is clear that in the case of $W_{11}/\omega_1^2\cong W_{22}/\omega_2^2\cong W_{12}/\omega_1\omega_2$ the quotient of the differences will be very sensitive to small variations of the cohesive energy densities. The smallness of l as compared with r is striking. Therefore it seems to be of interest whether other polymer-solvent systems give a similar result.[11]

The extension of a polymer coil of given molecular weight in solution appears to be quite dependent on the temperature and on the concentration of the polymer. Our results show that the radius of gyration in a solution of polystyrene $(M_n=1\,000\,000)$ in cyclo-

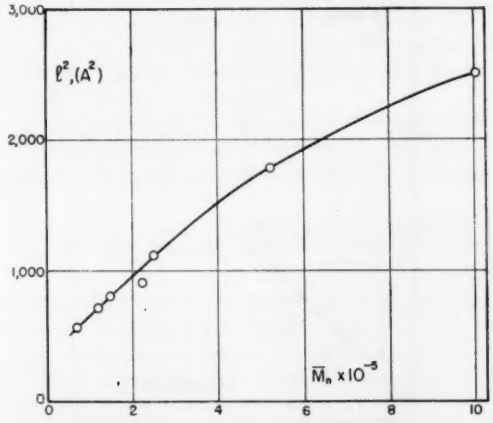

FIG. 5. Plot of interaction parameter against molecular weight of polystyrene, in cyclohexane.

[11] The system polyisobutylene-diisobutyl ketone is presently being investigated by the authors.

hexane, at the critical concentration, changes from 133 A near 30° to 169 A at 40°C. At infinite dilution (40°C) the radius of gyration for our sample G was estimated as 350 A. This result was obtained from slope and intercept of the limiting line at zero concentration in a Zimm plot. Under the condition that $r^2=R^2/6$, R being the end-to-end distance of the polystyrene coil, one calculates on the basis of the data reported by Notley and Debye[8] that r is approximately equal to 335 A for the same molecular weight if one interpolates for a temperature of 40°. Data by Krigbaum and Carpenter[12] lead to a result which is about 10% higher if one applies the relation $r_1^2/r_2^2=M_1/M_2$, and interpolates for 40°. The radii of gyration at infinite dilution, as obtained by these authors, likewise show an increase with temperature. The temperature dependence, expressed as $(1/r^2)[d(r^2)/dT]$, in our case was found to be approximately equal to $0.07°C^{-1}$ (40°, critical concentration). From the data by Krigbaum and Carpenter we estimated a temperature coefficient of $0.027°C^{-1}$ (40°, infinite dilution). Yet, the temperature dependence of these coefficients is not the same in both cases: around 33°, for instance, the two coefficients are about the same, viz., $0.08°C^{-1}$. We note again, that we assumed only r to vary with temperature, while l does not change with the temperature distance from the consolute point.

[12] W. R. Krigbaum and D. K. Carpenter, J. Phys. Chem. **59**, 1166 (1955).

ACKNOWLEDGMENT

The authors gratefully acknowledge the financial support given by the National Science Foundation and by the Office of Naval Research.

THE JOURNAL OF CHEMICAL PHYSICS VOLUME 33, NUMBER 6 DECEMBER, 1960

Heat Capacity of Ice at Low Temperatures

P. FLUBACHER,* † A. J. LEADBETTER,* ‡ AND J. A. MORRISON

Division of Pure Chemistry, National Research Council, Ottawa, Canada

(Received June 17, 1960)

The heat capacity of normal hexagonal ice has been measured over the temperature range 2° to 27°K with an estimated precision varying between ±2% at the lowest temperatures and ±0.2% at the higher temperatures. The results agree satisfactorily with those of earlier measurements in the region $T>10°K$, and do not significantly affect the value of the residual entropy of ice calculated by Giauque and Stout [W. F. Giauque and J. W. Stout, J. Am. Chem. Soc. **58**, 1144 (1936)]. Although the new results do not influence the existing thermodynamic description of ice, they provide information which is important in understanding its vibrational properties. In the first place, extrapolation of the results to $T=0°K$ yields a value of Θ_0, the Debye characteristic temperature corresponding to continuum behavior. This is found to agree satisfactorily with Θ (elastic) estimated from the elastic constants of ice. In the second place, complete $\Theta_D(T)$ curves can be constructed, and an examination of these, computed for different sizes of vibrational unit, enables the gross features of the lattice frequency spectrum of ice to be determined. The conclusion reached is that the three components of the spectrum, due respectively to translational and rotational vibrations of the water molecule and to intramolecular vibrations, are well separated. The contribution of the librational modes to the thermodynamic properties can be approximated rather well by a single frequency of 620 cm^{-1}.

INTRODUCTION

THE heat capacities of molecular crystals at very low temperatures ($T<10°K$) have received remarkably little attention. Most calorimetric work with such crystals has had as its object the determination of entropies, and a knowledge of the heat capacity down to solid hydrogen temperatures has been adequate for this purpose. However, in any attempt to use the heat capacity to derive information about the vibrational properties of the crystal lattices, measurements to much lower temperatures are very desirable.

Recently, Giguére[1] has drawn attention to the fact that at low temperatures ($T<100°K$) the heat capacity of ice departs markedly from that given by the Debye model. The question which Giguére raises is to what extent the heat capacity of ice should be considered anomalous. Giguére compares ice with solid H_2O_2, the heat capacity of which appears to follow the Debye model more closely, and concludes that the thermodynamic properties of ice are anomalous. It is important to note, however, that on general grounds[2] some variation in $\Theta_D(T)$ must be expected at low temperatures. In fact, $\Theta_D(T)$ should verge upon a constant value only in the region $T<\Theta_D/50$, which is appreciably below the lowest temperature reached in Giauque and Stout's experiments[4] and in the experi-

* National Research Council Postdoctorate Research Fellow.
† Present address: Reaktor Ltd., Würenlingen, Switzerland.
‡ Present address: Department of Physical and Inorganic Chemistry, The University, Bristol 8, England.

[1] P. A. Giguére, J. Phys. Chem. Solids **11**, 249 (1959).

[2] M. Blackman, *Handbuch der Physik*, edited by E. Flügge (Springer-Verlag, Berlin, 1955), Vol. 7, part 1, p. 325.

TABLE I. Measured heat capacities of ice.

T (°K)	C_p (cal/mole deg.)
Series I	
11.462	0.1018
12.549	0.1362
13.539	0.1728
14.509	0.2119
15.522	0.2561
16.502	0.3034
17.437	0.3459
18.957	0.4226
21.060	0.5348
23.108	0.6449
25.089	0.7503
27.034	0.8509
Series II(a)	
2.415	0.000640
2.895	0.001109
3.397	0.001860
3.914	0.002873
Series II(b)	
2.144	0.000418
2.586	0.000724
3.114	0.001278
3.651	0.002070
4.151	0.003180
4.650	0.004659
5.182	0.006486
5.738	0.009075
6.258	0.01261
6.724	0.01632
7.246	0.02123
7.907	0.02878
8.786	0.04141
9.871	0.06223
11.098	0.09154
12.228	0.1247
Series III	
12.431	0.1327
13.525	0.1711
14.625	0.2156
15.609	0.2588
16.567	0.3041
17.829	0.3666
19.742	0.4637
Series IV(a)	
4.741	0.004901
5.272	0.006829
5.799	0.009307
Series IV(b)	
2.686	0.000787
3.182	0.001406
3.669	0.002192
4.145	0.003080
Series IV(c)	
2.548	0.000655
3.089	0.001268
3.582	0.001975
4.044	0.002979
Series IV(d)	
2.798	0.000887
3.725	0.002319
4.759	0.004775
5.737	0.009629
6.735	0.01648
7.799	0.02731
8.898	0.04305
9.955	0.06396
11.109	0.09138

ments on H_2O_2. The question posed by Giguére therefore requires further investigation.

In the present paper we describe measurements of the heat capacity of ice down to 2°K. The results, together with those of Giauque and Stout,[4] show that the temperature dependence of $\Theta_D(T)$ of ice cannot be taken as unusual. It also becomes clear that the number of degrees of freedom assumed is important in the comparison of $\Theta_D(T)$ for different substances.

EXPERIMENTAL

The heat capacity measurements were made with a calorimeter assembly designed for experiments on condensed gases in the temperature range 2° to 300°K. A detailed description of the calorimeter will be given elsewhere.[3] It is sufficient to mention here that the working thermometers were a platinum resistance thermometer (for $T>11$°K) and a carbon thermometer (for $2°<T<11$°K). A consistent temperature scale for the thermometers was established using the calorimeter vessel as a gas thermometer.

The water used had been distilled from alkaline $KMnO_4$ and was degassed by several cycles of alternate freezing, pumping and melting. The sample (8.170g) was distilled into the calorimeter vessel and frozen rapidly after it had first been ensured that no condensed water was left in the filling tube. The ice was cooled to about 100°K over a period of five hours. While the vapor pressure of the ice was still appreciable, the temperature of the filling tube was kept well above that of the calorimeter vessel. No exchange gas was used inside the calorimeter vessel and no difficulty with long equilibrium times was experienced.

RESULTS

The measured heat capacities are given in Table I in the order of their determination and are shown graphically in Fig. 1 which is a plot of C/T^3 against T^2. The measurements in each series were made during the course of one day.

It will be noted that a distinction is made for the measurements in series II(a) which lie systematically above the others by about 9%. These results could not be reproduced and no satisfactory explanation for their departure was found. Between series II and III the ice specimen was warmed up to near its melting point and cooled again in roughly the same manner as for the initial cooling.

Previous heat capacity results obtained by Giauque and Stout[4] in the region $T>15°K$ and by Simon[5] for a narrow range around 10°K are also shown in Fig. 1. The agreement between these results and the present ones is quite acceptable.

[3] P. Flubacher, A. J. Leadbetter, and J. A. Morrison (to be published).

[4] W. F. Giauque and J. W. Stout, J. Am. Chem. Soc. **58**, 1144 (1936).

[5] Simon's results are quoted by Giauque and Stout.[4]

DISCUSSION

a. Zero Point Entropy

It now seems to be generally agreed that the finite zero point entropy of ice is due to frozen-in configurational disorder of the water molecules. Both theory and experiment suggest[6] that the freezing-in process occurs in the vicinity of liquid air temperatures. The effect of the present results on the numerical value of the zero point entropy determined previously[4] (0.82 cal/mole deg) is quite negligible. The total entropy change below 10°K is only 0.02 cal/mole deg.

b. Comparison with Elastic Properties

We next consider the behavior of the heat capacity in the limit as T approaches 0°K. We should expect to see C/T^3 approach a limiting value which, if only acoustic waves of long wavelength are being excited at the very low temperatures, should agree with C/T^3 calculated from the elastic constants of ice. The experimental results (Fig. 1) show that C/T^3 is changing rather rapidly even at the lowest temperatures; but a smooth extrapolation of the curve drawn through the experimental points to $T^2=0$ yields $(C/T^3)_0=4.00\times 10^{-6}$ cal/mole deg.[4] The elastic constants of ice have only been measured in the temperature range $-30°$ to 0°C, and so a considerable extrapolation is required to compare them with the low temperature thermal results. However, if the extrapolation is made using the mean velocity rather than the elastic constants, the uncertainty introduced is not large. Mean velocities were computed for us by Dr. O. L. Anderson of the Bell Telephone Laboratories; the average value at −16°C obtained from available elastic constant data[7-9] was $2.18\pm 0.02\times 10^5$ cm/sec and the temperature coefficient determined from the data of Bass *et al.*[9] was −0.00145 cm/sec deg. If we assume that the temperacoefficient is constant we obtain $v_m(0°K)=2.55\times 10^5$ cm/sec which corresponds to $(C/T^3)_0=3.47\times 10^{-5}$ cal/mole deg.[4] This differs from the result of the thermal measurements by about 13%. The actual difference must be less than this, however, because the third law of thermodynamics requires the temperature coefficient of the velocity to tend to zero as T approaches 0°K. We may thus conclude that the results of thermal and elastic measurements are in reasonable agreement, and hence that optical modes of very low frequency are not contributing appreciably to the measured heat capacity at the lowest experimental temperatures.

Usually, the above comparison is made in terms of limiting Debye characteristic temperatures, Θ_0 and Θ (elastic), a calculation of which involves the number of vibrational degrees of freedom per mole (although the *comparison* is independent of this quantity[2]). It will be shown below that the appropriate choice for the very low temperature region is $3N$ degrees of freedom per mole (where N is the number of atoms) and on this basis we obtain $\Theta_0=226°K$ and Θ (elastic) $<238°K$.

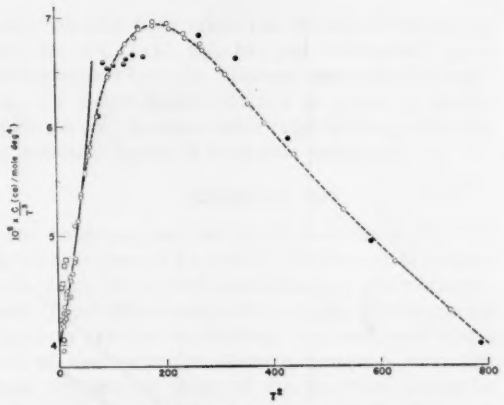

FIG. 1. A graph of C/T^3 against T^2 for ice. □ series II(a) and ○ other series, present results. ● Giauque and Stout.[4] ◒ Simon (quoted in footnote reference 4).

c. Vibrations of the Ice Lattice

Spectroscopic investigations[10] have shown that water molecules preserve their individuality in ice; for example, the three fundamental vibration frequencies of the molecule differ only slightly for water vapor and for ice. This means that there is only a slight coupling between inter- and intramolecular vibrations. Therefore, to a good approximation the contribution of the intramolecular vibrations to the thermodynamic properties may be considered independently. The fundamental frequencies in ice are so high (3252, 3143, and 1640 cm^{-1} [11]) that their contribution to the heat capacity is negligibly small below 200°K. Hence, below this temperature, the molar heat capacity of ice must be accounted for by $6N$ or less degrees of freedom ($3N$ for each of translational and rotational vibrations of the water molecules). The main problem is thus whether we can distinguish between the contributions of the two types of molecular vibration to the heat capacity. A simple approach is to examine $\Theta_D(T)$ graphs covering a wide temperature range; such graphs are shown in Fig. 2.

The values of $\Theta_D(T)$ were calculated from the results of the present work and that of Giauque and Stout.[4] Values of C_p-C_v were computed using thermal expansion coefficients reported by Powell,[12] and a constant value of the isothermal compressibility

[6] K. S. Pitzer and J. Polissar, J. Phys. Chem. **60**, 1140 (1956).
[7] F. Iona and P. Scherrer, Helv. Phys. Acta **25**, 35 (1952).
[8] R. E. Green and L. MacKinnon, J. Acoust. Soc. Am. **28**, 1292 (1956).
[9] R. Bass, D. Rossberg, and G. Ziegler, Z. Physik **149**, 199 (1957).
[10] For a summary see N. Ockman and G. B. B. M. Sutherland, Proc. Roy. Soc. (London) **A247**, 434 (1958).
[11] N. Ockman, Advances in Phys. **7**, 199 (1958).
[12] R. W. Powell, Proc. Roy. Soc. (London) **A247**, 464 (1958).

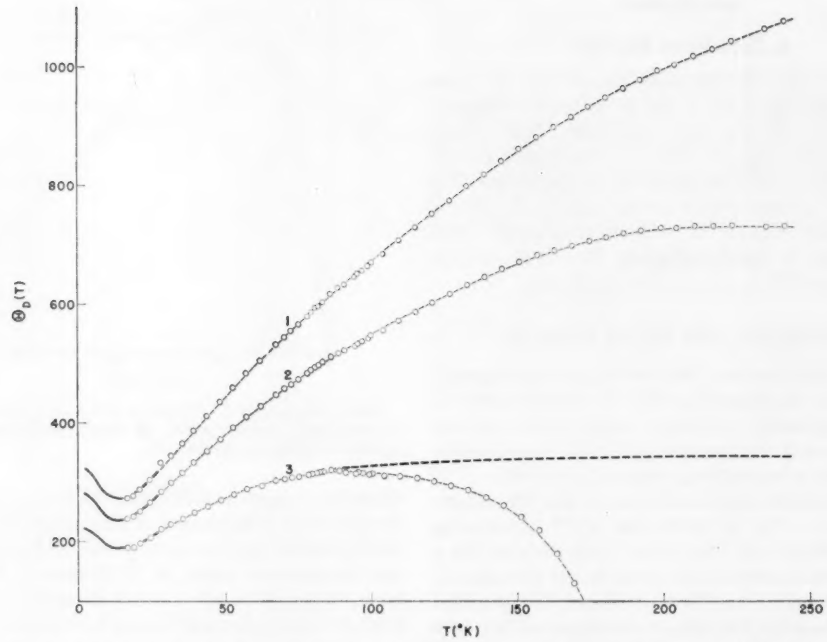

FIG. 2. Graphs of $\Theta_D(T)$ against T for different vibrational units. Curve 1, $9N$ vibrations; curve 2, $6N$ vibrations; curve 3, $3N$ vibrations. —— present results. ○ Giauque and Stout.[4] ------ extrapolation by means of the Thirring expansion.

(1.25×10^{-11} dynes/cm^2) corresponding to the elastic constants measured by Bass *et al.*[9] While the uncertainties in the expansion coefficients are large,[12,13] C_p-C_v is negligibly small below 80°K and only 1.4% of C_p at 200°K. It is therefore known sufficiently well for our present purpose which is to discuss the general shape of the $\Theta_D(T)$ curves.

Three curves are shown in Fig. 2 representing $3N$, $6N$, and $9N$ degrees of freedom per mole. $\Theta_D(T)$ for $9N$ degrees of freedom rises rapidly from a minimum at about 15°K and is still increasing markedly at the highest temperatures. This means that the general form of the lattice frequency spectrum as a whole departs strongly from that of a Debye spectrum. This can be accounted for in part by the fact that the $3N$ intramolecular vibrations are well separated from the remainder of the frequency spectrum.

The middle curve for $6N$ degrees of freedom also shows a very rapid rise at the lower temperatures; $\Theta_D(T)$ increases by about a factor of 3 between 15° and 150°K. This indicates that there is a further separation between other components of the spectrum, in particular those due to translational and rotational vibration of the molecules. The fact that the curve flattens off in the region $T>150$°K suggests that at such temperatures all $6N$ modes of vibration are contributing appreciably to the heat capacity.

[13] R. W. Powell, Advances in Phys. **7**, 276 (1958).

A clear separation between translational and librational branches of the frequency spectrum would have the consequence that over a range of low temperatures the $\Theta_D(T)$ curve for $3N$ degrees of freedom should show the behavior generally characteristic of simple solids. This proves to be so. The lowest curve in Fig. 2 shows that $\Theta_D(T)$ first decreases with increasing temperature to a minimum at about $T\sim\Theta_0/15$, then increases and flattens off in the vicinity of $T=\Theta_0/3$. These are characteristics of $\Theta_D(T)$ graphs of simple crystals (for examples, see footnote references 2, 14, and 15). In addition, the heat capacity in the region $T<\Theta_0/30$ can expressed in terms of the low temperature expansion

$$C=aT^3+bT^5+cT^7+\cdots \qquad (1)$$

(solid curve in Fig. 1).

The decrease in $\Theta_D(T)$ in the region $T>\Theta_0/3$ has been observed for some simple crystals[14,15] and has been ascribed[15,16] to the onset of anharmonicity in the lattice vibrations. Anharmonicity may indeed be a contributing factor in ice also, but when the $\Theta_D(T)$ curves for both $3N$ and $6N$ degrees of freedom are considered, we conclude that the dominant effect leading to the de-

[14] W. T. Berg and J. A. Morrison, Proc. Roy. Soc. (London) **A242**, 467 (1957).

[15] P. Flubacher, A. J. Leadbetter, and J. A. Morrison, Phil. Mag. **49**, 273 (1959).

[16] T. H. K. Barron, W. T. Berg, and J. A. Morrison, Proc. Roy. Soc. (London) **A242**, 478 (1957).

creasing $\Theta_D(T)$ for $3N$ degrees of freedom must be the excitation of the librational modes of vibration. This is confirmed by a further calculation.

The contribution of the translational modes in the region $T>80°K$ was estimated by an extrapolation using the Thirring expansion in a manner which has been described.[16] The course of the extrapolation is indicated by the heavy dashed portion of the lowest curve in Fig. 2. For the region $80°<T<200°K$ the difference between C_v (total) and C_v corresponding to the dashed curve was found to agree to better than 5% with an Einstein function representing $3N$ vibrations of frequency 620 cm^{-1}. This is of a magnitude expected for the librational frequencies in ice.[17] By comparing the heat capacities of H_2O ice and D_2O ice, Blue[18] has also concluded that librational contributions to the heat capacity become important in the region $T>80°K$.

Recently, Zajac[19] has studied thermal motion of the atoms in ice by investigating the effect of temperature on the reflection of x-rays in the range 0° to −90°C. He found that the thermal amplitudes of the oxygen atoms (and hence the translational motion of the water molecules) in ice could be represented by a single Debye characteristic temperature. This characteristic temperature is, of course, calculated from the Debye-Waller formula, and so to avoid confusion we indicate it by Θ_{DW}. In order to compare Θ_{DW} with the heat capacity results we note that it corresponds to the negative second moment of the lattice frequency spectrum, μ_{-2}. In particular,[2]

$$1/\Theta^2_{DW}=\tfrac{1}{3}(k/h)^2\mu_{-2} \qquad (2)$$

under the high temperature conditions of Zajac's experiments. A numerical value of μ_{-2} was computed from the measured heat capacities using a method which has been described.[16] The result $[6.29\times10^{-5}(h/k)^2]$, is equivalent to a characteristic temperature of 218°K, which is to be compared with $\Theta_{DW}=224\pm8°K$ obtained by Zajac. The agreement is much better than should be expected because thermal expansion of the lattice has only been taken into account through the correction of C_p to C_v. Θ_{DW} has been obtained at higher temperatures where the thermal expansion is large. Also, the Debye-Waller formula as given is strictly applicable only to monatomic cubic lattices, while ice is a molecular crystal of hexagonal symmetry.

[17] P. A. Giguére and K. B. Harvey, J. Mol. Spectroscopy **3**, 36 (1959).
[18] R. W. Blue, J. Chem. Phys. **22**, 280 (1954).
[19] A. Zajac, J. Chem. Phys. **29**, 1324 (1958).

SUMMARY

The foregoing analysis shows that the lattice frequency spectrum of ice consists of three main components which, to a good approximation, are well separated. These three components are the intramolecular vibrations and the translational and rotational vibrations of the molecules. More information than this about the detailed shape of the spectrum cannot be obtained from the heat capacity alone.[20] Hence, it may not be concluded that the librational portion of the spectrum consists of a single sharp peak at 620 cm^{-1}.

The deviation of the translational portion of the frequency spectrum of ice from a Debye spectrum is similar to deviations shown by spectra of simpler crystals. The low temperature heat capacity of ice cannot therefore be taken as anomalous as has been suggested by Giguére.[1] Instead, the $\Theta_D(T)$ graphs of the other substances discussed by Giguére, viz., H_2O_2, NH_3 and HCN, which showed agreement with the Debye model at low temperatures, should be viewed with reserve. In these substances librational motion of the molecules gives rise in general to some lower frequencies than in ice, and so it is probable that their low temperature heat capacities contain unseparable contributions from both translational and librational modes. If this is correct, it would be more appropriate to refer $\Theta_D(T)$ to more than $3N$ vibrations; such a change will produce $\Theta_D(T)$ curves rather like that of ice.

ACKNOWLEDGMENTS

We should like to thank Dr. T. H. K. Barron for very helpful comments and suggestions. Also, we have benefited from a number of discussions with Professor P. A. Giguére.

[20] T. H. K. Barron and J. A. Morrison, Proc. Roy. Soc. (London) **A256**, 427 (1960).

THE JOURNAL OF CHEMICAL PHYSICS VOLUME 33, NUMBER 6 DECEMBER, 1960

First-Order Phase Transitions of Six Normal Paraffins at Elevated Pressures

R. R. NELSON,* W. WEBB, AND J. A. DIXON

College of Chemistry and Physics, The Pennsylvania State University, University Park, Pennsylvania

(Received June 27, 1960)

First order phase transitions were investigated for *n*-nonane, *n*-dodecane, *n*-tridecane, *n*-pentadecane, *n*-octadecane, and *n*-tetracosane, at pressures up to 10 kilobars and temperatures up to 135°C. By a modification of standard piezometric techniques, phase transition pressures, as well as the associated isothermal isobaric volume changes were determined at approximately 25°C intervals. Correlations established between the melting temperatures and the specific volume changes associated with phase transitions and the *n*-paraffin chain lengths show a strong dependence upon whether the *n*-paraffin is of odd or even species. This dependence becomes more pronounced at higher pressures. The specific volume, enthalpy, and entropy changes showed no dependence upon chain length at the same melting temperature.

INTRODUCTION

SINCE 1947, the investigation of the volumetric and viscosity behavior of liquid hydrocarbons at high pressure and at a variety of temperatures has been pursued at the High Pressure Laboratory of the Pennsylvania State University. One of the principle objectives of this work has been to establish correlations between the high-pressure behavior of the liquid hydrocarbons and their structure. In this regard, isothermal compressions have been studied for 13 hydrocarbons and two binary mixtures of them by Cutler, McMickle, Webb, and Schiessler.[1] In addition, the temperature-pressure-structure effects on the viscosity of 20 high molecular weight hydrocarbons have been examined by Griest, Webb, and Schiessler[2] and by Lowitz, Spencer, Webb, and Schiessler.[3]

This paper presents an extension of the study of physical behavior at high pressure and the correlation of such behavior with molecular structure. Since this is to be the beginning of a systematic study of high-pressure phase transitions in pure hydrocarbons and correlation with structure, the compounds studied were *n*-paraffins which possess a relatively simple structure with only one variable within the series, molecular length.

The melting characteristics of a number of liquid hydrocarbons have been published by Bridgman,[4–8] Deffet,[9–11] Swallow and Gibson,[12] and Tammann.[13] However, the wide variety of structure and experimental ranges of pressure and temperature represented in these investigations make any structure correlations extremely difficult.

EXPERIMENTAL METHODS AND PROCEDURES

The experimental techniques employed were modifications of those used for the study of liquid compressibilities. The material under investigation was enclosed within a thin-walled lead capsule. The capsule was sealed within a metal bellows, the remaining volume of which was filled with a plasticizer, di-2-ethylhexyl adipate-dioctyl adipate (Adipol 2EH manufactured by Ohio Apex Company), as a pressure transmitting fluid. Changes in the longitudinal dimension of the bellows determined the compression of its total contents. First-order phase transitions in the material were evident as discontinuities in the change of the length of the bellows with pressure. The specific volume change associated with the transition was derived from the magnitude of this discontinuity and the weight of the sample.

Pressure System

The pressure system was capable of producing a pressure somewhat in excess of 10 kilobars within a working volume the dimensions of which are 14 cm long by 2.2 cm in diam. A primary pressure of 1300 bars was produced by a hand operated pump. Higher pressures were produced by subsequent use of either a 4:1 or 9.5:1 intensifier. Except for valve packings, all of the packings were of the Bridgman unsupported area type.[14]

Pressure measurement was based upon an American Instrument Company dead weight gauge with a capacity of about 3400 bars. For interpolation of pressure values within the capacity of the dead weight gauge, and for extrapolation of values beyond its capacity, a manganin wire pressure gauge[15,16] was used. The manganin wire gauge used in this study consisted of a spiral of 40 B and S gauge silk covered manganin wire which was helically wound on a lithograph limestone form in a manner suggested by the National Bureau of

* Present address: Department of Physics, Occidental College, Los Angeles, California.

[1] W. G. Cutler, R. W. McMickle, W. Webb, and R. W. Schiessler, J. Chem. Phys. **29,** 727 (1958).

[2] E. M. Griest, W. Webb, and R. W. Schiessler, J. Chem. Phys. **29,** 711 (1958).

[3] D. A. Lowitz, J. W. Spencer, W. Webb, and R. W. Schiessler, J. Chem. Phys. **30,** 73 (1959).

[4] P. W. Bridgman, Proc. Am. Acad. Arts Sci. **49,** 1 (1913).

[5] P. W. Bridgman, Proc. Am. Acad. Arts Sci. **59,** 141 (1923).

[6] P. W. Bridgman, Proc. Am. Acad. Arts Sci. **66,** 185 (1931).

[7] P. W. Bridgman, Proc. Am. Acad. Arts Sci. **67,** 1 (1931).

[8] P. W. Bridgman, Proc. Am. Acad. Arts Sci. **77,** 129 (1949).

[9] L. Deffet, Bull. soc. chim. Belges **44,** 41 (1935).

[10] L. Deffet, Bull. soc. chim. Belges **49,** 223 (1940).

[11] L. Deffet, Bull. soc. chim. Belges **51,** 237 (1942).

[12] J. C. Swallow and R. O. Gibson, J. Chem. Soc. **1934,** 440.

[13] G. Tammann, Ann. Physik **68,** 553 (1899).

[14] P. W. Bridgman, *The Physics of High Pressure* (G. Bell and Sons, Ltd., London, 1952).

[15] P. W. Bridgman, Proc. Am. Acad. Arts Sci. **47,** 321 (1911).

[16] P. W. Bridgman, Proc. Roy. Soc. (London) **A203,** 1 (1950).

Standards.[17] The length of manganin wire was about one meter and had a resistance of about 125 ohms. The changes in resistance were measured by a Carey-Foster bridge. Resistance changes in the manganin wire gauge due to temperature fluctuations were avoided by placing the gauge in the temperature controlled working volume of the high pressure system. Error in the measurement of absolute pressure was less than 10 bars at pressures below 1000 bars and less than 1% at pressures above 1000 bars.

Temperature Regulation

Phase transitions were investigated at seven temperatures, 15.56°, 37.78°, 60.00°, 79.44°, 98.89°, 115.00°, and 135.00°C. The working volume of the high-pressure system was immersed in a circulating bath of peanut oil, the temperature of which was controlled within 0.1°C of the desired value. The operating temperature was established using NBS calibrated mercury-in-glass thermometers. Owing to the thermal lag of the massive high pressure vessel, the temperature within the working volume probably fluctuated less than 0.05°C from the desired temperature.

Sample Encapsulation Procedure

The technique used in this study required that the material being investigated be sealed within a capsule. The capsule walls had to be capable of transmitting hydrostatic pressure and capable of withstanding extreme and repeated flexure without rupture. It was further required to make the seal without heating the capsule contents so that its high purity could be maintained.

It was found that a capsule made of pure lead possessed the required characteristics and that such a capsule could be adequately sealed by a cold-solder technique described by Bridgman.[18] A lead melting point standard supplied by the National Bureau of Standards proved to be of sufficient purity since no work-hardening of the lead was apparent after repeated flexure. The lead was extruded to form a thimble with a length of $1\frac{1}{8}$ in., a diameter of $\frac{7}{16}$ in., and a wall thickness of $\frac{1}{32}$ in. The thimble was partially filled with molten rosin which had previously been dissolved in ethyl alcohol, filtered, and heated to evaporate the alcohol in the filtrate. The rosin, when cooled, provided the capsule with sufficient rigidity so that it could be held in a lathe collet for the next operation, the closure of the open end of the thimble by a ball-shaped spinning tool. After closure a small opening with a conical edge was made with a $\frac{1}{16}$-in. standard 60° taper center drill. The rosin within the capsule was then removed by dissolving it with a fine jet of ethyl alcohol.

For filling, the clean capsule was placed in a cavity of a jig used for the sealing operation. The cavity provided a close fit to the capsule and was slightly deeper than the over-all length of the capsule. The liquid hydrocarbon sample was injected into the capsule by a hypodermic needle and allowed to overflow, submerging the capsule. The jig containing the sample and capsule was then subjected to a vacuum in order to remove air bubbles and dissolved gases from the sample.

The capsule was sealed by a lead rod which had been machined to a 60° conical point. Immediately after machining, the point was dipped into freshly prepared mercury-sodium amalgam, then fitted to the capsule opening. Alignment of the rod with the axis of the capsule was assured by the jig. A 2-kg weight was placed on the rod and left for at least a day to aid in the cold soldering. The sodium-mercury amalgam was prepared by dissolving five or six pieces of metallic sodium, each the size of a wheat grain, in about 10 g of mercury. After sealing, the rod was sawed off near its point leaving a filled capsule as shown in Fig. 1.

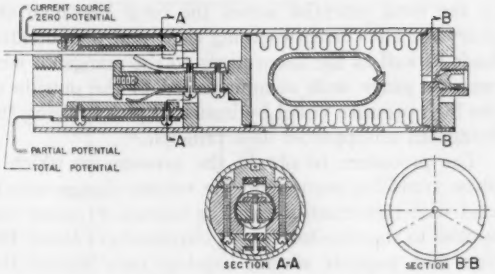

FIG. 1. Sectioned view of the densitometer showing the lead capsule enclosed within the bellows.

The weight of the sample was obtained by comparing the weight of the filled capsule with the weight of the lead comprising the capsule. The filled capsule was weighed before and after use to detect possible leakage of the capsule contents. Three phase transition determinations proved to be the average life of a capsule.

Measurement of Volume Changes

The instrument used for the measurement of volume changes associated with phase transitions at high pressure is a modification of the piezometer described by Cutler *et al.*[1] A sectioned view of the instrument, hereafter referred to as the *densitometer*, is shown in Fig. 1. Changes in the length of the bellows result in a longitudinal movement of an extension of the bellows upon which are mounted two opposed electrical contactors. The upper contactor bears upon a current-carrying slidewire. The electrical potential of the slidewire at the point of contact is transmitted to the exterior of the densitometer via the opposed contactor which slides along an insulated contact bar. By a calibration procedure, a correspondence can be established between the change in the volume of the bellows and a change in the ratio of the partial potential along the slidewire

[17] Natl. Bur. Standards Tech. News Bull. **40**, No. 7 (1956).
[18] P. W. Bridgman, Proc. Am. Acad. Arts Sci. U. S. **74**, 399 (1942).

to the total potential across the total length of the slidewire. The current-carrying leads and the potential leads as well as the connections to the manganin wire pressure gauge were communicated to the outside of the high pressure vessel by insulated pins utilizing the Bridgman unsupported area principle.[14]

The procedure to obtain the pressure at which a phase transition occurs and the volume change associated with this transition was as follows. Pressure was applied to the densitometer in increments of about 100 bars to a pressure several hundred bars beyond the highest pressure phase transition. Since superpression was present in many of the determinations, it was necessary to use the pressure at which melting occurred during decompression to obtain the thermodynamic equilibrium values for the transition pressure and volume changes. That these melting pressures were the equilibrium pressures was verified experimentally in every case by noting that melting could be stopped and refreezing obtained by increasing the pressure slightly, 10 to 20 bars, above the pressure at which melting was occurring. It was necessary to make this check before all of the solid had transformed otherwise superpression occurred again. The melting pressures were experimentally repeatable but the freezing pressures were not, that is the amount of superpression varies erratically. Decompression was in steps of about 50 bars until the expected transition pressure was approached, then the pressure was reduced in 20-bar increments. A transition was apparent as an isobaric, isothermal volume change of the bellows.

Corrections were applied to the volume change values obtained by the densitometer in order to compensate for changes in the size of the densitometer due to thermal and pressure effects. The total correction applied was less than 1% over the entire temperature and pressure ranges investigated.

To supplement the phase transition data at high pressure, atmospheric pressure phase transition data were obtained for those compounds for which such data were not available from the open literature. Standard dilatometric technique was used to obtain both the atmospheric pressure transition temperatures and the associated volume changes. The dilatometer was constructed so that mercury was in contact with the sample and would follow its volume changes. The mercury was communicated to a calibrated precision bore capillary enabling measurement of the isobaric, isothermal phase transition specific volume changes to a probable error of less than 0.001 cm^3/g. The temperature range of the dilatometer was, of course, limited to temperatures above the freezing point of mercury.

EXPERIMENTAL RESULTS

The transition pressure was taken as the interpolated pressure corresponding to the greatest volume change. The compounds used were of sufficient purity to make the lack of abruptness in the volume change negligible. The volume change associated with the phase transition was obtained by graphically determining the magnitude of the discontinuity in the volume-pressure curve. The uncertainty in the phase transition pressure corresponding to a particular temperature is not only dependent upon the uncertainty in pressure measurement but also upon the lack of sharpness of the discontinuity in the isothermal expansion curve. As the phase transition pressure is approached from a higher pressure, the volume change of the sample is not abrupt, resulting in a "knee" in the pressure-volume curve. The extent of the knee is a sensitive measure of the lack of purity of the sample,[14] and was used as such in this investigation. For all of the *n*-paraffins examined, the extent of the knee was small, 100 bars at most.

The phase transition pressure obtained from the data was the interpolated pressure at which the greater portion of the volume change took place. To obtain the best values for the phase transition pressures, the experimental values were smoothed graphically. The smoothed pressure values were obtained from the curve at temperatures corresponding to the original data. The rms deviation of the unsmoothed pressure from the smoothed values is 27 bars which is comparable to the uncertainty of the phase transition pressure for a single determination.

The smoothed values of the phase transition pressure and the corresponding values of the phase transition curve slopes are presented in Table I. In this tabulation, two solid phases of a single compound are denoted as solid I and solid II. Solid II is the solid form existing at pressure values where only one solid phase is present and solid I is the first solid form obtained in the atmospheric pressure freezing of the liquid. Figures 2 and 3 are phase diagrams of the *n*-paraffins exhibiting a solid phase transition, a curve with a smoothly varying slope is shown separating the liquid phase region from the solid phases. Although it is known from thermodynamics that a discontinuity in the slope of this curve exists at the triple point, the discontinuity was so small as to not be revealed by the experimental data.

The specific volume changes associated with the phase transitions were also smoothed and are presented in Table II. The rms deviation of the unsmoothed specific volume changes from the smoothed experimental values is 0.0014 cm^3/g. The specific volume change on fusion decreases with pressure by about 50% over a pressure range of 1–8000 bars and a temperature range of 15–135°C, if ΔV is the volume of the liquid minus the volume of the most dense solid. The ΔV curves are convex toward the pressure axis, suggesting that they do not approach zero.

The pressure-temperature transition curves are also convex toward the pressure axis. The slopes dp/dT almost double with increasing pressure in the temperature range of the experiments. The spans: 49.9 bar/°C to 98.9 bar/°C for n–C_{12} between 15.56°C, and 115°C, and 41.5 bar/°C to 79.9 bar/°C for n–C_{18} between

37.78°C and 135°C are typical. These also illustrate the general decrease of the slope of the transition curves with molecular weight.

These results are in agreement with those observed by Bridgman for hydrocarbons.

DISCUSSION

The shape of the melting curves for the *n*-paraffins as shown in Figs. 2 and 3 is typical of the melting curves

TABLE I. The smoothed transition pressures and the slopes of the transition curves. Atmospheric pressure transition temperatures, when obtained from the literature, are referenced accordingly.

Compound	Type of transition	Temperature (°C)	Pressure (bars)	(dP/dT) (bars/°C)
n-C_9	Liquid-solid I	−53.5[a]	1	74.6
		15.56	4805	87.8
	Solid I-solid II	...	1	...
		15.56	4965	
	Liquid-solid II	37.78	6795	94.9
		60.00	9030	105.5
n-C_{12}	Liquid-solid	−9.5[b]	1	43.1
		15.56	1175	49.9
		37.78	2390	57.0
		60.00	3775	65.7
		79.44	5155	74.7
		98.89	6712	86.1
		115.00	8192	98.9
n-C_{13}	Liquid-solid I	−5.3[c]	1	42.5
		15.56	1050	55.5
	Solid I-solid II	−17.9	1	41.1
		15.56	1442	45.7
	Liquid-solid II	37.78	2430	67.4
		60.00	4040	77.6
		79.44	5605	84.6
		98.89	7310	90.9
n-C_{16}	Liquid-solid I	9.9[b]	1	45.1
		15.56	280	47.7
		37.78	1400	55.1
	Solid I-solid II	−2.0	1	38.1
		15.56	704	41.6
		37.78	1664	46.8
	Liquid-solid II	60.00	2735	64.0
		79.44	4075	73.5
		98.89	5615	84.7
		115.00	7055	96.0
		135.00	9115	114.0
n-C_{18}	Liquid-solid	27.8[b]	1	38.4
		37.78	400	41.5
		60.00	1408	49.0
		79.44	2450	56.6
		98.89	3620	64.0
		115.00	4705	70.7
		135.00	6220	79.9
n-C_{24}	Liquid-solid I	50.3[c]	1	39.6
		60.00	405	41.8
	Solid I-solid II	48.1[c]	1	41.9
		60.00	416	41.9
	Liquid-solid II	79.44	1270	46.9
		98.89	2260	53.7
		115.00	3175	60.7
		135.00	4508	72.2

[a] F. D. Rossini *et al.*, *Selected Values of Physical and Thermodynamic Properties of Hydrocarbons and Related Compounds, American Petroleum Institute Project 44* (Carnegie Press, Pittsburgh, Pennsylvania, 1953).

[b] R. W. Schiessler and F. C. Whitmore, Ind. Eng. Chem. **47**, 1660 (1955).

[c] P. R. Templin, Ind. Eng. Chem. **48**, 134 (1956).

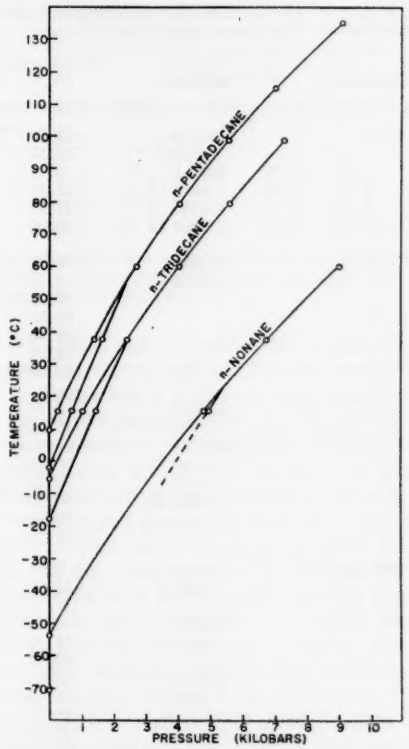

FIG. 2. Phase transition curves for the odd *n*-paraffins showing the existence of a solid phase modification. The solid-solid transition in *n*-nonane is not defined due to lack of experimental data below 15.56°C.

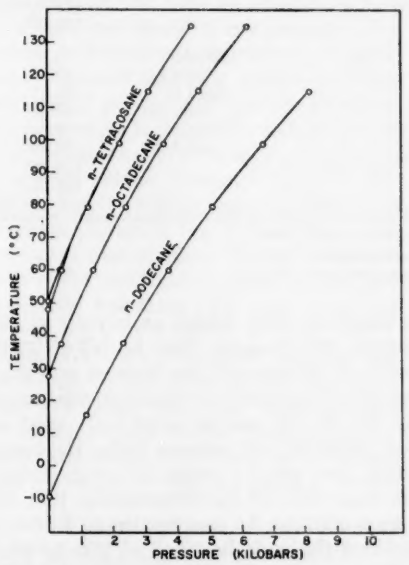

FIG. 3. Phase transition curves of the even *n*-paraffins.

TABLE II. The thermodynamic variables of first-order phase transitions in *n*-paraffins.

Compound	Type of transition	Temperature (°C)	ΔV (cm³/g)	ΔH (cal/g)	ΔU (cal/g)	ΔS (cal/g-°K)
n-C_9	Liquid-solid I	−53.5[a]	0.0737	28.83[a]	28.83	0.131
		15.56	0.0759	45.97	37.26	0.159
	Solid I-solid II	...	...	...	...	...
		15.56	0.0172	...	...	...
	Liquid-solid II	37.78	0.0714	50.34	38.75	0.162
		60.00	0.0696	58.45	43.43	0.175
n-C_{12}	Liquid-solid	−9.5[b]	0.1826	49.55	49.55	0.188
		15.56	0.1510	51.99	47.75	0.180
		37.78	0.1272	53.85	46.59	0.173
		60.00	0.1098	57.44	47.54	0.172
		79.44	0.0977	61.47	49.44	0.174
		98.89	0.0862	65.99	52.17	0.177
		115.00	0.0771	70.72	55.63	0.182
n-C_{13}	Liquid-solid I	−5.3[b]	0.1283	34.90	34.90	0.130
		15.56	0.1001	38.31	35.80	0.133
	Solid I-solid II	−17.9	0.0348	8.72	8.72	0.034
		15.56	0.0421	13.27	11.82	0.046
	Liquid-solid II	37.78	0.1188	59.48	52.59	0.191
		60.00	0.0948	58.56	49.41	0.176
		79.44	0.0832	59.30	48.16	0.168
		98.89	0.0710	57.37	44.97	0.154
n-C_{15}	Liquid-solid I	9.9[b]	0.1292	40.02	40.02	0.141
		15.56	0.1211	39.84	39.03	0.138
		37.78	0.0966	39.54	36.31	0.127
	Solid I-solid II	−2.0	0.0393	9.70	9.70	0.036
		15.56	0.0392	11.25	10.59	0.039
		37.78	0.0395	13.73	12.16	0.044
	Liquid-solid II	60.00	0.1127	57.41	50.05	0.172
		79.44	0.0949	58.77	49.53	0.166
		98.89	0.0803	60.45	49.68	0.162
		115.00	0.0708	63.04	51.11	0.162
		135.00	0.0619	68.81	55.33	0.169
n-C_{18}	Liquid-solid	27.8[b]	0.1953	53.95	53.95	0.179
		37.78	0.1800	55.48	53.76	0.178
		60.00	0.1456	56.82	51.92	0.170
		79.44	0.1249	59.56	52.25	0.168
		98.89	0.1090	62.00	52.57	0.166
		115.00	0.0994	65.18	54.01	0.167
		135.00	0.0901	70.19	56.80	0.172
n-C_{24}	Liquid-solid I	50.3[c]	0.1215[c]	37.18	37.18	0.115
		60.00	0.0975	32.45	31.51	0.097
	Solid I-solid II	48.1[c]	0.0662[c]	21.29	21.29	0.066
		60.00	0.0851	28.38	27.53	0.085
	Liquid-solid II	79.44	0.1465	57.89	53.45	0.164
		98.89	0.1237	59.06	52.37	0.159
		115.00	0.1127	63.43	52.88	0.163
		135.00	0.1037	73.01	61.85	0.179

[a] Footnote reference a, Table I.
[b] Footnote reference b, Table I.
[c] Footnote reference b, Table I.

of all substances which exhibit an increase of melting temperature with pressure. That is, $(dT/dP)>0$ and $(d^2T/dP^2)<0$. Bridgman[14] has pointed out that the existence of a critical point for the liquid solid transition requires that the ΔV and the latent heat vanish simultaneously while dT/dP remains finite. He concluded from data over greater ranges of temperature and pressure than those of this investigation that critical points were unlikely. An examination of Tables I and II shows that the latent heat and ΔV give no evidence of vanishing together, in fact most of the latent heats are increasing, in agreement with the findings of Bridgman. Whereas the present state of the theory of phase transition does not yield an analytical expression for the melting curve of compounds as complex as *n*-paraffins, an empirical expression would be of value in correlation studies. A number of types of simple functions have been examined which have either failed to describe adequately the experimental results, or are not conducive to fitting by experimental data. An empirical expression which adequately described the melting curve of a number of substances is that pro-

posed by Simon and Glätzel,[19] which may be written as

$$\ln(a+P)=c\ln T+b,$$

where T is the absolute melting temperature corresponding to the pressure, P, and a, b, and c are constants. The criterion for a fit to this expression is that $T(dP/dT)$ will vary linearly with pressure. Using this criterion, of all the melting curves of the *n*-paraffins studied, only that of *n*-octadecane seems to be satisfactorily described by the Simon-Glätzel equation. The values of the constants in this equation for *n*-octadecane are as follows:

$$a=3423 \text{ bars}$$

$$b=-11.269$$

$$c=3.4007.$$

With these values, the Simon-Glätzel equation yields freezing pressures which agree with the experimental values within an rms deviation of only 4 bars.

The phase diagrams shown in Figs. 2 and 3 do not show clearly the correlation between the melting curves

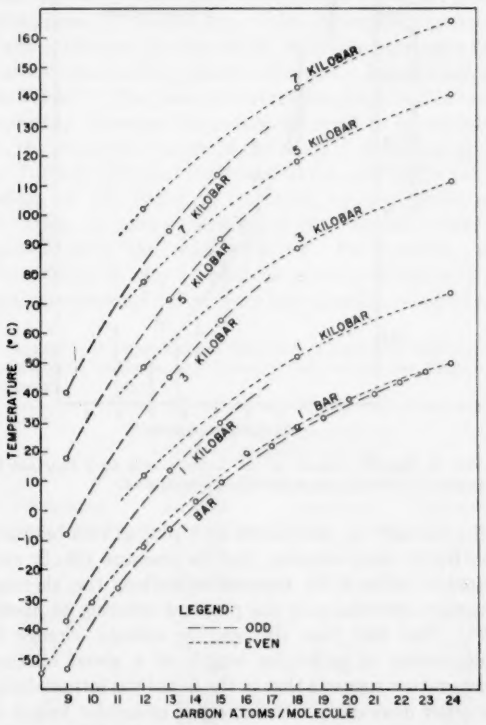

FIG. 4. Melting temperatures of *n*-paraffins shown as a function of molecular length. This is another representation of the melting data shown in Figs. 2 and 3 to illustrate the pronounced odd-even effect.

[19] F. Simon and G. Glätzel, Z. anorg. u. allgem. Chem. **178,** 309 (1929).

TABLE III. The melting temperatures of the *n*-paraffins at a series of elevated pressures.

Pressure (kilobars)	*n*-Paraffin					
	n-C_9	*n*-C_{12}	*n*-C_{13}	*n*-C_{15}	*n*-C_{18}	*n*-C_{24}
	°C					
1	−37.5	12.2	14.2	29.9	52.7	74.5
3	−7.8	48.8	45.9	64.8	89.3	112.1
5	17.9	77.6	72.1	92.2	118.9	142.0[a]
7	40.0	102.1	95.5	114.1	143.6[a]	166.5[a]

[a] These values were obtained by a graphical extrapolation of the experimentally determined melting curves.

of the *n*-paraffins and their molecular lengths. To show the correlation, the melting temperatures corresponding to the molecular length is plotted for a variety of pressures. Such a plot is shown in Fig. 4. The plotted values of the atmospheric pressure melting temperatures are those tabulated by Rossini *et al.*, see footnote reference a, Table I. The melting temperatures at elevated pressures were obtained graphically from the phase transition curves. These values are given in Table III. It is evident from Fig. 4 that at the same pressure, the melting temperature of an odd *n*-paraffin is lower than that obtained by an interpolation of the melting temperatures of the two adjacent even ones. Further, this effect increases with increasing pressure and decreases with increasing molecular length. King and Garner[20,21] have suggested that the alternation of melting points is due to the relative ability of the layers of odd- and even-numbered paraffins to pack in the crystal. If one accepts this hypothesis, the accentuations of the effect with increased pressure and/or with decreased molecular weight follow logically. Increased pressure decreases the total volume; this must be reflected in a decrease in free volume and thence in any property (e.g., melting) which is free-volume dependent. A direct consequence of decreased molecular weight is a higher ratio of ends (methyl groups) and therefore an accentuation of any effect which is due to the ends of the molecule.

The odd-even effect in *n*-paraffins is further exhibited in the specific volume changes associated with phase transitions. Specific volume changes presented in Table II are shown plotted in Fig. 5. Included in this figure are five points that represent the sum of the transition liquid to solid I and solid II, plotted at the pressure of the solid-solid transition. The five points are *n*-C_9, *n*-C_{13}, and *n*-C_{15} at 15.56°C, *n*-C_{15} at 37.78°C and *n*-C_{24} at 60.00°C. It is to be noted that these fall on the curves defined by the liquid to the solid phase where only one solid phase was found. There is a small error due to the compression of solid I, but using a reasonable estimate from Bridgman's[22] data on the compressions of solid hydrocarbons and the greatest pressure span

[20] A. M. King and W. E. Garner, J. Chem. Soc. **1936,** 1368.
[21] A. Müller, Proc. Roy. Soc. (London) **A120,** 433 (1928); *ibid.* **A127,** 417 (1930); *ibid.* **A128,** 514 (1932).
[22] P. W. Bridgman, Proc. Am. Acad. Arts Sci. **72,** 399 (1942).

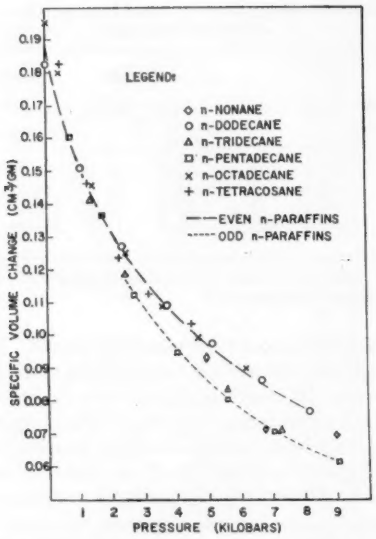

FIG. 5. Specific volume change associated with the melting of the *n*-paraffins. The odd-even effect is particularly evident at higher pressures although this is due, in part, to the increasing slope of the curves.

(424 bars for *n*-C_{15}) the maximum error does not exceed 2%. From the graph it is immediately evident that the plotted points determine two distinct curves, particularly at high pressures. One of these curves is through the points representing the values for the even *n*-paraffins and the other for the odd *n*-paraffins. Moreover, the specific volume change associated with the melting of the even *n*-paraffins is nearly the same for the same melting pressure although the corresponding melting temperatures are entirely different. A similar statement appears to be true for the odd *n*-paraffins. However, at the same melting pressure, the specific volume change of the odd *n*-paraffins is less than for the even ones, and this effect seems to increase with pressure. Such an odd-even effect is not exhibited by the specific enthalpy changes associated with the transition from the liquid to the most dense solid phase which are within an rms deviation of less than 2.5 cal/g of a smooth curve value at every melting temperature within the experimental range, regardless of molecular length. The enthalpy change increases monotonically with melting temperature and at a rate which increases with temperature. More conducive to interpretation is the variation of entropy change with melting temperature which, in the case of first-order phase transitions, may be obtained by dividing the enthalpy change by the corresponding melting temperature. The entropy change is found to exhibit a minimum with temperature as the independent variable. The minimum value appears at a melting temperature of about 95°C. This behavior may be interpreted as a competition between the liquid state ordering due to pressure effects and disorder induced by thermal agitation, the thermal disorder overwhelming the pressure ordering at about 95°C. The fact that the specific entropy change is independent of molecular length at a given melting temperature suggests that in the liquid the intramolecular order associated with increased molecular length is largely nullified by the intermolecular disorder present.

TABLE IV. The liquid phase specific volume of three *n*-paraffins at a variety of freezing pressures.

n-C_{12}		*n*-C_{15}		*n*-C_{18}	
Pressure (bars)	Specific volume (cm^3/g)	Pressure (bars)	Specific volume (cm^3/g)	Pressure (bars)	Specific volume (cm^3/g)
1	1.298	1	1.289	1	1.286
1175	1.234	280	1.270	400	1.260
2390	1.196	1400	1.318	1408	1.216
3775	1.169	2735	1.179	2450	1.181
5155	1.145	4075	1.148	3620	1.153
6712	1.126	5615	1.122	4705	1.133
8192	1.112	7055	1.103	6220	1.110

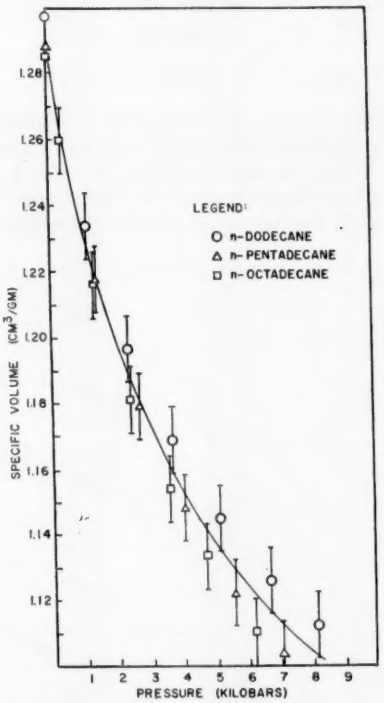

FIG. 6. Specific volume of the liquid phase as a function of pressure for three of the *n*-paraffins investigated.

Melting curve data were combined with compressibility data to obtain liquid phase specific volumes of *n*-dodecane, *n*-pentadecane, and *n*-octadecane at the freezing pressures corresponding to a number of different temperatures. Cutler *et al.*[1] investigated the liquid

state compressibilities of these compounds in temperature-pressure regions well away from their freezing point. By extrapolation of these data using the Tait equation,[23] the specific volumes at the freezing points were obtained. These data are presented in Table IV and are shown plotted in Fig. 6. Bounds of ± 0.01 cm^3/g are indicated on the plotted points to illustrate that at the same freezing pressure, but at different freezing temperatures, the liquid specific volumes of *n*-dodecane, *n*-pentadecane, and *n*-octadecane are the same within these bounds. For a given pressure the crystallization occurs at the same specific volume independent of chain length, and since for the two even-numbered compounds the change of volume on freezing is nearly the same, their solid specific volume are equal.

In addition to the specific volume changes, Table II also contains other thermodynamic variables associated with first-order phase transitions. The enthalpy change ΔH, the internal energy change ΔU, and the entropy change ΔS were obtained by application of the Clapeyron equation to the experimental data. Of particular interest is the enthalpy change because this also represents the heat of transition in first-order phase transitions. A comparison of the atmospheric pressure values obtained in this study with the corresponding values obtained by calorimetric methods is presented in Table V. The percent differences given in this table probably represent the maximum error to be expected in the calculated values of the heats of transition given in Table II. Of all of the variables required in the calculation of the heats of transition by the Clapeyron equation, probably the slope of the transition curve is known with the least precision. Furthermore, the uncertainty in this quantity is greatest at the ends of the experimental curve, since the actual drawing of the transition curve at its ends with a low density of experimental points required an extrapolation of the curvature trend.

TABLE V. A comparison of the heats of transition obtained by calorimetric methods and through the use of the Clapeyron equation.

Compound	Enthalpies of phase transition at atmospheric pressure (cal/g)		
	Calorimetric methods	Clapeyron equation	Difference (percent)
n-C_{12}	51.68[a]	49.55	4.4
n-C_{13}	36.94[a]	34.90	5.7
n-C_{15}	38.92[a]	40.02	2.8
n-C_{18}	58.21[a]	53.95	7.6
	57.64[b]	53.95	6.6
n-C_{24}	38.74[b]	37.18	4.1
	22.08[b,c]	21.29[c]	3.6

[a] Footnote reference a, Table I.
[b] A. A. Schraerer *et al.*, J. Am. Chem. Soc. **77**, 2017 (1955).
[c] These values correspond to solid-solid transitions.

[23] P. G. Tait, *Physics and Chemistry of the Voyage of HMS Challenger*, Vol. II, Part IV, S. P. LXI (1888).

TABLE VI. The extent of superpression in *n*-dodecane at a series of melting temperatures. The maximum error in the extent of superpression given in this table is ± 50 bars.

Temperature (°C)	Extent of superpression (bars)
15.56	Not observed
37.78	125
60.00	175
79.44	125
98.89	450
115.00	725

Although no effort was made to measure the extent of superpression in the *n*-paraffins, it was observed in most of the liquid-to-solid transitions. Superpression exists in a liquid which is at a pressure above the normal melting pressure at that temperature. Indicative of the trend of superpression with increasing melting temperatures are the data given in Table VI for *n*-dodecane. An examination of all the observed cases revealed that the superpression was definitely present in all compounds studied. The greatest superpression observed was 1200 bars, for nonane at 60°C, and the extent for all compounds was roughly proportional to the difference between the melting temperature at one atmosphere and the temperature under study. These facts are all consistent with the generally accepted view that the liquid-crystalline solid phase change is an ordering process.

SUMMARY

On the basis of the experimentally determined phase transition pressures and the corresponding transition temperatures, curves were drawn illustrating the interdependence of *n*-paraffin molecular length, the phase transition pressures and the transition temperatures. An analysis of this interdependence leads to the following conclusions. (1) At a given pressure, the melting temperature of an odd *n*-paraffin is lower than that obtained by interpolation of the melting temperatures of the adjacent even *n*-paraffins. Further, this effect increases with pressure and decreases with molecular length. (2) The existence of solid phase transitions in a *n*-paraffin is apparently independent of molecular weight or of whether it is of odd or even species. (3) Of the *n*-paraffins investigated, only *n*-octadecane exhibited a melting curve which could be accurately described by the Simon-Glätzel equation.

For at least three of the *n*-paraffins investigated, the specific volume of the liquid phase is nearly the same at the same freezing pressure. This behavior suggests that, at a particular pressure, fusion depends only upon the methyl group proximity and not upon molecular length.

An analysis of the specific volume changes which accompany phase transitions in *n*-paraffins indicates the following. (1) The specific volume changes associated with the melting of the even *n*-paraffins are nearly the same for a given melting pressure even though the corresponding melting temperatures are entirely different. A similar statement appears true for the odd *n*-paraffins. (2) At the same melting pressure, the specific volume change in the odd *n*-paraffins is less than for the even ones, and this effect increases with increasing pressure.

The specific entropy change associated with the transition from the most dense solid state to the liquid state is nearly the same for all of the *n*-paraffins investigated at the same melting temperature. Such an independence of molecular length suggests that, at the same melting temperature, the high intramolecular order of long chains is nullified by intermolecular disorder. This is also plausible on the basis of average intermolecular distance, since the liquid specific volume data at the melting temperature reveal that this distance is greater for longer chains. The entropy change exhibits a minimum value at a temperature of about 95°C, indicating that the liquid state ordering due to pressure effects is overwhelmed by thermal disorder at higher melting temperatures.

THE JOURNAL OF CHEMICAL PHYSICS VOLUME 33, NUMBER 6 DECEMBER, 1960

Infrared and Raman Spectra of Fluorinated Ethanes. XIII. 1,2-Difluoroethane*

PETER KLABOE† AND J. RUD NIELSEN

Department of Physics, University of Oklahoma, Norman, Oklahoma

(Received February 25, 1960)

The infrared absorption spectra of $CH_2F—CH_2F$ in the gaseous, liquid, and solid states have been obtained with a Perkin-Elmer double-pass spectrometer equipped with CsBr, NaCl, and LiF prisms. While the gas was studied in the spectral range from 6000 to 300 cm^{-1}, the liquid was examined from 6000 to 650 cm^{-1} and the solid from 3500 to 350 cm^{-1}. In addition, the infrared spectrum of the gas has been recorded at five different temperatures between 25°C and 180°C, and some of the absorption bands have been studied in solution in solvents of different polarities. The Raman spectrum of the liquid at −25°C and 35°C has been photographed with a 3-prism glass spectrograph and polarization measurements have been made. In all three states of aggregation the compound exists as a mixture of rotational isomers. The two isomeric forms (*trans* and *gauche*) are about equally stable in the gas, while the *gauche* configuration is more stable in the liquid state. Tentative assignments have been made of all fundamentals except the lowest fundamental of the *trans* isomer.

INTRODUCTION

THE vibrational spectra of a number of fluorinated ethanes having asymmetrical end groups have been studied with special reference to rotational isomerism.[1–3] It is of special interest to compare the spectra of $CH_2F—CH_2F$ with those of $CH_2Cl—CH_2Cl$ and $CH_2Br—CH_2Br$ which have been studied in great detail, particularly by Mizushima and co-workers.[4]

In the present paper infrared and Raman spectral data are reported for $CH_2F—CH_2F$, and the rotational isomerism exhibited by this compound is studied. A tentative assignment of all vibrational fundamentals for the *gauche* form, and all but the lowest fundamental for the *trans* form, has been carried out, and the spectra have been interpreted in detail.

EXPERIMENTAL RESULTS

The synthesis of $CH_2F—CH_2F$ in low yield by treating $CH_2Br—CH_2Br$ with HgF_2 has been reported by Henne and Renoll.[5] The sample was unstable, however, and exploded after 10 days. A synthesis of the compound (bp 30.7°C at 760 mm) has more recently been carried out by Edgell and Parts[6] from *p*-toluene sulfonic acid ester. The present sample (bp 31°C at 750 mm) was prepared by Dr. L. H. Beck in the laboratory of Professor A. L. Henne at Ohio State University following essentially Edgell's procedure.

A gas chromatogram showed the sample to contain less than 0.5% of more volatile impurities. A vapor density measurement at 28°C gave the molecular

* This work has been supported by the U. S. Atomic Energy Commission.

† Present address: Department of Chemistry, University of Oslo, Blindern, Oslo, Norway.

[1] R. E. Kagarise and L. W. Daasch, J. Chem. Phys. **23**, 113, 130 (1955).

[2] R. E. Kagarise, J. Chem. Phys. **23**, 207 (1955); *ibid.* **24**, 300, 1264 (1956); *ibid.* **26**, 380 (1957); *ibid.* **29**, 680 (1958).

[3] P. Klaboe and J. Rud Nielsen, J. Chem. Phys. **32**, 899 (1960).

[4] S. I. Mizushima, *Structure of Molecules and Internal Rotation* (Academic Press, Inc., New York, 1954).

[5] A. L. Henne and M. W. Renoll, J. Am. Chem. Soc. **58**, 889 (1936).

[6] W. F. Edgell and L. Parts, J. Am. Chem. Soc. **77**, 4899 (1955).

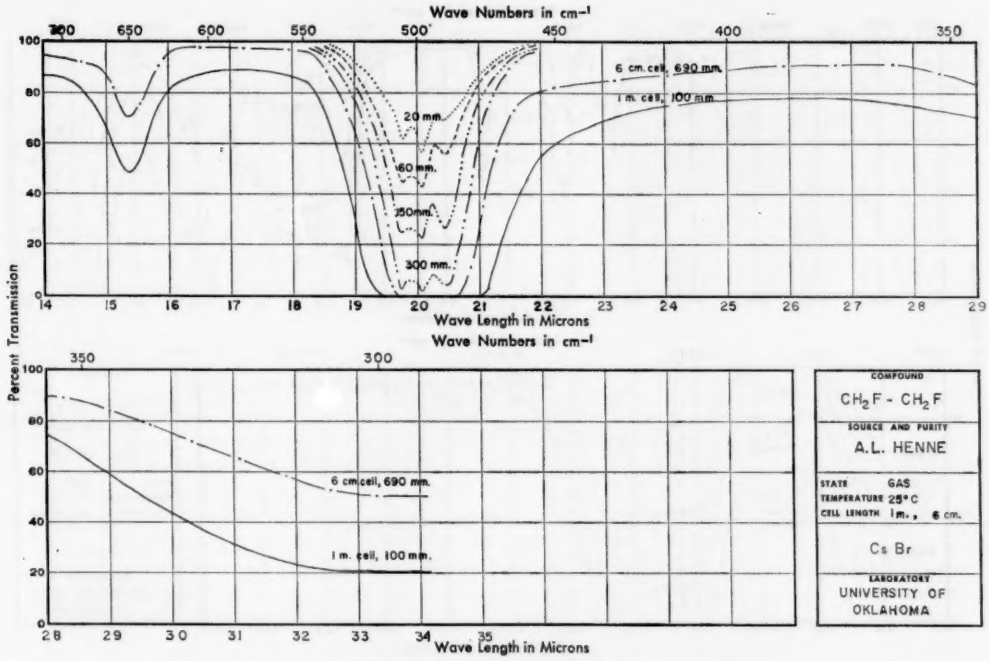

FIG. 1. Infrared absorption spectrum of gaseous $CH_2F—CH_2F$ (CsBr prism).

weight 65.2 which agrees quite well with the theoretical value 66.05. No explosion has occurred. No abnormal pressure in the sealed Raman tubes has been observed, nor any decomposition of the gas when heated to 180°C.

The infrared absorption spectrum of the gas at room temperature was recorded with the aid of a Perkin-Elmer model 112 spectrometer equipped with CsBr, NaCl, and LiF prisms and 6-cm, 10-cm, and 1-m cells. To study the rotational isomerism, the infrared spectrum of the gas in an electrically heated 10-cm cell was obtained also at 70°, 110°, 140°, and 170°C. The infrared spectrum of the pure liquid was obtained in sealed cells of thickness 0.0267 and 0.1043 mm. The spectral region from 800 to 1200 cm^{-1} was studied with the sample dissolved in different solvents, ranging from the nonpolar CCl_4 to the strongly polar nitromethane. Moreover, the infrared spectrum of the solid at −170°C was recorded by means of a low-temperature cell somewhat similar to that described by Lord *et al.*[7] The Raman spectrum of the liquid in a sealed Raman tube at 35°C and −25°C was photographed with an Applied Research Laboratories 3-prism glass spectrograph of reciprocal linear dispersion, 15 A/mm at 4358 A. Polarization measurements were made by the method of Crawford and Horwitz.[8] The infrared spectra are shown in Figs. 1–7, and the wave numbers of the observed absorption maxima (or "shoulders") are listed in Table I. The Raman spectral data are presented in Table II.

INTERPRETATION

From the work on $CH_2Cl—CH_2Cl$ and $CH_2Br—CH_2Br$,[4] one would expect $CH_2F—CH_2F$ to exist as an equilibrium mixture of *trans* and *gauche* isomers in the gaseous and liquid states and as a single rotational isomer in the crystalline state. However, $CH_2F—CH_2F$ seems to behave differently, and its spectra are more difficult to interpret than the spectra of the corresponding chlorine and bromine compounds. In the first place, none of the strong infrared bands present in the gaseous or liquid states disappear in the solid state at −170°C. Thus, both isomers are evidently present in the solid state. A similar situation has been reported by Kagarise and Daasch for $CFCl_2—CFCl_2$.[1] It is uncertain whether the existence of both isomers in the solid state must be interpreted as a simultaneous crystallization, or if the solid obtained is not crystalline but merely a glass or amorphous material, a possibility that has been discussed by Malherbe and Bernstein.[9] However, the large frequency and intensity differences observed in many cases between corresponding bands in liquid and solid $CH_2F—CH_2F$ indicate that the solid is crystalline.

[7] R. C. Lord, R. S. McDonald, and F. A. Miller, J. Opt. Soc. Am. **42**, 149 (1952).

[8] B. L. Crawford, Jr., and W. Horwitz, J. Chem. Phys. **15**, 882 (1947).

[9] F. E. Malherbe and H. J. Bernstein, J. Chem. Phys. **19**, 1607 (1951).

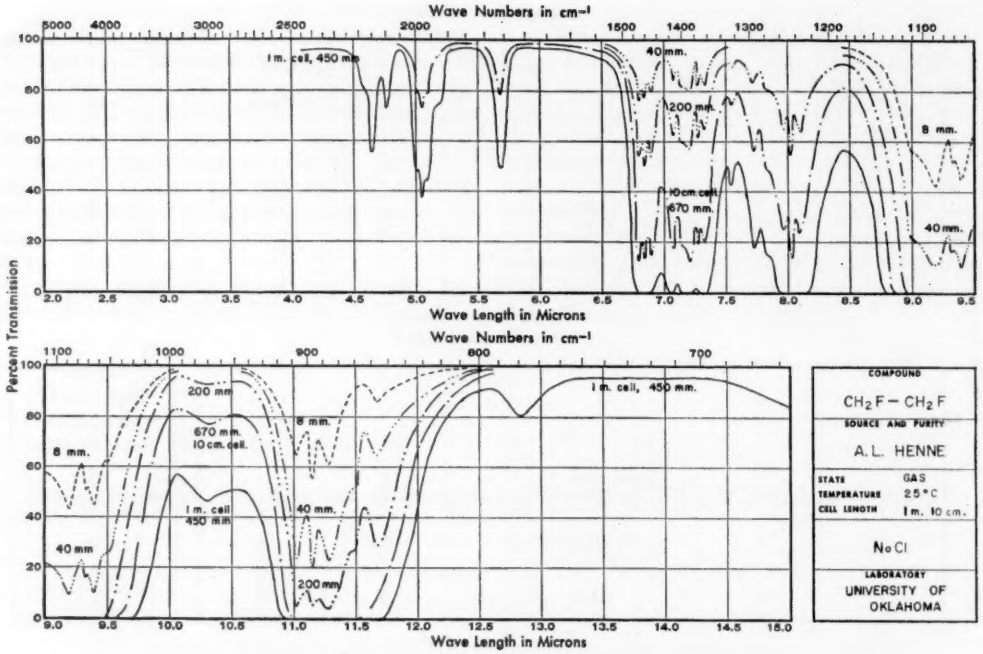

FIG. 2. Infrared absorption spectrum of gaseous $CH_2F—CH_2F$ (NaCl prism).

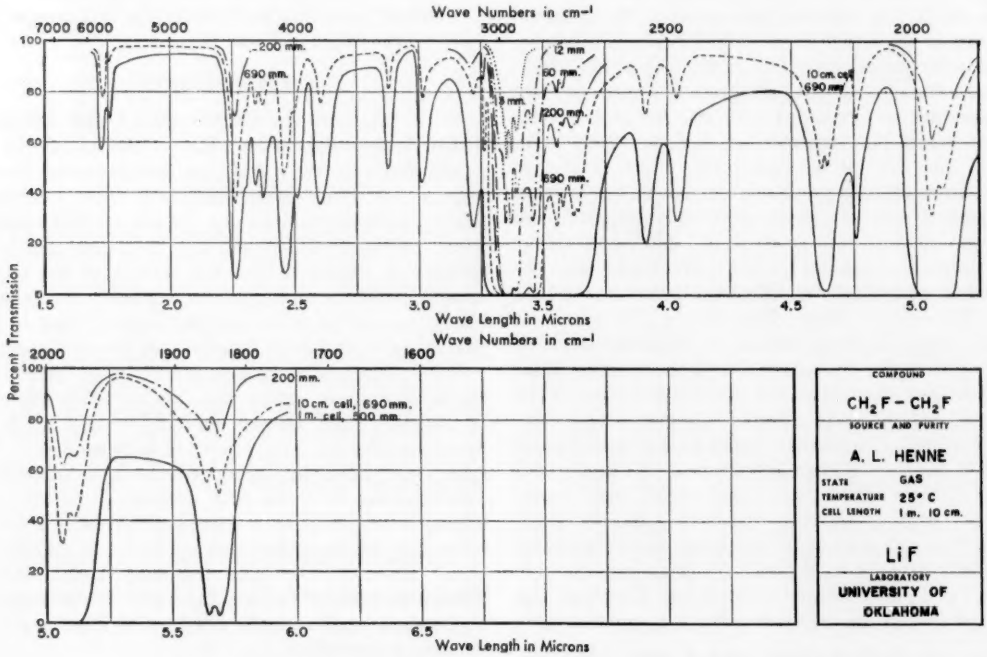

FIG. 3. Infrared absorption spectrum of gaseous $CH_2F—CH_2F$ (LiF prism).

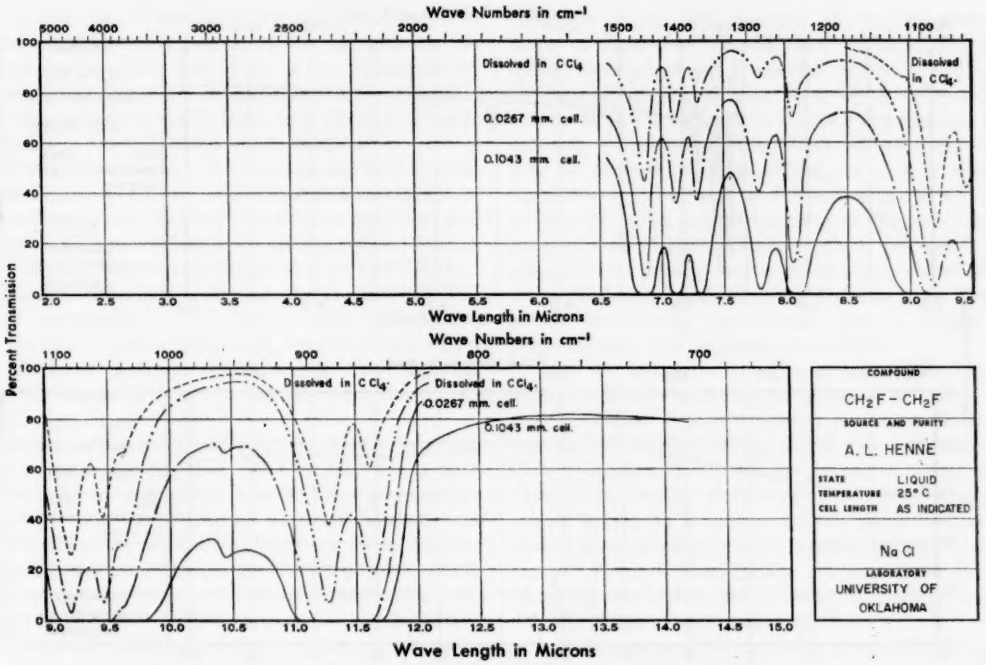

FIG. 4. Infrared absorption spectrum of liquid $CH_2F—CH_2F$ (NaCl prism).

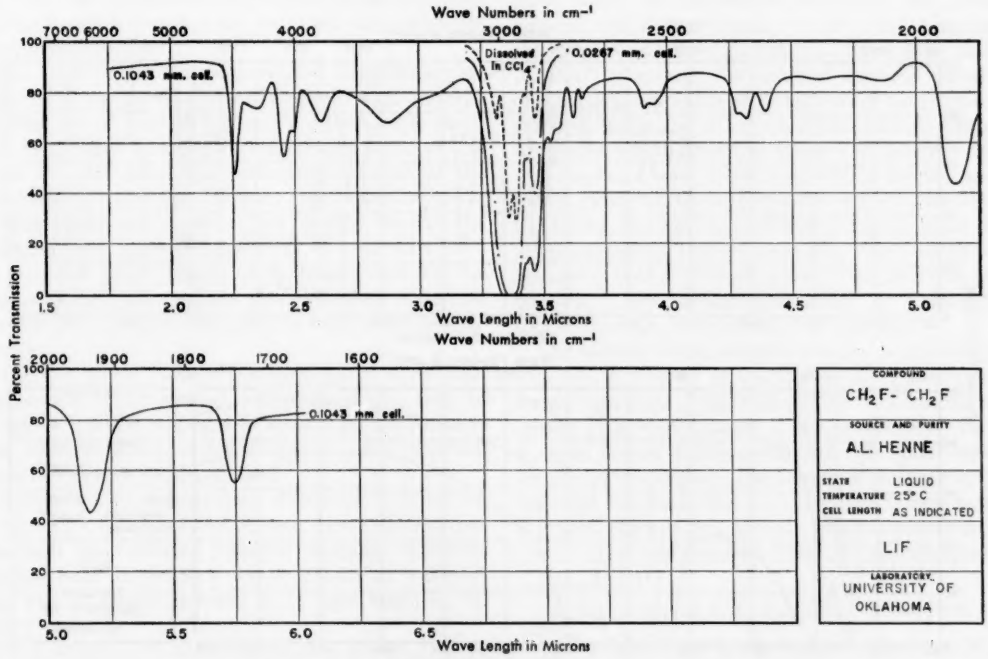

FIG. 5. Infrared absorption spectrum of liquid $CH_2F—CH_2F$ (LiF prism).

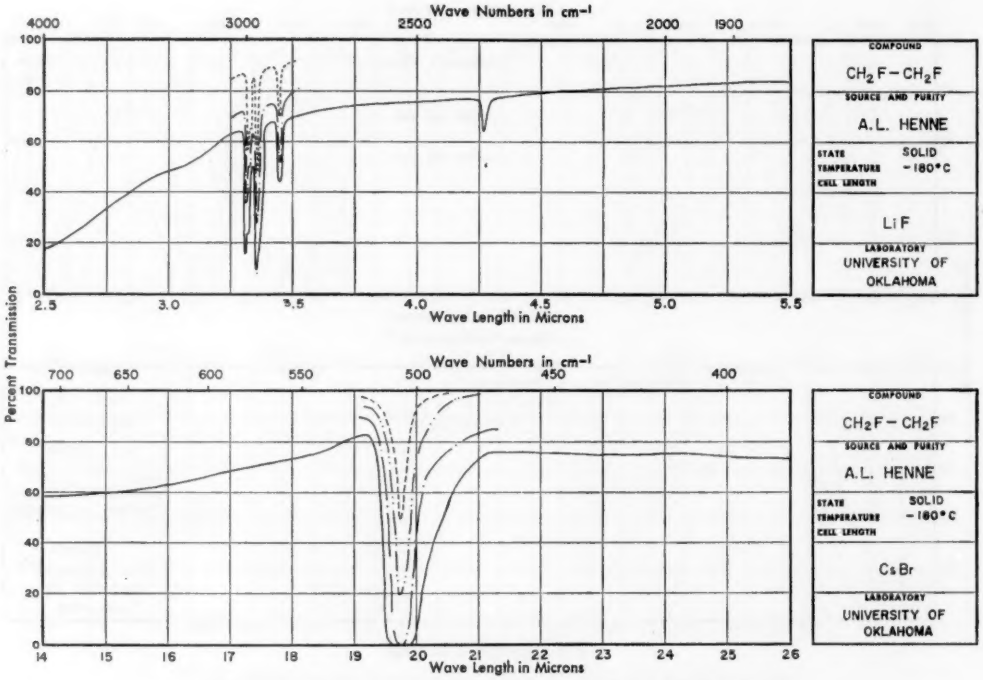

FIG. 6. Infrared absorption spectrum of solid $CH_2F—CH_2F$ (CsBr and LiF prisms).

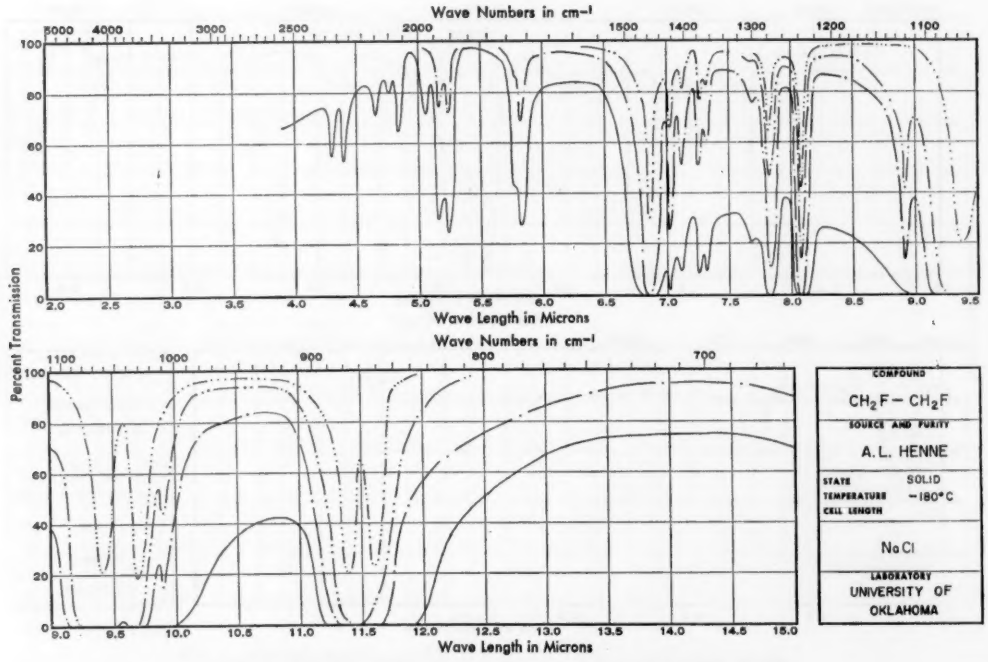

FIG. 7. Infrared absorption spectrum of solid $CH_2F—CH_2F$ (NaCl prism).

Secondly, even if the spectra are too rich in bands to be explained by the existence of one isomer only, the spectra are less rich than those of the corresponding chlorine and bromine compounds. It is therefore necessary to assume that a fairly large number of bands belonging to the different isomers overlap.

Thirdly, the existence of a *trans* isomer having symmetry C_{2h} should reveal itself by bands occurring in the infrared spectrum but not in the Raman spectrum, and *vice versa*. This mutual exclusion of infrared and Raman activities was observed for $CH_2Cl—CH_2Cl$ and $CH_2Br—CH_2Br$ and for other molecules of the form $CX_2Y—CX_2Y$ investigated.[1-3,10,11] The infrared and Raman spectra of the present compound, however, show only a few clear-cut instances where strong infrared bands have no counterpart in the Raman spectrum or *vice versa*.

In spite of these uncertainties, there seem to be strong reasons for assuming that $CH_2F—CH_2F$ exists as a mixture of *trans* and *gauche* isomers. Thus, a systematic intensity variation of certain infrared bands is observed when the sample is dissolved in solvents of different polarity. Furthermore, the temperature variations of the intensities of certain Raman bands recorded at 35°C and −25°C support this assumption.

The normal vibrations of the *trans* form of symmetry C_{2h} divide into symmetry species in the following manner: $6a_g+4a_u+3b_g+5b_u$. Vibrations of species a_u and b_u are active only in the infrared; vibrations of species a_g and b_g are active only in the Raman spectrum. Raman bands of species a_g are polarized, those of species b_g are depolarized.

The other isomer will consist of two enanthiomorphic forms of symmetry C_2 obtained from the *trans* form by rotating one of the CH_2F groups a certain angle about the C—C bond in either direction. The value of this angle will not affect the symmetry. Because of the electrostatic repulsion between the electronegative fluorine atoms and the attraction between fluorine and hydrogen, the angle will probably be less than 120°. On the other hand, because of the smaller radius of the fluorine atom, steric effects should be less important than in the corresponding chlorine and bromine compounds.

The two *gauche* forms will have identical vibrational frequencies. Their normal vibrations divide into 10 of species *a* and 8 of species *b*. All of them are active in both spectra. Raman bands of species *a* are polarized; those of species *b* are depolarized.

Assuming the internuclear distances C—C=1.54, C—F=1.37, C—H=1.093 A, and tetrahedral angles, one finds the following principal moments of inertia for the *trans* form: 30.9, 214.0, 234.2×10^{-40} g cm^2. The axis of largest moment is at right angle to the symmetry plane, and the axis of smallest moment makes an angle of 41°51′ with the C—C bond. Extrapolation from Badger and Zumwalt's curves[12] is not feasible because of the extreme form of the ellipsoid of inertia. Since the molecule is nearly a symmetrical top, however, the curves given by Gerhard and Dennison[13] may be applied to estimate the contours of the infrared bands. They give a *PR* separation of 16 cm^{-1} for parallel bands and an intensity of the zero branch equal to 0.12 of the intensity of the entire band. The perpendicular bands, on the other hand, should show no marked rotational branches, the zero branch completely dominating the contour. The a_u bands are perpendicular. The b_u bands are hybrids.

Since the exact configuration of the *gauche* form is unknown, a calculation of the moments of inertia and the prediction of band contours for this molecule is not feasible. A study of the model, however, indicates that the symmetry axis will be the axis of intermediate moment of inertia. Accordingly, bands of species *a* should have type *B* contours, while bands of species *b* should have contours that are hybrids between types *A* and *C*. There is considerable evidence from the infrared spectrum that *gauche* bands of species *b* have a *PR* separation of approximately 21 cm^{-1}.

It has been possible to make practically complete assignments of the vibrational fundamentals for both *trans* and *gauche* isomers. The assigned fundamentals are listed in Tables III and IV. The assignments are based mainly on the relative positions of the observed infrared and Raman bands, on the band contours of the infrared and the depolarization data of the Raman bands. Furthermore, the observed intensity variations of some Raman bands with increasing temperature in the liquid state and of certain infrared bands when the compound was dissolved in solvents of different dielectric constants were important criteria for the assignments. However, the large number of fundamentals and the strong overlapping in different regions make some of the assignments rather uncertain. This is particularly the case in the low-frequency part of the spectrum below 600 cm^{-1}. The assignments listed in Tables I–IV should therefore be considered as tentative.

The validity of the assignments may be tested by the sum rule derived by Mizushima, *et al.*[14] For the *gauche* isomer one finds $\sum \nu_i^2=49.36\times10^6$ and for the *trans* isomer $\sum \nu_i^2=49.23\times10^6$, if one assumes that the unassigned lowest fundamental has the same value as for the *gauche* isomer. The fact that the sum is 0.3% lower for the *trans* than for the *gauche* isomer may result from the fact that half of the fundamentals for the *trans* isomer are obtained from the Raman spectrum

[10] J. P. Zietlow, F. F. Cleveland, and A. G. Meister, J. Chem. Phys. **24,** 142 (1956).
[11] R. E. Kagarise and D. H. Rank, Trans. Faraday Soc. **48,** 394 (1952).
[12] R. M. Badger and L. R. Zumwalt, J. Chem. Phys. **6,** 711 (1938).
[13] S. L. Gerhard and D. M. Dennison, Phys. Rev. **43,** 197 (1933).
[14] S. Mizushima, T. Shimanouchi, I. Nakagawa and A. Miyake, J. Chem. Phys. **21,** 215 (1953).

TABLE I. Infrared spectral data for $CH_2F—CH_2F$ (in cm^{-1}).

Gas		Liquid		Solid		
Wave number	Description[a]	Wave number	Description[a]	Wave number	Description[a]	Interpretation[c]
295–340	w					a_u+a fundamentals
487, 498, 507	s			506	s	b fundamental
652	w					b_u fundamental
780	vw					a fundamental
857	s	[861][b]	vs	862	vs	a fundamental
871	w					$196+669=865B$
886, 897, 907	vs	[887]	vs	887	vs	b_u+b fundamentals
971	vw	954	vw			$196+780=976A$
				1009	w	$2\times506=1012A$
1051	vw	1039	w			$196+857=1053A$
1065	vs	[1057]	vs	1033	vs	b_u fundamental
1073	vw					
1088	vs	[1087]	vs	1061	vs	a fundamental
1112	m	1118	vw	1122	s	a fundamental
1234, 1246, 1255	s	1241	s	1240	s	b fundamental
1271, 1277	w					a fundamental
1295	m	1283	m	1277	s	b fundamental
1326	vw					$2\times669=1338A$
1365, 1376, 1386	s	[1373]	m	1369	w	b_u fundamental
				1379	w	$506+877=1383A$; ca $320+1061=1381A$
1402	s	[1406]	s	1406	w	a fundamental
1415	s			1423	s	a_u fundamental
1473, 1462, 1451	s	[1458]	s	1460	s	b fundamental
				1720	m	ca $320+1406=1726A$
1761	w	1740	w	1738	m	$498+1274=1772B$
1927	vw					$652+1285=1937A_u$
1963	w					$857+1112=1969A$; $669+1295=1964A$
1982	m	1938	m,b			$897+1088=1985B$
1996	w					$897+1112=2009B$
2101	w					$857+1246=2103B$
2152	m					$857+1295=2152B$
2163	m					$897+1274=2171B$; $2\times1088=2176A$
2476	w					$1065+1416=2481B_u$

TABLE I. (*Continued*)

Gas		Liquid		Solid		
Wave number	Description[a]	Wave number	Description[a]	Wave number	Description[a]	Interpretation[c]
		2532	vw			1241+1283=2524*A*
2556	w	2561	vw			1274+1295=2569*B*
2737	vw	2737	vw			
2746	m					1274+1462=2736*B*
2759	m	2760	vw			1295+1462=2757*A*
2796	w	2805	vw			1376+1416=2792B_u
2813	m	2829	vw			1415+1416=2831A_u
2895	s	[2887]	s	2901	s	*a* fundamental
2951	vs			2980	vs	b_u fundamental
2966	vs	[2953]	vs	3010	w	*b* fundamental
2987	vs	[2982]	vs	3018	vs	*b* fundamental
2994	w					a_u+*a* fundamentals
3001	w					
		3015	w			
3067	w					196+2895=3091*A*
3106	w					
3318	w					ca 320+2994=3314*A*
3476	w	3494	vw			498+2987=3485*A*
3843	vw	3837	vw			857+2987=3844*B*
3982	vw	4010	vw			1088+2895=3983*A*
4067	m	4072	w			1079+2994=4073A_u
4218	vw					1246+2987=4233*A*
		4237	vw			1241+2994=4235*B*
4270	vw					1285+2994=4279B_u
4338	vw					1376+2962=4338B_u
4417	m	4425	m			1462+2966=4428*A*
5692	vw					
5784	vw					2×2895=5790*A*

[a] The following abbreviations have been used: w, weak; m, medium; s, strong; b, broad; and v, very.

[b] Wave numbers enclosed in brackets are obtained in carbon tetrachloride solution.

[c] For brevity, the isomer, or isomers, to which a frequency is ascribed is not stated explicitly but is implied by the species assignment, a_u, b_u, A_u, and B_u referring to the *trans* and *a*, *b*, *A*, and *B* to the *gauche* isomer.

of the liquid phase. The empirical sum rule of Bernstein and Pullin[15] is also quite well satisfied, the sums being $\sum_i \nu_i = 24\,920$ for the *gauche* and $\sum_i \nu_i = 24\,739$ for the *trans* isomer.

In terms of the assigned fundamentals it has been possible to interpret all of the observed Raman bands and practically all of the infrared bands. These interpretations are given in Tables I and II. However, because of the large dependence of many of the frequencies upon the state of aggregation the correlation of several bands in the three spectra is difficult, and their interpretations are therefore rather uncertain. Most, if not all, of the very weak bands that have been left uninterpreted can be explained as ternary combination bands. However, in view of the large number of fundamentals, such interpretations are in most cases not unique and have therefore not been included in Table I.

ENTHALPY DIFFERENCE BETWEEN ROTATIONAL ISOMERS

All the stronger infrared bands assigned as fundamentals were recorded at 25°, 70°, 110°, 140°, and

[15] H. J. Bernstein and A. D. A. Pullin, J. Chem. Phys. **21**, 2188 (1953).

TABLE II. Raman spectral data for liquid $CH_2F—CH_2F$.

Wave number	Description[a]	Depolarization	Exciting Hg lines[b]	Interpretation[c]
196	vw		e	*a* fundamental
329	w	0.3	e	*a* fundamental
450	vw		e	b_g fundamental
502	w	0.8	e	*b* fundamental
669	vw		e	*b* fundamental
768	vw		e	*a* fundamental
804	w	p	e	a_g fundamental
858	vvs, sh	0.09	e,k,i	a_g+a fundamentals
881	vs	0.8	e,k,i	*b* fundamental
1049	s	0.5	e	a_g fundamental
1079	s, d	0.5	e,k	a_g+a fundamentals
1115	m	0.09	e	*a* fundamental
1244	s	0.8	e,k	*b* fundamental
1272	m,d		e	*a* fundamental
1285	s	0.8	e,k	b_g+b fundamentals
1416	w	0.5	e	a_g fundamental
1456	vs	0.7	e,k	*b* fundamental
2733	m	p	e	$2\times1373=2746A_g$
2806	m	p	e	$2\times1406=2812A$
2826	w	p	e	$2\times1416=2832A_g$
2895	s,sh	0.2	e,k,i	*a* fundamental
2962	vvs, sh	0.1	e,k,i	a_g+b fundamentals
ca. 2990	s,vd	0.7	e	b_g+a+b fundamentals

[a] For the abbreviations s, m, w, and v, see footnote a to Table I; sh, sharp; d, diffuse, p, polarized.
[b] The meanings of the Kohlrausch symbols for the Hg lines are e, 4358 A; k, 4047 A; i, 4078 A.
[c] Species a_g, b_g, and A_g refer to the *trans*, species *a*, *b*, and *A* to the *gauche* isomer.

TABLE III. Fundamental vibrational frequencies for *trans* $CH_2F—CH_2F$ (in cm^{-1}).[a]

Species	Infrared gas	Infrared liquid	Infrared solid	Raman liquid	Approximate motion
a_g				2962 vvs (0.1)	C—H stretching
a_g				1416 w (0.5)	CH_2F deformation
a_g				1079 s (0.5)	CH_2F deformation
a_g				1049 s (0.5)	C—F stretching
a_g				858 vvs (0.09)	C—C stretching
a_g				804 w (p)	Rocking
a_u	ca 2994 w				C—H stretching
a_u	1415 s		1423 s		CH_2F deformation
a_u	ca 320 w				Rocking
a_u					Torsion
b_g				ca 2990 s (0.7)	C—H stretching
b_g				1285 s (0.8)	CH_2F deformation
b_g				450 vw	Rocking
b_u	2951 vs		2980 vs		C—H stretching
b_u	1376 s	[1373][b] m	1379 w		CH_2F deformation
b_u	1065 vs	[1057] vs	1033 vs		C—F stretching
b_u	897 vs	[887] vs	887 vs		CH_2F deformation
b_u	652 w				Rocking

[a] For the meaning of the abbreviations used, see footnotes to Table I.
[b] Wave numbers enclosed in brackets are obtained in carbon tetrachloride solution.

170°C with the aid of a 10-cm gas cell. While the bands became broader at higher temperatures, no change in the integrated extinction of any band could be detected. The enthalpies of the two rotational isomers in the gaseous state must therefore be equal within the experimental error. A rough estimate based on Bernstein's graphical method[16] indicates that the upper limit of this error is approximately ±200 cal/mole.

In the liquid state, on the other hand, the intensities of some of the Raman bands were found to vary with temperature. The Raman tube was surrounded by a vacuum jacket and was cooled by a stream of cold nitrogen. Sets of exposures of durations 20 min, 1 hr and 3 hr were made at 35° and −25°C. Unfortunately, it was not possible to use lower temperatures, since the sample contained a small amount of an impurity which would freeze and make the sample turbid, thus producing a heavy background in the Raman spectrum.

The microphotometer traces of the Raman spectra showed that the bands at 881, 1115, and 1456 cm^{-1} were enhanced as the temperature was lowered, while

[16] H. J. Bernstein, J. Chem. Phys. **18**, 897 (1950).

TABLE IV. Fundamental vibrational frequencies for *gauche* $CH_2F—CH_2F$ (in cm^{-1}).[a]

Species	Infrared gas	Infrared liquid	Infrared solid	Raman liquid	Approximate motion
a	ca 2994 w			ca 2990 s (0.7)	C—H stretching
a	2895 s	[2887][b]s	2901 s	2895 s (0.2)	C—H stretching
a	1402 s	[1406]s	1406 w		CH_2F deformation
a	1274 w			1272 m	CH_2F deformation
a	1112 m	1118 vw	1122 s	1115 m (0.09)	CH_2F deformation
a	1088 vs	[1087]vs	1061 vs	1079 s (0.5)	C—F stretching
a	857 s	[861]vs	862 vs	858 vvs (0.09)	C—C stretching
a	780 vw			768 vvw	Rocking
a	ca 320 w			329 w (0.3)	Rocking
a				196 vw	Torsion
b	2987 vs	[2982]vs	3018 vs	ca 2990 s (0.7)	C—H stretching
b	2966 vs	[2953]vs	3010 vs	2962 vvs (0.1)	C—H stretching
b	1462 s	[1458]s	1460 s	1456 vs (0.7)	CH_2F deformation
b	1295 m	1283 m	1277 s	1285 s (0.8)	CH_2F deformation
b	1246 s	1241 s	1240 s	1244 s (0.8)	C—F stretching
b	897 vs	[887]vs	877 vs	881 s (0.8)	CH_2F deformation
b				669 vw	Rocking
b	498 s		506 s	502 w (0.8)	Rocking

[a] For the meaning of the abbreviations used, see footnotes to Table I.
[b] Wave numbers enclosed in brackets are obtained in carbon tetrachloride solution.

the bands at 858 and 1049 cm^{-1} decreased in intensity with decreasing temperature. The photographic intensity data were not accurate enough to calculate $\Delta H°$ for the liquid state. However, it was concluded that the bands at 881, 1115, and 1456 cm^{-1} are caused (at least predominantly) by the more stable isomer and the two other bands by the less stable isomer.

According to Onsager's theory of dielectrics,[17] the polar *gauche* isomer should have lower potential energy in the liquid than in the gas, while the nonpolar *trans* isomer should not suffer a change in potential energy on going from gas to liquid. Since the two isomers are found to have approximately the same energy in the gaseous state, the *gauche* form should be the more stable isomer in the liquid state. This is in accord with the assignments of the 5 Raman bands mentioned above: the 1456, 1115, and 881 cm^{-1} bands all have counterparts in the infrared spectrum and are ascribed to *gauche*, *gauche*, and *gauche*+*trans* (with *gauche* dominating), respectively; the 1049-cm^{-1} band, on the other hand, is assigned to the *trans* isomer, and the 858-cm^{-1} band, which has a counterpart in the infrared spectrum, is ascribed to both isomers (with the *trans* isomer dominating).

According to Onsager,[17] a spherical molecule of radius a and dipole moment μ loses the potential energy

$$E_r=[(\epsilon-1)/(2\epsilon+1)](\mu^2/a^3),$$

when transferred from vacuum ($\epsilon=1$) to a medium of dielectric constant ϵ. A rough estimate of the molecular value of $a\approx 2.3$ A has been assumed in the present calculations. Using the bond moments $\mu_{C-H}=0.4$ and $\mu_{C-F}=1.45$ D,[18] one finds the value 1.73D for the dipole moment of the *gauche* isomer (the same as for $CHF_2—CHF_2$),[3] provided one assumes an ideal *gauche* form obtained from the *trans* form by rotating one of the CH_2F groups 120° with respect to the other. In the actual *gauche* molecule, the dipole moment is probably somewhat smaller. The *trans* molecule has a center of symmetry and has zero dipole moment. When the compound is dissolved in solvents of different dielectric constants, the isomer equilibrium should change. This was verified by dissolving $CH_2F—CH_2F$ in the following solvents: cyclohexane, carbon tetrachloride, chloroform, acetonitrile, and nitromethane, the two first-mentioned being nonpolar, the last two strongly polar, and chloroform having an intermediate polarity. Only such bands of the sample could be studied that are very strong and not overlapped by solvent bands. The intensities of the infrared bands at 861, 887, 1057, and 1087 cm^{-1} were measured at different concentrations in different solvents, and their relative intensities were compared. The ratio between the extinctions of two bands was found to vary with the dielectric constant of the solvent in good agreement with Onsager's theory. From these variations it was concluded that the 861- and 1087-cm^{-1} bands are caused by the *gauche* and the 1057-cm^{-1} band by the *trans* isomer, while the band at 887 cm^{-1} is due to both isomers.

An indirect estimation of the enthalpy difference $\Delta H°$ between the *trans* and the *gauche* isomers in the liquid state was made as follows: It was assumed that the ratio of *gauche* to *trans* isomer is 2:1 in the gaseous state. Onsager's formula indicates a corresponding ratio of approximately 6:1 in cyclohexane, having a dielectric constant of 2.05. The intensity change between the *gauche* bands 1087 and 861 cm^{-1} and the *trans* band at 1057 cm^{-1} when the compound is dissolved in cyclohexane and in the pure liquid, indicates a *gauche-trans* ratio of 9:1 in the pure liquid state at room temperature. This ratio corresponds to a value of $\Delta H°\approx 900$

[17] L. Onsager, J. Am. Chem. Soc. **58**, 1486 (1936).
[18] C. P. Smyth, *Dielectric Behavior and Structure* (McGraw-Hill Book Company, Inc., New York, 1955).

TABLE V.

Compound	Phase	$H°(gauche) - H°(trans)$
$CH_2F—CH_2F$	gas	0 kcal/mole
	liquid	ca. −0.9
$CH_2Cl—CH_2Cl$[a]	gas	1.15
	liquid	0
$CH_2Br—Ch_2Br$[a]	gas	1.54
	liquid	0.72

[a] The values given for these compounds are averages of what are believed to be the most reliable of the previously reported values (see footnote reference 19).

cal/mole in the liquid state. Because the value is calculated using a number of assumptions, the figure should be considered as strictly approximate.

COMPARISON WITH $CH_2Cl—CH_2Cl$ AND $CH_2Br—CH_2Br$

It is of great interest to compare the results obtained here with those previously reported for $CH_2Cl—CH_2Cl$ and $CH_2Br—CH_2Br$.[19] In both of these compounds the *trans* isomer has the lower enthalpy in the gaseous phase. Because of the stabilization of the *gauche* form in the liquid state $H°$ (*gauche*) $- H°$ (*trans*) is smaller in this state. In the case of $CH_2Br—CH_2Br$ this difference is 0.72 kcal/mole, for $CH_2Cl—CH_2Cl$ it is zero, and for $CH_2F—CH_2F$ it is negative. As shown by Table V, the data obtained here for $CH_2F—CH_2F$ fit quite well with those for the two other compounds. It is seen that the *gauche* form becomes more stable as the substituted halogen changes from bromine to chlorine and from chlorine to fluorine. This is what would be expected if steric factors are largely responsible for the stability of the isomers. In a recent paper on $CH_2F—CH_2Cl$,[20] however, values are reported for $\Delta H°$ in the gaseous and liquid state which do not fit well into the table. For $CH_2F—CH_2Cl$,[20] the "*trans*" is reported to be more stable than the "*gauche*" both in the gaseous and the liquid states, the enthalpy differences being 60 and 470 cal/mole, respectively.

The different relative stabilities of the *trans* and *gauche* isomers for $CH_2F—CH_2F$, $CH_2F—CH_2Cl$, $CH_2Cl—CH_2Cl$, and $CH_2Br—CH_2Br$ may in part explain their different behavior on crystallizing. With the exception of $CH_2F—CH_2F$ they all crystallize in the *trans* (or "*trans*") form. In liquid $CH_2F—CH_2F$ the *gauche* isomer predominates, and the conversion to the *trans* form would require the addition of energy. Apparently, a mixed crystal of the two isomers is formed.

ACKNOWLEDGMENTS

The writers are indebted to Professor A. L. Henne and Dr. Leonard Beck for the preparation of the sample.

[19] Reference 4, p. 41.

[20] P. A. Bazhulin and L. P. Osipova, Optika i Spektroskopiya 6, 406 (1959).

Vapor Pressures and Related Thermodynamic Properties of the Isotopic Nitric Oxide Molecules*

JACOB BIGELEISEN

Chemistry Department, Brookhaven National Laboratory, Upton, New York

(Received June 15, 1960)

The large differences in thermodynamic properties of the isotopic NO molecules are interpreted in terms of the known structure of interacting dimers. It is shown that structural considerations alone suffice to calculate the relative O^{18} to N^{15} isotope effects on vapor pressure, heats of vaporization, and triple points. The calculated relative quantities are in excellent agreement with experiment. The properties of $N^{15}O^{18}$ are shown to be completely determined by those of $N^{14}O^{16}$, $N^{15}O^{16}$, and $N^{14}O^{18}$. The absolute value of the vapor pressure ratio of $N^{14}O^{16}/N^{15}O^{16}$ is calculated from spectral data in good agreement with experiment.

INTRODUCTION

RECENTLY Clusius and co-workers[1–4] have determined the difference in vapor pressures, heats of vaporization, and triple point temperatures of the isotopic NO molecules: $N^{14}O^{16}$, $N^{15}O^{16}$, $N^{14}O^{18}$, and $N^{15}O^{18}$ in the temperature range 111°–120°K. The effects observed are some tenfold that to be expected by extrapolation of the data on N_2, CO, and O_2 (cf. footnote 4, Fig. 2). This large effect is certainly to be ascribed to the fact that NO is known to form dimers in the liquid and solid state. A summary of some of the experimental vapor pressure data is given in Table I.

It is the purpose of the present paper to show that the difference in vapor pressures and heats of vaporization of all the isotopic NO molecules can be derived from the vapor pressure ratio of one pair, e.g. $\ln P_{N^{14}O^{16}}/P_{N^{15}O^{16}}$, without any arbitrary parameters. The difference in triple point temperatures of the various species obey a simple theoretical formula.[5] The calculation of the absolute difference in triple points requires knowledge of the change in structure on melting and will not be attempted. The difference in boiling points is derived from the difference in vapor pressures and heats of vaporization. Finally, an absolute calculation of the vapor pressure ratio from molecular data gives adequate agreement with the experimental data.

HEATS OF VAPORIZATION

Clusius, Schleich, and Vecchi[4] give empirical equations for the vapor pressure ratio of the form

$$\log P_{N^{14}O^{16}}/P_{N^{x}O^{y}}=(C/T)-b.$$

The difference in heats of vaporization given in Table I are 2.303 RC. Theory shows that, when the quantum effects are small, the vapor pressure ratio of isotopic molecules is of the form[5,6]

$$\ln P'/P=A/T^2. \tag{1}$$

Figure 1 shows that, in the range of temperatures studied, the logarithm of the vapor pressure ratio is linear in $1/T^2$. An extrapolation to zero in $\ln P'/P$ at infinite temperature is consistent with the experimental data. From Eq. (1) we obtain

$$\delta(\Delta H)_T\text{vap}=-2RT(\ln P'/P)_T. \tag{2}$$

We compare the observed and calculated difference in heats of vaporization in the middle of the temperature range (~115°K) in Table II. The agreement between the "experimental" and calculated heats of vaporization is almost within the limit of experimental error and shows that Eq. (1) is an adequate representation of the vapor pressure data. It is a tribute to the accuracy of the experimental data.

CORRELATION OF $N^{15}O^{16}$—$N^{14}O^{18}$—$N^{15}O^{18}$

The theory of the isotope effect on the vapor pressure gives the dependence of A in Eq. (1) on mass. It is

$$A\sim\sum_{\alpha}(\mu_\alpha'-\mu_\alpha)k_\alpha, \tag{3}$$

where μ_α' and μ_α are the reciprocals of the masses of the atoms in the molecule, k_α is a force constant associated with the displacement of the αth atom from its equilibrium position (it is actually the difference

TABLE I. Properties of isotopic NO molecules.

	$N^{15}O^{16}$	$N^{14}O^{18}$	$N^{15}O^{18}$
$\ln P(N^{14}O^{16})/P_{N^{x}O^{y}}$ at 115°K	0.0295	0.0406	0.0701
δ Triple point ($N^{x}O^{y}-N^{14}O^{16}$)	0.099°K	0.139°K	0.222°K
δ Boiling point ($N^{x}O^{y}-N^{14}O^{16}$)	0.228°K	0.313°K	0.528°K
δ Heat of vaporization ($N^{x}O^{y}-N^{14}O^{16}$) in cal mole^{-1}	14.1	20.4	33.5

* Research carried out under the auspices of the U. S. Atomic Energy Commission.

[1] K. Clusius and K. Schleich, Helv. Chim. Acta **41**, 1342 (1958).

[2] K. Clusius and K. Schleich, *Proceedings of the Second United Nations International Conference on the Peaceful Uses of Atomic Energy* (United Nations, Geneva, 1958), Vol. 4, 485 (P/255).

[3] K. Clusius, M. Vecchi, A. Fischer, and U. Piesbergen, Helv. Chim. Acta **42**, 1975 (1959).

[4] K. Clusius, K. Schleich, and M. Vecchi, Helv. Chim. Acta **42**, 2654 (1959).

[5] J. Bigeleisen, to be published.

[6] K. F. Herzfeld and E. Teller, Phys. Rev. **54**, 912 (1938).

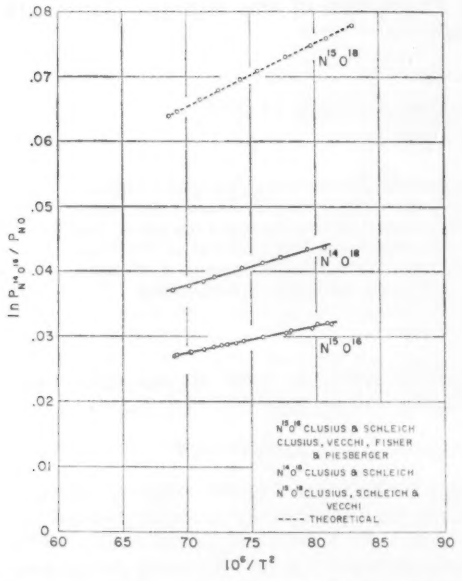

FIG. 1. Vapor pressure ratios $N^{14}O^{16}/N^{15}O^{16}$, $N^{14}O^{16}/N^{14}O^{18}$, $N^{14}O^{16}/N^{15}O^{18}$ ○ experimental data; — calculated from $N^{15}O^{16}$ and $N^{14}O^{18}$.

between such a quantity in the condensed phase and the gas phase), and the summation, $\sum_\alpha$, runs over the atoms in the molecule. It follows directly from Eqs. (1), (2), and (3)

$$\ln P_{N^{14}O^{16}}/P_{N^{15}O^{16}} \sim \left(\frac{1}{14}-\frac{1}{15}\right)k_N+\left(\frac{1}{16}-\frac{1}{18}\right)k_O$$

or

$$\ln P_{N^{14}O^{16}}/P_{N^{15}O^{18}} = \ln P_{N^{14}O^{16}}/P_{N^{15}O^{16}}+\ln P_{N^{14}O^{16}}/P_{N^{14}O^{18}}.$$

This is shown as the dotted line in Fig. 1 calculated using the experimental data on $\ln P_{N^{14}O^{16}}/P_{N^{15}O^{16}}$ and $\ln P_{N^{14}O^{16}}/P_{N^{14}O^{18}}$. The agreement is quantitative. Clusius, Schleich, and Vecchi[4] have found this relationship empirically. They write

$$P_{N^{14}O^{16}} \times P_{N^{15}O^{18}} = P_{N^{15}O^{16}} \times P_{N^{14}O^{18}}$$

and attribute the equality to the fact that the sum of the molecular weights on both sides of the equation is the same. This is a necessary but not sufficient condition. Any chemical reaction has the same molecular weights on both sides. Up through powers in $(h/kT)^2$ the relation between $N^{15}O^{18}$ and $N^{14}O^{16}$, $N^{14}O^{18}$, and $N^{15}O^{16}$ holds because of the fact that *there is isotope interchange between the same chemical species.* It also follows directly now that

$$\delta\Delta H(N^{14}O^{16}-N^{15}O^{18}) = \delta\Delta H(N^{14}O^{16}-N^{15}O^{16}) + \delta\Delta H(N^{14}O^{16}-N^{14}O^{18}),$$

which is verified by the experimental data in Table I.

The difference in triple point temperature depends on isotopic mass in a manner similar to the logarithm of the vapor pressure ratio.[5] Thus, the difference in triple point temperatures of $N^{15}O^{18}$ and $N^{14}O^{16}$ is predicted and found experimentally to be equal to the sum of the $N^{15}O^{16}$ and $N^{14}O^{18}$ differences. The boiling point difference follows from the vapor pressure ratios and heats of vaporization.

We now wish to consider the relative O^{18} and N^{15} effects. From Eqs. (1) and (3)

$$\frac{\ln P_{N^{14}O^{16}}/P_{N^{14}O^{18}}}{\ln P_{N^{14}O^{16}}/P_{N^{15}O^{16}}} = \frac{(\mu'-\mu)_O k_O}{(\mu'-\mu)_N k_N} = 1.46 k_O/k_N.$$

The structure of solid NO is one of randomly oriented dimers.[7,8] In the liquid the dimer is less than five percent dissociated.[9] The gas is completely dissociated into monomers. While the structure of dimer has not yet been uniquely established, qualitative molecular orbital considerations[10] favor the structure

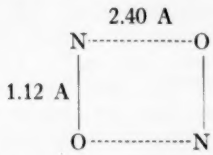

This is one of the structures derived from the x-ray data[7,8] but may be at variance with the infrared and Raman spectra of the liquid and solid.[11] The latter have not been definitively analyzed. A change from the rectangular head to tail dimer to a parallelogram will not affect the present discussion. The bent C_{2v} structure is not sufficiently well established to warrant detailed speculation. The present discussion, although based on the rectangular dimer, is not necessarily limited to this structure.

We have mentioned previously that k_α is the difference between k_α (liquid, solid) and k_α (gas). In the gas obviously k_O equals k_N. Let us consider the solid. The short N—O bond makes the same contribution to k_O (solid) and k_N (solid). The same is true for the long N—O bond. There may be a difference from k_{N-N}

TABLE II. Calculated and experimental differences in heat of vaporization of NO molecules (cal mole^{-1}).

	$N^{15}O^{16}$	$N^{14}O^{18}$	$N^{15}O^{18}$
"Experimental"	14.1	20.4	33.5
Calculated (Eq. (2)]	13.5	18.7	32.3

[7] W. L. Dulmage, E. A. Meyers, and W. N. Lipscomb, J. Chem. Phys. **19,** 1432 (1951).
[8] W. L. Dulmage, E. A. Meyers, and W. N. Lipscomb, Acta Cryst. **6,** 760 (1953).
[9] A. L. Smith and H. L. Johnston, J. Am. Chem. Soc. **74,** 4696 (1952).
[10] W. J. Orville-Thomas, J. Chem. Phys. **22,** 1267 (1954).
[11] A. L. Smith, W. E. Keller, and H. L. Johnston, J. Chem. Phys. **19,** 189 (1951).

and k_{O-O} of the dimer. These are definitely small contributions even compared to $k_{N-O(long)}$. We must now consider the interaction of dimers. Since the structure is a random one, obviously there is no strong preferential interaction, and the contribution to k_N and k_O from the interaction of dimers is the same. We conclude from structural considerations that k_N is very close to k_O. The predictions from this conclusion are compared with experiment in Table III.

The agreement between the calculated relative O^{18} and N^{15} effects and the experimental ones is excellent. What small discrepancy does exist may be attributed to the small contribution from the difference in the N—N and O—O interactions in the dimer. The present agreement lends further support to the head to tail structure of the dimer.

TABLE III. Relative O^{18} and N^{15} isotope effects in the vapor pressure of NO.

	Experimental	Calculated
$\dfrac{\ln P_{N^{14}O^{16}}/P_{N^{14}O^{18}}}{\ln P_{N^{14}O^{16}}/P_{N^{15}O^{16}}}$	1.38	1.46
$\dfrac{\delta\Delta H(N^{14}O^{18}-N^{14}O^{16})}{\delta\Delta H(N^{15}O^{16}-N^{14}O^{16})}$	1.45	1.46
$\dfrac{\delta T_{tr}(N^{14}O^{18}-N^{14}O^{16})}{\delta T_{tr}(N^{15}O^{16}-N^{14}O^{16})}$	1.40	1.46

VAPOR PRESSURE RATIO $N^{14}O^{16}/N^{15}O^{16}$

We have now shown that the vapor pressure ratios of $N^{14}O^{16}/N^{14}O^{18}$ and $N^{14}O^{16}/N^{15}O^{18}$ and the triple point temperatures of $N^{14}O^{18}$ and $N^{15}O^{18}$ can be described in terms of the vapor pressure ratio

$$N^{14}O^{16}/N^{15}O^{16}$$

and the triple points of $N^{14}O^{16}$ and $N^{15}O^{16}$. Further the difference heats of vaporization can all be correlated with the vapor pressure ratio of $N^{14}O^{16}/N^{15}O^{16}$. We shall now estimate the latter from molecular data.

The vapor pressure ratio can be written[5]

$$\ln P_{N^{14}O^{16}}/P_{N^{15}O^{16}}=\frac{1}{24}\left(\frac{1}{14}-\frac{1}{15}\right)\left(\frac{h}{kT}\right)^2(k_N)+\cdots. \quad (4)$$

We shall calculate k_N for a model of interacting dimers. The fact that the vapor pressure equation can be written in the form of Eq. (1) shows that the N—O bond of the monomer is to a high approximation the same in the dimer. This interaction therefore makes but a small contribution to k_N and will be neglected. Smith, Keller, and Johnston[11] have found three low-lying Raman frequencies in the spectrum of liquid NO. These are associated with the dimer. The fourth low-lying frequency is not definitely known. The frequencies associated with the stretching of the short NO bond are not much shifted from the gas, which further justifies our neglecting it. We shall assume that the square of the fourth low-lying frequency is equal to the average of the squares of the other three. It would have to deviate by a considerable amount to affect the present calculation. The contribution to k_N from the dimerization can be calculated from the approximation that the structure consists of four atoms of mass 15. This introduces a negligible error. The contribution of the dimerization to k_N is then

$$4k_N(\text{dimer})=(4/3)(15)\sum_{i=1}^{3}\omega_i^2.$$

The three frequencies associated with the dimer[11] are 167, 196, and 262 cm^{-1}. The contribution to k_N from the dimerization is thus calculated to be 69×10^4 cm^{-2}. This leads to a vapor pressure difference between $N^{14}O^{16}$ and $N^{15}O^{16}$ of

$$\ln P_{N^{14}O^{16}}/P_{N^{15}O^{16}}=\frac{1}{24}\left(\frac{hc}{kT}\right)^2\left(\frac{1}{14}-\frac{1}{15}\right)69\times10^4+\text{dimer}-\text{dimer}.$$

The numerical term above is 0.021 at 115°K. To this we must now add the effect due to the interaction of dimers. The latter has been estimated in two ways. In the first method we account for the displacements of the dimers in the lattice by a Debye spectrum and use $\theta_D=119$°K, which has been estimated by Johnston and Giauque[12] from heat capacity data. We assume that the rotations about the lattice points make a similar contribution. By the second method we extrapolate the vapor pressure data on N_2^{14}—$N^{14}N^{15}$, O_2^{16}—$O^{16}O^{18}$, $C^{12}O^{16}$—$C^{13}O^{16}$ with respect to temperature and mass. Both of these methods lead to $3\text{–}4\times10^{-3}$ in $\ln P'/P$ from the interaction of dimers. Thus we calculate $\ln P_{N^{14}O^{16}}/P_{N^{15}O^{16}}$ to be 0.025 at 115°K. The experimental value is 0.0295. The agreement is satisfactory and shows that the major contribution to the vapor pressure ratio arises from the relatively strong interaction when the monomers form dimers in the condensed state.

The difference in thermodynamic properties of the isotopic NO molecules, vapor pressures, heats of vaporization, and triple point temperatures have been quantitatively calculated in terms of a structure of interacting dimers. The relative isotope effects of $N^{15}O^{16}$, $N^{14}O^{18}$, and $N^{15}O^{18}$ have been calculated from structural considerations without the use of any experimental parameters.

[12] H. L. Johnston and W. F. Giauque, J. Am. Chem. Soc. **51**, 3194 (1929).

Quantum-Mechanical Calculation of Harmonic Oscillator Transition Probabilities in a One-Dimensional Impulsive Collision

KURT E. SHULER AND ROBERT ZWANZIG
National Bureau of Standards, Washington 25, D. C.

(Received June 6, 1960)

Quantum-mechanical vibrational transition probabilities $P_{i\to f}(\epsilon)$ for harmonic oscillators, undergoing impulsive hard sphere collisions along the line of centers with an incident atom with relative kinetic energy ϵ, have been computed by a machine (IBM-704) solution of the relevant Schrödinger equation. Curves for $P_{i\to f}(\epsilon)$ over a range of ϵ are presented for initial (i) and final (f) vibrational oscillator states $i, f=0, 1, 2$, and 3. It is shown that this model of an inelastic collision gives rise to appreciable vibrational transitions $v(i)\to v(f)$ with $|\Delta v|>1$ (in addition to $|\Delta v|=1$) in contrast to the Landau-Teller-Herzfeld adiabatic, first-order perturbation treatment which permits only transitions with $|\Delta v|=1$. This result is discussed in relation to the dissociation of diatomic molecules and to the adsorption of atoms on solids. Averaged transition probabilities $\bar{P}_{i\to f}(T)$ are computed for an incident beam of particles with a Maxwellian velocity distribution. It is pointed out that such averaged transition probabilities may give a misleading impression of the efficiency of translational-vibrational energy transfer if the $P_{i\to f}(\epsilon)$ show a resonance type of behavior, i.e., a strong dependence of $P_{i\to f}(\epsilon)$ on ϵ over a small interval of ϵ.

I. INTRODUCTION

IN order to develop quantitative treatments of rate and transport processes it is necessary to have information on energy transfer cross sections, particularly with respect to their dependence on the quantum states of the interacting species and on the various parameters which characterize the collisions.[1] There have been a number of calculations of energy transfer cross sections for the exchange of translational and vibrational energy in inelastic collisions between atoms and molecules. The classic treatment, on which most of these calculations are based, is that of Landau and Teller.[2] A quantum-mechanical version of the Landau-Teller theory has been developed over the past few years by K. F. Herzfeld and his co-workers.[3] The basic assumption underlying these treatments is that the maximum displacement X of the oscillator nuclei from their equilibrium separation r_e during the collision is small, compared to the "interaction distance" x between the incident atom and the center of the mass of the oscillator. Then the interaction energy $U(x-X)$ can be expanded as a power series in X about r_e in which terms of order X^2 or higher can be neglected. In this approximation, the vibrational transition probability matrix elements are linear in the nuclear displacement X and their evaluation leads, for harmonic oscillators, to the "selection rule" $\Delta v=\pm 1$, i.e., the collision can induce transitions only between neighboring vibrational levels v and $v\pm 1$.

Herzfeld and his co-workers have computed translational and vibrational transition probabilities for many diatomic molecules according to the above prescription and have found good agreement with experimental data obtained from ultrasonic dispersion and shock wave relaxation experiments (see footnote 3). It must be emphasized, however, that this agreement pertains in every case to transition between the first few vibrational levels, i.e., $v=0$, 1, and 2. Serious difficulties arise when the Landau-Teller assumption of small perturbation (i.e., $X\ll x$), which gives rise to the $\Delta v=\pm 1$ selection rule, and the assumption of near adiabacity of the collisions, which gives rise to a very inefficient transfer of translational to vibrational energy, are applied to problems where transitions to the higher vibrational levels play an important role. The following examples may be quoted. A calculation of the rate of collisional activation of a diatomic molecule A_2 to its "activated state" for dissociation using the selection rule $|\Delta v|=1$ and the Landau-Teller-Herzfeld values for the translational-vibrational transition probabilities results in an activation rate which is lower than the experimental one by several orders of magnitude (about 10^5 for the dissociation of I_2).[4] Analogous calculations by Herzfeld and Griffing[5] and by Herzfeld[6] using the $\Delta v=\pm 1$ selection rule gave similar results. Similar difficulties appear when one considers the processes of adsorption and desorption of atoms from solid surfaces. In this case the selection rule $|\Delta v|=1$ corresponds to one phonon processes (creation or destruction of one phonon) in the interaction of an atom with a surface.[7,8] Since the

[1] See, e.g., C. S. Wang-Chang and G. E. Uhlenbeck, "Transport Phenomena in Polyatomic Molecules," University of Michigan Publ. CM-681 (1951); M. A. Eliason and J. O. Hirschfelder, J. Chem. Phys. **30**, 1426 (1959).

[2] L. D. Landau and E. Teller, Physik. Z. Sowjetunion **10**, 34 (1936).

[3] For a detailed discussion see: K. F. Herzfeld and T. A. Litovitz, *Dispersion and Absorption of Ultrasonic Waves* (Academic Press, Inc., New York, 1959).

[4] E. W. Montroll and K. E. Shuler in *Advances in Chemical Physics*, edited by I. Prigogine (Interscience Publishers, Inc., New York, 1958), Vol. 1, p. 361.

[5] K. F. Herzfeld and V. Griffing, J. Phys. Chem. **61**, 844 (1957).

[6] K. F. Herzfeld in *Seventh Symposium (International) on Combustion* (Butterworths Scientific Publications, Ltd., London, 1959) p. 27. This calculation is for the dissociation of O_2.

[7] See, e.g., the series of papers of Lennard-Jones and co-workers in Proc. Roy. Soc. (London) (1936) and (1937). A summary of this work and detailed references are to be found in B. L. Bonch-Bruevich, Uspekhi Fiz. Nauk **40**, 369 (1950). (Technical Translation TT-509, National Research Council of Canada, Ottawa, 1954.)

[8] R. W. Zwanzig, J. Chem. Phys. **32**, 1173 (1960).

normal mode frequency spectrum of a lattice has an upper limit at the Debye frequency ν_m, the energy of a phonon has an upper limit equal to $k\theta_D$ where $\theta_D = h\nu_m/k$ is the Debye characteristic temperature. Since for many crystals θ_D is between 200 to 400°K, the phonon energy has a maximum of about 400 to 800 cal/mole. This energy is much too low for the desorption of strongly bound atoms in a one-step process and it is also much too low to account for the high heats of adsorption (presumably into the ground vibrational state) observed for both chemical and physical adsorption. The assumption of a $\Delta v = \pm 1$ "ladder climbing" process in the vibrational level system of the adsorbed atom-surface bond will, as in the gas phase case, lead to adsorption and desorption rates which are too low in comparison with the experimentally obtained values.

These difficulties suggest that, in addition to transitions with $|\Delta v| = 1$, the collisional transfer of translational and vibrational energy also proceeds by transitions with $|\Delta v| > 1$. If one considers anharmonic oscillators, then transitions with $|\Delta v| > 1$ are possible even within the linear interaction energy approximation. A calculation for anharmonic oscillator matrix elements with a linear interaction potential shows that the transition probabilities $P_{v,v\pm r}$ are proportional to x_e^{r-1} where x_e is the anharmonicity.[9] Since x_e is of the order of 10^{-2} to 10^{-3} for most diatomic molecules, it is evident that in this model transitions with $|\Delta v| > 1$ can not play any significant role in energy transfer rate processes.[10] Other attempts to use the Landau-Teller linearized interaction in higher orders of perturbation calculations would lead to similar results as evidenced from analogous optical transition calculations.

A more realistic approach to the calculation of translational-vibrational transition probabilities is to use the total interaction instead of a linearized interaction approximation. Such an approach is indicated particularly for collisions in which the kinetic energy of the incident atom is large compared to the vibrational quantum $h\nu$ of the oscillator and where the maximum displacement X of the oscillator nuclei from their equilibrium position will not be small compared to the "interaction distance" x. We have carried out such a calculation. For our model we have been able to show, that the probability per collision for a vibrational transition with $|\Delta v| > 1$ is of the same order of magnitude as that for a transition with $|\Delta v| = 1$.

II. CALCULATION OF THE TRANSITION PROBABILITIES $P_{i\to f}(\epsilon)$

We consider a one-dimensional system in which an incident atom interacts along the line of centers with a (rotationless) harmonic oscillator. For mathematical convenience we use a hard sphere potential between the incident atom and the struck atom of the oscillator so that we are dealing with an impulsive collision. Since such a collision may also be considered as one in which a very large force acts for a very short time, one is now no longer restricted to the adiabatic collisions of Landau and Teller in which the collision time is assumed to be long compared to the period of the vibration. This model of an impulsive inelastic collision has been considered previously by Jackson and Mott,[11] Castellan and Hulburt,[12] and by Widom[13] who have given approximate analytical solutions for some special cases using various simplifying assumptions. Since a general analytical solution to this problem appears to be intractable we have put our efforts into obtaining numerical solutions for various combinations of parameters using an IBM-704 computer.

We now proceed to a more formal description of the model, and the derivation of equations in a form suitable for machine computation. The diatomic molecule is represented by the harmonic oscillator Hamiltonian

$$H_0 = -(\hbar^2/2M)(\partial^2/\partial R^2) + \tfrac{1}{2}M\omega^2 R^2, \qquad (1)$$

where ω is the vibrational frequency of the oscillator, M is its mass, and R is the displacement of one of the atoms from its equilibrium position. The center of mass and the orientation of the molecule are fixed. The Hamiltonian for the incident atom is

$$H_1 = -(\hbar^2/2m)(\partial^2/\partial r^2). \qquad (2)$$

Its mass (which is "reduced" since the center of mass of the molecule has been fixed) is m and its position is r.

In a more realistic calculation than the present one the atom would interact with the molecule according to some potential energy function $U(r-R)$. In our model, however, we assume a rigid sphere interaction. It is well known that the singular rigid sphere potential energy can be conveniently and rigorously replaced by a boundary condition on the wave function $\Psi(r, R)$,

$$\Psi(r, R) \equiv 0 \qquad \text{if} \qquad r - R = \sigma, \qquad (3)$$

where σ is the distance of closest approach of the atom to the molecule. Note that the actual value of σ is of no consequence, since r can be replaced by $r-\sigma$ without affecting either H_0 or H_1. We shall assume that this substitution has already been made so that we can take $\sigma = 0$. The problem is thus to solve Schrödinger's equation

$$(H_0 + H_1)\Psi(r, R) = E\Psi(r, R) \qquad (4)$$

with the boundary condition

$$\Psi(R, R) \equiv 0. \qquad (5)$$

[9] R. Herman and K. E. Shuler, J. Chem. Phys. **21**, 373 (1953); **22**, 954 (1954).

[10] N. W. Bazley, E. W. Montroll, R. J. Rubin, and K. E. Shuler, J. Chem. Phys. **28**, 700 (1958); *ibid.* **29**, 1185 (1958).

[11] J. M. Jackson and F. N. Mott, Proc. Roy. Soc. (London) **A137**, 703 (1932).

[12] G. W. Castellan and H. M. Hulburt, J. Chem. Phys. **18**, 312 (1950).

[13] B. Widom, J. Chem. Phys. **30**, 238 (1959).

Since Schrödinger's equation for the present problem is separable in the coordinates r and R, the most general solution is a linear combination of products of harmonic oscillator wave functions, ψ_n,

$$H_0\psi_n(R)=E_n\psi_n(R) \qquad n=0, 1, 2\cdots$$
$$E_n=(n+\tfrac{1}{2})\hbar\omega \tag{6}$$

and free particle wave functions, $\exp(\pm ipr/\hbar)$. The solution which is consistent with a given total energy E, and which represents the scattering of a single incident wave with wave number $p_i/\hbar$ by a single initial oscillator state, is

$$\Psi(r, R)=A_i\psi_i(R)\exp[-(i/\hbar)p_ir]+\sum_f B_f\psi_f(R)\exp[(i/\hbar)p_fr]. \tag{7}$$

The momentum of the incident atom is $-p_i$, and $p_i>0$; the subscript i labels the initial oscillator state. In order that Ψ satisfy Schrödinger's equation, the momenta p_f must obey the condition

$$E_i+(1/2m)p_i^2=E_f+(1/2m)p_f^2 \tag{8}$$

for all f, where f labels the final oscillator state. Those states for which p_f^2 is negative must be included for completeness. If we take the positive root $p_f=+i(|p_f|^2)^{\frac{1}{2}}$, such states will decay exponentially with increasing r and will not appear in the asymptotic forms of the wave function. They are, however, essential for satisfying the boundary condition.

The probability of a transition in which the oscillator goes from state ψ_i to state ψ_f, while the momentum of the incident atom changes from $-p_i$ to $+p_f$, is

$$P_{i\to f}=(p_f/p_i)(|B_f|^2/|A_i|^2). \tag{9}$$

This is defined only for those transitions in which p_f is real. Since the amplitude of the incident wave determines the scattering uniquely, it is convenient to choose the normalization $A_i=1$. We have to find those coefficients B_f for which $\Psi(R, R)$ vanishes identically in R.

We follow the procedure introduced by Jackson and Mott.[11] This is to expand the wave function along the boundary in harmonic oscillator states

$$\Psi(R, R)=\sum_n c_n\psi_n(R)$$
$$c_n=\int_{-\infty}^{+\infty}dR\psi_n^*(R)\Psi(R, R). \tag{10}$$

Since $\Psi(R, R)$ vanishes identically, and since the functions $\psi_n(R)$ form a complete orthonormal set, the coefficients c_n must all vanish.

$$c_n=\int_{-\infty}^{+\infty}\psi_n^*(R)\exp[-(i/\hbar)p_iR]\psi_i(R)dR+\sum_f B_f\int_{-\infty}^{+\infty}\psi_n^*(R)\exp[+(i/\hbar)p_fR]\psi_f(R)dR=0 \tag{11}$$

for all n. This is an infinite set of inhomogeneous simultaneous linear equations in the variables B_f.

Subsequent numerical calculations will be greatly simplified if dimensionless variables are used. Distances R are expressed in terms of the characteristic harmonic oscillator length $(\hbar/M\omega)^{\frac{1}{2}}$, by

$$x=R(\hbar/M\omega)^{-\frac{1}{2}} \tag{12}$$

and energies are expressed in terms of $\hbar\omega$. The kinetic energy ϵ of the incident atom in these units is

$$\epsilon=(p_i^2/2m)/\hbar\omega. \tag{13}$$

We also introduce a symbol for the mass ratio

$$\gamma^2=2m/M. \tag{14}$$

Then it is easy to see that

$$p_iR/\hbar=\gamma x(\epsilon)^{\frac{1}{2}}$$
$$p_fR/\hbar=\gamma x(\epsilon+i-f)^{\frac{1}{2}}. \tag{15}$$

Using conventional matrix notation for the integrals, the equations for the B_f are

$$\sum_n\langle n\,|\exp[i\gamma x(\epsilon+i-f)^{\frac{1}{2}}]\,|f\rangle B_f=-\langle n\,|\exp(-i\gamma x\epsilon^{\frac{1}{2}}\,|\,i\rangle. \tag{16}$$

The integrals are easily evaluated for harmonic oscillators; we obtain (for arbitrary α)

$$\langle n\,|\exp(i\alpha x)\,|f\rangle=H_{nf}(\alpha)\exp(-\alpha^2/4) \tag{17}$$

where, if $n<f$,

$$H_{nf}(\alpha)=(f!n!)^{-\frac{1}{2}}\sum_{k=0}^{n}\binom{n}{k}f^{(k)}(\alpha i/\sqrt{2})^{f+n-2k} \tag{18}$$

and

$$f^{(k)}=f(f-1)\cdots(f-k+1).$$

If $n>f$, one merely exchanges f and n in this equation. The equations to be solved numerically for the B_f are then

$$\sum_f H_{nf}[\gamma(\epsilon+i-f)^{\frac{1}{2}}]\exp[\gamma^2(f-i)/4]B_f=-H_{ni}^*(\gamma\epsilon^{\frac{1}{2}}). \tag{19}$$

The requirement of conservation of current density is a useful check on the accuracy of the numerical work. This is given by

$$\sum_f{}'p_f\,|B_f|^2=p_i\,|A_i|^2 \tag{20}$$

or, since $|A_i|^2$ has been chosen to be unity,

$$\sum_f{}'[(\epsilon+i-f)/\epsilon]^{\frac{1}{2}}\,|B_f|^2=1 \tag{21}$$

where the sum $\sum'$ is restricted to those f for which p_f is real. (Imaginary values of p_f appear in the exponentially decaying part of the solution, and make no contribution to the current density as $r\to\infty$.) In the pres-

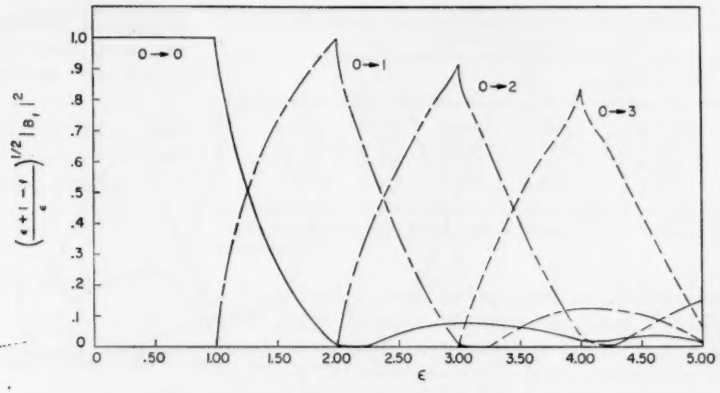

FIG. 1. The vibrational transition probability per collision $P_{i\to f}(\epsilon) = [(\epsilon+i-f)/\epsilon]^{\frac{1}{2}} |B_f|^2$ as a function of the (dimensionless) relative kinetic energy ϵ of the incident particles. Oscillator in initial vibrational state $i=0$.

ent notation the transition probabilities per collision are then

$$P_{i\to f}(\epsilon) = [(\epsilon+i-f)/\epsilon]^{\frac{1}{2}} |B_f|^2. \tag{22}$$

They depend implicitly on the mass ratio parameter γ through Eq. (19).

The set of simultaneous linear equations (19) has been solved numerically for the transition amplitudes B_f for initial (i) and final (f) oscillator levels $i, f = 0, 1, 2$, and 3, in the range $0<\epsilon<5$, and using $\gamma=1$. This value of γ corresponds, in the case of homonuclear oscillators, to a mass ratio of 7 which one would find (approximately) for systems like O_2+He or I_2+A. The above range of ϵ, the ratio of the kinetic energy of the incident particles to the vibrational energy of the oscillators, permits the computation of $P_{i\to f}(\epsilon)$ for transitions[14] up to $|i-f| = |\Delta v| = 4$.

The method of solution is described in this paragraph. For any given initial state i, Eqs. (19) form an infinite set of simultaneous linear equations in the unknown B_f. This infinite set was replaced by a finite set of order N, and these were solved on the IBM-704 computer. The order N was increased until convergence in $|B_f|^2$ was reached to three decimal places, for the physically important values of f. For ϵ around 1, the number N varied from 8 to 13 depending upon the value of i. Near $\epsilon=5$, N varied from 15 to 20. The upper limit on the number of equations had to be set at $N=20$ since computer overflow occurred in going past this number. Solutions for $P_{i\to f}(\epsilon)$ and $|B_f|^2$ were obtained at intervals of ϵ of 0.25 in the range $0<\epsilon<5$ except about the "resonance peaks" where the interval was taken as 0.05.

The results of these calculations are shown in Figs. 1 through 4 where we have plotted the normalized transition probabilities $P_{i\to f}(\epsilon)$ of Eq. (22) as a function of the dimensionless incident particle energy ϵ. *It will be noted that transitions with* $|\Delta v| = |i-f| > 1$ *are now strongly allowed.* The "resonance" behavior at $\epsilon=f+1$ is a quantum effect; the sharpness of the "resonance" peaks is probably attributable to the hard sphere interaction model.[15] Microscopic reversibility for the $P_{i\to f}(\epsilon)$ holds in the form

$$P_{a\to b}(\epsilon) = P_{b\to a}(\epsilon+a-b) \tag{23}$$

which reflects the condition for conservation of total energy [Eq. (8)] as written in dimensionless variables.

The results obtained above should be compared with those of Bartlett and Moyal[16] who computed the *exact* (analytical) transition probabilities for a quantum mechanical oscillator in an external field where the perturbing potential has the form $V=q\mathcal{E}(t)$, q is the oscillator coordinate and $\mathcal{E}(t)$ is an arbitrary function of the time. This calculation is valid for large as well as small perturbations. Bartlett and Moyal found a high probability for excitation with $|\Delta v| > 1$ in the case of large perturbations. Our work agrees with these findings in that excitations with $|\Delta v| > 1$ are highly probable for strong interaction.

III. TRANSITION PROBABILITIES FOR AN INCIDENT MAXWELLIAN BEAM OF PARTICLES. [DISTRIBUTION AVERAGED TRANSITION PROBABILITIES]

The transition probabilities per collision $P_{i\to f}(\epsilon)$ computed in Sec. II pertain to collisions of oscillators in state i with an incident monoenergetic beam of particles with energy ϵ. While it may be possible with modern molecular beam techniques to carry out inelastic scattering experiments with monoenergetic atomic beams, in the more usual experimental techniques the oscillators are in an essentially thermal environment. It is therefore of interest to convert our $P_{i\to f}(\epsilon)$ to $\bar{P}_{i\to f}(T)$ by integrating the $P_{i\to f}(\epsilon)$ over a Maxwellian velocity distribution corresponding to a thermal beam at the temperature T.

[14] It should be noted that conservation of current requires $\epsilon > |i-f|$ (for $i<f$) where $|i-f|$ is of course integral.

[15] Analogous resonance peaks appear in the theory of inelastic neutron scattering by harmonic oscillators. See e.g., G. Placzek, Phys. Rev. **86**, 377 (1952); G. Placzek and L. Van Hove, Nuovo cimento **1**, 233 (1955); G. C. Wick, Phys. Rev. **94**, 1228 (1954).

[16] M. S. Bartlett and J. E. Moyal, Proc. Cambridge Phil. Soc. **45**, 545 (1949).

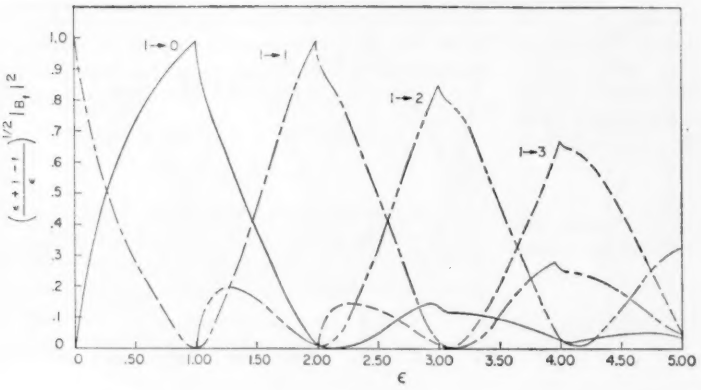

FIG. 2. The vibrational transition probability per collision $P_{i\to f}(\epsilon)=[(\epsilon+i-f)/\epsilon]^{\frac{1}{2}}|B_f|^2$ as a function of the (dimensionless) relative kinetic energy ϵ of the incident particles. Oscillator in initial vibrational state $i=1$.

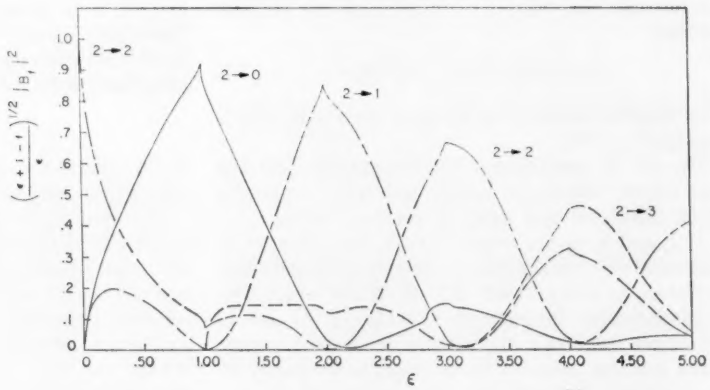

FIG. 3. The vibrational transition probability per collision $P_{i\to f}(\epsilon)=[(\epsilon+i-f)/\epsilon]^{\frac{1}{2}}|B_f|^2$ as a function of the (dimensionless) relative kinetic energy ϵ of the incident particles. Oscillator in initial vibrational state $i=2$.

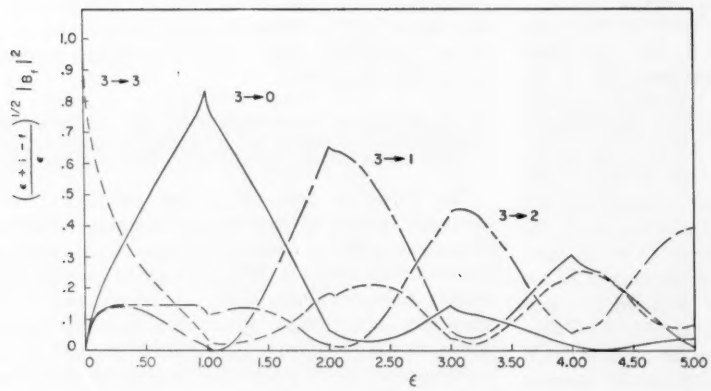

FIG. 4. The vibrational transition probability per collision $P_{i\to f}(\epsilon)=[(\epsilon+i-f)/\epsilon]^{\frac{1}{2}}|B_f|^2$ as a function of the (dimensionless) relative kinetic energy ϵ of the incident particles. Oscillator in initial vibrational state $i=3$.

In a one-dimensional *beam* with a Maxwellian distribution of velocities the fraction of atoms dN/N with velocities between v and $v+dv$ (or energies between ϵ and $\epsilon+d\epsilon$) is given by

$$dN/N=(m/kT)v\exp(-mv^2/2kT)dv$$
$$=(1/\phi)\exp(-\epsilon/\phi)d\epsilon, \quad (24)$$

where $\phi=kT/h\nu$. The temperature dependent transition probabilities $\bar{P}_{i\to f}(T)$ are given by

$$\bar{P}_{i\to f}(T)=\phi^{-1}\int_0^\infty P_{i\to f}(\epsilon)\exp(-\epsilon/\phi)d\epsilon. \quad (25)$$

Before evaluating Eq. (25) for some specific values of ϕ we wish to verify that the $\bar{P}_{i\to f}(T)$ obtained from Eq. (25) obey the principle of detailed balancing and

form a stochastic matrix.[17] Any physically meaningful set of transition probabilities must fulfill these two conditions. From Eq. (23) it follows that

$$\bar{P}_{b\to a}(T)=\phi^{-1}\int_0^\infty P_{b\to a}(\epsilon+a-b)\exp(-\epsilon/\phi)d\epsilon. \quad (26)$$

Setting $\epsilon+a-b=\epsilon'$, one can rewrite Eq. (26) as

$$\bar{P}_{b\to a}(T)$$

$$=\phi^{-1}\int_0^\infty P_{b\to a}(\epsilon')\exp[-(1/\phi)(\epsilon'+b-a)]d\epsilon'$$

$$=\phi^{-1}\exp[-(1/\phi)(b-a)]\int_0^\infty P_{b\to a}(\epsilon')\exp(-\epsilon'/\phi)d\epsilon'. \quad (27)$$

Since ϵ' in Eq. (27) is only an integration variable it can be replaced again by ϵ and a comparison of Eqs. (27) and (25) then shows that

$$\bar{P}_{a\to b}(T)\exp(-a/\phi)=\bar{P}_{b\to a}(T)\exp(-b/\phi). \quad (28)$$

If one now multiplies both sides of Eq. (28) by Z, the number of collisions per unit time, and recalls that for harmonic oscillators the equilibrium population n_j^{eq} of oscillators in level j is proportional to $\exp(-j/\phi)$, Eq. (28) can be written as

$$Z\bar{P}_{a\to b}(T)n_a^{eq}=Z\bar{P}_{b\to a}(T)n_b^{eq} \quad (29)$$

which is the familiar form of the detailed balancing relation. That set $\bar{P}_{i\to f}(T)$ forms a stochastic matrix can readily be verified by summing Eq. (25) over all f and then using relations (9) and (21) to obtain

$$\sum_f P_{i\to f}(T)=\sum_f\phi^{-1}\int_0^\infty P_{i\to f}(\epsilon)\exp(-\epsilon/\phi)d\epsilon$$

$$=\phi^{-1}\int_0^\infty\sum_f P_{i\to f}(\epsilon)\exp(-\epsilon/\phi)d\epsilon$$

$$=\phi^{-1}\int_0^\infty\exp(-\epsilon/\phi)d\epsilon=1. \quad (30)$$

It should be pointed out that attempts to convert the one-dimensional $P_{i\to f}(\epsilon)$ to $\bar{P}_{i\to f}(T)$ by integrating over a two-dimensional or three-dimensional incident Maxwellian beam lead to results which no longer obey the principle of detailed balancing. The moral of this observation is clear.

We have computed the transition probabilities $\bar{P}_{i\to f}(T)$ from Eq. (25) by numerical integration. Since these values were calculated only in the range $0<\epsilon<5$ the ϵ integration could only be carried out between these limits. It was therefore necessary to choose a value of ϕ for which $\exp(-\epsilon/\phi)$ becomes very small as $\epsilon\to 5$, so that there would be no significant contribution to $\bar{P}_{i\to f}(T)$ for $\epsilon>5$. We have computed $\bar{P}_{i\to f}(T)$ for $\phi=0.5$ which, for many diatomic oscillators such as N_2, O_2, or CO corresponds to a beam temperature of between 1000 to 1500°K.[18] The transition probability matrix $\bar{P}_{i\to f}(T)$ obtained for this value of ϕ is shown in Table I.

TABLE I. Distribution averaged vibrational transition probabilities $\bar{P}_{i\to f}(T)$ $[\phi=kT/\hbar\omega=0.5]$.

i	f 0	1	2	3	$\Sigma_f\bar{P}_{i\to f}(T)$[a]
0	0.923	0.071	0.008	0.001	1.003
1	0.528	0.471	0.022	0.002	1.023
2	0.441	0.158	0.413	0.017	1.029
3	0.373	0.119	0.127	0.395	1.014

[a] The deviation from unity of these sums is a measure of the accuracy of the numerical results.

A comparison of the $\bar{P}_{i\to f}(T)$ of Table I with the values calculated by Herzfeld and co-workers[3] shows a wide discrepancy for comparable transitions, i.e., transition with $\Delta v=\pm 1$. Whereas Herzfeld obtains values of $P_{1\to 0}(1000°K)$ in the range of 10^{-4} to 10^{-9} we find $P_{1\to 0}$ $(1000°K)\simeq 5\times 10^{-1}$. Such a comparison is, however, unrealistic. Herzfeld's calculations are based on the adiabatic, weak interaction model of Landau and Teller and will thus necessarily result in low values for $P_{i\to f}(T)$. Our model for an impulsive collision, which is nonadiabatic and involves a very strong interaction, will naturally give rise to much higher values of $\bar{P}_{i\to f}(T)$. The primary aim of this paper has not been to compute absolute values for $\bar{P}_{1\to 0}(T)$ for small perturbations. It has been instead to explore the consequences of a strong interaction model on the form of the $P_{i\to f}(\epsilon)$ and $\bar{P}_{i\to f}(T)$.

The significant comparison is between the values of $\bar{P}_{i\to f}(T)$ of Table I and the values of $\bar{P}_{i\to f}(\epsilon)$ of Figs. 1–4. Focusing our attention, for example, on the 1→0 transition, it appears from Table I that on the average essentially every second collision is effective in producing the de-excitation. From Fig. 2, however, we learn that while at $\epsilon=1$ essentially every collision produces the de-excitation, at $\epsilon=2.15$ about 5×10^4 collisions are required. For the transition 0→3 for instance, Table I shows that only 1 out of a 1000 collisions are effective while Fig. 1 shows that at $\epsilon=4$ essentially every collision is effective in producing this excitation. This apparent contradiction is of course due to the fact that the values of $\bar{P}_{i\to f}(T)$ in Table I have been obtained by averaging the $P_{i\to f}(\epsilon)$ over the thermal distribution (24). It is not clear how strongly this "resonance" type of behavior of $P_{i\to f}(\epsilon)$ with ϵ depends upon the impulsive hard sphere collision model. The calculations presented here, however, indicate the

[17] A stochastic matrix is a square matrix with non-negative elements and unit row sums. A properly defined set of transition probabilities, when written as a matrix, will form a stochastic matrix.

[18] With our dimensionless set of parameters $\phi=kT/\hbar\omega$ and $\epsilon=(p_i^2/2m)/\hbar\omega$ the temperature T of the incident Maxwellian beam of atoms can only be expressed in terms of the energy level spacing $\hbar\omega$ of the oscillators. The *mean* kinetic energy of a one-dimensional Maxwellian beam is $\phi/2$ in our dimensionless units.

desirability of carrying out experiments on vibrational excitation and deexcitation using monoenergetic incident beams to obtain $P_{i\to f}(\epsilon)$, rather than under the usual thermal conditions where very little information on the energy dependence of the inelastic scattering cross sections can be obtained.

IV. ACKNOWLEDGMENTS

We wish to acknowledge the many helpful contributions of Dr. D. J. Rubin. Our thanks are also due to Miss I. Stegun and Miss R. Zucker of our Computation Laboratory who programmed and carried out most skillfully the calculations presented in this paper.

THE JOURNAL OF CHEMICAL PHYSICS VOLUME 33, NUMBER 6 DECEMBER, 1960

Mass Spectrometric Determination of the Dissociation Energies of the Molecules AgAu, AgCu, and AuCu†

MARCEL ACKERMAN,* FRED E. STAFFORD,‡ AND JEAN DROWART

Laboratoire de Chimie Physique Moléculaire, Université Libre de Bruxelles, Brussels, Belgium

(Received May 16, 1960)

The vapors issuing from mullite and graphite Knudsen cells containing pure metals and alloys of the triad Cu—Ag—Au have been analyzed mass spectrometrically. From the experimental ratios of diatomic to monoatomic species and the vapor pressures of the elements, the following dissociation energies are obtained:

$D_0^0(Cu_2)=45.5\pm2.2$ kcal $\quad D_0^0(AgAu)=47.6\pm2.2$ kcal
$D_0^0(Ag_2)=37.6\pm2.2$ kcal $\quad D_0^0(AgCu)=40.7\pm2.2$ kcal
$D_0^0(Au_2)=51.5\pm2.2$ kcal $\quad D_0^0(AuCu)=54.5\pm2.2$ kcal

These are based on $\Delta H_{298}^{vap}=81.1$, 68.4, and 87.5 kcal/g-atom for Cu, Ag, and Au where D_0^0 of AgCu depends on the value for Cu, and D_0^0 of AgAu and AuCu on Au. The uncertainties quoted do not include the uncertainty in ΔH^{vap}.

INTRODUCTION

THE symmetric molecules Cu_2, Ag_2, and Au_2 have been identified and studied by optical spectroscopy in emission and absorption by Ruamps,[1] and by Kleman, Lindkvist, and Selin.[2,3] Vibration frequencies and dissociation energies from linear Birge-Sponer extrapolations were obtained. Drowart and Honig[4] and Schissel[5] used a mass spectrometric technique to study the species vaporizing from the pure metals. They identified the symmetric diatomic molecules and determined their heats of dissociation. Martynkevitch[6] apparently has observed triatomic copper ions above pure copper.

The asymmetric molecules AgAu, AgCu, and AuCu were observed spectroscopically by Ruamps.[7,8] The species AuCu was observed by Schissel,[5] while all three asymmetric molecules were observed by Ackerman.[9]

The present paper reports a mass spectrometric determination of the dissociation energies of the symmetric and asymmetric diatomic molecules in equilibrium with binary Cu-Ag-Au alloys. Particular emphasis has been placed on obtaining values of dissociation energies that are accurate relative to one another.

EXPERIMENTAL

Binary alloys were prepared by mixing together weighed quantities of the 99.9% pure metals and melting them in the mass spectrometer. The initial composition was generally about 90 at. % of the less volatile constituent. In all cases, the more volatile constituent was found to distill off quantitatively leaving behind the other constituent essentially pure.

The alloys were vaporized from electron-bombardment heated[10] Knudsen cells with 1-mm diam orifices and orifice-to-sample-surface ratio of about 1/100. In the early experiments, graphite Knudsen cells were

† This research has been supported in part by the Wright Air Development Center of the Air Research and Development Command, U. S. Air Force, through its European Office.

* Aspirant, Fonds National de la Recherche Scientifique, Belgium.

‡ Postdoctoral Fellow, National Science Foundation, United States.

[1] J. Ruamps, Compt. rend. **237**, 1489 (1954).

[2] B. Kleman and S. Lindkvist, Arkiv Fysik **8**, 333 (1954); *ibid.* **9**, 385 (1955).

[3] B. Kleman, S. Lindkvist and L. E. Selin, Arkiv Fysik **8**, 505 (1954).

[4] J. Drowart and R. E. Honig, J. Chem. Phys. **25**, 581 (1956); J. Phys. Chem. **61**, 980 (1957).

[5] P. Schissel, J. Chem. Phys. **26**, 1276 (1957).

[6] G. M. Martynkevitch, Vestnik Moskov Univ. Ser. Mat. Mekhan, Astron. Fiz. Khim. **13**, 151 (1958); Chem. Abstracts **53**, 5796h (1959).

[7] J. Ruamps, Compt. rend. **239**, 1200 (1954).

[8] J. Ruamps, *Colloquium Spectroscopium Internationale VI* (Amsterdam) (Pergamon Press, New York, 1956).

[9] M. Ackerman, Ind. chim. belge **25**, 523 (1960).

[10] W. A. Chupka and M. G. Inghram, J. Phys. Chem. **59**, 100 (1955).

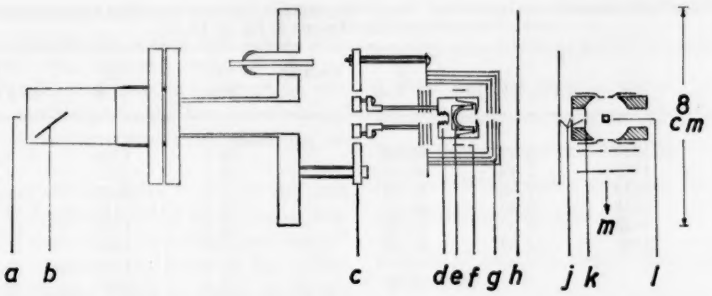

FIG. 1. Electron bombardment and ion source assembly, schematic. *a*, pyrometer window; *b*, magnetically operated shutter; *c*, pyrophyllite support; *d*, "blackbody" hole for temperature measurements; *e*, crucible—outer crucible in Mo, inner in mullite ($3Al_2O_3 \cdot 2SiO_2$); *f*, electron emission filament; *g*, radiation shields; *h*, movable beam defining slit; *j*, limiting collimation of molecular beam; *k*, ion source; *l*, beam of ionizing electrons.

used. However, particularly in the case of gold, during the course of an experiment the monomer intensity was observed to decrease appreciably and the dimer/monomer ratio, taken at constant temperature, similarly decreased by as much as a factor of 10. Examination of a ball of gold that remained after such an experiment showed that it was covered by a heavy layer of graphite, in contrast with the results of Rossman and Yarwood.[11] As a result, experiments were made using a molybdenum outer crucible and an impermeable mullite ($3A1_2O_3 \cdot 2SiO_2$) inner crucible, which proved to be satisfactory.

A Leeds and Northrup disappearing filament optical pyrometer was used to measure the brightness temperature of a hole drilled in the bottom of the molybdenum crucible. Calibrations for emissivity were obtained *in situ* and are given under "Treatment of Data."

The crucible and source arrangement are significantly different from those used previously in this laboratory and are shown in Fig. 1. The pyrometer window *a* is protected from deposits by the magnetically operated shutter *b*. The geometry used is such that the pyrometer objective is completely filled by light from the blackbody hole in the crucible *d*. The molecular beam limiting aperture is a 1-mm orifice at *j*. The density distribution of the deposit on a window on the far side of the source *k* is the same as that calculated for a 1-mm crucible orifice and the collimation at *j*. None of the molecular beam strikes any part of the source. A movable beam defining slit *h*, whose position is fixed by a micrometer screw, permits us to distinguish between ions formed from species in the molecular beam, from species possibly reevaporating from the radiation screens and from the residual gases in the source.[12]

Pumping speed in the region of the source and the furnace is about 10 liters/sec.

The ion source is the same as used previously.[4,13] Ions were formed by a 3- to 30-μA of 5- to 70-v electrons and accelerated to 2000 ev.

The ions formed were mass analyzed by a 20-cm radius of curvature, 60° sector, single focusing mass spectrometer with a resolving power of 1/700 (Rayleigh criterion). The ion current leaving the exit slit was further accelerated to 4500 ev, amplified by a nine-stage Ag-Mg secondary electron multiplier, and then measured by a vibrating reed amplifier and pen recorder. Species were identified[12] by mass, isotope ratio, appearance potential, and dependence of intensity on the position of the movable beam defining slit *h*.

EXPERIMENTAL DATA

In addition to the atoms, only the six symmetric and asymmetric diatomic molecules were observed. Table I presents the observed ratios of diatomic to monoatomic molecules corrected for ionization cross section and multiplier efficiency. The first column of the table indicates the number of the experiment; the second, the absolute temperature; the third, the ratio of molecule pressure to that of the *more* volatile atomic species; and the last, the value of the dissociation energy calculated by Eq. (1). Values indicated by footnote c are averages of 3 to 5 consecutive readings taken at a given temperature.

TREATMENT OF DATA

The dissociation energies $D_0°$ were calculated using the relation

$$D_0° = -RT \ln[I(Y)\sigma\gamma(XY)/I(XY)\sigma\gamma(Y)]p(X) - T\Delta[(F°-H_0°)/T], \quad (1)$$

where $I(Y)$ is the ion current due to species Y; σ the ionization cross section; γ the relative efficiency of the secondary electron multiplier; $p(X)$ the vapor pressure of the less volatile species X; and $(F°-H_0°)/T$ the free energy function.

[11] M. G. Rossman and J. Yarwood, Brit. J. Appl. Phys. **5**, 7 (1954).

[12] M. G. Inghram and J. Drowart, *Mass Spectrometry Applied to High Temperature Chemistry: Proceedings of a Conference, Asilomar, California* (1959).

[13] J. Drowart and P. Goldfinger, J. chim. phys. **55**, 721 (1958).

TABLE I. Corrected dimer/monomer ratios and calculated dissociation energies from ion intensities above pure metals (Experiments 19 and 20) and alloys (Experiments 4, 10, 14, 16, 17).

Column	(1) Exp.	(2) T°K	(3) $(XY/Y)\times10^4$	(4) D_0^0 kcal
Cu_2				
	20.1	1549	6.27	45.65
	20.6	1582	7.16	45.51
	20.5	1620	7.96	45.15
	20.2	1634	9.93	45.65
	20.3	1642	9.67	45.38
	20.4	1709	13.82	45.44
				mean 45.46
Ag_2				
	19.7	1336	7.47	37.93
	19.2	1352	8.69	38.03
	19.1	1356	6.85	37.32
	19.6	1419	11.43	37.62
	19.5	1447	12.02	38.13
	19.3	1479	13.10	36.99
	19.4	1502	15.10	37.05
				mean 37.58
Au_2[a]				
	14.1	1666	9.77	51.66[c]
	14.2	1722	11.06	51.65[c]
	14.3	1801	17.07	51.32[c]
	16.4	1658	9.57	52.23
	16.3	1703	7.25	50.43
	16.1	1734	14.73	52.34
	16.2	1742	13.14	51.78
	16.5	1777	12.21	50.92
	17.1	1694	11.72	52.21[c]
	17.3	1726	11.40	51.57[c]
	17.2	1778	14.53	51.53[c]
				mean 51.49
AgAu[a]				
	14.1	1568	3.67	48.17
	14.2	1575	3.17	46.32
	14.3	1667	7.00	48.26[c]
	14.4	1722	8.76	47.92[c]
	14.5	1798	11.77	47.76[c]
	17.1	1566	2.89	47.28
	17.2	1612	3.27	46.71
	17.3	1694	6.59	47.51[c]
	17.5	1726	9.31	47.86[c]
	17.4	1778	9.50	47.96[c]
	17.6	1788	8.82	46.61
				mean 47.58
AgCu[b]				
	04.1	1484	1.78	41.56[c]
	04.2	1632	2.85	41.20
	04.3	1674	4.27	39.90
	04.4	1770	7.16	39.77
	10.1	1565	5.16	42.76
	10.2	1583	3.01	40.66
				mean 40.65
AuCu[a]				
	16.5	1658	47.3	55.39
	16.4	1703	41.9	54.25[c]
	16.1	1725	48.0	54.32
	16.2	1734	43.6	53.83
	16.3	1742	53.3	54.43
	16.6	1781	62.8	54.49[c]
	16.7	1798	70.1	54.81[c]
				mean 54.50

[a] In experiments 14, 16, and 17 correction of 0.3, 0.7, and 0.3 kcal, respectively, have been added to D_0^0 to components for the reduced activity of gold in the alloys.

[b] 0.3 kcal has been added to D_0^0(AgCu) for the reduced activity of copper.

[c] Average of 3 to 5 consecutive measurements at the same temperature.

Values for the relative ionization cross sections of Cu and Ag were taken from Otvos and Stevenson.[14] The value for Au was calculated from data for a quantitative vaporization of a 15-mg Cu-Au (50 at. % Cu) alloy sample in the mass spectrometer with a classical collector. Equation (2) presents the relation between ion intensity and ionization cross section

$$\sigma(X)\gamma(X)S'=(s/G)(M/2\pi R)^{\frac{1}{2}}\Sigma_t I(X)T^{\frac{1}{2}}\Delta t, \qquad (2)$$

where γ is unity for a classical collector, S' is characteristic of the instrument, s is the area of the effusion orifice, G the number of grams evaporated, M the molecular weight, R the gas constant, T the absolute temperature, and t the time. When comparison is made between two substances evaporated simultaneously, S' and s cancel. The value obtained is

$$\sigma(\text{Au})/\sigma(\text{Cu})=35/18.4.$$

For the diatomic species it is assumed that[14]

$$\sigma(XY)=\sigma(X)+\sigma(Y).$$

[14] G. W. Otvos and D. P. Stevenson, J. Am. Chem. Soc. **78**, 546 (1956).

The multiplier efficiency, as a function of mass only, was determined experimentally from data for a mixture of rare gases and from quantitative vaporizations of alloys. Molecular effects were calculated as suggested by Stanton, Chupka and Inghram.[15] The values used are shown in Table II.

The temperature scale of the pyrometer was verified by observing the melting point of Cu, Ag, and Au. The experimental arrangement consisted of a block of graphite under a hydrogen atmosphere in an electrically heated quartz tube furnace. One hole in the graphite block served as a "blackbody" while an adjacent served as sample holder.

In addition, an *in situ* calibration described by Johnson, *et al.*[16] using the molybdenum cell in the mass spectrometer was performed. This involved measuring the crucible brightness temperature and ionic intensity of the species X^+ at some temperature just above the point of fusion. The heating power was reduced, the cooling curve recorded, and the brightness tempera-

[15] H. E. Stanton, W. A. Chupka and M. G. Inghram, Rev. Sci. Instr. **27**, 109 (1956).

[16] R. G. Johnson, D. E. Hudson, W. C. Caldwell, F. H. Spedding, and W. R. Savage, J. Chem. Phys. **25**, 917 (1956).

ture measured at the lower temperature. Interpolation of the intensities between the higher and lower temperatures measured was achieved using a plot of $\log I^+T$ vs $1/T$. The observed point of fusion of Au was 40° low. This was attributed to the low emissivity of the molybdenum. Corrections were made assuming an emissivity of 0.7.[17]

The heats of vaporization ΔH_{298}^{vap} of Cu, Ag, and Au were taken as 81.1, 68.4, and 87.5 kcal. Vapor pressures for Cu and Ag were taken from Stull and Sinke.[18] For gold there is a disagreement between the values given by Stull and Sinke, which is based on Hall's work,[19f] and the recent determinations of Nesmeianov, Smakhtin, and Lebedev,[19g] Edwards,[19h] and Rauh.[19i] Table III indicates the various values calculated for ΔH_{298}^{vap} for gold, based on the free energy functions of Stull and Sinke.[18]

TABLE II. Ionization cross sections and relative yield of the multiplier.

Species	Ionization cross section	Mult. yield × cross section
Cu	18.4	18.4
Cu_2	36.8	26.1
Ag	34.8	24.7
Ag_2	69.6	32.4
Au	35	16
Au_2	70	26
AgCu	53.2	29.3
AgAu	70	29
AuCu	53	23

The values of Harteck, and of Baur and Brunner have been interpreted by Hall as giving upper and lower limits, Harteck being high because of contamination of his surface (cf. Fraser[20]) and Baur and Brunner low because of inadequate emissivity corrections. We have chosen to use the average of the three most recent determinations, 87.5 kcal.

We have attempted also to measure directly the differences in heats of vaporization of Cu, Ag, and Au. The relation between the ionic intensities due to Cu or Ag and Au and the respective pressure is

$$p(\mathrm{Au})/p(\mathrm{Ag}) = I(\mathrm{Au})\sigma\gamma(\mathrm{Ag})a(\mathrm{Ag})/I(\mathrm{Ag})\sigma\gamma(\mathrm{Au})a(\mathrm{Au}), \quad (3)$$

TABLE III. ΔH_{298}^{vap} of gold (kcal/g-atom).

Ruff and Bergdahl (footnote reference 19a, 1919)	82.98
Ruff and Konschak (footnote reference 19b, 1926)	81.71
Harteck (footnote reference 19c, 1928)	91.22
Farkas (footnote reference 19d, 1929)	88.40
Baur and Brunner (footnote reference 19e, 1934)	78.12
Hall (footnote reference 19f, 1951)	84.70
Nesmeianov, Smakhtin, Lebedev (footnote reference 19g, 1957)	87.70
Edwards (footnote reference 19h, 1959)	87.20
Rauh (footnote reference 19i, 1959)	87.50
Selected average (last three values)	87.5

where p are the pressures and a the activities.[21] Unfortunately, the uncertainty in the activities of the more volatile component Cu or Ag, which activity ranged between 0.0 and 0.1, gives rise to estimated uncertainties in ΔH^{vap}(Au) of 1.5 to 2 kcal. The value obtained by this method is 87 kcal. Similarly, one quantitative vaporization experiment, using Eq. (2) to determine S', gives 87.3 kcal.

Free energy functions for the monoatomic species were taken from Stull and Sinke and were calculated[22] for diatomic species. The vibration frequencies were taken from the literature[1-3,7,8] and the interatomic distances are those estimated from the lattice parameters by Pauling.[23] The vibration frequencies used for Cu_2, Ag_2, Au_2, AgAu, AgCu, and AuCu are 266.1, 192, 191, 210, 250, and 250 cm^{-1} respectively, while the interatomic distances used are 2.34, 2.68, 2.68, 2.68, 2.51, and 2.51. Values of r based on the gaseous hydrides or on Ruamp's value of 2.50 A for Au_2 are systematically smaller but their use, even in the extreme, would not increase the

TABLE IV. Dissociation energies at 0°K of Ib symmetric and asymmetric molecules in kcal/mole.

	This work	Drowart Honig[a] recalc.	Schissel[b] recalc.	Spectr.[c] (Birge-Sponer)
Cu_2	45.5±2.2	46.5±2.3	46.2±2.3	48
Ag_2	37.6±2.2	37.8±2.3	38.2±2.3	42
Au_2	51.5±2.2	53.0±2.3	51.7±2.4	62
AgAu	47.6±2.2	...	...	...
AgCu	40.7±2.2	...	...	29
AuCu	54.5±2.2	...	...	64

[a] See footnote reference 4.
[b] See footnote reference 5.
[c] See footnote reference 1, 2, 7, 8.

[17] W. E. Forsythe, in *Temperature, Its Measurement and Control in Science and Industry*, edited by American Institute of Physics (Reinhold Publishing Corporation, New York, 1941), p. 1183.
[18] D. R. Stull and G. C. Sinke, Advances in Chem. Ser. **18**, (1956).
[19] (a) O. Ruff and G. Bergdahl, Z. anorg. Chem. **106**, 76 (1919); (b) O. Ruff and H. Konschak, Z. Elektrochem. **32**, 515 (1926); (c) P. Harteck, Z. physik Chem. **134**, 1 (1928); (d) A. Farkas, Z. physik Chem. **B5**, 467 (1929); (e) E. Baur and R. Brunner, Helv. Chim. Acta **17**, 958 (1934); (f) L. D. Hall, J. Am. Chem. Soc. **73**, 757 (1951); (g) Nesmeianov, Smakhtin and Lebedev, Doklady Akad. Nauk S.S.S.R. **112**, 700 (1957); (h) R. K. Edwards, private communication; (i) E. G. Rauh, unpublished data.
[20] R. G. J. Fraser, *Molecular Rays* (Cambridge University Press, New York, 1931).
[21] (a) Selected values for the thermodynamic properties of metals and alloys, Minerals Research Laboratory, University of California, Berkeley; (b) R. K. Edwards and J. H. Downing, J. Chem. Phys. **60**, 108 (1956).
[22] K. S. Pitzer, *Quantum Chemistry* (Prentice-Hall, Inc., Englewood Cliffs, New Jersey, 1953).
[23] L. Pauling, J. Am. Chem. Soc. **69**, 542 (1947).

TABLE V. Comparison of $D_0°(XY)$ with $\frac{1}{2}[D_0°(X_2)+D_0°(Y_2)]$ (Pauling's rule) and with the enthalpy of mixing for the alloys.

Species	$D_0°$ exp. kcal/mole	$D_0°$ calc. kcal/mole	Δ kcal/mole	ΔH^{mix} (liquid, $x=0.5$)[b]
AgAu	47.6±2.2	44.5	+3.1±1.7[a]	−1.1(1350°K)
AgCu	40.7±2.2	41.5	−0.8±1.7[a]	0.8(1428°K)
AuCu	54.5±2.2	48.5	+6.0±1.7[a]	−2.7(1550°K)

[a] Most probable error including ±1.4 kcal experimental error plus error in ΔH^{vap} (see text). This error is smaller than the uncertainties in the absolute values due to compensating errors.
[b] See footnote reference 21.

calculated D_0^0 by more than 1 kcal. Electronic states were assumed to be $^1\Sigma$.

THE DISSOCIATION ENERGIES

The values of the dissociation energies obtained by Drowart and Honig,[4] by Schissel,[5] and by ourselves are shown in Table IV. All these values are intercomparable since they have been recalculated using the same elemental heats of vaporization, free energy functions and assumptions about ionization cross section as stated above. All three are in excellent agreement with one another.

Schissel's results have been interpreted under the same assumption for the ionization cross sections used in interpreting D–H's and our own. This is $\sigma(X_2)=2\sigma(X)$, no further corrections being made for the difference in the energy of the ionizing electrons. The ratio of $\sigma\gamma(X_2)/\sigma\gamma(X)$ used in calculating the $D_0°$ shown in Table IV is taken to be 1.7, assuming his correction for multiplier efficiency to be 0.85. Actually, one would expect the ratio of γ for Cu_2/Cu to be smaller than 0.85, tending to bring our results into closer agreement. (Cf., Inghram *et al.*[24] for curves of γ as a function of mass, or Schissel's paper.[5])

$D_T°$ calculated from plots of $\ln p(X_2)/p(X)$ vs $1/T$, even though not dependent on instrumental sensitivities or free energy functions, are, as is well known, much less reliable than those from the third law. The $D_T°$'s calculated from our own and from the other's data tend to be ∼10 kcal higher than the third law $D_0°$is which is within the limits of error for the second law. The mass spectrometric results are considered to be in good accord with the linear Birge-Sponer extrapolations.

The probable error in the absolute value of our results calculated by the third law is estimated as follows: the scatter of the various experimental points for each molecule is about 0.5 kcal (this is ∼0.8 kcal for AgCu due to the smaller dimer-monomer ratio). The error due to an assumed uncertainty of 70% in the cross sections and multiplier efficiencies gives an uncertainty of 2 kcal at 1700°K; a systematic temperature error of 40° would give rise to 0.5 kcal for Au at 1700°K. No allowance is made for uncertainties in the free energy functions due to interatomic distances. Exclusive of uncertainties in the heats of vaporization, this gives rise to a most probable error of 2.2 kcal.

A quantity that is of interest is the difference Δ between the experimental $D_0°(XY)$ and the arithmetic mean of the energies for the symmetric molecules. Attempts were made to obtain this difference directly from the reaction $2XY \rightleftharpoons X_2+Y_2$; unfortunately, experimental conditions did not permit simultaneous observation of all three diatomic species. Since errors made in assuming ionization cross sections and in measuring temperatures would largely tend to cancel in taking differences, we estimate the error in $D_0°$ for this purpose as scatter, 0.5 kcal; cross sections and multiplier efficiencies, 1 kcal; temperature, 0.2 kcal, giving a most probable error of 1.1 kcal. The most probable error in the difference Δ is thus 1.4 kcal, exclusive of uncertainties in ΔH^{vap}.

Errors in the heats of vaporization of the atoms for, say, AgAu causes an error in the difference equal to $\delta\Delta H(\text{Ag})+\frac{1}{2}\delta\Delta H(\text{Au})$. Thus for the differences Δ (Table V), the total most probable error is ±1.7 kcal.

DISCUSSION OF RESULTS

Brewer and Searcy[25] have remarked that the dissociation energies for the six molecules of the copper triad should provide extremely interesting tests of bond theories. The first column of Table V shows the dissociation energies of the asymmetric molecules XY. The second column shows the arithmetic mean of $D_0°(X_2)$, and the third column the difference between the first two columns. Although there are significant differences, these differences are not larger than 15%. In particular, the two molecules containing Au are distinctly more stable than predicted by the mean of the symmetric molecules.

Such behavior may be interpreted in terms of a difference of electronegativity[26] for the three atoms. Electronegativity differences between Cu–Ag, Ag–Au, and Au–Cu are calculated to be 0, 0.4, and 0.5, in good agreement with earlier results of Haissinsky.[27]

[24] M. G. Inghram and R. J. Hayden, *A Handbook on Mass Spectrometry*, National Research Council Publ. 311, (1954); Inghram, Hayden and Hess in Natl. Bur. Standards Circ. 522, p. 257 (1953).

[25] L. Brewer and A. W. Searcy, Ann. Rev. Phys. Chem. **7**, 268 (1956).

[26] L. Pauling, *Nature of the Chemical Bond* (Cornell University Press, Ithaca, New York, 1941).

[27] M. Haissinsky, J. phys. **7**, 7 (1946).

This behavior may be attributed to the availability of d orbitals for bonding. Silver, which has the smallest energy of dissociation, also has the relatively most stable d shell indicated by the fact that the atom with next lower atomic number, Pd, has a $d^{10}s^0$ configuration while those preceding Cu and Au (Ni and Pt) have d^8s^2 and d^9s^1 configurations. The silver atom has relatively few low-lying d^9 excited levels[28] compared to Cu and Au, and silver compounds normally exhibit only the +1 valence. Similarly, as discussed below, there seems to be a distinct relation between bonding in the gas and in the condensed phase indicating that conclusions made about bond character in the condensed phase apply to the diatomic molecules.

It has been remarked by Pauling that the ratio $\Delta H^{vap}/D_0^\circ$ is approximately 2 for the group IA elements.[29] Similarly, using dissociation energies given by Herzberg,[30a], Chupka, *et al.*,[30b] and by ourselves, we have calculated the same ratio for the groups IIIB, III and IB. This ratio systematically is equal to ~ 2, which leads one to believe bonding in the gas and in the condensed phases is similar for these metals. Thus the stability of the row VI transition metals, apparently due to the d electrons, is observed also in $Au_2(g)$.

In view of the apparent relation between bonding in the gas phase and in the pure liquids, we have looked for a relation between the dissociation energies of the asymmetric molecules and the enthalpies of mixing. The systems Cu–Ag–Au are relatively well suited for such a comparison since the pure metals have the same structure and approximately the same radii. Furthermore the alloys have well determined and relatively simple phase diagrams. The enthalpies of mixing are shown in column 5 of Table V. There seems to be a qualitative relation between those enthalpies and the deviation Δ from Pauling's rule shown in column 4. Both gaseous and liquid AuCu are formed exothermically from Au_2 and Cu_2 and from the pure liquids, respectively. Similarly, gaseous and liquid AgAu are formed somewhat less exothermically and AgCu endothermically.

ACKNOWLEDGMENTS

We wish to thank Professor Paul Goldfinger for his constant encouragement and counsel. Miss J. Lemaire has greatly assisted us in making the calculations. Part of the equipment has been made available by the Comité Belge de Spectrométrie de Masse (I.R.S.I.A.).

[28] C. E. Moore, Natl. Bur. Standards Circ. 467, (1958).
[29] L. Pauling, J. chim. phys. **46**, 277 (1949).
[30] (a) G. Herzberg, *Molecular Spectra and Molecular Structure I; Diatomic Molecules* (D. Van Nostrand Company, Inc., Princeton, New Jersey, 1951). (b) Chupka, Berkowitz, Giese, and Inghram, J. Phys. Chem. **62**, 611 (1958).

THE JOURNAL OF CHEMICAL PHYSICS VOLUME 33, NUMBER 6 DECEMBER, 1960

Proton Magnetic Resonance Study of Barium Bromate Monohydrate*

A. A. SILVIDI AND J. W. MCGRATH

Department of Physics, Kent State University, Kent, Ohio

(Received June 22, 1960)

The proton magnetic resonance absorption spectrum of barium bromate monohydrate was obtained using a Pound-Watkins spectrometer. Results indicate that there is only one orientation of the water molecule in the crystal. The p–p distance is 1.61 ± 0.01 A and direction angles of the p–p vector are $\alpha_0=30°$, $\beta_0=95°$, and $\gamma_0=122°$. The experimental errors in these angles were $\pm3°$. Apparently the water molecule is oriented so as to form the complex, $O_{II\,Br}$— —H—O—H— — $O_{II\,Br}$, where O_{Br} are neighboring bromate oxygens. Results obtained for barium chlorate monohydrate were consistent with those for barium bromate monohydrate.

INTRODUCTION

THE crystal structure of barium bromate monohydrate was determined by x-ray diffraction by Kartha.[1] Because x-ray methods cannot locate the hydrogen atoms, their positions were measured by us as part of our general study[2–7] of the structure of the water molecule in hydrated compounds by the proton magnetic resonance technique developed by Pake.[8]

* Partially supported by the U. S. Air Force through the Air Force Office of Scientific Research.

[1] G. Kartha, Proc. Indian Acad. Sci. **A38**, 1 (1953).
[2] J. W. McGrath, A. A. Silvidi, and J. C. Carroll, Bull. Am. Phys. Soc. **3**, 349 (1958).
[3] A. A. Silvidi and J. W. McGrath, J. Chem. Phys. **30**, 1028 (1959).
[4] J. W. McGrath, A. A. Silvidi, and J. C. Carroll, J. Chem. Phys. **31**, 1444 (1959).
[5] A. A. Silvidi and J. W. McGrath, Bull. Am. Phys. Soc. **4**, 471 (1959).
[6] A. A. Silvidi and J. W. McGrath, J. Chem. Phys. **32**, 924 (1960).
[7] J. W. McGrath and A. A. Silvidi, J. Chem. Phys. **33**, 644 (1960).
[8] G. E. Pake, J. Chem. Phys. **16**, 327 (1948).

TABLE I. Comparison of the two isomorphous salts.

Direction Angles	Barium bromate monohydrate: From NMR data	Barium bromate monohydrate: Calculated from x-ray data	Barium chlorate monohydrate: From NMR data	Barium chlorate monohydrate: Calculated from x-ray data	Barium chlorate monohydrate: Spence's values
α_0	30±3°	24°30′	31±2°	25°25′	30°30′
β_0	95±3	90	89±2	90	90
γ_0	122±3	118	124±2	118°56′	124
p-p distance in A	1.61±0.01		1.61±0.01		1.56

EXPERIMENT

$Ba(BrO_3)_2 \cdot H_2O$ crystals are monoclinic with space group C_{2h}^6 and contain four molecules per unit cell. The crystals were grown by the evaporation method. Because of the low solubility of this compound, seven months were required to grow a crystal of approximately 0.5 cc in volume. The experimental equipment, the parameters and the method of analysis were the same as those described elsewhere.[3,4,7] The crystallographic c axis was the axis of rotation. Measurements were made at room temperature.

RESULTS

Figure 1 shows the Pake curve. The value of δ is 32±3° and that of ϕ_0 is −47±1°. The value of 2α was determined by a least-square deviation method. The best value of 2α (10.10 gauss) resulted in a value of r, the $p-p$ separation, of 1.61±0.01 A. The fact that there is only one Pake curve indicates that there is only one orientation of the water molecule in the crystal. By using values of δ and ϕ_0, the direction angles of the $p-p$ vector were determined. These are $\alpha_0=30°$, $\beta=95°$, and $\gamma_0=122°$. These angles are measured to the positive a, b, and c axes, respectively.

DISCUSSION

The $p-p$ direction can be computed if one assumes that the water hydrogen atoms form hydrogen bonds between the water oxygen and the nearest bromate oxygens. Such bonding appears to exist in other hydrated crystals.[4-7] The atomic positions given by Kartha[1] were used in the computation. Results are shown in Table I and good agreement exists between the direction angles measured by this NMR method and those computed. The H bond distance is 2.78 A, a value within the acceptable range of H bond distances.[9]

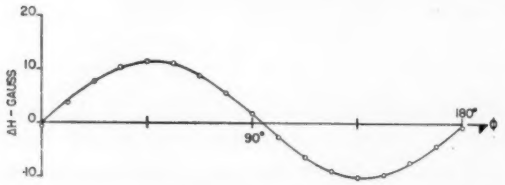

FIG. 1. Pake curve for barium bromate monohydrate when the c axis was the axis of rotation. The solid line is a plot of $\Delta H = 10.1[3\cos^2(\phi+\phi_0)\cos^2\delta-1]$ where ϕ_0 is −47° 15′ and δ is 32° 28′. The circles are experimental points. The initial orientation of the crystal was such that the $(1\bar{1}0)$ plane was parallel to H_0 the external field.

We computed the H—O—H angle from our value of r and an assumed value of 1 A for the O—H distance. The result was 107°. The $O_{II\ Br}$—O—$_{II\ Br}$ angle, computed from x-ray results, is 113°. It has been noted elsewhere that H bonds are often slightly bent.

These considerations suggest strongly that the hydrated water forms the complex $O_{II\ Br}$— —H—O—H— —$O_{II\ Br}$ in this compound.

Barium bromate monohydrate is isomorphous with barium chlorate monohydrate. A proton resonance study of the latter compound has been reported by Spence.[10] To check for consistency in structure between these two isomorphous salts, we made a similar study on barium chlorate monohydrate. These results are also shown in Table I. Results for the two salts are consistent. The direction angles are also in agreement with those given by Spence.[10] Our $p-p$ separation differs from that given by Spence. Since his article does not give a probable error in r, we are uncertain about the magnitude of the discrepancy. Our values of r are in good agreement with the values obtained from the study of eight other hydrates.

CONCLUSION

This proton magnetic resonance study of barium bromate monohydrate and barium chlorate monohydrate shows that there is only one orientation of the water molecule in these crystals. The $p-p$ distance and the direction angles are given in Table I. The water molecule is oriented by hydrogen bonding so as to form the complex O_{II}— —H—O—H— —O_{II} where the O_{II} symbol stand for the appropriate oxygen atoms in the bromate or chlorate ion.

[9] L. Pauling, *Nature of the Chemical Bond* (Cornell University Press, Ithaca, New York, 1940), p. 289.

[10] R. D. Spence, J. Chem. Phys. **23**, 1166 (1955).

Compression of Flexible Chain Molecules in Solution*

ROBERT SIMHA
Department of Chemistry, University of Southern California, Los Angeles, California
AND
J. L. ZAKIN†
Department of Chemical Engineering, New York University, New York

(Received May 23, 1960)

The compression of coiling molecules in good solvents at finite concentrations has been previously treated. However, the expressions were evaluated earlier by means of an expansion in the effective pressure acting on a coil. They are now presented in a form appropriate to include the range of reduced concentrations $c/c_0 \geq 1$. As an example volume ratios for polystyrene solutions in toluene are computed. They depend only slightly on molecular weight and amount to a reduction of about 30% in the most probable encompassed volume, at $c/c_0 = 1$.

I. INTRODUCTION

SEVERAL years ago we estimated[1] in a discussion of solution viscosities at moderate concentrations the compression of coils in good solvents which arises from a balance between intra- and intermolecular repulsions of chain segments. The expressions derived by us for the compression ratio were evaluated by using the first term of an expansion. For the concentration range of interest, however, when the coils are actually overlapping, this expansion, even including higher terms, is not adequate.[2] Compressions were estimated in this manner and compared with apparent reductions in coil volume derived from the derivatives of the viscosity concentration curves.[1] Although the results were not unreasonable, viscosities do not provide, in the manner used by us, an adequate measure for the reduction in coil volume.[3]

The purpose of the present paper is to present expressions for the compression without recourse to expansions and to evaluate these for some polymer-solvent systems by means of intrinsic viscosity and osmotic data. The bearing of these results on the viscosities of moderately concentrated solutions in good and poor solvents[1,3] will be considered at another occasion.

II. COMPRESSION RELATIONS

Let us consider first a polymer coil at infinite dilution. Following an argument given earlier,[1] we consider its configurations by placing the n constituent segments, each of excluded volume $\propto b_0^3$ into the volume $\propto R^3$ encompassed by the chain in an arbitrary configuration, characterized by a radius of gyration R. The parameter b_0, of course, varies with the nature of the solvent. On disregarding the links connecting the segments, that is, placing them at random into the available volume, and discarding terms $0(b_0^6/R^6)$, which excludes highly compact configurations, we arrive at the distribution function $W_0(r)$ for end to end distances r[1].

$$W_0(r) \propto r^2 \exp(-3r^2/2nb^2) \exp(-n^2b_0^3/2R^3). \quad (1)$$

The further development depends on the relation between r and R which is available only for a Gaussian chain, where[4] for an arbitrary r

$$R^2 = nb^2/12(1+r^2/nb^2). \quad (2)$$

Substitution of Eq. (2) into Eq. (1) and introduction of the expansion factor α_0 of the most probable value r_0 through

$$r_0^2/nb^2 = 2\alpha_0^2/3 \quad (3)$$

results in the following equation for α_0:

$$(1+2\alpha_0^2/3)^{5/2} - 1/\alpha_0^2(1+2\alpha_0^2/3)^{5/2} = (12^{\frac{1}{2}}/2)(b_0/b)^3 n^{\frac{1}{2}}. \quad (4)$$

If, on the other hand, we replace Eq. (2) by an "average" relation

$$R^2 = \lambda r^2, \quad (2a)$$

where λ represents a constant, the result is, as has been previously found[1]:

$$\alpha_0^5 - \alpha_0^3 = \tfrac{1}{2}(\tfrac{3}{2})^{5/2}(1/\lambda^{\frac{3}{2}})(b_0/b)^3 n^{\frac{1}{2}}. \quad (4a)$$

This is of the same form as Flory's[5] equation. A relation of type (4a) is alternatively derived, if in Eq. (1) the distribution in respect to R is assumed to be Gaussian for the unperturbed chain. This, again, is not exact.[6,7] It should be noted that the numerical value of the right hand side of Eq. (4) does not matter for our further purposes.

Consider now the distribution W_c at finite concentration. In a good solvent an osmotic compression will take place and the value of α be reduced below α_0, as given by Eqs. (4) or (4a). We approximated earlier[1]

* Part of a dissertation submitted in partial fulfillment of the requirements for the degree of Doctor of Engineering Science.
† Present Address: Socony Mobil Oil Company, Research Department, Brooklyn Laboratory, Brooklyn 22, New York.
[1] S. G. Weissberg, R. Simha, and S. Rothman, J. Research Natl. Bur. Standards **47**, 298 (1951).
[2] R. Simha, unpublished.
[3] J. L. Zakin, thesis, Dr. Eng. Sc., New York University, 1959; J. L. Zakin and R. Simha, preprints of papers presented at the Cleveland Meeting, Am. Chem. Soc. April, 1960.
[4] J. J. Hermans and J. Th. G. Overbeek, Rec. trav. chim. **67**, 761 (1948).
[5] P. J. Flory, J. Chem. Phys. **17**, 303 (1949).
[6] A. Isihara, J. Phys. Soc. Japan **5**, 201 (1950).
[7] P. Debye and F. W. Bueche, J. Chem. Phys. **20**, 1337 (1952).

TABLE I. Parameters used in Fig. 1.

$M_n\times10^5$	$[\eta]dl/g.$	α_0	$B_2\times10^4$, cm^3g^{-2}	$B_3\times10^8$, cm^6g^{-3}
6.0	2.026	1.424	3.50	21.0
1.5	0.732	1.264	4.78	7.6
0.4	0.278	1.145	6.38	2.1

the distribution by writing

$$W_e=W_0\exp\{-pV/kT\}, \qquad (1')$$

where $V=(4\pi/3)R^3$ and p represents an effective pressure acting on the coil, which will be a function of the polymer concentration. Equations (2) and (1′) yield for the most probable value of r:

$$(1+r^2/nb^2)^{5/2}-(\tfrac{3}{2}r^2/nb^2)(1+r^2/nb^2)^{5/2}+(12^{5/2}/16)(b_0/b)^3(r^2/nb^2)n^{\frac{1}{2}}-[\beta(nb^2)^{\frac{1}{2}}12^{-\frac{1}{2}}/8](1+r^2/nb^2)^3r^2=0,$$

with

$$\beta=4\pi/3(p/kT).$$

To bring this equation into a convenient form for application, we eliminate nb^2 through Eq. (3), introduce the volume ratio

$$V_e/V_0=(r/r_0)^3,$$

and transform the third term by means of Eq. (4). The result is:

$$\alpha_0^2(V_e/V_0)^{5/3}-V_e/V_0+(8^{-\frac{1}{2}}\beta r_0^3/\alpha_0)(V_e/V_0)^{5/3}\times[1+2\alpha_0^2/3(V_e/V_0)^{2/3}]^{\frac{1}{2}}=(V_e/V_0)^{5/3}(1+\tfrac{2}{3}\alpha_0^2)^{5/2}\times(\alpha_0^2-1)/[1+(2\alpha_0^2/3)(V_e/V_0)^{2/3}]^{5/2}. \qquad (4')$$

Alternatively, Eqs. (2a), (4a), and (1′) lead to the result given earlier in a somewhat different form, viz.,[5]

$$\alpha_0^2(V_e/V_0)^{5/3}+(3\beta_2/2)(V_e/V_0)^2r_0^3-V_e/V_0=\alpha_0^2-1, \qquad (4a')$$

with

$$\beta_2=\beta\cdot\lambda^{\frac{1}{2}}.$$

Both Eqs. (4′) and (4a′) are cast here in a form which permits direct evaluation of the volume ratio, provided the chain dimensions and expansion factor are known at infinite dilution from appropriate light scattering or viscosity data. To proceed, p must be expressed as a function of concentration. We establish the connection by substituting for the effective pressure p that part of the total osmotic pressure which arises from intermolecular interactions and can be formally expressed in terms of the second and higher virial coefficients, or

$$p=\Pi-\Pi_0=RT(B_2c^2+B_3c^3+\cdots), \qquad (5)$$

where Π_0 represents the van't Hoff term. Equations (4′) or (4a′) and (5) complete our description of the most probable coil configuration at finite concentrations. Two approximations are involved in this result. The first resides in the equivalence of the actual compression caused by intermolecular repulsions and that resulting from a uniform pressure effectively acting on a coil. At concentrations $c\approx c_0$, where close packing of the encompassed volumes is achieved, this assumption will be more adequate than at lower concentrations. Under these circumstances, this effective pressure exerted by the cage surrounding a given molecule must be closely related to the osmotic pressure difference, Eq. (5). We have postulated an actual equality. A more detailed treatment of the chain configuration in the appropriate range of concentrations is required to prove the extent to which this equality is valid.

Before proceeding, one may inquire at what pressure the intramolecular repulsion is just balanced by the intermolecular compression and the chain assumes once more the unperturbed dimensions, or

$$V_e/V_0=1/\alpha_0^3.$$

This occurs when β and β_2 obey the respective equations

$$\left.\begin{aligned}&\beta r_0^3=4.89\alpha_0(\alpha_0^2-1)(1+2\alpha_0^2/3)^{5/2}\\ \text{or}\quad&\beta_2 r_0^3=\tfrac{2}{3}\alpha_0^6(\alpha_0^2-1)\end{aligned}\right\}. \qquad (6)$$

We have shown earlier[1] that the compression $1-V_e/V_0$ varies as c^2 at relatively low concentrations. This will result in negative contributions to the fourth and higher virial coefficients.[1]

It is finally convenient both for the discussion of solution viscosities and the present effects, to introduce a reduced concentration variable. A natural choice is c_0, the concentration of incipient overlap of the encompassed average spherical coil volumes. For hexagonal packing, the result is[1]

$$c_0=2^{\frac{1}{2}}M_n/(8N_A)\langle R_2\rangle_{Av}^{-\frac{3}{2}},$$

where M_n, N_A and $\langle R^2\rangle_{Av}$ represent the number average molecular weight, Avogadro's number and the mean square radius of gyration. A corresponding (larger) c_0

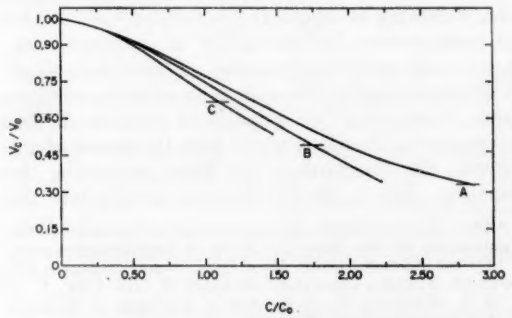

FIG. 1. Relative volume V_e/V_0 vs reduced concentration c/c_0, Eq. (4a′), for fractions of polystyrene described in Table I. A: $M_n=6.10^5$; B: $M_n=1.50.10^5$; C: $M_n=0.40.10^5$. Bars indicate coordinates corresponding to $\alpha=1$, $V_e/V_0=1/\alpha_0^3$.

could be defined in terms of the most probable value. This quantity is most simply expressed in terms of intrinsic viscosity, if we make use of the Fox-Flory expression,[8] in which $[\eta]$ is proportional to $\langle R^2\rangle_{Av}^{-\frac{3}{2}}$. Then

$$c_0 = 1.08/[\eta].$$

III. NUMERICAL RESULTS

We shall apply our equations to solutions of polystyrene in a good solvent, toluene. This is one of the systems for which viscosities over a range of concentrations up to $c/c_0 \approx 2$–3 were obtained.[1,3] It will serve to illustrate the magnitude of the effects to be encountered in good solvents and the usual range of molecular weights.

The parameters required in Eqs. (4′) or (4a′) are shown in Table I. The experimental second virial coefficients B_2 are based on those used in footnote reference 1, which appear to be averages of those given by several authors. Suitable plots of B_2 as a function of molecular weight may be used for interpolation. At least third virial coefficients are also required. They were estimated by means of a relationship[9] involving α_0. For details as well as more extensive results J. L. Zakin's thesis[3] may be consulted.

Figure 1 shows the results computed from Eq. (4a′). As concluded earlier,[1] the relative volumes vary only slightly with molecular weight at equivalent concentrations. The intramolecular repulsion is smaller but p larger for the smaller M. The expansion factor α, see Fig. 1., approaches unity in the region of c/c_0 between 1 and 3 in our range of molecular weights. Since the fourth and higher virial coefficients are not adequately known, the curves can not accurately be extended to higher concentrations. However, they will tend to level off since B_4 will be negative or smaller at any rate than for a rigid solute.

TABLE II. Compression ratios for $c/c_0 \approx 1$, with $\lambda^3 = 0.06$.[3]

$M_n \times 10^5$	c/c_0	V_e/V_0 Eq. (4′)	V_e/V_0 Eq. (4a′)
6.0	1.00	0.795	0.775
1.5	0.95	0.770	0.755
0.4	0.98	0.725	0.705

Finally we compare the results of Eqs. (4′) and (4a′) in two ranges of concentration. Table II shows the compressions to be practically identical for $c/c_0 \approx 1$. A further comparison is derived from the two relations (6) for various α_0's. When α_0 approaches unity, the ratio of β obtained from the first to that following from the second equation is 1.58, for $\lambda^3 = 0.06$,[3] indicating a less rapid decrease of V_e for the lowest molecular weight than in Fig. 1. When $\alpha_0 = 1.25$, the ratio is 0.86 and it decreases to 0.64 for $\alpha_0 = 1.424$, corresponding to $M_n = 6 \times 10^5$. Thus the differences between the highest and lowest molecular weight in Fig. 1 remain on the basis of Eq. (4′) or are reduced when $c/c_0 > 1$. Our evaluation of c_0 and α_0 from $[\eta]$ presupposes the proportionality of the latter with α_0^3. When a comparison with direct observations of the compression effect will be possible, it may be desirable to introduce corrections in expressing c_0 through the intrinsic viscosity, since these would vary with molecular weight.

ACKNOWLEDGMENT

One of us (J. L. Z.) gratefully acknowledges receipt of the Socony Mobil Employee Incentive Fellowship.

[8] T. G. Fox and P. J. Flory, J. Phys. Chem. **53**, 197 (1949).
[9] W. H. Stockmayer and E. F. Casassa, J. Chem. Phys. **20**, 1560 (1952).

THE JOURNAL OF CHEMICAL PHYSICS VOLUME 33, NUMBER 6 DECEMBER, 1960

Nuclear Magnetic Resonance Spectra of the ABX_3 Type: Field Dependence and Relative Signs of Spin-Spin Coupling Constants

VALDEMAR J. KOWALEWSKI* AND DORA G. DEKOWALEWSKI

Institute of Physics, University of Uppsala, Uppsala, Sweden

(Received December 14, 1959)

The ABX_3 spin system is studied as a function of applied magnetic field. A method for the determination of the relative signs of J_{AX} and J_{BX}, together with the relative chemical shifts and coupling constants is described. The results are applied to the *cis* crotonic acid, the *trans* crotonic acid, its methyl ester, and *N*-methylformamide. In the latter case it is shown that the relative chemical shift of the A and B protons can be estimated from the field behavior of the X_3 group of lines.

1. INTRODUCTION

IN connection with the interpretation of NMR spectra, the problem of the determination of the relative signs of some of the J-coupling constants sometimes arises. Dealing with one of these problems[1] the authors looked for significant features in the spectrum which would be more general than the correct fitting in a specific case. The problem in question was of a type which in the Bernstein, Pople, and Schneider[2] nomenclature is called ABX_3, but was rather obscured by the fact that the signal of the B proton was not visible at all due to the strong quadrupole effect of the neighboring nitrogen. The substance in question was *N*-methylformamide.

Some features were found and were tested with other substances (*cis* and *trans* crotonic acids and the methyl ester of *trans* crotonic acid). These results, when applied to *N*-methylformamide allowed not only the determination of the values and relative signs of two of the couplings, but also provided an estimate of the relative chemical shift of the missing B signal.

Anderson[3] has pointed out that the relative signs of some of the spin-spin couplings can be determined if there are at least three interacting groups of nuclei. Williams and Gutowsky[4,5] using this principle have determined relative signs of H–F couplings and several recent papers[6–8] report H–H couplings of different relative signs. In this connection the ABX case has been extensively studied[2,9] and some of the conclusions drawn here for the ABX_3 spin system have been known to apply to the ABX case.

2. EXPERIMENTAL

Spectra were taken at three different frequencies: 60, 40, and 25 Mc with two different kinds of spectrometers: the Varian model 4300 for 60 and 40 Mc and the Trübb-Tauber for 25 Mc. In all cases spinning samples were used as usual for high-resolution work. The substances used were commercially available and when impurities were found, such as in the *cis* crotonic acid, the substance was carefully distilled under vacuum and at low temperature. Samples were sealed into glass tubes under vacuum.

3. PROCEDURE FOR THE INTERPRETATION OF THE SPECTRA

The ABX_3 case was studied by Fessenden and Waugh[7] as an approximation of the ABC_3 case. In the ABX_3 approximation, the problem of the diagonalization of the Hamiltonian reduces to the solution of four quadratic equations which can be solved in the usual way.[9]

For the present purposes we need the explicit expressions of the frequencies and intensities of the lines. These are given in Table I, where ν_A and ν_B are the frequencies of A and B nuclei, respectively, referred to ν_X which is taken as zero. The J's are the spin-spin coupling constants and the other symbols are defined by[7]

$$R_+=\tfrac{1}{4}J_{AB}^2+[\tfrac{1}{2}(\nu_B-\nu_A)+\tfrac{3}{4}(J_{AX}-J_{BX})]^2$$
$$S_+=\tfrac{1}{4}J_{AB}^2+[\tfrac{1}{2}(\nu_B-\nu_A)+\tfrac{1}{4}(J_{AX}-J_{BX})]^2$$
$$S_-=\tfrac{1}{4}J_{AB}^2+[\tfrac{1}{2}(\nu_B-\nu_A)-\tfrac{1}{4}(J_{AX}-J_{BX})]^2$$
$$R_-=\tfrac{1}{4}J_{AB}^2+[\tfrac{1}{2}(\nu_B-\nu_A)-\tfrac{3}{4}(J_{AX}-J_{BX})]^2,$$

and the θ's by

$$\tan2\theta_1=J_{AB}/[(\nu_B-\nu_A)+\tfrac{3}{2}(J_{AX}-J_{BX})]$$
$$\tan2\theta_2=J_{AB}/[(\nu_B-\nu_A)+\tfrac{1}{2}(J_{AX}-J_{BX})]$$
$$\tan2\theta_3=J_{AB}/[(\nu_B-\nu_A)-\tfrac{1}{2}(J_{AX}-J_{BX})]$$
$$\tan2\theta_4=J_{AB}/[(\nu_B-\nu_A)-\tfrac{3}{4}(J_{AX}-J_{BX})].$$

* On leave of absence from Facultad de Ciencias Exactas, Universidad de Buenos Aires, Argentina.

[1] V. J. Kowalewski and D. G. de Kowalewski, J. Chem. Phys. **32**, 1272 (1960).

[2] H. J. Bernstein, J. A. Pople, and W. G. Schneider, Can. J. Chem. **35**, 65 (1957).

[3] W. A. Anderson, Phys. Rev. **102**, 151 (1956).

[4] G. A. Williams and H. S. Gutowsky, J. Chem. Phys. **25**, 1288 (1956).

[5] H. S. Gutowsky, C. H. Holm, A. Saika, and G. A. Williams, J. Am. Chem. Soc. **79**, 4596 (1957).

[6] S. Alexander, J. Chem. Phys. **28**, 358 (1958).

[7] R. W. Fessenden and J. S. Waugh, J. Chem. Phys. **30**, 944 (1959).

[8] A. D. Cohen and N. Sheppard, Proc. Royal Soc. (London) **A252**, 488 (1959).

[9] J. A. Pople, W. G. Schneider, and H. J. Bernstein, *High Resolution NMR Spectroscopy* (McGraw-Hill Book Company, Inc., New York, 1959), p. 135.

The angles $2\theta_i$ are not uniquely specified by their tangent since $\tan^{-1}x = 2\theta_i + n\pi \cdot n$ is usually taken equal to zero because the other values of n only change the relative order in which the eigenvectors are given.

To determine the parameters corresponding to a specific experimental spectrum the X_3 part is initially supposed nonexistent and the lines of the quadruplets corresponding to the A and B nuclei are averaged out. This gives the approximate position of the pure AB spectrum from which J_{AB} and $\delta_{AB}=\nu_A-\nu_B$ are calculated.[9] After deciding about the relative signs of J_{AX} and J_{BX} by some of the means described later the R's and S's are obtained taking the difference between the frequencies of the lines: $1-9=5-13=2R_+$, etc. (The relative signs of J_{AX} and J_{BX} must be determined *first* to allow for the correct labeling of the lines according to the transitions, Fig. 1 and Table I.) The average values of the several R's and S's are then put into their defining equations and the value of $|J_{AX}-J_{BX}|$ is found. This, together with the value of $|J_{AX}+J_{BX}|$ obtained from the X part of the spectrum gives us J_{AX} and J_{BX}. These initial values need usually only a slight adjustment to fit the observed spectrum correctly.

4. DISCUSSION

With the above formulas a spectrum of a typical ABX_3 type was calculated for all possible assignments of signs. Figure 1 shows what happens with the spectrum of the A and B protons. The results can be summed up as follows:

(1) As in the ABX case no change in the spectrum occurs if the sign of J_{AB} alone is changed or if all of them are changed simultaneously [Fig. 1(a)]; (2) If J_{AX} and J_{BX} are of different signs, no matter which is the positive and which is the negative one, the spectrum looks like Fig. 1(b).

An interesting feature about the relative intensities of the lines within the quadruplets should be noted: If we neglect the binomial coefficient factors which affect the intensities of these lines, in the B group of lines of the spectrum of Fig. 1(a) ($|J_{AX}| < |J_{AX}|$) the intensities of the two quadruplets slope outwards, while in the corresponding (b) spectrum they slope inwards, forming alternatively a "roof" and a "valley." Thus, for an ABX_3 case in which the lines of the B group are fully resolved (and $\delta_{AB} \gg J_{AB}$) the inspection of the intensities contour should give indication about the relative signs of J_{AX} and J_{BX}. The same holds for the ABX case, as can be seen in the spectrum of the 1,4 difluoro 2,3,5 trichlorobenzene[4] and, as it may be shown,[10] for the ABX_2 case.

The relative signs of J_{AX} and J_{BX} can also be inferred from the X_3 group. Sometimes, as in the ABX case, by simple inspection of frequencies and relative intensities, but much better by studying the changes which this group of lines undergoes when the magnetic field is changed or, what is equivalent, using different spectrometer frequencies.

[10] D. G. deKowalewski and V. J. Kowalewski, J. phys. radium (to be published).

TABLE I. Frequencies and relative intensities for the system ABX_3.

		Relative intensities
	A transitions	
1	$\frac{1}{2}(\nu_A+\nu_B)-\frac{1}{2}J_{AB}-\frac{3}{4}(J_{AX}+J_{BX})-R_+$	$1-\sin 2\theta_1$
2	$\frac{1}{2}(\nu_A+\nu_B)-\frac{1}{2}J_{AB}-\frac{1}{4}(J_{AX}+J_{BX})-R_+$	$3(1-\sin 2\theta_2)$
3	$\frac{1}{2}(\nu_A+\nu_B)-\frac{1}{2}J_{AB}+\frac{1}{4}(J_{AX}+J_{BX})-S_-$	$3(1-\sin 2\theta_3)$
4	$\frac{1}{2}(\nu_A+\nu_B-\frac{1}{2}J_{AB}+\frac{3}{4}(J_{AX}+J_{BX})-R_-$	$1-\sin 2\theta_4$
5	$\frac{1}{2}(\nu_A+\nu_B)+\frac{1}{2}J_{AB}-\frac{3}{4}(J_{AX}+J_{BX})-R_+$	$1+\sin 2\theta_1$
6	$\frac{1}{2}(\nu_A+\nu_B)+\frac{1}{2}J_{AB}-\frac{1}{4}(J_{AX}+J_{BX})-S_+$	$3(1+\sin 2\theta_2)$
7	$\frac{1}{2}(\nu_A+\nu_B)+\frac{1}{2}J_{AB}+\frac{1}{4}(J_{AX}+J_{BX})-S_-$	$3(1+\sin 2\theta_3)$
8	$\frac{1}{2}(\nu_A+\nu_B)+\frac{1}{2}J_{AB}+\frac{3}{4}(J_{AX}+J_{BX})-R_-$	$1+\sin 2\theta_4$
	B transitions	
9	$\frac{1}{2}(\nu_A+\nu_B)-\frac{1}{2}J_{AB}-\frac{3}{4}(J_{AX}+J_{BX})+R_+$	$1+\sin 2\theta_1$
10	$\frac{1}{2}(\nu_A+\nu_B)-\frac{1}{2}J_{AB}-\frac{1}{4}(J_{AX}+J_{BX})+S_+$	$3(1+\sin 2\theta_2)$
11	$\frac{1}{2}(\nu_A+\nu_B)-\frac{1}{2}J_{AB}+\frac{1}{4}(J_{AX}+J_{BX})+S_-$	$3(1+\sin 2\theta_3)$
12	$\frac{1}{2}(\nu_A+\nu_B)-\frac{1}{2}J_{AB}+\frac{3}{4}(J_{AX}+J_{BX})+R_-$	$1+\sin 2\theta_4$
13	$\frac{1}{2}(\nu_A+\nu_B)+\frac{1}{2}J_{AB}-\frac{3}{4}(J_{AX}+J_{BX})+R_+$	$1-\sin 2\theta_1$
14	$\frac{1}{2}(\nu_A+\nu_B)+\frac{1}{2}J_{AB}-\frac{1}{4}(J_{AX}+J_{BX})+S_+$	$3(1-\sin 2\theta_2)$
15	$\frac{1}{2}(\nu_A+\nu_B)+\frac{1}{2}J_{AB}+\frac{1}{4}(J_{AX}+J_{BX})+S_-$	$3(1-\sin 2\theta_3)$
16	$\frac{1}{2}(\nu_A+\nu_B)+\frac{1}{2}J_{AB}+\frac{3}{4}(J_{AX}+J_{BX})+R_-$	$1-\sin 2\theta_4$
	X transitions	
$17=-23$	$\frac{1}{2}(J_{AX}+J_{BX})$	12
$18=-24$	$\frac{1}{2}(J_{AX}+J_{BX})$	12
$19=-25$	$\frac{1}{2}(J_{AX}+J_{BX})$	12
$20=-26$	R_+-S_+	$12\cos^2(\theta_1-\theta_2)$
$21=-27$	S_+-S_-	$12\cos^2(\theta_2-\theta_3)$
$22=-28$	S_--R_-	$12\cos^2(\theta_3-\theta_4)$
	Combinations	
$29=-32$	R_++S_+	$12\sin^2(\theta_1-\theta_2)$
$30=-33$	S_++S_-	$12\sin^2(\theta_2-\theta_3)$
$31=-34$	S_-+R_-	$12\sin^2(\theta_3-\theta_4)$

In Fig. 2 is shown the aspect of the X_3 group as given for the ABX_3 approximation calculated for a series of spectrometer frequencies and for two hypothetical sets of parameters: $\delta_{AB}=0.15$ ppm, $J_{AB}=10$ cps, $J_{AX}=+5.0$ cps, and for $J_{BX}=+1.0$ and -1.0 cps. The following features of this group should be noted: there are 18 lines, 12 simple transitions, and six combinations. The latter are usually of feeble intensity (except for low spectrometer field intensities) and far away from the main group and have been neglected in the present calculation though, when observed, can be

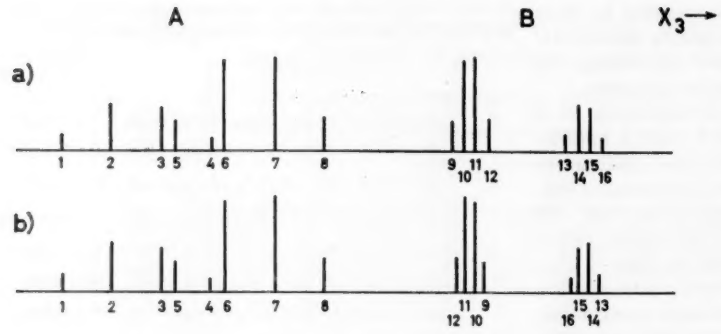

FIG. 1. Parts A and B of a calculated spectrum of the ABX_3 type. (a) J_{AX} and J_{BX} of the same sign. (b) J_{AX} and J_{BX} of different sign. $\nu_X=0$; $\nu_A=5.0$ ppm; $\nu_B=4.0$ ppm; $J_{AB}=15.7$ cps; $J_{AX}=7.0$ cps; $J_{BX}=\pm 1.7$ cps.

useful because they give immediately the sum of the R's and S's. Out of the 12 simple transitions, six give rise to *one doublet only* whose splitting value gives directly $|J_{AX}+J_{BX}|$ *independently of the applied field*, (transitions 17, 18, 19, 23, 24, and 25). The aspect of the lines due to the remaining transitions depends on the field and on δ_{AB}; they are more spread out the smaller is δ_{AB}. For sufficiently high field values and for $\delta_{AB}\gg J_{AB}$ (or rather, as will be shown later, for $\delta_{AB}\gg|J_{AX}-J_{BX}|$) these six transitions are all of almost the same frequency and give rise to another doublet symmetric with the preceding one (Fig. 2). The intensity of this doublet depends, in practice, on the amount of overlapping of the several components and may sometimes equal that of the field-independent one. It can be shown that in the limit the splitting of this doublet is equal to $|J_{AX}-J_{BX}|$, thus giving rise to a simple first-order theory spectrum.

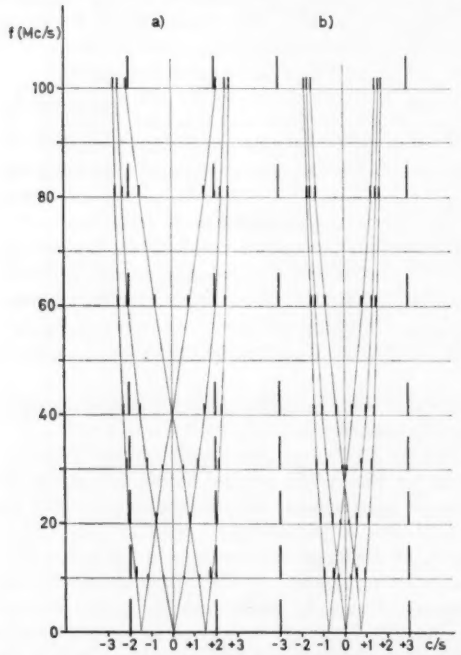

FIG. 2. X part of a hypothetical ABX_3 spectrum as function of spectrometer frequency. $\delta_{AB}=1.0$ ppm; $J_{AB}=10.0$ cps; $J_{AX}=5.0$ cps; (a) $J_{BX}=-1.0$ cps; (b) $J_{BX}=+1.0$ cps.

If both J_{AX} and J_{BX} are of the same sign the spectrum looks like Fig. 2(b) and the external lines are the field-independent ones. If they are of opposite signs the spectrum is given by Fig. 2(a) and the internal lines are now the field-independent ones. An experiment at two different spectrometer frequencies can thus give immediate indication about the relative signs of both couplings. If for example starting at 40 Mc a spectrum taken at 25 Mc shows that the external lines have moved inwards, we may say that a situation of two different signs is present. The inward movement of the internal lines is not, however, a proof of the quality of both signs, because it might just happen that δ_{AB}, or the field, is not large enough.[11] In this case it is necessary to apply a larger field (if possible) and look for an outward movement of the lines.

It may be seen from Fig. 2 that for sufficiently low field values, or rather for low enough δ_{AB}, two of the lines are of zero frequency (in the $\nu_X=0$ coordinates system) giving rise to a central line in the middle of the doublet.[7] The condition for this to occur can be obtained by equating to zero the transitions 21, 22, and 23, respectively, from Table I. One solution, common for all these transitions, is $J_{AX}=J_{BX}$. In this case the group appears as a triplet *independently of the applied field*.

The other solutions are: (1) $\nu_A-\nu_B=J_{AX}-J_{BX}$; (2) $\nu_A=\nu_B$; (3) $\nu_A-\nu_B=J_{BX}-J_{AX}$. If $|J_{AX}|>|J_{BX}|$ then solution (1) occurs at some definite value of the applied field, solution (2) occurs only for zero field and solution (3) corresponds to a reversal of the field.

A nice example of solution (1) is provided by the trans propenylbenzene for which the above formulas give a crossover frequency of 35.6 Mc.

5. APPLICATIONS

Methyl Ester of *trans* Crotonic Acid

A spectrum of this substance taken at 40 Mc may be seen, together with the calculated one, on Figs. 3

[11] This feature was also observed by R. Hoffman working with tiophenes (private communication).

FIG. 3. Observed and calculated spectra of the A and B protons of the methyl ester of *trans* crotonic acid. Frequency: 40 Mc. The lines marked r are rotational sidebands. Field increasing from left to right.

and 4, and the aspect of the methyl group alone at 25 Mc on Fig. 5. (As the values used for calculation purposes are averages from several spectra it is not possible to obtain perfect agreement between the calculated and any one of the observed spectra). At both frequencies the X_3 group appears as a quadruplet, the ratio b/a of the splittings being 1.56 at 40 Mc and 1.4 at 25 Mc. This, together with the intensities contour of the B proton spectrum was taken as a proof of a "different signs" situation. We propose the following set of parameters for this substance:

$J_{AB}=15.4\pm0.1$ cps

$J_{AX}=\pm(7.0\pm0.1)$ cps $\qquad \delta_{AB}=1.075\pm0.01$ ppm

$J_{BX}=\mp(1.6\pm0.1)$ cps $\qquad \frac{1}{2}(\nu_A+\nu_B)=4.504\pm0.01$ ppm

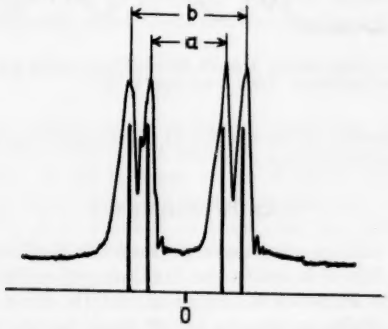

FIG. 4. Methyl group of the substance of Fig. 3. Same conditions.

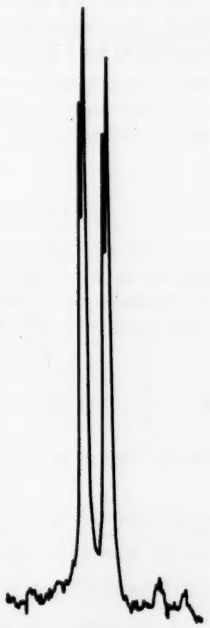

FIG. 5. Same as Fig. 4 but at 25 Mc. Field increasing from right to left.

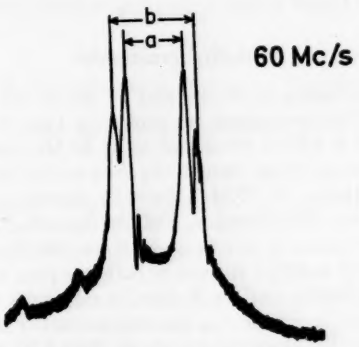

FIG. 6. Methyl group of the N-methylformamide at 60 Mc. Field increasing from left to right.

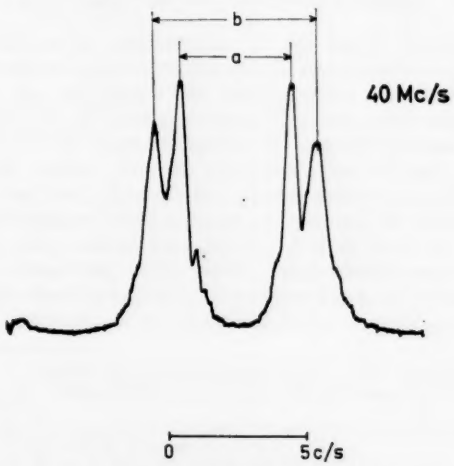

FIG. 7. Same as Fig. 6 at 40 Mc. Different scales for both axes. Field from left to right.

Trans Crotonic Acid

For this substance the intensities contour alone was assumed proof enough of the existence of different signs. The proposed parameters are:

$J_{AB}=14.9\pm0.1$ cps

$J_{AX}=\pm(6.7\pm0.1)$ cps $\quad\delta_{AB}=1.210\pm0.01$ ppm

$J_{BX}=\mp(1.7\pm0.1)$ cps $\quad\frac{1}{2}(\nu_A+\nu_B)=4.450\pm0.01$ ppm.

Cis Crotonic Acid

As in *trans* crotonic acid, the intensities were the deciding factor. The proposed parameters are:

$J_{AB}=11.4\pm0.1$ cps

$J_{AX}=\pm(7.5\pm0.1)$ cps $\quad\delta_{AB}=0.660\pm0.01$ ppm

$J_{BX}=\mp(1.9\pm0.1)$ cps $\quad\frac{1}{2}(\nu_A+\nu_B)=3.992\pm0.01$ ppm.

N-Methylformamide

Spectra taken at 60, 40, and 25 Mc of the methyl group of this substance are shown in Figs. 6–8. The ratio b/a is 1.44 at 60 as well as at 40 Mc, showing a first-order spectrum, though the lines are not all of the same intensity. At 25 Mc, $b/a=1.2$, showing the presence of two different signs. The corresponding J-couplings were found to be: $J_{AX}=\pm5.0$ cps and $J_{BX}=\mp0.9$ cps. As the A signal appears as only one peak of about 5-cps half-width and the B signal is missing it was not possible to determine J_{AB}. δ_{AB} was estimated from the frequency behavior to be about 1.25–1.30 ppm, a value similar to the one found in substances of similar chemical structure.[1]

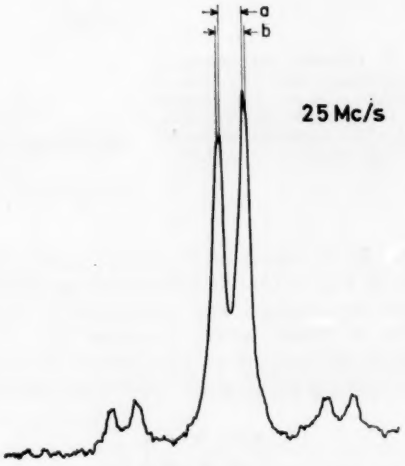

FIG. 8. Same as Fig. 6 at 25 Mc. Different scales and strong rotational sidebands. Field from right to left.

ACKNOWLEDGMENTS

The authors are grateful to Professor Kai Siegbahn for his kind hospitality and facilities put at their disposal, to Professor R. Freyman and Dr. P. Bommer for the 25-Mc spectra, to Dr. P. Diehl for the 60-Mc spectrum, and to Dr. R. Hoffman for useful comments during the work.

One of us (V.J.K.) is indebted to the Consejo Nacional de Investigaciones Científicas y Técnicas (Argentina) for a grant.

Gradient Dependence of Intrinsic Viscosity of Freely Flexible Linear Macromolecules

ANTON PETERLIN*

Department of Chemistry, Wayne State University, Detroit 2, Michigan†

(Received July 8, 1960)

In laminar flow the randomly coiled macromolecule expands nonuniformly. The averaged distances between close-by chain elements increase much slower than those between elements situated far away on the molecular chain. Because the latter move in opposite direction and the former in the same one, yielding a negative and positive contribution respectively to hydradynamic interaction, the nonuniform expansion results in a much faster decrease of negative terms. As a consequence hydrodynamic interaction first increases with the gradient yielding an initial drop in intrinsic viscosity proportional to the square of the gradient. With persisting coil expansion, however, the positive terms too decrease so far that the viscosity, after reaching a minimum, rises again and eventually surpasses the initial value at zero gradient. The increase is coming to an end when the rms end-to-end distance approaches the extended length of the molecule.

ACCORDING to Kramers,[1] intrinsic viscosity of randomly coiled linear macromolecules reads

$$[\eta]=(N_A\Lambda/6M)\sum_{i=1}^{Z}\langle r_i^2\rangle=(N_AZR^2/6M)\Lambda, \quad (1)$$

with Λ hydrodynamic resistance coefficient of the statistically independent segment, Z number of such segments, r_i the distance of ith segment from the center of mass, and R the gyration radius of the macromolecule. Z is assumed so large that the difference between Z and $Z+1$ may be neglected.

Hydrodynamic interaction reduces Λ to Λ^*. With the assumption that the average distribution of intrachain distances has spherical symmetry one obtains

$$\Lambda\mathbf{v}_j=\Lambda_j^*\mathbf{v}_j+a\sum_{k=1}^{Z}\Lambda_k^*\mathbf{v}_k\langle 1/r_{jk}\rangle \quad (2)$$

$a=\Lambda/6\pi$, r_{jk} distance between the jth and kth segment. In the sum k assumes all values from 1 to Z except j. The velocities $\mathbf{v}_j$ and $\mathbf{v}_k$ are mean values obtained after averaging over all possible configurations leading to the same end-to-end vector $\mathbf{r}_{1Z}$. In laminar flow one has

$$\mathbf{v}_1=-\mathbf{v}_Z$$
$$\mathbf{v}_j=(1-2j/Z)\mathbf{v}_1=(2j/Z-1)\mathbf{v}_Z. \quad (3)$$

The system Eq. (2) of Z linear equations for the Z unknowns Λ_j^* may be transformed into an integral equation and the solution obtained by expansion in the corresponding Fredholm series. The first term yields the average Λ^* over all Λ_j^*

$$\Lambda=\Lambda^*\left[1+(8a/Z^2)\sum_{j=1}^{Z/2}\sum_{k=1}^{Z}{}'(Z-2k)\langle 1/r_{jk}\rangle\right]. \quad (4)$$

In that which follows we shall limit us to this approximation.

In an undisturbed Gaussian coil, i.e., at the Θ point and $G=0$, one has

$$\langle 1/r_m\rangle=(6/\pi)^{\frac{1}{2}}/h_m$$
$$h_m=\langle r_m^2\rangle^{\frac{1}{2}}=b\cdot m^{\frac{1}{2}}$$
$$m=|j-k| \quad (5)$$

b length of the segment. In such a case, Eq. (4) reads

$$\Lambda=\Lambda_0^*[1+(2aZ^{\frac{1}{2}}/b)(6/\pi)^{\frac{1}{2}}S] \quad (6)$$

with

$$S=\sum_{m=1}^{Z/2}(m/Z)^{-\frac{1}{2}}-2\sum_{1}^{Z}(m/Z)^{\frac{1}{2}}-2\sum_{1}^{Z/2}(m/Z)^{\frac{1}{2}}+2\sum_{Z/2}^{Z}(m/Z)^{\frac{1}{2}}. \quad (7)$$

Replacing the sums by integrals one obtains $S=0.598$ so that the intrinsic viscosity turns out to be[2]

$$[\eta]=(N_AZR^2/6M)\Lambda/[1+1.196(6/\pi)^{\frac{1}{2}}aZ^{\frac{1}{2}}/b]. \quad (8)$$

With proper consideration of the higher terms of Fredholm series expansion one obtains a smaller value[3] for the coefficient 1.196, and this value also varies a little with Z. For not too small Z, a very good value is two-thirds, which we shall use in that which follows.[4,5]

In laminar flow the macromolecular coil gets expanded and oriented; the solution exhibits streaming birefringence. With constant Λ^*, however, the intrinsic viscosity remains unchanged.[6–8] Just as much as the restoring force of the coiled macromolecule increases more than linearly with the gradient G as a consequence of deformation, its contribution to shearing stress

* On leave of absence from Department of Physics, Ljubljana University, Yugoslavia. The author is indebted to SKNE, Belgrade, Yugoslavia for a research grant which made this work possible.

† Present address: Physikalisches Institut, Technische Hochschule, München, Germany.

[1] H. A. Kramers, J. Chem. Phys. **14,** 415 (1946).

[2] A. Peterlin, International Congress, *Les grosses molécules en solution* (Paris, 1948), p. 70; Diss. acad. Ljubljana (3A) **1,** 48 (1950).

[3] J. Kirkwood and J. Riseman, J. Chem. Phys. **16,** 565 (1948).

[4] A. Peterlin, J. Polymer Sci. **5,** 473 (1950).

[5] Y. Ikeda, J. Phys. Soc. Japan **12,** 378 (1957).

[6] J. J. Hermans, Physica **10,** 777 (1943).

[7] A. Peterlin, J. Polymer Sci. **8,** 621 (1952).

[8] B. H. Zimm, J. Chem. Phys. **24,** 269 (1956).

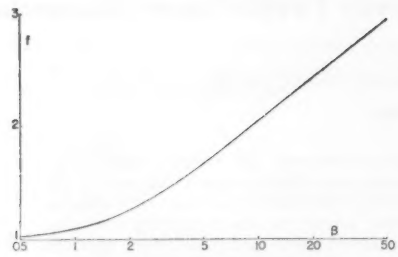

FIG. 1. $f(\beta)$ from Eq. (14) over $\log\beta$.

diminishes with orientation so that intrinsic viscosity does not change with the gradient.

Deformation, however, changes the intramolecular distances and this results in a change of Λ^* according to Eq. (4). Under the simplifying condition that the average $\Lambda^*(G)$ can be used independently on molecular orientation—one hence neglects the variation of interaction with compression and dilatation respectively occuring twice during every full rotation of macromolecule in the laminar flow—the change of shape can be determined from the free end distribution function which, in the case of freely flexible coil, reads

$$\phi(x', y', z') = (\mu/\pi)^{\frac{3}{2}}(1+\beta^2)^{-\frac{1}{2}} \exp\{-\mu[(1+2\beta^2)x'^2 - 2\beta x'y' + y'^2 + (1+\beta^2)z'^2]/(1+\beta^2)\} \quad (9)$$

with

$$\mu = 3/2h_0^2 = 3/2b^2Z$$

$$\beta = M[\eta]\eta_0 G/N_A kT, \quad (9a)$$

where η_0 is the viscosity of the solvent. When transforming to the main axes of refracting index, one obtains

$$\phi(x, y, z) = (\mu/\pi)^{\frac{3}{2}}(abc)^{-1} \exp\{-\mu[(x/a)^2 + (y/b)^2 + (z/c)^2]\}, \quad (10)$$

where

$$a^2 = 1+\beta^2+\beta(1+\beta^2)^{\frac{1}{2}}$$

$$b^2 = 1+\beta^2-\beta(1+\beta^2)^{\frac{1}{2}}$$

$$c^2 = 1.$$

The average square of the end-to-end distance and the average of the inverse distance turn out to be

$$h^2 = h_0^2(1+2\beta^2/3) = b^2Z(1+2\beta^2/3)$$

$$\langle 1/r_Z\rangle = (6/\pi)^{\frac{1}{2}}h^{-1}F(k, \phi)/[2\beta(1+\beta^2)^{\frac{1}{2}}]^{\frac{1}{2}} \quad (11)$$

with $F(k, \phi)$ elliptic integral of the first kind with

$$k^2 = \tfrac{1}{2}[1+\beta/(1+\beta^2)^{\frac{1}{2}}]$$

$$\sin^2\phi = \beta/k^2(1+\beta^2)^{\frac{1}{2}}.$$

The intramolecular distances r_{jk} and their averages follow from the corresponding averaged distribution functions[9]

$$\phi_m(x, y, z) = (\mu_m/\pi)^{\frac{3}{2}}(a_m b_m c_m)^{-1} \exp\{-\mu_m[(x/a_m)^2 + (y/b_m)^2 + (z/c_m)^2]\}, \quad (12)$$

where

$$\mu_m = 3/2b^2m$$

$$a_m^2 = a^2/(Z-1)\cdot[(m-1)+(Z-m)/(1+2\beta^2/3)]$$

$$b_m^2 = b^2/(Z-1)\cdot[(m-1)+(Z-m)/(1+2\beta^2/3)]$$

$$c_m^2 = 1/(Z-1)\cdot[(m-1)+(Z-m)/(1+2\beta^2/3)].$$

One obtains

$$\langle 1/r_m\rangle = (6/\pi)^{\frac{1}{2}}(bm^{\frac{1}{2}})^{-1}\{1+[(m-1)/(Z-1)]2\beta^2/3\}^{-\frac{1}{2}} \times F(k, \phi)[(1+2\beta^2/3)/2(1+\beta^2)^{\frac{1}{2}}]^{\frac{1}{2}} \quad (13)$$

in complete analogy with Eq. (11). The additional factors mean that the less extension in flow the closer the segments are in the chain.

By substituting the averages from Eq. (13) into Eq. (4) and introducing the half-empirical factor $\frac{2}{3}$ instead of 1.198, one obtains

$$\Lambda = \Lambda^*[1+\tfrac{2}{3}(6/\pi)^{\frac{1}{2}}(aZ^{\frac{1}{2}}/b)f(\beta)S(\beta)/0.598], \quad (14)$$

where

$$f(\beta) = F(k, \phi)[(1+2\beta^2/3)/2\beta(1+\beta^2)^{\frac{1}{2}}]^{\frac{1}{2}} = 1+\beta^2/10-\beta^4/168+\cdots$$

$$S(\beta)/0.598 = \left[\sum_{m=1}^{Z/2}(m/Z)^{-\frac{1}{2}} - 2\sum_{1}^{Z}(m/Z)^{\frac{1}{2}} - 2\sum_{1}^{Z/2}(m/Z)^{\frac{1}{2}} + 2\sum_{Z/2}^{Z}(m/Z)^{\frac{1}{2}}\right] \cdot\{1+[(m-1)/(Z-1)]2\beta^2/3\}^{-\frac{1}{2}}/0.598 = 1+0.0524\beta^2-0.0255\beta^4+\cdots.$$

The function $f(\beta)$ is plotted in Fig. 1 and the weight function of the terms to be summed up in S in Fig. 2. The first function is unity at $\beta=0$ and very slowly increases with β, its asymptotic value being proportional to $\ln\beta$. The second function very distinctly shows the specific role of chain segments in laminar flow. Nearest neighbors move in the same direction and hence by hydrodynamic interaction reduce the resistance parameter Λ. Segments farther apart, however, move in opposite direction and therefore by interaction increase Λ. At $\beta=0$ both effects result in a decrease of Λ to Λ_0^*, the decrease being substantially smaller than in the case of sedimentation where all segments move in the same direction and hence all contribute toward a decrease of Λ. The respective coefficients are $\frac{2}{3}$ [intrinsic viscosity, Eq. (14)] and 8/3 (sedimentation).

[9] A. Peterlin, W. Heller, and M. Nakagaki, J. Chem. Phys. **28**, 470 (1958).

With nonvanishing β the additional factor in S affects the single terms the more the higher m. As a first consequence the contribution from negative terms goes down more rapidly than that of positive ones so that S increases in spite of increased intramolecular distances. At still higher β the contribution of negative terms is not more significant so that now the increase in intersegmental distances results in a drop of S. This decrease is partly compensated by the slow but steady increase of $f(\beta)$ with β so that the product fS after the initial steep rise first reaches a maximum and then very slowly decreases.

Intrinsic viscosity as function of gradient turns out to be

$$[\eta]/[\eta]_0=(1+e)/(1+\xi e)$$
$$=1-0.1524[e/(e+1)]\beta^2+\cdots, \quad (15)$$

where

$$e=(6/\pi)^{\frac{1}{2}}(2aZ^{\frac{1}{2}}/3b)$$
$$\xi=f(\beta)\,S(\beta)/0.598.$$

The factor $aZ^{\frac{1}{2}}/b$ is nearly equal to $a_0P^{\frac{1}{2}}/b_0$ with a_0 the hydrodynamic radius, b_0 the effective length of monomer unit, and P the degree of polymerization. In most cases to which the presented calculation may be applied P is so large that unity can be neglected against e. Equation (15) then reads

$$([\eta]/[\eta]_0)_{P\to\infty}=1/\xi=1-0.1524\beta^2+0.0593\beta^4-\cdots. \quad (16)$$

In Fig. 3 this function is plotted over β together with that corresponding to $e=10$. The difference is very small and hardly matters when compared with other neglections made in the derivation of Eq. (15). After the initial drop which is rather marked, due to the high value of numerical coefficient at β^2, intrinsic viscosity reaches a minimum value of $0.65[\eta]_0$ at $\beta=5.2$ and

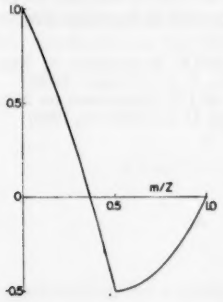

FIG. 2. The weight function by which the factors

$$1/(m/Z)^{\frac{1}{2}}[1+2\beta^2(m-1)/3(Z-1)]^{\frac{1}{2}}$$

in S [Eq. (14)] have to be multiplied. It shows the cooperative character of hydrodynamic interaction of close neighbors (m small) and the opposite influence of segments far away on the chain ($m\to Z$).

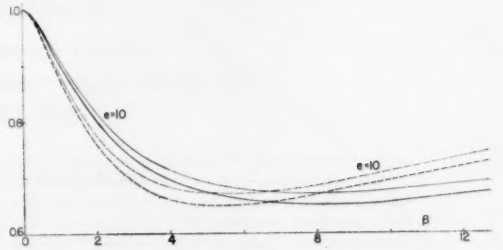

FIG. 3. Relative intrinsic viscosity $[\eta]/[\eta]_0$ with $e/(e+1)=1$ [Eq. (16)] and $e=10$ [Eq. (15)] over β (broken line) and β_0 (full line).

then very slowly increases. It has again the initial value at $\beta\sim 34$, but does not stop increasing.

When comparing with experiment one has to take care of the change of $[\eta]$ in Eq. (9a) connecting β and G. Usually one plots experimental values $[\eta]/[\eta]_0$ over G or the generalized parameter β_0

$$\beta_0=M[\eta]_0\eta_0G/N_AkT=([\eta]_0/[\eta])\beta. \quad (17)$$

The change from β to β_0 (Fig. 4) does not affect the initial decrease with β^2. But it changes the coefficients of all higher terms in the series expansion, Eq. (16), shifts the minimum to higher value of the gradient, and increases the slope of subsequent increase of intrinsic viscosity. In a plot of $[\eta]/[\eta]_0$ over β_0, the influence of e is still a little less marked as it is in a plot over β (Fig. 3).

At this derivation of gradient dependence of intrinsic viscosity one must not forget the limitations of the model. The density functions of Eqs. (9), (10) and (11) rather well represent the segment distribution in laminar flow as may be seen from the similarity with the corresponding density function in normal coordinates of Rouse's model[10]

$$\phi=A\cdot\exp\left\{-(3/2b^2)\sum_{k=1}^{Z}\frac{\mu_k}{1+\beta^2/\lambda_k^2}\left[\xi_k^2-(2\beta/-\lambda_k)\xi_k\eta_k+\left(1+\frac{2\beta^2}{\lambda_k^2}\right)\eta_k^2+(1+\beta^2/\lambda_k^2)\xi_k^2\right]\right\}, \quad (18)$$

where A is the normalization factor, and μ_k and λ_k are the eigenvalues of spring forces in the segment and of hydrodynamic interaction tensor, respectively.[8] But all these distribution functions are limited to so small β values that the rms end-to-end distance h is still substantially smaller than the extended length L of the macromolecule. According to Eq. (11), this condition requires

$$b^2Z(1+2\beta^2/3)\ll b_{\text{mon}}{}^2P^2\cos^2(\alpha/2)$$
$$\beta^2\ll 1.5[\tfrac{1}{2}(1-\cos\alpha)\cdot(1-\langle\cos\phi\rangle)/(1+\langle\cos\phi\rangle)P-1], \quad (19)$$

[10] P. E. Rouse, Jr., J. Chem. Phys. **21**, 1272 (1953).

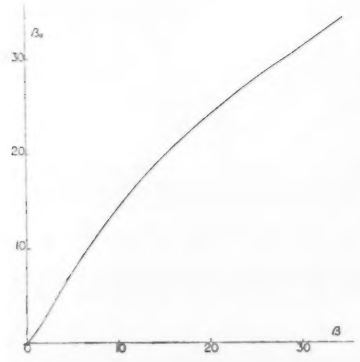

FIG. 4. β_0 over β.

b_{mon} is the geometrical length of monomer unit, $180-\alpha$ is the valency angle between consecutive monomers, and ϕ is the angle of rotation around the chemical bond. Therefore, the calculated values of gradient dependence of intrinsic viscosity are strictly valid, but for an infinite Z. With finite Z, saturation effects occur. The molecule rapidly approaches full extension $h=L$ and cannot extend over this length. Therefore, the intrinsic viscosity at still higher β has to decrease with increasing orientation and finally reaches a limit $[\eta]_\infty$ nearly equal to that corresponding to rigid, rod-like particles at maximum orientation.

A further effect completely neglected in this treatment is the *anisotropy* of hydrodynamic interaction which, without any consideration of coil expansion in flow, already yields a decrease in intrinsic viscosity.[11,5] In the present notation it would affect the factor $N_A Z R^2/6M$ and hence, at least at small values of β, provide for an additional drop in $[\eta]$. Without any more detailed analysis it is hard to predict what its effect will be at high β.

Streaming birefringence observations[12] lead Cerf[13] to the explicit consideration of coil rigidity (*inner friction*) which prevents free expansion of coil according to Eq. (11). This effect also results in reduction of intrinsic viscosity and very likely, at least at low solvent viscosity, prevents the final rise due to the increasing coil extension.

A reasonable comparison with experiments will be possible when all the effects on intrinsic viscosity, i.e., anisotropy of hydrodynamic interaction, change of coil shape by the competing influence of hydrodynamic forces and of inner friction of macromolecular chain, and non-Gaussian character of intrachain distances, will be properly taken into account. Any partial agreement is only misleading because it conceals the existing deficiencies of any treatment presented until now. But it is absolutely necessary to perform as complete calculations as possible of single approximate models in order to see in which direction the final synthesis has to be attempted.

In this connection, we wish to mention the very characteristic observations of dilatancy, i.e., viscosity increase with gradient, by Selby[14] on lubricating oils with macromolecular improver added, and by Merrill[15] on polyisobutylene solutions in benzene, a very poor solvent close to the Θ point. In the first case, the hydrodynamic forces in the extremely viscous solvent, $\eta_0 \sim 10^4$ poise, permitting one to obtain high β values at relatively low gradients, very likely so far overcome the inner friction of the macromolecule that the coil expands much more than in low-viscosity solvents, $\eta_0 \sim 0.01$ poise, and hence yields a gradient dependence similar to that in Fig. 3. In the second case, one has to admit an exceptionally high coil flexibility. Both observations, of course, were made at too high concentrations so that the measured viscosity cannot be interpreted yet as intrinsic viscosity. Therefore, one does not know how much of the effect is due to isolated macromolecule and how much to the intermolecular interaction. But they give a hint that under special conditions the non-Newtonian intrinsic viscosity may show an increase with the gradient when the deforming forces are strong enough for proper extension of macromolecular coil in laminar flow.

[11] M. Čopič, J. chim. phys. **53**, 440 (1956); A. Peterlin and M. Čopič, J. Appl. Phys. **27**, 434 (1956).
[12] R. Cerf, J. chim. phys. **47**, 663 (1950); H. Schwander and R. Cerf, Helv. Chim. Acta **34**, 436 (1951); J. Leray, J. Polymer Sci. **23**, 167 (1957).
[13] R. Cerf, J. phys. radium **19**, 122 (1958).
[14] T. W. Selby, ASTM Symposium on Non-Newtonian Viscometry, Washington, D. C. (October, 1960).
[15] E. W. Merrill, ASTM Symposium on Non-Newtonian Viscometry, Washington, D. C. (October, 1960).

THE JOURNAL OF CHEMICAL PHYSICS VOLUME 33, NUMBER 6 DECEMBER, 1960

Molecular Orbital Treatment of Hydrogen with Central Potentials and Modified Boundary Conditions*

JAMES M. PEEK† AND EDWIN N. LASSETTRE

Department of Chemistry, The Ohio State University, Columbus, Ohio

(Received April 6, 1960)

A model is proposed for a homonuclear diatomic molecule in which each electron is treated as moving in the field which would prevail for an isolated atom but with boundary conditions which require that either the one electron eigenfunction, or its normal derivative, vanishes along a plane perpendicular to the line of centers and passing through the midpoint. The model is tested by applying it to molecular hydrogen. The assumed potential is compared to that computed from a Heitler-London function, using a suggestion of Slater, and the energy of the ground state of hydrogen is computed as a function of internuclear distance. Employing the model throughout (i.e., without averaging the exact Hamiltonian) a dissociation energy of 5.65 ev is obtained and an equilibrium internuclear distance of 1.7 a.u. is predicted.

IN the Wigner-Seitz[1] treatment of solids the effect of the environment of a given atom, on the electronic eigenfunction, is replaced by a boundary condition which is then applied to a Schrödinger equation whose potential function is chosen as that for the *isolated* atom. While considering an electron impact problem we have been led to consider the possibility that a similar (but modified) model may be applied to homonuclear diatomic molecules. As far as the boundary conditions are concerned an appropriate set can easily be formulated. Since the molecular orbitals are either symmetric or antisymmetric with respect to reflection through a plane perpendicular to the line of centers, and passing through the midpoint, it follows that the function or its derivative normal to the plane must vanish along the plane. Thus we can consider only the half-space to one side of this plane provided that either one or the other of the above conditions is applied, to an appropriate Schrödinger equation, as boundary conditions on the dividing plane. The validity of adopting in this half-space the potential for an isolated atom is, however, open to serious question since the charge distributions around each nucleus depart considerably from spherical symmetry. The effect on the electronic eigenfunctions of the error in potential introduced by this assumption is probably compensated to some extent by forcing the correct boundary conditions on the solution. However, this compensation cannot be complete unless the actual potential closely approaches the assumed potential everywhere except for a thin layer near the boundary plane. Whether this is correct can be determined either by studying the potential field in some preliminary, and approximate, way or by trial and comparison with experiment. Both have been tried on the hydrogen molecule and the results are given in the following paper.

1. CALCULATION OF APPROXIMATE POTENTIAL FUNCTION

A molecular orbital theory based on the assumption of independent electron distributions does not lead to an isolated atom potential even at large internuclear distances and hence is unsuited to the present application. Slater has, however, described a method for the calculation of one-electron potential functions which is not confined to single configuration molecular orbital functions.[2] We have used this method, together with a Heitler-London function for hydrogen, in the calculation of an approximate potential. The Heitler-London function is employed because the actual wave function for hydrogen approaches this at large internuclear distances and hence the potential will presumably approach the free atom potential at large internuclear distances. Slater's formula for the potential is as follows:

$$V_e(x_1) = \frac{\int u^*(x_1, x_2, \cdots x_n)\left[\sum_{j=2}^{n}(e^2/r_{1j})\right]u(x_1, x_2, \cdots x_n)d\tau'}{\int u^*(x_1, x_2, \cdots x_n)u(x_1, x_2, \cdots x_n)d\tau'}. \quad (1)$$

Here u is the eigenfunction for a system of n electrons, r_{1j}, is the distance between electrons 1 and j, and the prime on $d\tau'$ indicates a volume element for all particles except the positional coordinates of particle 1. The integrations in both numerator and denominator are extended over the spin coordinates of all particles and over the positional coordinates of all particles except

* Supported in part by the Geophysics Research Directorate of the Air Force Cambridge Research Center.

† Kettering Foundation Fellow 1958–1959.

[1] E. Wigner and F. Seitz, Phys. Rev. **43**, 804 (1933); **46**, 509 (1934).

[2] J. C. Slater, Phys. Rev. **91**, 528 (1953).

the first. The potential is that due to electronic repulsion only and the attraction between the first electron and the nuclei must be added to obtain the complete potential.

The Heitler-London function is as follows:

$$a(1)b(2)+a(2)b(1). \tag{2}$$

where a, b are $1s$ hydrogen atom orbitals (normalized) centered, respectively, around nuclei a and b. The spin function is omitted. Insertion of (2) into Eq. (1) gives (in a.u.)

$$V_e(x_1)=\frac{a^2(1)\int[b^2(2)/r_{12}]d\tau_2+2a(1)b(1)\int[a(2)b(2)/r_{12}]d\tau_2+b^2(1)\int[a^2(2)/r_{12}]d\tau_2}{a^2(1)+2a(1)b(1)\int a(2)b(2)d\tau_2+b^2(1)}. \tag{3}$$

When the internuclear distance is large, and electron 1 is near nucleus a, then the integral in the first term of the numerator approaches $1/r_b$ and the remaining terms in the numerator, as well as the last two terms in the denominator, become negligible. Hence V_e approaches $1/r_b$. When the nuclear attraction term $-1/r_a-1/r_b$ is added, the total potential becomes $-1/r_a$, which is the isolated atom potential. In the vicinity of the other nucleus the potential approaches $-1/r_b$. At intermediate internuclear distances none of these terms are obviously negligible and we have calculated the potential by evaluating each integral. The second integral in the numerator was evaluated in the usual way using the expansion of $1/r_{12}$ in spheroidal coordinates and integrating term by term. Equipotentials have been calculated at one internuclear distance, 1.4 a.u., and are shown in Fig. 1. The potential shown is the total (electron repulsion and attraction by the nuclei).

If the potential to the left of the symmetry plane were that of the isolated atom, then the equipotentials would be circles. This is a fair approximation except in the vicinity of the symmetry plane. Deviations from the Coulomb law are shown more accurately in Fig. 2 where $-V$ is shown as a function of $1/r_b$ along each of three directions radiating from nucleus b; the first (curve A) along the line be of Fig. 1, the second (B) along bd perpendicular to the line of centers, and the third (C) along bc. If the Coulomb law were an accurate approximation the curve should be a straight line of slope 45 degrees. This is quite accurately approached by curve B. Curve A deviates only slightly from such a line. Curve C deviates more markedly from the straight line although it approaches the line asymptotically at small values of r_b and the most serious deviations occur, as expected, in the immediate vicinity of the midpoint of the line of centers. On the whole, the simple potential, $-1/r_b$, approximates the calculated potential considerably better than might have been expected, and the deviations become serious only within about 0.2 a.u. of the symmetry plane. We have therefore employed $-1/r_b$ as an approximation to the potential and the boundary conditions mentioned in the introduction.

It is important to note that there are no undetermined parameters in this assumed potential. If, therefore, the major factors contributing to the stability of the hydro-

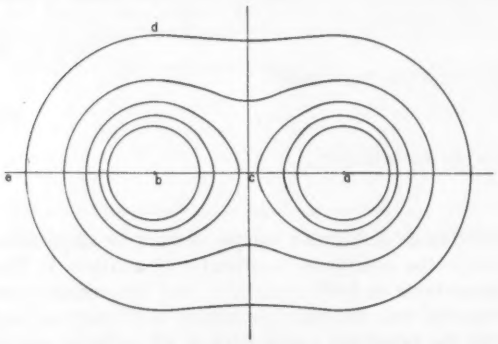

FIG. 1. Equipotential lines for the hydrogen molecule at an internuclear distance of 1.4 a.u.

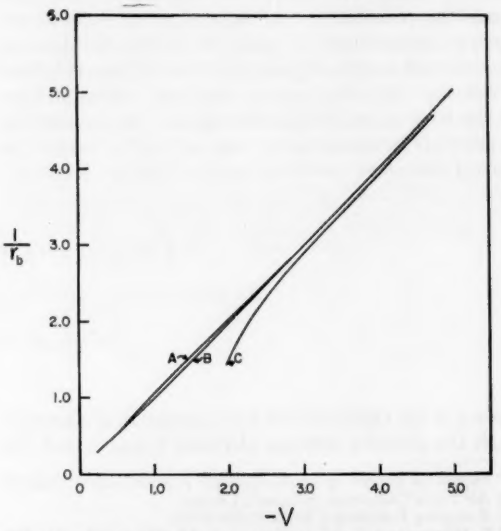

FIG. 2. $-V$ vs $1/r_b$. Curves A, B, and C refer to the respective lines be, bd, and bc of Fig. 1.

TABLE I. The parameters A, p and the one-electron energy E as a function of R for the σ_g and σ_u states.

	σ_g state			σ_u state		
R	A	p	$-E$	A	p	$-E$
0.05	0.0516	0.0524	0.5487			
0.10	0.1047	0.1088	0.5918			
0.30	0.3469	0.3484	0.6743	−1.5324	0.1646	0.1505
0.50	0.6391	0.5825	0.6786	−1.1915	0.3004	0.1805
0.60	0.8024	0.6944	0.6696			
0.70	0.9742	0.8029	0.6578	−0.8066	0.4707	0.2261
0.80	1.1563	0.9078	0.6437			
0.90	1.3561	1.0120	0.6321			
1.00	1.5625	1.1124	0.6187	−0.1010	0.7857	0.3087
1.20	2.0168	1.3094	0.5952			
1.40	2.5266	1.5019	0.5754	1.1281	1.2477	0.3971

gen molecule have been isolated in this model, then a straightforward and self-consistent calculation of the molecular energy from this model must lead to at least semiquantitative agreement with experiment.

A further test of the wave functions, calculated from this potential, can be made by computing the average of the exact Hamiltonian for hydrogen. Although this calculation has been reserved for future research, it seems desirable at this point to call attention to the importance of configuration interaction in the evaluation of this average. This arises because the use of a Heitler-London function [Eq. (2)] implies, in the usual sense of molecular orbital theory, a configuration interaction.[3] This strongly suggests that the functions, obtained by using the potential $-1/r_b$, are most appropriately employed in computing an average of the exact Hamiltonian when used in conjunction with a configuration interaction treatment. The approximation of Eq. (2) implies a configuration interaction between $\sigma_g^2(1s)$ and $\sigma_u^2(1s)$. The recent researches of Rahman,[4] Harris,[5] and McLean, Weiss, and Yoshimine[6] show that other configurations are also of importance if precise results are to be obtained.

2. ONE-ELECTRON EIGENFUNCTIONS AND EIGENVALUES

Treating only the half-space to the left of the symmetry plane[7] (Fig. 1) the Schrödinger equation is (in a.u.)

$$\nabla^2\Psi+2(E+1/r_b)\Psi=0. \tag{4}$$

Variables are separable in prolate spheroidal coordinates

$$\mu=(r_a-r_b)/r_{ab}, \qquad \lambda=(r_a+r_b)/r_{ab}, \qquad \phi$$

where r_{ab} is the internuclear distance. On substituting $\Psi=\Lambda(\lambda)M(\mu)\exp(im\phi)$, we find for the separated equations

$$(d/d\lambda)[(\lambda^2-1)(d\Lambda/d\lambda)]+\{-p^2\lambda^2+2R\lambda-[m^2/(\lambda^2-1)]+A\}\Lambda=0 \tag{5}$$

$$(d/d\mu)[(1-\mu^2)(dM/d\mu)]+\{p^2\mu^2+2R\mu-[m^2/(1-\mu^2)]-A\}M=0 \tag{6}$$

where A is a separation parameter.
Here $p^2=-(\frac{1}{2})r_{ab}^2E$, $R=(\frac{1}{2})r_{ab}$. The boundary conditions on Eq. (5) are that Λ be bounded at $\lambda=1$ and vanish at $\lambda=\infty$. The symmetry plane for the molecule is given by $\mu=0$.

A. Calculation of Eigenvalues

Equation (5) can be solved using a method due to Jaffe.[8,9] Equation (6) has been treated by A. H. Wilson[10] subject to the conditions that M be bounded at $\mu=1$ and $\mu=-1$. Wilson's analysis is also applicable in the present case, but the second of the preceding conditions must be replaced either by the requirement that (at $\mu=0$).

$$M=0 \tag{7}$$

or

$$dM/d\mu=0. \tag{8}$$

Equation (7), when applied to a solution of (6) bounded at $\mu=1$, provides a functional relation between p and A. A second relation, expressed as an infinite continued fraction, is given by Jaffe's solution to Eq. (5). Values

[3] C. A. Coulson, *Valence* (Oxford University Press, New York, 1952). See also C. A. Coulson and I. Fischer, Phil. Mag. **40**, 386 (1940).
[4] A. Rahman, Physica **23**, 31 (1957).
[5] F. Harris, J. Chem. Phys. **27**, 812 (1957).
[6] A. D. McLean, A. Weiss, and M. Yoshimine, Revs. Modern Phys. **32**, 211 (1960).
[7] The potential for the entire space is given by the equation

$$V=\begin{cases}-1/r_b \text{ when } r_a>r_b\\ -1/r_a \text{ when } r_a<r_b.\end{cases}$$

In prolate spheroidal coordinates (see text)

$$V=\{-1/[R(\lambda-|\mu|]\}$$

where $|\mu|$ denotes the absolute value of μ and both cases

$$(r_a>r_b,\ r_a<r_b)$$

are included. This potential is obviously symmetric with respect to reflection.
[8] G. Jaffe, Z. Physik **87**, 535 (1934).
[9] D. R. Bates, K. Ledsham, and A. L. Stewart, Trans. Roy. Soc. (London) **A246**, 215 (1953–1954).
[10] A. H. Wilson, Proc. Roy. Soc. (London) **A118**, 617 (1927).

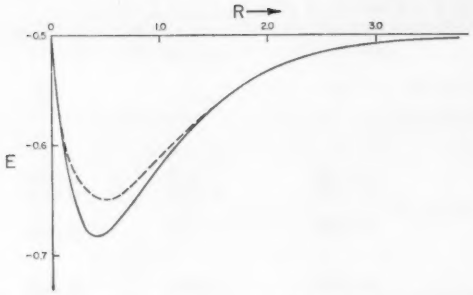

FIG. 3. The one-electron energy E (a.u.) for the σ_g state (solid line). The dotted curve is an approximation computed by a variation method.

of p and A which simultaneously satisfy these two equations are the eigenvalues associated with the antisymmetric eigenfunctions. Eigenvalues associated with the symmetric eigenfunctions are obtained when Eq. (7) is replaced by (8). These simultaneous equations were solved, for the two lowest energy states, by a successive approximation method. A desk calculator was used at two internuclear distances. Final calculations were carried out with an IBM 650 digital computer. Numerical values of E, A, p for several values of R are given in Table I, for each of the two lowest energy stages σ_g and σ_u. The values are correct to three significant figures, the fourth figure is uncertain.

It is evident from Table I that the energies of both states approach a common limit, $-\frac{1}{2}$, at large R. As the internuclear distance decreases, starting from large R, the energy of the σ_g state decreases and the energy of the σ_u state increases. The two states are, therefore, bonding and antibonding, respectively. In this respect, the model is qualitatively correct.

The energy of the σ_g state is shown (solid curve) as a function of R in Fig. 3. (The dotted curve is calculated by a variation method using the variation function $e^{-R\lambda}\cosh R\mu$.) The assumed potential, $-1/r_b$, must depart from the true one electron potential by progressively larger amounts as the internuclear distance decreases and at $R=0$ the departure is extreme. This is indicated in the figure by the fact that the limiting energy at $R=0$, calculated from the model, is $-\frac{1}{2}$, whereas for the actual molecule this one electron energy should approach to that for an electron in the helium atom, -1.84 a.u.[11] In view of this large discrepancy, little weight can be attached to the minimum in the curve of Fig. 3. Fortunately, this occurs at an internuclear distance so much smaller than the experimentally observed internuclear distance for hydrogen that a substantial error in the calculated energy has little significance.

TABLE II. Coefficients of the Laguerre expansion of the σ_g wave function, assuming that $b_3=0$, and the altered value of A shown as a function of R.

R	A	b_0	b_1	b_2
0.50	0.6411	1.0000	0.03415	0.00704
0.60	0.8039	1.0000	0.02946	0.00528
0.70	0.9755	1.0000	0.02427	0.00311
0.80	1.1559	1.0000	0.02147	0.00327
1.00	1.5617	1.0000	0.01560	0.00124
1.20	2.0159	1.0000	0.01173	0.00153

B. Expansion in Laguerre Series

In the eigenvalue calculations, thus far described, the methods outlined above are quite satisfactory. When, however, the eigenfunctions are used for the calculation of average values (as in the next section) a decided disadvantage of the power series expansion of Jaffe becomes evident. Definite integrals are encountered which have not been previously tabulated. This is not, of course, an insurmountable difficulty. However, by expanding in a series of Laguerre polynomials these difficulties can be avoided entirely. The procedure employed is outlined below.

TABLE III. Average value of $1/r_a$ and total molecular energy tabulated as a function of R.

R	$\langle 1/r_a\rangle_{Av}$	$-E_T$
0.50	0.7168	1.071
0.60	0.6501	1.157
0.70	0.5920	1.194
0.80	0.5448	1.207
1.00	0.4675	1.204
1.20	0.4106	1.184

The solution to Eq. (5) is expressed in the following form:

$$\Lambda=[(r^2/4p^2)+(r/p)]^{m/2}e^{-r/2}\sum_{n=0}^{\infty}b_nL_n^{(m)}(r). \quad (9)$$

Here $r=2p(\lambda-1)$, $L_n^{(m)}(r)$ is an associated Laguerre polynomial as defined by Szegö,[12] and the b_n are expansion coefficients. Substituting in Eq. (5) leads to the following three term recurrence formula for the coefficients

$$n(\sigma-n+1)b_{n-1}-\{u+2R+(m+1-4p)n+(\sigma-n)(2n+m+1)\}b_n+(n+m+1)(\sigma-n+m)b_{n+1}=0 \quad (10)$$

where $u=A-p^2+(m+1)(m-2p)$. It can be shown that the solution to (5) which is bounded at $\lambda=1$ and $\lambda=\infty$ also approaches zero exponentially as $\lambda\to\infty$. Hence the conditions for convergence of the Laguerre series[12] are satisfied in this case.

When p, A (for given R) are known then (10) gives the expansion coefficients b_n. In our first calculations the pairs of values for p, A from Table I were employed.

[11] W. S. Wilson and R. B. Lindsay, Phys. Rev. **47**, 681 (1935).
[12] G. Szegö, *Orthogonal Polynomials* (American Mathematical Society, New York, 1939), p. 96.

The calculated values of b_n obtained in this way passed through a minimum and then began to rise rapidly. This behavior resulted from the fact that the eigenvalues of p, A were calculated only to three significant figures and thus are only approximations to the actual eigenvalues, which are no doubt transcendental numbers. Thus the b_n's tend to approach, at large n, the coefficients of a Laguerre series which does not represent the eigenfunction and which, in fact, may be divergent. An accurate representation of the eigenfunction by Laguerre series then requires a pair of values of p, A which are self-consistent with higher accuracy. This behavior is apparently connected with the extreme rapidity of convergence of the Laguerre series. We have approached the problem of calculating the expansion coefficients by arbitrarily assigning the value zero to the coefficients of the series above a certain value, k say. Then (10) constitutes a set of linear homogeneous equations, and approximations to the eigenvalues (which become more accurate as k increases) are obtained as roots of the polynomial found by equating to zero the determinant of the coefficients of the b_n's. For the lowest energy state it is never necessary to retain more than three terms in the series. It was most convenient to solve for A and this was done, using in each case the values of p from Table I. The values of A and of the coefficients b_n are given in Table II. These were obtained with a desk calculator in all cases. Comparison with Table I shows that the values of A differ in the fourth significant figure. Although this is unimportant in energy calculations it has an important effect on the coefficients of the series expansion as discussed in the foregoing.

3. MOLECULAR ENERGY

The eigenvalues described in the preceding section provide the energy of one electron in the hydrogen molecule to the degree of accuracy of which the model is capable. Twice the one-electron energy (E of Table I), plus nuclear repulsion, does not give the molecular energy because, in doubling the energy of one electron, the repulsion between electrons is counted twice. If we subtract from $-1/r_b$ the term $-1/r_a-1/r_b$ (which gives the attraction of the nuclei for the electron considered) the result, $1/r_a$, gives the repulsion between the electron considered and the remaining electron which was tacitly assumed in adopting the potential function $-1/r_b$. The average value of $1/r_a$ is therefore the appropriate electronic repulsion which must be subtracted from twice the one electron energy to give the total electronic energy consistent with our model.

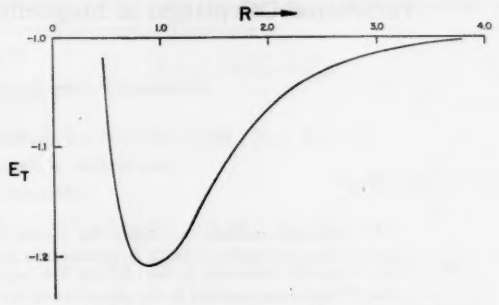

FIG. 4. Total molecular energy E_T as a function of R.

Using the Laguerre series for Λ (see Sec. 2) and the power series expansion for M, obtained from Wilson's formulas,[9] the average value of $1/r_a$ has been calculated as a function of internuclear distance for the lowest energy state (σ_g). The average values are shown in Table III together with the molecular energy $E_T=2E+1/2R-\langle 1/r_a\rangle_{Av}$. This energy is also shown as a function of R in Fig. 4. This curve has a minimum at $2R=1.7$ a.u. and the depth of the minimum is 5.65 ev. These are to be compared with the observed internuclear distance of 1.4 a.u. and the hydrogen dissociation energy of 4.75 ev. The calculated dissociation energy is too large. This does not contradict any variation theorem since we have not averaged the exact Hamiltonian.

The calculation of dissociation energy and equilibrium internuclear distance, outlined in the foregoing, is a self-consistent deduction from the model. Once the potential function is assumed, these results follow without further approximation. In view of the extreme nature of the assumed potential, the discrepancy between theory and experiment does not seem excessive. Further test of the model, by averaging the exact Hamiltonian, seems to be amply justified. Such calculations are now in progress, together with an additional study of another potential function suggested by the results of Sec. 1. A detailed comparison with the results of other investigators, on the hydrogen molecule, will be made when these results are reported.

It is interesting that a model based on a free atom potential (and appropriately modified boundary conditions) can account, even semiquantitatively, for the stabilities of systems as different as an alkali metal and a diatomic molecule with an electron pair bond.

ACKNOWLEDGMENT

We are greatly indebted to Dr. James M. Stewart for assistance in programming the IBM 650 computer.

Variational Calculation of Magnetic Hyperfine Interaction. Nitrogen Atom

T. P. DAS*

Department of Chemistry, Columbia University, New York

AND

A. MUKHERJEE†

Saha Institute of Nuclear Physics, Calcutta, India

(Received March 3, 1960)

A variational method, employing the unrestricted Hartree-Fock approximation, is proposed for the calculation of isotropic magnetic hyperfine constants in paramagnetic atoms and ions with unpaired electrons in non-S states and in free radicals. The method is applied to the ground state of the nitrogen atom. The N^{14} hyperfine constant in the ground state is calculated to be $+7.3$ Mc as compared to the recent experimental value of $+10.4509\pm0.0003$ Mc. Reasons for the discrepancy are discussed.

I. INTRODUCTION

IN the paramagnetic ions of the transition metal and rare earth elements, the unpaired electrons are in d and f states and one would expect, on the basis of the restricted Hartree-Fock model, a zero spin density at the nucleus and consequently a zero hyperfine constant, A. A similar situation would be expected for the nitrogen atom in its ground state, the unpaired electrons having a configuration $2p^3(^4S_{\frac{3}{2}})$. For aromatic free radicals, the siutation is similar. The unpaired electron is usually in a π-orbital state and would be expected to produce a zero spin density at a proton situated in the nodal plane of the π orbital. However, if the nucleus has a finite magnetic moment, a hyperfine splitting is observed in the electron spin resonance spectrum in all these cases[1–3] for atoms and ions of the transition metal and rare earth groups, the earliest explanation[4] offered was based on configuration interaction. It was shown that even in the ground state, small admixtures of configuration in which the S electrons of the atom were in triplet states, were present beside the predominant configuration in which the spins of the s electron were paired. Application of this method to Mn^{55} in Mn^{++} ion gave a value of A which was smaller by a factor of ten than experiment. Subsequently, the experimental value of A was more successfully explained[5,6] using the unrestricted Hartree-Fock approximation for the ground state of the Mn^{++} ion. In free radicals the explanation[7–9] of the hyperfine interaction was based on π—σ bonding in the wave function for the free radicals. A number of detailed calculations based on this idea have been reported for the CH_3 radical.[10–12] The relation between the unrestricted Hartree-Fock approximation in molecular orbital theory and the π—σ bonding theory has recently been discussed qualitatively.[13]

In the unrestricted Hartree-Fock approximation,[5,6] the spatial parts of the wave functions for inner electron states with spin parallel (α) and antiparallel (β) to the outer unpaired electrons, are assumed to be different. The difference arises because the one electron potential for an electron in the spin state α differs from that for an electron in the spin state β. The reason for this difference in one-electron potentials is that the α electron has an exchange interaction with the outer unpaired electrons while the β electron does not.[5] This difference in potentials may be conveniently termed an exchange polarization potential. One can write the one-electron radial differential equations for the spatial parts of the wave functions for $nS\alpha$ and $nS\beta$ states using the conventional Hartree-Fock procedure.[5] Alternatively, one can construct a differential equation for the difference in the radial parts of the wave function for the $nS\alpha$ and $nS\beta$ states, regarding the exchange polarization potential as a first-order perturbation.[6] Analogous to this latter procedure, one could obtain the difference in the radial wave functions by minimizing[14] the second-order change in energy due to the exchange polarization potential. The latter procedure would be useful for free radicals where no convenient differential equations can be set up. However, application of such a variational method to the nitrogen atom yields[14] a result for A of

* Supported by the U. S. Atomic Energy Commission. Address after September 1, 1960: Government of India Atomic Energy Establishment, Trombay, Apollo Pier Road, Bombay 1, India.

† Holder of Government of India, Department of Atomic Energy Junior Fellowship. Present address: Department of Chemistry, Columbia University, New York.

[1] B. Bleaney and K. W. H. Stevens, Repts. Progr. in Phys. **16,** 138 (1953).

[2] M. A. Heald and R. Beringer, Phys. Rev. **96,** 645 (1954).

[3] B. Venkataraman and G. K. Fraenkel, J. Chem. Phys. **24,** 737 (1956).

[4] A. Abragam, J. Horowitz, and M. H. L. Pryce, Proc. Roy. Soc. (London) **A230,** 169 (1955).

[5] G. W. Pratt, Jr., Phys. Rev. **102,** 1303 (1956); J. H. Wood and G. W. Pratt, Jr., Phys. Rev. **107,** 995 (1957).

[6] V. Heine, Phys. Rev. **107,** 1002 (1957); see the Appendix of this paper for the relation between the unrestricted Hartree-Fock approximation and the symmetrical configuration interaction approach of Abragam, Horowitz, and Pryce. Also see R. M. Sternheimer, Phys. Rev. **86,** 316 (1952).

[7] H. M. McConnell, J. Chem. Phys. **24,** 764 (1956).

[8] R. Bersohn, J. Chem. Phys. **24,** 1066 (1956).

[9] S. I. Weissman, J. Chem. Phys. **25,** 890 (1956).

[10] M. Karplus, J. Chem. Phys. **30,** 15 (1959).

[11] J. Higuchi and S. Aono, J. Chem. Phys. **32,** 52 (1960).

[12] A. Padgett and M. Krauss, J. Chem. Phys. **32,** 189 (1960).

[13] H. M. McConnell and D. B. Chesnut, J. Chem. Phys. **28,** 107 (1958).

[14] A. Mukherjee and T. P. Das (unpublished).

+23.0 Mc as compared to the experimental value[15,16] of +10.4509±0.0003 Mc. The large result is due to correlation effects principally between the two electrons in each *ns* shell, which are neglected in the Hartree-Fock approach.[17] These effects are pronounced in the regions where there is appreciable overlap between the unpaired $2p$ electrons and the $1S$ and $2S$ electrons. It is expected that a variational method which gives more weight to the region around the nucleus, where the effects of correlation would be expected to be less pronounced, will give a better value of A. The purpose of this paper is to discuss such a method and apply it to nitrogen atom. The method is simple enough so that it can be extended to free radicals using molecular orbital wave functions. It avoids the requirement of a knowledge of the wave functions and energies of excited states of the free radical that is necessary when using conventional perturbation theory. In Sec. II, the variational method is described and in Sec. III, an application is made to the N^{14} hyperfine interaction in nitrogen atom.

II. THEORY OF THE VARIATIONAL METHOD

The variational method used in this paper is discussed in all generality in earlier papers.[18] For purposes of clarity, a few of the important points of the method will be reproduced here before applying them to the specific problem of magnetic hyperfine interaction.

Consider a system described in its ground state by a wave function Ψ_0 and a Hamiltonian $\mathcal{H}_0$, subjected to two first-order perturbing forces described by Hamiltonians $\mathcal{H}_e$ and $\mathcal{H}_N$, which are assumed to be real as is the case in the problem under consideration. Let the first-order perturbations in the wave function due to $\mathcal{H}_e$ and $\mathcal{H}_N$ be given by $\delta\Psi$ and $\Delta\Psi$, respectively. Then the requisite first-order equations for $\delta\Psi$ and $\Delta\Psi$ are

$$(\mathcal{H}_0-E_0)\delta\Psi=-(\mathcal{H}_e-E_e)\Psi_0, \tag{1}$$

$$(\mathcal{H}_0-E_0)\Delta\Psi=-(\mathcal{H}_N-E_N)\Psi_0, \tag{2}$$

where

$$E_e=\langle\Psi_0\,|\,\mathcal{H}_e\,|\,\Psi_0\rangle, \tag{3}$$

and

$$E_N=\langle\Psi_0\,|\,\mathcal{H}_N\,|\,\Psi_0\rangle. \tag{4}$$

The energy of the system correct to second-order, under the action of the two perturbations is given by

$$E_0+E_1+E_2=\frac{\langle\Psi_0+\delta\Psi+\Delta\Psi\,|\,\mathcal{H}_0+\mathcal{H}_e+\mathcal{H}_N\,|\,\Psi_0+\delta\Psi+\Delta\Psi\rangle}{\langle\Psi_0+\delta\Psi+\Delta\Psi\,|\,\Psi_0+\delta\Psi+\Delta\Psi\rangle},$$

where E_1 and E_2 are the first-order and second-order changes in energy. Therefore

$$E_2=E_{ee}+E_{NN}+E_{eN}, \tag{5}$$

where

$$E_{ee}=2\langle\Psi_0\,|\,\mathcal{H}_e\,|\,\delta\Psi\rangle+\langle\delta\Psi\,|\,\mathcal{H}_0-E_0\,|\,\delta\Psi\rangle-2E_e\langle\Psi_0\,|\,\delta\Psi\rangle, \tag{6}$$

$$E_{eN}=2\langle\Psi_0\,|\,\mathcal{H}_e\,|\,\Delta\Psi\rangle+2\langle\delta\Psi\,|\,\mathcal{H}_0-E_0\,|\,\Delta\Psi\rangle+2\langle\Psi_0\,|\,\mathcal{H}_N\,|\,\delta\Psi\rangle-2E_e\langle\Psi_0\,|\,\Delta\Psi\rangle-2E_N\langle\Psi_0\,|\,\delta\Psi\rangle, \tag{7}$$

$$E_{NN}=2\langle\Psi_0\,|\,\mathcal{H}_N\,|\,\Delta\Psi\rangle+\langle\Delta\Psi\,|\,\mathcal{H}_0-E_0\,|\,\Delta\Psi\rangle-2E_N\langle\Psi\,|\,\Delta\Psi\rangle. \tag{8}$$

The terms involving E_e and E_N in Eqs. (6) to (8) drop out if we use the usual orthogonality conditions

$$\langle\Psi_0\,|\,\delta\Psi\rangle=\langle\Psi_0\,|\,\Delta\Psi\rangle=0, \tag{9}$$

which express the condition that the perturbed wave function be normalized to first order. Also it can be seen that, if we minimize E_{ee} with respect to variations in $\delta\Psi$, we get the perturbation equation (1) and if we minimize E_{NN} with respect to $\Delta\Psi$, we get perturbation equation (2). If we minimize E_{eN} with respect to variations in $\delta\Psi$ and $\Delta\Psi$, we get both Eqs. (1) and (2). When one is interested in the second-order energy due to one of the perturbations alone, $\mathcal{H}_e$ for example, then $\delta\Psi$ can be obtained either by solving Eq. (1) directly or by minimizing E_{ee} with respect to variation parameters in a suitably chosen variational form for $\delta\Psi$. Once $\delta\Psi$ is obtained, E_{ee} can be calculated using the equation

$$E_{ee}=\langle\Psi_0\,|\,\mathcal{H}_e\,|\,\delta\Psi\rangle, \tag{10}$$

which follows from Eqs. (1) and (6). Such a procedure has often been used for calculation of electric and magnetic polarizabilities.[19] To calculate E_{eN}, two alternative procedures could be used. The first procedure, referred to hereafter as method 1, is to obtain either $\delta\Psi$ or $\Delta\Psi$ as above and then evaluate E_{eN} from the relation

$$E_{eN}=2\langle\Psi_0\,|\,\mathcal{H}_N\,|\,\delta\Psi\rangle=2\langle\Psi_0\,|\,\mathcal{H}_e\,|\,\Delta\Psi\rangle, \tag{11}$$

which follows from Eqs. (1), (2), and (7). Method 1 has been used previously for calculation of nuclear magnetic shielding, antishielding of nuclear quadrupole moments in ions, and indirect nuclear spin-spin interaction in molecules.[20] The other alternative procedure referred to hereafter as method 2, is to use suitable

[15] L. W. Anderson, F. M. Pipkin, and J. C. Baird, Phys. Rev. **116**, 87 (1959).

[16] W. Holloway and R. Novick, Phys. Rev. Letters **1**, 367 (1957).

[17] D. R. Hartree, *Calculation of Atomic Structures* (John Wiley & Sons, Inc., New York, 1957), p. 153.

[18] T. P. Das and R. Bersohn, Phys. Rev. **102**, 733 (1956); Phys. Rev. **115**, 897 (1959); See the Appendix of the first paper and Sec. I of the second paper.

[19] See for example, J. Tillieu and G. Guy, Compt. rend. **239**, 1203 (1954); **240**, 1402 (1956); E. Ishiguro, T. Arai, M. Mizushima, and M. Kotani, Proc. Phys. Soc. (London) **A65**, 178 (1952) and also footnote 18.

[20] R. M. Sternheimer and H. M. Foley, Phys. Rev. **102**, 731 (1956); B. R. McGarvey, J. Chem. Phys. **27**, 68 (1957); D. E. O'Reilly, J. Chem. Phys. **32**, 1007 (1960); footnote 18.

variational forms for both $\delta\Psi$ and $\Delta\Psi$ and minimize E_{eN} as given by Eq. (7) with respect to variational parameters in these functions. With the functions $\delta\Psi$ and $\Delta\Psi$ calculated in this manner, the minimum value of E_{eN} is given by

$$E_{eN}=\langle\Psi_0\,|\,\mathcal{H}_N\,|\,\delta\Psi\rangle+\langle\Psi_0\,|\,\mathcal{H}_e\,|\,\Delta\Psi\rangle. \qquad (12)$$

The two methods can be simply described in the following manner. In method 1, we determine the first-order deformation in Ψ_0 due to $\mathcal{H}_e$ (or $\mathcal{H}_N$) alone and in this perturbed state, we compute the expectation value of $\mathcal{H}_N$ (or $\mathcal{H}_e$) to get $\langle\Psi_0+\delta\Psi\,|\,\mathcal{H}_N\,|\,\Psi_0+\delta\Psi\rangle$, the second-order part of which is given by Eq. (11). In method 2, we determine both deformations $\delta\Psi$ and $\Delta\Psi$ simultaneously and obtain the contribution from both these functions to the second-order energy E_{eN}. Such a method has previously[21] been used in the calculation of the proton magnetic shielding and indirect spin-spin coupling constants in the hydrogen molecule. The relative merits of the two methods from the point of view of accuracy, depend on the nature of the problem to which they are applied.

The specific problem of magnetic hyperfine interaction, that we are here interested in, will now be cast in the language of the general treatment outlined above. Around a nucleus A are three electrons. Two of these electrons are in states which have opposite spins, but have the same spatial wave function Ψ_b in the restricted Hartree-Fock approximation. The third electron is in a state which has spatial wave function Ψ_a that vanishes at nucleus A. In the restricted Hartree-Fock approximation, one therefore expects to have a zero spin density at nucleus A even when Ψ_b is finite[22] at A. Henceforth, we shall refer to the b state with spin parallel to the a state as $b\alpha$ and the b state with spin antiparallel as $b\beta$. In the restricted Hartree-Fock approximation, the electrons in states $b\alpha$ and $b\beta$ are assumed to experience the same one-electron potential. In the unrestricted Hartree-Fock approximation, account is taken of the difference in the potentials experienced by the electrons in $b\alpha$ and $b\beta$ states. This difference may be obtained as follows. The exchange interaction energy between electrons in the $b\alpha$ and $a\alpha$ states is

$$K_{ab}=-\int\psi_a(1)\psi_b(2)r_{12}^{-1}\psi_a(2)\psi_b(1)d\tau_1 d\tau_2(e^2/a_0), \qquad (13)$$

where e is the electronic change and a_0 the Bohr radius. There is no exchange interaction energy between electrons in $b\beta$ and $a\alpha$ states due to the orthogonality of the spin functions. The exchange interaction energy K_{ab} may be considered as arising out of an electron potential $\mathcal{H}_e$ defined by

$$K_{ab}=\int\psi_b(1)\mathcal{H}_e(1)\psi_b(1)d\tau_1.$$

Therefore

$$\mathcal{H}_e(1)=-[\psi_a(1)/\psi_b(1)]\int\psi_b(2)r_{12}^{-1}\psi_a(2)d\tau_2(e^2/a_0), \qquad (14)$$

$\mathcal{H}e$ is then the first-order exchange polarization potential leading to a difference $\delta\psi_b$ between the spatial parts of the wave functions for $b\alpha$ and $b\beta$ states. In addition, the electrons in $b\alpha$ and $b\beta$ states are subject to the Fermi contact potential due to the magnetic moment of nucleus A, namely

$$\mathcal{H}_N=\tfrac{8}{3}(16\pi\beta\hbar)\gamma_A\mathbf{I}\cdot\mathbf{S}\delta(\mathbf{r}_A)a_0^{-3}, \qquad (15)$$

where β = Bohr magneton, γ_A = magnetogyric ratio of nucleus A, $\mathbf{I}\hbar$ = spin angular momentum of nucleus A, $\mathbf{S}\hbar$ = spin angular momentum of electron, and $\delta(\mathbf{r})$ = three-dimensional Dirac δ function with $\mathbf{r}$ measured from nucleus A. The second-order energy E_{eN} then gives us the indirect hyperfine interaction energy between the nucleus A and the unpaired electron in a α state brought about by the combined effect of the exchange interaction of electrons in $a\alpha$ and $b\alpha$ states, and the magnetic interaction of the electron in the $b\alpha$ state with the nuclear magnetic moment. We could again follow either of the two methods outlined above. Method 1, that of determining $\delta\psi_b$ and using Eq. (11), has been the one used previously[5–12] for paramagnetic ions and free radicals. In our earlier variational calculation on the nitrogen atom,[14] we used this method and minimized E_{ee}. As mentioned in the introduction, this procedure leads to an overestimation of E_{eN} due to the pronounced effect of electron correlation[23] in the region from which we get the maximum contribution to E_{ee}. Alternatively, we could still use method 1, but determine $\Delta\psi_b$ by minimizing E_{NN}, thereby weighting the region near the nucleus significantly, where the effect of correlation is relatively less important. However, it is not possible to use this method in the nonrelativistic approximation because E_{NN} is infinite. If relativistic effects and the finite distribution of charge within the nucleus were taken into account, E_{NN} would of course be finite.[24] In some cases, as for example, the CH bond, to be discussed in the succeeding paper,[25] $\Delta\psi_b$ can be obtained from available experimental data such as the C^{13}—H^1 indirect spin-spin coupling constant.

Method 2 has advantages over both of the above alternatives of method 1 because, (a) like E_{NN}, the

[21] M. J. Stephen, Proc. Roy. Soc. (London) **A243**, 270, 274 (1957).

[22] As examples, for lithium atom in the $1s^22p$ configuration, ψ_a and ψ_b correspond respectively to $1s$ and $2p$ wave functions while for proton hyperfine interaction in a CH fragment, ψ_a refers to the wave function of the unpaired π electron state and ψ_b to the wave function for the σ orbitals constituting the CH bond.

[23] A. Mukherjee and T. P. Das, Phys. Rev. **111**, 1479 (1958); see the discussion on effects of electron correlation in Sec. II of this paper.

[24] Reference 18, Sec. III D and Appendix B of second paper.

[25] R. A. Bernheim and T. P. Das, J. Chem. Phys. **33**, 1813 (1960), following paper.

quantity to be minimized, E_{eN}, is less sensitive to the effect of electron correlation than E_{ee}, and (b) E_{eN} is not infinite in the nonrelativistic approximation as contrasted to E_{NN}. We have employed method 2 in our calculation on the nitrogen atom in Sec. III. For $\delta\psi_b$ and $\Delta\psi_b$, we have made use of the variational forms

$$\delta\psi_b = f\psi_b,$$
$$\Delta\psi_b = F\psi_b. \tag{16}$$

The advantage[18] in choosing variational functions of the form (16) is that the various matrix elements in Eq. (7) require only expectation values over the ground state wave function, which in this case is the restricted Hartree-Fock wave function ψ_b. For atoms,[26] a convenient form for f is

$$f = \sum_i \lambda_i r_A{}^i, \tag{17}$$

where i takes up integral values starting from zero, but $i=1$ is omitted to avoid a divergence in the term $\langle \delta\psi_b \mid \mathcal{H}_0 - E_0 \mid \Delta\psi_b \rangle$. The λ_i are the variational parameters with which we minimize E_{eN}. For the case where ψ_b is a two-centered molecular orbital, a suitable extension of Eq. (17) would be

$$f = \sum_i (\lambda_i r_A{}^i + \mu_i r_B{}^i), \tag{18}$$

where A and B refer to the two nuclei, and λ_i and μ_i are variational parameters. For the function F, one of the following alternative forms could be chosen.

$$F = \xi\delta(\mathbf{r}_A) + \sum_i \xi_i r_A{}^i, \tag{19}$$

$$F = (\xi_{-1}/r_A) + \xi \log_e r_A + \sum_i \xi_i r_A{}^i, \tag{20}$$

ξ_{-1}, ξ, and ξ_i being variational parameters. The summation in i extends over integral values starting from $i=0$. The form (19) was previously used[21] to calculate the indirect spin-spin coupling constant in HD molecule. The form (20) is suggested by the exact solution of Eq. (2) for the $1s$ state of hydrogen atom, which has the form[27]

$$(-r_A{}^{-1} + 2\log_e r_A + 2r_A)e^{-r_A}.$$

However the use of the form (19) greatly simplifies the integrals involved in Eq. (7) for E_{eN}. One objection could be raised against using the form (19) for F, namely that $\psi_b + \Delta\psi_b$ is not square integrable if we keep the term $\langle \Delta\psi_b \mid \Delta\psi_b \rangle$ in $\langle \psi_b + \Delta\psi_b \mid \psi_b + \Delta\psi_b \rangle$. However, we are interested in E_{eN} which involves $\Delta\psi_b$ only in first order and so the divergence of $\langle \Delta\psi_b \mid \Delta\psi_b \rangle$ is of no consequence to us.[24]

From the calculated value of E_{eN}, we obtain the hyperfine constant A in the spin-Hamiltonian $Ah\mathbf{I}\cdot\mathbf{s}$ for the $a\alpha$ electron using the relation

$$E_{eN} = (Ah/2)I_z.$$

In the general case, where there is more than one unpaired electron, A would be given by

$$A = E_{eN}/SI_s h, \tag{21}$$

where S is the total spin of the atom or the molecule and the state of the atom under consideration is that where $m_s = S$.

III. N^{14} MAGNETIC HYPERFINE CONSTANT IN NITROGEN ATOM

The N^{14} hyperfine constant in nitrogen atom in the ground state was calculated using method 2 of Sec. II based on extremizing E_{eN}. Since there are two paired states $1s$ and $2s$ in this case, which may become mixed with one another by the action of the perturbations $\mathcal{H}_e$ and $\mathcal{H}_N$, a slight modification of the method of Sec. II was necessary in order to permit us to handle the $1s$ and $2s$ states separately. To be able to do so, we require $\delta\psi_{1s}$ and $\Delta\psi_{1s}$ to be orthogonal to ψ_{2s} and $\delta\psi_{2s}$ and $\Delta\psi_{2s}$ to be orthogonal to ψ_{1s}. We, therefore, impose the following conditions on the variation functions f_1, f_2, F_1, and F_2,

$$\langle \psi_{1s} \mid f_1 \mid \psi_{2s} \rangle = \langle \psi_{1s} \mid f_2 \mid \psi_{2s} \rangle = \langle \psi_{1s} \mid F_1 \mid \psi_{2s} \rangle$$
$$\langle \psi_{1s} \mid F_2 \mid \psi_{2s} \rangle = 0. \tag{22}$$

In f_1, f_2, F_1, and F_2, the suffices refer to the state which is being perturbed.

As in Eqs. (17) and (19), the following expressions were used for the f_n and F_n,

$$f_n = (\lambda_{n_0} + \lambda_{n_2} r^2 + \lambda_{n_3} r^3 + \lambda_{n_4} r^4),$$
$$F_n = (\eta a_0{}^2/4\pi e^2)\{\xi_{n_0} + \xi_n[\delta(r)/r^2] + \xi_{n_1} r + \xi_{n_2} r^2\}, \tag{23}$$

where $\eta = \frac{1}{3}(16\pi\beta\hbar\gamma_N{}^{14} I_z)$, $\gamma_N{}^{14}$ representing the magnetogyric ratio of N^{14}, $I_z\hbar$ the z component of the nuclear spin, and $\delta(r)$ the radial δ function. Equation (9) then yields the following relations

$$\lambda_{n_0} = -\frac{\lambda_{n_2}\langle r^2\rangle_n + \lambda_{n_3}\langle r^3\rangle_n + \lambda_{n_4}\langle r^4\rangle_n}{\langle r^0\rangle_n}$$
$$\xi_{n_0} = -\frac{\xi_n\langle (1/r^2)\delta(r)\rangle_n + \xi_{n_1}\langle r\rangle_n + \xi_{n_2}\langle r^2\rangle_n}{\langle r^0\rangle_n}, \tag{24}$$

where $\langle\ \rangle_n$ refers to expectation values over ψ_{nS}. Equations (22) yield the relations

$$\lambda_{n_2} = -\frac{\lambda_{n_3}\langle r^3\rangle_{12} + \lambda_{n_4}\langle r^4\rangle_{12}}{\langle r^2\rangle_{12}}$$
$$\xi_n = -\frac{\xi_{n_1}\langle r\rangle_{12} + \xi_{n_2}\langle r^2\rangle_{12}}{\langle \delta(r)/r^2\rangle_{12}}, \tag{25}$$

[26] E. G. Wikner and T. P. Das, Phys. Rev. **107**, 497 (1957).
[27] C. Schwartz, Ann. Phys. (N. Y.) **6**, 156 (1959).

where

$$(\text{Op.})_{12}=\int\psi_{1S}\,\text{Op.}\psi_{2S}d\tau. \tag{26}$$

Using Eqs. (7) and (23) for the $m_s=\frac{3}{2}$ state when the spins of the three $2p$ electrons are all parallel, we then get

$$\begin{aligned}E_{eN}=(\eta a_0^{-3}/8\pi)\sum_n[&-(4\lambda_{n_2}\xi_n\langle\delta(r)/r^2\rangle_n\\&-2\lambda_{n_2}\xi_{n_1}\langle r\rangle_n-4\lambda_{n_2}\xi_{n_2}\langle r^2\rangle_n\\&-3\lambda_{n_2}\xi_{n_1}\langle r^2\rangle_n-6\lambda_{n_2}\xi_{n_2}\langle r^3\rangle_n\\&-4\lambda_{n_4}\xi_{n_1}\langle r^3\rangle_n-8\lambda_{n_4}\xi_{n_2}\langle r^4\rangle_n)\\&+2(\xi_{n_0}G_{nn}{}^0+\xi_{n_1}G_{nn}{}^1+\xi_{n_2}G_{nn}{}^2-\lambda_{n_0}\langle\delta(r)/r^2\rangle_n)],\end{aligned} \tag{27}$$

where

$$G_{nn}{}^p=\int_0^\infty\int_0^\infty P_{2p}(r)\,P_{nS}(r)r^pU_1(r,t)\,P_{2p}(t)\,P_{nS}(t)\,drdt, \tag{28}$$

with

$$P_{2p}(r)=r\psi_{2p}(r)\quad\text{and}\quad P_{nS}(r)=r\psi_{nS}(r),$$

and

$$\begin{aligned}U_1(r,t)&=(t/r^2)\quad\text{for}\quad t<r,\\&=(r/t^2)\quad\text{for}\quad t>r,\end{aligned}$$

$\psi_{ns}(r)$ and $\psi_{2p}(r)$ are the radial parts of the wave functions ψ_{ns} and ψ_{2p}.

In deducing Eq. (27) we have made use of the relation[18]

$$(\mathcal{H}_0-\mathcal{E}_n)\psi_{nS}=0,$$

which yields

$$(V_n-\mathcal{E}_n)=\hbar^2\Delta^2\psi_{nS}/2ma_0^2\psi_{nS},$$

V_n and $\mathcal{E}_n$ representing the zero-order (restricted Hartree-Fock) one-electron potential and one-electron energy in nS state. Using Eqs. (24) and (25), λ_{n_0}, ξ_{n_0}, λ_{n_2}, and ξ_n are eliminated from Eq. (26) and for each $nS\alpha$ state, we are left with an expression for E_{eN} involving linear terms in λ_{n_3}, λ_{n_4}, ξ_{n_1}, and ξ_{n_2} and products $\lambda_{n_4}\xi_{n_1}$, $\lambda_{n_4}\xi_{n_2}$, $\lambda_{n_4}\xi_{n_1}$, and $\lambda_{n_4}\xi_{n_2}$. Setting

$$\partial E_{eN}/\partial\lambda_{n_3}=\partial E_{eN}/\partial\xi_{n_1}=\partial E_{eN}/\partial\lambda_{n_4}=\partial E_{eN}/\partial\xi_{n_2}=0, \tag{29}$$

we obtain linear equations in these parameters which can be easily solved. Substituting the values of the parameters satisfying these linear equations in Eq. (27) for E_{eN}, the hyperfine constant A in cycles is then obtained using Eq. (11) with $S=\frac{3}{2}$.

The restricted Hartree-Fock functions ψ_{1S} and ψ_{2S} were taken from the published calculations of Hartree and Hartree.[28] The integrals involved in Eqs. (24), (25), and (27) were obtained correct to four significant figures on a desk computer. For the $1s$ state, the result of the calculation is

$$E_{eN}(1S)=-(\eta a_0^{-3}/4\pi)\,(2.544), \tag{30}$$

and for $2S$ state

$$E_{eN}(2S)=+(\eta a_0^{-3}/4\pi)\,(2.976). \tag{31}$$

Using Eq. (21) and remembering that $A(\text{H}^1)$ in the hydrogen atom is 1420 Mc and[29] $(\gamma_{\text{N}^{14}}/\gamma_{\text{H}^1})=0.07224$, we obtain

$$\begin{aligned}A(1S)&=-\tfrac{1}{6}\times2.544\times(\gamma_{\text{N}^{14}}/\gamma_{\text{H}^1})\times1420\text{ Mc}=-43.1\text{ Mc}\\A(2S)&=+\tfrac{1}{6}\times2.976\times(\gamma_{\text{N}^{14}}/\gamma_{\text{H}^1})\times1420\text{ Mc}=+50.4\text{ Mc}.\end{aligned} \tag{32}$$

The sum of these contributions then yields $A=+7.3$ Mc for the whole atom as compared to the recent experimental value[15,16] of $A=+10.4509\pm0.0003$. The agreement between our calculated and experimental values is quite good considering the fact that A is the difference of two large numbers.

While it is possible that other variational forms for f_n and F_n might give better agreement with experiment, there are two reasons why excellent quantitative agreement with experiment is not to be expected. One of these reasons is that our procedure is not strictly self-consistent. This is because, in applying Eq. (7) directly to the $1S\alpha$ and $2S\alpha$ states of the nitrogen atom to obtain the expression E_{eN} as in Eq. (23), we have neglected both the change in the one-electron potential experienced by the $1s\alpha$ electron which is produced by the perturbations $\delta\psi_{2s}$ and $\Delta\psi_{2s}$ in the wave function for the $2S\alpha$ state and the corresponding change in the one-electron potential for the $2S\alpha$ state due to perturbations $\delta\psi_{1S}$ and $\Delta\psi_{1S}$ in the $1S\alpha$ wave function. However, including these changes would hopelessly complicate the calculation, and there is some reason to expect that their effects on E_{eN} are small. The main contribution to E_{eN} comes from the region near the nucleus, and in this region, the one-electron potential originates mainly from the nuclear charge and the changes in the one-electron potential of the above type are relatively less significant than in regions removed from the nucleus.

The second source of error is the neglect of correlation between the electrons which, though less serious near the nucleus than away from it, could nevertheless affect the results of calculation appreciably. There is evidence from calculations on the helium atom and from other sources[30] that correlation effects increase the charge density near the nucleus above that predicted by Hartree-Fock calculations and this would increase our calculated result in the right direction. To properly take account of such correlations, interelec-

[28] D. R. Hartree and W. Hartree, Proc. Roy. Soc. (London) **A193**, 299 (1948).

[29] N. F. Ramsey, *Nuclear Moments* (New York, 1953), p. 79.

[30] See for example, Fig. 4 of footnote 23 for the helium atom and Table III of J. Chem. Phys. **27**, 1 (1957) for the boron atom.

tronic coordinates like r_{12} would have to be introduced into the wave functions of the perturbed and unperturbed states, making calculations much harder.

IV. CONCLUSION

The variational method discussed in this paper was arrived at in the quest for a method which would permit a relatively simple calculation of the hyperfine interaction constants in free radicals. In order to test the method it was applied to the nitrogen atom. It is hoped that in the future, someone will solve the self-consistent unrestricted Hartree-Fock differential equations[5] for the nitrogen atom when a comparison could be made with our approximate result. No such differential equations can be conveniently set up for free radicals because orbitals with more than one center are involved. Earlier quantitative methods have either been extremely laborious, requiring detailed valence-bond calculations[10] involving π—σ bonding or have used conventional perturbation theory requiring a knowledge of excitation energies.[13] It is hoped that the fair success of the present method as applied to the nitrogen atom will evoke interest in applying it to simple free radicals. Our method only requires a knowledge of the zero-order wave functions for the free radical which do not take the π—σ interaction into account. The method used in this paper will probably be more successful for proton hyperfine constants in free radicals since no differences between almost equal and opposing contributions are involved as in the case of the nitrogen atom.

ACKNOWLEDGMENTS

The authors are grateful to Professor R. Bersohn and Dr. R. A. Bernheim for helpful discussions.

THE JOURNAL OF CHEMICAL PHYSICS VOLUME 33, NUMBER 6 DECEMBER, 1960

Relation between the Proton Hyperfine Interaction and the C^{13}—H^1 Spin-Spin Coupling in Free Radicals*

R. A. BERNHEIM AND T. P. DAS†

Department of Chemistry, Columbia University, New York

(Received March 3, 1960)

It is shown that the C^{13}—H^1 spin-spin coupling constant $J(C^{13}$—$H^1)$ and the proton hyperfine constant $Q(H^1)$ in a free radical can be considered as interdependent, and that they both can be estimated by calculating the perturbation produced in the electronic wave functions by the magnetic moment of the proton. For a C—H fragment with an unpaired π electron on the carbon atom an approximate relation is established between $Q(H^1)$ and $J(C^{13}$—$H^1)$. Using the experimental value of $J(C^{13}$—$H^1)$ for the benzene molecule, $Q(H^1)$ is found to have a negative sign and order of magnitude agreement with experiment.

IN the preceding paper,[1] (referred to as I hereafter), it has been pointed out that the process which leads to an indirect hyperfine interaction between an unpaired electron and a nucleus can be described in two ways. For a C—H fragment with an unpaired π electron on the carbon atom, the hyperfine interaction between the π electron and the proton is usually explained as arising out of an exchange polarization[2–5] of the σ states by the π electron. Alternatively, the proton magnetic moment could deform the σ states, the deformation being communicated to the π electron by an exchange interaction with the σ electron of the same spin. Using this latter concept to calculate the hyperfine interaction energy would involve evaluating Eq. (11) of I,

$$E_{EN}=2\langle\psi_b \mid \mathcal{H}_E \mid \Delta\psi_b\rangle,$$

where ψ_b stands for the σ-state wave function and $\Delta\psi_b$ the perturbation in the σ-state wave function by the proton magnetic moment. We shall also show how $\Delta\psi_b$ can be determined approximately from the value of the C^{13}-H^1 indirect spin-spin coupling constant.

The experimental data relevant to the problem considered here are[6] $J(C^{13}-H^1)=159$ cps for benzene and[7] $Q(H^1)=-63$ Mc for a proton in a C—H bond of an aromatic compound when an unpaired π electron is localized on the carbon atom.

* This work was supported by the U. S. Atomic Energy Commission.

† Address after September 1, 1960: Government of India Atomic Energy Establishment, Trombay, Apollo Pier Road, Bombay 1, India.

[1] T. P. Das and A. Mukherjee, J. Chem. Phys. **33**, 1808 (1960).
[2] H. M. McConnell, J. Chem. Phys. **24**, 764 (1956).
[3] R. Bersohn, J. Chem. Phys. **24**, 1066 (1956).
[4] B. Venkataraman and G. K. Fraenkel, J. Chem. Phys. **24**, 737 (1956).
[5] S. I. Weissman, J. Chem. Phys. **25**, 890 (1956).
[6] P. C. Lauterbur, J. Chem. Phys. **26**, 217 (1957).
[7] H. M. McConnell and D. B. Chesnut, J. Chem. Phys. **28**, 107 (1958).

There are three perturbing Hamiltonians[1] acting on an electron in a $\sigma\alpha$ state of the C—H bond:

$$\mathcal{H}_E = -[\psi_\pi(1)/\psi_\sigma(1)]\int\psi_\sigma(2)r_{12}^{-1}\psi_\pi(2)d\tau_2(e^2/a_0) \quad (1)$$

$$\mathcal{H}_H = \lambda_H a_0^{-3}\mathbf{I}_H\cdot\mathbf{S}\delta(\mathbf{r}_H) \quad (2)$$

$$\mathcal{H}_C = \lambda_C a_0^{-3}\mathbf{I}_C\cdot\mathbf{S}\delta(\mathbf{r}_C), \quad (3)$$

where

$$\lambda_H = (16/3)\pi\beta\hbar\gamma_H$$

and

$$\lambda_C = (16/3)\pi\beta\hbar\gamma_C. \quad (4)$$

Here $\mathcal{H}_E$ is the additional exchange polarization potential which is felt by the electron in the $\sigma\alpha$ state over that in the $\sigma\beta$ state, $\mathcal{H}_H$ is the Fermi contact potential due to the proton magnetic moment and $\mathcal{H}_C$ that due to the C^{13} magnetic moment, γ_H and γ_C represent the magnetogyric ratios of the H^1 and C^{13} nuclei, respectively, $\mathbf{I}_H$ and $\mathbf{I}_C$ the nuclear spin vectors, $\mathbf{S}$ the π-electron spin vector, $\delta(\mathbf{r}_H)$ and $\delta(\mathbf{r}_C)$ δ functions centered on the proton and carbon nucleus, β the Bohr magneton, e the electronic charge, and a_0 the radius of the first Bohr orbit in the hydrogen atom.

Here ψ_σ and ψ_π denote the unperturbed wave functions for the σ state and π state, respectively, $\Delta\psi_\sigma$ denotes the perturbation in the wave function of the $\sigma\alpha$ electron by $\mathcal{H}_H$. Using the aforementioned Eq. (11) of I, we now have

$$E_{HC} = 2\langle\psi_\sigma \mid \mathcal{H}_C \mid \Delta\psi_\sigma\rangle \quad (5)$$

and

$$E_{EH} = 2\langle\psi_\sigma \mid \mathcal{H}_E \mid \Delta\psi_\sigma\rangle. \quad (6)$$

E_{HC} is related to $J(C^{13}\text{-}H^1)$ and E_{EH} to $Q(H^1)$. Both $J(C^{13}\text{-}H^1)$ and $Q(H^1)$ could be obtained if $\Delta\psi_\sigma$ were known. Also, if $\Delta\psi_\sigma$ was approximated by a function containing one unknown parameter, we could determine the parameter using Eq. (5) together with the experimental value of $J(C^{13}\text{-}H^1)$. The resulting $\Delta\psi_\sigma$ can then be used together with Eq. (6) to determine $Q(H^1)$.

From I, a suitable form for $\Delta\psi_\sigma$ with one adjustable parameter would be

$$\Delta\psi_\sigma = [b\delta(\mathbf{r}_H)+b_0]\psi_\sigma\lambda_H a_0^{-3}I_{Hz}, \quad (7)$$

where b_0 is related to b by

$$\langle\psi_\sigma \mid \Delta\psi_\sigma\rangle = 0,$$

leading to

$$b_0 = -b\psi_\sigma^2(H). \quad (8)$$

Using Eq. (5), we then get

$$E_{HC} = \lambda_H\lambda_C a_0^{-6}\langle\psi_\sigma \mid \delta(\mathbf{r}_C) \mid [b\delta(\mathbf{r}_H)+b_0]\psi_\sigma\rangle I_{Hz}I_{Cz}$$
$$= \lambda_H\lambda_C a_0^{-6}b_0\psi_\sigma^2(C)I_{Hz}I_{Cz}$$
$$= -\lambda_H\lambda_C a_0^{-6}b\psi_\sigma^2(H)\psi_\sigma^2(C)I_{Hz}I_{Cz}.$$

Therefore,

$$J(C^{13}\text{-}H^1) = -(b\lambda_H\lambda_C/a_0^6h)\psi_\sigma^2(H)\psi_\sigma^2(C) \text{ cycles}. \quad (9)$$

Equation (9) predicts the experimentally found[8] linear dependence of $J(C^{13}\text{—}H^1)$ upon the s character of the C—H bond if the dependence of b and $\psi_\sigma^2(H)$ upon the hybridization of the carbon orbitals is assumed to be negligible. This is a valid assumption since both b and $\psi_\sigma^2(H)$ are properties of the electron distribution at the proton.

Now, from Eqs. (1), (6), and (7), we get

$$E_{EH} = -\frac{\lambda_H e^2 b_0 I_{Hz}}{a_0^4}\iint\psi_\pi(1)\psi_\sigma(1)r_{12}^{-1}\psi_\pi(2)\psi_\sigma(2)d\tau_1 d\tau_2. \quad (10)$$

Therefore,

$$Q(H^1) = 2E_{EH}/I_{Hz}h = [2\lambda_H e^2 b\psi_\sigma^2(H)/ha_0^4]G, \quad (11)$$

where G denotes the exchange integral on the right-hand side of Eq. (10). Combining Eqs. (9) and (11), we get

$$Q(H^1) = [-2a_0^2e^2/\lambda_C\psi_\sigma^2(C)]GJ(C^{13}\text{-}H^1), \quad (12)$$

which relates $Q(H^1)$ to $J(C^{13}\text{-}H^1)$.

To test the validity of Eq. (12), it was compared with experimental data in the following manner. The orbital ψ_σ is assumed to be composed of an sp^2 hybrid C-atom orbital and a contracted H-atom $1s$ orbital with an effective nuclear charge $z_H = 1.2$. The number 1.2 was chosen by comparison with the case of the H_2 molecule[9] where z_H has been found to be 1.193 and with the HF molecule[10] where z_H is found to be 1.322. The ionic character was assumed equal to zero. Then

$$\psi_\sigma = (\psi_{C\sigma}+\psi_H)/[2(1+S)]^{\frac{1}{2}},$$

where

$$\psi_{C\sigma} = (\psi_{2S}+\sqrt{2}\psi_{2p_z})/\sqrt{3}$$

and

$$S = \langle\psi_{C\sigma} \mid \psi_H\rangle. \quad (13)$$

For ψ_{2S} and ψ_{2p_z}, the atomic wave functions calculated by Tubis[11] were used. The C–H distance R was taken as that in benzene, namely 1.08 A. We then obtain

$$\psi_\sigma^2(C) = 0.183. \quad (14)$$

Introducing this in Eq. (12) and evaluating the constants yields

$$Q(H^1) = -64.07GJ(C^{13}\text{-}H^1) \text{ Mc}, \quad (15)$$

where G is in units of e^2/a_0 and $J(C^{13}\text{-}H^1)$ is in cycles. The sign of $Q(H^1)$ is found to be negative, assuming $J(C^{13}\text{-}H^1)$ to have a positive sign (as is expected when the main contribution is given by the hyperfine interaction mechanism[12]).

[8] J. N. Shoolery, J. Chem. Phys. **31,** 1427 (1959).
[9] C. Coulson, Trans. Faraday Soc. **33,** 1479 (1937).
[10] R. A. Ballinger, Mol. Phys. **2,** 139 (1959).
[11] A. Tubis, Phys. Rev. **102,** 1049 (1956).
[12] N. F. Ramsey, Phys. Rev. **91,** 303 (1953).

To obtain numerical agreement with experiment, we require $G=0.0062\ e^2/a_0$ which is 0.17 ev. The integral G may be broken down into the following integrals:

$$G=[1/2(1+S)][\tfrac{2}{3}\langle\pi p\mid p\pi\rangle+\tfrac{1}{3}\langle\pi s\mid s\pi\rangle + (\sqrt{2}/3)\langle\pi p\mid s\pi\rangle+\langle\pi H\mid H\pi\rangle +\tfrac{2}{3}\langle\pi p\mid H\pi\rangle+\tfrac{1}{3}^{-1}\langle\pi s\mid H\pi\rangle], \quad (16)$$

where π, p, and s refer to $2p_\pi$, $2p_z$, and $2s$ orbital on the carbon atom, and H refers to the $1s$ orbital on the hydrogen atom. $\langle\alpha\beta\mid\gamma\delta\rangle$ refers to the exchange integral

$$\iint\alpha(1)\beta(2)r_{12}^{-1}\gamma(1)\delta(2)d\tau_1 d\tau_2.$$

Semi-empirical values can be used for the first, second, and fourth integrals of Eq. (16).[13] The third integral vanishes. The fifth and sixth integrals are tabulated for Slater orbitals on the carbon atom and for a hydrogen atomic orbital with $z_H=1.0$ by Kotani *et al.*[14] Using these values we obtain $G=0.97$ ev. This value would be reduced if Tubis orbitals were used for the carbon atom and a contracted orbital ($z_H=1.2$) were used for the hydrogen atom. It can be concluded that the value of $Q(H^1)$ calculated from the approximate relation, E . (12), seems to agree only in order of magnitude with experiment.

[13] D. H. Anderson, Ph.D. thesis, University of Illinois, 1959.
[14] M. Kotani, A. Amemiya, E. Ishiguro, and T. Kimura, *Table of Molecular Integrals* (Maruzen Co., Ltd., Tokyo, 1955).

To obtain a more accurate value of $Q(H^1)$, the variational procedure of I would have to be used, including more parameters in $\Delta\psi_\sigma$. The function $\Delta\psi_\sigma$ obtained in this way could also be used to calculate $J(C^{13}\text{-}H^1)$ using Eq. (5). It is to be noted that the variational calculation does not necessarily require the use of the semiempirical assumption[7]

$$A(H^1)=Q\rho,$$

where ρ is the density of the π orbital on the carbon atom of the C—H bond. To be more general, and to compute $A(H^1)$ directly, ψ_π in Eq. (1) would have to be a molecular orbital involving a linear combination of the π-atomic orbitals associated with all the carbon atoms in the aromatic system. The calculation would then become more laborious and would entail the estimation of exchange integrals about more than two centers.

The hyperfine constant $Q(C^{13})$ for the carbon nucleus in a C—H fragment could also be computed by the procedure outlined in I. A calculation of $Q(C^{13})$ would have to include perturbations due to $\mathcal{H}_C$ in the $1s^2$ shell and in the three σ bonds of the carbon atom in a free radical. Since four orbitals are involved in the interaction instead of only one as in the case of $Q(H^1)$, an approximate equation similar to Eq. (12) can no longer be obtained.

ACKNOWLEDGMENTS

The authors are grateful to R. Bersohn and M. J. Stephen for helpful discussions.

THE JOURNAL OF CHEMICAL PHYSICS VOLUME 33, NUMBER 6 DECEMBER, 1960

Critical Solution Phenomenon in Two-Component Liquid Systems. The System Water-Ethylene Glycol Mono-Isobutyl Ether

DE F. P. RUDD*

Department of Chemistry, Lincoln University, Lincoln University, Pennsylvania

AND

B. WIDOM

Department of Chemistry, Cornell University, Ithaca, New York

(Received July 6, 1960)

The system water-ethylene glycol mono-isobutyl ether is studied in the neighborhood of its lower critical mixing point, and it is found that the two lines in a Cox-Herington plot have slopes which, to within a small experimental error, are of exactly equal magnitude. The lower critical solution point is found to be at 25.8°C and 30.4 weight percent ether. It is shown that in an earlier study of this system by Cox and Cretcher there were probably significant impurities in the ether. A theorem derived by Rice for a one-component fluid is extended to binary systems, and it allows one to conclude from the symmetry of the Cox-Herington plot that at the critical solution temperature the chemical potential of either component, as a function of composition, has a discontinuous fourth derivative at the critical composition, the discontinuity being a simple reversal of sign.

INTRODUCTION

IT was found by Cox and Herington[1] that the coexistence curve in the temperature-composition plane for two-phase equilibrium in binary liquid systems could be represented by

$$|T-T_c|^{\frac{1}{3}}=\alpha\log\{[x/(1-x)][(1-x_c)/x_c]\},\quad x>x_c$$
$$|T-T_c|^{\frac{1}{3}}=-\beta\log\{[x/(1-x)][(1-x_c)/x_c]\},\quad x<x_c. \tag{1}$$

In these equations T is the temperature and x is the mole fraction of one of the two components, T_c and x_c being the values of T and x at the critical point. The quantities α and β are positive constants characteristic of the system. Equations of this form hold equally well in the neighborhood of both upper and lower critical solution points.

As the critical point is approached Eq. (1) takes on the limiting form

$$|T-T_c|^{\frac{1}{3}}=[\alpha/x_c(1-x_c)](x-x_c),\quad x>x_c$$
$$|T-T_c|^{\frac{1}{3}}=[\beta/x_c(1-x_c)](x_c-x),\quad x<x_c, \tag{2}$$

which is the familiar statement[2] that the coexistence curve is cubic. Equation (1) should be looked upon[3] as an empirical extension of Eq. (2), reducing to the latter as the critical point is approached but remaining numerically accurate much further from the critical point than is the case with the limiting equations. It may be noted in passing that there is nothing fundamental about the choice of mole fraction as composition variable, and that Eqs. (1) and (2) continue to hold with the same values of α and β when x is a mass fraction.

In most of the cases to which Eq. (1) was applied by Cox and Herington, they found that $\alpha\approx\beta$. It will now be seen that it is a matter of some interest to decide whether or not α and β are exactly equal.

For a pure fluid, Rice[4] showed that the critical isotherm in the pressure-density plane and the coexistence curve in the temperature-density plane are closely related. We derive in the Appendix the analogous relation for binary systems: Let μ be the chemical potential of the component of mole (or mass) fraction x, let the coexistence curve in the $T-x$ plane be given by

$$T-T_c=g(x-x_c), \tag{3}$$

where g is a function such that $g(0)=0$, and let the critical isotherm in the $\mu-x$ plane be given by

$$\mu-\mu_c=f(x-x_c), \tag{4}$$

where f is a function such that $f(0)=0$. Then as $x\to x_c$,

$$f(x-x_c)\sim-(\partial^2\mu/\partial T\partial x)_c(x-x_c)g(x-x_c), \tag{5}$$

where $(\partial^2\mu/\partial T\partial x)_c$ is the limiting value of $\partial^2\mu(T, x)/\partial T\partial x$ when the critical point is approached through the one-phase region. The asymptotic relation (5) applies at both upper and lower critical mixing points. It is just Rice's theorem, with the pressure replaced by μ and the density by x.

According to Eq. (2), the coexistence curve is cubic, with a discontinuity in its third derivative at the critical composition. It then follows from Eq. (5) that the critical isotherm is quartic, with a discontinuity in its fourth derivative at the critical composition.[3] These discontinuities are simply changes of sign if $\alpha=\beta$, but changes of both sign and magnitude if $\alpha\neq\beta$. If it could be established experimentally that $\alpha=\beta$ then this

* National Science Foundation Science Faculty Fellow at Cornell University, 1959–1960.

[1] J. D. Cox and E. F. G. Herington, Trans. Faraday Soc. **52**, 926 (1956).

[2] B. H. Zimm, J. Chem. Phys. **20**, 538 (1952).

[3] O. K. Rice, J. Phys. Chem. **64**, 976 (1960).

[4] O. K. Rice, J. Chem. Phys. **23**, 169 (1955).

would go a long way toward characterizing the singularity at the critical point and it would provide a simple goal for a statistical mechanical theory.

It is easy to conjecture that $\alpha=\beta$ from the tabulation of Cox and Herington,[1] but then it becomes important to establish in some, at least, of the cases where α and β appear unequal, that the discrepancy is due to experimental error. One of the larger discrepancies occurs at the lower critical solution point of the system water-ethylene glycol mono-isobutyl ether, for which Cox and Herington report

$$2.303\alpha=3.8$$

$$2.303\beta=4.4,$$

when, in Eq. (1), x is the fraction of the ether, and temperatures are in °C. These numbers were calculated from the original data of Cox and Cretcher.[5] We have redetermined the relevant portion of the coexistence curve for this system, using a carefully purified sample of the ether, and we find

$$2.303\alpha=4.25\pm0.05$$

$$2.303\beta=4.18\pm0.05,$$

so that the conclusion $\alpha=\beta$ appears justified.

THE SYSTEM WATER-ETHYLENE GLYCOL MONO-ISOBUTYL ETHER NEAR ITS LOWER CRITICAL SOLUTION POINT

Materials

The water used was conductance water. Mono-isobutyl ether of ethylene glycol[6] was prepared from ethylene chlorohydrin by method B of Cretcher and Pittenger.[7] The ether was fractionated on a spinning band fractionating column rated at 20 theoretical plates. Purity was checked with a vapor chromatograph and impurities estimated by peak areas. On this basis the five samples used ranged in purity from 99.87–99.95 mole %. Impurities probably identified were water, isobutyl alcohol, and ethylene glycol. One major high-boiling impurity present in some samples at 0.05–0.08 mole % was not identified but was probably the ether hydroperoxide. Another impurity in barely detectable amount was not identified. Samples of ether were kept in evacuated vessels.

Method of Measurement

Water and ether were weighed into sample tubes which were then evacuated and closed off by stopcock. The silicone grease used had no effect on temperatures of phase separation as shown in three separate experiments.

The tubes were placed in a stirred water bath and were rocked. Temperature was raised by a heater and the rise could be controlled to within 0.005°C/min when desired. Temperature was usually lowered by small additions of cold water to the bath. Phase mixing and phase separation were observed visually. The thermometer was graduated in 0.01°C, and calibrated at 0°C and at 32.37°C.

Temperatures of mixing and of phase separation were separately reproducible to 0.01°C when within 8° of T_c, and were within 0.01° of each other when close to T_c but were as much as 0.3° apart when far from T_c. Values of temperature reported are averages of two mixing and two phase separation temperatures. It was very difficult to observe the temperature of phase separation above 37°C because the amount of one phase and its change with temperature were very small. This was a major source of error at temperatures far from the critical.

It was noted that during the measurements material from the bottom of the sample tubes was distilling onto the side walls. The distilled material was of different composition than the residue since the phase separation temperature could be changed from 0.01° to 0.5°C by vigorous shaking. All samples were therefore shaken by hand during actual measurement.

Results

Table I lists the results obtained in this experiment. The uncertainties in column 4 were estimated as the composite effects of (i) impurities, (ii) difference between temperatures of mixing and of phase separation, (iii) uncertainty in locating the point of mixing or of phase separation, (iv) distillation of material onto the walls of the sample tube. No measurements were made below $T_c+0.42$°C since the uncertainty in $T-T_c$ would then have been of the order of magnitude of $T-T_c$ itself.

Our estimate of the uncertainty due to impurities, 0.1°, was based on a systematic study of the effects of various impurities. It was noted that isobutanol, used as a solvent in preparation of the ether, gives on a mole percent basis a larger change of phase separation temperature than do any of the other impurities likely to be present in the ether. Roughly 1% of isobutanol in the ether causes a lowering of 0.5°C in solutions which are 25 and 50 weight % ether, and of 0.75°C at 12.5 weight % ether. It was also observed that the phase separation temperature of a sample 28% by weight of ether was lowered 0.15°C after the solution was allowed to stand 8 days in a closed, but not evacuated, container. A sample of ether showing negligible impurity (~0.01 mole %), showed, by vapor chromatography, 0.13% after 2 hrs of exposure to air. However, material maintained in vacuum showed negligible change in

[5] J. D. Cox and L. H. Cretcher, J. Am. Chem. Soc. **48**, 451 (1926).

[6] Some of our earlier exploratory work was done with an ether sample supplied by the Olin Mathieson Chemical Corporation, whose courtesy we wish to acknowledge.

[7] L. H. Cretcher and W. H. Pittenger, J. Am. Chem. Soc. **46**, 1503 (1924).

TABLE I. Column 1 identifies the ether sample, column 2 is the weight percent ether in the solution, column 3 is the temperature (in °C) which, with the composition of column 2, locates a point on the coexistence curve, and column 4 is the estimated uncertainty in this temperature (in °C).

1	2	3	4	1	2	3	4
5	11.20	38.10	0.90	5	40.60	26.28	0.10
4	12.50	34.13	0.60	3	42.10	26.44	0.10
4	13.50	32.20	0.20	2	44.00	26.91	0.10
1	14.40	30.98	0.20	4	45.80	27.33	0.11
4	15.45	29.41	0.20	2	48.30	28.33	0.13
2	17.00	28.21	0.13	3	51.20	29.74	0.15
4	18.60	27.31	0.11	3	53.10	30.80	0.25
2	20.10	26.89	0.10	3	55.50	33.21	0.35
5	21.20	26.44	0.10	3	58.00	35.15	0.40
5	22.50	26.21	0.10	3	60.90	37.45	0.50

purity in 24 hrs, and there was no difference between observations made in vacuum and those made immediately after admitting air.

A Cox-Herington plot of the data in Table I is given in Fig. 1, and the results derived from it are in the last line of Table II. The uncertainties listed in column 4 of Table I were alternately added to and subtracted from the temperatures in column 3, and the points so calculated are the extremes of the vertical line segments in the figure. In the corresponding plot given by Cox and Herington for the lower critical solution point of the system water-2,6 lutidine the points appear to lie much closer to the lines than in the present case; but this is only because the points they plotted came from a smoothed coexistence curve whereas we have plotted our original data.

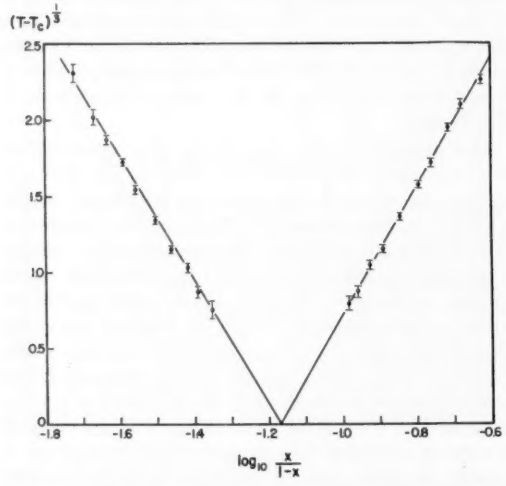

Fig. 1. Cox-Herington plot of the coexistence curve of the system water-ethylene glycol mono-isobutyl ether, near the lower critical solution point. Temperatures are in °C and x is the mole fraction of the ether.

The critical temperature was found by trial and error as that temperature T_c which made the straight lines in the plot cross at $(T-T_c)^{\frac{1}{3}}=0$. This method is very sensitive and a change in the assumed T_c of 0.05°C was distinguished with ease, in spite of the experimental scatter. The critical composition was determined from the crossing point. The "best" straight lines were fitted to the data by eye, and the uncertainties ±0.05 quoted for 2.303 α and 2.303 β represent the extremes through which the lines can be rotated and still fit the data at all reasonably.

Comparing the three sets of results in Table II it becomes clear that there were significant impurities in the ether used by Cox and Cretcher. Indeed, Chakhovskoy[8] and Onken[9] have previously inferred the presence of impurities in the ethylene glycol mono-

TABLE II. Derived results and comparisons. T_c is the lowest temperature (in °C) at which phase separation occurs, and is the lower critical solution temperature when the components are pure. x_c is the weight percent ether in the solution that shows phase separation at T_c. α and β refer to Eq. (1) in which x is the fraction of ether and temperatures are in °C.

Ether purity	T_c	x_c	2.303β	2.303α
Very impure[a]	24.2	25.2	5.3	3.2
Cox and Cretcher[b]	24.6	26.8	4.4	3.8
99.87–99.95 mole %	25.8±0.1	30.4	4.18±0.05	4.25±0.05

[a] These are our data with an ether sample that was two years old and was part of a lot produced for industrial use. It was shown to be very impure by vapor chromatography.

[b] Footnote 5. The purity is unknown.

n-butyl ether used by Cox and Cretcher for a parallel solubility study, and which they had prepared in the same way as its isobutyl analog.

APPENDIX. RICE'S THEOREM FOR BINARY SYSTEMS

Let the coexistence curve in the $T-x$ plane and the critical isotherm in the $\mu-x$ plane be given by Eqs. (3) and (4), respectively. Then it is to be shown that they are connected by the asymptotic relation (5).

In the one-phase region the chemical potential is $\mu(T, x)$, and if it is assumed that at the critical point $\partial\mu(T, x)/\partial T$ and $\partial^2\mu(T, x)/\partial T\partial x$ exist and neither is zero, then in the neighborhood of the critical point

$$\mu(T, x)\sim\mu_c+(\partial\mu/\partial T)_c(T-T_c)+(\partial^2\mu/\partial T\partial x)_c(T-T_c)(x-x_c)+f(x-x_c), \quad (6)$$

this being consistent with the critical isotherm given by Eq. (4). In the two-phase region the chemical potential is a function only of T, say $\nu(T)$, and if it is

[8] N. Chakhovskoy, Bull. soc. chim. Belges **65**, 474 (1956).

[9] U. Onken, Z. Elektrochem. **63**, 321 (1959).

assumed that at the critical point $d\nu(T)/dT$ exists and is not zero, then in the neighborhood of the critical point

$$\nu(T)\sim\mu_c+(d\nu/dT)_c(T-T_c). \quad (7)$$

The last assumption which is necessary is that

$$(\partial\mu/\partial T)_c=(d\nu/dT)_c. \quad (8)$$

This is the analog of what in one-component fluid systems is a well-established fact: The slope of the critical isochore in the pressure-temperature plane is continuous at the critical point. (The portion of the critical isochore which is below the critical point is, of course, just the vapor pressure curve.) So far as we know, Eq. (8) has never been experimentally established for binary systems, but its correctness is hardly in doubt.

In complete generality, independently of any of the above assumptions, the equation of the coexistence curve in the $T-x$ plane is

$$\mu(T,x)=\nu(T) \quad (9)$$

which can be made explicit by solving for x as a function of T or for T as a function of x. From Eqs. (6)–(9) it follows that near the critical point the coexistence curve is given by

$$T-T_c\sim-f(x-x_c)/(\partial^2\mu/\partial T\partial x)_c(x-x_c). \quad (10)$$

The asymptotic relation (5), which was to be derived, then follows from Eqs. (3) and (10).

THE JOURNAL OF CHEMICAL PHYSICS VOLUME 33, NUMBER 6 DECEMBER, 1960

Scattering of Metastable Helium Atoms in Helium, Neon, and Argon*

G. M. SMITH† AND E. E. MUSCHLITZ, JR.

Department of Chemistry, University of Florida, Gainesville, Florida

(Received January 29, 1960)

Total collision cross sections for the scattering of metastable 2^3S and 2^1S He atoms in helium, neon, and argon have been measured using a thermal-energy atomic beam in which a fraction of the helium atoms are excited by electron bombardment. The excited particles are detected by measuring the secondary electron emission from metal surfaces. The cross sections for the scattering of the triplet atoms are larger than for the singlet in each case. For neon the difference is considerably greater than the estimated experimental error, indicating a large difference in the interaction potentials.

INTRODUCTION

OUR present knowledge of intermolecular forces has been obtained largely by analyzing experimental determinations of macroscopic properties such as viscosity and diffusion, which depend on these forces. This requires a well-founded theory connecting the intermolecular forces with the observed bulk properties as well as good experimental data. Molecular-beam experiments provide a much more direct method of studying these forces. A beam of unidirectional particles can be formed by suitable collimation. The scattering of such a beam can then be observed either by measuring the intensity of the beam as it passes through a gas at a low pressure or by observing the intensity as a function of the scattering angle using a suitable detecting device. The properties of the individual particles can be observed in this manner, thus eliminating the necessity of relating intermolecular forces to bulk properties.

A collision between particles is classified as elastic or inelastic, depending upon whether or not they survive the collision without a change in internal energy. Inelastic collisions may involve a rearrangement or exchange of the atoms that compose the reactant particles or simply an exchange of energy involving the internal energy of one or both of them. For each type of two-body collision process, a collision cross section may be defined which is a measure of the probability of the process concerned. The magnitude of these cross sections is governed by the nature of the forces exerted between the colliding particles and their relative velocities. The total cross section is the sum of all of these subsidiary cross sections. Experiments of this type have provided considerable fundamental information concerning the nature of particle collisions and of the forces exerted between individual particles.[1] The techniques involved provide the only direct means for obtaining this knowledge, which is essential for a complete understanding of chemical reactions.[2]

* This research was supported by a grant from the National Science Foundation.

† Present address: Los Alamos Scientific Laboratory, Los Alamos, New Mexico.

[1] H. S. W. Massey and E. H. S. Burhop, *Electronic and Ionic Impact Phenomena* (Oxford University Press, New York, 1952).

[2] S. Datz and E. H. Taylor, *Recent Researches in Molecular Beams* E. Estermann, Editor (Academic Press, Inc., New York, 1959).

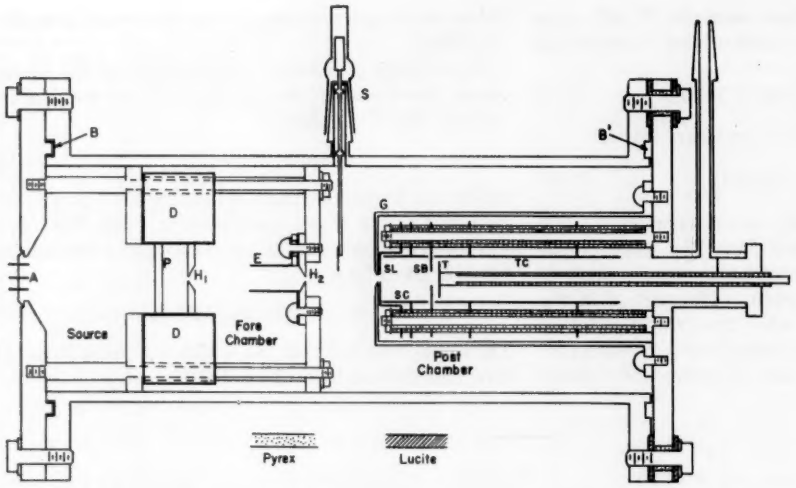

FIG. 1. Cross section of apparatus.

We are concerned here with the measurement of total absorption cross sections for collisions of excited He atoms in helium, neon, and argon. Some of the atoms in gaseous helium are excited to both the 2^1S and 2^3S metastable states by electron bombardment. The 2^2S state of helium is 19.82 ev above the ground state, and the 2^1S state is 20.61 ev above the ground state. An atomic beam of the He atoms is produced and allowed to enter a collision chamber in which a gas is introduced at a low pressure. The scattering of the metastable He atoms is then observed by measuring the electron current ejected by the excited atoms when they arrive at metal detector surfaces. In general, both elastic and inelastic collisions of the excited atoms occur.

EXPERIMENTAL

A. Apparatus

The four separate chambers of the apparatus are shown in Fig. 1. The atomic beam was produced by introducing helium gas through a capillary leak into the source, where it effused through the first defining hole, H_1, into the fore chamber. Some of the atoms were excited before leaving the source region by an electron beam which passed directly behind H_1. The fraction of the atoms traveling in the proper direction then passed through the second defining hole H_2 and formed a pencil-shaped beam 0.5 mm in diam. The beam entered the scattering region, where the collision experiments were performed, through a hole in the cylindrical can G which separates the scattering region from the post chamber.

Since it was necessary to introduce gas into both the source and the scattering region while scattering measurements were being made, quite rapid pumping speeds were required to maintain sufficiently low pressures in the fore and post chambers. This was accomplished by using a differential pumping system of two high-speed mercury diffusion pumps attached to these chambers through large Dewar-type liquid-air traps. These pumps were backed by a two-state mercury-diffusion pump of standard design and a mechanical pump. An auxiliary vacuum system was used for gas manipulation and pressure measurements.

Excitation of the helium was accomplished by electron bombardment. Figure 2 shows plate P of Fig. 1 with all the elements of the electron gun attached. Electrons were produced by thermionic emission from a directly heated filament F. The filament was an iridium ribbon thoriated by cataphoretic deposition as described by Muschlitz.[3] It was mounted on the nickel jaws G, which were insulated from the plate P by spacers constructed of lava. Electrons were accelerated by the anode S-1, passed through S-2 into the equipotential region N, and were collected by a catcher C. The electrode R was maintained at a negative potential to help direct electrons emitted from the filament through S_1. A copper-constantan thermocouple was used to measure the temperature in the source directly behind the electron catcher. The temperature determined in this way was probably low, but this position of the couple was chosen because it was shielded from direct radiation from the filament, which would have given temperatures much larger than the correct value. The electron beam was confined by a magnetic field of approximately 200 gauss, which was produced by two Alnico magnets D (Fig. 1). A potential was applied across plates E in the fore chamber, to deflect from the beam any charged particles that were produced in the source. The entire source and the plates supporting the beam-defining holes could be removed from the vacuum chamber if necessary, without disturbing the alignment of the defining holes. Good

[3] E. E. Muschlitz, Jr., J. N. Ratti, and H. O. Randolph (to be published).

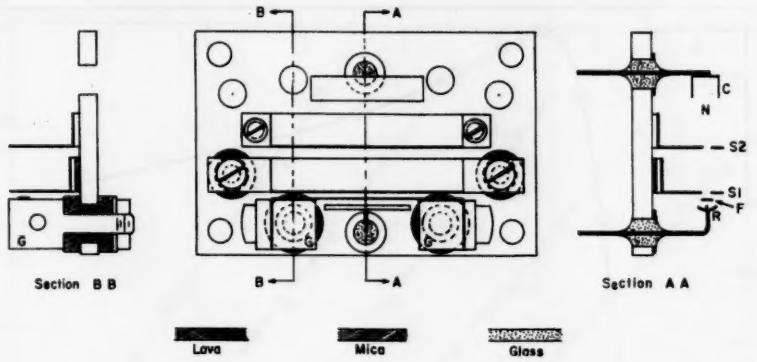

FIG. 2. Electron gun.

pressure differentials were obtained between different chambers by machining the 0.25-in. thick disks that separate the chambers to extremely close tolerances with respect to the chamber wall. A magnetically operated shutter S was placed directly behind the second defining hole so that the beam could be interrupted to obtain a zero reading.

The scattering elements were mounted on four rods at 90°. They were insulated from the mounting rods by Pyrex sleeves and from one another by Pyrex spacers. Cylindrical symmetry was used throughout the scattering region. The scattering elements were heavily gold plated, to obtain surfaces which had the same electron-ejection efficiency.

Electrical connections through the chamber walls were made with Kovar-glass headers, except for the target, which was enclosed in a Pyrex sleeve and sealed with Apiezon W sealing wax. Current measurements were made with a Cary Instruments vibrating-reed electrometer. Maximum sensitivity was 1×10^{-14} amp for full-scale deflection of the output meter, using an input resistance of 10^{11} ohms. A Weston model 931 0−0.1 ma full scale ammeter was used to measure the output of the electrometer.

Complete shielding of the leads from the scattering region was necessary. All the leads were enclosed in a copper envelope, which was connected directly to the electrometer head. A specially constructed switch, similar in design to one described by Simons and coworkers,[4] was used in order to make the measurement of currents to each of the scattering elements possible with one electrometer. It was constructed so that contact was made between amalgamated copper strips and mercury pools.

B. Measurements

Helium was introduced into the system through a trap which contained degassed charcoal at liquid-air temperature. It was estimated that the impurities in this gas amounted to less than one part in 10^3. Furthermore, this gas was used only in the source where the impurities were likely to be ionized and deflected from the beam. The gas samples used in the scattering region were taken from flasks of reagent-grade gas supplied by the Air Reduction Sales Company. Reported impurities were less than one part in 10^4. Pressures in the scattering region were measured with a McLeod gauge with an estimated accuracy of 1%. The vacuum obtainable in a reasonable amount of time was 5×10^{-6} mm. After introduction of gas into the source and scattering region, the pressure in the fore chamber and post chamber was about 10^{-5} mm. The helium pressure in the source region was 0.1 mm Hg or less. Scattering gas pressures ranged from 1 to 30×10^{-4} mm Hg.

The beam entered the scattering region through a 0.75-mm hole in can G and passed through a slightly larger hole in the scattering cylinder lid SL. The metastable atoms could then be detected at the scattering cylinder SC and the scattering cylinder bottom SB or the target T, depending on whether the scattered or unscattered fraction of the beam was to be measured.

In the preliminary experiments on beam behavior all measurements of the electron current ejected by metastable atoms (hereafter referred to as metastable current) were made at the target with a potential of +19.2 v on the other scattering elements and with the scattering region evacuated. The metastable current was found to be directly proportional to the electron current in the electron beam. As was expected, the metastable current varied linearly with the pressure in the source at low pressures and fell off at high pressures. This deviation from linearity is caused by an increase in pressure in the fore chamber and subsequent scattering of the beam in that region. At the higher pressures, the flow from the first defining hole becomes hydrodynamic, so that a true molecular beam is not produced.

Figure 3 is the experimental appearance potential curve observed for metastable He atoms. It is the sum of the appearance potential curves for the 2^1S and 2^3S states of helium. This curve compares favorably with the total metastable appearance potential curve

[4] J. H. Simons, H. T. Francis, C. M. Fontana, and R. S. Jackson, Rev. Sci. Instr. **13**, 419 (1942).

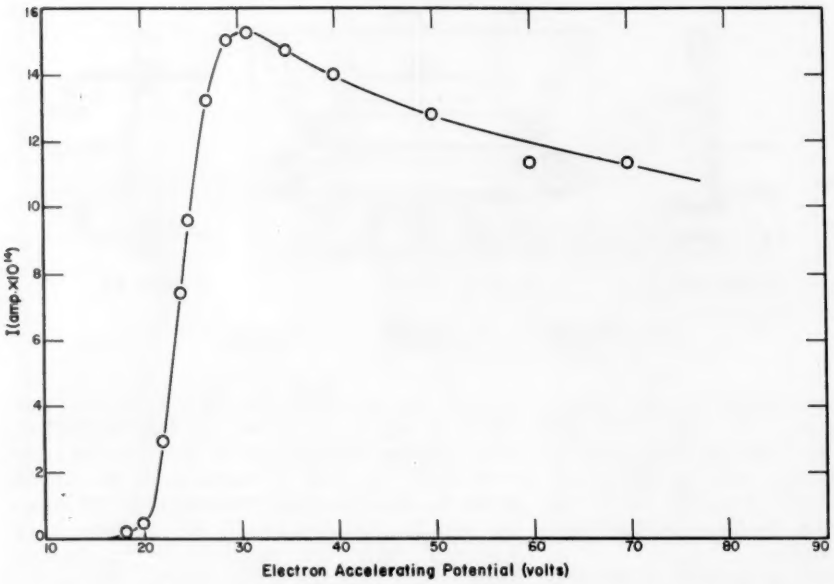

FIG. 3. Appearance potential curve for metastable helium atoms.

given by Frost and Phelps,[5] if allowance is made for the energy distribution of our electron beam. A retarding potential curve showed the total energy spread to be ± 3 ev.

The scattering experiments were performed by introducing a gas into the scattering region at a known pressure and measuring the beam intensity. To obtain the total beam intensity entering the scattering region, it was necessary to measure three currents. The metastable current to the target i_T was measured with a potential of $+13$ v on SB and SC. The current i_{SL} to SL was measured with the same potential on SB and SC. SB and SC were then made 13 v negative with respect to ground, and the sum of the currents i_S to T and SL measured. The scattering-path length was taken as the distance between the left surface of SL and the left surface of SB (2.17 cm). Then i_T is a measure of the unscattered fraction of the beam, and the sum of i_S and i_{SL} is a measure of the scattered fraction of the beam. The elements to which current measurements were made were held at ground potential. TC was held at -13 v, to prevent the migration of electrons to it. The metastable current corresponding to the total beam intensity entering the scattering region i_0 was taken as the sum of the three measured currents.

Between experiments the apparatus was filled to one atmosphere with dry helium. No appreciable variation with time was observed in the ejected-electron currents under identical source conditions. Apparently, the electron-ejection efficiency of the gas-covered gold surfaces remained reasonably constant.

Photons originating in the source region may contribute to the measured current i_T by photoelectric emission; however, i_T was reduced to essentially zero for a scattering gas pressure at which the majority of any photons present should still have been detected, since the cross sections for their absorption by the gas are relatively small.[6] In order to confirm this observation, a thin collodion-film window similar to that described by Stebbings[7] was constructed and mounted on the magnetically operated shutter (S of Fig. 1). Such a window should not absorb an appreciable fraction of any photons in the beam. The window was found, however, to be just as effective in stopping the beam as the metal shutter itself.

C. Treatment of Experimental Data

The atomic beam consists of He atoms in the 2^1S and 2^3S metastable states plus atoms in the 1^1S ground state. Atoms excited to other states decay by electric dipole radiation to one of these states in times of the order of 10^{-8} sec, so that the proportion of these species in the beam, by the time it arrives at the collision chamber, is negligibly small. The method of detection is insensitive to atoms in the ground state, and we may assume that the scattering of the metastable particles is independent of the presence of ground-state atoms in the beam. Thus if I_{01} and I_{03} are the intensities of the singlet and triplet metastable atoms at the entrance to the collision region, and I_1 and I_3 are the intensities in the beam at the distance along the beam path $l=2.17$ cm, then

$$I_1 = I_{01} \exp(-\sigma_1 N l p) \qquad (1)$$

[5] L. S. Frost and A. V. Phelps, Westinghouse Research Report 6-94439-6-R3 (1957).

[6] J. B. Hasted and P. Mahadevan, Proc. Roy. Soc. (London) **A249,** 42 (1958).

[7] R. E. Stebbings, Proc. Roy. Soc. (London) **A241,** 270 (1957).

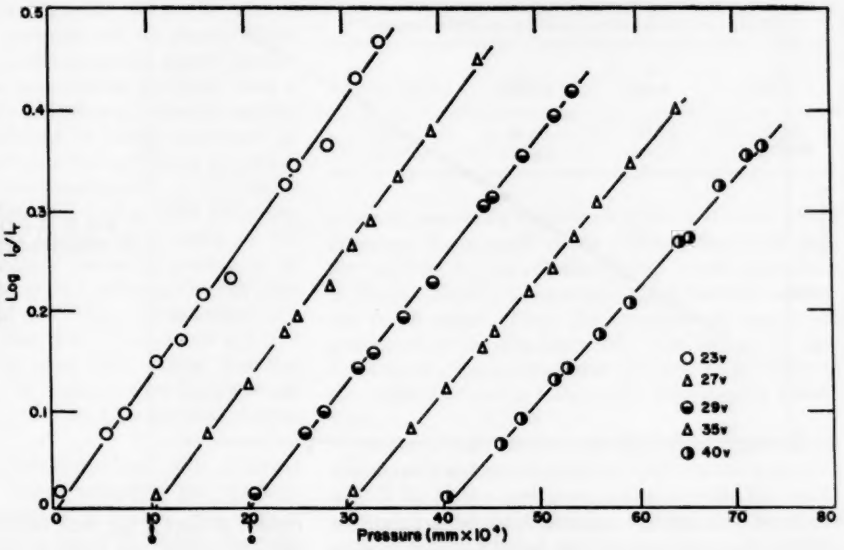

FIG. 4. Log i_0/i_T vs p for the scattering of metastable helium atoms in neon for various exciting electron energies. (*Note*: The abscissas for the curves at the higher energies have been displaced to the right.)

and

$$I_3 = I_{03} \exp(-\sigma_3 Nlp), \tag{2}$$

where σ_1 and σ_3 are the total absorption cross sections for the singlet and triplet metastable atoms in cm², p is the pressure in mm Hg at 0°C, and N is the number of scattering gas particles per cc at 1 mm Hg and 0°C. We designate the total cross sections defined in this way as absorption cross sections in order to emphasize the difference between them and the mean collision cross section $\bar{Q}$. (See footnote reference 1, pp. 389–390.) If the average velocity of the scattering gas atoms could be neglected compared to that of the beam atoms, the two cross sections would be the same.

The two metastable species eject electrons from metal surfaces with different efficiencies, so that the currents i_0 and i_T defined previously must be expressed as

$$i_0 = \gamma_1 I_{01} + \gamma_3 I_{03} \tag{3}$$

and

$$i_T = \gamma_1 I_1 + \gamma_3 I_3, \tag{4}$$

where γ_1 and γ_3 are the electron-ejection efficiencies. Substituting Eqs. (1) and (2) into (4) and defining $R = \gamma_3 I_{03}/\gamma_1 I_{01}$, we obtain

$$i_0/i_T = (1+R)/[\exp(-\sigma_1 Nlp) + R\exp(-\sigma_3 Nlp)]. \tag{5}$$

This equation does not allow the ready evaluation of σ_1 or σ_3 unless $\sigma_1 = \sigma_3 = \sigma$, in which case

$$\sigma = \ln(i_0/i_T)/Nlp. \tag{6}$$

At sufficiently low pressures, Eq. (5) may be simplified by expanding the exponentials and neglecting terms in the second and higher powers of p,

$$(i_0/i_T) = (1+R)/[(1-\sigma_1 Nlp) + R(1-\sigma_3 Nlp)].$$

On taking the logarithm of both sides and rearranging,

$$\ln(i_0/i_T) = -\ln\{1-[(\sigma_1+R\sigma_3)/(1+R)]Nlp\} \cong [(\sigma_1+R\sigma_3)/(1+R)]Nlp. \tag{7}$$

A plot of $\ln i_0/i_T$ vs p at low pressures should yield a straight line with a slope m, given by

$$m = [(\sigma_1+\sigma_3 R)/(1+R)]Nl. \tag{8}$$

By determining m as a function of the electron energy, and hence the composition of the beam, values of m as a function of R may be obtained. On rearranging Eq. (8),

$$(1+R)m/l = N\sigma_1 + RN\sigma_3. \tag{9}$$

A plot of $(1+R)m/l$ vs R yields a straight line with a slope $N\sigma_3$ and an intercept on the ordinate of $N\sigma_1$.

D. Experimental Results

Figure 4 is a plot of $\log i_0/i_T$ for scattering of metastable helium in neon vs pressure for various energies of the electron beam. The change in slope with increasing electron energy indicates a difference in cross section for the two metastable species. Figure 5 is a plot of $(1+R)m/l$ vs R for a range of values of R that is probable at the electron energy corresponding to each value of m. A straight line was drawn so as to interpret each of these subsidiary lines. $A \pm 20\%$ range of values of R was taken centered on the value of 0.5 for γ_3/γ_1 reported by Dorrestein[8] for a platinum surface and appropriate values of I_{03}/I_{01} taken from the excitation functions of metastable helium given by Frost and Phelps.[5] The straight line from which the cross sections were calculated is restricted to narrow limits such that

[8] R. Dorrestein, Physics **9**, 433, 447 (1942).

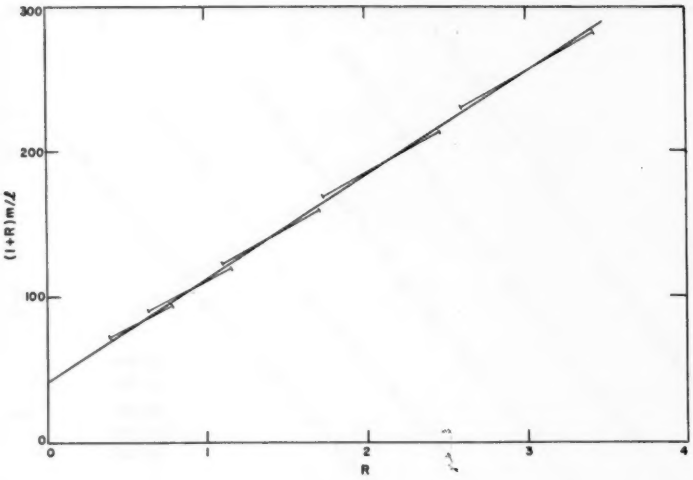

FIG. 5. $(1+R)m/l$ vs R for the scattering of metastable helium atoms in neon.

the cross sections are estimated to be accurate to $\pm 10\%$. The total cross section for 2^1S helium in neon is 29×10^{-16} sq cm, and that for 2^3S helium in neon is 50×10^{-16} sq cm. The total cross sections for metastable helium in helium were evaluated in the same manner and found to be 49×10^{-16} sq cm for 2^3S helium and 37×10^{16} sq cm for 2^1S helium. The uncertainty in the results is due primarily to the uncertainty in the ratio of γ_3 to γ_1. Unfortunately, this ratio has not been measured for a gold surface. Stebbings[7] has determined γ_3 for a gas-covered gold surface as 0.29, and Hasted and Mahadevan[6] give $\gamma_3=0.26$ for a gas-covered platinum surface, which compares favorably with Dorrestein's value of 0.24. It is not unreasonable to assume, then, that γ_3/γ_1 is the same on both surfaces, since γ_3 is nearly the same on both; however, if σ_1 and σ_3 are nearly the same, the calculated values are essentially independent of R. Furthermore, at the higher electron energies, I_{03}/I_{01} decreases as the electron energy increases[5]; so that if m decreases with increasing electron energy, as our results indicate, $\sigma_3>\sigma_1$, a conclusion which is independent of the value of R.

The ionization potential of argon is 15.75 ev, and therefore ionization of argon by metastable helium is possible. Since the sum of the three metastable currents can no longer be taken as the total beam intensity, because the ions and electrons resulting from ionization were collected with 100% efficiency while metastable atoms eject electrons with much smaller efficiencies, it was necessary to correct the ionization current to get it on the same basis as the metastable current. This correction was based on the fraction of each metastable species in the beam and its ejection efficiency.

In the cases of helium and neon, where no ionization occurred, i_{ST} was small and did not vary with the scattering gas. In argon, a large majority of the ionizing collisions would occur in the front part of the scattering region, so that if i_{SL} were measured with SB and SC positive, all of the positive ions would be collected at SL and included in this current. With SB and SC negative, i_{SL} was negative and was the sum of electron currents resulting from ionization and ejection of electrons from SB and SC by elastically scattered metastable atoms. The total beam intensity was calculated from the three metastable currents and the corrected ionization current i_I. It was then possible to calculate the total scattering cross sections for metastable helium in argon in the same manner as before and, they were found to be 58×10^{16} sq cm for 2^3S helium and 51×10^{-16} sq cm for 2^1S helium.

DISCUSSION

Since the excitation energy of the metastable states of helium is large, various inelastic collisions between a metastable He atom and another atom are possible:

$$\mathrm{He}^*+X\rightarrow \mathrm{He}+X^* \qquad (10)$$

$$\mathrm{He}^*+X\rightarrow \mathrm{He}+X+h\nu \qquad (11)$$

$$\mathrm{He}^*+X\rightarrow \mathrm{He}+X^++e^- \qquad (12)$$

$$\mathrm{He}(2^1S)+X\rightarrow \mathrm{He}(2^3S)+X. \qquad (13)$$

The conditions of the experiment eliminate three-body collisions from consideration.

The first of these equations is an exchange of excitation energy, and the second is a collision-induced radiative transition where $h\nu$ represents a photon. Equation (12) is a particular case of (10) in which the excitation energy of the metastable atom is large enough to ionize the struck atom. Equation (13) is a collision in which a 2^1S He atom is converted into a 2^3S He atom. The reverse reaction is not possible for collisions at thermal energies.

The cross section for the collision-induced radiative transition [Eq. (11)] should be small, since the proba-

bility of such collisions depends upon the kinetic energy of the colliding particles and the energy difference between the metastable state and nearby radiating states, so that the perturbation resulting from a collision of a metastable He atom at thermal energies is not likely to be sufficient to induce radiation. In fact, Phelps and Molnar[9] and Phelps,[10] using an optical absorption method for the determination of metastable atom concentrations with time in a gaseous discharge, found the cross section for the destruction of 2^1S helium in a collision with a normal He atom to be 3×10^{-20} sq cm and that of 2^3S helium to be less than 10^{-22} sq cm. They found no evidence for reaction (13). Therefore, we assume that these processes do not contribute materially to the total cross section. Reaction (10) does contribute to the cross sections in helium and in neon. Reaction (12) contributes to the cross sections in argon.

The experimental results obtained with a source temperature of 66°C and a scattering gas temperature of 27°C are summarized in Table I. The angular resolution of the apparatus was 6.3°. This is the angle subtended by the radius of the hole in SB, a, at the entrance to the scattering region, i.e., $\tan^{-1}(a/l)=6.3°$. As the angular definition is increased, the cross sections should increase to some finite limit at zero angle. Preliminary experiments at higher angular resolution showed a rapid increase in the cross section for the scattering of metastable He atoms in helium as the resolution was increased.

It is evident that the cross section is larger for 2^3S helium than for 2^1S helium in each of the scattering gases. The only cases for which any calculation of these cross sections is available are those of 2^1S helium and 2^3S helium in helium. Buckingham and Dalgarno[11] have found that the interaction is repulsive for both species at large distances leading to essentially the same mean collision cross sections at thermal energies, $\bar{Q}=160\times10^{-16}$ sq cm at 27°C. At somewhat smaller interaction distances, the 2^3S interaction is slightly more repulsive than the 2^1S. The results reported here, obtained with relatively low angular resolution, correspond to scattering at larger angles (and hence closer distances of approach of the colliding particles) than the majority of the collisions which would contribute to the calculated cross section, which includes scattering at all angles. Thus, the experimental results are considered to be consistent with the theoretical predidction of a large interaction between an He atom in the *triplet* metastable state and a ground-state helium atom.

TABLE I. Total absorption cross sections for thermal-energy metastable helium atoms in various gases (sq cm$\times10^{16}$).

Beam Atom	σ Helium	σ Neon	σ Argon
2^3S He	49±5	50±5	58±9
2^1S He	37±4	29±3	51±7

Stebbings[7] and Hasted and Mahadevan[8] have determined total absorption cross sections for the scattering of 2^3S He in the rare gases, using a molecular beam-scattering apparatus with a resolution of 0.5°. These authors used a gaseous discharge as a source of metastable atoms. Their results are applicable to the triplet metastable state only insofar as the collision cross section for deexcitation of 2^1S He by collision with thermal-energy electrons in the discharge is very large.[10] They obtained 149×10^{-16} sq cm and 144×10^{-16} sq cm, respectively, for the scattering of 2^3S He in He. A comparison of these results with the result reported here (49×10^{-16} sq cm) is indicative of the large number of collisions taking place at small angles.

The cross sections we obtained for the two metastable states of helium in neon are different, even considering the extreme limits of experimental error. The larger total cross section for 2^3S He might be due to an exchange of excitation energy as shown in Eq. (10); however, Phelps[12] in his survey of gaseous discharge studies reported a value of 2×10^{-17} sq cm for the cross section for destruction of 2^3S He atoms in two-body collisions with neon atoms. This is small compared to the total cross section, so the difference in the total cross sections can only be caused by a difference in the interaction potentials and should encourage further theoretical calculations.

[9] A. V. Phelps and J. P. Molnar, Phys. Rev. **89**, 1202 (1953).
[10] A. V. Phelps, Phys. Rev. **99**, 1307 (1955).
[11] R. A. Buckingham and A. Dalgarno, Proc. Roy. Soc. (London) **A213**, 327 and 506 (1952).
[12] A. V. Phelps, Westinghouse Scientific Paper 6-94439-6-P3 (1957).

THE JOURNAL OF CHEMICAL PHYSICS VOLUME 33, NUMBER 6 DECEMBER, 1960

Electron Spin Resonance Line Shape of a Polycrystalline CH Radical

ROLAND LEFEBVRE

Centre de Mécanique Ondulatoire Appliquée, Paris, France

(Received May 31, 1960)

A formula is derived for the electron spin resonance line shape of a polycrystalline sample containing the CH π-electron radical. The assumption is made in this derivation that the spectrum of the radical in a specific orientation is made up of Gaussians. The line shapes are calculated at the X, K, and J bands, and shown to be rather different for a sufficiently small component line width.

INTRODUCTION

THE electron spin resonance (ESR) spectra of organic radicals in solutions can be interpreted in terms of the contact interactions between the unpaired electron distribution and the nuclei of nonzero spin.[1] The ESR spectra of a radical trapped in a crystal is complicated by the presence of dipole-dipole interactions, which average out to zero in liquids.[2] The lines are anisotropic and new selection rules must be formulated.[3–5] The spectra of a polycrystalline or amorphous sample is a superposition of the spectra corresponding to radicals in various orientations. Such superpositions have been calculated for the nuclear resonance spectra of polycrystalline materials.[6,7] We wish in this note to present a similar calculation for the line shape of the ESR spectra of a polycrystalline CH π-electron radical[8] such as might be obtained for instance from x-ray irradiated Malonic acid.[3] The procedure which will be followed can be extended to more complicated cases. The main assumption is that the spectrum of an individual radical is made up of Gaussians. A treatment in two steps of the line shape for the same system has been proposed by H. Sternlicht[9]: (a) assuming the spectrum of the individual radical to be made up of Dirac functions; (b) weighting the line shape obtained in this manner by a Gaussian function. This expression for the line shape was only used to treat the case where the spin of the proton is quantized along the direction of the external magnetic field. This will not be so in most experimental conditions. The present formulation reduces the line shape function to a double integral which has been programmed for the IBM 704.

LINE SHAPE FORMULA

The ESR spectra of a CH π-electron radical has been treated by McConnell, Heller, Cole, and Fessenden.[3] We shall briefly summarize the main results of the theory here. The spin Hamiltonian can be written

$$\mathrm{H}=h\,|\,\nu_e\,|\,\mathbf{S}_H-h\nu_p\mathbf{I}_H+h(A\mathbf{S}_z\mathbf{I}_z+B\mathbf{S}_z\mathbf{I}_z+C\mathbf{I}_y\mathbf{S}_y). \quad (1)$$

In (1) $|\,\nu_e\,|$ and ν_p are the resonance frequencies of the electron and the proton in the external magnetic field, given by

$$|\,\nu_e\,|=h^{-1}g_0\,|\,\beta\,|\,H_0 \quad (2)$$

$$\nu_p=h^{-1}g_p\beta_N H_0. \quad (3)$$

In Eqs. (2) and (3) g_0 and g_p are the electron and proton g factors, $|\,\beta\,|$ the absolute value of the electron Bohr magneton, β_N the nuclear magneton, H_0 the intensity of the applied external magnetic field. A, B, and C from Eq. (1) are the principal values of the tensor combining contact and dipole-dipole interactions. The xyz reference system is that in which this tensor assumes a diagonal form. $\mathbf{S}$ and $\mathbf{I}$ are the electron and proton spin operators of components $\mathbf{S}_x$, $\mathbf{S}_y$, $\mathbf{S}_z$ and $\mathbf{I}_x$, $\mathbf{I}_y$, $\mathbf{I}_z$ in the xyz axes. $\mathbf{S}_H$ and $\mathbf{I}_H$ are the components of these spin operators along the direction of the external magnetic field.

In an external magnetic field of such magnitude that S_H is a good quantum number, the spectrum is a symmetrical quartet, centered on the electron resonance frequency $|\,\nu_e\,|$. This quartet is made up of two doublets, the four absorption frequencies being given by the relations

$$\nu_1=|\,\nu_e\,|+\tfrac{1}{2}(\nu'-\nu'')$$

$$\nu_2=|\,\nu_e\,|-\tfrac{1}{2}(\nu'-\nu'') \quad (4)$$

$$\nu_3=|\,\nu_e\,|+\tfrac{1}{2}(\nu'+\nu'')$$

$$\nu_4=|\,\nu_e\,|-\tfrac{1}{2}(\nu'+\nu''). \quad (5)$$

In (4), ν' and ν'' are, for given values of ν_p, A, B, and C, the following functions of θ and ϕ, the polar angles which determine the direction of the external magnetic field with respect to the xyz axes,

$$\nu'=[(\nu_p-\tfrac{1}{2}A)^2\cos^2\theta+(\nu_p-\tfrac{1}{2}B)^2\sin^2\theta\cos^2\phi+(\nu_p-\tfrac{1}{2}C)^2\sin^2\theta\sin^2\phi]^{\frac{1}{2}} \quad (6)$$

$$\nu''=[(\nu_p+\tfrac{1}{2}A)^2\cos^2\theta+(\nu_p+\tfrac{1}{2}B)^2\sin^2\theta\cos^2\phi+(\nu_p+\tfrac{1}{2}C)^2\sin^2\theta\sin^2\phi]^{\frac{1}{2}}. \quad (7)$$

[1] See e.g., D. J. E. Ingram, *Free Radicals as Studied by Electron-Spin Resonance* (Butterworths Scientific Publications, Ltd., London, 1958).
[2] S. I. Weissman, J. Chem. Phys. **22,** 1378 (1954).
[3] H. M. McConnell, C. Heller, T. Cole, and R. W. Fessenden, J. Am. Chem. Soc. **82,** 766 (1960).
[4] N. M. Atherton and D. H. Whiffen, Mol. Phys. **3,** 1 (1960).
[5] I. Miyagawa and W. Gordy, J. Chem. Phys. **32,** 255 (1960).
[6] G. E. Pake, J. Chem. Phys. **16,** 327 (1948).
[7] E. R. Andrew and R. Bersohn, J. Chem. Phys. **18,** 159 (1950).
[8] "π-electron radical" is used here as defined by H. M. McConnell and J. Strathdee, Mol. Phys. **2,** 129 (1959).
[9] H. Sternlicht (to be published).

The doublet corresponding to (4) has a relative intensity of $\cos^2(\xi/2)$, that corresponding to (5) a relative intensity of $\sin^2(\xi/2)$, where the angle ξ is given by the relation

$$\cos\xi=\frac{\nu_p^2-\frac{1}{4}[A^2\cos^2\theta+B^2\sin^2\theta\cos^2\phi+C^2\sin^2\theta\sin^2\phi]}{\nu'\nu''}. \tag{8}$$

The spectrum is field-dependent because of the presence of ν_p in (6)–(8).

We now assume that a radical in a specific orientation has a spectrum made up of four Gaussians, centered at the four absorption frequencies, and having the relative weights given previously. We consider that this modification can take into account conveniently the various causes of broadening. A normalized Gaussian function can be written

$$f(\nu)=\lambda^{-1}(2/\pi)^{\frac{1}{2}}\exp(-2\nu^2/\lambda^2), \tag{9}$$

where λ is the width between the points of maximum and minimum slope. Thus the normalized line shape for a given orientation is given by

$$\begin{aligned}h(\nu)=(2\lambda)^{-1}(2/\pi)^{\frac{1}{2}}[&\cos^2(\xi/2)\{\exp[-2(\nu-\nu_1)^2/\lambda^2]\\&+\exp[-2(\nu-\nu_2)^2/\lambda^2]\}\\&+\sin^2(\xi/2)\{\exp[-2(\nu-\nu_3)^2/\lambda^2]\\&+\exp[-2(\nu-\nu_4)^2/\lambda^2]\}].\end{aligned} \tag{10}$$

To calculate the value at ν of the line shape function in the polycrystalline sample, where all orientations are assumed to be equally probable, we multiply (10) by the probability for θ to be between θ and $\theta+d\theta$ and ϕ between ϕ and $\phi+d\phi$,

$$P(\theta,\phi)d\theta d\phi=(1/4\pi)\sin\theta d\theta d\phi \tag{11}$$

and integrate over all values of θ and ϕ. The normalized shape function for the polycrystalline sample is

$$\begin{aligned}g(\nu)=(1/8\pi\lambda)(2/\pi)^{\frac{1}{2}}&\int_0^{\pi}d\theta\int_0^{2\pi}d\phi\\&\times\sin\theta[\cos^2(\xi/2)\{\exp[-2(\nu-\nu_1)^2/\lambda^2]\\&+\exp[-2(\nu-\nu_2)^2/\lambda^2]\}\\&+\sin^2(\xi/2)\{\exp[-2(\nu-\nu_3)^2/\lambda^2]\\&+\exp[-2(\nu-\nu_4)^2/\lambda^2]\}].\end{aligned} \tag{12}$$

This double integral over the sphere has been programmed for the IBM 704 electronic computer. The parameters in the program are ν_p, the proton resonance frequency in the external magnetic field, the constants A, B, and C of the spin Hamiltonian, and the component linewidth λ.

SECOND AND FOURTH MOMENTS

The various moments of a magnetic resonance spectrum for a polycrystalline substance can be obtained by averaging over all orientations those calculated for a specific direction.[10] Such moments can sometimes be useful for extracting information from complex spectra. We shall now derive the second and fourth moments corresponding to the shape function (12).

For given values of θ and ϕ the second moment corresponding to the spectra as described by Eqs. (5)–(8) is[3]

$$\langle(\Delta\nu)^2\rangle_\nu=A^2\cos^2\theta+B^2\sin^2\theta\cos^2\phi+C^2\sin^2\theta\sin^2\phi. \tag{13}$$

The subscript ν means that an average has been made over the absorption frequency. After averaging over θ and ϕ, there is the relation

$$\langle\langle(\Delta\nu)^2\rangle_\nu\rangle_{\theta,\phi}=\tfrac{1}{3}(A^2+B^2+C^2). \tag{14}$$

Similarly the fourth moment in a specific orientation is

$$\begin{aligned}&\langle(\Delta\nu)^4\rangle_\nu\\&=\cos^2(\xi/2)(\nu'-\nu'')^4+\sin^2(\xi/2)(\nu'+\nu'')^4\\&=4\{(A^2\cos^2\theta+B^2\sin^2\theta\cos^2\phi+C^2\sin^2\theta\sin^2\phi)\\&\quad-(A\cos^2\theta+B\sin^2\theta\cos^2\phi+C\sin^2\theta\sin^2\phi)^2\}\nu_p^2\\&\quad+\{A^2\cos^2\theta+B^2\sin^2\theta\cos^2\phi+C^2\sin^2\theta\sin^2\phi\}^2.\end{aligned} \tag{15}$$

Averaging (15) over all directions gives

$$\begin{aligned}&\langle\langle(\Delta\nu)^4\rangle_\nu\rangle_{\theta,\phi}\\&\quad=\tfrac{8}{15}\{(A^2+B^2+C^2)-(AB+AC+BC)\}\nu_p^2\\&\quad+\{\tfrac{1}{5}(A^4+B^4+C^4)+\tfrac{2}{15}(A^2B^2+A^2C^2+B^2C^2)\}.\end{aligned} \tag{16}$$

Owing to the occurrence of ν_p in (15) and (16), the fourth moments are field-dependent, unlike the second moments.

The second and fourth moments referring to the shape function calculated with a Gaussian component line can easily be shown to be related to those by the expressions

$$\langle\langle(\Delta\nu)^2\rangle_\nu\rangle_{\theta,\phi}^{(\lambda)}=\langle\langle(\Delta\nu)^2\rangle_\nu\rangle_{\theta,\phi}+\lambda^2 \tag{17}$$

$$\langle\langle(\Delta\nu)^4\rangle_\nu\rangle_{\theta,\phi}^{(\lambda)}=\langle\langle(\Delta\nu)^4\rangle_\nu\rangle_{\theta,\phi}+6\lambda^2\langle\langle(\Delta\nu)^2\rangle_\nu\rangle_{\theta,\phi}+3\lambda^4. \tag{18}$$

The relations (17) and (18), in addition to indicating the dependence of the second and fourth moments upon external magnetic field intensity and component linewidth, can serve as tests for the line shapes obtained through numerical integration of formula (12).

SOME EXAMPLES

We shall adopt in the following the values of A, B, and C calculated by McConnell and Strathdee[11] by combining the principal values of the tensor expressing the dipole-dipole interaction derived from an unpaired electron distribution represented by a $2p\pi$ Slater or-

[10] See, e.g., E. R. Andrew, *Nuclear Magnetic Resonance* (Cambridge University Press, New York, 1956), p. 160.

[11] H. M. McConnell and J. Strathdee, Mol. Phys. **2**, 129 (1959).

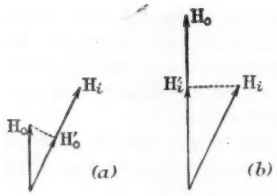

FIG. 1. Magnetic fields for cases a and b in the limiting approximation. The internal magnetic field reverses its sign when the electron flips its spin.

bital, with the value of the contact term deduced from experimental results in liquids. These values are close to those which have been derived later[3,4,12,13] from experimental measurements made on monocrystals containing trapped organic radicals. Expressed in megacycles per second (Mc), these constants are

$$A=-21 \text{ Mc}, \qquad B=-69 \text{ Mc}, \qquad C=-103 \text{ Mc}.$$

Experimental measurements are very often made at one of the following electron resonance frequencies.[5]

X band 9500 Mc corresponding to $H_0\sim$ 3400 gauss

K band 24 100 Mc corresponding to $H_0\sim$ 8600 gauss

J band 34 000 Mc corresponding to $H_0\sim$12 150 gauss.

The spectra of the individual radical is strongly dependent upon the intensity of the external magnetic field.[3,5] The various situations can be roughly pictured as

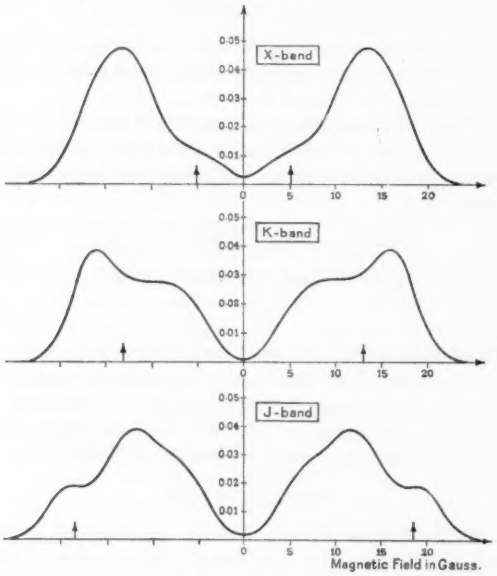

FIG. 2. The three line shapes at X, K, and J band for a component linewidth of 4 gauss. The arrows indicate the position of the proton resonance.

[12] D. K. Ghosh and D. H. Whiffen, Mol. Phys. **2**, 285 (1959).
[13] N. M. Atherton and D. H. Whiffen, Mol. Phys. **3**, 103 (1960).

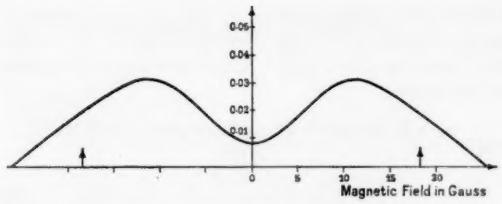

FIG. 3. The line shape at J band for a component linewidth of 8 gauss. The arrows indicate the position of the proton resonance.

follows: (a) when the external magnetic field is somewhat smaller than the internal magnetic field acting on the proton (as is the case for the X-band spectra), the inner doublet is of weak intensity and has a separation of approximately twice the resonance frequency of the proton in the magnetic field H_0' (cf. Fig. 1), the projection of the external magnetic field H_0 along the direction of the internal magnetic field H_i. The outer doublet is of strong intensity and has a separation of approximately twice the proton resonance frequency in the field H_i. (b) When H_0 is of somewhat larger intensity than H_i (as is the case for the J-band spectra), the outer doublet is of weak intensity and has a separation of approximately twice the proton resonance frequency in H_0. The inner doublet is of strong intensity and has a separation of approximately twice the proton resonance frequency in H_i', the projection of H_i along the direction of H_0. (c) At K band, the two fields are of comparable magnitude, and at some orientations the two doublets can have the same intensity. At the limit of a large difference between the intensities of H_0 and H_i, the weak doublets completely disappear.

In Fig. 2 are given the line shapes obtained from formula (12) for the three cases. The line shapes are given as functions of the intensity of the external magnetic field rather than as functions of the frequency. The component linewidth [that is λ formula (9)] was tentatively taken to be 4 gauss. In general lines in the ESR spectra of radicals trapped in a monocrystal are broader than those obtained from liquids; however, if the monocrystalline substance is not perfect, there will be a broadening due to the variation in orientation. This broadening should not be taken into account in a calculation for the polycrystal.

The main features of the line shapes can be under-

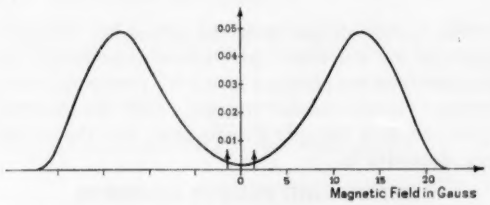

FIG. 4. The line shape for a field $H_0\sim$860 gauss, and a component linewidth of 4 gauss.

TABLE I. Second and fourth moments.

λ	band	Second moments: Numerical integration	Second moments: From formula (17)	Fourth moments: Numerical integration	Fourth moments: From formula (18)
4	X	686.87 gauss^2	686.87 gauss^2	6350 10^2 gauss^4	6350 10^2 gauss^4
4	K	686.87 gauss^2	686.87 gauss^2	6843 10^2 gauss^4	6842 10^2 gauss^4
4	J	686.88 gauss^2	686.87 gauss^2	7420 10^2 gauss^4	7421 10^2 gauss^4
8	J	734.83 gauss^2	734.87 gauss^2	9467 10^2 gauss^4	9466 10^2 gauss^4

stood on the basis of the consideration made previously. The arrows show the position of the proton resonance frequency ν_p in the external magnetic field for the three cases. In the X-band and J-band cases there are slight humps in the neighborhood of ν_p, which are due to the fact that at most orientations there is a weak but relatively isotropic absorption in these regions. This is more pronounced in the J-band case where the weak bands are strictly isotropic in the limiting approximation. In addition the line shape in this case conforms to the general rule formulated by Sternlicht[9] for the case where I_H is a good quantum number (which is already nearly the case at most orientations): the peak to peak separation is equal to the absolute value of the constant having the middle value, among A, B, and C. In this problem this is $|B|$, which is equal to 24.7 gauss. In the K-band case the spectra is roughly made up of two doublets of comparable intensity.

The possibility of observing these differences in the line shape should of course be strongly dependent upon the value of the component linewidth. To test this the calculation was repeated for the J-band case with $\lambda=8$ gauss. Figure 3 shows the line shape obtained in this manner. The spectrum is now a broad doublet. The bands in the region of the proton resonance frequency have now completely disappeared.

As a last example Fig. 4 shows the line shape for $\lambda=4$ and a rather small external magnetic field ($\sim$860 gauss). The spectrum is now a doublet, with a peak to peak separation of 27 gauss.

Table I compares the moments obtained through expressions (17) and (18) with those calculated by numerical integration from the line shapes given in Figs. 2 and 3. It will be seen that the agreement is very satisfactory.

CONCLUSIONS

Before deciding about the sort of information that can be extracted from ESR polycrystalline spectra, it will be necessary to make calculations on more complex radicals. The question of the component linewidth might also be quite crucial here. A number of spectra have been reported in the literature for polycrystalline or amorphous substances containing organic radicals,[14] but in these radicals there was interaction between the odd electron and more than one proton. The difficulty of interpreting such spectra is well illustrated by the case of γ-irradiated glycollic acid. Work on the polycrystalline material had given a spectrum[15] which apparently could be explained as resulting from interaction with one proton only. Later work[4] on a single crystal has shown that in fact there is in addition a weaker but non-negligible interaction with another proton.

ACKNOWLEDGMENTS

This work resulted from a visit to the group of Professor H. M. McConnell to whom the author would like to express his deep appreciation. The program for the IBM 704 was written by G. Bessis and his collaboration is most gratefully acknowledged. Finally Dr. Sternlicht was most kind in sending me a copy of his paper prior to publication.

[14] E.g., B. Smaller and M. S. Matheson, J. Chem. Phys. **28**, 1169 (1958); M. Zeldes and R. Livingston, *ibid.* **30**, 40 (1959).
[15] P. M. Grant, R. B. Ward, and D. H. Whiffen, J. Chem. Soc. **1958**, 4635.

THE JOURNAL OF CHEMICAL PHYSICS VOLUME 33, NUMBER 6 DECEMBER, 1960

Nuclear Spin Conservation in Ortho-Para Hydrogen Conversion

DOYLE BRITTON AND Z Z. HUGUS, JR.

Department of Chemistry, University of Minnesota, Minneapolis, Minnesota

(Received February 3, 1960)

The details of statistics of the nuclear spin states in the ortho-para hydrogen conversion by hydrogen atoms are considered. It is shown that the observed rate of conversion is 5/6 the rate of formation of the transition state if H_3 is linear. The factor is 8/9 is H_3 if an equilateral triangle.

NUCLEAR SPIN CONSERVATION IN ORTHO-PARA HYDROGEN CONVERSION

THE interconversion of ortho and para hydrogen by the reaction

$$H+o\text{-}H_2=H+p\text{-}H_2 \tag{1}$$

has been of considerable theoretical and experimental interest since the early work of Farkas.[1] The rate constant for the reaction has been defined by

$$-[d(p\text{-}H_2)/dt]=k(H)[(p\text{-}H_2)-(p\text{-}H_2)_{equil}], \tag{2}$$

where k has been interpreted as if the products, statistically, were

$$H+o\text{-}H_2\Rightarrow\tfrac{3}{4}o\text{-}H_2+\tfrac{1}{4}p\text{-}H_2 \tag{3a}$$

$$H+p\text{-}H_2\Rightarrow\tfrac{3}{4}o\text{-}H_2+\tfrac{1}{4}p\text{-}H_2 \tag{3b}$$

which leads to the conclusion that the observed rate constant is equal to the rate constant for the formation of the transition state (see Appendix I). This suggestion, that the products in each of the individual reactions are the same as the products in the overall reaction, was first made by Pelzer and Wigner,[2] and has been used repeatedly since.[3] It is our contention that the effects of nuclear spin conservation and atom exchange have been incorrectly considered, and the distribution of products from the specific reactions is not that given by (3a) and (3b).

If the high-temperature limit is considered so that energy difference between the various states can be ignored, in a vanishingly small magnetic field there are two nuclear states for an H atom.[4] These have nuclear spin projections $+\frac{1}{2}$ and $-\frac{1}{2}$ and will be referred to here often as α and β. These are four possible nuclear states for a hydrogen molecule. If the symbol $\alpha\beta$ is read as the first nucleus in spin state α and the second in spin state β the four states are $\alpha\alpha$, $\alpha\beta+\beta\alpha$, $\beta\beta$, and $\alpha\beta-\beta\alpha$. The first three are the possible states of o-H_2; the last is the only state of p-H_2. Therefore the products of the following eight collisions must be considered.

$$\alpha+\alpha\alpha \tag{4a}$$

$$\beta+\alpha\alpha \tag{4b}$$

$$\alpha+(\alpha\beta+\beta\alpha) \tag{4c}$$

$$\beta+(\alpha\beta+\beta\alpha) \tag{4d}$$

$$\alpha+\beta\beta \tag{4e}$$

$$\beta+\beta\beta \tag{4f}$$

$$\alpha+(\alpha\beta-\beta\alpha) \tag{4g}$$

$$\beta+(\alpha\beta-\beta\alpha). \tag{4h}$$

In reaction (4a) or (4f) it would appear that the products are the same as the reactants, since selection rules forbid transitions between the various nuclear spin projections except in a strong, inhomogeneous magnetic field. A comparison of the rate constants for $o-p$ conversion in the presence of paramagnetic molecules shows that the magnetic field due to the H atom is not large enough to cause the observed rate. Therefore we will assume, as Pelzer and Wigner did,[2] that the nuclear spin projection quantum number must be conserved. The difference comes in the treatment of the collisions involving different nuclear spin states.

Pelzer and Wigner assumed that the H atom approached in an end on manner and that exchange of end atoms always took place so that in (4b), for example,

$$\beta+\alpha\alpha\rightarrow\beta\alpha+\alpha$$

and that $\beta\alpha$ should be interpreted as an equal mixture of $\alpha\beta+\beta\alpha$ and $\alpha\beta-\beta\alpha$. In reaction (4c) or (4g) they assumed that as the H atom approached, the H_2 molecule, now in an asymmetric environment, became either $\alpha\beta$ or $\beta\alpha$, both equally likely, and predicted the products of exchange on this basis which gives Eqs. (3a) and (3b).

It does not seem that the exchange of atoms is necessary for the $o-p$ conversion, but only that a transition state be formed in which the various nuclear states can mix. Two possibilities occur here. The first is that

[1] A. Farkas, Z. physik. Chem. (Leipzig) **10B**, 419 (1931). For recent work, and more complete references, see R. E. Weston, Jr., J. Chem. Phys. **31**, 892 (1959), or I. Shavitt, J. Chem. Phys. **31**, 1359 (1959).

[2] H. Pelzer and E. Wigner, Z. physik Chem. (Leipzig) **15B**, 445 (1932). In particular see p. 470.

[3] For example, A. Farkas, *Orthohydrogen, Parahydrogen and Heavy Hydrogen* (Cambridge University Press, New York, 1935), p. 66; L. Farkas and E. Wigner, Trans. Faraday Soc. **32**, 708 (1936).

[4] Since experiments are carried out with no precautions to ensure the absence of terrestrial magnetic fields the question of whether these states maintain their identity in the complete absence of a field seems a philosophical one and not essential to the argument given here.

TABLE I. Probability of distribution of formation of product for triangular H_3 transition state.

Reactants \ Products	$\alpha+\alpha\alpha$	$\alpha+(\alpha\beta+\beta\alpha)$	$\alpha+(\alpha\beta-\beta\alpha)$	$\beta+\alpha\alpha$	$\alpha+\beta\beta$	$\beta+(\alpha\beta+\beta\alpha)$	$\beta+(\alpha\beta-\beta\alpha)$	$\beta+\beta\beta$
$\alpha+\alpha\alpha$	1							
$\alpha+(\alpha\beta+\beta\alpha)$		$\frac{1}{3}$	$\frac{1}{3}$	$\frac{1}{3}$				
$\alpha+(\alpha\beta-\beta\alpha)$		$\frac{1}{3}$	$\frac{1}{3}$	$\frac{1}{3}$				
$\beta+\alpha\alpha$		$\frac{1}{3}$	$\frac{1}{3}$	$\frac{1}{3}$				
$\alpha+\beta\beta$					$\frac{1}{3}$	$\frac{1}{3}$	$\frac{1}{3}$	
$\beta+(\alpha\beta+\beta\alpha)$					$\frac{1}{3}$	$\frac{1}{3}$	$\frac{1}{3}$	
$\beta+(\alpha\beta-\beta\alpha)$					$\frac{1}{3}$	$\frac{1}{3}$	$\frac{1}{3}$	
$\beta+\beta\beta$								1

complete mixing of the spin state occurs. This would be the case if the transition state were an equilateral triangular H_3. Here only the sum of the spin projections need be considered, since all products with the same sum of spin projections as the reactants would be equally likely. The probabilities of the various reactants going to the various products are shown in Table I. Inspection of Table I will show that the net reaction products are

$$H+o\text{-}H_2 \Rightarrow \tfrac{7}{9}o\text{-}H_2+\tfrac{2}{9}p\text{-}H_2 \qquad (5a)$$

$$H+p\text{-}H_2 \Rightarrow \tfrac{2}{3}o\text{-}H_2+\tfrac{1}{3}p\text{-}H_2. \qquad (5b)$$

Thus, there is a larger probability of retaining the original configuration than the equilibrium distribution would predict. This means that the observed rate is not the rate of formation of the transition state but is actually less. According to Eq. (9), derived in Appendix I, $k=\frac{8}{9}k_t$, where k_t is the rate of formation of the transition state.

The second possibility is that in the transition state there is not complete equivalence of the three H atoms, but only two of the three are equivalent. This could be the linear H_3 transition state. Here the situation is a little less clear and the various possibilities of the transition state must be considered in detail. These are eight: $\alpha\alpha\alpha$, $\alpha\alpha\beta+\beta\alpha\alpha$, $\alpha\alpha\beta-\beta\alpha\alpha$, $\alpha\beta\alpha$, $\alpha\beta\beta+\beta\beta\alpha$, $\alpha\beta\beta-\beta\beta\alpha$, $\beta\alpha\beta$, and $\beta\beta\beta$. The probabilities of forming these various states from the various sets of reactants are shown in Table II, where the rows can be read as the probabilities of a given set of final products from a given transition state.

When the decomposition of the transition states is considered, then Table III, which shows the distribution of products from reactants, can be constructed. Inspection of Table III shows that the net reaction products are

$$H+o\text{-}H_2 \Rightarrow \tfrac{19}{24}o\text{-}H_2+\tfrac{5}{24}p\text{-}H_2, \qquad (6a)$$

$$H+p\text{-}H_2 \Rightarrow \tfrac{5}{8}o\text{-}H_2+\tfrac{3}{8}p\text{-}H_2. \qquad (6b)$$

This makes $k=\frac{5}{6}k_t$, which is an even greater effect than for the triangular transition state. The difference between this and the result of Pelzer and Wigner is a consequence of the fact that they only considered a transition state to have been formed if there was an exchange of atoms (although not necessarily a net change of spins).

If the spin of an individual nucleus is greater than $\frac{1}{2}$ one more complication arises. That is the question

TABLE II. Probability distribution of formation of transition states for linear H_3.[a]

Reactants \ Transition state	$\alpha\alpha\alpha$	$\alpha\alpha\beta+\beta\alpha\alpha$	$\alpha\alpha\beta-\beta\alpha\alpha$	$\alpha\beta\alpha$	$\beta\alpha\beta$	$\alpha\beta\beta+\beta\beta\alpha$	$\alpha\beta\beta-\beta\beta\alpha$	$\beta\beta\beta$
$\alpha+\alpha\alpha$	1							
$\alpha+(\alpha\beta+\beta\alpha)$		$\frac{1}{4}$	$\frac{1}{4}$	$\frac{1}{2}$				
$\alpha+(\alpha\beta-\beta\alpha)$		$\frac{1}{4}$	$\frac{1}{4}$	$\frac{1}{2}$				
$\beta+\alpha\alpha$		$\frac{1}{2}$	$\frac{1}{2}$	0				
$\alpha+\beta\beta$					0	$\frac{1}{2}$	$\frac{1}{2}$	
$\beta+(\alpha\beta+\beta\alpha)$					$\frac{1}{2}$	$\frac{1}{4}$	$\frac{1}{4}$	
$\beta+(\alpha\beta-\beta\alpha)$					$\frac{1}{2}$	$\frac{1}{4}$	$\frac{1}{4}$	
$\beta+\beta\beta$								1

[a] It is worth noting that if the middle symbol in each transition state is omitted (i.e., $\alpha\beta\alpha$ is read as $\alpha\alpha$, and $\alpha\alpha\beta+\beta\alpha\alpha$ is read as $\alpha\beta+\beta\alpha$) this table gives the distribution of products predicted by Pelzer and Wigner.

TABLE III. Probability distribution of formation of products for linear H_3.

Reactants \ Products	$\alpha+$ $\alpha\alpha$	$\alpha+$ $(\alpha\beta+\beta\alpha)$	$\beta+$ $(\alpha\beta-\beta\alpha)$	$\alpha+$ $\alpha\alpha$	$\alpha+$ $\beta\beta$	$\beta+$ $(\alpha\beta+\beta\alpha$)	$\beta+$ $(\alpha\beta-\beta\alpha)$	$\beta+$ $\beta\beta$
$\alpha+\alpha\alpha$	1							
$\alpha+(\alpha\beta+\beta\alpha)$		$\frac{3}{8}$	$\frac{3}{8}$	$\frac{1}{4}$				
$\alpha+(\alpha\beta-\beta\alpha)$		$\frac{3}{8}$	$\frac{3}{8}$	$\frac{1}{4}$				
$\beta+\alpha\alpha$		$\frac{1}{4}$	$\frac{1}{4}$	$\frac{1}{2}$				
$\alpha+\beta\beta$					$\frac{1}{2}$	$\frac{1}{4}$	$\frac{1}{4}$	
$\beta+(\alpha\beta+\beta\alpha)$					$\frac{1}{4}$	$\frac{3}{8}$	$\frac{3}{8}$	
$\beta+(\alpha\beta-\beta\alpha)$					$\frac{1}{4}$	$\frac{3}{8}$	$\frac{3}{8}$	
$\beta+\beta\beta$								1

whether transitions of type $\alpha+(\alpha\gamma+\gamma\alpha)\Rightarrow\alpha+\beta\beta$ are possible, where α, β, and γ are spin states such that the spin projection, $\alpha+\gamma=2\beta$. In our opinion transitions of this type would not occur within a reasonable probability since they conserve the spin projection by two simultaneous transitions.

If such transitions are forbidden the factor of $\frac{5}{6}$ which was found for spin $\frac{1}{2}$ in the linear case becomes $\frac{11}{12}$ for spin 1 and $\frac{14}{15}$ for spin $\frac{3}{2}$. The factor of $\frac{5}{6}$ which was found for the triangular case for spin $\frac{1}{2}$ becomes $\frac{7}{8}$ for spin 1 and $\frac{9}{10}$ for spin $\frac{3}{2}$.[5] The spin 1 case would apply to ortho-para conversion in deuterium.

ACKNOWLEDGMENT

We would like to thank the Research Corporation and the Office of Ordnance Research, U. S. Army for support.

APPENDIX I

The general relationship between the proportions of ortho and para hydrogen in the products and the ratio of the observed rate constant to the rate of formation of the transition state is derived. Let k_t be the rate constant for the formation of the transition state from one atom and one molecule and x and y be the fractions of o-H_2 in the products from o-H_2 and p-H_2, respectively.

$$H+o\text{-}H_2\xrightarrow{k_t}H_3\Rightarrow x\ o\text{-}H_2+(1-x)\,p\text{-}H_2 \qquad (7a)$$

$$H+p\text{-}H_2\xrightarrow{k_t}H_3\Rightarrow y\ o\text{-}H_2+(1-y)\,p\text{-}H_2. \qquad (7b)$$

Since at equilibrium there is no net change in the relative amounts of o-H_2 and p-H_2 at the high temperature limit

$$(1-y)/(1-x)=3/1 \text{ or } y=3x-2$$

$$(\tfrac{2}{3}\leqslant x\leqslant 1 \text{ must be true}).$$

The net rate of disappearance of p-H_2 is

$$\begin{aligned}-[d(p\text{-}H_2)/dt]&=-(1-x)k_t(H)[(o\text{-}H_2)-o\text{-}H_{2\,equil}]\\&\quad+(1-y)k_t(H)[(p\text{-}H_2)-(p\text{-}H_2)_{equil}]\\&=4(1-x)k_t(H)[(p\text{-}H_2)-(p\text{-}H_2)_{equil}].\end{aligned} \qquad (8)$$

If this is compared with Eq. (2),

$$k=4(1-x)k_t. \qquad (9)$$

[5] If transitions $\alpha+(\alpha\gamma+\gamma\alpha)\Rightarrow\alpha+\beta\beta$ were allowed the factors would be 20/21 for spin 1 and 439/450 for spin $\frac{3}{2}$.

THE JOURNAL OF CHEMICAL PHYSICS VOLUME 33, NUMBER 6 DECEMBER, 1960

Intermolecular Coupling of Vibrations in Molecular Crystals: A Vibrational Exciton Approach*

R. M. HEXTER

Mellon Institute, Pittsburgh, Pennsylvania

(Received November 2, 1959)

A vibrational exciton theory is developed which parallels in many ways the electronic exciton theory originally put forward by Davydov and amplified by Craig and Hobbins and by Fox and Schnepp. The kernel of the theory is the adoption, following Davydov again, of a transition-dipole—transition-dipole interaction as the potential which perturbs the isolated molecule energies and which thereby couples the motions of pairs of molecules in a crystal. As a result of the quantitative application of this theory, molecular dipole derivatives of several of the parallel modes of methyl chloride are obtained from the correlation field splittings of the corresponding fundamentals in the spectrum of solid methyl chloride. An isotope effect upon correlation field splittings is reported and is accounted for in terms of the same theory. A general method of testing the theory in terms of this isotope effect is suggested. The effect of intermolecular transition dipole coupling on intensities is derived and compared with the ratio of the dipole derivatives obtained from the correlation field splittings to those obtained from absolute intensity studies in the gas phase. The possible use of other bases for correlation field splittings is also discussed.

INTRODUCTION

THE existence of correlation field splittings of nondegenerate vibrational bands of molecular crystals was first predicted by Hornig[1] and Winston and Halford.[2] Observations of such splittings have been reported many times.[3] There have been, unfortunately, few instances[4,5] wherein the magnitude of these splittings for each of the several bands of one crystal have been intercompared or compared with the other principal source of vibrational splittings—those of *degenerate* molecular modes by the decreasing symmetry of the *local* field of a molecule upon its condensation.[2,6]

Recently Decius[7] has made use of a theory of intermolecular coupling of vibrational modes *via* a transition-dipole—transition-dipole interaction, which could form a basis for calculation of the correlation field splitting. The first proposal of an interaction of this form was made by Davydov,[8] with whose name the general phenomenon of correlation field splittings[9] is often associated. A careful exposition of this theory, with special application to the *electronic* Davydov splitting, in molecular crystals constructed of "sheets" of molecules, has been made by Craig and Hobbins.[10] A more general extension of the theory has been made by Fox and Schnepp.[11] In connection with the interpretation of certain complex infrared spectra of crystalline carbonates,[7a] nitrates,[7a,b] and borates,[7c] in which isotopic substitution of some of the central atoms (C, N, or B) of these planar and trigonal ions has been made, Decius has essentially made use of a one-dimensional form of the same theory. The geometry of the problem is somewhat simplified by the choice of these carbonates, nitrates, and borates, as some of the several anions of one unit cell are situated in parallel planes and others are coplanar; in addition, one of the interanionic distances is considerably shorter than the other. As a consequence, the problem can be idealized in terms of linear chains of molecules. In these systems, where there is little isotopic substitution, this geometry permits only one member of the resultant correlation field doublet to be spectroscopically active.

It is the purpose of this article to extend this model to specific crystals which contain molecules having only axial symmetry and have their molecules oriented with respect to one another such that no distinct chains of molecules are obvious. Instead, a two-dimensional network of molecules forms a good idealization of the crystal.

THEORY

In the following, we shall follow the development due to CH and to a considerable extent the symbolism will be that of CH, with the reminder that all wave functions used herein are *vibrational* rather than electronic, as in CH. It will be seen that our knowledge of harmonic oscillator wave functions leads to simple and reasonable results for the many interaction integrals embodied in the general theory, and which, when the

* This research was supported in part by the U. S. Air Force through the Air Force Office of Scientific Research of the Air Research and Development Command.

[1] D. F. Hornig, J. Chem. Phys. **16,** 1063 (1948).

[2] H. Winston and R. S. Halford, J. Chem. Phys. **17,** 607 (1949).

[3] Representative references are G. C. Pimentel, A. L. McClellan, W. B. Person, and O. Schnepp, J. Chem. Phys. **23,** 234 (1955), and S. Zwerdling and R. S. Halford, *ibid.* **23,** 2221 (1955).

[4] R. M. Hexter, J. Chem. Phys. **25,** 1286 (1956).

[5] D. A. Dows, J. Chem. Phys. **29,** 484 (1958).

[6] R. S. Halford, J. Chem. Phys. **14,** 8 (1946).

[7] (a) J. C. Decius, J. Chem. Phys. **22,** 1941, 1946 (1954); (b) **23,** 1290 (1955); (c) **25,** 1184 (1956).

[8] A. S. Dovydov, *Theory of Light Absorption of Molecular Crystals,* (Institute of Physics, Ukranian Academy of Sciences, Kiev, Ukranian SSR, 1951), translation by Max Oppenheimer, Jr., and Michael Kasha (to be published by McGraw-Hill Book Company, Inc., New York).

[9] A. S. Davydov, J. Exptl. Theoret. Phys. (U.S.S.R) **18,** 210 (1948).

[10] D. P. Craig and P. C. Hobbins, J. Chem. Soc. **1955,** 539 (hereafter referred to as CH).

[11] D. Fox and O. Schnepp, J. Chem. Phys. **23,** 767 (1955).

wave functions are electronic, cannot at present be simply evaluated.

As a primitive but instructive example, we consider the change in the ground state energy of a molecular system upon crystallization. The "molecules" may be first taken to be simple one-dimensional harmonic oscillators. The crystal's vibrational ground state is defined as a product of all individual molecules' vibrational eigenfunctions,

$$\Phi_G=\varphi_1\varphi_2\varphi_3\cdots\varphi_N, \tag{1}$$

where

$$\varphi_i=\mathfrak{N}_0\exp(-\gamma Q^2/2);\quad \mathfrak{N}_0=(\gamma/\pi)^{1/4};\quad \gamma=4\pi^2\nu/h. \tag{2}$$

According to first-order perturbation theory,

$$E_G=\sum_k w_k+\sum_l\sum_k\int\varphi_l\varphi_k V_{lk}\varphi_l\varphi_k d\tau, \tag{3}$$

where $w_k=h\nu/2$. We shall postpone the formulation of V_{lk} until a later section. What distinguishes this from the related electronic problem is found upon substitution of (2) in (3) (together with the particular V_{lk} we shall ultimately adopt) yielding a relation of the form

$$E_G=\sum_k w_k+\sum_j(K_j/R_j^3)\sum_l\sum_k\mu_l^0\mu_k^0, \tag{4}$$

where μ_i^0 is the permanent dipole moment of the ith molecule. R_j is a fundamental distance of one possible chain of molecules in the crystal, the members of which are not translationally equivalent, and K_j is a trigonometric factor characteristic of this jth chain. We shall obtain a related result for crystal excited state energies, which will permit the prediction that condensation of nonpolar molecules should result in few, if any, shifts of their active vibrational frequencies. This simple consequence of (2) will be further discussed below.

The excited state functions of the crystal are not so easily stated as with (1). Rather we define, again as in CH, the function

$$\phi_p=\varphi_1\varphi_2\varphi_3\cdots\varphi_p'\cdots\varphi_N, \tag{5}$$

where $\varphi_1\cdots\varphi_N$ are ground state wave functions as in (2), but φ_p' is a first excited harmonic oscillator wave function ($v=1$)

$$\varphi_p'=\mathfrak{N}_1\exp(-\gamma Q^2/2)\cdot H_1(\gamma^{\frac{1}{2}}Q) \tag{6}$$

$$\mathfrak{N}_1=2^{-\frac{1}{2}}(\gamma/\pi)^{1/4}.$$

Such states as (5) are not states of definite energy, but may form such by being taken as bases of an orthonormal set,

$$\Phi_r=\sum_{l=1}^{N}a_{rl}\phi_l, \tag{7}$$

Φ_r is an *exciton wave function*, in which the vibrational excitation may be pictured as the exciton. The quantity $a_{rl}^*a_{rl}$ measures the extent that the vibrational excitation is localized on the lth molecule. Here Φ_r may also be viewed as a determinantal function of the φ_i's in which the vibrational excitation, rather than electron coordinates, is permuted among the molecules. Again by first-order perturbation theory the energy of the state Φ_r may be stated, in secular determinant form, wherein the diagonal terms are the counterparts of the coulomb energy, and the off-diagonal terms

$$I_{pq}=(\varphi_p'\varphi_q\mid V_{pq}\mid\varphi_p\varphi_q'), \tag{8}$$

those of the exchange energy, in the many-electron problem. As in the exposition due to CH, it is more useful to state the excitation energy E_r-E_G, again in secular determinant form. The results are the same with the exception that there is an outgrowth of (4) and the paragraph subsequent to it.

The diagonal elements of E_r-E_G are of the form

$$w_p'-w_p+D-\Delta E, \tag{9}$$

where

$$w_p'=\tfrac{3}{2}h\nu, \tag{10}$$

and

$$D=\sum_l{}'\{(\varphi_p'\varphi_l\mid V_{pl}\mid\varphi_p'\varphi_l)-(\varphi_p\varphi_l\mid V_{pl}\mid\varphi_p\varphi_l)\}. \tag{11}$$

Thus D measures the *shift* of the spectrum upon crystallization. In the same sense as (4) it is only the difference of the square of the permanent moment of the molecule in its ground and first excited states and vanishes identically for nonpolar molecules.

The off-diagonal elements of E_r-E_G remain as in (8). Evaluation of (8) is facilitated by the definition of *unit cell wave functions*[12]

$$\gamma^{\alpha,\beta}=(2)^{-\frac{1}{2}}(\phi_p\pm\phi_{p+1}), \tag{12}$$

such that the pth and the $(p+1)$st molecules share the occupancy of a bimolecular unit cell. Having thus evoked the basic entity of a crystal, the Φ_r may be constructed in the usual manner, using the Bloch form[13]

$$\Phi^{\alpha,\beta}(k_a,k_b,k_c)=(2/N)^{\frac{1}{2}}\sum_{\mu,\nu,\omega}\exp[i(k_a\cdot a\mu+k_b\cdot b\nu+k_c\cdot c\omega)]\times\gamma^{\alpha,\beta}(\mu,\nu,\omega), \tag{13}$$

where

$$\left.\begin{matrix}0\le\mu\le M_a\\0\le\nu\le M_b\\0\le\omega\le M_c\end{matrix}\right\};\quad M_aM_bM_c=N/2,$$

[12] The upper sign applies to α and the lower to β.

[13] Equation (13) is the counterpart to Eq. (5) of Fox and Schnepp.[11] The CH procedure introduces the matrix B_k^g of Fox and Schnepp [implicit in (12)] prior to the formation of Bloch functions, whereas Fox and Schnepp generate the functions (13) in the reverse order. This order is of no consequence.

and

$$k_a = 2\pi\sigma/M_a \cdot a, \quad \text{etc.},$$

and

$$\sigma = 0, \pm 1, \pm 2, \cdots, +M_a/2.$$

All the foregoing may be repeated for molecules with more normal coordinates than one, because of the orthogonality of these coordinates. The most important change in this development will be in the form of (8), in which each wave function φ becomes a product wave function of the $3n-6$ orthogonal harmonic oscillator functions of the molecule. The interaction potential will become V_{pl}^{ij}, where i and j denote a pair of normal modes of the molecules p and l, respectively. If we assume that such couplings take place only between *like* normal modes of two molecules, the original orthogonality will be retained. There is abundant experimental evidence for the *lack* of such mode-mixing upon crystallization.

As an example of how the orthogonality is retained we may examine the dynamics of a bimolecular unit cell of a system of nonlinear triatomic molecules. We construct symmetry coordinates of the unit cell by taking linear combinations of the normal coordinates of the isolated molecules, as dictated by the symmetry operations of the unit cell,

$$S_i^+ = (2)^{-\frac{1}{2}}(Q_{i1} + Q_{i2}), \tag{14}$$

$$S_i^- = (2)^{-\frac{1}{2}}(Q_{i1} - Q_{i2}). \tag{15}$$

Here S_i^+ and S_i^- are the symmetry coordinates associated with the in-phase and out-of-phase vibrations of the two molecules of the unit cell, associated with the motion of the isolated molecule having frequency ν_i. The first or lettered subscript on the Q's refers to the numbering of the normal coordinates in the isolated molecule; the second, or numbered subscript refers to the numbering of the molecule in the unit cell. The array of Eqs. (14), (15), etc. forms a matrix equation $\mathbf{S}=\mathbf{UQ}$, where $\mathbf{S}$ is the (column) matrix of symmetry coordinates of the unit cell, and $\mathbf{Q}$ is the (column) matrix of molecular normal coordinates.

$$\mathbf{Q} = \begin{vmatrix} Q_{11} \\ Q_{21} \\ Q_{31} \\ Q_{12} \\ Q_{22} \\ Q_{32} \end{vmatrix}. \tag{16}$$

$\mathbf{U}$ is the matrix of a unitary transformation constructed in the usual manner[14] from the character table of the appropriate symmetry group, in this case, that of the unit cell:

$$\mathbf{U} = 2^{-\frac{1}{2}} \left|\begin{array}{cccccc} 1 & & & 1 & & \\ & 0 & & & 0 & \\ & 1 & & & 1 & \\ 0 & & & 0 & & \\ & & 1 & & & 1 \\ \hline 1 & & & -1 & & \\ & 0 & & & 0 & \\ & 1 & & & -1 & \\ 0 & & & 0 & & \\ & & 1 & & & -1 \end{array}\right| = \mathbf{U}^\dagger. \tag{17}$$

We now define the force constant matrix for the unit cell $\mathbf{F}$ in terms of normal coordinates of each of the molecules in the unit cell. We treat first only those motions derived from the nondegenerate molecular vibrations (ν_1, ν_2, ν_3). By assumption we expect interaction force constants between Q_{11} and Q_{12} to be relatively large, but interactions between Q_{11} and Q_{22}, or between Q_{11} and Q_{21} to be negligible. Consequently,

$$\mathbf{F} = \begin{vmatrix} \Lambda_1^0 & 0 & 0 & F_1 & 0 & 0 \\ & \Lambda_2^0 & 0 & 0 & F_2 & 0 \\ & & \Lambda_3^0 & 0 & 0 & F_3 \\ & & & \Lambda_1^0 & 0 & 0 \\ & \text{(symmetric)} & & & \Lambda_2^0 & 0 \\ & & & & & \Lambda_3^0 \end{vmatrix}. \tag{18}$$

The Λ^0 values are defined as $\Lambda^0 = 4\pi^2(\nu_i^0)^2$, where the ν_i^0 are the "isolated molecule" frequencies (from mixed crystal studies, wherein the solvent is as similar to the solute as possible, but is not identical). The F_i's are then the interaction force constants to be related to the potential given in Eq. (8).[15]

If we transform coordinates from "isolated molecule" normal coordinates to the symmetry coordinates of the unit cell, using the unitary transformation $\mathbf{U}$, we find

[14] E. Bright Wilson, J. C. Decius, and P. C. Cross, *Molecular Vibrations* (McGraw-Hill Book Company, Inc., New York, 1955), p. 119.

[15] In terms of these normal coordinates, the Wilson $\mathbf{G}$ matrix for the unit cell will be the identity matrix, by the definition of normal coordinates. $\mathbf{G}$-matrix elements connect only those coordinates with common atoms. Since we are not including in our potential energy expression, any *new* coordinates, such as lattice coordinates, there can be no new G elements, and in terms of the molecular *normal* coordinates, $\mathbf{G}=\mathbf{E}$.

the new $\overline{\mathbf{F}}$ matrix:

$$\overline{\mathbf{F}}=\begin{pmatrix}\Lambda_1^0+F_1 & & & & & \\ & \Lambda_2^0+F_2 & & & & \\ & & \Lambda_3^0+F_3 & & & \\ & & & \Lambda_1^0-F_1 & & \\ & & & & \Lambda_2^0-F_2 & \\ & & & & & \Lambda_3^0-F_3\end{pmatrix}. \tag{19}$$

Thus, we see that these symmetry coordinates are also the normal coordinates of the unit cell, under the assumptions we have made and we can proceed to use (8), etc., for each normal mode of a polyatomic molecule separately.

We shall apply (8), (13), etc. first to a system that may be well approximated as an "infinite sheet" crystal. The system will be solid methyl chloride, which does in fact have such a structure.[16] Examination of this structure demonstrates that the interactions responsible for the correlation field splittings are primarily between molecules within each sheet and not between molecules in different sheets (see below).

The treatment due to CH[10] was developed for such a system and was applied to the problem of the Davydov splittings in the electronic spectrum of crystalline anthracene. The planar lattice of concern to CH was square; ours will be rectangular. Furthermore, the CH treatment was first restricted to nearest-neighbor interactions. The results of including more distant interactions were also given, and were obtained by direct and presumably laborious calculation. In the following, we also begin with nearest-neighbor interactions and will then extend our calculations to include second-to-nearest-neighbor interactions. We then show that this should be sufficient, for all practical purposes.

For the infinite sheet crystal, with nearest-neighbor interactions only, we follow CH again and first define the excitation energy of a single unit cell, $\Delta E_u^{\alpha,\beta}$. We note that in CH_3Cl(s) the plane of interest is the bc plane; hence our terminology differs somewhat from theirs,

$$\Delta E_u^{\alpha,\beta}=\Delta w+D\pm A, \tag{20}$$

where

$$A=(\phi_p \mid V_{p,p+1} \mid \phi_{p+1})=(\varphi_p'\varphi_{p+1} \mid V_{p,p+1} \mid \varphi_p\varphi_{p+1}').$$

A is defined as the interaction between a molecule at a lower left-hand corner of a unit cell and another at the center of the *same* unit cell. Then

$$\Delta E^{\alpha,\beta}(k_b, k_c)=\Delta E_u^{\alpha,\beta}+\sum_{\mu,\nu\neq 0,0}\exp[i(k_b\cdot b\nu+k_c\cdot c\omega)]\times\int\gamma_{0,0}^{\alpha,\beta}H\gamma_{\nu,\omega}^{\alpha,\beta}d\tau. \tag{21}$$

Direct evaluation of (21) then yields[17]

$$\Delta E^{\alpha,\beta}(k_b, k_c)=\Delta E_u^{\alpha,\beta}+2\cos(k_b\cdot b)H_b^{\alpha,\beta}+2\cos(k_c\cdot c)H_c^{\alpha,\beta}+2\cos(k_b\cdot b+k_c\cdot c)H_{bc}^{\alpha,\beta}. \tag{22}$$

By explicit calculation of the integral in (21), it is found that

$$H_b^{\alpha,\beta}=B\pm\tfrac{1}{2}A', \tag{23}$$

$$H_c^{\alpha,\beta}=C\pm\tfrac{1}{2}A', \tag{24}$$

and

$$H_{bc}^{\alpha,\beta}=\pm\tfrac{1}{2}A. \tag{25}$$

In (23) and (24), H_b and H_c represent the integral in (21), evaluated for unit cell wave functions of *cells* that neighbor one another along the **b** and **c** axes, respectively. B and C represent, respectively, the interaction integrals I_{lk} [Eq. (8)] between translationally equivalent molecules along the **b** and **c** axes. A is defined by (20). A' is a similar interaction to A, but is between the molecule at a corner of a unit cell and the one at the center of the cell beneath it. H_{bc} represents the integral in (21) evaluated for neighboring unit cells along the diagonal (**b**+**c**). It is interesting to note that the interaction between cells along the diagonal (**b**−**c**) identically vanishes, as those cells contain no molecular pairs that are nearest neighbors. For the allowed transition $k_b=k_c=0$,

$$\Delta E^{\alpha}(0,0)-\Delta E^{\beta}(0,0)=E^{\alpha}(0,0)-E^{\beta}(0,0), \tag{26}$$

$$=4(A+A'), \tag{27}$$

which is analogous to the quantity "8C" CH obtained for the square lattice. Equation (27) is the "Davydov splitting"; as a consequence of the translational symmetry, it does not depend on the B and C interactions. Equation (26) is a consequence of the lack of degeneracy of the ground state [see Eq. (1)].

Before proceeding to second-to-nearest-neighbor interactions, we shall consider the form of the interaction potential V_{lk}. We shall assume, along with Davydov,[5] that it is given by the form[18]

$$V_{lk}=(\mu_l\mu_k/R_{lk}^3)(\cos\theta_{lk}-3\cos\theta_l\cos\theta_k), \tag{28}$$

$$=-(\mu_l\mu_k/R_{lk}^3)\times[2\cos\theta_l\cos\theta_k-\sin\theta_l\sin\theta_k\cos(\phi_l-\phi_k)]. \tag{29}$$

The various angles used in (29) are defined (Fig. 1).

[16] R. D. Burbank, J. Am. Chem. Soc. **75**, 1211 (1953).

[17] Equation (21) is the analog of Eqs. (6)+(8) of Fox and Schnepp.[11]

[18] The terminology in this section is more in keeping with that used in footnote reference 14, than that originally used by Davydov.

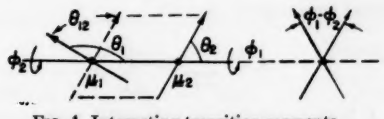

FIG. 1. Interacting transition moments.

The dipole moments μ_i are expanded as a power series in the normal coordinates, with only the first two terms retained, as usual. Again we neglect interactions between *different* normal modes,

$$\mu_i=\mu_i^0+(\partial\mu/\partial Q_i)_0 Q_i. \tag{30}$$

R_{lk} is *assumed* to be the separation of the centers of gravity of the interacting molecules. As a consequence of the properties of integrals of the harmonic oscillator wave functions,[19] we can easily evaluate the interaction integrals A and A'. As an example, by substitution of (29) and (30) into the definition of A, we obtain

$$\begin{aligned}A_i&=(\varphi_p'\varphi_{p+1}\mid V_{p,p+1}\mid\varphi_p\varphi_{p+1}')\\&=KR^{-3}(\varphi_1^*\varphi_0^*\mid[\mu_l^0+(\partial\mu/\partial Q_l)_0Q_l]\\&\qquad\cdot[\mu_k^0+(\partial\mu/\partial Q_k)_0Q_k]\mid\varphi_0\varphi_1)\\&=KR^{-3}\{[\langle1\mid\mu_l^0\mid0\rangle+\langle1\mid(\partial\mu/\partial Q_l)_0Q_l\mid0\rangle]\\&\qquad\cdot[\langle0\mid\mu_k^0\mid1\rangle+\langle0\mid(\partial\mu/\partial Q_k)_0Q_k\mid1\rangle]\}\\&=KR^{-3}\{[(\partial\mu/\partial Q_l)_0\langle1\mid Q_l\mid0\rangle]\\&\qquad\cdot[(\partial\mu/\partial Q_k)_0\langle0\mid Q_k\mid1\rangle]\}\\&=KR^{-3}(\partial\mu/\partial Q_i)^2(2\gamma_i)^{-1}.\end{aligned}\tag{31}$$

In (31), $\gamma_i=4\pi^2\nu_i^0/k$ and ν_i^0 is as defined previously [following (18)]. K is the trigonometric factor of (29) and R is the separation of the centers of gravity of the molecules which share the A interaction. Similar substitution of (29) and (30) into (3) yields (4); the same substitution into (11) leads to the conclusion (*vide supra*) concerning the small magnitude of the shift term, D. The K factor will be the same for all normal modes which belong to the same vibrational species in the isolated molecule, such as the three parallel modes of CH_3Cl, ν_1, ν_2, and ν_3. On combining (27), (31), and a similar relationship for A_i', we obtain the Davydov splitting for each parallel mode i as

$$E_i^\alpha(0,0)-E_i^\beta(0,0)=(\partial\mu/\partial Q_i)^2(2\gamma_i)^{-1}\cdot4(a_i+a_i'), \tag{32}$$

where a_i and a_i' are the appropriate trigonometric factors for the A and A' interactions, divided by the respective factors R_{lk}^3.

The exciton band, bounded by $E^\alpha(0,0)$ and $E^\beta(0,0)$, is usually symmetric about $h\nu_i^0$, as a result of the shift term D being approximately zero. This was observed by Hornig and Hiebert[20] in studies of solid HCl and HBr which also have sheetlike crystal structures, similar to that of CH_3Cl. Our own investigations of CH_3I in CD_3I have demonstrated the same feature, as will be shown. When this is true, $2\nu_i^0$ may be replaced by $\nu_i^\alpha+\nu_i^\beta$. As a result, (32) may be manipulated to yield

$$\lambda_i^\alpha-\lambda_i^\beta=4(\partial\mu/\partial Q_i)^2(a_i+a_i'), \tag{33}$$

where $\lambda_i=4\pi^2\nu_i^2$.

The inclusion of *all* pairwise interactions, however remote, demands the general form[10]

$$\Delta E^{\alpha,\beta}=\Delta w+\mathfrak{D}+\sum_p I_{lp}\pm\sum_m I_{lm}. \tag{34}$$

In (34) Δw has the same significance as before, but $\mathfrak{D}$ is a generalized version of its ancestor D. The first summation is over translatory equivalent molecules and the second summation is over *all* chains of translatory nonequivalent molecules.

In applying (34) to second-to-nearest-neighbor interactions, Fig. 2 will be of help. Aside from the continuation of the A and A' chains, there are four new ones established called, respectively, E and E', F and F'. It is first observed that along the A chain the second-nearest neighbor is translationally equivalent to the molecule at the origin, and it can be easily demonstrated that the interactions of these two molecules makes its contribution to $\sum_p I_{lp}$, and not to $\sum_m I_{lm}$. Nevertheless, within this first shell of neigh-

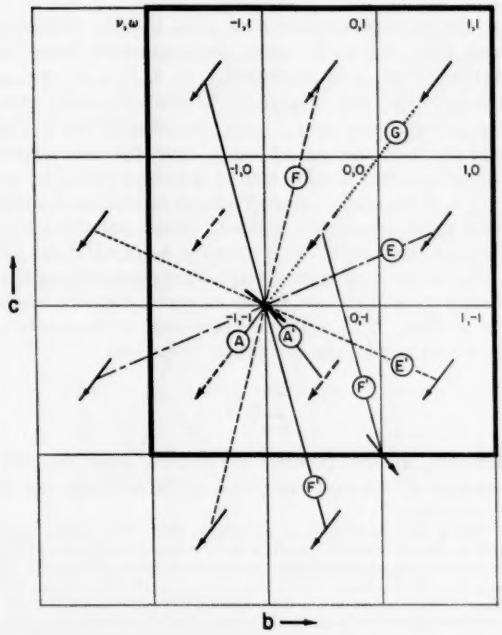

FIG. 2. First-nearest-neighbor unit cells; second-nearest-neighbor intermolecular interactions. [For meaning of E, E', etc., see text.]

[19] Footnote reference 14, p. 290.

[20] D. F. Hornig and G. L. Hiebert, J. Chem. Phys. **27**, 752 (1957).

boring unit cells surrounding the one at the origin, the *next* member of the A chain does contribute to $\sum_m I_{lm}$. The consequent interaction is called G.

On applying (21), it is found that the Davydov splitting, to this approximation, is given by

$$E^{\alpha}(0,0)-E^{\beta}(0,0)$$
$$=(\partial\mu/\partial Q_i)^2\cdot(1/2\gamma_i)[4a_i+4a_i'+2(e+e'+f+f')+2g], \tag{35}$$

or, alternatively,

$$\lambda_i^{\alpha}-\lambda_i^{\beta}$$
$$=(\partial\mu/\partial Q_i)^2[4a_i+4a_i'+2(e+e'+f+f')+2g]. \tag{36}$$

Here e, f, etc. bear the same relationship to E, F, etc. as did a to A and a' to A'.

From simple trigonometry it is learned that

$$e=e' \tag{37}$$

$$f=f'. \tag{38}$$

By virtue of the R_k^{-3} factor of V_{lk}, and the identity of the trigonometric dependencies of the G and A interactions,

$$g=a/27. \tag{39}$$

In a square lattice

$$e+e'+f+f'=0, \tag{40}$$

in addition to

$$a+a'=0. \tag{41}$$

In the rectangular lattice of CH_3Cl, (40) and (41) have finite values. By using the parameters found by Burbank,[16] we have evaluated a, a', e, e', f, f', and g. The results are $4(a+a)'=4.520\times10^{22}$ cm^{-3} and $4(a+a')+2(e+e'+f+f')+2g=4.222\times10^{22}$ cm^{-3}. The next cycle of cells (ν or $\omega=\pm2$) modifies the trigonometric term to the sum $4(a+a'+e+e'+f+f'+g+g')$, if we neglect all new chains encountered other than those previously defined, except for $g'=a'/27$. The numerical value of this sum is 4.424×10^{22} cm^{-3}.[21]

The inclusion of more distant interactions will hardly change these numbers. As an example, consider again the A chain. If all of its members were to be counted, we should require the evaluation of the sum

$$\sum_{n=1}^{\infty}n^{-3}.$$

However, as was pointed out earlier, only the odd members of this sum contribute to the splitting, hence the actual sum needed is

$$KR^{-3}\sum_{n=1}^{\infty}(2n-1)^{-3},$$

where K is the constant trigonometric parameter of the chain and R is the separation of the first member from the origin. The sum

$$\sum_{n=1}^{\infty}(2n-1)^{-3},$$

may be shown to be, in the limit, $\frac{7}{8}$ of the sum

$$\sum_{n=1}^{\infty}n^{-3}.$$

Furthermore, the latter sum, while it cannot be put in closed form, can be shown to be $1.20205690\cdots$.[22] It can be easily shown that the sum

$$\sum_{n=1}^{2}(2n-1)^{-3}$$

is within 1% of

$$\tfrac{7}{8}\sum_{n=1}^{\infty}n^{-3}.$$

Accordingly there seems to be no reason for extending our calculations to further members of these chains. Indeed, the next member of the E chain is not encountered until the cell $\nu=3$, $\omega=1$ is reached, while the next member of the F chain is met at cell $\nu=1$, $\omega=5$. Finally, were the sheet continuous and isotropic, we could replace these sums by integrals over R. The population of any one shell at radius R would then be $2\pi RdR$ and the total interaction integral will be of the form

$$\int_1^{\infty}R^{-2}dR,$$

which is unity. Thus there need be no great concern over the divergence of the total interaction as $R\to\infty$.

The values of λ_i^{α} and λ_i^{β} were calculated from data on ν_1 and ν_2 of CH_3Cl obtained by Dr. Marilyn E. Jacox.[23] Because of the difficulty with the interpretation of ν_3 discussed by Dows, Dr. Jacox obtained λ_3^{α} and λ_3^{β} from a study of CH_3Cl^{35}. The results are given in Table I and are compared with those of Dickson *et al.*[24] The values of $|\partial\mu/\partial Q_i|$ (crystal) have been calculated using the geometric factor obtained when the nearest intersheet pair interactions are included. The dimensions of the $|\partial\mu/\partial Q_i|$ reported here differ from those used by Dickson *et al.*[24] because of a trivial difference in the definition of the dimensions of the electric moment.

[21] While the idealization of an infinite sheet crystal has been used, we should examine the effect of including at least some of the interactions between molecules in different sheets. When this is done, the contribution of the nearest pairs is such as to change the geometric factor just given from 4.424×10^{22} cm^{-3} to 4.428×10^{22} cm^{-3}. The effect of this change is to decrease the calculated dipole derivatives by less than 1% from the values derived by neglecting such interactions. All other intersheet pairs contribute considerably less. Consequently the infinite sheet idealization is a good approximation.

[22] K. Knopp, *Theory and Application of Infinite Series* (Hafner Publishing Company, New York, 1947), p. 554.

[23] I am indebted to Dr. Jacox for this data.

[24] A. D. Dickson, I. M. Mills, and B. Crawford, J. Chem. Phys. **27**, 445 (1957).

TABLE I.

	Crystal	Gas	Crystal/Gas
$\lvert \partial\mu/\partial Q_1 \rvert$	180 esu/g$^{\frac{1}{2}}$	56.3 esu/g$^{\frac{1}{2}}$ cm	3.19
$\lvert \partial\mu/\partial Q_2 \rvert$	149	31.6	4.71
$\lvert \partial\mu/\partial Q_3 \rvert$	82.2	57.5	1.43

EFFECT OF ISOTOPIC SUBSTITUTION ON CORRELATION FIELD SPLITTING

It has been previously claimed,[4] on the basis of the data of Mador and Quinn,[25] that CH_3I and CH_3Cl are isomorphous. Dows' observation of the quartet-structure of ν_5 of CH_3I completely obviates this crystal structural assignment and henceforth there is no basis for interpreting the spectrum of CH_3I in this light.

Figure 3 illustrates $\nu_5^{CH_3I}$ in a CD_3I solution. There is no doubt that the large separation in the quartet ($\sim$25 cm^{-1}) is due to the local field, or site group, effect and that the smaller splitting ($\sim$5 cm^{-1}) is due to the correlation field. Figure 4 illustrates $\nu_5^{CD_3I}$ in pure CD_3I. At a spectral resolution of less than 0.6 cm^{-1}, there is no evidence of a quartet. The CD_3I used in this experiment was 98.78% pure,[26] the impurities being $\sim$1% CD_2HI and $\sim$0.1% CDH_2I. At these concentrations, the correlation field splitting should be hardly changed.

Because of the proportionality of the splitting, $h\Delta\nu$, to the factor $(\partial\mu/\partial Q_j)^2\gamma_j^{-1}$, as indicated by (32) and (35), it follows that

$$\Delta\nu_j/\Delta\nu_j{}^i=(\nu_{j,0}{}^i/\nu_{j,0})\,(p_j/p_j{}^i)^2, \tag{42}$$

where $p=\partial\mu/\partial Q$ and the superscript denotes the indicated quantities of the isotopically substituted molecule. This relationship has been separately derived by Dows.[27] It is well known that the dipole derivatives p_j change upon isotopic substitution,[24] hence as indicated by (42), the effect first noted with ν_5 of CD_3I is to be expected.

Upon any amount of isotopic dilution, a complicated distribution of sizes of clusters of "light" and "heavy" molecules is created. For a one dimensional crystal this distribution is the Flory distribution.[28] For two- and three-dimensional crystals, the analogous problem has never been solved. Nevertheless, in a one-to-one solid solution of a molecule and its isotopically substituted modification, the distributions for each kind of molecule must be identical. As $(p_j/p_j{}^i)^2$ is identically the ratio of the intensity of the jth fundamental of a molecule to that of the same fundamental of the isotopically substituted molecule, (42) may be tested by measuring the splittings $\Delta\nu_j$ and $\Delta\nu_j{}^i$ in the pure solids, the mean frequencies $\nu_{j,0}$ and $\nu_{j,0}{}^i$ in the one-to-one mixture and the relative intensities $I_j/I_j{}^i$ in the same mixture. It is important, of course, that the isotopic substitution does not change the symmetry of the molecule.

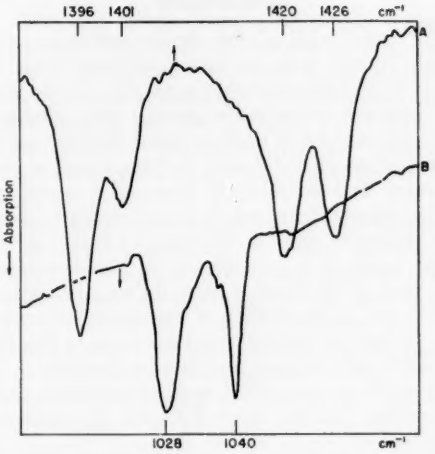

FIG. 4. Curve A, ν_5 of CH_3I solid; curve B, ν_5 of CD_3I solid.

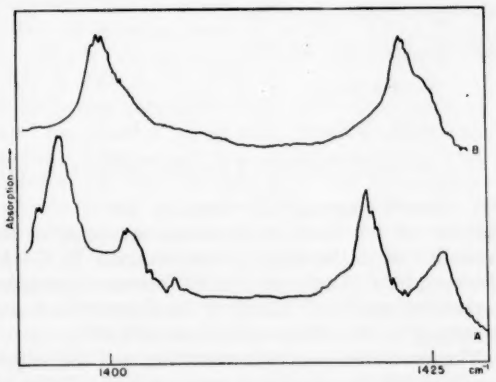

FIG. 3. ν_5 of CH_3I: curve A, pure CH_3I solid; curve B, in a CD_3I solution (10 mole% CH_3I).

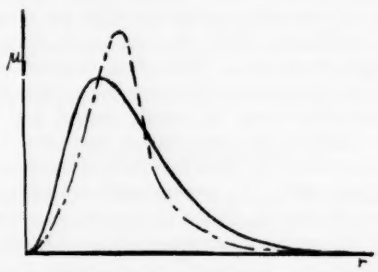

FIG. 5. Change of dipole moment vs internuclear separation (schematic). ——— gas; – – – – condensed phase.

[25] I. L. Mador and R. S. Quinn, J. Chem. Phys. **20,** 1837 (1952).
[26] We are indebted to Dr. W. H. Hamill of the University of Notre Dame for this analysis.
[27] D. A. Dows (private communication).
[28] P. J. Flory, J. Am. Chem. Soc. **58,** 1877 (1936).

DISCUSSION

The magnitudes of the dipole derivatives found (Table I) may seem at first surprisingly large. The values range from somewhat more than one to almost five times the values in the gaseous state. Similar enhancement was found by Hornig and Hiebert[20] for HCl. On the other hand, we note that the coupling theory presented here is stated in terms of a considerable modification of the system's wave functions. That we can continue to speak of the quantity $\partial\mu/\partial Q$ on a molecular basis is a consequence of the translational symmetry of the crystal. Nevertheless, the electronic distribution in the vicinity of any molecular center is changed upon crystallization. The change in the dipole derivative reflects the change in wave function.

Coulson[29] has proposed a mechanism for this change by recalling that the strict definition of a molecule's dipole moment is

$$\mu=\int \mathbf{r}\rho(\mathbf{r})\,d\tau, \tag{43}$$

where $\rho(\mathbf{r})$ is the charge density of the molecule at the terminus of the vector $\mathbf{r}$ from the origin. If we choose the origin at the center of mass of the molecule, we conclude that small changes in $\rho(\mathbf{r})$ at the periphery of the molecule will make large changes in μ and likewise in its derivative. It is easily shown that (43) is invariant to translation of the origin, provided the molecule has no net charge. While condensation may change[30] the total dipole moment of the molecule by, say, 10%, it is at least as reasonable that the dipole derivative may be more strongly affected. A possible illustration of such a situation is shown in Fig. 5.[31]

Enhancement of the dipole derivative should be accompanied by a similar enhancement of the absorption intensity, as indicated by (42). Recent studies by Person and Swenson[32] indicate a threefold *decrease* in the total absolute intensity of the infrared spectrum of benzene upon crystallization. The changes in p_j given in Table I are inconsistent with this observation.

Because of the resonant nature of the assumed coupling law, it is worthwhile to compare the intensity of a gas of uncoupled oscillators with one of pairwise coupled oscillators, where the coupling is via a transition-dipole interaction. While this problem is often treated in elementary quantum-mechanics treatises, the interaction *energy* is usually sought and is also usually obtained by perturbation methods. For the present purposes, the wave functions of the ground and first excited states of a coupled pair of oscillators are necessary, in order to obtain the transition probability.

The wave equation for two coupled oscillators, where the coupling force varies as $C(x-y)$, where x and y are the individual oscillator positions, is the only separable Schrödinger equation for the motion of interacting particles.[33] If the intramolecular and intermolecular force constants are denoted, respectively, by K and C, the wave equation may be easily shown to take the form

$$(\hbar^2/2M)[(\partial^2\psi/\partial x^2)+(\partial^2\psi/\partial y^2)]$$
$$+[E-\tfrac{1}{2}(K+C)(x^2+y^2)+Cxy]\psi=0. \tag{44}$$

With the substitutions

$$C=-2fe^2/R^3, \qquad K+C=K',$$

where f is an oscillator strength, e the electronic charge, and R the intermolecular distance, (44) assumes the form usually utilized in primitive van der Waals energy calculations,

$$(\hbar^2/2M)[(\partial^2\psi/\partial x^2)+(\partial^2\psi/\partial y^2)]$$
$$+[E-(K'/2)(x^2+y^2)-(2fe^2/R^3)xy]\psi=0. \tag{45}$$

The solution of (44) is[33]

$$\psi_{mn}(\xi,\eta)=\frac{(\beta\beta_+)^{1/4}}{(\pi 2^{m+n}m!n!)^{\frac{1}{2}}}$$
$$\times\exp(-\tfrac{1}{2}\beta\xi^2-\tfrac{1}{2}\beta_+\eta^2)H_m(\xi\beta^{\frac{1}{2}})H_n(\eta\beta_+^{\frac{1}{2}}) \tag{46}$$

where $\beta^2=MK/\hbar^2$, $\beta_+^2=MK'/\hbar^2$, $\xi=2^{-\frac{1}{2}}(x+y)$, $\eta=2^{-\frac{1}{2}}(x-y)$, and the $H_m(\xi\beta^{\frac{1}{2}})$ and $H_n(\eta\beta_+^{\frac{1}{2}})$ are Hermite polynomials of degree m and n, respectively. On using the definitions

$$I_1=\iint\psi_{00}\xi\psi_{10}d\xi d\eta, \qquad I_2=\iint\psi_{00}\eta\psi_{01}d\xi d\eta,$$

and

$$I_0=\int\psi_{0x}x\psi_{1x}dx,$$

where the latter is the $(1\leftarrow 0)$ matrix element for the uncoupled oscillator, we find

$$\Delta I^2/I_0^2=(I_1^2+I_2^2-I_0^2)/I_0^2$$
$$=(\beta/\beta_+)-1$$
$$=(K/K')^{\frac{1}{2}}-1$$
$$=-\tfrac{1}{2}(C/K)+\tfrac{3}{8}(C/K)^2-\tfrac{1}{16}(C/K)^3+\cdots. \tag{47}$$

We observe that $\Delta I^2/I_0^2$ vanishes for $C=0$. Also $\Delta I^2/I_0^2\to\infty$ for $C\to K$. In addition, according to the definition of C, for large f and/or small R, $C\to K$; however, for $C/K=0.1$, only a 5% increase in intensity is predicted and for $C/K\cong 10^{-3}$,[34] the intensity increases according to (47) will be of the order of 0.05%.

The inconsistency of this prediction, and the magnitudes of the dipole derivatives obtained (Table I) (and of Person's and Swenson's results) is difficult to

[29] C. A. Coulson, Spectrochim. Acta **14**, 161 (1959).
[30] C. P. Smyth, *Dielectric Behavior and Structure* (McGraw-Hill Book Company, Inc., New York, 1955), p. 48.
[31] We are grateful to Dr. A. D. Buckingham for this example.
[32] W. B. Person and C. A. Swenson (private communication).
[33] P. M. Morse and H. Feshbach, *Methods of Theoretical Physics* (McGraw-Hill Book Company, Inc., New York, 1953), p. 1718.
[34] It can be shown, using (19) and (32), that this is the order of magnitude of the ratio C/K.

reconcile. The assumption that the oscillators interact solely via a transition dipole mechanism should, of course, be questioned. Calculations of the dipole energy and of the total electrostatic energy of, for example, a pair of HCl molecules 3 A apart shows that the dipole energy is a good approximation for the total electrostatic energy. Considering the slight changes in the distances during vibration, the transition-dipole interaction should be a suitable model.

In the original development of this theory by Davydov,[8] the additional effect of interaction between higher multipoles is treated. The interaction between two 2 l-pole moments of course varies with $R^{-(2l+1)}$ so that further terms in the multipole expansion should be far less important than the dipole-dipole term. Davydov[8] also treats the contribution of changes in the exchange repulsion forces. These are functions of the intramolecular normal coordinates, and hence also change in the course of a molecular vibration; however, as the exchange repulsion energy is usually assumed to have an exponential dependence on the intermolecular separation, and as this can be approximated, in the region of the usual intermolecular distances in crystals by a function which falls off with distance not slower than R^{-9}, it should hardly be of the importance of the transition dipole interaction.

Dows[35] has pointed out that in methyl chloride the hydrogen atoms are considerably closer than the molecular centers, so that the changes in the exchange repulsion forces between the hydrogen atoms may form another basis for calculation of correlation field splittings. To do this, Dows uses de Boer's functions for the exchange repulsion energy[36] for the several atoms involved in the interactions of two hydrogen molecules. The parameters of de Boer's function were obtained from direct calculation of Coulomb and exchange integrals for hydrogen atoms by Hirschfelder and Weygandt.[37] De Boer finds these parameters suitable for H···H distances from $4a_0$ to $10a_0$ (2.12–5.29 A). The closest (intermolecular) H···H distance in CH_3Cl is 2.87 A. In order to compare the over-all intermolecular potential energy with experiment, de Boer[36] has found a power series representation of the exponential form which has explicit trigonometric dependence, but which is valid only over the range $6a_0$ to $8a_0$ (3.15–4.23 A) and which is not at all valid for particular intermolecular orientations. To the spatial average of this function reasonable r^{-6} and r^{-8} dispersion energies are added and the results are compared with a Lennard-Jones potential with force constants obtained from the second virial coefficient of H_2 gas at low density. As this data rarely gives reliable values for the energy in the repulsive region (H···H distance less than 3 A) and as the angular dependent exchange repulsion function used by de Boer was not intended to be of great accuracy in this region, the parameters of de Boer's exponential exchange repulsion should not be expected to apply in solid CH_3Cl. In Dows'[35] use of the repulsive potential to account for the correlation splittings he suggests an amendment of the de Boer parameters.

Balescu[38] has derived a modification of the Lennard-Jones potential *for molecules* which has the virtue of accounting for a number of thermodynamic properties of molecules which are markedly different from those of monatomic substances.[39] Balescu expresses the interaction of a pair of molecules in terms of the n^2 interactions of each molecule's n peripheral atoms, wherein the latter interactions are assumed to be given by a (6–12) potential. The resultant molecular interaction is no longer of the simple (6–12) form. As an example, for a fluid of symmetrical tetrahedral molecules, the first corrective terms include an r^{-8} attractive term and an r^{-14} repulsive term. The result is mainly the *enhancement of the repulsive term*, especially at small intermolecular distances. Accordingly, the *fitting* of a (6–12) potential to virial coefficient data does not justify a theoretical intermolecular potential curve which may be in agreement with it.

CONCLUSIONS

The ease of manipulation of the vibrational exciton theory presented here, with few approximations (other than first-order perturbation theory) makes for an infectious confidence in its ultimate results. Nevertheless, there is at present no conclusive demonstration of the origin of correlation field splittings. No doubt both transition dipolar interaction and exchange repulsion should be treated in a unified manner. The observation of an isotope effect on a correlation field splitting has been quantitatively rationalized with the transition dipole model. To further test this theory of these splittings, isotope effects upon the relative intensities of fundamentals of small molecules in one-to-one solid solutions with their isotopic modifications will be of great value. In addition the progress of this area of molecular spectroscopy would be immeasurably advanced were there available more known crystal structures of small polyatomic molecules than merely that of CH_3Cl.

ACKNOWLEDGMENTS

It is the author's pleasure to gratefully acknowledge the many discussions and correspondence he has had concerning this subject with Professor W. B. Person, Professor D. A. Dows, and Professor J. C. Decius.

[35] D. A. Dows, J. Chem. Phys. **32,** 1342 (1960).
[36] J. de Boer, Physica **9,** 363 (1942).
[37] J. O. Hirschfelder and C. N. Weygandt, J. Chem. Phys. **6,** 806 (1938).
[38] R. Balescu, Physica **22,** 224 (1956).
[39] I. Prigogine, *The Molecular Theory of Solutions* (North-Holland Publishing Company, Amsterdam, 1957), Chap. XIII.

THE JOURNAL OF CHEMICAL PHYSICS VOLUME 33, NUMBER 6 DECEMBER, 1960

Proton Spin Coupling by Pi Electrons

MARTIN KARPLUS*

Noyes Chemical Laboratory, University of Illinois, Urbana, Illinois

(Received June 6, 1960)

A theoretical formulation is developed for the pi-electron contribution, $A_{HH'}(\pi)$, to the spin coupling between pairs of protons in hydrocarbon molecules. By means of the correspondence between the σ–π interaction in unsaturated molecules and related free radicals, the proton spin coupling is expressed in terms of hyperfine constants and triplet state energies. With known values for these quantities, $A_{HH'}(\pi)$ is found to be in agreement with experimental measurements available for molecules in which the pi electrons are expected to dominate the coupling. Of particular interest are the large couplings (1.3–8 cps) calculated for certain systems with protons separated by three or four carbon atoms. Also absolute signs are predicted by the theory, with $A_{HH'}(\pi)$ equal to -6.7 cps for allene and $+7.8$ cps for butatriene.

INTRODUCTION

THE theoretical study of chemical shifts and spin-coupling constants measured by NMR[1] is of considerable interest because of the intimate connection between these parameters and the molecular electron distribution. Although exact calculations will have to await the availability of accurate wave functions, approximate methods can serve to provide a framework for the interpretation of the experimental results. One such method is the valence-bond theory which has been applied to the coupling constants in saturated hydrocarbons.[2] For pairs of protons on the same carbon atom or adjacent carbon atoms, a second-order perturbation calculation has yielded results in reasonable agreement with the measured values. Further, a sensitive dependence of the coupling constant on structural parameters (HCH′ angle,[3] HCC′/CC′H′ dihedral angle[4]) was predicted by the theory and verified by experiment. The same valence-bond treatment has been used also for vicinal protons in unsaturated molecules,[4] such as ethylene and substituted benzenes. Only the sigma electrons were considered and their deviations from perfect pairing were shown to provide the dominant contribution to the coupling constants, which are equal to +5–11 cps for *cis*-protons and +10–18 cps for *trans*-protons.

From recent measurements on unsaturated molecules, coupling constants for protons three or four carbons apart (HCCCH′ and HCCCCH′) have been found to be in the range 1.3 to 7 cps.[5] Since the sigma-electron contribution is expected to be less than 0.5 cps for such protons, the question of the origin of the large coupling constants has focused attention on the pi electrons.[6] For aromatic molecules, McConnell[7a] has considered the pi-electron terms and estimated that their contribution is only on the order of 0.5 cps for vicinal protons and even less for those separated by a larger number of carbon atoms. Since this conclusion is not necessarily applicable to the nonaromatic compounds in which the surprisingly large coupling constants were observed, a reexamination of the pi-electron terms is desirable.

In this paper a second-order perturbation treatment is developed for the calculation of the pi-electron contribution to the proton coupling constant. The coupling interaction between the protons and the pi orbitals is shown to arise from σ-π exchange terms in the Hamiltonian operator. Recognition of the correspondence between these exchange terms and those occurring in related pi-electron radicals makes possible a considerable simplification of the theory. The resulting formulation is applied to a number of pi-electron systems. Both the magnitude and sign of the proton coupling constants are determined and compared with the available experimental measurements.

THEORETICAL FORMULATION

For a pair of protons (H, H′) in a $^1\Sigma$ molecule, the nuclear spin interaction energy can be written in the

* Alfred P. Sloan Foundation Fellow. Present address: Columbia University, New York, New York.

[1] J. A. Pople, W. G. Schneider, and H. J. Bernstein, *High Resolution Nuclear Magnetic Resonance* (McGraw-Hill Book Company, Inc., New York, 1959).

[2] M. Karplus, D. H. Anderson, T. C. Farrar, and H. S. Gutowsky, J. Chem. Phys. **27,** 597 (1957); M. Karplus and D. H. Anderson, *ibid.* **30,** 6 (1959); S. Alexander, Bull. Research Council Israel **7F,** 95 (1958); E. Hiroike, J. Phys. Soc. Japan **15,** 270 (1959).

[3] H. S. Gutowsky, M. Karplus, and D. M. Grant, J. Chem. Phys. **31,** 1278 (1959).

[4] M. Karplus, J. Chem. Phys. **30,** 11 (1959). In this reference, as well as the papers of footnote references 2 and 3, a mean excitation energy approximation was introduced, which has recently been questioned by A. D. McLachlan [J. Chem. Phys. **32,** 1263 (1960)]. It has been shown [M. Karplus, *ibid.* **33,** 941 (1960)] that a perturbation procedure corresponding to that employed here for pi electrons can be used to justify the mean excitation energy approximation for the systems to which it has been applied.

[5] See Table II for references to the measured values.

[6] R. A. Hoffman, Mol. Phys. **1,** 326 (1958); E. B. Whipple, J. H. Goldstein, and W. E. Stewart, J. Am. Chem. Soc. **81,** 4761 (1959); M. Kreevoy (private communication).

[7] (a) H. M. McConnell, J. Mol. Spectroscopy **1,** 11 (1957); J. Chem. Phys. **30,** 126 (1959); (b) T. P. Das (private communication) has used a related method for the carbon-hydrogen σ-bond coupling.

form[8]

$$\Delta E_{HH'}=2\sum_T \frac{\langle\Psi_S \mid \xi\sum_k\delta(\mathbf{r}_{kH})\mathbf{S}_k\cdot\mathbf{I}_H \mid \Psi_T\rangle\langle\Psi_T \mid \xi\sum_l\delta(\mathbf{r}_{lH'})\mathbf{S}_l\cdot\mathbf{I}_{H'} \mid \Psi_S\rangle}{E_S-E_T}, \quad (1)$$

where $\xi=(8\pi\beta_e\beta_N g_e g_H/3)$, Ψ_S and Ψ_T are ground-state singlet and excited-state triplet wave functions with energies E_S and E_T, respectively, and the other symbols conform to the standard notation. Of the several terms in the molecular Hamiltonian that lead to coupling between nuclear spins, we have included only the contact term because it is known to make the dominant contribution for protons.[8,9] From Eq. (1) the isotropic coupling $A_{HH'}$, which is the quantity that is generally measured in solution NMR, can be written

$$A_{HH'}=(2/3h)\sum_T \frac{\langle\Psi_S \mid \xi\sum_k\delta(\mathbf{r}_{kH})\mathbf{S}_k \mid \Psi_T\rangle\cdot\langle\Psi_T \mid \xi\sum_l\delta(\mathbf{r}_{lH'})\mathbf{S}_l \mid \Psi_S\rangle}{E_S-E_T}. \quad (2)$$

For a determination of $A_{HH'}(\pi)$, the pi-electron contribution to the coupling constant $A_{HH'}$, the wave functions Ψ_S and Ψ_T must be expressible in a form that separates sigma and pi electrons. Such a separation requires that the σ-π exchange interaction is small compared to the σ-σ and π-π energy terms in the molecule.[10] Since this is a basic assumption in the usual treatment of the pi-electron spectra of aromatic molecules, it has been discussed rather frequently. A lucid formulation of the "pi-electron approximation," which is utilized in the development of this paper, has been given by Lykos and Parr.[11] Neglecting the σ-π exchange terms, we approximate Ψ_S by the function ψ_{0s} of the form

$$\psi_{0s}={}^1\Sigma(1, 2, \cdots, n_a)\ {}^1\Pi(n_{a+1}, n_{a+2}, \cdots, n)\ ({}^1\Sigma\,{}^1\Pi)_s. \quad (3)$$

Here ${}^1\Sigma(1, 2, \cdots, n_a)$ is an antisymmetric singlet function of the coordinates of the n_a sigma electrons and ${}^1\Pi(n_{a+1}, n_{a+2}, \cdots, n)$ is an antisymmetric singlet function for the $(n-n_a)$ pi electrons. The product function ψ_{0s}, which is not antisymmetric with respect to interchange of sigma and pi electrons, is taken to be the lowest energy eigenfunction of the molecular n-electron Hamiltonian,

$$\mathcal{H}=\mathcal{H}(\sigma)+\mathcal{H}(\pi)+\sum_{\sigma,\pi}(e^2/r_{\sigma\pi}), \quad (4)$$

where $\mathcal{H}(\sigma)$ and $\mathcal{H}(\pi)$ are, respectively, the complete sigma-electron and pi-electron Hamiltonian operators (without nuclear spin interactions) and the sum over σ, π corresponds to the Coulomb repulsion between the sigma and pi electrons. The function ${}^1\Sigma$ includes, in principle, all of the sigma-electron correlation, but only an average Hartree-type interaction with the pi electrons, as is evident from the simple product used for ψ_{0s} in Eq. (3); a similar statement applies to the ${}^1\Pi$ function. With the neglect of σ-π exchange, we can write the corresponding eigenfunctions of $\mathcal{H}$ that involve spin excitations in the form $\psi_{0t}\sim({}^1\Sigma\,{}^3\Pi)_t$, $({}^3\Sigma\,{}^1\Pi)_t$, etc.

In all cases considered here, the orbitals on the protons H and H′ whose coupling is being determined are taken to be part of the sigma-electron system; e.g., the methyl protons of methyl acetylene are classified as part of the sigma system, with the pi designation restricted to the four pi electrons in the C—C triple bond. Consequently, an accurate calculation of $A_{HH'}(\sigma)$, the sigma contribution to the coupling constant, can be made directly by substitution of ψ_{0s} for Ψ_S and the sigma-electron triplets $({}^3\Sigma\,{}^1\Pi)_t$ for Ψ_T in Eq. (2). By integrating out the pi-electron terms, we obtain

$$A_{HH'}(\sigma)=(2/3h)\sum_t \frac{\langle({}^1\Sigma)_s \mid \xi\sum_k\delta(\mathbf{r}_{kH})\mathbf{S}_k \mid ({}^3\Sigma)_t\rangle\cdot\langle({}^3\Sigma)_t \mid \xi\sum_l\delta(\mathbf{r}_{lH'})\mathbf{S}_l \mid ({}^1\Sigma)_s\rangle}{E_s^0-E_t^0}, \quad (5)$$

where $E_s^0-E_t^0$ is the zero-order energy corresponding to the excitation from ψ_{0s} to ψ_{0t}. With the function ${}^1\Sigma$ approximated by a valence-bond expression and the perturbation sum reduced by the average energy approximation, Eq. (5) has been used previously for ethylenic systems.[4]

An attempt to obtain $A_{HH'}(\pi)$ by the corresponding procedure of introducing the functions $({}^1\Sigma\,{}^1\Pi)_s$ and $({}^1\Sigma\,{}^3\Pi)_t$ for Ψ_S and Ψ_T, respectively, in Eq. (2) would yield a completely meaningless result [$A_{HH'}(\pi)\cong 0$ cps]. This follows from the fact that the correlation between the spins of sigma and pi electrons, which is essential to the sigma-proton coupling, has been neglected in constructing the functions ψ_{0s} and ψ_{0t}. To introduce the required spin correlation, a perturbation treatment of the σ-π exchange interaction can be employed. We write the exchange perturbation oper-

[8] N. F. Ramsey, Phys. Rev. **91,** 303 (1953).
[9] M. J. Stephens, Proc. Roy. Soc. (London) **A243,** 274 (1957); E. Ishiguro, Phys. Rev. **111,** 203 (1958).
[10] R. McWeeny, Proc. Roy. Soc. (London) **A223,** 306 (1954); **A237,** 358 (1956).
[11] P. J. Lykos and R. G. Parr, J. Chem. Phys. **24,** 1166 (1956).

ator $\mathcal{H}_{\sigma\pi}'$ in the form

$$\mathcal{H}_{\sigma\pi}'=-\sum_{\sigma,\pi}(e^2/r_{\sigma\pi})\,P_{\sigma\pi}, \tag{6}$$

where the sum over σ, π ranges over all the sigma and pi electrons and $P_{\sigma\pi}$ is the transposition operator for each pair. The first-order singlet function ψ_{1s} is given by the equation

$$\psi_{1s}=\psi_{0s}+\sum_{s'}\frac{\langle\psi_{0s'}\,|\,\mathcal{H}_{\sigma\pi}'\,|\,\psi_{0s}\rangle}{E_s^0-E_{s'}{}^0}\psi_{0s'} \tag{7}$$

and, correspondingly, the first-order triplet functions ψ_{1t} are

$$\psi_{1t}=\psi_{0t}+\sum_{t'}\frac{\langle\psi_{0t'}\,|\,\mathcal{H}_{\sigma\pi}'\,|\,\psi_{0t}\rangle}{E_t^0-E_{t'}{}^0}\psi_{0t'}. \tag{8}$$

Here E_s^0, $E_{s'}{}^0$ and E_t^0, $E_{t'}{}^0$ represent the zero-order energies of the functions ψ_{0s}, $\psi_{0s'}$ and ψ_{0t}, $\psi_{0t'}$, respectively. Substituting ψ_{1s} and ψ_{1t} for a typical matrix element of Eq. (2), we have, to second-order,

$$\langle\Psi_S\,|\,\xi\sum_k\delta(\mathbf{r}_{kH})\mathbf{S}_k\,|\,\Psi_T\rangle=\sum_{s'}\frac{\langle\psi_{0s}\,|\,\mathcal{H}_{\sigma\pi}'\,|\,\psi_{0s'}\rangle\langle\psi_{0s'}\,|\,\xi\sum_k\delta(\mathbf{r}_{kH})\mathbf{S}_k\,|\,\psi_{0t}\rangle}{E_s^0-E_{s'}{}^0}$$
$$+\sum_{t'}\frac{\langle\psi_{0s}\,|\,\xi\sum_k\delta(\mathbf{r}_{kH})\mathbf{S}_k\,|\,\psi_{0t'}\rangle\langle\psi_{0t'}\,|\,\mathcal{H}_{\sigma\pi}'\,|\,\psi_{0t}\rangle}{E_t^0-E_{t'}{}^0}. \tag{9}$$

To simplify Eq. (9), we have to consider the form of the functions and operators involved. The function ψ_{0s} is given by Eq. (3) and the triplets ψ_{0t} that contribute to the pi-electron coupling are of the form $(^1\Sigma\,{}^3\Pi)_t$. Since the direct overlap of pi orbitals with the coupled protons is negligibly small and the operator

$$[\xi\sum_k\delta(\mathbf{r}_{kH})\mathbf{S}_k]$$

is nonzero only for matrix elements between sigma-electron singlet and triplet functions, the states $\psi_{0s'}$ and $\psi_{0t'}$ that have to be included in the perturbation sum are given by the expressions

$$\psi_{0s'}=(^3\Sigma\,{}^3\Pi)_{s'},\qquad \psi_{0t'}=(^3\Sigma\,{}^1\Pi)_{t'}. \tag{10}$$

On introducing these into Eq. (9) and integrating out the pi-electron functions in the spin matrix elements, we obtain

$$\langle\Psi_S\,|\,\xi\sum_k\delta(\mathbf{r}_{kH})\mathbf{S}_k\,|\,\Psi_T\rangle=\sum_{s'}\frac{\langle(^1\Sigma\,{}^1\Pi)_s\,|\,\mathcal{H}_{\sigma\pi}'\,|\,(^3\Sigma\,{}^3\Pi)_{s'}\rangle\langle(^3\Sigma)_{s'}\,|\,\xi\sum_k\delta(\mathbf{r}_{kH})\mathbf{S}_k\,|\,(^1\Sigma)_t\rangle}{E_s^0-E_{s'}{}^0}$$
$$+\sum_{t'}\frac{\langle(^1\Sigma)_s\,|\,\xi\sum_k\delta(\mathbf{r}_{kH})\mathbf{S}_k\,|\,(^3\Sigma)_{t'}\rangle\langle(^3\Sigma\,{}^1\Pi)_{t'}\,|\,\mathcal{H}_{\sigma\pi}'\,|\,(^1\Sigma\,{}^3\Pi)_t\rangle}{E_t^0-E_{t'}{}^0}. \tag{11}$$

Since the exact form of the wave functions in Eq. (11) depends on the particular molecule under consideration, a separate calculation appears to be required for each case; however, a more general treatment is possible for systems in which the functions $\psi_{0s'}$ and $\psi_{0t'}$ can be expressed in terms of a localized bond description. In the valence-bond approach, this would require that deviations from perfect pairing be small; in molecular-orbital theory, an equivalent orbital approximation would have to be valid. With this restriction it is possible to classify the $^3\Pi$ states in terms of broken pi bonds and to determine the σ-π interactions from localized fragment models. For the molecules of interest here, only two types of fragments have to be considered. One contains a proton bonded to a carbon that forms a pi bond (H—C′=C″···) and the other has a methyl or methylene proton next to a pi bond (H—C—C′=C″···). In both fragments, the important $^3\Pi$ function is the one with the pair of pi electrons in the carbon-carbon double-bond forming a triplet. To obtain an estimate of the σ-π interaction, the HC′=C″ fragment could be treated as a four-electron problem (two electrons in the H—C′ σ-bond and two in the C′—C″ π-bond or triplet) and the HCC′=C″ fragment as composed of six electrons (two in the H—C σ-bond, two in the C—C′ σ-bond, and two in the C′—C″ π-bond or triplet).

Rather than performing the $\mathcal{H}_{\sigma\pi}'$ perturbation calculation for the fragments, we develop a device similar to that assumed valid by McConnell in his study of aromatic compounds.[7a,b] This is based on an approximate relationship between the fragment matrix elements required for Eq. (11) and the proton hyperfine splitting in the pi-electron radicals formed by "removing" one electron from the fragments (the pi electron of C″ in H—C′=C″ and H—C—C′=C″). For these radicals the ground state is the doublet function Ψ_D, which leads to a hyperfine matrix element of the form $\langle\Psi_D\,|\,\xi\sum_k\delta(\mathbf{r}_{kH})S_{zk}\,|\,\Psi_D\rangle$. The zero-order approximation ψ_{0d} to Ψ_D is the function $(^1\Sigma\,{}^2\Pi)_d$. By means of the perturbation operator $\mathcal{H}_{\sigma\pi}'$, excited states

$\psi_{0d'}$ are introduced and we can write the first-order doublet function ψ_{1d} in the form

$$\psi_{1d}=\psi_{0d}+\sum_{d'}\frac{\langle\psi_{0d'}\mid 3\mathcal{C}_{\sigma\pi}'\mid\psi_{0d}\rangle}{E_d^0-E_{d'}^0}\psi_{0d'}, \tag{12}$$

where E_d^0 and $E_{d'}^0$ are the zero-order doublet state energies. To calculate the hyperfine splitting only the functions $\psi_{0d'}$ of the form $(^3\Sigma\,^2\Pi)_{d'}$ have to be included in the perturbation sum. Substitution of these into the usual strong field matrix element leads to the expression

$$\langle\Psi_D\mid\xi\sum_k\delta(\mathbf{r}_{kH})\,S_{kz}\mid\Psi_D\rangle=2\sum_{d'}\frac{\langle(^1\Sigma\,^2\Pi)_d\mid 3\mathcal{C}_{\sigma\pi}'\mid(^3\Sigma\,^2\Pi)_{d'}\rangle\langle(^3\Sigma)_{d'}\mid\xi\sum_k\delta(\mathbf{r}_{kH})\,S_{kz}\mid(^1\Sigma)_d\rangle}{E_d^0-E_{d'}^0}. \tag{13}$$

To compare Eq. (13) with Eq. (11), we consider each element in turn. (Also a simple valence-bond picture of the relationship between the $3\mathcal{C}_{\sigma\pi}'$ terms is given in the Appendix.) Within the localized approximation, we have

$$\begin{aligned}\langle(^3\Sigma)_{d'}\mid\xi\sum_k\delta(\mathbf{r}_{kH})\,S_{kz}\mid(^1\Sigma)_d\rangle&=\langle(^3\Sigma)_{s'}\mid\xi\sum_k\delta(\mathbf{r}_{kH})\,S_{kz}\mid(^1\Sigma)_t\rangle\\&=\langle(^3\Sigma)_{t'}\mid\xi\sum_k\delta(\mathbf{r}_{kH})\,S_{kz}\mid(^1\Sigma)_s\rangle,\end{aligned} \tag{14}$$

since the same sigma-electron functions are involved in the matrix elements. Corresponding results hold for the other spin-operator components S_{kx} and S_{ky}, with appropriate choices of the spin functions. The relationship between the matrix elements

$$\langle(^1\Sigma\,^2\Pi)_d\mid 3\mathcal{C}_{\sigma\pi}'\mid(^3\Sigma\,^2\Pi)_{d'}\rangle$$

for the radical and

$$\langle(^1\Sigma\,^1\Pi)_s\mid 3\mathcal{C}_{\sigma\pi}'\mid(^3\Sigma\,^3\Pi)_{s'}\rangle,$$

$$\langle(^3\Sigma\,^1\Pi)_{t'}\mid 3\mathcal{C}_{\sigma\pi}'\mid(^1\Sigma\,^3\Pi)_t\rangle$$

for the fragments, depends on the form of the functions $^1\Pi$ and $^3\Pi$. On approximating the functions in terms of the atomic pi orbitals π' and π'' centered on carbons C′ and C″, respectively, we have, with formal neglect of overlap,

$$^2\Pi(1)=\pi'(1)\alpha(1), \tag{15a}$$

$$\begin{aligned}^1\Pi(1,2)=&[2(1+\lambda)^{\frac{1}{2}}]^{-1}\{\pi'(1)\pi''(2)+\pi''(1)\pi'(2)\\&+\lambda[\pi'(1)\pi'(2)+\pi''(1)\pi''(2)]\}\\&\times\{\alpha(1)\beta(2)-\beta(1)\alpha(2)\},\end{aligned} \tag{15b}$$

$$\begin{aligned}^3\Pi(1,2)=&\tfrac{1}{2}\{\pi'(1)\pi''(2)-\pi''(2)\pi'(1)\}\\&\times\{\alpha(1)\beta(2)+\beta(1)\alpha(2)\},\end{aligned} \tag{15c}$$

where the spin function written for $^3\Pi(1, 2)$ is the one contributing to Eq. (14) and λ in $^1\Pi(1, 2)$ is a parameter determining the ratio of ionic and covalent contributions. For a simple molecular orbital, the parameter λ is equal to unity. Introduction of the functions into the matrix elements leads to the result

$$\begin{aligned}&\langle(^1\Sigma\,^1\Pi)_s\mid 3\mathcal{C}_{\sigma\pi}'\mid(^3\Sigma\,^3\Pi)_{s'}\rangle\\&\quad=\langle(^3\Sigma\,^1\Pi)_{t'}\mid 3\mathcal{C}_{\sigma\pi}'\mid(^1\Sigma\,^3\Pi)_t\rangle\\&\quad\cong(1+\lambda)^{-\frac{1}{2}}\langle(^1\Sigma\,^2\Pi)_d\mid 3\mathcal{C}_{\sigma\pi}'\mid(^3\Sigma\,^2\Pi)_{d'}\rangle.\end{aligned} \tag{16}$$

The sign ($\cong$) is used because the equality involves the neglect of a number of small integrals, as well as the localized approximation (see Appendix). Finally considering the excited states appearing in Eqs. (11) and (13), we see that the zero-order energy differences are related by expressions of the form

$$E_s^0-E_{s'}^0=E_d^0-E_{d'}^0+E^0(^1\Pi)-E^0(^3\Pi) \tag{17a}$$

and

$$E_t^0-E_{t'}^0=E_d^0-E_{d'}^0+E^0(^3\Pi)-E^0(^1\Pi), \tag{17b}$$

where $E^0(^1\Pi)$ and $E^0(^3\Pi)$ are the energies of the singlet and triplet pi states appearing in Eqs. (15b) and (15c). On introducing the symbols $\Delta\sigma$ and $\Delta\pi$ defined by the equations,

$$\Delta\sigma=E_d^0-E_{d'}^0,\qquad\Delta\pi=E^0(^3\Pi)-E^0(^1\Pi), \tag{18}$$

and making use of Eqs. (14)–(17), we find that

$$\begin{aligned}&\langle\Psi_S\mid\xi\sum_k\delta(\mathbf{r}_{kH})\,S_{kz}\mid\Psi_T\rangle\\&=(1+\lambda)^{-\frac{1}{2}}\frac{(\Delta\sigma)^2}{(\Delta\sigma)^2-(\Delta\pi)^2}\langle\Psi_D\mid\xi\sum_k\delta(\mathbf{r}_{kH})\,S_{kz}\mid\Psi_D\rangle.\end{aligned} \tag{19}$$

Since the hyperfine constant a_H is given by the expression

$$a_H=(2/h)\,\langle\Psi_D\mid\xi\sum_k\delta(\mathbf{r}_{kH})\,S_{kz}\mid\Psi_D\rangle, \tag{20}$$

Eq. (19) can be rewritten,

$$\begin{aligned}&\langle\Psi_S\mid\xi\sum_k\delta(\mathbf{r}_{kH})\,S_{kz}\mid\Psi_T\rangle\\&\quad=\tfrac{1}{2}(1+\lambda)^{-\frac{1}{2}}(h)\frac{(\Delta\sigma)^2}{(\Delta\sigma)^2-(\Delta\pi)^2}a_H.\end{aligned} \tag{21}$$

Substitution of this result and the corresponding ones for the other spin components into Eq. (2) specialized

TABLE I. Hyperfine constants.

Radical fragment	a_H (cps)
H—$\dot{C}(sp^2)$[a]	-65×10^6[b]
H—$\dot{C}(sp)$[a]	-95×10^6[c]
H—C—$\dot{C}$	$+150\cos^2\phi\times10^6$[d,e]

[a] The symbols (sp^2) and (sp) indicate the hybridization of the carbon C—H bond orbital.
[b] See footnote references 13–16.
[c] M. Karplus (unpublished calculations).
[d] The angle ϕ is the angle between the H—C—$\dot{C}$ plane and the $\dot{C}$ π-orbital axis.
[e] See footnote references 18–20.

for $A_{HH'}(\pi)$ leads to the formula[12]

$$A_{HH'}(\pi)=h\sum_T\left\{\frac{[\Delta\sigma(T)]^2}{[\Delta\sigma(T)]^2-[\Delta\pi(T)]^2}\right\}\times\left\{\frac{[\Delta\sigma'(T)]^2}{[\Delta\sigma'(T)]^2-[\Delta\pi(T)]^2}\right\}\times\frac{a_H(T)a_{H'}(T)}{2[(1+\lambda)(1+\lambda')]^{\frac{1}{2}}\Delta\pi(T)},\quad(22)$$

where the index T has been introduced to indicate that different fragments may have to be used for each pi-electron triplet that contributes to the coupling constant. Also, the unprimed quantities are associated with the fragment for proton H and the primed quantities with the fragment for proton H′ [the $\Delta\pi(T)$ terms are the same for the primed and unprimed fragments].

Equation (22) is the desired relationship between $A_{HH'}(\pi)$ and the proton hyperfine constants $a_H(T)$ and $a_{H'}(T)$. With experimental values for $a_H(T)$ and $a_{H'}(T)$, and estimates for the excitation energies and molecular-orbital parameters involved, Eq. (22) can be used to evaluate the magnitude of $A_{HH'}(\pi)$ for molecules that can be treated in terms of the fragment models. Since the sign of $a_H(T)$ and $a_{H'}(T)$ are known in some systems, the absolute sign of $A_{HH'}(\pi)$ can be determined from Eq. (22). ($A_{HH'}$ is taken as positive when the antiparallel nuclear spin orientation leads to a lower energy state than the parallel orientation.) Although only relative signs have been measured experimentally, comparison with the theoretical values can be used to test the consistency of the results.

APPLICATIONS

To determine $A_{HH'}(\pi)$ for a series of hydrocarbon molecules, we simplify Eq. (22) by evaluating the factors that can be expected to remain relatively constant. We assume that a pure molecular orbital description is valid for the pi-electron singlet state and set $\lambda=\lambda'=1$. Since in all cases considered here, the $^1\Sigma\rightarrow{}^3\Sigma$ excitation is primarily localized in a C—H bond, $\Delta\sigma(T)$ is on the order of 9–12 ev while $\Delta\pi(T)$ is in the range 6–8 ev (see the following). With these estimates, we find

$$\left\{\frac{[\Delta\sigma(T)]^2}{[\Delta\sigma(T)]^2-[\Delta\pi(T)]^2}\right\}\left\{\frac{[\Delta\sigma'(T)]^2}{[\Delta\sigma'(T)]^2-[\Delta\pi(T)]^2}\right\}\times[(1+\lambda)(1+\lambda')]^{\frac{1}{2}}\cong1,\quad(23)$$

and

$$A_{HH'}(\pi)=2.1\times10^{-15}\sum_T\frac{a_H(T)a_{H'}(T)}{\Delta\pi(T)},\quad(24)$$

where $A_{HH'}(\pi)$, $a_H(T)$, and $a_{H'}(T)$ are expressed in units of cps and $\Delta\pi(T)$ in ev. In this form Eq. (24) can be used to estimate $A_{HH'}(\pi)$ simply from measured hyperfine constants and triplet state energies.

Table I lists values of the hyperfine constants for radical species related to the H—C′=C″ and H—C—C′=C″ fragments. In each case the value of a_H is that corresponding to a single unpaired electron on the carbon C. For H—$\dot{C}(sp^2)$, a large number of electron spin resonance measurements[13] and theoretical calculations[14] are available. The relative constancy of a_H found in a variety of compounds containing the H—C radical fragment has demonstrated the important result that the $\mathcal{H}_{\sigma\pi}'$ perturbation is not sensitive to the remainder of the molecule.[15] Although the sign of a_H cannot be determined by solution electron resonance studies, it is known to be negative for H—C(sp^2) from detailed measurements in oriented single crystals.[16] For H—C(sp), a simple variation calculation of a_H, comparable to that used for the H—C(sp^2) radical,[14] leads to the listed value of -95×10^6 cps.[17] The value of a_H in the H—C—C radical fragment has been studied in a number of irradiated systems and found to be

[12] Equation (22) makes clear what is implied by the average energy approximation (ΔE) used previously in spin-coupling calculations (see footnote reference 4). If only one triplet state contributes significantly to the sum over T, ΔE is to be identified with $\Delta\pi(T)$, which is always positive, and the sign of $A_{HH'}(\pi)$ is determined by the sign of the product $a_H(T)a_{H'}(T)$. If several terms have to be included in the sum over T, but in all of these $a_H(T)a_{H'}(T)$ has the same sign, ΔE is again definitely positive and corresponds to the appropriate average over the $\Delta\pi(T)$ values. This is the situation that occurs in the sigma-electron treatments of footnote references 2–4. Only if the various $a_H(T)a_{H'}(T)$ terms that are important have different signs or the localized approximation breaks down does the problem envisaged by McLachlan arise and a perturbation sum have to be used instead of the average energy approximation.

[13] G. K. Fraenkel and B. Segal, Ann. Rev. Phys. Chem. **10**, 435 (1959).
[14] H. M. McConnell, J. Chem. Phys. **24**, 764 (1956); H. S. Jarrett, *ibid.* **25**, 1289 (1956); M. Karplus, *ibid.* **30**, 15 (1959).
[15] H. M. McConnell and D. B. Chesnut, J. Chem. Phys. **28**, 107 (1958).
[16] D. K. Ghosh and D. H. Whiffen, Mol. Phys. **2**, 285 (1959); H. M. McConnell, C. Heller, T. Cole, and R. W. Fessenden, J. Am. Chem. Soc. **82**, 766 (1960).
[17] The author wishes to thank a referee for pointing out that this calculation is in good agreement with the measured value obtained for irradiated methyl acetylene by Poole and Anderson [J. Chem. Phys. **31**, 346 (1959)].

TABLE II. Proton spin-coupling constants.

Separation of protons	$A_{HH'}(\pi)$ (cps) (theoret)[i]	$A_{HH'}$(cps) (exptl)[i]
1. Two carbons		
(a) H—C=C—H	+1.5	5–11 (cis) 10–18 (trans)[b]
(b) H—C≡C—H	+4.6	9.1[c]
2. Three carbons		
(a) H—C=C—C—H	−1.7	−1.4 to −1.8[d]
(b) H—C≡C—C—H	−3.7	−2.1 to −2.9[e]
(c) H—C=C=C—H	−6.7	6.1 to 7.0[f] (unknown sign)
3. Four carbons		
(a) H—C—C=C—C—H[a]	+2.0	1.2 to 1.5[g] (unknown sign)
(b) H—C—C≡C—C—H[a]	+2.9	2.9[h] (unknown sign)
(c) H—C=C=C=C—H	+7.8	...

[a] Independent rotation of the two C—H groups is assumed. If certain relative orientations are weighted unequally in some molecules, a corresponding alteration of the coupling constant would result.

[b] See footnote references 3 and 6.

[c] See footnote reference 2.

[d] See footnote reference 26.

[e] See footnote reference 27. Also, E. B. Whipple, J. H. Goldstein, L. Mandell, G. S. Reddy, and G. R. McClure, J. Am. Chem. Soc. **81**, 1321 (1959).

[f] E. B. Whipple, J. H. Goldstein, and L. Mandell, J. Chem. Phys. **30**, 1109 (1959); E. B. Whipple, J. H. Goldstein, and W. E. Stewart, J. Am. Chem. Soc. **81**, 4761 (1959).

[g] See footnote reference 28(b).

[h] N. Muller and D. E. Pritchard, J. Chem. Phys. **31**, 768 (1959).

[i] The signs determined theoretically are absolute values, while those for the experimental results are relative to the HCCH coupling, which is taken to be positive in agreement with theoretical calculations.

equal to $\sim 75\times 10^6$ cps.[18] In all of the measured compounds, the hydrogen was freely rotating about the C—C line and the observed a_H value is an average over this rotation. From theoretical considerations,[19] the hyperfine constant is known to vary approximately as $\cos^2\phi$, where ϕ is the angle between the Ċ pi-orbital and the H—C—Ċ plane. Consequently, a_H is equal to $+150\cos^2\phi\times 10^6$ cps for H—C—Ċ, with the positive sign determined both by theory[19] and experiment.[20] Although the H—C—Ċ hyperfine constant also has a dependence on the σ-bond hybridization of the carbon orbitals, the variation is expected to be less than in the H—Ċ case and is neglected here.

Because of the forbidden character of the singlet-triplet transition relatively little is known about the pi-electron triplet state energies in simple organic molecules. For ethylene there is an observation of some bands at 6.0–6.5 ev which have been assigned to the triplet-state excitation.[21] A variety of theoretical calculations[22] indicate that the lowest triplet state is between 4.5 and 6.0 ev. For acetylene there are no experimental observations. However, the most reliable theoretical estimates[23] place the lowest $^3\Pi_u$ states between 6 and 10 ev. For lack of more critical data, we choose $\Delta\pi(T)=6.0$ ev for the ethylenic and $\Delta\pi(T)=8.0$ ev for the acetylenic compounds.

With the numerical values for $a_H(T)$ in Table I and the $\Delta\pi(T)$ values in the previous paragraph, $A_{HH'}(\pi)$ can be determined by means of Eq. (24) for a variety of compounds. The results obtained are given in Table II, which is arranged according to the number of carbon atoms between the coupled protons. For protons two carbons apart (H—C—C—H), it is known from calculations on ethylene[4] that the σ-bond contribution to $A_{HH'}$ is large and positive (+6 cps for *cis*-and +11 cps for *trans*-protons). Thus $A_{HH'}(\pi)$ is only a small part of the coupling in this case. In acetylene, $A_{HH'}(\pi)$ is apparently a larger fraction of the total coupling, since $A_{HH'}(\sigma)$ equals ~ 7 cps from a MO calculation.[2] When there are three or more carbon atoms separating the coupled protons, $A_{HH'}(\sigma)$ has been shown to be very small by experimental measurements in saturated molecules[24] and by some valence-bond calculations[25] [$|A_{HH'}(\sigma)|\leq 0.5$ cps]. For such distant interactions,

[18] W. Gordy and C. G. McCormick, J. Am. Chem. Soc. **78**, 3244 (1956); R. Bersohn, J. Chem. Phys. **24**, 1066 (1956); B. Smaller and M. S. Matheson, *ibid.* **28**, 1169 (1958).

[19] A. D. McLachlan, Mol. Phys. **1**, 233 (1958); D. B. Chesnut, J. Chem. Phys. **29**, 43 (1958).

[20] A. Forman, J. N. Murrell, and L. E. Orgel, J. Chem. Phys. **31**, 1129 (1960).

[21] W. J. Potts, Jr., J. Chem. Phys. **23**, 65 (1955).

[22] See, for example, R. Pariser and R. G. Parr, J. Chem. Phys. **21**, 767 (1953); K. Ohno and T. Itoh, *ibid.* **23**, 1468 (1955); W. Kolos, *ibid.* **27**, 591 (1957).

[23] I. G. Ross, Trans. Faraday Soc. **48**, 973 (1953); J. Serre, Compt. rend. **242**, 1469 (1956).

[24] P. T. Narasimhan (private communication; T. Shimizu, S. Matsuoka, S. Hafferi, and K. Seudo, J. Phys. Soc. Japan **14**, 683 (1959).

[25] M. Karplus (unpublished calculations).

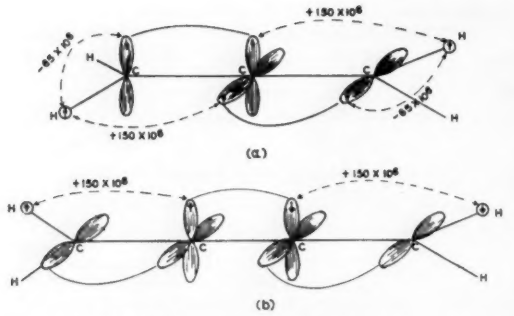

FIG. 1. Diagram of proton coupling in (a) allene and (b) butatriene. The arrows represent electron spins; (—) indicates the π-bond pairing of electrons; and (---) the σ–π perturbation interaction of electrons.

the pi-electron terms are expected to make the dominant contribution to the coupling constant; that is, $A_{HH'}(\pi) \cong A_{HH'}$. Comparing the experimental $A_{HH'}$ values with the $A_{HH'}(\pi)$ results obtained from Eq. (24) for protons separated by three or four carbon atoms, we see that the agreement is quite satisfactory (see Table II). Perhaps more important than the individual quantitative results are certain observed ratios of coupling constants which follow from the theory independent of the exact constants used in the formula. In Table II, we have both theoretically and experimentally,

$$-(2a) \cong (3a) \cong -\tfrac{1}{2}(2b) \cong \tfrac{1}{2}(3b) \cong -\tfrac{1}{4}(2c) \cong \tfrac{1}{4}(3c).$$

Also for the two systems (allyl group[26] and methyl acetylene[27]) in which relative signs have been determined, the experimental values (relative to the HCCH′ coupling as positive) are consistent with the absolute sign of the theoretical results.[28] Studies[29] of H—C≡C—C—H′ systems indicate that the magnitude of the coupling depends on the *cis* or *trans* arrangement of H and CH′ with respect to the double-bond. Since the pi-electron theory values are the same for *cis* and *trans* protons, the observed differences must result from sigma contributions and would be expected to be no larger than 1 cps.

Of particular interest are the large $A_{HH'}(\pi)$ magnitudes and opposite signs obtained theoretically for allene ($H_2C{=}C{=}CH_2$) and butatriene ($H_2C{=}C{=}C{=}CH_2$). To clarify the interactions involved, a diagrammatic representation of the coupling terms is given in Fig. 1. In allene, $A_{HH'}(\pi)$ receives contributions from two interaction paths, each of which is composed of one H—Ċ(sp^2) radical and one H—C—Ċ radical hyperfine coupling. Further, the two paths are additive because of the parallel spin-orientation of the two electrons in the central carbon pi orbitals (Hund's rule). The net result of the opposite signs of the $3\mathcal{C}_{\sigma\pi}'$ perturbation in radical fragments H—Ċ and H—C—Ċ is a parallel orientation of the proton spins ($A_{HH'}(\pi) \cong A_{HH'} < 0$). By contrast, in the four-carbon system there is only a single important interaction path consisting of a pair of H—C—Ċ radical hyperfine couplings, which result in antiparallel proton spin orientation ($A_{HH'}(\pi) \cong A_{HH'} > 0$). To confirm the analysis given here it would be most useful to have available the relative sign of the coupling in some substituted allene and both the magnitude and sign of the coupling in butatriene.

For the next higher cumulene

$$(H_2C{=}C{=}C{=}C{=}CH_2),$$

$A_{HH'}$ should be considerably reduced from the allene and butatriene values. Qualitatively, $A_{HH'}$ would be expected to be on the order of 0.5 cps with the exact value depending on the extent of conjugation between the pairs of double-bonds. This suggests that such long-range couplings can be used to "measure" the amount of conjugation in unsaturated molecules.[30]

The large pi-electron contributions found for certain systems by the theory presented here are in striking contrast to the small values that have been estimated for aromatic molecules.[7a] The difference between the two sets of results arises not from alterations in the basic formulation[30] but from the types of interactions present in the molecules considered. In all cases dealt with in this paper, the pi-electron bond involved is a complete bond (bond-order unity) as compared with the partial bonding found in aromatic molecules. Also, more than one interaction path exists in some of the systems (e.g., allene, acetylene). Where methyl or methylene groups are present, they often are "fixed" with respect to the pi-electron plane, such that the angle ϕ is zero and a sizeable a_H value results. By a combination of one or more of these factors, there are obtained theoretical coupling constants in agreement with the large values found experimentally for unsaturated molecules.

ACKNOWLEDGMENTS

I wish to thank Dr. D. E. Applequist and Dr. P. T. Narasimhan for helpful discussions.

APPENDIX

To present a simple valence-bond picture of the effect of $3\mathcal{C}_{\sigma\pi}'$ and the comparison between the singlet and

[26] S. Alexander, J. Chem. Phys. **28**, 355 (1958); J. Waugh, *ibid.* **30**, 944 (1958); C. N. Banwell, A. D. Cohen, N. Sheppard, and J. J. Turner, Proc. Chem. Soc. **1959**, 266.

[27] P. T. Narasimhan and M. T. Rogers, J. Chem. Phys. (to be published). The relative sign determination is based on a study of ethyl acetylene.

[28] *Note added in proof.* Prof. R. A. Hoffman (private communication) has kindly informed me that measurements for compounds of the type HC≡CCH and HCC≡CCH yield relative signs in agreement with the theoretical results.

[29] (a) F. S. Mortimer, J. Mol. Spectroscopy **3**, 340 (1959); (b) R. R. Fraser, Can. J. Chem. **38**, 549 (1960).

[30] An extension of Eqs. (22) and (24) to conjugated and aromatic pi-electron systems is straightforward. With the simplified expression [Eq. (24)], results very close to those estimated by McConnell [J. Mol. Spectroscopy **1**, 11 (1957)] would be obtained for aromatic systems.

doublet state interaction, we consider a four-electron fragment H—C′=C″. There are two structures: the perfect pairing structure ψ_{0s} with the $H-\sigma'$ bond and a $\pi'-\pi''$ bond, and the structure $\psi_{0s'}$ with an $H-\pi''$ bond and a $\sigma'-\pi'$ bond. Here H is a 1s orbital on hydrogen, σ' and π' are a sp^2-hybrid orbital and a pi orbital on carbon C′, and π'' is a pi orbital on carbon C″. By perturbation theory, the contribution $c_{0s'}$ made by the structure ψ_{0s} is found to be

$$c_{0s'}=\tfrac{1}{2}\frac{[\sigma',\pi']-[H,\pi']+[H,\pi'']-[\sigma',\pi'']}{[H,\sigma']-[\pi',\pi'']-[\sigma',\pi']-[H,\pi'']}, \quad \text{(A1)}$$

where $[A, B]$ is the exchange integral

$$[A, B]=\int A(1)B(2)\mathfrak{H}B(1)A(2)d\tau_1 d\tau_2. \quad \text{(A2)}$$

For the radical in the doublet state resulting from the removal of the π'' electron, the corresponding coefficient $c_{0d'}$ has the form

$$c_{0d'}=\tfrac{1}{2}\frac{[\sigma',\pi']-[H,\pi']}{[H,\sigma']-[\sigma',\pi']}. \quad \text{(A3)}$$

As the integrals $[H, \pi'']$ and $[\sigma', \pi'']$ are both very small, the only significant difference between the formulas for $c_{0s'}$ and $c_{0d'}$ is the presence of the integral $[\pi', \pi'']$ in the denominator of Eq. (A2). With semiempirical integrals used previously for the methyl radical[14] ($[H,\sigma']=-3.92$ ev, $[H,\pi']=0.75$ ev, $[\sigma',\pi']=1.26$ ev) and the value of -0.90 ev for $[\pi', \pi'']$, we find $c_{0s'}=-0.53$ and $c_{0d'}=-.065$, in reasonably close agreement. For the corresponding triplet states, the effect of $[\pi', \pi'']$ is to make the coefficient $c_{0t'}$ somewhat larger than $c_{0d'}$, which compensates for the $c_{0s'}$, $c_{0d'}$ difference.

THE JOURNAL OF CHEMICAL PHYSICS VOLUME 33, NUMBER 6 DECEMBER, 1960

Lattice Heat Capacity of the Rare Earths. Heat Capacities of Yttrium and Lutetium from 15–350°K*

L. D. JENNINGS,† R. E. MILLER, AND F. H. SPEDDING

Institute for Atomic Research and Department of Chemistry, Iowa State University, Ames, Iowa

(Received June 1, 1960)

The heat capacities of lutetium and yttrium have been measured and are found to have the same dependence on a reduced temperature as does that of lanthanum. The lattice heat capacities are given by Θ values of 130.7, 166.0, and 213.7 for La, Lu, and Y and the corresponding electronic heat capacities are given by γ values of 100, 95, and 85×10^{-4} joules/g atom-deg^2.

INTRODUCTION

IN order to carry out a program directed toward understanding the process of magnetic ordering in the rare-earth metals with the aid of heat capacity measurements, it is necessary to estimate the lattice and electronic contributions to the heat capacity. This estimate has been made with the aid of the heat capacity of lanthanum,[1,2] but it is desirable to establish whether or not the form of the nonmagnetic heat capacity is the same for all rare-earth metals. Strictly speaking, the only nonmagnetic trivalent rare earths are lanthanum and lutetium, but one would expect that yttrium would have approximately the same bonding parameters and hence a lattice heat capacity that differs only in temperature scale from that of the rare earths. We have measured the heat capacities of lutetium and yttrium and find that, to the accuracy desired for estimating the form of the magnetic heat capacity of the other rare earths, the lattice parts have the same dependence on a reduced temperature as does the heat capacity of lanthanum.

EXPERIMENTAL

We made use of the same adiabatic calorimeter employed for previous rare-earth samples.[3] The sample can was essentially a copy of the can used with terbium which has also been described previously.[4]

The procedures used for the ion exchange separation of the rare-earth salts[5] and the reduction of the an-

* Contribution No. 892. This work was performed in the Ames Laboratory of the U. S. Atomic Energy Commission.

† Present address: Ordnance Materials Research Office, Watertown, Massachusetts.

[1] D. H. Parkinson, F. E. Simon, and F. H. Spedding, Proc. Roy. Soc. (London) **A207**, 137 (1951).

[2] A. Berman, M. W. Zemansky, and H. A. Boorse, Phys. Rev. **109**, 70 (1958).

[3] M. Griffel, R. E. Skochdapole, and F. H. Spedding, J. Chem. Phys. **25**, 75 (1956).

[4] L. D. Jennings, R. M. Stanton, and F. H. Spedding, J. Chem. Phys. **27**, 909 (1957).

[5] J. E. Powell and F. H. Spedding, U. S. Atomic Energy Commission Rept. ISC-617 (1955).

TABLE I. Thermodynamic functions of yttrium joules/(g atom-deg).

T, °K	C_p	S^0	$(H^0-H_0^0)/T$	$(-F^0-H_0^0)/T$
5	0.06	0.064	0.026	0.038
10	0.23	0.150	0.081	0.069
15	0.79	0.322	0.197	0.125
20	1.89	0.693	0.476	0.217
30	5.29	2.063	1.479	0.584
40	8.95	4.121	2.892	1.229
50	12.19	6.478	4.439	2.039
60	14.80	8.953	5.965	2.988
70	16.84	11.398	7.379	4.019
80	18.43	13.757	8.664	5.093
90	19.71	16.006	9.822	6.184
100	20.71	18.136	10.862	7.274
120	22.14	22.054	12.631	9.423
140	23.17	25.541	14.065	11.476
160	23.98	28.686	15.255	13.431
180	24.63	31.547	16.259	15.288
200	25.10	34.169	17.122	17.057
220	25.46	36.577	17.862	18.715
240	25.78	38.805	18.508	20.297
260	26.05	40.880	19.079	21.801
273.15	26.24	42.169	19.422	22.747
280	26.31	42.820	19.587	23.233
298.15	26.52	44.476	20.005	24.471
300	26.54	44.643	20.043	24.640
320	26.74	46.362	20.455	25.907
340	26.92	47.989	20.830	27.159

hydrous fluoride[6] have been described previously. The metals were vacuum-cast in tantalum crucibles and machined to make a snug fit in the calorimeter can.

Spectrographic analysis showed the yttrium sample to contain impurities of Dy, Gd, Ca, Mg, and Cr but to contain not more than about 0.5% total of these metals. Vacuum fusion showed the sample to contain about 150 ppm carbon, and 250 ppm nitrogen. Chemical analysis completed since taking the heat capacity data showed the sample to contain 0.44% Ta and 0.97% yttrium oxyfluoride. The sample weighed 214.79 g.

Spectrographic analysis showed the lutetium sample to contain small amounts of Y, Sc, Yb, Tm, Ca, Cr, Fe, Cu, Si, and Mg; but to contain not more than about 0.2% total of these metals. Vacuum fusion showed the sample to contain about 100 ppm carbon and 800 ppm nitrogen. Chemical analysis completed since taking the heat capacity data showed the sample to contain 1.62% Ta and 1.97% lutetium oxyfluoride. The sample weighed 455.63 g.

The tantalum and oxyfluoride were detected by dissolving the rare-earth metal with nitric acid and analyzing the insoluble residue. The tantalum was not observed in spectrographic analyses because of interferences and the oxyfluoride gives no detectable lines. We now believe that most of the rare-earth samples whose heat capacities have been measured did contain a significant amount of tantalum. Recent analysis of the terbium and thulium samples used in measurements in this laboratory showed them to contain small amounts of tantalum but no oxyfluoride.

[6] A. H. Daane and F. H. Spedding, J. Electrochem. Soc. **100,** 442 (1953).

RESULTS

The results of the individual measurements of $\Delta H/\Delta T$ as a function of the average temperature have been deposited with the Library of Congress.[7]

Smooth curves were drawn through the points and extrapolated to absolute zero using the low-temperature dependence of the Debye temperature of lanthanum as a guide. Representative values which were taken from these curves and corrected for the heat capacity of the tantalum and oxyfluoride impurities are given in Tables I and II. The values of the thermodynamic functions were then calculated by numerical integration and are given in Tables I and II.

Inasmuch as the tantalum and the oxyfluoride form separate phases, it is possible to correct for their presence if the individual heat capacities are known. The heat capacity of tantalum has been measured by Sterett and Wallace.[8] Unfortunately, no data on the heat capacities of the oxyfluorides exist. The heat capacities of the oxyfluorides were estimated by the

TABLE II. Thermodynamic functions of lutetium joules/(g atom-deg).

T, °K	C_p	S^0	$(H^0-H_0^0)/T$	$(-F^0-H_0^0)/T$
5	0.10	0.063	0.036	0.027
10	0.49	0.225	0.145	0.080
15	1.67	0.607	0.425	0.182
20	3.66	1.346	0.977	0.369
30	8.47	3.746	2.673	1.073
40	12.71	6.793	4.677	2.116
50	15.84	9.973	6.613	3.360
60	18.10	13.072	8.309	4.723
70	19.74	15.993	9.866	6.127
80	20.98	18.712	11.179	7.533
90	21.93	21.241	12.323	8.918
100	22.59	23.587	13.318	10.269
120	23.64	27.802	14.954	12.848
140	24.40	31.506	16.252	15.254
160	24.97	34.802	17.307	17.495
180	25.42	37.769	18.184	19.585
200	25.78	40.457	18.926	21.531
220	26.03	42.936	19.561	23.375
240	26.25	45.210	20.109	25.101
260	26.50	47.322	20.591	26.731
273.15	26.63	48.633	20.379	27.754
280	26.69	49.293	21.020	28.273
298.15	26.85	50.975	21.369	29.606
300	26.88	51.141	21.404	29.737
320	27.04	52.881	21.751	31.130
340	27.17	54.523	22.066	32.457

[7] A copy of these results in tabular form may be had by requesting Document No. 6320 from the ADI Auxiliary Publications Project, Photoduplication Service, Library of Congress, Washington, D. C., and by remitting $1.25 for photoprints or $1.25 for 35-mm microfilm. Advance payment is required. Make checks or money orders payable to: Chief, Photoduplication Service, Library of Congress, Washington, D. C.

[8] K. F. Sterrett and W. F. Wallace, J. Am. Chem. Soc. **80,** 3176 (1958).

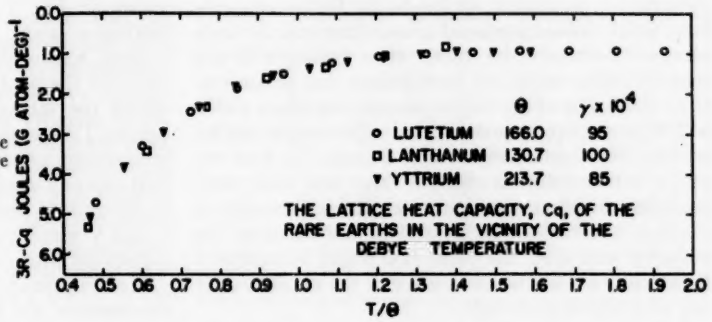
3R-Cq JOULES (G ATOM-DEG)⁻¹
T/Θ
Θ γ x 10⁴
LUTETIUM 166.0 95
LANTHANUM 130.7 100
YTTRIUM 213.7 85
THE LATTICE HEAT CAPACITY, Cq, OF THE RARE EARTHS IN THE VICINITY OF THE DEBYE TEMPERATURE

FIG. 1. Lattice heat capacity C_q of the rare earths in the vicinity of the Debye temperature.

following approximation, suggested by the work of Hofmann *et al.*[9]

$$C_x = n[f_D(\Theta_r/T) + f_D(\Theta_o/T) + f_D(\Theta_f/T)],$$

where C_x is the approximate heat capacity of the compound, n is the number of moles of the compound present, $f_D(\Theta/T)$ is the Debye function; and Θ_r, Θ_o, and Θ_f are estimated Debye temperatures for the rare earth, oxygen, and fluorine atoms, respectively. The Debye temperature of the rare-earth atoms was assumed to be that found for each metal in these measurements. The Debye temperatures for the oxygen and fluorine atoms were estimated by roughly averaging values found for these atoms in several compounds by Hofmann *et al.*[9] The values used were 1000 and 650 for oxygen and fluorine, respectively. On treating the samples as mixtures of three phases, rare-earth metal, tantalum, and rare-earth oxyfluoride, the results were corrected for the presence of the tantalum and oxyfluoride impurities.

The net corrections to yttrium for the tantalum and oxyfluoride impurities varied from 0 to 0.6% of the heat capacity. The net corrections to lutetium varied from 0 to 1.3% of the heat capacity, except at temperatures below 25°K where the corrections increased to about 2%. We have estimated that these corrections for impurities are correct to 10–15% of their values. Most of the error is due to the uncertainty in the heat capacity values used for the oxyfluorides. This would mean that the corrected results could still be in error by as much as 0.1–0.2% due to the tantalum and oxyfluoride impurities.

We estimate the precision of our results from the scatter of points about the smooth curves. For yttrium this scatter did not amount to more than about 0.2% at temperatures from 30° to 300°K except for six points which were within 0.3% of the smooth curve. For lutetium the scatter did not amount to more than about 0.1% in the range 30° to 300°K except for two points which were within 0.2% of the smooth curve. The precision for both samples dropped to 0.3% at 20°K and 2% at 15°K and also dropped to 0.3% at 350°K due to increased difficulty in maintaining adiabatic conditions.

The accuracy for the data is thought to be about the same as the precision for the actual sample used. We estimate then that the error in heat capacity of either sample would not exceed about 0.3% above 30°K of which 0.1–0.2% arises from the uncertainty in the corrections for impurities. The error in the entropy at room temperature of either sample should not exceed 0.25 joules/g atom-deg of which 0.10 arises from the uncertainty in the extrapolation below 13°K. The error in the enthalpies of either sample should not exceed 0.25% above 100°K. The absolute accuracy of the results would of course be dependent upon purity conditions not corrected.

DISCUSSION

In order to reduce the results for lanthanum, lutetium, and yttrium to the same form, it is necessary to

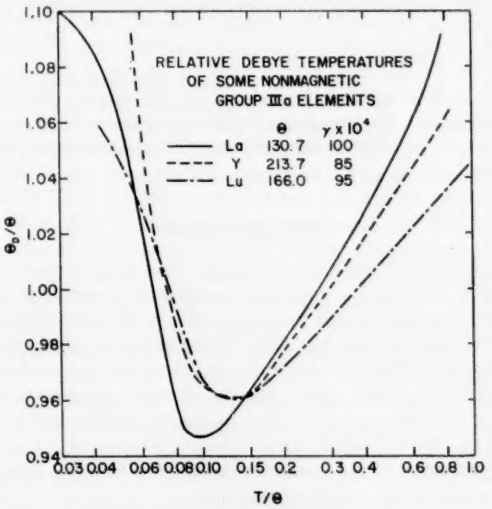

FIG. 2. Relative Debye temperatures of some nonmagnetic group IIIa elements.

[9] J. A. Hofmann, A. Paskin, K. J. Tauer, and R. J. Weiss, J. Phys. Chem. Solids **1**, 45 (1956).

determine a parameter, similar to the Debye temperature, which defines a reduced temperature scale for each element. Because of its utility when dealing with the magnetic rare earths, we have chosen this parameter, Θ, as that value of the Debye temperature which yields a Debye entropy equal to the experimental lattice entropy near room temperature. Because the heat capacity is practically its classical value near room temperature, the exact temperature at which the match is made is not critical. If, instead of the entropy, the enthalpy were used, the value of Θ would be increased by about 3%, but the consistency of the results would not be modified appreciably.

Before evaluating Θ, it is necessary to establish the contribution of the conduction electrons to the heat capacity. We assume that this contribution has the form: $C=\gamma T$. Since very low temperature results are not yet available, we evaluate γ in the following way. We make the preliminary estimate that the electronic contribution is the same as it is in lanthanum and are thus able to make a first approximation to the value of Θ. We then choose a new value of γ so that the lattice heat capacity, C_q, of La, Lu, and Y is the same function of T/Θ at temperatures near and above Θ, where the contribution of γT is appreciable. That we get good agreement over a wide range of temperature as shown in Fig. 1 encourages us to believe that this method is valid.

Thus, having chosen a corrected value for γ, we can calculate the final value of Θ. It is then convenient to depict the lattice heat capacity by plotting Θ_D/Θ, against T/Θ, as shown in Fig. 2. Here Θ_D is the Debye temperature which yields the actual value of the lattice heat capacity at any temperature. This value may then be determined from tables of $C(\Theta_D/T)$.[10] The values of Θ and γ which were used are given in the tables incorporated with the figures.

If one's primary interest is in the entropy near room temperature, the bulk of the information is contained in the curves of Fig. 2 in the range of T/Θ of 0.1 to 0.5, as the contribution at the lower temperatures is small and the contribution at higher temperatures in nearly independent of Θ. If attention is focused on the enthalpy, the important range is even smaller. It may be appreciated then, in view of the fact that a 2% difference among the curves of Fig. 2 means only a 6% difference in the heat capacity at low temperatures and less at higher temperatures, that the lattice heat capacity of La, Lu, and Y may be well described by a single function of a reduced temperature.

[10] Landolt-Bornstein, *Physikalische-Chemische Tabellen, Erste Ergänzungsband* (Julius Springer, Berlin, 1927), p. 705.

THE JOURNAL OF CHEMICAL PHYSICS VOLUME 33, NUMBER 6 DECEMBER, 1960

Temperature Variation of the Linewidth in Nonresonant Microwave Absorption*

JAMES E. BOGGS, A. P. DEAM, AND JOE M. KING

Department of Chemistry and Electrical Engineering Research Laboratory, The University of Texas, Austin 12, Texas

(Received July 22, 1960)

The linewidth parameter $\Delta\nu/p$ for nonresonant microwave absorption in CH_3Cl and in $CHCl_2F$ has been determined at five temperatures between 10° and 150°C from cavity measurements of dielectric dispersion in the gases as a function of pressure at a frequency of 402 Mc. The linewidth is found to be proportional to $T^{-1.5}$, as opposed to the $T^{-1.0}$ dependence predicted by Anderson's theory of collision broadening.

INTRODUCTION

At all but the lowest pressures, the width of spectral lines in the microwave region is determined by collision broadening due to the effects of intermolecular collisions in the gas. The phenomenon is of general interest in that it inherently contains information about molecular force fields out to distances considerably greater than can be studied by kinetic theory methods. The line half-width $\Delta\nu$ is directly proportional to gas pressure, and the linewidth parameter $\Delta\nu/p$ is characteristic of the colliding molecules.

Anderson's quantum mechanical treatment of pressure broadening[1] has been successful in treating both self-broadening in ammonia and the broadening of ammonia lines by foreign gases. Anderson's theory predicts that the line-broadening constant should vary as $T^{-1.0}$ in the case of dipole-dipole interactions and as a lower power of temperature, down to a limit of $T^{-0.5}$, for shorter range forces.

Anderson's theory has not been successful[2] in the prediction of the magnitude of the linewidth parameter

* This work has been supported by Office of Naval Research. The results were reported in part at the 1960 spring meeting of the American Physical Society, Washington, D. C., April, 1960.

[1] P. W. Anderson, Phys. Rev. **75**, 1450L (1949); **76**, 647 (1949); **80**, 511 (1950).

[2] G. Birnbaum, Ph.D. dissertation, George Washington University, 1956.

for nonresonant spectra. Such spectra arise from the pressure-broadening of very low frequency lines into the observable frequency region, and have been studied either by direct measurement of microwave absorption[3,4] or by examining the frequency variation of the permittivity of the gas.[5,6] Birnbaum and Maryott[7] have been able to correlate the observed nonresonant line widths for a number of gases by means of a classical consideration of the torque existing between two colliding dipoles. Their approach predicts a temperature variation of $T^{-1.5}$ for the linewidth parameter, rather than the $T^{-1.0}$ predicted by Anedrson's theory in the case of dipole-dipole interactions.

In a recent paper, Maryott, Estin, and Birnbaum have reported measurements of the temperature variation of the linewidth parameter for the symmetric-top molecules CHF_3, CH_3F, and $CClF_3$.[8] Their results substantiate the $T^{-1.5}$ dependence for CHF_3 and CH_3F for which dipole-dipole interaction would be expected to predominate. Our results, on different gases and determined by a quite different experimental method, support their conclusions which are of fundamental importance to an adequate theory of collision broadening.

EXPERIMENTAL

The apparatus used to obtain the results reported here was the same as that used in previous experiments[6] except for the modifications described in the following. Briefly, the dielectric constant of the gas is determined at different pressures and temperatures by observing the operating frequency of an oscillator which is locked to the resonant frequency of a cavity containing the gas to be studied. The linewidth parameter for nonresonant absorption is then calculated as previously described.[6]

For the present experiments, the frequency of the 400-Mc oscillator was translated to approximately 6 Mc with a Gertsch FM-3 frequency meter and the resulting beat observed on a radio receiver while the difference frequency was determined with a low-frequency standard. Stability of the over-all system has been observed to be $\pm 10^{-6}$ over several hours. Resolution was better than 2.5×10^{-7}.

It has been pointed out by the authors[6] that when a Pound system, such as is used here, is considered in detail, it is found that the frequency generated by the oscillator is not entirely dependent upon the resonant frequency of the gas-filled cavity. A particular difficulty in interpreting the output of the oscillator as a function of cavity resonant frequency arises when the gas in the cavity exhibits high dissipation. Since the coupling to the cavity is fixed geometrically, the coupling coefficient will vary with cavity Q. The system cannot *practically* be made to respond only to the imaginary component of the cavity reflection coefficient alone. As a result, an error arises in the evaluation of the dielectric constant which may be of significant importance if the gas is particularly lossy. No attempt has been made to study this phenomenon in detail other than to evaluate the scatter obtained for different tuneup procedures. Fluoroform has a higher loss than either of the gases used in the present study, and it was found that in the region of maximum loss it was not uncommon to obtain values for the polarization differing $\pm 1\%$ when operating with different tuneup procedures. As a result of the coupling problems encountered when measuring gases with high loss, it appears that care must be used when a Pound system is used to measure dielectric constants.

TABLE I. Parameters for the dielectric dispersion of CH_3Cl and $CHCl_2F$ at various temperatures.

	CH_3Cl		$CHCl_2F$	
T (°C)	$\frac{\Delta\nu}{p}$	$\frac{P_0-P_\infty}{P_0-P_D}$	$\frac{\Delta\nu}{p}$	$\frac{P_0-P_\infty}{P_0-P_D}$
10°	4.62	0.101	3.09	0.26
40°	4.19	0.097	2.66	0.27
80°	3.27	0.100	2.06	0.27
120°	2.93	0.100	1.84	0.27
150°	2.68	0.100	1.64	0.27

RESULTS

The dielectric polarization of methyl chloride and of dichlorofluoromethane was measured at pressures from 50 to 800 mm, at five temperatures between 10° and 150°C, and at the fixed frequency of 402 Mc. At each temperature the molar polarization was plotted as a function of pressure and parameters of the Cole-Cole equation chosen to give the best fit. At high pressure the polarization approaches the low-frequency value, while at low pressure it approaches the value which it would have at frequencies above the region of dispersion. The linewidth parameter is found by dividing the measuring frequency, 402 Mc, by the pressure at which the molar polarization is midway between its extremes. One check on the accuracy of the data is the consistency of the extrapolated high-pressure and zero-pressure values of the molar polarization. Figure 1 shows these quantities for methyl chloride plotted against reciprocal temperature. The circles on the upper line are the extrapolated high-pressure values, which should be the ordinary static values of molar polarization. The line drawn is taken from low-frequency dielectric constant measurements by Fuchs.[9] It can be seen that the agreement is good.

[3] W. D. Hershberger, J. Appl. Phys. **17,** 495 (1946).
[4] G. Birnbaum, J. Chem. Phys. **27,** 360 (1957).
[5] J. E. Boggs, J. Am. Chem. Soc. **80,** 4235 (1958).
[6] J. E. Boggs and A. P. Deam, J. Phys. Chem. **64,** 248 (1960).
[7] G. Birnbaum and A. A. Maryott, J. Chem. Phys. **29,** 1422 (1958).
[8] A. A. Maryott, A. Estin, and G. Birnbaum, J. Chem. Phys. **32,** 1501 (1960).
[9] O. Fuchs, Z. Physik **63,** 824 (1930).

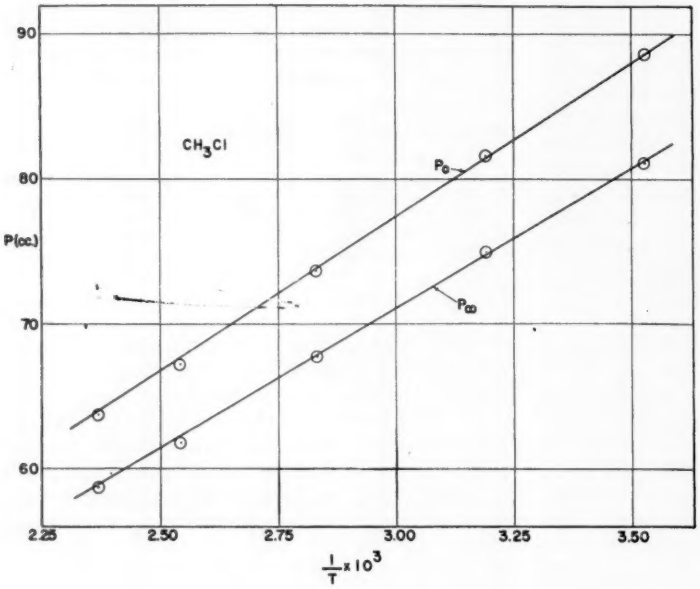

FIG. 1. Molar polarization of CH_3Cl vs reciprocal temperature. The upper line is a plot based on previous low-frequency dielectric constant measurements; the points on it are the present high-pressure extrapolated values. The lower line is calculated from the upper one; the points on it are the present low-pressure extrapolated values.

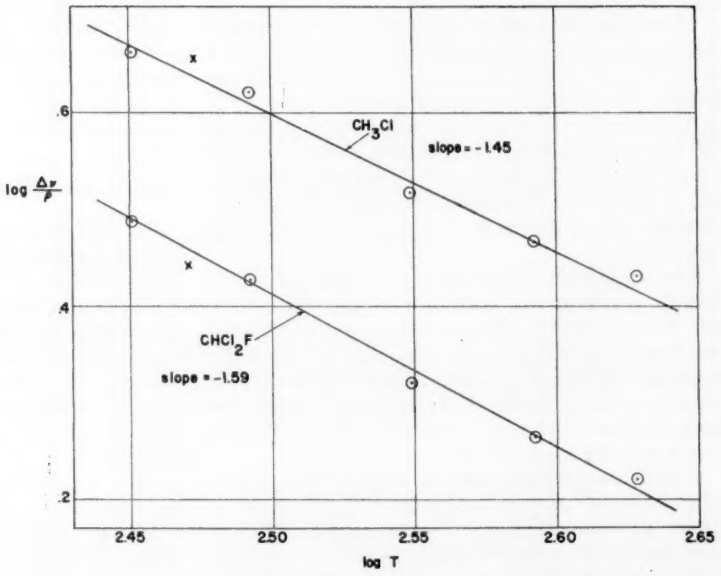

FIG. 2. Logarithm of the line-broadening constant vs logarithm of temperature. The circles represent measurements from this paper. The crosses are an earlier determination by Birnbaum at 26°. The slope of the line gives n in $\Delta\nu/p = kT^n$.

For a symmetric top rotor, such as methyl chloride,

$$\frac{P_0 - P_\infty}{P_0 - P_D} = (1/\mu^2)\Sigma f_{JK} \mid \mu_{JK} \mid^2$$

where P_0 is the static molar polarization, P_∞ is the polarization at high frequency, P_D is the distortion polarization found by extrapolating to zero reciprocal temperature, μ is the dipole moment, f_{JK} is the fractional number of molecules occupying the JK rotational energy level, and $\mid \mu_{JK} \mid$ is the dipole moment matrix element for inversion.[6] For methyl chloride, the sum on the right has been evaluated as 0.097.[10] The lower line in Fig. 1 shows that value of P_∞ calculated from this relationship and the low-frequency measurements by Fuchs. The points on the lower line are the extrapolated zero-pressure values of the molar polarization obtained in the present experiments.

[10] J. E. Walter and W. D. Hershberger, J. Appl. Phys. **17**, 814 (1946).

The results of the measurements at various temperatures are shown in Table I, which gives the derived values of the line-broadening constant and the ratio $(P_0-P_\infty)/(P_0-P_D)$. For the asymmetric rotor $CHCl_2F$, the polarization ratio has not been calculated from molecular parameters, but it should be constant, as the experiments have indicated it is.

To determine the exponential variation of the line-broadening parameter with temperature, the logarithm of the parameter is plotted against the logarithm of the absolute temperature in Fig. 2. The circles represent the value measured in the present work while the two crosses show the values determined at the single temperature of 26° by Birnbaum.[4] The determined values, $T^{-1.45}$ for CH_3Cl and $T^{-1.59}$ for $CHCl_2F$, are not thought to be significantly different from $T^{-1.5}$, but a $T^{-1.0}$ dependence would be far beyond experimental error.

CONCLUSIONS

The temperature dependence of the linewidth parameter as well as the absolute magnitude of the linewidth parameter predicted by the Anderson theory of collision broadening is not in agreement with experiment for nonresonant absorption. The correlation of linewidths by Birnbaum and Maryott does predict the correct temperature dependence, but it cannot give a complete prediction of the magnitude of the parameter. At the present time there does not appear to be a satisfactory theory of collision broadening that is applicable to nonresonant absorption.

THE JOURNAL OF CHEMICAL PHYSICS VOLUME 33, NUMBER 6 DECEMBER, 1960

Infrared Spectra and Structure of the Isomers of N_2F_2†

RUSSELL H. SANBORN

Lawrence Radiation Laboratory, University of California, Livermore, California

(Received June 17, 1960)

The isomers of N_2F_2 have been characterized in the past by their reactivity towards mercury. Investigation of the infrared spectra showed that inactive N_2F_2 is *trans*-1,2-difluorodiazine and may be identified by the single strong band centered at 989 cm^{-1}, with *PQR* structure. Active N_2F_2 resembles 1,1-difluorodiazine instead of a *cis*-isomer. This conclusion was reached by considering the mass spectrum, the chemical reactivity, and both the position of the infrared bands and their shapes. 1,1-difluorodiazine may be identified by strong bands at 1524 (*PR*), 952 (*PQR*), 896 (*PR*), and 737 (*PQR*) cm^{-1}, respectively. Normal coordinate analyses using the Wilson *FG*-matrix method were performed on both isomers.

INTRODUCTION

N_2F_2 was first prepared by Haller[1] in 1942 by the decomposition of fluorine azide. The electron diffraction pattern of this sample was determined by Bauer[2] in 1947. He assumed a 50–50% mixture of *cis*- and *trans*-isomers, and fitted the data with an N—F bond distance of 1.44 A, the N=N double bond 1.25 A, and the FNN angle 115°.

N_2F_2 has recently been made in substantial quantities in our laboratory by maintaining an electric discharge in a stream of nitrogen trifluoride in the presence of mercury vapor.[3] Gas chromatography with a silica-gel column maintained at a low temperature separates two fractions, each with a molecular weight of 66, corresponding to N_2F_2, but with vastly different chemical reactivity. One fraction reacts rapidly with mercury and explosively with diborane, the other does not. The infrared spectra of the two fractions differ markedly. From the infrared spectrum, the inactive form is readily interpreted as *trans*-1,2-difluorodiazine. The active form is best described as 1,1-difluorodiazine.

EXPERIMENTAL

The infrared spectra were recorded on a Perkin-Elmer model 21 infrared spectrophotometer equipped with NaCl and CsBr optics. Ten-centimeter cells with NaCl or CsBr windows were used.

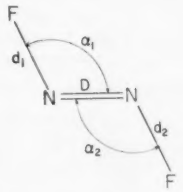

FIG. 1. *Trans*-1,2-N_2F_2 molecule.

Trans-1,2-difluorodiazine

Trans-1,2-difluorodiazine, diagrammed in Fig. 1, is a planar molecule with a center of symmetry and consequently of C_{2h} symmetry. It has three fundamental vibrations of species A_g, one of A_u and two of B_u. The

† This work was done under the auspices of the U. S. Atomic Energy Commission.

[1] J. F. Haller, Ph.D. thesis, Cornell University, 1942.

[2] S. H. Bauer, J. Am. Chem. Soc. **69**, 3104 (1947).

[3] J. W. Frazer, J. Inorg. & Nuclear Chem. **11**, 166 (1959).

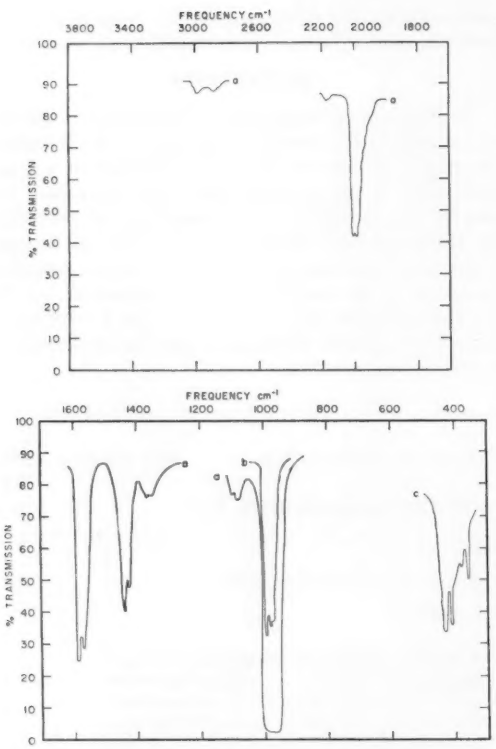

FIG. 2. Infrared spectrum of inactive N_2F_2. Pressures (mm of Hg): (a) 279; (b) 4.1; (c) 113.

A_g fundamental frequencies are active only in the Raman spectrum, and are forbidden in the infrared spectrum. These fundamentals are: ν_1, symmetric N—F stretch; ν_2, N=N double-bond stretch; and ν_3, symmetric

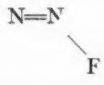

bend. The B_u and A_u fundamentals are allowed in the infrared spectrum. The B_u fundamentals are: ν_4, asymmetric N—F stretch; and ν_5, asymmetric

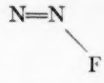

bend. The single A_u mode, ν_6, is the torsion out of the plane of the molecule.

TABLE I. Infrared bands of *trans*-1,2-difluorodiazine.

ν_{obs} (cm^{-1})	Intensity[a]	Assignment	Symmetry species
2975	vw	$2\nu_1+\nu_3+\nu_6$	A_u
2871	vw	$\nu_1+\nu_5+4\nu_6$	B_u
2159	vw	$\nu_1+\nu_5+2\nu_6$	B_u
1996	m	$\nu_2+\nu_6$	A_u
1581	m	$\nu_3+\nu_4$	B_u
1434	m	$\nu_1+\nu_5$	B_u
1366	m	$\nu_1+\nu_6$	A_u
1097	w		
989	vs	ν_4	B_u
421	m	ν_5	B_u
360	m	ν_6	A_u

[a] vw=very weak; m=medium; w=weak; vs=very strong.

TABLE II. Fundamental vibrations of *trans*-1,2-difluorodiazine.

Symmetry species	Fundamental	Frequency (cm^{-1})	Vibration
A_g	ν_1	1010	N—F symmetric stretch
A_g	ν_2	1636	N=N stretch
A_g	ν_3	592	N=N—F symmetric bend
B_u	ν_4	989	N—F asymmetric stretch
B_u	ν_5	421	N=N—F asymmetric bend
A_u	ν_6	360	Torsion

The observed infrared spectrum of the inactive form of N_2F_2 is presented in Fig. 2. The single strong band in the N—F stretching region between 850 and 1050 cm^{-1} identifies the isomer as *trans*-1,2-N_2F_2. The observed infrared bands with intensities and assignments are presented in Table I. The inactive fundamentals of species A_g were obtained from observed combinations with fundamentals of species A_u and B_u. The fundamentals of each symmetry class are given in Table II.

A normal coordinate analysis using the molecular parameters of Bauer[2] was performed by the Wilson *FG*-matrix method.[4] Calculation of the potential constants of the molecule involves solution of the secular determinant

$$|FG-\lambda E|=0$$

for each symmetry class. F is the potential energy matrix, G the kinetic energy matrix, E the unit matrix, and λ the eigenvalues of each determinant. Values of λ are calculated from the observed frequencies by the relation $\lambda=4\pi^2c^2\nu^2$, where ν is the observed frequency in cm^{-1}, and c is the velocity of light. The potential constants are adjusted to give good fit of the experimental frequencies.

TABLE III. Symmetry coordinates of *trans*-1,2-difluorodiazine.

d = N—F = 1.44 A
D = N=N = 1.25 A
α = $\angle$FNN = 115°

A_g:

$R_1=[\frac{1}{2}^{\frac{1}{2}}](\Delta d_1+\Delta d_2)$
$R_2=\Delta D$
$R_3=[\frac{1}{2}^{\frac{1}{2}}](\Delta\alpha_1+\Delta\alpha_2)$

B_u:

$R_4=[\frac{1}{2}^{\frac{1}{2}}](\Delta d_1-\Delta d_2)$
$R_5=[\frac{1}{2}^{\frac{1}{2}}](\Delta\alpha_1-\Delta\alpha_2)$

A_u:

$R_6=\Delta\gamma$

[4] E. B. Wilson, Jr., J. Chem. Phys. **7**, 1047 (1939); **9**, 76 (1941).

TABLE IV. Elements of the potential energy matrix of *trans*-1,2-N_2F_2.[a]

Species A_g:

$$F_{11}=f_d+f_{dd}$$
$$F_{12}=F_{21}=2^{\frac{1}{2}}f_{dD}$$
$$F_{13}=F_{31}=df_{d\alpha}'$$
$$F_{22}=f_D$$
$$F_{23}=F_{32}=2^{\frac{1}{2}}Df_{D\alpha}'$$
$$F_{33}=dD(f_\alpha'+f_{\alpha\alpha}')$$

Species B_u:

$$F_{44}=f_d-f_{dd}$$
$$F_{45}=F_{54}=df_{d\alpha}'$$
$$F_{55}=dD(f_\alpha'-f_{\alpha\alpha}')$$

Species A_u:

$$F_{66}=dDf_\gamma'$$

[a] The subscripts refer to the internal coordinates of the molecule. γ refers to the angle of the out-of-plane torsional vibration.

Table III contains the symmetry coordinates of each class; Table IV, the elements of F; and Table V, the elements of G.

There are only six experimental frequencies to determine nine potential constants, so that an exact calculation of the potential constants is impossible. Interactions between the two N—F bonds, and also the two FNN angles, were considered negligible in setting up the A_g and B_u matrices. The constant $f_{D\alpha'}$ was arbitrarily given the small positive value 0.20, and the other potential constants were varied until a reasonable fit of the experimental frequencies was obtained.

Table VI gives the values used for the potential constants and the calculated frequencies of the fundamental vibrations of *trans*-1,2-difluorodiazine. The force constants are in units of millidynes per angstrom.

1,1-Difluorodiazine

The active form of N_2F_2 could have either of the other two possible structures considered by Bauer.[2] They are presented in Figs. 3 and 4 as a *cis*-isomer and 1,1-difluorodiazine, a molecule with a separation of charge. The evidence is strongly against a *cis*-isomer.

The mass spectra of the two isomers, normalized against the mass "47" peaks, are given in Table VII.

TABLE V. Elements of the kinetic energy matrix of *trans*-1,2-N_2F_2.[a]

Species A_g:

$$G_{11}=\mu_F+\mu_N$$
$$G_{12}=G_{21}=2^{\frac{1}{2}}(\mu_N\cos\alpha)$$
$$G_{13}=G_{31}=(-2\mu_N/D)\sin\alpha$$
$$G_{22}=2\mu_N$$
$$G_{23}=G_{32}=-2^{\frac{1}{2}}(\mu_N/d)\sin\alpha$$
$$G_{33}=(\mu_F/d^2)+\mu_N[(4/D^2)+(1/d^2)-(4\cos\alpha/dD)]$$

Species B_u:

$$G_{44}=\mu_F+\mu_N$$
$$G_{45}=G_{54}=0$$
$$G_{55}=(d^2)^{-1}(\mu_F+\mu_N)$$

Species A_u:

$$G_{66}=(2/d^2\sin^2\alpha)(\mu_F+\mu_N)$$

[a] μ is the reciprocal of the mass of the atom in question. F=fluorine, N=nitrogen, cos=cosine and sin=sine.

TABLE VI. *Trans*-1,2-N_2F_2 potential constants and calculated frequencies.

f_d=4.60 md/A	f_{dd}=0	$f_{d\alpha}'$=0.42 md/A
f_D=11.10 md/A	f_{dD}=0.95 md/A	$f_{D\alpha}'$=0.20 md/A
f_α'=1.02 md/A	$f_{\alpha\alpha}'$=0	f_γ'=0.29 md/A

	Obs (cm^{-1})	Calc (cm^{-1})
ν_1	1010	1012
ν_2	1636	1638
ν_3	592	585
ν_4	989	989
ν_5	421	421
ν_6	360	360

Once the first fluorine atom is removed the patterns are quite similar. This can be seen by normalizing against the mass "28" peak instead of the "47" peak. For the active form to be this *cis*-isomer, the difference in the patterns would have to arise from the strain caused by having the two fluorines on the same side of the N=N double bond. Models of a *cis*-isomer indicate strong spatial as well as electronic interaction between the two fluorines, which raises the added possibility that a *cis*-isomer could not form at all.

A search for the microwave spectrum of the active N_2F_2 was made by Professor R. J. Myers of the University of California, Berkeley, but no lines could be found. Professor Myers concluded that the dipole moment must be less than 0.1 debye units. This information does not make either proposed form preferable, since NF compounds in general have small dipole moments. NF_2 has a dipole moment of 0.234 debye units[5] and N_2F_4 has one of 0.26 debye units.[6]

Both the *cis*-isomer and 1,1-difluorodiazine are of C_{2v} symmetry. Only the out-of-plane torsional vibration in the *cis*-isomer is forbidden in the infrared. The shapes of the infrared bands, presented in Fig. 5, are irreconcilable with a *cis*-isomer. The strong band at 737 cm^{-1} does not fit a *cis*-isomer. This band should be a bending fundamental, but, from the experience with *trans*-N_2F_2, all bending fundamentals should have much lower frequencies. The calculated moments of inertia of a *cis*-isomer and 1,1-difluorodiazine, using the molecule dimensions that fit the electron diffraction data of Bauer,[2] are shown in Table VIII. The molecules are assumed to be in the xz plane, with the z axis parallel to the N=N double bond. The smallest moment of inertia of a *cis*-isomer is parallel to the N=N double bond. Thus the N=N double-bond stretching vibration of the *cis*-isomer should show appreciable PQR structure.[7] Only infrared bands with P and R branches

FIG. 3. *Cis*-1,2-N_2F_2 isomer.

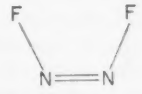

[5] M. Mashima, J. Chem. Phys. **24**, 489 (1956).
[6] D. R. Lide, Jr., and D. E. Mann, J. Chem. Phys. **31**, 1129 (1959).
[7] R. M. Badger and L. R. Zumwalt, J. Chem. Phys. **6**, 711 (1938).

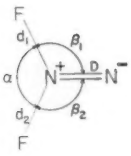

FIG. 4. 1,1-Difluorodiazine molecule.

TABLE VII. Mass spectra of N_2F_2 isomers. "47" patterns.

Mass peak	Ion	Inactive N_2F_2	Active N_2F_2
14	N^+	26.26	13.38
19	F^+	6.37	8.60
23.5	NNF^{++}	0.16	0.52
28	NN^+	99.02	58.73
33	NF^+	11.76	5.53
47	NNF^+	100.00	100.00
66	$FNNF^+$	21.56	0.16

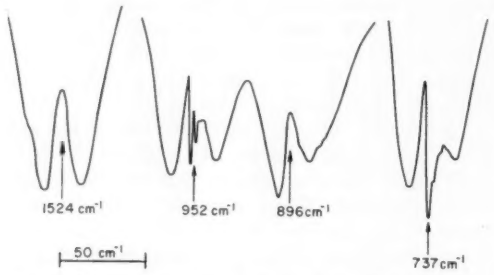

FIG. 5. Shapes of the strong infrared bands of active N_2F_2.

TABLE VIII. Moments of inertia of *cis*-1,2-N_2F_2 and 1,1-N_2F_2.

	cis-1,2-N_2F_2
N—F = 1.44 A	$I_z = A = 45.58$ (g cm² × 10^{40})
N=N = 1.25 A	$I_x = B = 113.3$ $(A/B) = 0.402$
∠FNN = 115°	$I_y = C = 158.9$
	1,1-N_2F_2
N—F = 1.44 A	$I_z = A = 58.9$
N=N = 1.25 A	$I_x = B = 107.5$ $(A/B) = 0.548$
∠FNF = 130°	$I_y = C = 166.4$

in the N=N double bond stretching regions are observed. The strongest band in this region is the one at 1524 cm^{-1}. Two bands corresponding to N—F stretching vibrations are observed at 952 and 896 cm^{-1}. The band at 952 cm^{-1} has a split *Q* branch with a separation of 3 cm^{-1}, while the band at 896 cm^{-1} has *PR* structure. In general, asymmetric stretching vibrations appear at higher frequencies than do the symmetric vibrations since more energy is required. In the case of a *cis*-isomer, the change in dipole moment of the asymmetric N—F stretch is parallel to the N=N double bond, and the band at 952 cm^{-1} fits this vibration nicely; however, the structure of the band is much different from the

TABLE IX. Comparison of bending frequencies of COF_2 and 1,1-N_2F_2.

Vibration	COF_2	1,1-N_2F_2
ν_3	626 cm^{-1}	552 cm^{-1}
ν_5	584	573
ν_6	774	737

band at 1524 cm^{-1}, which would have to be assigned to the N=N double-bond stretching vibration. Here the dipole moment change is also along the N=N double bond. They should show the same structure if the active form is the *cis*-isomer. In cases of *cis-trans* isomerism, in general, the only change in the potential function describing the fundamental vibrations is different values of the interaction constants. There are no similarities between the spectra of *trans*-N_2F_2 and active N_2F_2, suggesting that, if the active isomer were *cis*-, severe changes also occur in the principal force constants, which is contrary to what one would expect.

1,1-difluorodiazine could easily have the mass spectrum of the active isomer. The fact that there is no mass peak of 52 corresponding to NF_2 simply means that the N—F bond is very much weaker than the N=N bond. A molecule with two opposing centers of

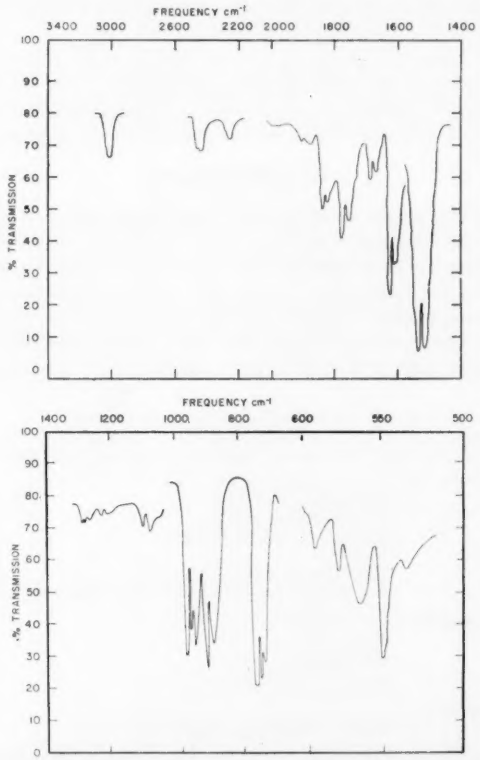

FIG. 6. Infrared spectrum of active N_2F_2. Pressures were not measured.

negative charge, as in

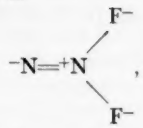

would be expected to have a small dipole moment. The intermediate moment of inertia of 1,1-difluorodiazine, referring to Table VIII, is along the N=N double bond. Vibrations in which the change in dipole moment is parallel to the axis of this moment of inertia have bands with *PR* structure.[7] Thus the N=N double-bond stretching and symmetrical N—F stretching vibrations are easily assigned to the bands at 1524 cm^{-1} and 896 cm^{-1}, respectively. The asymmetric N—F stretching vibration is parallel to the smallest moment of inertia, and the *PQR* structure of the band at 952 cm^{-1} fits this vibration.

TABLE X. Infrared spectrum of 1,1-difluorodiazine.

ν_{obs} (cm^{-1})	Shape	Intensity[a]	Assignment	Symmetry species
3023	*PR*	vw	$\nu_2+\nu_3+\nu_4$	B_1
2465	*PQR*	vw	$\nu_2+\nu_4$ $(2\nu_4+\nu_5)$	B_1
2420	*PR*	vw	$\nu_1+\nu_2$	A_1
2259	?	vw	$\nu_2+\nu_6$	B_2
1988	?	vvw	$\nu_1+2\nu_3$	A_1
1895	?	vvw	$2\nu_4$	A_1
1834	*PR*	w	$2\nu_5+\nu_6$	B_2
1774	*PR*	m	$2\nu_1$	A_1
1683	*PR*	w	$\nu_4+\nu_6$?	A_2
1619	*PR*	m	$\nu_1+\nu_6$	B_2
1524	*PR*	s	ν_2	A_1
1287	?	vw	$\nu_3+\nu_6$	B_2
1225	?	vvw		
1096	*PR*	vw	$2\nu_3$	A_1
952	*PQR*	vs	ν_4	B_1
896	*PR*	vs	ν_1	A_1
737	*PQR*	vs	ν_6	B_2
573	*PQR*?	vw	ν_5	B_1
552	*PR*	w	ν_3	A_1

[a] v=very; w=weak; m=medium; s=strong.

1,1-difluorodiazine is isoelectronic with carbonyl fluoride, COF_2. The bending frequencies assigned to 1,1-N_2F_2 are compared in Table IX with the corresponding bands in COF_2.[8] The similarity in the positions of the frequencies, especially of the out-of-plane mode ν_6, supports the existence of 1,1-difluorodiazine.

The complete infrared spectrum of active N_2F_2 is presented in Fig. 6. Table X gives the experimental frequencies, intensities and assignments of the bands. Table XI gives the assignment of the fundamentals of each symmetry class with a description of the vibration. The bands at 2420, 2465, and 3023 cm^{-1} were investigated with a small grating in place of the Littrow mirror in the Perkin-Elmer model 112 equipped with a KBr prism. The *P* branch of the ν_5 vibration at 573 cm^{-1} is assumed to be overlapped by the ν_3 doublet at 552 cm^{-1}.

TABLE XI. Fundamental vibrations of 1,1-difluorodiazine.

Symmetry species	Fundamental	Frequency (cm^{-1})	Vibration
A_1	ν_1	896	N—F symmetric stretch
A_1	ν_2	1524	N=N stretch
A_1	ν_3	552	F—N—F symmetric bend
B_1	ν_4	952	N—F asymmetric stretch
B_1	ν_5	573	F—N—F symmetric bend
B_2	ν_6	737	Out-of-plane bend

Two different normal coordinate analyses were attempted on 1,1-difluorodiazine, but only five of the six vibrations could be exactly calculated. No accurate structural data and only six experimental frequencies prevented any better fit than this. The most general harmonic force field used by Lindeman and Wilson[9] for the mixed halides of boron, requires 13 potential constants for an exact representation. Because of a large amount of interaction between vibrations in fluorine-containing compounds, most of the potential constants representing these interactions are required. This puts the necessary number of constants greater than the number of experimental points. Lovell, Stephenson, and Jones[8] used a combination of valence force terms and central force terms, amounting to six constants, to treat carbonyl fluoride, COF_2. This type of treatment of 1,1-N_2F_2, using the molecular parameters of *trans*-1,2-N_2F_2 and the potential constants shown, gave the calculated frequencies in Table XII. The good agreement satisfies the infrared spectrum of the active isomer of N_2F_2.

SUMMARY

The infrared spectrum of the inactive isomer of N_2F_2 was interpreted as that of *trans*-1,2-difluoridiazine. The active isomer of N_2F_2 was shown to be 1,1-difluorodiazine on consideration of chemical, mass-spectral, dipole-moment, and infrared-spectral evidence.

TABLE XII. 1,1-Difluorodiazine potential constants and calculated frequencies.

$F_d=3.354$	$F_\alpha=1.500$	$F_\gamma=0.326$
$F_D=8.700$	$F_\beta=0.364$	$K=0.750$

	Obs (cm^{-1})	Calc (cm^{-1})
ν_1	896	898
ν_2	1524	1524
ν_3	552	529
ν_4	952	952
ν_5	573	573
ν_6	737	737

[8] R. J. Lovell, C. V. Stephenson, and E. A. Jones, J. Chem. Phys. **22**, 1953 (1954).

[9] L. P. Lindeman and M. K. Wilson, J. Chem. Phys. **24**, 242 (1956).

ACKNOWLEDGMENTS

The author would like to thank Jack Frazer for preparing and purifying the N_2F_2 samples; Miss Patricia Cogswell for determining the mass spectra; and Dr. Edward Catalano and Dr. Earl Worden for critically reviewing the paper.

THE JOURNAL OF CHEMICAL PHYSICS VOLUME 33, NUMBER 6 DECEMBER, 1960

Vibrational Spectra of Orthorhombic Metaboric Acid

J. L. PARSONS

Scientific Laboratory, Ford Motor Company, Dearborn, Michigan

(Received May 27, 1960)

Infrared absorption spectra have been obtained in the 430 to 4000 cm^{-1} region for $B_3O_3(OH)_3$, $B_3{}^{10}O_3(OH)_3$, and $B_3O_3(OD)_3$, as polycrystalline mulls and, in the case of $B_3O_3(OH)_3$, as a single crystal section. A partial Raman spectrum has been obtained for $B_3O_3(OH)_3$ in the polycrystalline form. The spectral data have been interpreted in terms of the vibrations of the $B_3O_3(O^-)_3$ unit, with the D_{3h} symmetry of the unit perturbed by the crystal's potential field, plus the motions of the hydrogen atoms. The latter are regarded as those of an infinite chain which has a factor group isomorphic with the point group D_{2h}.

INTRODUCTION

THE vibrational spectra of orthorhombic metaboric acid were of interest in connection with an investigation of the vibrational spectra of vitreous $B_2O_3 \cdot xH_2O$.[1] The spectra were also interesting because they could be expected to exhibit effects resulting from (1) perturbation of the molecular symmetry by the potential field of the crystal and (2) coupling between identical atomic configurations.

Tazaki[2,3] has determined the crystal structure of orthorhombic metaboric acid and has shown that the crystal has the space group $V_h{}^{16}=D_{2h}{}^{16}$ (Pnam). The unit cell has the dimensions $a=8.01$ A, $b=9.79$ A, $c=6.24$ A and contains four $B_3O_3(OH)_3$ ring shaped molecules. The molecules are arranged in a layer structure, being joined within each layer by hydrogen bonds and with two of the molecules of the unit cell in one layer. The arrangement within one of the layers is shown in Fig. 1. In each $B_3O_3(OH)_3$ molecule, the average O–O distance is 2.37 A, the B–O distance 1.37 A and, although not determined by x rays, the O–H distance can be expected to be approximately 1 A. The average O–H—O distance between adjacent molecules is 2.74 A. The layers are separated by the comparatively large distance of 3.12 A with only van der Waals forces between them so that the crystal is readily cleaved parallel to the layers, i.e., parallel to the c face.

Goubeau and Hummel[4] have recently published an analysis of the infrared absorption spectra of orthorhombic metaboric acid and deuterated orthorhombic metaboric acid based on D_{3h} symmetry for the $B_3O_3(O^-)_3$ unit. However, they did not obtain the spectra of $B_3{}^{10}O_3(OH)_3$ and of $B_3O_3(OH)_3$ as a single crystal section. In addition, while there is broad agreement between their report and this work, significant differences occur in the spectra and in the interpretations of the spectra. The differences are discussed later.

EXPERIMENTAL

Analytical reagent grade powdered boric acid, $B(OH)_3$, was used to prepare all samples except boron-10 substituted orthorhombic metaboric acid, $B_3{}^{10}O_3(OH)_3$. The latter was prepared from boric acid for which the boron content was given as 96.6% boron-10 by the source for this material, the Oak Ridge National Laboratory. Polycrystalline orthorhombic metaboric acid was prepared by heating 0.5 to 1.5 g of powdered boric acid in a small open vessel for 24 hours at 100°C.[2] Single crystals of $B_3O_3(OH)_3$ were obtained by placing a few grams of polycrystalline orthorhombic metaboric acid in a sealed tube and heating the tube in an oven at 170–175°C.[5] After several weeks rhombic plates, up to 3 mm on a side, had formed on the wall of the tube. The nature of the single crystal as well as the polycrystalline samples was determined by means of their x-ray powder patterns.[3] To obtain deuterated orthorhombic metaboric acid, $B_3O_3(OD)_3$, boric acid was first dehydrated in a platinum crucible at about 1000°C to form boron oxide glass, B_2O_3. The B_2O_3 was then dissolved in 99.5% D_2O at 55°C in a dry nitrogen atmosphere. The temperature of the solution was lowered to 0°C, the liquid decanted, and the remaining material dried in a stream of warm dry

[1] J. L. Parsons and M. E. Milberg, J. Am. Ceram. Soc. **43**, 326 (1960).
[2] H. Tazaki, J. Sci. Hiroshima University **A10**, 37 (1940).
[3] H. Tazaki, J. Sci. Hiroshima University **A10**, 55 (1940).
[4] J. Goubeau and D. Hummel, Z. physik. Chem. Neue Folge **20**, 15 (1959).
[5] F. C. Kracek, G. W. Morey, and H. E. Merwin, Am. J. Sci. **235A**, 143 (1938).

nitrogen. The material thus obtained was estimated by means of its infrared spectrum to be approximately 99% $B(OD)_3$. Polycrystalline $B_3O_3(OD)_3$ was then prepared by heating $B(OD)_3$ as described above. D_2O–H_2O exchange was reduced during this step by heating the $B(OD)_3$ in a stream of nitrogen which had first passed through a trap cooled with liquid nitrogen and then over D_2O before reaching the sample.

A Perkin-Elmer model 13 spectrophotometer equipped with NaCl and KBr prisms and a Perkin-Elmer model 137 spectrophotometer were used to obtain spectra in the region between 430 cm^{-1} and 4000 cm^{-1}. Spectra of the polycrystalline materials were run as mulls in Nujol or hexachlorobutadiene, the latter material being used to expose those regions of the spectrum obscured by the Nujol. To obtain the spectrum of a single crystal, the crystal was cleaved parallel to the *c* face into several thin sections which were then mounted on a KBr window with paraffin wax and polished in place[6] with a dry ground glass plate until a useful spectrum was obtained. The polishing operation deposited polycrystalline material between the single crystal sections and the spectrum was obviously distorted by reflection and scattering losses but it still served to reveal those absorptions associated with vibrations parallel to the *c* face.

The partial Raman spectrum[7] of a polycrystalline sample of $B_3O_3(OH)_3$ was obtained using the complementary interference filter method of Brandmüller.[8] Attempts to obtain the Raman spectrum were seriously hampered by strong fluorescence so that only two strong lines were ultimately recorded. It cannot be said with certainty whether the fluorescence was primarily from the $B_3O_3(OH)_3$ or whether it should be attributed to impurities. Although the apparatus yielded an excellent Raman spectrum of polycrystalline boric acid, when the same boric acid was converted to polycrystalline $B_3O_3(OH)_3$, strong fluorescence appeared. However, the fluorescence was reduced when the $B_3O_3(OH)_3$ was prepared from $B(OH)_3$ which had first been recrystallized from water solution several times.

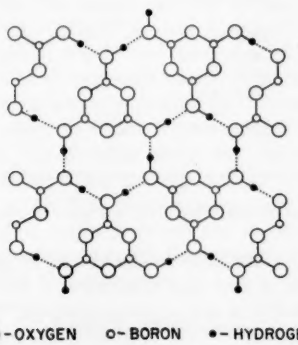

FIG. 1. The structure of a single layer of the orthorhombic metaboric acid crystal. Hydrogen bonds are shown by dotted lines.

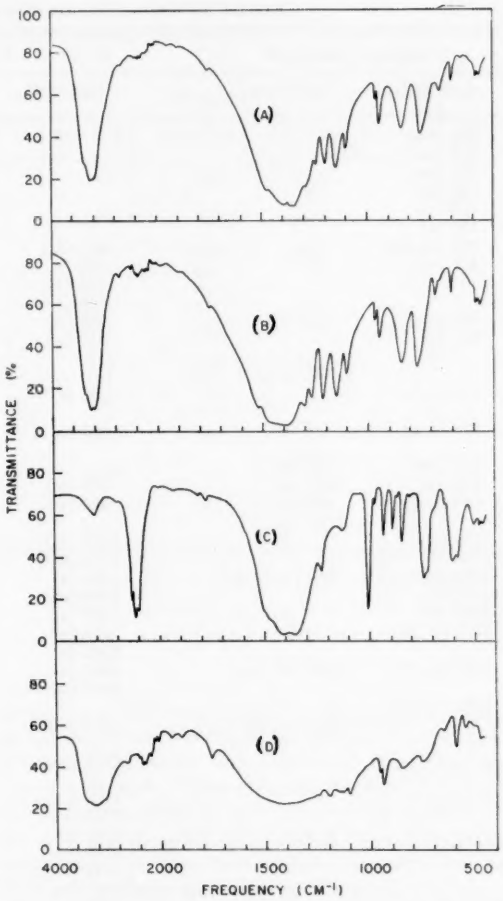

FIG. 2. Infrared spectra of orthorhombic metaboric acid. A, $B_3O_3(OH)_3$, (polycrystalline mull in Nujol and hexachlorobutadiene); B, $B_3{}^{10}O_3(OH)_3$, (polycrystalline mull in Nujol and hexachlorobutadiene); C, $B_3O_3(OD)_3$, (polycrystalline mull in Nujol and hexachlorobutadiene); D, $B_3O_3(OH)_3$, single crystal, radiation incident perpendicular to the layer shown in Fig. 1.

RESULTS

The infrared absorption spectra of polycrystalline $B_3O_3(OH)_3$, $B_3{}^{10}O_3(OH)_3$, $B_3O_3(OD)_3$, and a single crystal of $B_3O_3(OH)_3$ with the incident radiation perpendicular to the *c* face, are shown in Fig. 2. The frequencies of the observed absorption maxima, the corresponding values reported by Goubeau and Hummel,[4] and the Raman data are listed in Table I. These spectra differ from those reported in footnote reference

[6] D. E. Bethell and N. Sheppard, Trans. Faraday Soc. **51,** 9 (1955).

[7] The Raman work was performed by Dr. R. C. Taylor of the University of Michigan, under a contract with the Ford Motor Company.

[8] J. Brandmüller, Z. angew. Physik **5,** 95 (1953).

TABLE I. Infrared and Raman spectra (cm^{-1}) of orthorhombic metaboric acid.

Goubeau and Hummel[a]		This work			Raman
$B_3O_3(OH)_3$	$B_3O_3(OD)_3$	$B_3O_3(OH)_3$	$B_3{}^{10}O_3(OH)_3$	$B_3O_3(OD)_3$	$B_3O_3(OH)_3$
262 (vw)					
268 (vw)					
274 (vw)					
280 (m)					
415 (m)					
456 (s)					
462 (m, sh)		462 (m)	463 (m)	456 (m)	
476 (m)		478 (w, sh)	482 (w, sh)	474 (w, sh)	
		504 (vw)	504 (vw)	499 (m)	
		548 (vw)		577 (w)	
591 (m)		595 (w)	600 (w)	600 (s, b)	598±3 (s)
645 (s)		650 (w)	650 (vw)	639 (w)	
			675 (w)	680 (w)	
	718 (s, b)			727 (m)	
735 (s, b)		745 (s, b)	761 (s, b)	739 (s, b)	
				805 (vw)	
825 (s, b)	835 (w)	833 (s, b)	835 (s, b)	842 (m)	819±5 (s)
				865 (vw)	
885 (vw)	880 (w)			887 (m)	
942 (m)	925 (w)	939 (m)	942 (m)	930 (m)	
960 (vw)	970 (vw)	956 (w)	960 (w)	972 (w)	
	1005 (m)			1004 (s)	
1110 (w)		1099 (m)	1099 (m)		
		1132 (m)			
1150 (m)	1160 (w, b, sh)	1147 (s)	1153 (s)	1126 (w)[b]	
1200 (s)		1196 (m)	1212 (s)		
1245 (w)		1239 (s)	1267 (m)	1226 (w)	
1290 (w, sh)		1289 (w)	1300 (m)		
		1342 (vs)			
1375 (vs, vb)	1350 (vs, vb)	1360 (vs)		1358 (vs, b)	
		1397 (vs, vb)	1385 (vs, vb)	1407 (vs, b)	
1450 (s, vb)			1451 (vs, vb)	1441 (m, b)	
	1475 (w, sh)	1473 (m)		1477 (m, b)	
			1523 (m)	1504 (m, b)	
		1754 (vw)	1754 (vw)	1775 (vw)	
				1812 (vw)	
		1905 (vw)	1892 (vw)		
		1942 (vw)	1976 (vw)	1930 (vw)	
		2041 (vw)	2041 (vw)	2008 (vw)	
		2088 (vw)	2088 (vw)		
		2151 (vw)			
		2188 (vw)	2179 (vw)	2193 (vw)	
		2227 (vw)	2227 (vw)	2227 (vw)	
		2294 (vw)			
		2342 (vw)	2353 (vw)	2398 (s)	
		2415 (vw)	2410 (vw)	2454 (s)	
		2475 (vw)	2485 (vw)	2506 (s)	
		2646 (vw)	2717 (vw)	2825 (vw)	
		3195 (s)	3195 (s)		
		3257 (s)	3257 (s)	3215 (w)[b]	
		3356 (s)	3356 (s)		

[a] See reference 4.

[b] Absorption resulting from residual OH groups. vs, very strong; s, strong; m, medium; w, weak; vw, very weak; b, broad; vb, very broad; sh, shoulder; sp, sharp.

4. In particular, their infrared spectrum of $B_3O_3(OH)_3$ appears to be modified by the absorptions of boric acid.[4,6] This would explain why they have reported a very weak absorption at 885 cm^{-1} and strong absorptions at 645, 1196, and 1450 cm^{-1} in contrast to those reported in this work for the same regions, namely, 885 cm^{-1} (absent), 650 cm^{-1} (weak), 1196 cm^{-1} (medium), and 1397 cm^{-1} (very strong).

INTERPRETATION

The complete analysis of the infrared and Raman spectra of orthorhombic metaboric acid in terms of the fundamental vibrational modes of the crystal requires consideration of the four molecules of the crystalline unit cell, that is, a factor group analysis.[9,10] However, it has been shown[10,11] that, in general, the main features of the spectra of molecular crystals can be interpreted in terms of the molecular and site point groups associated with the center of gravity of the molecular unit.

[9] S. Bhagavantam and T. Venkatarayudu, *The Theory of Groups and Its Application to Physical Problems* (Andhra University, Waltair, India, 1951).

[10] H. Winston and R. S. Halford, J. Chem. Phys. **17**, 607 (1949).

[11] R. S. Halford, J. Chem. Phys. **14**, 8 (1946).

TABLE II. Selection rules, description of normal vibrations and frequency (cm^{-1}) assignments for the $B_3O_3(O^-)_3$ skeleton of orthorhombic metaboric acid for point group D_{3h}.

Species and activity	Description of normal vibration	Assignment[a]	Infrared $B_3O_3(OH)_3$	Infrared $B_3{}^{10}O_3(OH)_3$	Infrared $B_3O_3(OD)_3$	Raman $B_3O_3(OH)_3$
	[b]Symmetric B–OH[c] stretching	ν_1	1239	1267	1226	
A_1'	[b]Trigonal deformation of the B_3O_3 ring	ν_2	[d]	[d]	805	819
Raman	[b]Ring breathing (B–OH groups in phase)	ν_3	595	600	577	598
A_2'	[b]B atoms twisting against the O atoms	ν_4	1473	1523	1441	
Inactive	[b]OH groups twisting against the ring	ν_5	478	482	474	
	B–OH stretching	ν_6	1397	1451	1407	
E'	Ring stretching	ν_7	1342, 1360	1385	1358	
Infrared Raman	Ring stretching	ν_8	939	942	930	
	Ring angle bending	ν_9	462	463	456	
	B–OH rocking	ν_{10}	280[e]			
A_2''	Out-of-plane ring mode (B and O atoms out of phase)	ν_{11}	745	761	727, 739	
Infrared	B–OH wagging (OH groups in phase)	ν_{12}	(200)[f]			
E''	[b]B–OH wagging	ν_{13}	650	675	639	
Raman	Out-of-plane ring mode	ν_{14}	(215)[f]			

[a] Numbering follows the Herzberg scheme.
[b] Vibrations active under the site group symmetry C_{2v}.
[c] Oxygen atoms not in ring distinguished as OH groups.
[d] Obscured by strong OH absorption.
[e] From footnote reference 4.
[f] Estimated from data in footnote reference 14 and combination bands.

Unfortunately, as a result of the orientation of the hydrogen atoms relative to the $B_3O_3(O^-)_3$ skeleton, both the $B_3O_3(OH)_3$ molecule and its site in the orthorhombic crystal have, strictly speaking, very low symmetry. Nevertheless it is still possible to simplify the analysis of the spectra. As Hornig and Plumb[12] have pointed out in the case of boric acid, in a first approximation the vibrations of the $B_3O_3(OH)_3$ molecule may be divided into two classes, the vibrations of the heavy atom skeleton, $B_3O_3(O^-)_3$, and the motions of the hydrogen atoms, which are then treated separately. This division of vibrations is possible because the mass of the hydrogen atom is much less than the mass of the oxygen atom to which it is bonded.[13] In this approximation, the skeletal vibrations should be relatively insensitive to the arrangement of the hydrogen atoms. As a further simplification, the symmetry properties of a single layer of the crystal structure will be considered, since all the strong forces act between atoms in the same layer.

Skeletal Vibrations

The molecular symmetry of the $B_3O_3(O^-)_3$ unit is D_{3h} and the site symmetry in the $B_3O_3(O^-)_3$ layer lattice is C_{2v}. The nature of the vibrations of the $B_3O_3(O^-)_3$ skeleton will be determined essentially by the D_{3h} symmetry of the unit, while the lower order local symmetry C_{2v} of the potential field of the layer can be expected to perturb the molecular symmetry causing the selection rules to be less strict and the degenerate modes to be split. The correlation between the species of the D_{3h} point group and those of C_{2v} is shown in Fig. 4. The species, activity, description and frequency assignments of the fundamental vibrations of the $B_3O_3(O^-)_3$ skeleton are shown in Table II.

When the masses and forces involved are similar, the $B_3O_3(O^-)_3$ skeletal frequencies can be expected to resemble those assigned to corresponding vibrations in similar molecules of D_{3h} symmetry, such as 1,3,5-trifluorobenzene ($C_6H_3F_3$),[14] *s*-triazine ($C_3H_3N_3$),[15] 1,3,5-trideuterobenzene ($C_6H_3D_3$),[16] and other compounds containing the boroxole ring B_3O_3.[4,17] The frequency assignments shown in Table II have been made to agree as far as possible with the interpretations in the references just cited as well as with the experimental data reported here.

The two strong Raman lines near 819 and 598 cm^{-1} have been assigned to two of the totally symmetric vibrations of the $B_3O_3(O^-)_3$ group, the other expected

[12] D. F. Hornig and R. C. Plumb, J. Chem. Phys. **26,** 637 (1957).
[13] R. C. Lord and F. A. Miller, Appl. Spectroscopy **10,** 115 (1956).
[14] J. R. Nielsen, Ching-yu Liang, and D. C. Smith, Discussions Faraday Soc. **No. 9,** 177 (1950).
[15] J. E. Lancaster and N. B. Colthup, J. Chem. Phys. **22,** 1149 (1954); R. F. Stamm and J. E. Lancaster, *ibid.* **22,** 1280 (1954).
[16] C. R. Bailey, C. K. Ingold, H. G. Poole, and C. L. Wilson, J. Chem. Soc. **149,** 222 (1946); C. R. Bailey, J. B. Hale, N. Herzfeld, C. K. Ingold, A. H. Leckie, and H. G. Poole, *ibid.* **149,** 255 (1946).
[17] J. Goubeau and H. Keller, Z. anorg. u. allgem. Chem. **272,** 303 (1953).

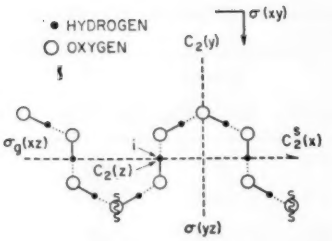

FIG. 3. Part of infinite chain formed by the hydrogen and oxygen atoms in $B_3O_3(OH)_3$, with the associated symmetry elements of the factor group isomorphic with the point group D_{2h}. C_2-twofold axis, C_2^s-twofold screw axis, σ-mirror plane, σ_g-glide plane, i-center of inversion. The repeating unit is shown between wavy vertical lines. Hydrogen bonds are shown by dotted lines. Hydrogen atoms are shown midway between the oxygen atoms to illustrate the D_{2h} symmetry on which the analysis of the hydrogen motions is based.

strong line[4,17] near 1200 cm^{-1} being obscured by fluorescence. Although these three fundamentals of species A_1' are forbidden in the infrared under D_{3h} selection rules, according to the C_{2v} site symmetry they are allowed. Therefore sharp weak absorptions in the infrared spectra have been assigned to the vibrations of this species, as shown in Table II. It can be expected that the ν_1 and ν_3 vibrations, involving principally symmetric breathing motion of the B-OH groups, will be more affected by the site symmetry and thus be more active in the infrared than the ν_2 vibration, a trigonal deformation of the ring. It may be noted that the symmetric breathing vibration of the BO_3 triangle in boric acid is active in the infrared even though it is theoretically allowed only by the symmetry of the factor group.

Some infrared activity might also be expected from species A_2' vibrations. Although most of the information published on this type of vibration is speculative in nature, weak to medium absorptions at 478 and 1473 cm^{-1}, for which no better alternative explanations could be found, have been assigned to this type of vibration.

The infrared spectrum obtained with the incident radiation perpendicular to the c face reveals that the absorptions at 650, 745, 833, and part of the absorption at 1147 cm^{-1} are associated with out-of-plane vibrations. The absorption at 745 cm^{-1} is strong and shows the expected isotope shifts for a boron-oxygen vibration. Therefore it has been assigned to the out-of-plane ring mode, species A_2''. The absorption at 650 cm^{-1} is shifted to 675 cm^{-1} in the spectrum of $B_3{}^{10}O_3(OH)_3$ which indicates that it should be assigned to a boron-oxygen vibration. However, the B-OH wagging fundamental (species A_2'') should be at a much lower frequency[14] but the corresponding E'' fundamental should appear in the 600 cm^{-1} region. Therefore, the absorption at 650 cm^{-1} has been assigned to the B-OH wagging vibration (species E'') which has become active in the infrared as a result of the site symmetry. The spectrum of $B_3O_3(OD)_3$ shows that the other two out-of-plane absorptions are associated with hydrogen motion.

The remaining medium or strong absorptions, which are relatively unaffected by deuteration, have been assigned to vibrations of species E' in a fairly straightforward manner. Apparently the degeneracy of ν_7 has been removed by the site symmetry so that a doublet appears (1342 and 1360 cm^{-1}). Classifying the absorption at 939 cm^{-1} as an E' fundamental deserves some comment. Although the associated normal vibration has been described as a ring stretching vibration, it is unusually sensitive to the masses of the ring substituents. The corresponding fundamental appears at 1485, 1407, and 1124 or 993 cm^{-1} in the infrared spectra of benzene, 1,3,5-trideuterobenzene and 1,3,5-trifluorobenzene, respectively. It is therefore not surprising to find this fundamental displaced so far from the other ring stretching absorption at 1360 cm^{-1}, since the latter shows very little sensitivity to ring substitution (1596, 1573, and 1610 cm^{-1} for the three compounds just cited).

Hydrogen-Oxygen Vibrations

The spectrum of the deuterated material shows that the remaining strong absorptions involve principally motion of the hydrogen atoms. Unlike the interpretation of the skeletal vibrations, analysis of the hydrogen-oxygen vibrations in terms of a single molecule of $B_3O_3(OH)_3$ is not a suitable procedure because the motions of the hydrogen atoms in the various molecules are strongly coupled through hydrogen bonds. This condition necessitates the choice of a different basic unit in order to predict the hydrogen spectrum.

The hydrogen atoms form part of infinite hydrogen-oxygen chains as shown in Figs. 1 and 3. In these chains, strong coupling forces exist between adjacent hydrogen atoms through hydrogen bonds. On the other hand, because of the difference in masses, the hydrogen motions are largely uncoupled from the boron-oxygen vibrations and the chains are isolated from each other by the relatively massive $B_3O_3(O^-)_3$ groups. It therefore seemed appropriate to choose an isolated hydrogen-oxygen chain as the basic unit for analyzing the hydrogen motions.

Tobin[18] has suggested that the effect of strong coupling in one direction in a molecular crystal might be treated as if the system had a line group type symmetry. This symmetry treatment has been applied in the case of the hydrogen-oxygen chain. The repeating unit in the chain is shown between the wavy lines in Fig. 3. Those symmetry elements which reproduce the repeating unit, with translations regarded as identity, constitute a factor group of the line group. In this case the factor group is isomorphic with the point group C_{2v} but the chain is close to having a factor group iso-

[18] M. C. Tobin, J. Chem. Phys. **23**, 891 (1955).

TABLE III. Selection rules, description of hydrogen motions and frequency (cm^{-1}) assignments for the hydrogen-oxygen chain for the factor group isomorphic with the point group D_{2h}.

Species and activity	Description of hydrogen motion	Assignment	Infrared $B_3O_3(OH)_3$	Infrared $B_3{}^{10}O_3(OH)_3$	Infrared $B_3O_3(OD)_3$
A_g Raman	Stretching	$\nu_1{}^H$			
	In-plane bending	$\nu_2{}^H$			
B_{1g} Raman	Stretching	$\nu_3{}^H$			
	In-plane bending (R_z)	$\nu_4{}^H$			
B_{2g} Raman	Out-of-plane bending (R_y)	$\nu_5{}^H$			
B_{3g} Raman	Rotation about the chain axis (R_x)	0			
A_u Inactive	Out-of-plane bending	$\nu_6{}^H$			
	Out-of-plane bending	$\nu_7{}^H$			
B_{1u} Infrared	Out-of-plane bending	$\nu_8{}^H$	833	835	600
	Translation (T_z)	0			
B_{2u} Infrared	Stretching	$\nu_9{}^H$	3356	3356	2506
	In-plane bending	$\nu_{10}{}^H$	1196	1212	1004
	In-plane bending	$\nu_{11}{}^H$	1147	1153	887
	Translation (T_y)	0			
B_{3u} Infrared	Stretching	$\nu_{12}{}^H$	3257	3257	2454
	Stretching	$\nu_{13}{}^H$	3185	3195	2398
	In-plane bending	$\nu_{14}{}^H$	1099	1099	842
	Translation (T_x)	0			

morphic with the point group D_{2h}. Since the optical activity of the hydrogen motions observed in this investigation agrees with the selection rules based on D_{2h} symmetry, it would appear that, as a result of the hydrogen bonding, the electric moment of the hydrogen-oxygen configuration transforms according to D_{2h} rather than C_{2v} symmetry. Therefore, in order to analyze the hydrogen spectrum, the chain was assumed to have D_{2h} symmetry. The symmetry elements of the factor group are shown in Fig. 3. The hydrogen motions are then readily classified in terms of the irreducible representations (symmetry species) of the factor group by the usual procedure for group analysis.[9]

The species, activity, description and assignment of the hydrogen motions are shown in Table III. The assignment of the three hydrogen stretching frequencies and the three in-plane bending frequencies to specific O-H vibrations must be regarded as tentative. The in-plane bending vibration represented by the absorption at 1196 cm^{-1} ($\nu_{10}{}^H$) in the $B_3O_3(OH)_3$ spectrum deserves special comment. This fundamental exhibits considerable interaction with a boron-oxygen vibration as shown by the shift from 1196 cm^{-1} to 1212 cm^{-1} for $B_3{}^{10}O_3(OH)_3$ and to 1004 cm^{-1} (expected frequency 920 cm^{-1}) for $B_3O_3(OD)_3$. The intensity was also greatly enhanced by deuteration, indicating that the interaction had increased through resonance, so that the interacting boron-oxygen vibration is probably the ν_8 (species E') vibration represented by the absorption at 939 cm^{-1} in the $B_3O_3(OH)_3$ spectrum. According to the assignments made here both ν_8 and $\nu_{10}{}^H$ belong to the species A_1 of the subgroup C_{2v} (see Fig. 4).

Combinations and Overtones

Several very weak to medium infrared absorptions listed in Table I which have not already been assigned, can be interpreted as combination or overtone bands. Possible assignments for most of these absorption bands are listed in Table IV. Some of the absorptions have been left unassigned because it was felt that the complete Raman spectrum, especially the displacements due to the hydrogen vibrations, as well as the far infrared spectrum, were needed to complete the interpretation of the weak absorptions.

Several of the combination bands appearing in the

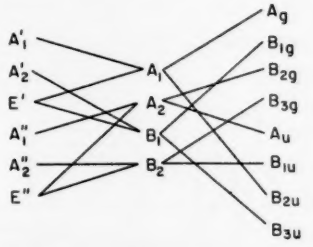

FIG. 4. Correlation chart between the symmetry species of the group C_{2v} and the groups D_{2h} and D_{2h}. The $C_2(y)$ axis of both D_{2h} and D_{2h} becomes the twofold axis of C_{2v} and the z coordinate is normal to the plane of the molecule in each case.

TABLE IV. Interpretation of combination and overtone bands in the infrared spectrum of orthorhombic metaboric acid, $B_3O_3(OH)_3$.

Observed frequency in cm^{-1}	Interpretation
415[a]	(200)+(215)=415 (E')
548	2×280[a]=560 ($A_1'+A_2'+E'$)
956	(215)+745=960 (E')
1132	?
1289	?
1754	?
1905	?
1942	595+1360=1955 (E')
2041	939+1099=2038
2088	939+1147=2086
2151	939+1196=2135
2188	819+1360=2179 (E') 939+1239=2178 (E')
2227	819+1397=2216 (E')
2294	939+1360=2299 ($A_1'+A_2'+E'$)
2342	939+1397=2336 ($A_1'+A_2'+E'$)
2415	939+1473=2412 (E')
2475	?
2646	1239+1397=2636 (E')

[a] From footnote reference 4.

various spectra deserve special comment. The assignment of the 1004 cm^{-1} and the 930 cm^{-1} absorptions in the spectrum of the deuterated material to ν_{10}^H and ν_8, respectively, is substantiated by the evidence from combination bands, since the 930 cm^{-1} frequency combines with 842, 887, and 1004 cm^{-1} to give three frequencies close to the absorption frequencies observed at 1775, 1812, and 1930 cm^{-1}. If the roles of the 1004 and 930 cm^{-1} frequencies were reversed, the above combinations could not be formed.

As stated previously the normal incidence spectrum [Fig. 2(D)] shows that part of the absorption at 1147 cm^{-1} is associated with an out-of-plane vibration. This must be a combination band since it is very unlikely that an out-of-plane ring or hydrogen vibration would occur at such a high frequency. While no precise assignment could be made, it is suggested that this out-of-plane absorption results from ν_8^H (833 cm^{-1}) combining with a rotary vibration of the hydrogen-oxygen chain.

DISCUSSION

Goubeau and Hummel[4] assigned absorptions at 476 cm^{-1} and 591 cm^{-1} to out-of-plane vibrations (species A_2'') and absorptions at 735 and 1150 cm^{-1} to in-plane vibrations (species E'), whereas the single crystal spectrum shows that the first two should be assigned to in-plane vibrations and the other two absorptions to out-of-plane vibrations. It should be noted that in both reports, part of the absorption at 1150 cm^{-1} has been assigned to an O-H in-plane vibration. They have assigned an absorption at 645 cm^{-1} to an out-of-plane hydrogen vibration. As already noted, the assignment of the absorption at 650 cm^{-1} in this report to a boron-oxygen vibration is based on the shift to 675 cm^{-1} in the spectrum of $B_3{}^{10}O_3(OH)_3$. The assignment of the broad, strong, absorption reported here at 1397 cm^{-1} to a B-OH stretching vibration (species E'), rather than combination bands as in footnote reference 4, is based on its response to B^{10} substitution and expected broadening as a result of splitting of the degenerate frequency, the B^{10} isotope shift of ν_6 and ν_7 and possible interaction with lattice vibrations.

Several other differences occur in our respective interpretations of the spectra of both $B_3O_3(OH)_3$ and $B_3O_3(OD)_3$ but it does not seem appropriate to pursue the comparison further here. It should be apparent that the frequency assignments have been greatly facilitated by the single crystal and isotope spectra. This points up the desirability of even more extensive experimental data such as the Raman and far infrared spectra of the same materials.

ACKNOWLEDGMENTS

The author wishes to thank Dr. M. E. Milberg and Dr. A. D. Brailsford of this laboratory and Dr. R. C. Taylor of the University of Michigan for participating in several helpful discussions of this work and also to acknowledge his indebtedness to Dr. Milberg for suggesting the investigation and supplying the single crystal of orthorhombic metaboric acid.

Letters to the Editor

THE Letters to the Editor section is subdivided into three parts entitled Communications, Comments and Errata, and Notes. These three sections are all subject to the same limitations on length. The textual material of each Letter is limited to a number of words equal to 950 minus the following; (a) 200 words for each average-sized figure: (b) 50 words for each displayed equation: (c) 7 words for each line of table including headings and horizontal rulings. No proof will be sent to the authors of "Communications" and "Comments and Errata." Proof will be sent to the authors of "Notes." The publication charge for Letters is $30 per page, with a minimum of $30 per Letter, If honored, the Institution will be entitled to 100 reprints without covers. See issues of May–September, 1957, for descriptions of categories.

Communications

The Raman Spectrum of Gaseous CF_4†

B. MONOSTORI AND A. WEBER

Department of Physics, Fordham University, New York

(Received September 8, 1960)

ALTHOUGH the infrared and Raman spectra of the halogenated methanes have been extensively studied, there have been only two investigations of the Raman spectrum of tetrafluoromethane.[1,2] Claassen[2] has investigated the Raman spectrum of the gas under moderate dispersion and resolving power.

As part of a program on the rotation-vibrational Raman spectra of polyatomic molecules, we have photographed the Raman spectrum of CF_4 and report at this time some preliminary results of the study. The spectra were photographed with a Jarrell-Ash 21-ft concave grating spectrograph capable of a dispersion of approximately 5 A/mm (26 cm^{-1}/mm at 4358 A). Excitation of the Raman spectrum was accomplished by means of the techniques developed by Welsh[3] and Stoicheff.[4] The gas pressure was 2 atm and the spectra were photographed on Kodak 103a-J plates with exposure times up to 48 hrs and slit widths of 60 and 80 μ. A smoothed microphotometer trace of the spectrum is

TABLE I. Raman spectrum of tetrafluoromethane (CF_4).

Wavenumber (cm^{-1})	Assignment
418	$(O-P)_{max}$
435.0	Q } $\nu_2(e)$
451	$(R-S)_{max}$
467	$\nu_1-\nu_2$ (E)
624	$(O-P)_{max}$
631.2	Q } $\nu_4(f_2)$
638	$(R-S)_{max}$
866.8	$2\nu_2(A_1+E)$
908.5	$\nu_1(a_1)$
1234	$\nu_3(f_2)^{13}CF_4$
	F_2
1258	} $2\nu_4(A_1+E+F_2)$
1263	(A_1+E)
1273	$(O-P)_{max}$
1283.0	Q } $\nu_3(f_2)$
1294	$(R-S)_{max}$
1314	?
1324	?

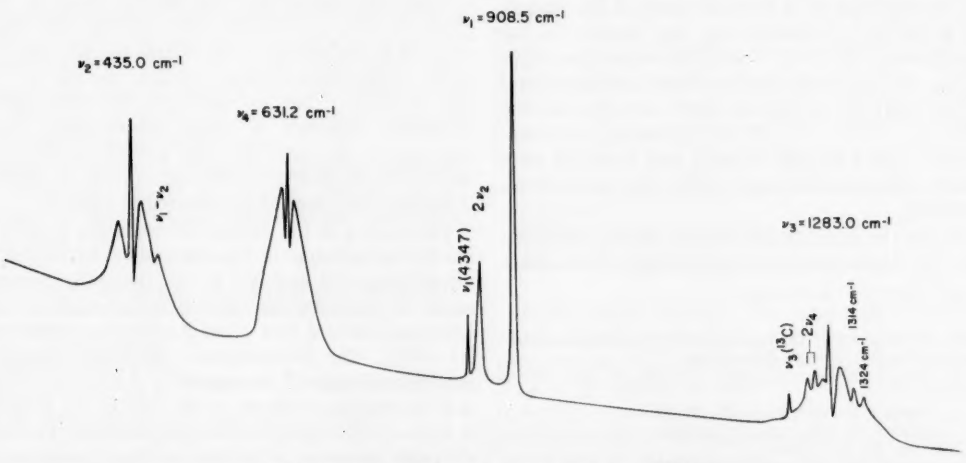

FIG. 1. Raman spectrum of gaseous tetrafluoromethane.

shown in Fig. 1 and the wavenumbers of the bands are listed in Table I. The wavenumbers of the Q-branches were determined with a comparator whereas weak bands and the maxima of the broad rotational branches were measured on microphotometer traces.

The fundamental vibrations occur at $\Delta\nu_1=908.5$ cm^{-1} (a_1), $\Delta\nu_2=435.0$ cm^{-1} (e), $\Delta\nu_3=1283.0$ cm^{-1} (f_2), and $\Delta\nu_4=631.2$ cm^{-1} (f_2). The rotation-vibration bands are seen to be partially resolved. The separation of the maxima of the rotational branches of the ν_2 band is 33 cm^{-1} which is somewhat greater than that expected on the basis of the theoretical expression

$$(\Delta\nu)_{\max}=4.5(BkT/hc)^{\frac{1}{2}}\text{ cm}^{-1}$$

derived by Placzek and Teller.[5] Thus, using Hoffman and Livingston's[6] value of 1.317 A for the C—F bond length and a gas temperature of 323°K, the separation is predicted to be 29.6 cm^{-1}. Weak grating ghosts expected to fall near the positions of the R−S maximum, and expecially the $O-P$ maximum of ν_4, cause the intensities of these maxima to be enhanced. The triply degenerate ν_3 band is quite complex. Its resolution may prove difficult since it is perturbed by the overtone $2\nu_4(A_1+E+F_2)$. The peak at 1234 cm^{-1} is suggested as the ν_3 band of the $^{13}CF_4$ molecule.[7] The peaks at 1314 cm^{-1} and 1324 cm^{-1} are at present not accounted for and may be spurious. Unfortunately the quality of the present spectrograms is not particularly good in this region due to the "grass" type of grating ghosts which begin to appear in this region in long exposures.

The interesting aspect here is the direct evaluation of the Coriolis coupling coefficients whose determination by means of the rotation-vibrational Raman spectrum is more favorable in this case than when determined by means of the more commonly used infrared absorption technique. Thus, the spacings of the lines in the $S^+(\Delta J=+2)$ and $0^-(\Delta J=-2)$ series of the Raman band is $2B(2+\zeta_i)$ whereas the line spacing in the infrared band is $2B(1-\zeta_i)$. Using the values $\zeta_3=+0.84$ and $\zeta_4=-0.35$ as determined by Edgell and Moynihan[8] from the study of the infrared band contours, the line spacings would be $\Delta\nu=1.09$ cm^{-1} (Raman) and $\Delta\nu=0.06$ cm^{-1} (I.R.) for the ν_3 band, and $\Delta\nu=0.63$ cm^{-1} (Raman) and $\Delta\nu=0.52$ cm^{-1} (I.R.) for the ν_4 band, respectively.

Work on the rotation-vibrational Raman spectrum of CF_4 with improved apparatus yielding higher resolution and dispersion is in progress.

† This work is aided by the support of the Research Corporation and the National Science Foundation.

[1] D. M. Yost, E. N. Lassetre, and S. T. Gross, J. Chem. Phys. **4,** 325 (1935).
[2] H. H. Claassen, J. Chem. Phys. **22,** 50 (1954).
[3] H. L. Welsh, E. J. Stansbury, J. Romanko, and T. Feldman, J. Opt. Soc. Am. **45,** 338 (1955).
[4] B. P. Stoicheff, Can. J. Phys. **32,** 330 (1954).
[5] G. Placzek and E. Teller, Z. Physik, **81,** 209 (1933).
[6] W. W. Hoffman and R. L. Livingston, J. Chem. Phys. **22,** 565 (1953).
[7] J. Goubeau, W. Bues, and F. W. Kampmann, Z. anorg. u. allgem. Chem. **283,** 123 (1956).
[8] W. F. Edgell and R. E. Moynihan, J. Chem. Phys. **27,** 155 (1957).

The Biradical Paradox*

HARDEN M. MCCONNELL†

Gates and Crellin Laboratories of Chemistry,‡ California Institute of Technology, Pasadena, California

(Received October 10, 1960)

REITZ and Weissman[1] have reported that in large biradicals such as Tschitschibabin's hydrocarbon (Tbb) the rate of spin exchange between the two triphenylmethyl groups is small compared to the observed C^{13} nuclear hyperfine splittings, $\Delta\nu\sim100$ Mc. Such observations suggest that the ground-state singlet-triplet splittings ΔU are small compared to $h\Delta\nu$. But theoretical calculations[2] indicate that at most nuclear configurations $|\Delta U|\gg h\Delta\nu$. We suggest here an explanation of this apparent paradox.

Let θ be an intramolecular nuclear coordinate representing, for example, the relative angle of rotation of the two phenyl groups about the central bond in Tbb. Let $S_0(\theta)$, $T_1(\theta)$, $T_0(\theta)$, $T_{-1}(\theta)$ be the energies of the singlet and triplet manifold of states in the absence of nuclear hyperfine and spin-orbit interactions. Note that $\Delta U=T_0-S_0$. For brevity represent the *magnitudes* of the nuclear hyperfine and *effective* spin-orbit Hamiltonian operators by $h\Delta\nu$ and ξ, and let δ be the larger of the two. Here $\xi\sim|\mathbf{g}_1-\mathbf{g}_2|\beta H_0$ where $\mathbf{g}_1$ and $\mathbf{g}_2$ are the spectroscopic splitting factor tensors for the two halves of the biradical. Divide the intramolecular potential surface into two regions, I and II. In I, $|\Delta U|<|\delta|$, and in II, $|\Delta U|>|\delta|$. On relative rotation of the planes of the central phenyl groups (or other conjugated π-electron systems) we may not only find a region I, but we may find that this region is thermally accessible at room temperature. Assume that this is the case and that solvent viscosity plus large-molecule inertia is sufficient to hold the biradical in region I for a time long compared to $(2\pi\Delta\nu)^{-1}$.

The ratio η of the number of molecules in I to the number of molecules in II is determined by the relative magnitudes of δ and ΔU in the thermally accessible region of the intramolecular potential surface, crude estimates indicate that η could easily be in the range 0.1−10%. The paramagnetic resonance spectra of molecules in region I correspond to slow spin exchange, and the resonance spectra of the bulk of the molecules in region II correspond to fast spin exchange. The essential point, however, is that the spectra of molecules in I are sharp and the spectra of molecules in II are *broad*.

Briefly, the argument is this. In region I, δ removes the S_0, T_0 degeneracy and the relaxation rate is typical of that of a normal monoradical. The stationary state functions $\psi(S_0)+\psi(T_0)$ and $\psi(S_0)-\psi(T_0)$ in this region may, however, be regarded as involving a coherent (fixed relative phase) interconversion of the $\psi(S_0)$ and $\psi(T_0)$ states at a rate $\sim h^{-1}\delta$. In region II there is an *effective* degeneracy of the S_0 and T_0 states, the electronic energy difference ΔU being made up by low frequency nuclear motions in these "loose" biradicals. Here again the $S_0 \rightleftharpoons T_0$ interconversion is expected to be of the order of $h^{-1}\delta$ (if $kT \gtrsim \Delta U$), but now the process is essentially random in character. Thus, in II, magnetic dipole transitions from T_{-1} or T_{+1} to T_0 are broad (width $\sim h^{-1}\delta$) because of the intercombination relaxation between T_0 and S_0. If δ is determined by the hyperfine interactions themselves, then rapid exchange spectra will show no well-resolved hyperfine structure. If the spin-orbital contribution is larger, $\delta=\xi \gg h\Delta\nu$, the rapid exchange spectra may not be detectable at room temperature. Of course there is an additional source of broadening due to the changing relative values of δ and ΔU in the transition region between $|\Delta U| \gg \delta$ and $|\Delta U| \ll \delta$.

This idea, which will be discussed more quantitatively elsewhere, appears to be consistent with experimental observations. For example, the apparent loss of resonance intensity with decreasing temperature[1] is due to depopulation of the cross-over region I, irrespective of whether or not the lowest electronic state is singlet or triplet. This may account for the otherwise surprising loss of apparent resonance intensity[1] in 1,3-*bis*-(diphenylmethylenyl)-benzene at the lower room temperatures, since one would suspect on theoretical grounds that this molecule should have a triplet ground state. The present proposal suggests that the resonance spectrum of this and related biradicals should "reappear" at very low temperatures (e.g., liquid He) where the rate of the $S_0 \rightleftharpoons T_0$ process is severely reduced and show a fast-exchange spectrum. We also suggest the possibility of observing *broad* unresolved *fast-exchange spectra* in any of these biradicals in liquids at room temperature, perhaps at high rf powers where the slow-exchange spectra are saturated.

I wish to express my sincere thanks to Professor S. I. Weissman, Dr. H. S. Jarrett, and Dr. R. W. Warring for many helpful conversations concerning this problem.

* Sponsored by the National Science Foundation, by the Office of Ordnance Research, U. S. Army, and by the U. S. Public Health Service.
† Alfred P. Sloan Fellow.
‡ Contribution No. 2638.
[1] D. C. Reitz and S. I. Weissman, J. Chem. Phys. **33**, 700 (1960).
[2] H. M. McConnell, J. Chem. Phys. **33**, 115 (1960).

Comments and Errata

Strength of the N—N Bond in Tetrafluorohydrazine

CHARLES B. COLBURN AND FREDERIC A. JOHNSON

Rohm and Haas Company, Redstone Arsenal Research Division, Huntsville, Alabama

(Received September 1, 1960)

LOUGHRAN and Mader[1] recently reported that the bond dissociation energy of the F_2N—NF_2 bond in tetrafluorohydrazine undergoing electron bombardment is 1.3±0.3 ev. This value was based on the appearance potential of the NF_2^+ ion and the appearance potential of the NF^+ ion assuming that the fragmentation processes are

$$e+N_2F_4 \rightarrow NF_2^+ + NF + F^- + e$$

and

$$e+N_2F_4 \rightarrow NF^+ + NF + F^- + F + e.$$

We have studied the dissociation of

$$N_2F_4 \rightleftarrows 2NF_2(l)$$

by two independent methods: (a) measurement of pressure variation with temperature at constant volume and (b) the temperature dependence of the uv absorption at 260 mμ (due to absorption by NF_2). These studies have given values for reaction (1) of $\Delta H = +19.2$ kcal. $\Delta S = 38.6$ eu. The details of these studies will appear at a later date.

TABLE I.

Species	*m/e*	Relative Abundance I[a]	II[b]	III[c]	IV[d]
$N_2F_4^+$	104	...	...	2.2%	0.2%
$N_2F_3^+$	85	...	...	6.6%	1.3%
$N_2F_2^+$	66	...	...	7.4%	0.7%
NF_2^+	52	57.6%	90.6%	100 %	100 %
N_2F^+	47	...	...	7.8%	0.7%
NF^+	33	100 %	100 %	40.6%	134.5%
N_2^+	28	0.2%	7.7%	5.0%	1.7%
F^+	19	6.6%	4.7%	3.5%	6.9%
NF^{++}	16.5	0.3%	...	...	...
N^+	14	11.4%	8.5%	6.4%	12.8%

[a] Reference 1.
[b] Reference 2.
[c] This work (ionization chamber at room temperature).
[d] This work (ionization chamber at approximately 170°C).

These values indicate that under the conditions which normally prevail in mass spectrometer ionization sections, N_2F_4 will be completely dissociated into NF_2. It is significant that the two published mass spectra of tetrafluorohydrazine[1,2] do not show a mass peak for any of the following ions, $N_2F_4^+$(*m/e* 104), $N_2F_3^+$(*m/e* 85), $N_2F_2^+$(*m/e* 66), and N_2F^+(*m/e* 47).

We have recently obtained a mass cracking pattern of tetrafluorohydrazine with the heaters in the ionization chamber turned off, i.e., ionization chamber approximately room temperature instead of its normal operating temperature of about 170°C. The four available mass cracking patterns of tetrafluorohydrazine are given in Table I.

It is apparent from these spectra that the inconsistency between them is due to the difference in the position of the equilibrium $N_2F_4 \rightleftarrows 2NF_2$ in the samples being analyzed. It is also suggested that the appearance potential measured by Loughran and Mader AP $(NF_2^+) = 11.8 \pm 0.2$ ev is simply the ionization potential of NF_2.[3] This number is in good agreement with the value estimated by Reese and Dibeler[4] of 11.0 ev for the ionization of the NF_2 radical.

The authors wish to express their appreciation to Al Kennedy for the mass spectral cracking patterns reported herein and to Dr. Carl Bumgardner for valuable discussions on the above problems. This work was performed under the sponsorship of the Army Ordnance Corps.

[1] E. D. Loughran and C. Mader, J. Chem. Phys. **32,** 1578 (1960).
[2] C. B. Colburn and A. Kennedy, J. Am. Chem. Soc. **80,** 5004 (1958).
[3] After consideration of our N—N bond energy, Loughran and Mader agree that the value of 11.8 ev is probably the ionization potential of NF_2. They suggest the following set of mechanisms:

m/e	A.P.	Postulated Mechanism
52	11.8	$NF_2 = NF_2^+$ thus $IP(NF_2) = 11.8$
33	15.0	$NF_2 = NF^+ + F$
		Thus $AP(NF^+) = IP(NF) + D(FN—F)$
		$= 12.0 + 2.7$
		$= 14.7.$

There was also a break in their appearance potential curve for m/e 52 at 12.5 ev and they suggest the process $N_2F_4 \rightarrow NF_2 + NF_2^+$ which gives an N—N bond strength of 16–25 kcal/mole in excellent agreement with that reported herein; however, another possibility is an excited state of the NF_2^+ ion. (Private communication to the authors from C. L. Mader and E. D. Loughran.)
[4] R. M. Reese and V. H. Dibeler, J. Chem. Phys. **24,** 1175 (1956).

Analysis of Reactive Scattering in Crossed Molecular Beams*

DUDLEY R. HERSCHBACH

Department of Chemistry and Lawrence Radiation Laboratory, University of California, Berkeley, California

(Received September 19, 1960)

IN their recent paper, *Variation of a Chemical Reaction Cross Section with Energy,* Greene, Roberts, and Ross[1] report a study of the K+HBr→H+KBr reaction in crossed molecular beams. The K velocity was selected mechanically and the HBr velocity spread diminished by holding the source at a low temperature. The ratio of the scattered intensity of KBr to elastically scattered K, observed at a laboratory angle of 35°, appeared to rise sharply above the background at a relative initial kinetic energy (RIKE, in kcal/mole) of 1.4, reach a maximum at 3.3, and thereafter decline. We wish to point out several effects that must be taken into account in the interpretation of these results and similar experiments.

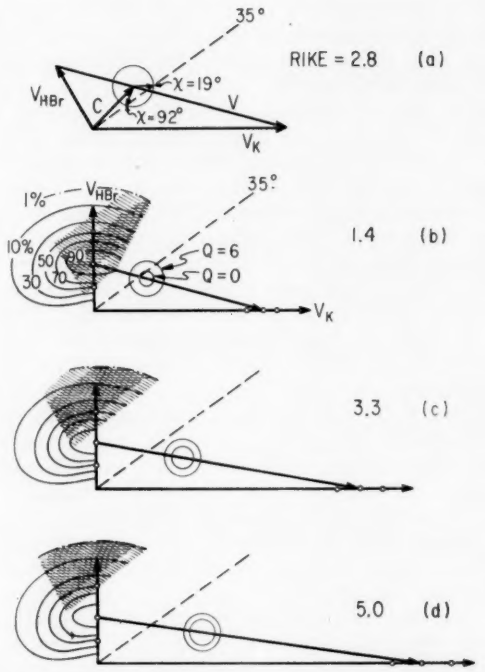

FIG. 1. Constructions to find (a) χ values that contribute to 35° yield for given Q (radius of sphere); (b, c, d) effect of remaining spread in beam speeds and intersection angles.

There are problems even if the intersecting beams are regarded as entirely monochromatic in speed and direction. The reaction probability as expressed in the differential cross section, $\sigma(v, v', \chi)$, depends upon[2] the magnitude of the initial and final relative velocity vectors, $\mathbf{v}$ and $\mathbf{v}'$, and the angle between them, χ. If the collision yield is measured at a fixed laboratory angle while the speed of one of the beams is varied, the orientation of $\mathbf{v}$ and the center of mass vector $\mathbf{c}$ with respect to the direction of observation will be continually changing. This causes the dependence on v and the dependence on χ to be superposed in the results. Calculations show the effect is quite serious; for the example of Fig. 1(a), the two values of χ that

contribute to the yield at 35° in the laboratory undergo large changes, to 38° and 123°, when RIKE is raised 25% by increasing v_K.

The recoil velocity of KBr relative to the center of mass is small: $(M_H/M)v' \simeq (1/120)v'$. From energy balance, $v' = [2(E+Q)/\mu']^{\frac{1}{2}}$, where E is RIKE and Q is the internal energy converted into translational energy of separation of the products. The maximum possible value of Q is only about 6 kcal/mole in this reaction.[3] Thus one finds that the recoil velocity vector of the KBr is confined within the small sphere indicated in Fig. 1(a). Even for completely specified initial conditions there will always be some distribution of internal excitation in the product molecules, i.e., distribution of Q-values (spheres of various radii), and a corresponding distribution in values of χ that contribute at a given laboratory angle.

TABLE I. Analysis of energy variation.

Nominal RIKE	Central v_K 10^4 cm/sec	KBr Recoil Velocity $Q=0$	KBr Recoil Velocity $Q=6$	Range and most probable RIKE $Q=0$
0.5	3.65	0.18	0.62	0.2– 1.0; 0.4
1.4	6.48	0.29	0.66	0.6– 2.8; 1.6
3.3	10.21	0.44	0.75	2.7– 5.7; 4.2
5.0	12.48	0.54	0.81	3.9– 7.7; 6.1
7.0	14.73	0.65	0.88	6.0–10.6; 8.1

Figures 1(b), (c), (d) and Table I demonstrate that the RIKE scale used in reference 1 must be modified. This scale ("nominal" in Table I) was calculated for perpendicular collisions, using the most probable v_{HBr} at 152°K and v_K at the center of the triangular intensity distribution transmitted by the selector. As shown by the diagrams, KBr from such collisions could not appear at 35° in the laboratory when RIKE is above about 3 (since then, spheres for $Q \lesssim 6$ no longer intercept the 35° line). The shaded areas (single shading for $Q=6$; double for $Q=0$) indicate the range of $\mathbf{v}_{HBr}$ vectors which could yield KBr at 35°. Conservation of momentum and energy requires the endpoints of $\mathbf{v}_{HBr}$ vectors to fall between lines roughly parallel to the 35° line; the areas are further delimited by the partial collimation of the HBr (±30°, a rather wide spray[4]) and by the 1% intensity level. The contour lines give the percentage of the peak intensity as computed from the Maxwellian and the cosine distributions. Table I lists the derived range in RIKE. These are conservative estimates, based on the 10% contour and $Q=0$ rather than the maximal $Q=6$; allowance is made for the remaining spread in v_K and the contribution of out-of-plane scattering (not included in Fig. 1). It will be noted that at a nominal RIKE of 1.4, a substantial number of collisions have RIKE as high as 2.8, near the activation energy determined from the temperature variation,[5] so that the appearance of the threshold in this experiment at a low nominal RIKE is perhaps not surprising. Furthermore, the systematic shift of the shaded areas relative to the contour lines shows that as RIKE increases, the yield at 35° must be increasingly attenuated, and eventually will disappear, regardless of the actual form of the energy dependence of the cross section.

We thank E. F. Greene, R. W. Roberts, and J. Ross for helpful correspondence.

* Support received from the Alfred P. Sloan Foundation and the U. S. Atomic Energy Commission is gratefully acknowledged.

[1] E. F. Greene, R. W. Roberts, and J. Ross, J. Chem. Phys. **32**, 940 (1960).

[2] See, for example, M. A. Eliason and J. O. Hirschfelder, J. Chem. Phys. **30**, 1426 (1959).

[3] Obtained from the difference in dissociation energies of KBr and HBr, $D_0° = 4.2 \pm 1.1$ kcal/mole [A. G. Gaydon, *Dissociation Energies* (Chapman and Hall, Ltd., London, 1953)] plus three times the most probable rotational energy of HBr, 0.15 kcal/mole at 152°K.

[4] Private communication from Professor Greene.

[5] E. H. Taylor and S. Datz, J. Chem. Phys. **23**, 1711 (1955), and private communication.

Erratum: Electronic Structure of Nitric Oxide

[J. Chem. Phys. **30**, 673 (1959)]

H. BRION AND C. MOSER

Centre de Mécanique Ondulatoire Appliquée, Paris, France

AND

M. YAMAZAKI

Department of Physics, Yamagata University, Yamagata Prefecture, Japan

(Received October 10, 1960)

CHANGES, as follows, should be made in the above article: Table VI, third calculation,

$$\Phi_{3\sigma} = \cdots\cdots + 0.1944\, 2p\sigma_0,$$

Equation (18), $= 0.9691\psi_0 - 0.1342\psi_3 - 0.1237\psi_4$

$$+ 0.0934\psi_4' - 0.0699\psi_5 + 0.0704\psi_5'$$

$$+ 0.0326\psi_6 - 0.0697\psi_6' - 0.0555\psi_7,$$

Table VII, column configuration interaction,

Total energy (a.u.) -128.847

Binding energy (ev) $+1.3$,

Table IX, reverse the values given for $2p\pi_N 2p\pi_0$,

Page 680,

the dipole moment is found to be $0.27D(N^-O^+)$.

Erratum and Addendum: Substituted Methanes. XXIX. Vibrational Spectra, Potential Constants, and Calculated Thermodynamic Properties for Dibromochlorofluoromethane and Bromodichlorofluoromethane

[J. Chem. Phys. **31**, 1633 (1959)]

ROBERT L. GILBERT, EDWARD A. PIOTROWSKI, JEROME M. DOWLING, AND FORREST F. CLEVELAND

Spectroscopy Laboratory, Department of Physics, Illinois Institute of Technology, Chicago, Illinois*

(Received September 23, 1960)

ROBERT L. Hubbard (Physics Department, University of North Carolina) has brought to our attention the fact that the potential energy constants given by us for CBr_2ClF and $CBrCl_2F$ [J. Chem. Phys. **31**, 1633 (1959)] are not completely correct. These constants do reproduce the observed wave numbers, but they do not fulfill the redundancy conditions of the Gold, Dowling, Meister method.[1]

In rechecking our calculations, we found that we had inadvertently published preliminary sets of constants for these molecules. However, these sets, given in Tables IV and V of our paper, differ from the correct sets only in the interaction constants. Nevertheless, for clarity and convenience all the constants are given in the revised Tables IV and V given here. These tables therefore supersede the Tables IV and V of our paper.

We are thankful to Mr. Hubbard for his assistance in the rectification of this error.

TABLE IV (revised). Potential energy constants for CBr_2ClF.[a]

Bond stretching and bond-bond interaction constants (md/A)		Bond-angle interaction constants (md/rad)		Angle bending and angle-angle interaction constants (md A/rad²)	
f_b	2.76500[b]	f_b^{bc}	0.25167	f_{bb}	0.89816
f_f	5.31000	$f_b^{b'c}$	−0.25833	f_{bc}	0.91893
f_c	3.49588	f_b^{bb}	0.31167	f_{bf}	0.91682
f_b^b	0.33500	f_b^{bf}	0.19667	f_{cf}	1.17260
f_c^f	0.81000	f_b^{cf}	−0.28833	f_{bc}^{bb}	−0.17411
f_b^f	0.65000	$f_b^{b'f}$	−0.21333	$f_{bf}^{b'f}$	−0.26318
f_b^c	0.32250	f_f^{bc}	−0.16167	$f_{bc}^{b'c}$	−0.14107
		f_f^{bb}	−0.18166	f_{bf}^{bc}	−0.14277
		$-f_f^{bf}$	0.16833	f_{cf}^{bc}	−0.21823
		f_f^{cf}	0.16833	f_{cf}^{bf}	−0.18060
		f_c^{bc}	0.28167	$f_{bc}^{b'f}$	−0.24277
		f_c^{bb}	−0.26833	f_{cf}^{bb}	−0.37494
		f_c^{bf}	−0.26833	f_{bf}^{bb}	−0.08751
		f_c^{cf}	0.24167		

[a] The symbols for the potential constants are in the descriptive notation of Davis *et al.*, reference 8: b=C—Br, f=C—F, c=C—Cl, bc=Br—C—Cl, bf=Br—C—F, etc., and b and b' represent different C—Br bonds.

[b] This number of significant figures is not justified by the accuracy of the observed wave numbers, but is necessary to give the best reproduction of the observed wave numbers and to secure internal consistency in the calculations.

TABLE V (revised). Potential energy constants for $CBrCl_2F$.[a]

Bond stretching and bond-bond interaction constants (md/A)		Bond-angle interaction constants (md/rad)		Angle bending and angle-angle interaction constants (md A/rad²)	
f_c	3.44639	f_c^{cf}	0.24883	f_{cc}	0.86611
f_b	3.40551	$f_c^{c'f}$	−0.28917	f_{cf}	1.08733
f_f	5.25100	f_c^{cc}	0.29883	f_{bc}	0.91822
f_c^c	0.26122	f_c^{bc}	0.29883	f_{bf}	0.87735
f_b^f	0.66000	f_c^{bf}	−0.29117	f_{cc}^{cf}	−0.21699
f_b^c	0.33000	$f_c^{bc'}$	−0.26617	$f_{bc}^{bc'}$	−0.13180
f_c^f	0.81000	f_b^{cf}	−0.26750	$f_{cf}^{c'f}$	−0.13322
		f_b^{cc}	−0.24250	f_{bc}^{cf}	−0.19404
		f_b^{bc}	0.28250	f_{bf}^{cf}	−0.23904
		f_b^{bf}	0.21250	f_{bc}^{bf}	−0.13595
		f_f^{cf}	0.14333	$f_{bc}^{c'f}$	−0.30404
		f_f^{cc}	−0.17667	f_{bf}^{cc}	−0.12738
		f_f^{bc}	−0.12666	f_{bc}^{cc}	−0.15238
		f_f^{bf}	0.14333		

[a] The footnotes to Table IV apply also to this table, except that here c and c' represent different C—Cl bonds.

* Publication No. 143.

[1] R. Gold, J. M. Dowling, and A. G. Meister, J. Mol. Spectroscopy **2**, 9 (1958).

Erratum: Improved Molecular Orbitals and the Valence Bond Theory

[J. Chem. Phys. **33**, 301 (1960)]

A. C. HURLEY

Division of Chemical Physics, C.S.I.R.O. Chemical Research Laboratories, Melbourne, Australia

(Received September 23, 1960)

ON page 301, line 4 should read "$\theta_1=2^{-1}\{\,|\,\sigma_g\bar{\sigma}_u'\,|+|\,\sigma_u'\bar{\sigma}_g\,|\,\}$, (1)."

On page 301, line 8, "$\zeta'(\pm\zeta)$" should read "$\zeta'(\neq\zeta)$."

On page 301, line 20, "$\theta_1{}^{\theta''}$" should read "θ_1."

On page 302, line 9, "$\zeta\pm\zeta'$" should read "$\zeta\neq\zeta'$."

On page 302, line 19, "$B\,'\Sigma_u^+$" should read "$B\,^1\Sigma_u^+$."

On page 302, line 24, "$\theta_2=2^{-\frac{1}{2}}\,|\,\{\sigma_g'\cdots$" should read "$\theta_2=2^{-\frac{1}{2}}\{\,|\,\sigma_g'\cdots$."

On page 302, lines 37 and 38 should read:

$$"s=0.5662+1012/(1268R-2164),$$

$$q=(32-4s-s^2-5s^3)/(32-16s)."$$

The following sentence should be inserted after line 7 in the second column of page 302:

"A similar analysis may be applied to the $^3\Sigma_u^+$ state of H_2."

Notes

Lattice Dimensions of NbC as a Function of Stoichiometry

C. P. Kempter, E. K. Storms, and R. J. Fries

Los Alamos Scientific Laboratory, University of California, Los Alamos, New Mexico

(Received August 15, 1960)

THE variation of the lattice constant of NbC has been studied by Umanski,[1] Brauer, Renner, and Wernet,[2] Brauer and Lesser,[3] Elliott,[4] Storms and Krikorian,[5] Fries,[6] and Kempter and Nadler.[7] Precision lattice-constant determination techniques were employed only in the last three investigations.

In an attempt to improve the analytical curve of lattice constant (a_0) vs C/Nb molar ratio for the entire NbC phase range, the data of the last three investigations were combined with additional high C/Nb molar ratio points obtained by heating mixtures of niobium and graphite. The general preparative method has been described in detail by Storms, Krikorian, and Kempter.[8] Lattice constants were determined on an IBM 704 computer by the method of Vogel and Kempter[9] or of Hess,[10] assuming systematic errors in $\Delta a_0/a_0$ directly proportional to $\phi\tan\phi$, where ϕ is the complement of the Bragg angle. All measurements were made at 25°C using a 12.00-cm symmetrical-back-reflection-focusing camera with iron-filtered cobalt radiation or a 11.459-cm Debye-Scherrer camera with nickel-filtered copper radiation. The refraction correction (0.000100 A for Cu radiation and 0.000135 A for Co radiation) was added to normalize all lattice constant values. All specimens were analyzed for niobium, total carbon, and free carbon by the methods described by Kriege.[11] The 41 specimens covered a combined C/Nb molar ratio range of 0.700 to 0.996, and had a niobium plus total carbon analytical summation of 99.85% or greater. Additional information on the impurities present and their effect on lattice parameter can be found in the work cited in footnotes 5 and 12.

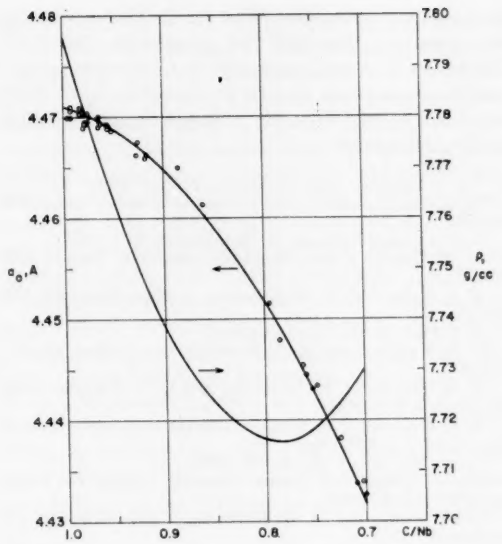

FIG. 1. Lattice constant and theoretical density vs C/Nb molar ratio for NbC.

Polynomial least-squares fits of $(a_0-4.4)$ vs C/Nb, with each point statistically weighted as the reciprocal of the standard deviation of a_0, squared, were determined on an IBM 704 computer. Subtraction of 4.4 A from each a_0 value avoided any rounding errors. The only fit which gave a smooth curve with no inflection points in the experimental range was the quadratic. The y intercept was $a_0=4.4710\ \pm 0.0001_5$ A. The quadratic equation is

$$a_0=4.09847+0.71820(\text{C/Nb})-0.34570\ (\text{C/Nb})^2,$$

and is shown in Fig. 1. It must be emphasized that this is an empirical equation applicable to the C/Nb molar ratio range 0.700–0.996 for NbC (NaCl-type) specimens that are essentially homogeneous and free from impurities.

A plot of the theoretical densities (calculated from the equation) vs C/Nb molar ratio is also shown in Fig. 1. The phase reaches a minimum density of 7.716 g/cc at $NbC_{0.785}$, an intermediate density of 7.730 g/cc at $NbC_{0.700}$, and a maximum density of 7.796 g/cc (by extrapolation) at $NbC_{1.000}$. The density of Nb_2C (hexagonal) is about 7.95 g/cc, and that of Nb (body-centered cubic) is 8.53 g/cc. It is apparent that the density of the NbC phase cannot necessarily be used to define unambiguously the lattice constant or C/Nb molar ratio.

The authors thank R. H. Moore and R. E. Vogel for their assistance with the application of the iterative

least-squares technique; Miss D. L. Cooper for her assistance with the IBM 704 calculations, Dr. O. H. Kriege, Dr. E. Van Kooten, and G. C. Heasley for their analytical assistance and D. D. Crecelius, L. A. Wahman, B. Lee, and Mrs. M. J. Jorgensen for their film-reading assistance.

[1] Ya. S. Umanski, Zhur. Fiz. Khim. **14,** 332 (1940).
[2] G. Brauer, H. Renner, and J. Wernet, Z. anorg. Chem. **277,** 249 (1954).
[3] G. Brauer and R. Lesser, Z. Metallkunde **50,** 8 (1959).
[4] R. P. Elliott, Armour Research Foundation Report, ARF 2120-4 (May, 1959).
[5] E. K.Storms and N. H. Krikorian, J. Phys. Chem. **63,** 1747 (1959).
[6] R. J. Fries (unpublished research).
[7] C. P. Kempter and M. R. Nadler, J. Chem. Phys. **32,** 1477 (1960).
[8] E. K. Storms, N. H. Krikorian, and C. P. Kempter, Anal. Chem. (to be published).
[9] R. E. Vogel and C. P. Kempter, Los Alamos Scientific Laboratory Report LA-2317 (April, 1959).
[10] J. B. Hess, Acta Cryst. **4,** 209 (1951).
[11] O. H. Kriege, Los Alamos Scientific Laboratory Report LA-2306 (March, 1959).
[12] E. K. Storms and N. H. Krikorian, J. Phys. Chem. (to be published).

The Ultraviolet Spectrum of Triptycene

CHARLES F. WILCOX, JR.

Department of Chemistry, Cornell University, Ithaca, New York

(Received August 11, 1960)

RECENTLY the preparation of bicyclo-[2.2.2]-2,5,7-octatriene, I, "barrelene," has been reported[1] as well as an interpretation of the 45-mμ bathochromic shift of the ultraviolet absorption of its three ethylene chromophores.[2] This interpretation ascribes the shift principally to the interaction between locally excited ethylene transitions, with a minimal role being played by the electron-transfer process. It is interesting to compare these interactions in "barrelene" with those of triptycene, II, first, because of the obvious structural analogy, and second, because qualitative considerations have led to the suggestion that ionic structures involving transfer of charge between benzene

I II

rings play a major role in determining the near ultraviolet spectrum of triptycene.[3] In the present note it is shown from a slightly more quantitative point of view that (1) a crude model predicts no shift in the near ultraviolet; (2) the shift is, in fact, small when the appropriate reference compound is selected; and (3) the residual shifts can be accounted for by the interaction of locally excited states without invoking interbenzene charge-transfer interactions.

The spectrum of triptycene has been investigated theoretically by the use of the Longuet-Higgins and Murrell model, which treats π-electron transitions of coupled chromophores in terms of local and charge-transfer excitations.[4] This approach has the advantage of not only being numerically simple, but, perhaps more importantly, it ascribes changes of spectra in the greater part to interactions which already have a role in the organic chemist's conceptual framework.

In carrying out preliminary calculations, several simplifying assumptions have been made: (1) that all important local and charge-transfer states can be adequately described in terms of single electron excitations between the highest energy bonding and lowest-energy nonbonding orbitals of benzene[4]; (2) that these orbitals are oriented so that the transition moment of the long wavelength $\alpha(^1L_b)$ band is perpendicular to the threefold axis of triptycene[5]; (3) that all penetration integrals may be ignored; (4) that the resonance integral between any pair of π-core atoms is proportional to the corresponding overlap integral; and finally (5) that interbenzene repulsion $(pp \mid qq)$ terms may be evaluated theoretically from Slater nodeless orbitals.

With these assumptions, and the C_{3h}(orbital) symmetry of triptycene, one can conclude immediately that the long wavelength local α bands should not be displaced. This lack of shift, which contrasts with the predicted and observed shift in "barrelene," arises from the fact that in the assumed form of the α transition the two components of the transition dipole act in opposite directions so that the interaction terms cancel. This prediction agrees reasonably well with experiment: triptycene in ethanol[3,6] shows bands (log ε in parentheses) at 264 mμ (sh.~3.3), 271 mμ (3.55), 279 mμ (3.67), while *o*-xylene in ethanol has band maxima at 263 mμ (2.44) and 271 mμ (2.35).[7] A plausible origin of this 8-mμ shift will be considered below.

The calculation of λ max for the triptycene bands related to the $p(^1L_a)$, β (^1B_b), $\beta'(^1B_a)$ bands of benzene is more involved. If it is assumed that an alcoholic solution of *o*-xylene has a *p* band at 210 mμ, and β bands at 190 mμ, as it does in the vapor,[8,9] it is predicted that triptycene will have *p*-derived bands at 206 mμ and 214 mμ (doubly degenerate). From this same set of calculations comes the result that the longest wavelength component of the β sextet should lie at 200 mμ. In fact, triptycene shows a strong band at 211 mμ (log ε 4.80). This might be the displaced long-wavelength β component *or* the 214 mμ forbidden band which has become allowed by vibrational interaction with the immediately adjacent β-derived band.

These preliminary calculations provide a gross inter-

pretation to the ultraviolet spectrum of triptycene, but they fail to account for the 0.1-ev bathochromic shift of the α-band or its enhanced absorptivity. If the effect of penetration integrals are included, it is calculated that the degenerate triptycene α bands will split with two components moving out to 274 mμ. Furthermore, if it is assumed that the substituents add about 10% of β-band character to the α band[10] then the agreement with experiment is excellent. These modifications also account nearly quantitatively for the enhanced absorptivity. Whatever the exact details of the 0.1-ev shift, however, the important point here is that the near ultraviolet spectrum of triptycene shows an accountably smaller (by a factor of 5) bathochromic shift than does "barrelene." Moreover, the present approach can be extended to triptycene derivatives, for which it can be predicted that their near-ultraviolet spectrum should be closely approximated (within a few tenths of an electron volt) by the sum of the spectra of the separate three chromophores. In a similar fashion, triptycene analogs in which one of the benzene rings is replaced by some other type of chromophore, should show chromophoric additivity. These extensions will be discussed in detail elsewhere.

[1] H. Zimmerman and R. Paufler, J. Am. Chem. Soc. **82,** 1514 (1960).
[2] C. F. Wilcox, Jr., S. Winstein, and W. McMillan, J. Am. Chem. Soc. (to be published).
[3] P. D. Bartlett and E. S. Lewis, J. Am. Chem. Soc. **72,** 1005 (1950).
[4] H. C. Longuet-Higgins and J. N. Murrell, Proc. Phys. Soc. (London) **A68,** 601 (1955).
[5] A. L. Sklar, Revs. Modern Phys. **14,** 232 (1942).
[6] A. C. Craig and C. F. Wilcox, Jr., J. Org. Chem. **24,** 1619 (1959).
[7] The choice of *o*-xylene rather than benzene as a model system is dictated by the observations that variously substituted alkyl benzenes show similarly located α bands which are considerably displaced from the λ max of benzene.
[8] F. A. Matsen, W. W. Robertson, and R. L. Chvoke, Chem. Revs. **41,** 273 (1947).
[9] J. R. Platt and H. B. Klevens, Chem. Revs. **41,** 301 (1947).
[10] L. Goodman, I. Ross, and H. Shull, J. Chem. Phys. **26,** 474 (1957); L. Goodman and H. Shull, *ibid.* **27,** 1388 (1957).

The Effect of Hydrogen Bonding on the Intensity of the CD Raman Band of $CDCl_3$

D. G. Rea

California Research Corporation, Richmond, California

(Received August 22, 1960)

THE formation of a hydrogen bond manifests itself in many ways. Thus, in the infrared spectra of the participating species there are many changes from the nonhydrogen-bonded system.[1] A prominent feature of the infrared spectrum is the large intensification of the fundamental band of the *X*-H stretching mode. Some measurements on the corresponding Raman band of phenol in an inert solvent in this laboratory indicated a completely different behavior, with a possible decrease in band intensity. Due to the breadth of the association band, phenol is a poor molecule to study. Accordingly, to obtain quantitative data on the effect of H-bond formation on the Raman intensity, measurements were made on chloroform-*d* dissolved in several bases. The infrared spectra of these systems[2,3] show very large increases in the intensity of the CD stretching band when in an H-bonded complex.

The chemicals originally were of high purity and, in certain cases, were further purified by distillation or passage through a column of silica gel. The only impurity in the $CDCl_3$, as determined by mass spectrometric and infrared analysis, was 3.9% $CHCl_3$. For the intensity measurements solutions 10% by volume of $CDCl_3$ in the base were prepared. The data referred to in footnote 1 indicate that for this concentration essentially all of the $CDCl_3$ is complexed.

TABLE I. The integrated intensity of the CD stretching band of chloroform-*d* in various bases.

Base	Relative Raman intensity	Adjusted relative Raman intensity	Relative infrared intensity	
			Reference 2	Reference 3
Chloroform-*d*	1.00	1.00	1.00	1.00
Carbon tetrachloride	0.90	0.88		0.81
Diethyl ether	0.77	1.09	11.5	
Acetone	0.82	1.12	12.5	8.7
Dioxane	0.82	0.93	18.0	
Benzene	1.21	1.04		5.0
o-Xylene	1.49	1.28		
m-Xylene	1.31	1.15		
p-Xylene	1.43	1.26		
Mesitylene	1.51	1.29		5.1

The Raman intensity measurements were made with a Cary Model 81 Raman spectrophotometer using either a Pyrex or lime-glass tube (volume 4.5 ml), the choice depending on the refractive index of the solution. The integration interval varied from 60–100 cm^{-1}. A correction for the optical effect of the refractive index was applied.[4] The spectral slit width, measured as in work cited in footnote 4, was 4.1 cm^{-1} at 2252 cm^{-1}. The temperature of the solutions was estimated to be 25–28°C.

The data on the changes in the band position and the observed half-width agreed within experimental error with the infrared data. The greatest difference was 3 cm^{-1}. However, the integrated intensity behaves much differently, as is seen in Table I. The intensity in column 3 is that in column 2 multiplied by an addi-

tional refractive-index factor. This factor has a refractive-index dependence which makes the adjusted intensity of the C=C band in the normal *l*-olefins constant. Its use should minimize residual refractive-index effects.[5]

The adjusted intensities are unity within experimental error except for the xylenes and mesitylene. The increase for these bases may be due to a solvent effect similar to that observed for CCl_4 in benzene[5] or to a contribution of the aromatic molecule in the complex.

The theoretical implications of the constancy of the Raman band intensity, while the infrared band increases by an order of magnitude, have not been studied.

[1] G. C. Pimentel and A. L. McClellan, *The Hydrogen Bond* (W. H. Freeman and Company, San Francisco, 1960), Chap. 3.
[2] R. C. Lord, B. Nolin, and H. D. Stidham, J. Am. Chem. Soc. **77**, 1365 (1955).
[3] C. M. Huggins and G. C. Pimentel, J. Chem. Phys. **23**, 896 (1955).
[4] D. G. Rea, J. Opt. Soc. Am. **49**, 90 (1959).
[5] D. G. Rea, J. Mol. Spectroscopy **4**, 507 (1960).

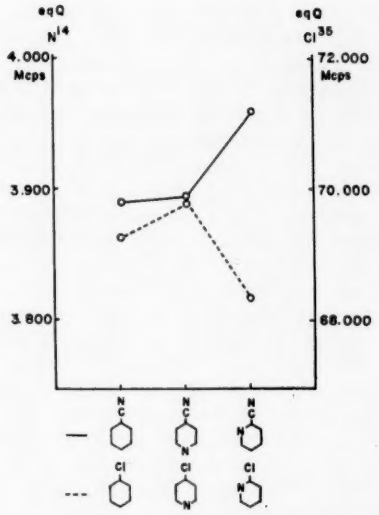

FIG. 2. Comparison of the coupling constants eq$Q$ of similar compounds.

N^{14} Pure Quadrupole Resonances of Several Nitriles*

HISAO NEGITA AND P. J. BRAY

Department of Physics, Brown University, Providence, Rhode Island

(Received July 25, 1960)

STUDIES have been made of N^{14} pure quadrupole resonances of trichloracetonitrile, isonicotinonitrile, picolinonitrile, and benzonitrile at 77°K using a Pound-Watkins[1,2] recording spectrometer. A Zeeman modulation field[3] of 60–70 gauss replaced the 20–30 gauss fields previously employed.[4–6] The N^{14} resonance frequencies, quadrupole coupling constant eq$Q$, and electric field gradient asymmetry parameter η are given for each compound in Table I.

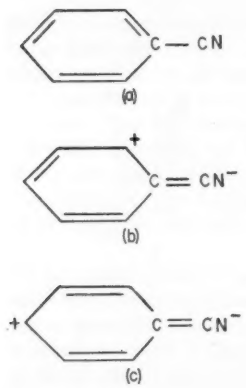

FIG. 1. Resonance structures for benzonitrile.

The N^{14} coupling constant of trichloroacetonitrile, 4.052 Mc, is higher than that of acetonitrile,[6] 3.738 Mc, but is very close to that of hydrocyanic acid,[6] 4.018 Mc. The lower value in acetonitrile may be attributed[6] to the contribution of the structure $^{+}HCH_2{=}C{=}N^{-}$ by hyperconjugation.[7] Hyperconjugation is not possible in hydrocyanic acid and trichloroacetonitrile. The contribution of the ionic structure $^{-}ClCCl_2{=}C{=}N^{+}$ in trichloroacetonitrile is assumed small because the electronegativities[8] of Cl and N are equal and the Cl^{35} coupling constants[9] of CCl_3CN (83.068–83.459 Mc) are higher than those[10] of CCl_4 (80.930–81.634 Mc). In this regard, the value of 1.450 A recently proposed[11] for the C—C distance in Cl_3CCN is puzzling. This value is essentially that reported[12] for the C—C distance in CH_3CCN (1.460 A) where the carbon-carbon double bond contained in the hyperconjugation structure $^{+}HCH_2{=}C{=}N^{-}$ shortens the C—C distance. (The ordinary C—C single bond distance is 1.54 A.) The earlier value[11] of 1.515 A for the C—C distance in Cl_3CCN is preferable in light of the lack of resonance structures containing the carbon-carbon double bond.

The C—C distance[13] of 1.419 A in benzonitrile [Fig. 1(a)] is substantially shorter than the usual carbon-carbon single bond distance. This evidence for the resonance structures [Figs. 1(b) and 1(c)] containing the necessary carbon-carbon double bond indicates that the N^{14} coupling constant should be reduced and the asymmetry parameter increased in this molecule. The data of Table I confirm this expectation.

Values are not available for the carbon-carbon bond distances in isonicotinonitrile and picolinonitrile. However, nitrogen is more electronegative than carbon and its replacement of carbon in the ring should suppress the resonance structures [Figs. 1(b), (c)]. This effect is presumably exhibited in the increase of eqQ (Fig. 2) and decrease of η (Table I) shown by isonicotinonitrile and picolinonitrile in comparison with benzonitrile. It is puzzling, however, that η for isonicotinonitrile is quite small rather than a value intermediate between the asymmetry parameters of benzonitrile and picolinonitrile.

TABLE I. N^{14} Pure nuclear quadrupole resonances of several nitriles at 77°K.

Compound	Resonance frequency (Mc)	Coupling constant (Mc)	Asymmetry parameter (%)
Trichloroacetonitrile, CCl_3CN	3.0337±0.0002 3.0444±0.0002	4.0521±0.0003	0.53±0.02
Isonicotinonitrile, 4-$C_5H_4N(CN)$	2.9073±0.0002 2.9353±0.0002	3.8951±0.0003	1.44±0.02
Picolinonitrile, 2-$C_5H_4N(CN)$	2.8978±0.0002 3.0396±0.0002	3.9583±0.0003	7.16±0.02
Benzonitrile, C_6H_5CN	2.8098±0.0002 3.0183±0.0002	3.8854±0.0003	10.73±0.02

Figure 2 also displays the Cl^{35} coupling constants[14–16] for molecules similar to three nitriles of Table I but with Cl replacing CN. The inductive effect of the ring nitrogen[15] is responsible for the increase of the Cl^{35} coupling constant in 4-chloropyridine over the value in chlorobenzene. An inductive effect is also present in 2-chloropyridine but is outweighed by an increase in the double-bond character of the C—Cl bond which lowers eqQ substantially.[15,16]

* This work supported by a grant from the National Science Foundation.

[1] G. D. Watkins, Ph.D. thesis, Harvard University, 1952.
[2] R. V. Pound and W. D. Knight, Rev. Sci. Instr. **21,** 219 (1950).
[3] H. G. Dehmelt, Am. J. Phys. **22,** 110 (1954).
[4] P. A. Casabella and P. J. Bray, J. Chem. Phys. **28,** 1182 (1958).
[5] P. A. Casabella and P. J. Bray, J. Chem. Phys. **29,** 1105 (1958).
[6] Hisao Negita, P. A. Casabella, and P. J. Bray, J. Chem. Phys. **32,** 314 (1960).
[7] J. W. Baker, *Hyperconjugation* (Oxford University Press, New York, 1952), p. 27.
[8] L. Pauling, *Nature of the Chemical Bond* (Cornell University Press, Ithaca, New York, 1948).
[9] R. Livingston, J. Phys. Chem. **57,** 496 (1953).
[10] J. D. Graybeal and C. D. Cornwell, J. Phys. Chem. **62,** 483 (1958).
[11] W. Zeil, Z. Elektrochem. **60,** 752, 1204 (1956).
[12] M. Kessler, H. Ring, R. Trambarulo, and W. Gordy, Phys. Rev. **79,** 54 (1950).
[13] D. R. Lide, J. Chem. Phys. **22,** 1577 (1954).
[14] R. Livingston, Phys. Rev. **82,** 289 (1951).
[15] P. J. Bray, S. Moskowitz, H. O. Hooper, R. G. Barnes, and S. L. Segel, J. Chem. Phys. **28,** 99 (1958).
[16] S. L. Segel, R. G. Barnes, and P. J. Bray, J. Chem. Phys. **25,** 1286 (1956).

Spin Densities in Several Odd Alternant Radicals*

H. H. DEARMAN† AND H. M. MCCONNELL‡

Gates and Crellin Laboratories of Chemistry,§ California Institute of Technology, Pasadena, California

(Received August 15, 1960)

IN this note we report the unpaired electron spin distribution in the benzyl, α-methylnaphthenyl, β-methylnaphthenyl, and trivinylmethyl radicals calculated using simple valence-bond theory. This method has been previously employed to calculate the spin densities in triphenylmethyl[1] and perinaphthenyl.[2] By *simple* valence bond theory we mean that all ionic or long-bond structures have been neglected, and that exchange integrals involving atoms separated by more than one bond have been set equal to zero. The rules for evaluation of the matrix elements of the spin-density operator and other details of this calculation for odd alternant radicals have been presented previously.[2]

The diagonal elements of the atomic orbital spin density matrix for these radicals are given in Fig. 1. For benzyl, α-methylnaphthenyl, and β-methylnaph-

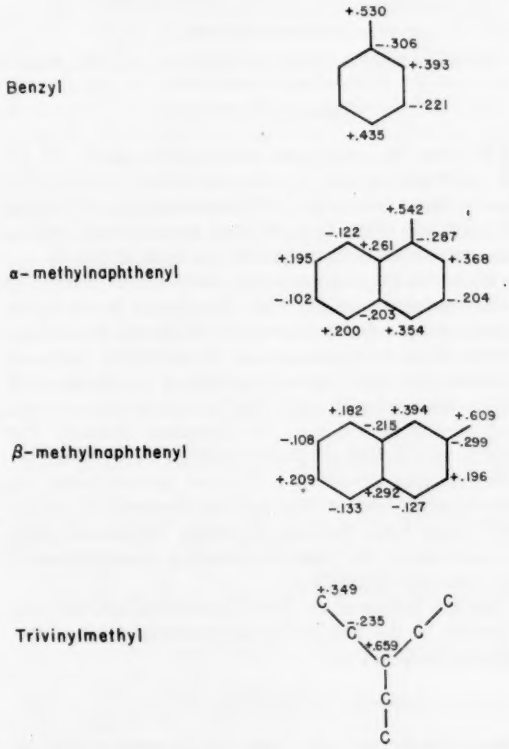

FIG. 1. Calculated spin densities in odd-alternant hydrocarbon radicals.

thenyl the results of the valence-bond energy calculation of Pauling and Wheland[3] have been employed. These authors report the ratios of the coefficients of the principal VB structures, and we have determined the coefficients themselves by normalization. The ground-state function for trivinylmethyl is obtained by solution of the 2×2 secular equation.

It is hoped that these spin densities will be helpful in the interpretation of the proton hyperfine structure of the electron resonance spectra of these or prototype radicals.

* Sponsored by the National Science Foundation, by the U.S. Public Health Service and by the Office of Ordnance Research, U.S. Army.
† Dow Chemicals Fellow.
‡ Alfred P. Sloan Fellow.
§ Contribution No. 2620.
[1] P. Brovetto and S. Ferroni, Nuovo cimento **5**, 142 (1957).
[2] H. M. McConnell and H. H. Dearman, J. Chem. Phys. **28**, 51 (1958).
[3] L. Pauling and G. W. Wheland, J. Chem. Phys. **1**, 362 (1933).

Calculated Band Intensities for CO_2 from Infrared Dispersion Data

BERTRAM SCHURIN

Geophysics Research Directorate, Lawrence G. Hanscom Field, Bedford, Massachusetts

(Received July 27, 1960)

IN order to obtain an independent check on the reported values for the intensities of the CO_2 fundamental bands the 1924 dispersion data of Torsten Wetterblad[1] (Fig. 1) have been recalculated, and an alternate set of band intensities has been obtained.

Wetterblad's measurements were made using the hollow-prism technique with the change in deviation produced by a change in pressure of the gas in a hollow prism taken as a measure of the refractive index. A constant deviation monochromator of the Wadsworth design was used with a 60° NaCl prism 70 mm in height and 55 min in width as the dispersing element. The source was a Nernst glower with an iron-constantan thermocouple joined to a Paschen galvanometer for the detecting system. The required spectral slit widths were quite large, because of energy limitations (Fig. 1), and where the index is changing rapidly there is less certainty in the data.

For the harmonic oscillator approximation the contribution to the index is directly related to the integrated absorption Ai,

$$\Delta_i(n-1)=(1/2\pi^2)[A_i/(\nu_i^2-\nu^2)], \qquad (1)$$

where Ai is in cm^{-2} atm^{-1} and ν is the wave number in cm^{-1}. Wetterblad fitted his data to a sum of terms related to (1). An examination of the fit between the

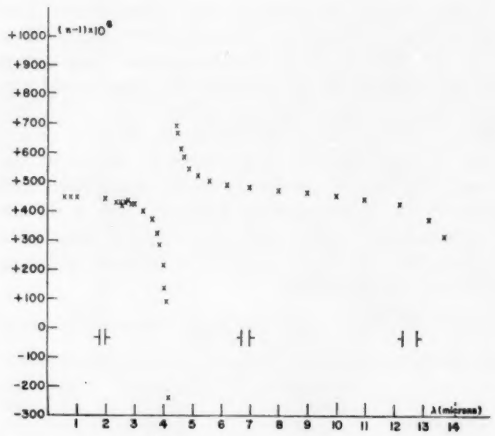

FIG. 1. Refractive index measurements for CO_2 (Wetterblad).

experimental results and the predicted curve indicated a large discrepancy in the region of the 4.27 μ band (Fig. 2). The errors, however, were not in a direction one would expect from the normal slit effects but involved a shift in either wavelength setting or the choice of ν_i.

In recalculating the data the measurements of Cuthbertson and Cuthbertson[2] have been taken for the absolute value of the index at the NaD lines. This has required lowering Wetterblad's data some 1.5%. The value of ν_i for the 4.27 μ band has been shifted to 2370 cm^{-1} for best agreement with the data. However, the contributions to the index are weighted as $1/(\nu_i^2-\nu^2)$, and one would not expect to fit (1) with the true band center. The agreement for the recalculated data is indicated in Fig. 2.

The recalculated band intensities at 273° K are $A(4.27\text{-}\mu)=2970\pm60$ cm^{-2} atm^{-1} and $A(15\text{-}\mu)=240\pm5$ cm^{-2} atm^{-1}. The value for the 15-μ band is in complete agreement with the most recent absorption measurements[3,4] while the 4.27-μ band value is some 10% higher than previously reported.[5,6] In view of the

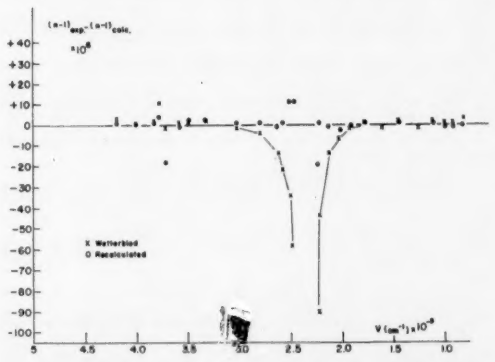

FIG. 2. Fit between experimental and calculated index value.

excellent agreement at 15 μ the dispersion calculations argue that our estimate for the 4.27-μ band intensity based on the absorption data has been too low.

[1] T. Wetterblad, thesis, Uppsala, 1924 (values quoted I.C.T. VII, 9).
[2] C. Cuthbertson and M. Cuthbertson, Proc. Roy. Soc. **A97**, 152 (1920).
[3] L. D. Kaplan and D. I. Eggers, J. Chem. Phys. **25**, 876 (1956).
[4] J. Overend, M. J. Youngquist, E. C. Curtis, and B. Crawford, J. Chem. Phys. **30**, 532 (1959).
[5] D. I. Eggers and B. L. Crawford, Jr., J. Chem. Phys. **19**, 1554 (1951).
[6] D. R. Weber, J. Holm, and S. S. Penner, J. Chem. Phys. **29**, 1820 (1952).

Dipole Moments of Hydrocarbons

DAVID R. LIDE, JR.*

William Ramsay and Ralph Forster Laboratories, University College, London W.C. 1

(Received August 1, 1960)

THERE has been considerable discussion[1] on the relative importance of hybridization changes and electron delocalization effects in determining bond lengths, energies, and other molecular properties. The presence of significant electric dipole moments in toluene and propylene has traditionally been used as an argument in support of hyperconjugation in these molecules. However, Petro has proposed in a recent paper[2] that the dipole moments of unsaturated hydrocarbons may be explained equally well in terms of a set of bond moments which depend upon the degree of hybridization of the carbon atom. It is the purpose of this note to point out certain additional experimental evidence which relates to this question.

From microwave investigations of propylene and methylallene[3] information has been obtained on the orientation, as well as on the magnitude of the dipole moment. While the interpretation is subject to certain ambiguities, it is very probable that the dipole moment vector in both molecules makes an angle α of about 30° with the CC single bond (and correspondingly, a 30° angle with the CC double bond). In any event α cannot be less than 28° in methylallene and 14° in propylene. Now if, for simplicity, we assume 120° valence angles at the double-bonded carbon atoms (and this assumption is certainly valid[3] within 3° or 4°), the picture developed by Petro predicts that the moment will be parallel to the CC single bond, so that $\alpha=0$. On the other hand Crawford[4] has carried out a crude molecular orbital calculation of hyperconjugation effects in propylene. The calculated charge densities predict $\alpha=18°$, in rather better agreement with the observed value. We cannot expect closer agreement from such a calculation; the important point is that the excess negative charge on the number one carbon atom, which will always occur in this delocalization picture whatever the details of the calculation, tends to rotate the dipole moment toward the observed orientation.

A further test of the two theories is provided by the dipole moments of the butene isomers. For isobutene, $(CH_3)_2C{:}CH_2$, the hybridization picture predicts a total moment equal in magnitude to that of propylene (0.36 D), again assuming 120° valence angles[5]; for *cis*-butene-2, $(CH_3)\,CH{:}CH(CH_3)$, the predicted moment is larger by a factor of $\sqrt{3}$, or 0.63 D. While no calculations of hyperconjugation effects in these molecules have been carried out, it is possible to make qualitative predictions. In isobutene the charge transfer produced by the two CH_3 groups is in the same direction, so that one expects the moment to be larger than that of propylene; in *cis*-butene-2, however, the CH_3 groups compete with each other in their influence on the double bond, and a smaller moment should result. The observed moment of isobutene[6] is 0.50 D, about 40% greater than that of propylene; the moment of *cis*-butene-2 has not been measured, but the failure to observe a strong microwave spectrum[6] shows that it must be smaller (and probably much smaller) than the propylene moment. The hyperconjugation picture is again in better accord with the facts.

We may conclude that the simple bond-moment picture proposed by Petro does not satisfactorily explain the dipole moments of unsaturated hydrocarbons. There is strong evidence that a significant part of the polarity resides in the double bond itself. Hyperconjugation appears to be the most reasonable explanation for this result, but the possibility that some still different factor is involved cannot be excluded. Finally, the presence of non-negligible moments in saturated hydrocarbons (0.132 D in isobutane,[7] 0.081 D in propane[8]) makes it clear that several factors must contribute to the net dipole moment. Unless one takes the dubious step of attributing the moments of the paraffins to second-order hyperconjugation, some other factor such as hybridization must be invoked, and this will also make a contribution in the unsaturated compounds. Therefore, considerable caution must be exercised in the quantitative interpretation of dipole moments in terms of an electron delocalization picture.

* National Science Foundation Senior Postdoctoral Fellow, 1959–60, on leave from the National Bureau of Standards, Washington 25, D. C.

[1] M. J. S. Dewar and A. N. Schmeising, Tetrahedron **5**, 166 (1959); R. S. Mulliken, *ibid.* **6**, 68 (1959); B. Bak and L. Hansen-Nygaard, J. Chem. Phys. **33**, 418 (1960). See also A. D. Walsh, Trans. Faraday Soc. **43**, 60 (1947).
[2] A. J. Petro, J. Am. Chem. Soc. **80**, 4230 (1958).
[3] D. R. Lide and D. E. Mann, J. Chem. Phys. **27**, 868, 874 (1957).
[4] V. A. Crawford, J. Chem. Soc. **1953**, 2061.
[5] No reasonable change in valence angles can alter these arguments in any essential way.
[6] V. W. Laurie (private communication).
[7] D. R. Lide and D. E. Mann, J. Chem. Phys. **29**, 914 (1958).
[8] D. R. Lide, J. Chem. Phys. (to be published).

Carbon-13 Hyperfine Splittings in Semiquinones*

D. C. Reitz, F. Dravnieks, and J. E. Wertz

School of Chemistry, University of Minnesota, Minneapolis, Minnesota

(Received August 5, 1960)

THE electron-spin resonance spectra of 2,5-dihydroxysemiquinone [I in Fig. 1(a)] and semiquinone [II in Fig. 1(b)] exhibit hyperfine splittings consistent with the number of ring protons on each molecule. In addition, there are lines of weak intensity in both spectra which may be attributed to the natural abundance of C^{13} in ring carbon atoms. (The natural labeling will be approximately 4% at position 1 and 2% at position 2.)

Figure 1(a) shows the hyperfine spectrum of I at high gain. Two pairs of weak triplets are centered upon the central triplet. Although the innermost pair of triplets partially overlaps the central signal, those lines which are resolved appear to have twice the intensity of the corresponding lines of the outermost pair of triplets. The intensity ratio of the central signal to the weak satellites is within 5% of the value expected on the basis of the natural abundance of C^{13}. From these considerations we assign the following measured splittings to the protons and carbon atoms: $a_H = 0.79$

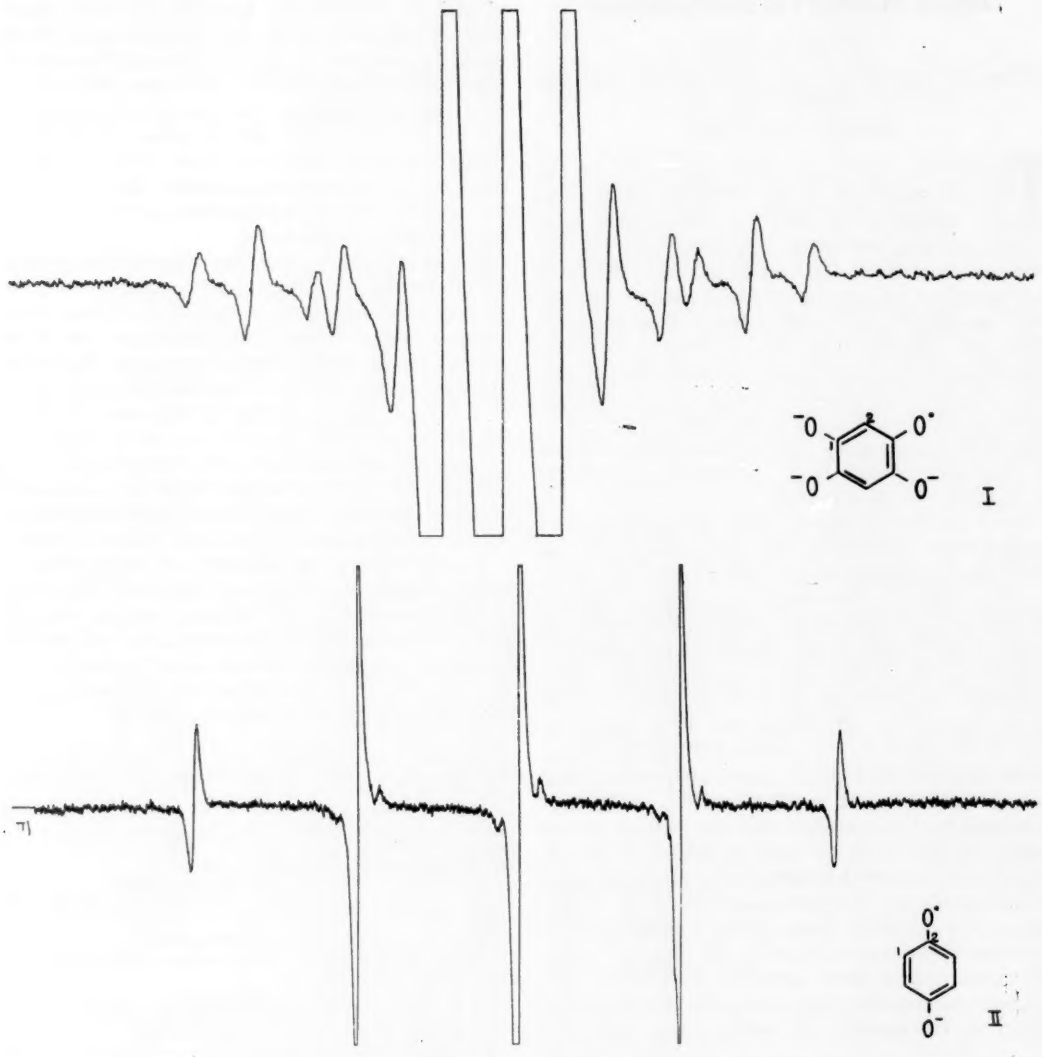

Fig. 1. (a) ESR spectrum of I; (b) ESR spectrum of II.

gauss, $a_{C_1}=2.82$ gauss, and $a_{C_2}=6.62$ gauss.

Only one C^{13} splitting is observed in II. Fig. 1(b) shows the proton hyperfine spectrum of II. Centered around the base of each line is a weak pair of poorly resolved lines. No other lines due to C^{13} could be observed in the spectrum as far as 100 gauss on either side of the central line. Although accurate intensity measurements could not be made, the best assignment of splittings appears to be: $a'_H=2.35$ gauss, $a'_{C_1}\approx 0.6$ gauss, $a'_{C_2}\approx 0$. (The primes differentiate these quantities from those of I.)

Tuttle[1] has shown that an isotropic hyperfine interaction a_i at either a ring carbon or proton of a π radical may be related to the π-spin densities ρ_i through the empirical expression

$$a_i=k_i\rho_i+\sum_j k_{ij}\rho_j,$$

where ρ_j is the spin density at atoms adjacent to i.

Calculations of k_{ij} for an isolated aromatic C—H bond predict a negative value for k_{C-H},[2] and experimentally k_{C-H} has been found to be approximately equal for the C—H bonds of many aromatic hydrocarbon radicals.[3,4]

From these considerations one may expect that the k_i for similar atoms and the k_{ij} for similar bonds in π radicals will be approximately equal. The measured C^{13} splittings in I and II may then be expressed as

$$a_{C_i}=k_C\rho_i+k_{C-C}\sum_j\rho_j+k_{C-O}\rho_0.$$

Two of the six ρ_i in these four equations may be calculated directly from the proton splittings, using $k_{C-H}=-26$ gauss. Thus $\rho_2=(-0.79/-26)=0.03$, $\rho_1'=-2.35/-26=0.09$. Since the sum of the π densities for each molecule must be unity, two of the remaining four densities may be eliminated. The remaining unknown quantities are then k_C, k_{C-C}, k_{C-O}, ρ_0' or ρ_2', ρ_0 or ρ_1, and the absolute signs of the a_{C_i}.

If we assume that the value of k_C determined by Tuttle from the α- and β-C^{13} splittings of naphthalene[1] is approximately equal to the semiquinone k_C value, then several solutions are possible. There is, however, only one solution which yields negative values for both k_{C-C} and k_{C-O} and positive values for all the ρ_i. This results when we choose $a_{C_1}=+2.82$; $a_{C_2}=-6.62$, $a_{C_1}'=-0.6$, and $a_{C_2}'=0$. The solutions change very little if we put $a_{C_1}'=0$ and $a_{C_2}'=-0.6$.

The naphthalene experiments allow two sets of constants, depending on the choice of signs. If $a_{C_\alpha}=7.1$ gauss, and $a_{C_\beta}=1.2$ gauss, then $k_C=40.5$ and $k_{C-C}=-5.9$. If $a_{C_\alpha}=7.1$ gauss and $a_{C_\beta}=-1.2$ gauss, then $k_C=45.6$ and $k_{C-C}=-17.1$. Using $k_C=40.5$ and the above values for the a_{C_i} in the semiquinone relationships, k_{C-C} is calculated to be -21 gauss; and if we choose $k_C=45.6$, then $k_{C-C}=-23$ gauss. Thus, there is fair agreement with the latter set of naphthalene constants.

The values determined for the remaining quantities are $k_0=-4.7$, $\rho_0=0.062$, $\rho_1=0.173$, $\rho_2=0.030$, $\rho_0'=0.206$, $\rho_1'=0.090$, $\rho_2'=0.113$. These latter three values may be compared to the same quantities calculated from simple molecular orbital theory by Bersohn.[5] The MO spin densities for II are $\rho_0'=0.221$, $\rho_1'=0.078$, and $\rho_2'=0.123$.

Although both the MO and the present calculations are very crude, the agreement between the two suggests that the constants k_{C-H}, k_{C-C}, and k_C are good approximations to similar constants in the semiquinones.

We are grateful to Dr. A. van Roggen for bringing the semiquinone C^{13} splitting to our attention.

* This research was supported in part by the Air Force Office of Scientific Research, Aeromedical Section.

[1] T. R. Tuttle, Jr., J. Chem. Phys. **32**, 1579 (1960).
[2] H. M. McConnell and D. B. Chesnut, J. Chem. Phys. **28**, 107 (1958).
[3] E. de Boer and S. I. Weissman, J. Am. Chem. Soc. **80**, 4549 (1958).
[4] S. I. Weissman, T. R. Tuttle, and E. de Boer, J. Phys. Chem. **61**, 28 (1957).
[5] R. Bersohn, J. Chem. Phys. **24**, 1066 (1956).

Electronegativity Effects of Hybridized Carbon Atoms

M. G. Brown

Department of Education, Nottingham University, Nottingham, England

(Received June 13, 1960)

ELECTRONEGATIVITY differences between atoms in bonds have been postulated to correlate the differences between the observed and calculated (arithmetic or geometric) mean bond properties.[1] Bond properties for C—X bonds (X=H, halogen, C, O, N) have been correlated with the various states of hybridization of the carbon atom.[2,3] Insofar as electronegativities have at least a correlative function, then such a correlation is to be expected between bond properties of C—X bonds containing variously hybridized carbon atoms and the electronegativity differences for the carbon atoms and X atoms. Several scales of electronegativities have been published for carbon atoms in different states of hybridization,[4] so that some estimate of the electronegativity effects can be attempted.

Lengths of C—X bonds (X=H, halogen; Csp^3, Csp^2, Csp) have been derived using some suggested values for the radii of hybridized carbon atoms (see Table 6 of reference, footnote 3). Differences between the derived values of bond lengths and the corresponding average observed values (see Table 3 of reference, footnote 3) are given in Table I. Carbon atom electronegativities have been calculated by the method of

Wilmhurst,[4] but using the radii of the relevant *external* single bond[3] to obtain the electronegativity of the appropriate orbital. Electronegativity differences for the atoms of these bonds are also recorded in Table I.

TABLE I. Differences Δd between calculated arithmetic mean and average observed bond lengths and electronegativity differences Δx for C—X bonds (X=H, halogen).

	C—H			C—Cl		
	sp^3	sp^2	sp	sp^3	sp^2	sp
Δd:	0.048	0.022	0.00	−0.005	0.016	0.05
Δx:	0.53	0.76	0.86	−0.37	−0.14	−0.04
	C—Br			C—I		
	sp^3	sp^2	sp	sp^3	sp^2	sp
Δd:	−0.013	0.0	0.034	−0.035	0.015	0.027
Δx:	−0.17	0.06	0.16	0.13	0.36	0.46

$\Delta x=(x_C-x_X)$, with values of x_H and x_{hal}.[4]
x_C: Me—, 2.63; CH_2=CH—, 2.86; CH≡C—, 2.96. (See text for calculation.)
$\Delta d=(d_{calc}-d_{obs})$. Values from data in Tables 3 and 6 of reference, footnote 3.

The values presented in Table I exhibit trends that are unexpected from simple considerations,[1] assuming constant x_C and x_X values for each bond with a given type of carbon atom or X atom. Thus, for C—H bonds, Δx increases while Δd decreases; and for the C—Cl bond, Δx decreases while Δd increases. In view of the fact that even Csp^3-halogen bonds with chlorine, bromine, and iodine show an expansion relative to the standards, it appears that effects often ascribed simply to electronegativity effects are not not always easily explicable.[5,6]

TABLE II. Values of Δd and Δx for C—F bonds.

	d (calc)	d (obs)	d	x
Csp^3—F:	1.482	1.392 (1.32)	0.09 (0.16)[a]	−1.37
Csp^2—F:	1.443	1.333	0.11	−1.14
Csp—F:	1.40	1.27	0.13	−1.04

d (calc) from r_F=0.71 and r_C from ref. 3

d (obs) Csp^2—F and Csp^2—F from ref. 3; Csp—F from E. E. Aynsley, R. E. Dodd, and R. Little, Proc. Chem. Soc., **265,** 1959; J. K. Tyler and J. Sheridan, *ibid.*, **119,** 1960.

[a] The figure in the bracket is for C—F bond in CF_4.

Recently available data for the C—F bond lengths allow us to carry out similar derivations for them. There is a severe complication in this case, however, because of the marked difference in bond length for the C—F bond in CH_3F and in CF_4. However, the data in Table II show that simple electronegativity arguments are inadequate. Bent[6] has recently discussed the C—F bond.

The significance of the values in Tables I and II may be severely questioned on the basis, first, that the original hybridized radii allow too much for hybridization effects in their derivation from C—C bonds. Second, the values of the electronegativities of the hybridized carbon atoms are very uncertain. However, use of larger carbon atom radii can only accentuate the trends noticed.

Further comment on the trends noted here must await more precisely determined values of carbon and X-atom electronegativities or until hybridization effects[6,7] and conjugation effects are more surely separated in fixing carbon radii.

[1] L. Pauling, *The Nature of the Chemical Bond* (Cornell University Press, Ithaca, New York, 1945), Chap. 2, p. 58.
[2] A. J. Petro, J. Am. Chem. Soc. **80,** 4230 (1958).
[3] M. G. Brown, Trans. Faraday Soc. **55,** 694 (1959).
[4] H. O. Pritchard and H. A. Skinner, Chem. Revs. **55,** 745 (1955); J. K. Wilmhurst, J. Chem. Phys. **27,** 1129 (1957).
[5] T. L. Cottrell and L. E. Sutton, Proc. Roy. Soc. (London) **A218,** 333 (1953).
[6] H. A. Bent, J. Chem. Phys. **33,** 304 (1960).
[7] J. Duchesne, J. Chem. Phys. **20,** 540 (1952).

On the Isomerization of *n*-Butyl Radicals

ALVIN S. GORDON AND JAMES R. MCNESBY*

Chemistry Division, U. S. Naval Ordnance Test Station, China Lake, California

(Received August 15, 1960)

IN a recent publication Kerr and Trotman-Dickenson[1] have studied the reactions of *n*-butyl radicals generated via the photolysis of *n*-valeraldehyde. They observe propene in their products and ascribe it to an intraradical abstraction of a hydrogen followed by a pyrolytic breakdown,

$$\dot{C}H_2CH_2CH_2CH_3 \rightarrow CH_3CH_2\dot{C}HCH_3 \rightarrow \dot{C}H_3 + CH_3CH{=}CH_2. \quad (1)$$

Some time ago[2] we reported on the reaction of CD_3 radicals with $CH_3CD_2CD_2CH_3$. Two butyl radicals are formed in this reaction, $\dot{C}H_2CD_2CD_2CH_3$ and $CH_3\dot{C}DCD_2CD_3$. The most important pyrolytic reactions of these radicals result in the formation of ethene and propene. The deuterium marking of the ethene (only d_2) and propene (only d_3) was interpreted as involving the simple breaking of the two butyl radicals. In particular, no propene-d_4 was observed in the products, thus showing that the isomerization reaction involving a shift of a D atom along the carbon skeleton,

$$\dot{C}H_2CD_2CD_2CH_3 \rightarrow CH_2D\dot{C}DCD_2CH_3 \rightarrow CH_2DCD{=}CD_2 + \dot{C}H_3 \quad (2)$$

does not occur when there is a relatively easy alternative path. Kerr and Trotman-Dickenson[1] now propose, on the basis of their mechanism, that our results may

be interpreted in terms of reaction (1) as

$$\dot{C}H_2CD_2CD_2CH_3 \rightarrow CH_2DCD_2\dot{C}DCH_3$$

$$\rightarrow CH_3CD{=}CD_2 + \dot{C}H_2D, \quad (3)$$

since they observe that the product ratio of methane/propene = 1. We have examined the isotopic content of the methane fraction in our work in terms of this interpretation. The results are reported in Table I and show no CH_2D_2 within the limits of the reading error of the mass spectra peaks. It should be noted that

TABLE I. Methane analyses as percentages from reaction of CD_3 with $CH_3CD_2CD_2CH_3$.[a]

	T °C					
	399.8	450.8	356.4	355.6	402.4	450.0
CD_4	48.4	44.3	63.4	45.9	35.5	50.2
CD_3H	18.6	17.6	19.5	24.8	19.3	15.8
CD_2H_2	0.0	0.0	0.0	0.0	0.0	0.1
CDH_3	24.1	27.8	13.2	19.0	29.6	26.4
CH_4	8.9	10.3	3.9	10.3	15.6	7.5

[a] Three different mixes of acetone-d_6/$CH_3CD_2CD_2CH_3$ were used in these experiments.

the methyl radical abstracts deuterium more readily than hydrogen ($CD_4/CD_3H > 2$) under our experimental conditions. Our results were obtained in a temperature range which overlaps the range in which Kerr and Trotman-Dickenson[1] worked. The results show clearly that reaction (1) does not occur in this temperature range at a rate measurably competitive with simple carbon-carbon rupture. We have previously reported evidence[3] that alkyl radicals are probably isomerized via a reaction analogous to reaction (1) when the "activated complex" involves a ring of five or six atoms. The four-atom "complex" in reaction (1) is not formed, presumably due to the strain involved in the ring.

At the temperatures used in the work of Kerr and Trotman-Dickenson the products should contain evidence of the attack of hydrocarbon radicals on all the hydrogens of *n*-valeraldehyde. The main attack will be on the aldehydic hydrogen, followed by attack on the hydrogens on the carbon α to the aldehyde group, then the equivalent hydrogens on the β and γ carbons, and lastly, the hydrogens on the methyl group.

The equivalence of the methane and propene observed by Kerr and Trotman-Dickenson may be the result of a free radical abstraction of the equivalent *n*-valeraldehyde hydrogen atoms on the β and γ carbons

$$R + CH_3CH_2CH_2CH_2CHO$$

$$\rightarrow RH + CH_3\dot{C}HCH_2{:}CH_2CHO \quad (4)$$

$$R + CH_3CH_2CH_2CH_2CHO$$

$$\rightarrow RH + CH_3{:}CH_2\dot{C}HCH_2CHO, \quad (5)$$

where : indicates the subsequent cleavage point of the large radical produced in reactions (4) and (5).

* Present address: National Bureau of Standards, Washington 25, D. C.

[1] J. A. Kerr and A. F. Trotman-Dickenson, J. Chem. Soc. **323**, 1602 (1960).

[2] J. R. McNesby, C. M. Drew, and A. S. Gordon, J. Chem. Phys. **24**, 1260 (1956).

[3] A. S. Gordon and J. R. McNesby, J. Chem. Phys. **31**, 853 (1959).

Optical Rotatory Dispersion of Transition-Metal Complexes

SATORU SUGANO*

Bell Telephone Laboratories, Inc., Murray Hill, New Jersey

(Received June 22, 1960)

IN 1956, Moffitt[1] discussed theoretically, optical rotatory dispersion of transition-metal complex ions, namely, $[MY_3]^{3+}$ (M = Cr, Co; Y = ethylene diamine, oxalate ion), where each Y ion bridges between two of the six octahedral ligand sites, giving D_3 symmetry. He concluded that the optical rotatory dispersion may be attributed to a first-order asymmetric distortion of the octahedral *d*-orbitals due to the odd-parity ligand field associated with the system. We wish to point out here that this mechanism is incorrect: dihedral transition-metal complexes can *not* attain their optical rotatory power from such asymmetric distortions. This conclusion is *independent* of the specific transition-metal ion involved.

The proof is given by the use of symmetry arguments as follows: The quantum mechanical theory gives the formula[2]

$$R_{\Gamma\Gamma'} = \mathrm{Im}\sum_{\gamma\gamma'}(\Gamma\gamma \mid \mathbf{P} \mid \Gamma'\gamma') \cdot (\Gamma'\gamma' \mid \mathbf{m} \mid \Gamma\gamma), \quad (1)$$

for the rotational strength of the $\Gamma \pm \Gamma'$ band.[3] Here, $\mathbf{P}$ is an electric dipole and $\mathbf{m}$ is a magnetic dipole vector, γ and γ' denote the degenerate components, referred to the fourfold axes of the octahedron, of the Γ and Γ' states, respectively. In order to have nonvanishing matrix elements of $\mathbf{P}$, we take into account the first-order asymmetric distortion of the Γ and Γ' states due to the odd-parity ligand field perturbation

$$V = \sum_{\Gamma^*\gamma^*} C_{\Gamma^*\gamma^*} V_{\Gamma^*\gamma^*}, \quad (2)$$

which is invariant under transformations with the symmetry of the system. Then, factorizing[4] the matrix

elements into their radial and angular (the Wigner coefficients) parts and rearranging them in a suitable way, we find

$$R_{\Gamma\Gamma'}=\mathrm{Im}\sum_{\alpha_u'\Gamma_u'\Gamma^*}A(\Gamma\Gamma'\Gamma^*\alpha_u'\Gamma_u')$$
$$\times[\sum_{\gamma^*\gamma'\gamma_u'}C_{\Gamma\cdot\gamma^*}(\Gamma_u'\gamma_u'\mid\Gamma'\gamma'\Gamma^*\gamma^*)$$
$$\times\{\sum_{\gamma\gamma^\dagger}(\Gamma_u'\gamma_u'\mid\Gamma_uT_1\gamma^\dagger)(\Gamma'\gamma'\mid\Gamma\gamma T_1\gamma^\dagger)\}]$$
$$+\mathrm{Im}\sum_{\alpha_u''\Gamma_u''\Gamma^*}B(\Gamma\Gamma'\Gamma^*\alpha_u''\Gamma_u'')$$
$$\times[\sum_{\gamma^*\gamma\gamma_u''}C_{\Gamma\cdot\gamma^*}(\Gamma\gamma\mid\Gamma_u''\gamma_u''\Gamma^*\gamma^*)$$
$$\times\{\sum_{\gamma'\gamma^\dagger}(\Gamma_u''\gamma_u''\mid\Gamma'\gamma'T_1\gamma^\dagger)(\Gamma\gamma\mid\Gamma'\gamma'T_1\gamma^\dagger)\}],\quad(3)$$

where A and B are the factors not depending upon the component γ's, and the other factors, the Wigner coefficients for the cubic group, are already known.[5] The excited states of odd-parity are represented by $\alpha_u'\Gamma_u'\gamma_u'$ and $\alpha_u''\Gamma_u''\gamma_u''$, which are admixed respectively with the $\Gamma'\gamma'$ and $\Gamma\gamma$ states by perturbation (2). By the use of orthogonality relations between the Wigner coefficients, the expressions in the first and the second $\{\ \}$ brackets are reduced to $\delta(\Gamma_u'\gamma_u',\ \Gamma'\gamma')$ and $\delta(\Gamma_u''\gamma_u'',\ \Gamma\gamma)$, respectively. The Kronecker delta applies only to species symbols $\Gamma\gamma$ and not to parities. Therefore, the vanishing or nonvanishing of Eq. (3) depends upon the value of the Wigner coefficient $(\Gamma\gamma\mid\Gamma\gamma\Gamma^*\gamma^*)$, which is, irrespective of $\Gamma\gamma$ and γ^*, zero for the case of interest here, $\Gamma^*=T_1,\ T_2$.

For the dihedral system we are considering, $V_{A_{1u}}$ and $(V_{T_{2u}\xi}+V_{T_{2u}\eta}+V_{T_{2u}\zeta})$ are invariant under the symmetry operation, but, since $V_{A_{1u}}$ appears first in the ninth-order in the power expansion with respect to r, it may be safely neglected. The only remaining term in (2) is, therefore, the latter term with $\Gamma^*=T_{2u}$, which gives no contribution to the rotational strength as proved already. It should be noticed that our perturbing field is identical to the $\mathcal{V}_3$ Moffitt adopted in his paper.

Besides Moffitt's mechanism the conceivable first-order mechanism which might be supposed to give nonvanishing rotational strengths is the vibronic interaction, but it does not work again if we assume that the interaction is only appreciable with the vibrational modes coming from the T_{1u} and T_{2u} vibrations of the undistorted octahedral framework, because the same symmetry arguments as mentioned above can be applied.

In such a linear vibronic mechanism, there are arguments relevant to the rotation, other than those symmetry arguments presented here, but we do not touch upon them now, although discussions on them seem as important as the symmetry arguments.[6] Further studies on the vibronic mechanism are necessary, together with those on the contribution of the higher-order distortion of d-orbitals to the rotatory dispersion.[6]

The author would like to express his thanks to Dr. A. D. Liehr for criticizing the manuscript.

* On leave from Physics Department, Tokyo University, Tokyo, Japan.

[1] W. Moffitt, J. Chem. Phys. **25,** 1189 (1956).
[2] E. U. Condon, Revs. Modern Phys. **9,** 432 (1937).
[3] We, as does Moffitt, neglect here the effect of dihedral splittings of the cubic states $\Gamma\gamma$ and $\Gamma'\gamma'$, assuming that the magnitudes of the splittings are small compared with the width of the dispersion curve.
[4] Y. Tanabe and H. Kamimura, J. Phys. Soc. Japan **13,** 394 (1958).
[5] Y. Tanabe and S. Sugano, J. Phys. Soc. Japan **9,** 753 (1954).
[6] S. Sugano, (to be published).

Behavior of the Free Radicals Trapped in Gamma-Irradiated Compounds Which Contain Hydrogen Bonds

ZENICHIRO KURI, YUZURU FUJIWARA,* HISASHI UEDA,† AND SHOJI SHIDA

Japanese Association for Radiation Research on Polymers, Tokyo, Japan

(Received July 12, 1960)

SINCE free radicals are in general very reactive, it is very difficult to store them, except in vacuum.

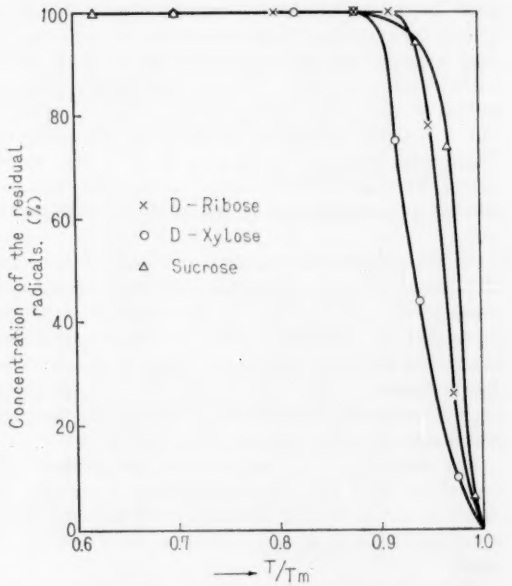

FIG. 1. Concentration of the residual radicals from d-ribose, d-xylose, and sucrose after heating for 10 min at each temperature. The abscissa is the ratio of the heating temperature to the melting point (°K).

Therefore, the free radicals formed in polymers, which have been gamma-irradiated in vacuum in a state of powder or thin film, usually suffer from oxidation when exposed to air after irradiation, to produce peroxide radicals which are soon transformed into carbonyl groups.[1–3] This means that even free radicals trapped in the solid state cannot survive in open air.

However, we found that the triplet electron-spin resonance (ESR) spectrum of free radicals formed in gamma-irradiated polyvinyl alcohol (PVA) did not change, even on exposure to air. Moreover, strikingly, the ESR pattern of this radical is affected neither by exposure to scavengers, such as Cl_2, I_2, NO, SO_2, or H_2S, nor by simultaneous irradiation together with these gases. But this does not mean that the radical itself is chemically unreactive. The following experiments will suggest an alternative interpretation.

In the first place, when the irradiated PVA was heated above the glass transition temperature or swollen with water to stimulate the segmental motion of the polymer, the ESR pattern of the radical soon disappeared, perhaps by recombination. On the other hand, the irradiated polymer can be grafted with some vinyl monomers, such as styrene or methylmethacrylate, in the presence of water.[4] The failure of the radical from PVA to react with scavenger accordingly seems to be due to some factor other than exceptional stability. We carried out similar experiments using other compounds. Cellulose, starch, arabinose, ribose, xylose, glucose, fructose, sorbose, galactose, sucrose, cellobiose, lactose, inulin, and glutamic acid were irradiated in the powdery state. The radicals formed here were found to be as stable in air as that of PVA. In particular, the radicals in crystalline organic substances, such as sucrose and fructose, are not affected by oxygen or by temperatures below the melting point. At the melting point they decay sharply, as shown in Figs. 1 and 2. Nevertheless, when 1 g irradiated sucrose at the dosage of 10^7 r was dissolved into 10 cc of 10% acrylamide solution, the monomer was completely polymerized. From these experiments, it is seen that the stability of the radicals formed in sucrose indicates not their nonreactivity with the scavengers but their impermeability to gases. If the whole matrix of the radicals is broken up into pieces by dissolution, the pieces begin to move freely and to react with the scavenger or vinyl monomer.

All these compounds have hydroxyl groups forming intermolecular hydrogen bonds, and such insensibility to the scavengers is not seen in any other molecular and polymer radicals at ordinary temperatures. Therefore, the result may be caused by the network of intermolecular hydrogen bonds which will prevent penetration of the gases.

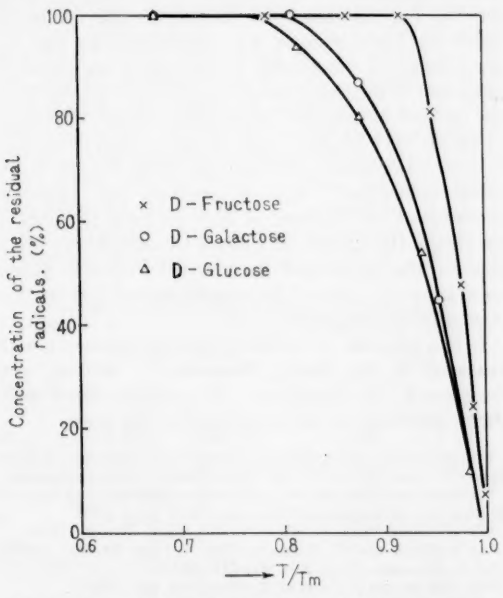

FIG. 2. Concentration of the residual radicals from *d*-fructose, *d*-galactose, and *d*-glucose after heating for 10 min at each temperature. The abscissa is the ratio of the heating temperature to the melting point (°K).

* On leave from Kurashiki Rayon Company, Ltd. Umeda, Kita-ku, Osaka, Japan.
† On leave from Toyo Spinning Company, Ltd., Dojima, Kita-ku, Osaka, Japan.

[1] R. J. Abraham and D. H. Whiffen, Trans. Faraday Soc. **54,** 129 (1958).
[2] H. Rexroad and W. Gordy, J. Chem. Phys. **30,** 399 (1959).
[3] Z. Kuri, H. Ueda, and S. Shida, J. Chem. Phys. **33,** 371 (1960).
[4] I. Sakurada, T. Okada, and E. Kugo, Isotopes and Radiation (Japan) **2,** 296, 306, 316 (1959).

Power Series Expansions of Vibrational Potentials. I. The Heitler-London Potential for H_2†*

CHARLES L. BECKEL

Department of Physics, Georgetown University, Washington, D. C.

(Received August 25, 1960)

THE recent work of Herzberg and co-workers on H_2[1] and HD[2] has emphasized the inadequacy of existing methods for interpreting vibrational data on diatomic molecules. The behavior of vibrational energy difference curves is not understood in detail. In an attempt to shed further light on this behavior, the author has expanded in a Dunham series[3] a simple model of a covalent vibrational potential, the Heitler-London

potential[4] for H_2. This paper reports the results of the expansion.

With the aid of the WPA tables[5] the Heitler-London electronic energy was computed at nuclear separations $r/a_0=1.45$, 1.50, 1.55, 1.60, 1.63, 1.64, 1.65, 1.66, 1.70, 1.75, 1.80, and 1.85, a_0 being the Bohr radius for the H atom. A cubic expression fitted at 1.63, 1.64, 1.65, and 1.66 was used to determine the equilibrium separation r_e. The coefficients of Dunham's power series were determined by fitting the energies at 1.45, 1.50, 1.55, 1.60, 1.65, 1.70, 1.75, 1.80, and 1.85, and Dunham's expressions were used to determine the spectroscopic constants. These are shown in Table I. The spectroscopic constants, in Dunham's notation, are listed at the left with the more common symbols shown in parentheses. All the Heitler-London constants are accurate to within one in the last digit. The experimental constants, from Herzberg and Howe,[1] are listed with the same number of digits as the Heitler-London values. The H-L constants Y_{10}, Y_{20}, Y_{01}, Y_{11}, and Y_{02} are all of the same sign, but smaller than the experimental values. This is associated with the fact that the Heitler-London potential is not deep enough and its r_e is too large. The H-L Y_{30}, however, has a sign opposite to the experimental value. This means that the Heitler-London ΔG vs v curve has a negative curvature at low vibrational quantum number, while the experimental first-energy difference curve has a positive curvature. It is of interest to compare the Heitler-London dissociation energy with the value predicted by linear extrapolation using the H-L vibrational constants. The result $D_0/D_{\text{lin}}=0.801$ indicates that the H-L potential has rapidly converging vibrational levels at high v. In 1946 Gaydon[6] found that for a large number of nonionic molecules the experimental ratio D_0/D_{lin} averaged $\sim$0.80.

TABLE I. Constants for the ground electronic state of H_2.

Constant	Heitler-London potential	Experimental
$Y_{10}(\omega_e)$	3804 cm^{-1}	4400 cm^{-1}
Y_{20} $(-\omega_e x_e)$	−116 cm^{-1}	−121 cm^{-1}
Y_{30} $(\omega_e y_e)$	−1.1 cm^{-1}	+0.7 cm^{-1}
Y_{01} (B_e)	44.28 cm^{-1}	60.86 cm^{-1}
Y_{11} $(-\alpha_e)$	−2.10 cm^{-1}	−3.08 cm^{-1}
Y_{02} $(-D_e)$	−0.02400 cm^{-1}	−0.04657 cm^{-1}
r_e	0.86919 A	0.74116 A
D_0	2.923 ev	4.478 ev

The e^2/r term, the nuclear attraction integral, and the Coulomb integral of the H-L potential converge only in the range $0<r<2r_e$ when expanded about r_e. The coefficients shown in Table II tend to confirm that cancellations do not occur and that $0<r<2r_e$ is the range of convergence of the H-L power series. The coefficients show no convergence. Above $n=2$ they are close to values obtained from an expansion of e^2/r alone.

To ensure rapid convergence of a power series fitted to numerical values of a vibrational potential, one must not use too wide a range of r. On the other hand, if the range of r is too narrow, the $(r-r_e)^n/r_e^n$ become negligible and prevent determination of their coefficients at small n. In the present work, the range of r was chosen so that the $n=9$ term was the first negligible one. The value of $(r-r_e)^8/r_e^8$ was nonnegligible, but small enough to prevent its coefficient from having much accuracy. As n decreased, the $(r-r_e)^n/r_e^n$ became larger and the coefficients more accurate. This is shown in Table II. The $n=6$ coefficient was the highest one of interest here, since the $n=7, 8, \cdots$, coefficients are not needed to determine Y_{30}.

TABLE II. Coefficients of $(r-r_e)^n/r_e^n$ in e^2/a_0 units.

n	Heitler-London	e^2/r
2	+0.37224±0.00001	+0.60881
3	−0.62466±0.00002	−0.60881
4	+0.66295±0.00005	+0.60881
5	−0.645±0.001	−0.60881
6	+0.63±0.01	+0.60881
7	−0.67±0.07	−0.60881
8	+1.2±0.7	+0.60881

It is worth noting that even if the vibrations of the H_2 molecule were exactly governed by the Heitler-London potential, spectroscopic data would not yield the Y_{10}, Y_{20}, Y_{30} values shown in the middle column of Table I. This is because, for a light molecule like H_2, the number of vibrational Y's required, for accuracy consistent with that of the data, is always greater than the number of empirical vibrational energy differences available.[7] The higher Y's are dropped from consideration with the result that the remaining Y's are incorrectly determined. This is precisely the situation encountered by Herzberg *et al.*,[1,2] in their analyses of the H_2 and HD ultraviolet spectra. Obviously, an expression for the vibrational energies other than a power series in $v+\frac{1}{2}$ is required for unambiguous determination of vibrational properties.

It is a pleasure to acknowledge conversations with Professor G. H. Dieke, Professor V. Griffing, and Professor E. R. Lippincott, and correspondence with Dr. G. Herzberg on the background of this work.

† Supported by grants from the Georgetown University Alumni Research Fund and the U.S. Air Force Office of Scientific Research.

* A report on this work was made at the Symposium on Molecular Structure and Spectra, Columbus, Ohio, June, 1960.

[1] G. Herzberg and L. L. Howe, Can. J. Phys. **37,** 636 (1959).

[2] R. A. Durie and G. Herzberg, Can. J. Phys. **38,** 806 (1960).

[3] J. L. Dunham, Phys. Rev. **41,** 721 (1932).

[4] W. Heitler and F. London, Z. Physik **44,** 455 (1927).

[5] Work Projects Administration, *Tables of the Exponential Function, Tables of Sine, Cosine, and Exponential Integrals, Tables of Natural Logarithms,* (New York, 1939, 1940, 1941).

[6] A. G. Gaydon, Proc. Phys. Soc. (London) **58,** 525 (1946).

[7] A. S. Coolidge, H. M. James, and E. L. Vernon, Phys. Rev. **54,** 726 (1938).

Power Series Expansions of Vibrational Potentials. II. Two Classical Potentials for Ionic Molecules*†

EDWARD J. FINN AND CHARLES L. BECKEL

Department of Physics, Georgetown University, Washington, D. C.

(Received August 25, 1960)

VIBRATIONS in diatomic molecules are not yet well enough understood to permit reliable extrapolation from known energy levels to unknown ones. In a previous note[1] some vibrational properties associated with a simple covalent potential were described. In this note the results of a similar study are reported for two simple ionic potentials. These results were obtained through use of Dunham's power series technique.[2]

TABLE I. Test of applicability of ionic potentials to indium halides.

	$-Y_{20}$ (cm^{-1})			D_i (ev)		
Molecule	*A*	*B*	exp[a]	*A*	*B*	exp[b]
InF	4.38	2.85	2.64	6.6	7.3	7.6
InCl	1.88	1.11	1.01	5.4	6.3	6.5

[a] See footnote 4.
[b] C. L. Beckel, J. Chem. Phys. **24**, 923 (1956).

The first ionic potential that was expanded consisted of an exponential repulsion term and a $1/r$ Coulomb attraction term. Values computed with this potential are labeled "*A*" in Tables I and II. The second expansion (values labeled "*B*") was of a potential that retained these two terms and added an attractive $1/r^4$ polarizability term. These two potentials are simplified forms of that proposed by Rittner,[3] higher-order polarizability terms and the Van der Waals $1/r^6$ term here being neglected. In the case of potential *A*, the two adjustable parameters were determined by experimental values of r_e and ω_e.[4] For potential *B* an additional parameter, the average polarizability of the ions, necessitated the use of an additional experimental constant. This was chosen to be $Y_{11}(-\alpha_e)$.[4]

TABLE II. Y_{30} and D_i/D_{1in} from the ionic potentials.

	Y_{30} (cm^{-1}) $\times 10^3$		D_i/D_{1in}	
Molecule	*A*	*B*	*A*	*B*
LiF	+29.0	+35.0	2.40	2.50
LiI	+21.0	+7.0	2.69	2.29
NaI	+3.4	+1.6	2.87	2.43
InF	+25.0	+5.9	3.30	2.40
InCl	+7.7	+1.3	3.32	2.27

The two potentials were applied to three alkali halides and two indium monohalides. It is well known that potentials of the type considered here are applicable to alkali halides.[3,5-7] It appears from Table I that such ionic potentials are also useful for Group III monohalides, since reasonable values of Y_{20} and D_i (the energy of dissociation into ions) are obtained for InF and InCl, particularly in case *B*.

A study of the Dunham terms reveals certain general results. For potential *A*, Y_{20} is always negative, Y_{11} is negative if $Q>4.5\times10^6$, and Y_{30} is positive if $Q>3.4\times10^6$, where Q is the product $\mu\omega_e^2r_e^3$ (amu cm^{-2} A^3). For the alkali and indium halides, $Q>10^7$. When the $1/r^4$ term is included, it is not easy to state such simple conditions; nevertheless, all computed Y_{20}'s and Y_{11}'s were negative, and all Y_{30}'s were positive. Table II contains the calculated values of Y_{30} and the ratio of D_i to the energy of dissociation, D_{1in}, obtained by linear extrapolation from the curve constants. The fact that all Y_{30}'s are positive shows that the ΔG vs v curves for the potentials considered here have, as might be expected, a positive curvature at small v. This is in contrast with the results reported in the preceding note.[1] For all but LiF, the Y_{30} computed when polarizability is taken into account is smaller than when englected. This indicates that polarizability of ions leads to less positive curvature of the ΔG curves at low v than would be present if ions were not polarizable. The results for LiF illustrate the fact that computed polarizabilities are very sensitive to the spectroscopic constants used to determine potential *B*. Potential *A* applied to LiF yielded an α_e 5% below the experimental value. When potential *B* was fitted to the experimental α_e, the average polarizability for Li^+ and F^- was computed to be negative. In contrast with the Heitler-London potential,[1] all the ratios of D_i/D_{1in} are >1; in fact, considerably so. Thus, it is seen that these ionic potentials lead to very slow convergence of vibrational levels. Introduction of polarizability speeds up the convergence somewhat. This is more noticeable for InF and InCl, since In^+ is more polarizable than the alkalis.

Both ionic potentials, when expanded in a Taylor series about r_e, converge only in the range $0<r<2r_e$. However, for heavy molecules such as the alkali and Group III monohalides, Dunham's expansion has rapidly converging terms and is therefore useful for a large number of vibrational levels.

* Supported in part by a grant from the U.S. Air Force Office of Scientific Research.

† Parts of this note were reported at the Symposium on Molecular Structure and Spectra, Columbus, Ohio, June 1960.

[1] C. L. Beckel, J. Chem. Phys. **33**, 1885 (1960).

[2] J. L. Dunham, Phys. Rev. **41**, 721 (1932).

[3] E. S. Rittner, J. Chem. Phys. **19**, 1030 (1951).

[4] The experimental constants were taken from the following sources. LiF: rotational and vibrational data both from G. L. Vidale, Aerophysics Research Memo-No. 32, General Electric Aerosciences Laboratory, Philadelphia, Pennsylvania (1959); LiI and NaI: rotational data from work cited in footnote 5, vibrational data from work cited in footnote 6; InF: rotational and vibrational data both from R. F. Barrow, D. V. Glaser, and P. B. Zeeman, Proc. Phys. Soc. (London) **A68**, 962 (1955); InCl:

rotational data from A. H. Barrett and M. Mandel, Phys. Rev. **99**, 666 (1955); vibrational data from G. Herzberg, *Molecular Spectra and Molecular Structure* (D. Van Nostrand Company, Inc. Princeton, New Jersey, 1950), Vol. 1.
[5] A. Honig, M. Mandel, M. L. Stitch, and C. H. Townes, Phys. Rev. **96**, 629 (1954).
[6] W. Klemperer and S. A. Rice, J. Chem. Phys. **26**, 618 (1957); **27**, 573 (1958).
[7] Y. P. Varshni, Trans. Faraday Soc. **53**, 132 (1957).

Increasing the Intensity of C^{13} NMR Signals by a Flowing-Sample Method

S. Forsén and A. Rupprecht

Research Group for NMR, Division of Physical Chemistry, The Royal Institute of Technology, Stockholm, Sweden

(Received May 3, 1960)

THE only stable isotope of carbon with nonzero spin is C^{13} which, with a spin of one half, is quite suitable for NMR spectroscopy although its low natural abundance (1.1%) gives a low signal-to-noise ratio.[1] It will be shown that the use of flowing samples offers a means of increasing the signal strength of C^{13}.

In 1951 Suryan[2] studied the PMR absorption signal of water, which had previously been magnetically polarized, flowing steadily through a resonance coil. He found that the signal amplitude at first increased with increasing flow rate, reaching a constant value at higher rates of flow corresponding to a fivefold increase in intensity over the signal from a stationary sample. The energy absorption of the flowing sample is higher due to a lower over-all saturation factor, caused by the continuous supply of unsaturated nuclei.

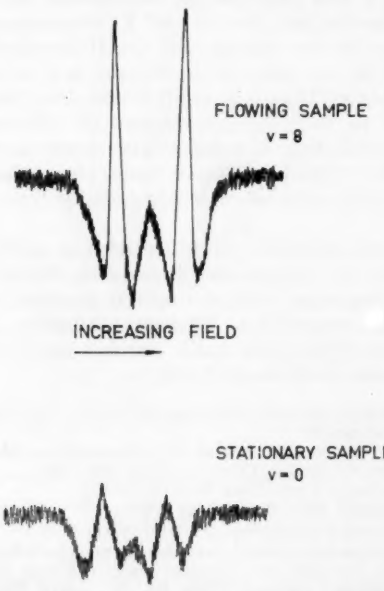

FIG. 1. C^{13} NMR spectrum of benzene (the derivative of the dispersion mode with negative sign). v = Rate of flow through rf coil in cm/sec.

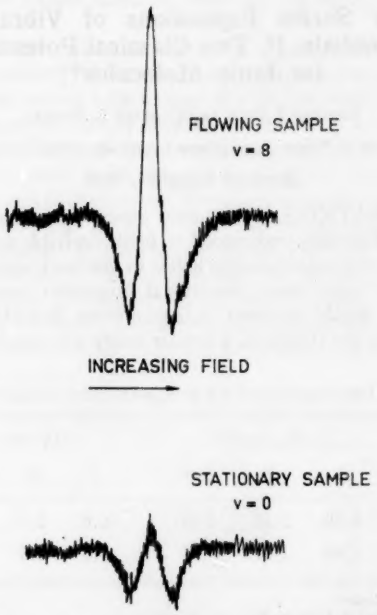

FIG. 2. C^{13} NMR spectrum of carbon tetrachloride (the derivative of the dispersion mode with negative sign). v = Rate of flow through rf coil in cm/sec.

The method has been explored by other investigators,[3–9] some of whom used it mainly for the purpose of increasing the signal-to-noise ratio of weak proton signals.[4,6]

The C^{13} measurements were carried out on a Varian V–4200 B Wide Line NMR-spectrometer at 7.8 Mc and a magnetic field of about 7300 gauss. A screwpump maintained a steady flow of liquid through a 1.1-liter vessel made of nylon mounted in the 1.75-in. gap of the 12-in. magnet. The polarized liquid passed directly from the vessel to the resonance coil. As in stationary C^{13} measurements the dispersion mode was used, since the slow relaxation easily leads to saturation in the absorption mode.[1] The signals were thus recorded as the derivative of the dispersion mode and being taken with negative sign, bear some resemblance to the absorption mode itself.

As predicted by theory,[2] the signal-to-noise ratio increased with increasing flow rate v and reached a constant maximum value at about $v = 7$ cm/sec. Figure 1 shows the spectrum of natural benzene for a stationary and a flowing sample, respectively, recorded under the following approximate conditions:

Rf field (H_1) = 0.005 gauss
Sweep rate of static magnetic field = 0.3 gauss/min
Sweep field amplitude (peak-to-peak) = 0.08 gauss,
Sweep field frequency = 20 cps.

The flowing benzene sample gives peaks about three times the height of those given by the stationary one. Under stationary conditions the components of the doublet, caused by the indirect spin-spin interaction of each carbon with its attached proton, are unequal in intensity due to the magnetization transfer effect discussed by McConnell.[1,10,11] With flowing samples, however, the components of the doublet appear with equal intensity.

Figure 2 shows the spectrum of carbon tetrachloride (which theoretically should show 13 peaks) recorded under the same conditions as given above. Only a single line is observed, presumably due to the chlorine quadrupole moment which blots out all evidence of spin coupling.

The flowing sample method should be well adapted to the high-resolution observation technique (applied to C^{13} by Lauterbur[1,12] and Holm[13]) where the use of higher rf fields is possible and may result in a further increase of the C^{13} signal intensity.

Thanks are due to Dr. Erik Forslind for valuable discussions and to the Knut and Alice Wallenberg Foundation for the gift of the NMR apparatus.

[1] P. C. Lauterbur, Ann. N. Y. Acad. Sci. **70**, 841 (1957).
[2] G. Suryan, Proc. Indian Acad. Sci. **A33**, 107 (1951).
[3] P. M. Denis, G. J. Béné, and R. C. Extermann, Arch. sci. (Geneva) **5**, 32 (1952).
[4] A. L. Bloom and J. N. Shoolery, Phys. Rev. **90**, 358 (1953).
[5] C. Sherman, Phys. Rev. **93**, 1429 (1954).
[6] A. M. J. Mitchell and G. Phillips, Brit. J. Appl. Phys. **7**, 67 (1956).
[7] A. Z. Hrynkiewicz and T. Waluga, Acta Phys. Polon. **XVI**, 381 (1957).
[8] K. Antonowicz, Bull. intern. acad. polon. sci., Classe III, **5**, 813 (1957).
[9] K. Antonowicz, Bull, intern. acad. polon. sci., Classe III, **5**, 1069 (1957).
[10] H. M. McConnell and D. D. Thompson, J. Chem. Phys. **26**, 958 (1957).
[11] H. M. McConnell and D. D. Thompson, J. Chem. Phys. **31**, 85 (1959).
[12] P. C. Lauterbur, J. Chem. Phys. **26**, 217 (1957).
[13] C. H. Holm, J. Chem. Phys. **26**, 707 (1957).

The Single-Stage Fractionation Factor for the System Oxygen vs Cobalt Di-(Salicylal)-Ethylenediimine-Oxygen*

L. L. Brown and J. S. Drury
Chemistry Division, Oak Ridge National Laboratory, Oak Ridge, Tennessee

(Received July 29, 1960)

THE single-stage fractionation factor for the oxygen isotopes O^{16}–O^{18} has been measured at room temperature for the system oxygen (gas) vs cobalt di(salicylal)-ethylenediimine-oxygen. Equilibrations by two methods gave concordant results. The observed enrichment factor, $\alpha - 1$, differed by a factor of two from that reported by Panchenkov *et al.*[1] Our value using the first method is 1.013 ± 0.002, $\alpha = (O^{18}/O^{16})$ gas/(O^{18}/O^{16}) solid, and by the second method 1.012 ± 0.002. The heavy-oxygen isotope enriches in the gas phase. Panchenkov *et al.*, reported a single-stage fractionation factor of 1.032 ± 0.02. His multistage data yielded estimates of α from 1.024 to 1.030. Our experimental methods follow.

The solid chelate was prepared by the method of Bailes and Calvin.[2] The active form was made by recrystallizing the solid from pyridine. Method *A*[3] used a 30-cm long cylindrical tube of 120 ml capacity. Approximately 3 g of the pyridinated chelate was placed in the tube and then heated to 170°C with constant pumping at 10 μ. The resulting light brown solid was cooled to 26° under vacuum and saturated with oxygen at a pressure of 75 cm Hg. About 160 ml of oxygen was required. As oxygen was absorbed, the solid turned black. After 40 hr, with the tube horizontal and the solid spread along its length, samples of the gas phase were taken by expanding it directly into evacuated break-seal tubes. The residual gas was pumped off and the reactor warmed to desorb the oxygen from the solid. Samples of this gas also were collected. The isotopic composition of samples obtained from each phase, as well as the feed oxygen, was determined by measuring mass peaks 32 and 34 with a 6-in. 60°-sector mass spectrometer.

TABLE I. Isotope ratios and separation factors.

Method *A*	O^{16}/O^{18}	α[a]
Gas	479.7±0.6	1.013±0.002
Solid	486.0±0.4	(95% C.I.)
Feed	482.4±0.2	
Method *B*	**Ratio O_2^{34}/O_2^{32}**	
Gas solid	1.0050	1.0124
Feed solid	1.0074	
Gas solid I		1.0129
II		1.0113
		Average 1.012$_2$

[a] $\alpha = (O^{18}/O^{16})$ gas/(O^{18}/O^{16}) solid.

Method *B* used a spherical reactor of 138 ml volume. It was loaded with 1.98 g of oxygenated chelate, which is easier to handle than the pyridinate. The oxygen was removed by pumping at 10 μ with the reactor immersed in 70° water. When cooled to room temperature the reactor was instantaneously pressurized to 75.7 cm with oxygen feed gas. (Actually, a mixture of 86.7% O_2 and 13.3% N_2 was used, but the nitrogen is inert

toward the complex.) After absorption by the solid, the oxygen distribution was: $O_2(gas)/O_2(solid) = 1.38$. After 46 hr the gas was sampled and the excess pumped off. Then the solid was sampled by warming it and using a Topler pump to collect the released oxygen in a sample tube. Samples were analyzed on a 6-in., 60°-sector ratio mass spectrometer. Results are given in Table I.

It should be noted in passing that the isotopic fractionation which occurs in this system is a quantum-mechanical effect and is not due to a steric effect; that is, to differences in the molecular volumes of the isotopic oxygen molecules, as claimed by Panchenkov *et al.* Although in principle molecules containing different isotopes should exhibit differences in molecular volume, this effect diminishes rapidly with increasing atomic number and is of practical importance only for the isotopes of hydrogen.

* This paper is based on work performed for the U.S. Atomic Energy Commission by Union Carbide Corporation.

[1] G. M. Panchenkov, A. M. Tolmachev, and V. B. Kondratova, Zh. Fiz. Khim. **33**, 734–5 (1959); Chem. Abstracts **53**, 21246a (1959).

[2] R. H. Bailes and M. Calvin, J. Am. Chem. Soc. **69**, 1886 (1947).

[3] This was reported in Chemical Separation of Isotopes Semi-Annual Progress Report, ORNL-2097 (1955).

Author Index to Volume 33

(References with (L) are to Letters to the Editors.)

Ackerman, Marcel, Fred E. Stafford, and Jean Drowart. Mass spectrometric determination of the dissociation energies of the molecules AgAu, AgCu, and AuCu—1783

Adams, G. B., Jr. (see Graven, W. M.)—954(L)

Albrecht, Andreas C. "Forbidden" character in allowed electronic transitions—156

——On the assignment of the lowest triplet state in benzene—937(L)

——Vibronic calculations in benzene—169

Alder, B. J. and T. E. Wainwright. Studies in molecular dynamics. II. Behavior of a small number of elastic spheres—1439

——(see Hrostowski, H. J.)—980

Allnatt, Alan R. and Stuart A. Rice. On the dynamical theory of diffusion in crystals. V. Random-walk treatment of the heat of transport—573

Allport, John J. (see Robben, Frank)—630(L)

Ameer, George (see Babrov, Harold)—145

Amme, Robert C. and Sam Legvold. Vibrational transitions and the intermolecular potential—91

——(see Calvert, J. B.)—1270(L)

Anderson, D. H. (see Brown, Thomas H.)—720

Anderson G. R. (see Wexler, S.)—850

Anderson, M. E., G. E. Pake, and T. R. Tuttle, Jr. Proton resonance in diphenyl picryl hydrazyl—1581(L)

——, **P. J. Zandstra, and T. R. Tuttle, Jr.** Proton resonance shifts in pyrene mononegative ion at 4.2°K—1591(L)

Arai, S., S. Sato, and S. Shida. Mercury photosensitized decomposition of cyclohexane at high temperatures—1277(L)

Arai, Tadashi. Theorem on separability of electron pairs—95

Arase, Elizabeth M. and Robert D. Hatcher. Frequency distribution and the specific heat of NaCl at low temperatures—1703

Arking, A. (see Bradley, R. C.)—764

Aronson, J. R., R. C. Lord, and D. W. Robinson. Far infrared spectrum and structure of disiloxane—1004

Auer, P. L. and S. Tamor. Statistical mechanics of the nonuniform gas—1426

Babrov, Harold, George Ameer, and William Benesch. Molecular collision cross sections from infrared absorption measurements—145

Bak, Børge and Lise Hansen-Nygaard. Molecular structure correlations—418

Baldeschwieler, John D. and George C. Pimentel. Light-induced *cis-trans* isomerization of nitrous acid formed by photolysis of hydrazoic acid and oxygen in solid nitrogen—1008

Baldwin, H. W. and H. Taube. Flow adaptation of the isotopic dilution method for the study of ionic hydration—206

Baldwin, Robert L. (see Kirkwood, John G.)—1505

Balwit, J. S. (see Lawton, Elliott, J.)—395, 405

Banks, E. (see Mandel, G.)—192

Banyard, K. E. Diamagnetism as a test of wave functions for some simple molecules—832

Bartell, L. S., Kozo Kuchitsu, and R. J. de Neui. Equilibrium bond lengths in methane and deuteromethane as determined by electron diffraction and spectroscopic methods—1254(L)

Basile, L. J. and A. Weinreb. Transfer of excitation energy in solid solutions of anthracene-polystyrene and 9,10-diphenylanthracene-polystyrene—1028

Basu, Sadhan (see Chakravorty, Animesh)—1266(L)

——(see Majumdar, Dilip Kuman)—1199

Bauer, Ernest and Morris Salkoff. Three-body recombination of oxygen atoms—1202

Bauer, S. H., Tadashi, Ino, and Richard F. Porter. Molecular structure of lithium chloride dimer. Thermodynamic functions of Li_2X_2(X = Cl, Br, I)—685

——(see LaVilla, Robert E.)—182

Bauman, R. P. (see Mandel, G.)—192

Beam, John E. and H. L. Davis. Energy levels of a slightly asymmetric top—1255(L)

Bearman, Richard J. and Peter F. Jones. Statistical mechanical theory of the viscosity coefficients of binary liquid solutions—1432

Beaumont, D. W. (see Scatchard, G.)—1292

Beckel, Charles L. Power series expansions of vibrational potentials. I. The Heitler-London potential for H_2—1885(L)

——(see Finn, Edward J.)1887(L)

Beers, D. S. (see Bradley, R. C.)—764

Begun, G. M. and W. H. Fletcher. Partition function ratios for molecules containing nitrogen isotopes—1083

Belles, Frank E. (see Brabbs, Theodore A.)—307(L)

Benesch, William (see Babrov, Harold)—145

Bennett, R. G. (see Dayton, I. E.)—179

Benson, R. E. (see Phillips, W. D.)—607(L)

Benson, Sidney W. On the existence of energy chains in ozone decomposition—939(L)

—— On the existence of polyoxides of hydrogen—306(L)

Bent, Henry A. Bond shortening by electronegative substituents—1260(L)

—— Correlation of bond shortening by electronegative substituents with orbital hybridization—1259(L)

—— Electronegativities from comparison of bond lengths in AH and AH^+—1258(L)

—— Explanation of the nonadditivity of bond lengths—304(L)

Bergmann, Ernst D. (see Yaroslavsky, Samuel)—635(L)

Berkowitz, Joseph, David J. Meschi, and William A. Chupka. Heterogeneous reactions studied by mass spectrometry. II. Reaction of Li_2O(s) with H_2O(g)—533

—— (see Meschi, David J.)—530

Berlman, Isadore B. Efficiency of energy transfer in a solution of PPO in xylene—1124

Bernheim, Robert A. and T. P. Das. Relation between the proton hyperfine interaction and the C^{13}—H^1 spin-spin coupling in free radicals—1813

—— (see Brown, Thomas H.)—1593(L)

Bernstein, Richard B. Quantum mechanical (phase shift) analysis of differential elastic scattering of molecular beams—795

—— (see Hoffman, Morton Z.)—526

—— (see Schumacher, Hugo)—584

Bestul, A. B. and D. H. Blackburn. Condensation coefficient of arsenic trioxide glass—1274(L)

Bigeleisen, Jacob. Vapor pressures and related thermodynamic properties of the isotopic nitric oxide molecules—1774

Birdwell, B. F. and George W. Crawford. Gamma radiolysis of propane—928

Birtley, W. B. (see Rank, D. H.)—323, 327

Blackburn, D. H. (see Bestul, A. B.)—1274(L)

Blais, Normand C. and Joseph B. Mann. Ionization of Cu, Ag, and Au by electron impact—100

Blauer, G. and H. Linschitz. Metastable states of acridine orange in solution—937(L)

Blinder, S. M. Orientation dependence of magnetic hyperfine structure in free radicals—748
Blume, Philip (see Ettinger, Raymond)—1597(L)
Boggs, J. E., A. P. Deam, and J. M. King. Temperature variation of the linewidth in nonresonant microwave absorption—1852
Bolling, G. F. Some thermal data for Bi_2Te_3—305(L)
Bose, Monisha (see Labes, Mortimer M.)—868
Brabbs, Theodore A., Steven A. Zlatarich, and Frank E. Belles. Limitations of the reflected-shock technique for studying fast chemical reactions—307(L)
Bradley, R. C., A. Arking, and D. S. Beers. Secondary positive ion-emission from platinum—764
Brady, George W. Structure in ionic solutions. IV—1079
Bray, P. J. (see Hooper, H. O.)—334
—— (see Negita, Hisao)—1876(L)
Brinkley, S. R., Jr. (see Richardson, J. M.)—1467
Brion, H., C. Moser, and M. Yamazaki. Erratum: Electronic structure of nitric oxide—1871(L)
Britton, Doyle and Z Z. Hugus, Jr. Nuclear spin conservation in ortho-para hydrogen conversion—1830
—— (see Lipscomb, William N.)—275
Broadhurst, Martin G. Theoretical dielectric behavior of an ethyl stearate-heneicosane mixture—221
—— **and Edwin R. Fitzgerald.** Dielectric behavior and crystal structure of ethyl and vinyl stearate—210
Brout, R. (see Buff, Frank P.)—1417
Brown, David A. Metal-metal bonding in dicobalt hexacarbonyl diphenylacetylene—1037
Brown, L. L. and J. S. Drury. The single-state fractionation factor for the system oxygen vs cobalt di(salicylal)-ethylenediimine-oxygen—1889(L)
Brown, M. G. Electronegativity effects of hybridized carbon atoms—1881(L)
Brown, Thomas H., D. H. Anderson, and H. S. Gutowsky. Spin densities in organic free radicals—720
——, **Robert A. Bernheim, and H. S. Gutowsky.** Temperature dependence of proton relaxation times in aqueous solution of paramagnetic ions. II. $CrCl_3$—1593(L)
Broyles, A. A. Radial distribution functions from the Born-Green integral equation—456
Büchler, Alfred (see Klemperer, William)—1534
Buff, Frank P. and R. Brout. Some tests of the superposition approximation in the liquid phase—1417
Bumble, S. and J. M. Honig. Utilization of order-disorder theory in physical adsorption. I. Fundamental equations—424
Bunker, Don L. Erratum: Mechanics of atomic recombination reactions—617(L)
Burns, John H., Darrell W. Osborne, and Edgar F. Westrum, Jr. Heat capacity of uranium tetrafluoride from 1.3° to 20°K and the thermodynamic functions to 300°K. Calorimeter for the range 0.8° to 20°K—387
Burns, R. P. (see Grimley, R. T.)—308(L)

Cahn, J. W. (see Sears, G. W.)—494
Calvert, J. B. and R. C. Amme. Multiple velocity dispersion in halomethane gas mixtures—1270(L)
Calvo, Crispin. On the molecular nature of the dielectric anomalies in thiourea—1720
Cann, John R. Effect of binding of ions and other small molecules on protein structure. VIII. On isomerization of serum albumin in acidic media—1410
Carlin, R. L. (see Piper, T. S.)—608(L), 1208
Carlson, F. F., G. J. King, and B. S. Miller. Hyperfine structure of *F*-center spin resonance in sodium azide—1266(L)
Carpenter, D. K. (see Krigbaum, W. R.)—921
Carpenter, G. B. Density of the bonding electrons in diamond —300(L)
Castellan, Gilbert W. (see Singer, Sister Judith Mary)—633(L)
Chaiken, R. F. Comments on hypervelocity wave phenomena in condensed explosives—760
Chakravorty, Animesh and Sadhan Basu. Crystal spectra of chromium *tris*-acetyl acetone—1266(L)
Chan, Sunney I., John Zinn, Jose Fernandez, and William D. Gwinn. Trimethylene oxide. I. Microwave spectrum, dipole moment, and double minimum vibration—1643
——, **John Zinn, and William D. Gwinn.** Double minimum vibration in trimethylene oxide—295(L)
Chantry, George W. and Robert A. Plane. Bond polarizability components—634(L)
—— **and R. A. Plane.** CN stretching bands in the Raman spectra of some group Ib and group IIb complex cyanides —736
Chesnut, D. B. Cl^{35} NMR contact shifts in aqueous cobaltous chloride solutions—1234
—— **and G. J. Sloan.** Paramagnetic resonance absorption of triphenylmethyl—637(L)
Choi, Sang-Il and John Ross. Quantum corrections for transport coefficients—1324
Chupka, William A. (see Berkowitz, Joseph)—533
—— (see Meschi, David J.)—530
Cimino, A. E. Molinari, and G. G. Volpi. Comment on the homogeneous exchange reaction between hydrogen and deuterium—616(L)
Claassen, Howard H. and Bernard Weinstock. Search for a Jahn-Teller effect in IrF_6—436
Cleveland, Forrest F. (see Gilbert, Robert L.)—1872(L)
Clinton, William L. Forces in molecules. I. Application of the virial theorem—1603
—— Note on the internal rotation problem—632(L)
Coggeshall, Norman D. Quantitative relations in the mass spectra of *n*-paraffins—1247
Cohen, Arthur (see Strehlow, Roger A.)—618(L)
Colburn, Charles B. and Frederic A. Johnson. Strength of the N—N bond in tetrafluorohydrazine—1869(L)
Cole, R. H. (see Johnston, D. R.)—1310
Coleman, Bernard D. and Clifford Truesdell. On the reciprocal relations of Onsager—28
Coll, H. (see Debye, P.)—1745
Connelly, B. T. (see Porter, Gerald B.)—81
Conradi, J. J. (see Parker, D. J.)—629(L)
Coogan, C. K. (see Stalinski, B.)—933(L)
Cook, Denys, Stephen J. Kuhn, and George A. Olah. Infrared spectra of complexes of NO_2F with BF_3, PF_5, and SbF_5—1669
Crapo, L. M. and C. H. Sederholm. NMR analysis of CF_3CF_2CFICl: Example of an unexpected spin-coupling constant—1583(L)
Crawford, George W. (see Birdwell, B. F.)—928
Crowe, R. W. and J. C. Devins. Sparking potential and molecular structure of unsaturated hydrocarbon gases—413
—— (see Devins, J. C.)—1578(L)
Cubicciotti, Daniel. Erratum: Lattice energies of the alkali halides and the electron affinities of the halogens—1579(L)
Curtiss, C. F. (see Hollinger, Henry B.)—1386
Cvetanović, R. J. Temperature dependence of the rates of addition of oxygen atoms to olefins—1063

Dahler, J. S. (see O'Toole, J. T.)—1487, 1496
Dailey, B. P. Halogen bond character in the alkyl halides—1641
Dalby, F. W. (see Dayton, I. E.)—179
Danti, Alfred, W. J. Lafferty, and R. C. Lord. Far infrared spectrum of trimethylene oxide—294(L)
Das, T. P. and A. Mukherjee. Variational calculation of magnetic hyperfine interaction. Nitrogen atom—1808
—— (see Bernheim, R. A.)—1813
Davidson, D. W. (see Grant, R. F.)—1712

Davidson, Ernest R. First excited $^1\Sigma_u^+$ state of H_2. A double-minimum problem—1577(L)
Davies, D. W. Separation theorem for degenerate eigenvalues —781
Davis, H. L. (see Beam, John E.)—1255(L)
Dayton, I. E., F. W. Dalby, and R. G. Bennett. Radiative lifetime of the $B\ ^2\Sigma^+$ state in N_2O^+—179
Deam, A. P. (see Boggs, J. E.)—1852
Dearman, H. H. and H. M. McConnell. Spin densities in several odd alternant radicals—1877(L)
—— (see McLachlan, A. D.)—65
Debye, P., H. Coll, and D. Woermann. Critical opalescence of polystyrene in cyclohexane—1745
deKowalewski, Dora G. (see Kowalewski, Valdemar J.)—1793
deNeui, R. J. (see Bartell, L. S.)—1254(L)
Devins, J. C. and R. W. Crowe. Electric strength of methane and deuteromethane—1578(L)
—— (see Crowe, R. W.)—413
Devlin, J. P. (see Hisatsune, I. C.)—714
Dibeler, Vernon H. (see Herron, John T.)—1595(L)
Dickey, Fred P. (see Rogge, William H.)—453
Dieke, G. H. and D. F. Heath. Structure of the infrared Y bands of N_2—432
—— (see Varsanyi, F.)—1616
Dixon, J. A. (see Nelson, R. R.)—1755
Douglass, Dean C. (see McCall, David W.)—777
Dowling, Jerome M. (see Gilbert, Robert L.)—1872(L)
Dows, David A. Infrared spectra of crystalline CD_3Cl and CD_3Br—1742
Dravnieks, F. (see Reitz, D. C.)—1880(L)
Dressler, K. and O. Schnepp. Absorption spectra of solid methane, ammonia, and ice in the vacuum ultraviolet—270
—— (see Schnepp, O.)—49
Drickamer, H. G. (see Minomura, S.)—290
—— (see Zahner, J. C.)—1625
Drowart, Jean (see Ackerman, Marcel)—1783
Drury, J. S. (see Brown, L. L.)—1889(L)
—— (see Palko, A. A.)—779
Dubois, Jean T. Primary processes in the gaseous photolysis of polyatomic molecules. I. Biacetyl—229
Dudek, Gerald O. H^1—P^{31} spin coupling in phosphate esters —624(L)
Dunlop, Peter J. (see Kirkwood, John G.)—1505
Dupuis, Marc, Robert Mazo, and Lars Onsager. Surface specific heat of an isotropic solid at low temperatures—1452

Eastman, D. P. (see Rank, D. H.)—323, 327
Edlén, B. Isoelectronic extrapolation of electron affinities—98
Ehrlich, Gert and F. G. Hudda. Observation of adsorption on an atomic scale—1253(L)
Eisenstein, J. C. Spectrum of ReF_6—1530
Eisner, Melvin (see Mitchell, Richard W.)—86
Elias, L. (see Morgan, J. E.)—930(L)
Elliott, Norman. Interatomic distances in FeS_2, CoS_2, and NiS_2—903
Elliott, Reed O. (see Kempter, Charles P.)—837
Emerson, Merle T., Ernest Grunwald, and Robert A. Kromhout. Proton-transfer studies by nuclear magnetic resonance. I. Diffusion control in the reaction of ammonium ion in aqueous acid—547
Emslie, Alfred G. (see Klemperer, William)—1534
Epstein, A. and B. S. Wildi. Erratum: Electrical properties of poly-copper phthalocyanine—618(L)
Erikson, Ted A. and R. J. Tykodi. Thermodynamics, stationary states, and steady-rate processes. VI. Forced vaporization of selected liquids—46
Ettinger, Raymond, Philip Blume, Andrew Patterson, Jr., and Paul C. Lauterbur. C^{13} chemical shifts in CO and CO_2—1597(L)
Evans, J. C. (see Scherer, James R.)—314(L)
Evers, E. Charles. On the structure of dilute solutions of metals—618(L)
Evett, Arthur A. Second-order perturbation calculation of the hindered rotator model for adsorbed hydrogen—789

Fallon, Robert J., Joseph T. Vanderslice, and Edward A. Mason. Erratum: Potential curves for HF and LiH—944(L)
—— (see Tobias, Irwin)—1638
Fernandez, Jose (see Chan, Sunney I.)—1643
Fessenden, Richard W. and Robert H. Schuler. EPR observation of steady-state ethyl radical concentration in radiolysis of liquid ethane—935(L)
Finn, Edward J. and Charles L. Beckel. Power series expansions of vibrational potentials. II. Two classical potentials for ionic molecules—1887(L)
Fite, Wade L. (see Stebbings, R. F.)—1226
Fitts, Donald D. (see Kirkwood, John G.)—1317
Fitzgerald, Edwin R. (see Broadhurst, Martin G.)—210
Fixman, Marshall. Density correlations, critical opalescence, and the free energy of nonuniform fluids—1357
—— Osmotic pressure of moderately concentrated polymer solutions—370
—— Ultrasonic attenuation in the critical region—1363
Fletcher, W. H. (see Begun, G. M.)—1083
Flood, E. A. (see Kuroda, H.)—952(L)
Flubacher, P., A. J. Leadbetter, and J. A. Morrison. Heat capacity of ice at low temperatures—1750
Forsén, S. and A. Rupprecht. Increasing the intensity of C^{13} NMR signals by a flowing sample method—1888(L)
Fotland, Richard A. Photoconductivity and photolysis in cadmium iodide—956(L)
Fox, J. W. and A. C. H. Smith. Viscosity of mixtures of hydrogen and water vapor at 295°K—623(L)
Fox, R. E. Multiple ionization in argon and krypton by electron impact—200
Freeman, G. R. Energy transfer in liquid hydrocarbons excited by γ rays—957(L)
—— Radiolysis of cyclohexane. I. Pure liquid cyclohexane and cyclohexane-benzene solutions—71
Frey, H. M. (see Harrington, R. E.)—1271(L)
Friedman, E. and W. Low. Effect of thermal treatment of paramagnetic resonance spectra of rare earth impurities in calcium fluoride—1275(L)
Fries, R. J. (see Kempter, C. P.)—1873(L)
Frisch, H. L. (see Helfand, E.)—1379
Frosch, R. P. (see Wright, M. R.)—934(L)
Fujiwara, Yuzuru (see Kuri, Zenichiro)—1884(L)
Fumi, F. G. and M. P. Tosi. Madelung constants of the cubic Perovskite structures—1

Gans, Paul J. Open first-order stochastic processes—691
Garrett, C. G. B. Quantitative considerations concerning catalysis at a semiconductor surface—966
Geller, S. Crystal structure of β-Ga_2O_3—676
Geske, David H. (see Maki, August H.)—825
Giddings, J. Calvin and Spencer L. Seager. Rapid determination of gaseous diffusion coefficients by means of gas chromatography apparatus—1579(L)
Gilbert, Robert L., Edward A. Piotrowski, Jerome M. Dowling and Forrest F. Cleveland. Erratum and Addendum: Substituted methanes. XXIX. Vibrational spectra, potential constants, and calculated thermodynamic properties for dibromochlorofluoromethane and bromodichlorofluoromethane—1872(L)
Gilliam, O. R. (see Shuskus, A. J.)—622(L)
Glarum, Sivert H. Dielectric relaxation of isoamyl bromide—639
—— Dielectric relaxation of polar liquids—1371

Glasel, Jay A. Near-infrared absorption spectra of ortho- and para-H_2O in solid xenon and argon—252
Glew, David N. (see Walkley, John)—621(L)
Glick, R. E. and D. F. Kates. Quantum-mechanical approximations to chemical systems—308(L)
Gold, L. Peter (see Wharton, Lennard)—1255(L)
Golden, S. and H. C. Longuet-Higgins. On temporal evolution of isolated dynamical systems—1479
Goldfarb, Theodore D. and George C. Pimentel. Chemiluminescence of ethylene formed probably from methylene in an inert matrix—105
Golding, R. M. Ultraviolet and structural studies of polythionates—1666
Goodman, Lionel (see Hoyland, J. R.)—946(L)
—— See Krishna, V. G.)—381
Gordon, Alvin S. and James R. McNesby. On the isomerization of *n*-butyl radicals—1882(L)
Gordy, Walter (see Miyagawa, Ichiro)—1599
Gosting, Louis J. (see Kirkwood, John G.)—1505
Gouterman, Martin. A theory for the triplet-triplet absorption spectra of porphyrins—1523
Grad, Harold. On molecular chaos and the Kirkwood superposition hypothesis—1342
Grant, R. F., D. W. Davidson, and Peter Gray. Dielectric study of some liquid alkyl nitrites—1712
Graven, W. M., R. E. Salomon, and G. B. Adams, Jr. Absorption spectra of anodic niobium oxide films—954(L)
Gray, Peter (see Grant, R. F.)—1712
Green, H. S. (see Hurst, C. A.)—1059
Green, John W., Duncan E. Poland, and John L. Margrave. Thermodynamic properties of unipositive gaseous elemental ions—35
—— (see Iczkowski, Raymond P.)—1261(L)
Green, Melville S. On the theory of the critical point of a simple fluid—1403
Greenberg, J. and Leander J. Hallgren. Infrared absorption spectra of alkali metal nitrates and nitrites above and below the melting point—900
Grimley, R. T., R. P. Burns, and Mark G. Inghram. Mass-spectrometric study of the osmium-oxygen system—308(L)
Gruen, Dieter M. (see Satten, Robert A.)—1140
Grunwald, Ernest, Photios J. Karabatsos, Robert A. Kromhout, and E. Lee Purlee. Proton-transfer studies by nuclear magnetic resonance. II. Rate constants and mechanism for the reaction $CH_3NH_3^+ + OH_2 + NH_2CH_3$ in aqueous acid—556
—— (see Emerson, Merle T.)—547
Gschneidner, Karl A., Jr. (see Kempter, Charles P.)—837
Gunn, Stuart R. and Russell H. Sanborn. Heats of formation of BF_2Cl and $BFCl_2$—955(L)
Gutmann, Joel R. and Max Wolfsberg. Equilibrium in the exchange of tritium between ammonia and hydrogen and the zero-point energy difference between NH_3 and NH_2T—1592(L)
Gutowsky, H. S. (see Brown, Thomas H.)—720, 1593(L)
—— (see Schug, John C.)—843
—— (see Stalinski, B.)—933(L)
Gwinn, William D. (see Chan, Sunney I.)—295 (L), 1643
—— (see LeBlanc, Oliver H., Jr.)—598

Haake, C. H. (see Kemeny, G.)—783
Hall, G. G. Ambiguity in the determination of self-consistent bond orders—953(L)
Hallgren, Leander J. (see [illegible] J.)—900
Halsey, G. D., Jr. (see Vo[illegible] 1132
Hansen, K. and D. P. [illegible]ng. Thickness of shock fronts in argon—913
Hansen-Nygaard, [illegible]ise (see Bak, Børge)—418
Harrah, L. A. and D. W. Mayo. Rotational isomerism involving the 2-3 carbon-carbon bond of the 1-alkenes—298(L)
Harrington, R. E., B. S. Rabinovitch, and H. M. Frey. Decomposition of activated *sec*-butyl radicals from different sources and unimolecular reaction theory—1271(L)
——, **B. S. Rabinovitch, and M. R. Hoare.** Collisional deactivation of vibrationally excited *sec*-butyl-d_1 radicals produced by chemical activation—744
Harris, Robert A. and Stuart A. Rice. Kinetic theory of the moderately dense rigid-sphere fluid. IV. Fluxes of matter, momentum, and energy in a mixture—1047
—— **and Stuart A. Rice.** Kinetic theory of the moderately dense rigid-sphere fluid. V. Relaxation in momentum space—1055
Harteck, Paul (see Mannella, Gene G.)—636(L)
Hatcher, Robert D. (see Arase, Elizabeth M.)—1703
—— (see Neuberger, Jacob)—265
Hause, C. D. (see Mann, Glen A.)—1117
Heath, D. F. (see Dieke, G. H.)—432
Helfand, Eugene. On inversion of the linear laws of irreversible thermodynamics—319
——, **H. Reiss, H. L. Frisch, and J. L. Lebowitz.** Scaled particle theory of fluids—1379
Herron, John T. Rate of reaction of nitrogen atoms with ethylene—1273(L)
—— **and Vernon H. Dibeler.** Mass spectrum and appearance potentials of tetrafluorohydrazine—1595(L)
Herschbach, Dudley R. Analysis of reactive scattering in crossed molecular beams—1870(L)
Hertzberg, Martin (see Ortenburger, Irene B.)—579
Hexter, R. M. Intermolecular coupling of vibrations in molecular crystals: a vibrational exciton approach—1833
Higashimura, T. (see Takeda, M.)—631(L)
Higdon, William T. (see Hight, Robert, Jr.)—1656
Hight, Robert, Jr., William T. Higdon, and Paul W. Schmidt. Small angle x-ray scattering study of sodium montmorillonite clay suspensions—1656
Hijikata, Katsunori (see Lin, Chun C.)—878
Hildebrand, Joel H. (see Walkley, John)—621(L)
Hirschfelder, Joseph O. Classical and quantum mechanical hypervirial theorems—1462
——(see Stogryn, Daniel E.)—942(L)
Hirth, J. P. (see Ives, M. B.)—517
Hisatsune, I. C., J. P. Devlin, and Yasuo Wada. Infrared spectra of some unstable isomers of N_2O_4 and N_2O_3—714
Hoare, M. R. (see Harrington, R. E.)—744
Hobey, W. D. and A. D. McLachlan. Dynamical Jahn-Teller effect in hydrocarbon radicals—1694
Hochstrasser, Robin M. Electronic absorption spectrum of diphenylene in substitutional solid-solid solution—950(L)
—— Polarization of the first two electronic transitions of pyrene—459
Hoffman, Morton Z. and Richard B. Bernstein. Relative quenching cross sections in the reaction of $Hg(6^3P_1)$ atoms with isotopic N_2O molecules—526
Hoffman, Ragnar A. Analysis of high-resolution NMR spectra by iterative methods—1256(L)
Hollinger, Henry B. and C. F. Curtiss. Kinetic theory of dense gases—1386
Holmberg, Robert W., Ralph Livingston, and William T. Smith, Jr. Paramagnetic-resonance study of hyperfine interactions in single crystals containing α,α-diphenyl-β-picrylhydrazyl—541
Holøien, E. On excited bound states of negative atomic ions—310(L)
—— Remarks on doubly excited states of the negative atomic hydrogen ion—301(L)
—— Some remarks on the electron affinity of atomic lithium—309(L)
Honig, J. M. (see Bumble, S.)—424
Hooper, H. O. and P. J. Bray. Induction studies in several groups of halogen-containing organic compounds by their Cl^{35}, Br^{79}, or Br^{81} pure quadrupole resonance spectra—334

Hornig, D. F. (see Hansen, K.)—913
Hoyland, J. R. and Lionel Goodman. A modification of Koopmans' theorem for conjugated hydrocarbons—946(L)
Hrostowski, H. J. and B. J. Alder. Evidence for internal rotation in the fine structure of the infrared absorption of oxygen in silicon—980
Hudda, F. G. (see Ehrlich, Gert)—1253(L)
Hugus, Z Z., Jr. (see Britton, Doyle)—1830
Hummer, David G. (see Stebbings, R. F.)—1226
Hurley, A. C. Improved molecular orbitals and the valence bond theory—301(L); erratum—1872(L)
Hurst, C. A. and H. S. Green. New solution of the Ising problem for a rectangular lattice—1059
Hurzeler, H. (see Morrison, J. D.)—821

Ibers, James A. Comments on Carpenter's Paper "Density of the bonding electrons in diamond"—299(L)
——, **Junji Kumamoto, and Robert G. Snyder.** Structure of potassium hydroxide: an x-ray and infrared study—1164
—— (see Snyder, Robert G.)—1171
—— (see Stevenson, D. P.)—762
Iczkowski, Raymond P., John L. Margrave, and John W. Green. Absorption spectrum of chlorine in the vacuum ultraviolet—1261(L)
Ikeda, R. M. Flash-absorption spectroscopy of free radicals in shock waves—311(L)
Imamura, Y. (see Takeda, M.)—631(L)
Inghram, Mark G. (see Grimley, R. T.)—308(L)
—— (see Morrison, J. D.)—821
Ino, Tadashi (see Bauer, S. H.)—685
Inokuti, Mitio. Molecular size distribution and gelation of irradiated copolymers—1607
Ives, M. B. and J. P. Hirth. Dissolution kinetics at dislocation etch pits in single crystals of lithium fluoride—517

Jennings, L. D., R. E. Miller, and F. H. Spedding. Lattice heat capacity of the rare earths. Heat capacities of yttrium and lutetium from 15–350°K—1849
Johnson, Frederic A. (see Colburn, Charles B.)—1869(L)
Johnson, Lauren G. Microwave spectrum of quinuclidine—949(L)
Johnston, D. R., G. J. Oudemans, and R. H. Cole. Dielectric constants of imperfect gases. I. Helium, argon, nitrogen, and methane—1310
Johnston, Harold S. (see Rapp, Donald)—695
Jones, Llewellyn H. Equilibrium constant for isotope exchange in ammonia from infrared spectra—1585(L)
Jones, Peter F (see Bearman, Richard J.)—1432
Joshi, S. K. Number of 3*d* electrons in iron—1261(L)
Joy, Hubert W. and W. F. Libby. Size effects among isotopic molecules—1276(L)

Kaneko, M. (see Krigbaum, W. R.)—921
Karabatsos, Photîos J. (see Grunwald, Ernest)—556
Karo, Arnold M. Lattice vibrations in alkali halide crystals. II. Potassium and rubidium halides; cesium fluoride—7
Karplus, Martin. "Average energy approximation" in spin-coupling calculations—941(L)
—— Note on the internal-rotation barrier in ethanic compounds—316(L)
—— Proton spin coupling by pi electrons—1842
Kates, D. F. (see Glick, R. E.)—308(L)
Keffer, Frederic. The effective ionic charge in CdS—1267(L)
Kegeles, Gerson (see Kirkwood, John G.)—1505
Keller, Joseph M. Conduction electrons in sodium tungsten bronze—232
Kemeny, G. and C. H. Haake. Activator center in magnesium fluorogermanate phosphors—783
Kemp, J. C. Electron spin resonance in neutron-irradiated calcite—1269(L)
Kempter, Charles P., Reed O. Elliott, and Karl A. Gschneidner, Jr. Thermal expansion of delta and epsilon zirconium hydrides—837
—— **and M. R. Nadler.** Preparation and crystal structures of RuC and OsC—1580(L)
——, **E. K. Storms, and R. J. Fries.** Lattice dimensions of NbC as a function of stoichiometry—1873(L)
—— (see McGuire, Joseph C.)—1584(L)
Kikuchi, Chihiro and L. M. Matarrese. Paramagnetic-resonance absorption of ions with spin 5/2: Mn^{++} in calcite—601
King, G. J. (see Carlson, F. F.)—1266(L)
King, J. M. (see Boggs, J. E.)—1852
Kingery, W. D. (see Oishi, Y.)—480, 905
Kirkwood, John G., Robert L. Baldwin, Peter J. Dunlop, Louis J. Gosting, and Gerson Kegeles. Flow equations and frames of reference for isothermal diffusion in liquids—1505
—— **and Donald D. Fitts.** Statistical mechanics of transport processes. XIV. Linear relations in multicomponent systems—1317
—— (see Stillinger, Frank H., Jr.)—1282
—— (see Wojtowicz, Peter J.)—1299
Kiser, Robert W. Estimation of the ionization potential and dissociation energy of molecular astatine—1265(L)
Kivelson, Daniel. Theory of ESR linewidths of free radicals—1094
Klaboe, Peter and J. Rud Nielsen. Erratum: Infrared and Raman spectra of fluorinated ethanes. XII. 1,1,2,2,-tetrafluoroethane—617(L)
—— **and J. Rud Nielsen.** Infrared and Raman spectra of fluorinated ethanes. XIII. 1,2-difluoroethane—1765
Klein, H. Michael (see Milne, Thomas A.)—1628
Klemperer, William, W. G. Norris, Alfred Büchler, and Alfred G. Emslie. Infrared spectra of lithium halide monomers—1534
—— (see Wharton, Lennard)—1255(L)
Kneubühl, Fritz Kurt. Line shapes of electron paramagnetic resonance signals produced by powders, glasses, and viscous liquids—1074
Kohin, Barbara C. Molecular rotation in crystals of N_2 and CO—882
Kohn, Harold W. Paramagnetic studies of radiation damage in silica gel—1588(L)
Korvezee, A. E. and J. L. Meyering. Erratum: Validity and consequences of Schreinemakers' theorem on ternary distillation lines—304(L)
Kowalewski, Valdemar J. and Dora G. deKowalewski. Nuclear magnetic resonance spectra of the ABX_3 type: field dependence and relative signs of spin-spin coupling constants—1793
Kraemer, L. M. Cuprous halide films on alkali halide crystals—991
Krauss, M. and B. J. Ransil. Some intra-atomic correlation correction studies—840
Kretschmer, C. B. and H. L. Petersen. Recombination kinetics of atomic oxygen at room temperature—948(L)
Krigbaum, W. R., D. K. Carpenter, M. Kaneko, and A. Roig. Theory of dilute high polymer solutions. II—921
Krisher, Lawrence C. Errata: Microwave spectrum of acetyl cyanide—304(L)
—— Microwave spectrum, barrier to internal rotation, and quadrupole coupling of acetyl bromide—1237
Krishna, V. G. and Lionel Goodman. Solvent effects on $n \rightarrow \pi^*$ transitions in pyrazine—381
Kromhout, Robert A. (see Emerson, Merle T.)—547
—— (see Grunwald, Ernest)—556
Kuchitsu, Kozo (see Bartell, L. S.)—1254(L)
Kuebler, N. A. (see Nelson, L. S.)—610(L)
Kuhn, Stephen J. (see Cook, Denys)—1669
Kumamoto, Junji (see Ibers, James A.)—1164
—— (see Snyder, Robert G.)—1171

Kuppermann, Aron and John G. Larson. Nonmolecular nature of nitric-oxide-inhibited thermal decomposition of *n*-butane—1264(L)
Kurata, Michio, Walter H. Stockmayer, and Antonio Roig. Excluded volume effect of linear polymer molecules—151
Kuri, Zenichiro, Yuzuru Fujiwara, Hisashi Ueda, and Shoji Shida. Behavior of the free radicals trapped in gamma-irradiated compounds which contain hydrogen bonds—1884(L)
Kurita, Yukio (see Miyagawa, Ichiro)—1599
Kuroda, Haruo. Absorption spectra of photo-oxide of meso-naphthodianthrene—1586(L)
—— **and E. A. Flood.** Effect of oxygen on semiconductivities of mesonaphthodianthrene and mesonaphthodianthrone—952(L)

Labes, Mortimer M., Robert Sehr, and Monisha Bose. Organic semiconductors. II. The electrical resistivity of organic molecular complexes—868
LaBudde, C. D. and R. C. Sahni. Study of molecular integrals. II. Three-center one-electron and two-electron integrals—1022
—— (see Sahni, R. C.)—1015
Lafferty, W. J. (see Danti, Alfred)—294(L)
Landesman, H. (see Shapiro, I.)—1590(L)
Larson, John G. (see Kuppermann, Aron)—1264(L)
Lassettre, Edwin N. (see Peek, James M.)—1803
Laurie, Victor W. (see LeBlanc, Oliver H., Jr.)—598
—— (see Norris, James A.)—1256(L)
Lauterbur, Paul C. (see Ettinger, Raymond)—1597(L)
LaVilla, Robert E. and S. H. Bauer. Molecular structure of iodine heptafluoride—182
Lawton, Elliott J., J. S. Balwit, and R. S. Powell. Paramagnetic-resonance studies of irradiated high-density polyethylene. I. Radical species and the effect of environment on their behavior—395
——, **J. S. Balwit, and R. S. Powell.** Paramagnetic-resonance studies of irradiated high-density polyethylene. II. Effect of irradiation dose on the radical species trapped at room temperature—405
Leadbetter, A. J. (see Flubacher, P.)—1750
LeBlanc, Oliver H., Jr. Hole and electron drift mobilities in anthracene—626(L)
——, **Victor W. Laurie, and William D. Gwinn.** Microwave spectrum, structure, and dipole moment of formyl fluoride—598
Lebowitz, J. L. (see Helfand, E.)—1379
Lefebvre, Roland. Electron spin resonance line shape of a polycrystalline CH radical—1826
—— (see McLachlan, A. D.)—65
Lefebvre-Brion, H. C. M. Moser, and R. K. Nesbet. The $^1\Sigma^+$ excited states of carbon monoxide—931(L)
Legvold, Sam (see Amme, Robert C.)—91
—— (see Valley, L. M.)—627(L)
Lehmann, Walter J., Charles O. Wilson, Jr., and I. Shapiro. Infrared spectra of alkyldiboranes. III. 1,2-dimethyl- and 1,2-diethyldiboranes—590
Levy, Paul W. (see Shuskus, A. J.)—622(L)
Libby, W. F. Optical transparency and resistance to flash heating—1588(L)
—— (see Joy, Hubert W.)—1276(L)
Lide, David R., Jr. Dipole moments of hydrocarbons—1879(L)
—— Microwave spectrum, structure, and dipole moment of propane—1514
—— Structure of the isobutane molecule; change of dipole moment on isotopic substitution—1519
Lifson, Shneior and Irwin Oppenheim. Neighbor interactions and internal rotations in polymer molecules. IV. Solvent effect on internal rotations—109
Lin, Chun C., Katsunori Hijikata, and Michiko Sakamoto. Electronic structure and hyperfine structure constants of NO molecule—878
Lind, S. C. (see Rudolph, P. S.)—705
Linder, Bruno. Continuum-model treatment of long-range intermolecular forces. I. Pure substances—668
Linschitz, H. (see Blauer, G.)—937(L)
Lippincott, Ellis R. (see Steele, D.)—1242
—— (see Vanderslice, Joseph T.)—614(L)
Lipscomb, William N. and Doyle Britton. Valence structure of the higher borides—275
Livingston, Ralph and A. J. Weinberger. Atomic and molecular hydrogen yields from irradiated acids—499
—— (see Holmberg, Robert W.)—541
Long, Maurice W., Quitman Williams, and T. L. Weatherly. Microwave spectrum of $CFCl_3$—508
Longuet-Higgins, H. C. (see Golden, S.)—1479
Lord, R. C. (see Aronson, J. R.)—1004
—— (see Danti, Alfred)—294(L)
Lounasmaa, O. V. Application of Ehrenfest equations to liquid-vapor and liquid-solid mixtures of He^4—443
Low, W. Absorption lines of Cr^{3+} in ruby—1162
—— (see Friedman, E.)—1275(L)
Lund, L. H. X-ray scattering by a cell-model liquid—1086

MacCallum, C. J. Comment on dynamical theory of electrosedimentation—1263(L)
Machacek, Milos and Charles W. Scherr. Simple configuration interaction wave functions. III. Three-electron atomic system: an analytic study—242
Mackenzie, J. D. and W. K. Murphy. Structure of glass-forming halides. II. Liquid zinc chloride—366
Mahan, Bruce H. Photolysis of carbon dioxide—959
Mahendroo, P. P. (see Nolle, A. W.)—863
Mahler, W. and E. L. Muetterties. F^{19} spectra of phosphorus (V) fluorides—636(L)
Maisch, William G. (see Vanderslice, Joseph T.)—614(L)
Majumdar, Dilip Kuman and Sadhan Basu. Charge transfer and fluorescence quenching—1199
Maki, August H. and David H. Geske. Electron-spin resonance of electrochemically generated free radicals. Isomeric dinitrobenzene mononegative ions—825
Mandel, G., R. P. Bauman, and E. Banks. Electronic transitions of rare earth ions in the infrared region—192
Mangelsdorf, Paul C., Jr. Transport processes in liquid alloys. II. The electrical force on an ion—1151
Mann, D. E. and B. A. Thrush. On the absorption spectrum of CF_2 and its vibrational analysis—1731
Mann, Glen A. and C. D. Hause. Magnetic rotation spectra of nitric oxide in the near infrared—1117
Mann, Joseph B. (see Blais, Normand C.)—100
Mannella, Gene G., Robert R. Reeves, and Paul Harteck. Surface catalyzed excitation with N and O atoms—636(L)
Manning, Francis S. and William P. Manning. Derivation of thermodynamic relations for three-dimensional systems—1554
Manning, William P. (see Manning, Francis S.)—1554
Margolis, Jack S. (see Satten, Robert A.)—618(L)
Margrave, John L. (see Green, John W.)—35
—— (see Iczkowski, Raymond P.)—1261(L)
Mason, Edward A. (see Fallon, Robert J.)—944(L)
—— (see Vanderslice, Joseph T.)—492, 614(L)
Matarrese, L. M. (see Kikuchi, Chihiro)—601
Matheson, M. S. (see McMillan, J. A.)—609(L)
Mayer, Joseph E. Ensembles of maximum entropy—1484
Mayo, D. W. (see Harrah, L. A.)—298(L)
Mazo, Robert (see Dupuis, Marc)—1452

McCall, David W. and Dean C. Douglass. Nuclear magnetic resonance in solid adamantane—777
McConnell, Harden M. Biradical paradox—1868(L)
—— Theory of singlet-triplet splittings in large biradicals—115
—— (see Dearman, H. H.)—1877(L)
—— (see Sternlicht, H.)—302(L)
McGrath, J. W. and A. A. Silvidi. Proton-magnetic-resonance study of barium bromide monohydrate—644
—— (see Silvidi, A. A.)—1788
McGrath, W. D. Production of vibrationally excited S_2 in the isothermal flash photolysis of S_2Cl_2—279(L)
McGuire, Joseph C. and Charles P. Kempter. Preparation and properties of scandium dihydride—1584(L)
McInteer, B. B. and M. J. Reisfeld. Thermal-diffusion-column shape factors for the Lennard-Jones (12-6) potential—570
McLachlan, A. D. Valence-bond resonance structures for a triplet state—663
——, **H. H. Dearman, and R. Lefebvre.** Theory of hyperfine interactions in aromatic radicals—65
—— (see Hobey, W. D.)—1694
McLaren, G. A. (see Parker, D. J.)—629(L)
McMahon, Paul E. (see Schug, John C.)—843
McMillan, J. A., M. S. Matheson, and B. Smaller. Paramagnetic resonance of gamma-irradiated single crystals of ice at 77°K—609(L)
McNesby, James R. (see Gordon, Alvin S.)—1882(L)
McRae, E. G. A vibrational effect on the polarization of molecular crystal fluorescence—932(L)
Melton, C. E. Charge transfer reactions producing intrinsic chemical change: methyl, methylene, and hydrogen radicals produced from argon and methane reactions—647
—— **and P. S. Rudolph.** Transient species in the radiolytic polymerization of cyanogen—1594(L)
Meschi, David J., William A. Chupka, and Joseph Berkowitz. Heterogeneous reactions studied by mass spectrometry. I. Reaction of $B_2O_3(s)$ with $H_2O(g)$—530
—— (see Berkowitz, Joseph)—533
Meyer, Norman J. Multiple vibrational relaxation in gaseous dibromomethane—487
Meyering, J. L. (see Korvezee, A. E.)—304(L)
Miller, Brian S. Identification of colloidal sodium in sodium azide—889
—— (see Carlson, F. F.)—1266(L)
Miller, R. E. (see Jennings, L. D.)—1849
Milne, Thomas A. and H. Michael Klein. Mass spectrometric study of heats of dimerization of alkali chlorides—1628
Minomura, S. and H. G. Drickamer. Effect of pressure on the *M* center in alkali halide crystals—290
Mitchell, Richard W. and Melvin Eisner. Nuclear spin-lattice relaxation in solutions—86
Mitoff, S. P. Comments on Dr. Schmalzried's Letter—941(L)
Miyagawa, Ichiro, Yukio Kurita, and Walter Gordy. Electron spin resonance of an irradiated single crystal of N-acetylglycine—1599
Moffitt, William (see Witkowski, Andrzej)—872
Molinari, E. (see Cimino, A.)—616(L)
Monostori, B. and A. Weber. Raman spectrum of gaseous CF_4—1867(L)
Monse, E. U. Calculation of equilibrium constants for several isotope exchange reactions involving N_2O_4—312(L)
Monson, Philip R. (see Robben, Frank)—630(L)
Moore, Neal. Energy of interaction of two helium atoms—471
Moore, W. and M. Silver. Generation of free carriers in photoconducting anthracene. I—1671
Morgan, J. E., L. Elias, and H. I. Schiff. Recombination of oxygen atoms in the absence of O_2—930(L)
Morrison, J. A. (see Flubacher, P.)—1750
Morrison, J. D., H. Hurzeler, Mark G. Inghram, and H. E. Stanton. Threshold law for the probability of excitation of molecules by photon impact. A study of the photoionization efficiencies of Br_2, I_2, HI, and CH_3I—821
Moser, C. M. (see Brion, H.)—1871(L)
—— (see Lefebvre-Brion, H.)—931(L)
Moser, J. B. (see Whitmore, D. H.)—917
Muetterties, E. L. (see Mahler, W.)—636(L)
Muha, George M. and Philip A. Vaughan. Structure of the complex ion in aqueous solutions of zirconyl and hafnyl oxyhalides—194
Mulliken, Robert S. Lowest triplet states of ethylene—1596(L)
—— Some neglected subcases of predissociation in diatomic molecules—247
—— (see Phillipson, P.)—615(L)
Murphy, W. K. (see Mackenzie, J. D.)—366
Murthy, C. R. K. and R. D. Spence. Nuclear magnetic relaxation in a strongly associated liquid—945(L)
Muschlitz, E. E., Jr. (see Smith, G. M.)—1819
Myers, Rollie J. and E. Bright Wilson, Jr. Application of symmetry principles to the rotation-internal torsion levels of molecules with two equivalent methyl groups—186

Nadler, M. R. (see Kempter, Charles P.)—1580(L)
Nakagawa, Ichiro (see Thorson, Walter R.)—994
Narasimhan, P. T. and Max T. Rogers. Nuclear magnetic resonance spectra of systems of the A_3B_2C type: proton magnetic resonance spectra and the absolute signs of the proton-proton spin coupling constants in ethyl acetylene and ethyl mercaptan—727
Negita, Hisao and P. J. Bray. N^{14} pure quadrupole resonances of several nitriles—1876(L)
Nelson, L. S. and N. A. Kuebler. Kinetic absorption spectra recorded through flash-heated grids—610(L)
Nelson, R. R., W. Webb, and J. A. Dixon. First-order phase transitions of six normal paraffins at elevated pressures—1755
Nesbet, R. K. (see Lefebvre-Brion, H.)—931(L)
Nettleton, R. E. Casimir coefficients and minimum entropy production—237
Neuberger, Jacob and Robert D. Hatcher. Frequency spectrum for a two-dimensional lattice—265
Nielsen, J. Rud (see Klaboe, Peter)—617(L), 1765
Nolle, A. W. and P. P. Mahendroo. Effects of pressure on proton spin-lattice relaxation in several degassed organic liquids—863
Norris, James A. and Victor W. Laurie. Erratum: Energy levels of a slightly asymmetric top—1256(L)
Norris, W. G. (see Klemperer, William)—1534

Ogg, Richard A., Jr. (see Ortenburger, Irene B.)—579
Oishi, Y. and W. D. Kingery. Oxygen diffusion in periclase crystals—905
—— **and W. D. Kingery.** Self-diffusion of oxygen in single crystal and polycrystalline aluminum oxide—480
Okamura, S. (see Takeda, M.)—631(L)
Olah, George A. (see Cook, Denys)—1669
Onsager, Lars (see Dupuis, Marc)—1452
Oppenheim, Irwin (see Lifson, Shneior)—109
Ore, Aadne. Quantum yield for energy transfer by resonance—31
Ortenburger, Irene B., Martin Hertzberg, and Richard A. Ogg, Jr. Secondary reactions in a gas discharge—579
—— (see Rapp, Donald)—1230
Osborne, Darrell W. (see Burns, John H.)—387
O'Toole, J. T. and J. S. Dahler. Boltzmann equation and inverse collisions—1487
—— **and J. S. Dahler.** Molecular friction in dilute gases—1496
Otterson, Dumas A. On the presence of NaOH in crystalline NaCl—227

Oudemans, G. J. (see Johnston, D. R.)—1310
Overend, John and James R. Scherer. Transferability of Urey-Bradley force constants. IV. Methyl halides—446
—— (see Scherer, James R.)—314(L), 1680

Padmini, P. R. K. L., K. Subba Rao, and B. Ramachandra Rao. Molar sound velocity in inorganic acids—1268(L)
Pake, G. E. (see Anderson, M. E.)—1581(L)
—— (see Rogers, R. N.)—1107
Palko, A. A. and J. S. Drury. Separation of boron isotopes. IV. The methyl sulfide-BF_3 system—779
Pappalardo, R. Note on the optical absorption of $MnCl_2$ and $MnBr_2$—613(L)
—— **and D. L. Wood.** Spectrum of Yb^{3+} in yttrium gallium garnet—1733
Parker, D. J., G. A. McLaren, and J. J. Conradi. Observation of the Overhauser effect on carbon-13 nuclear resonance signals—629(L)
Parr, Robert G. Three remarks on molecular orbital theory of complex molecules—1184
—— (see Saturno, Antony F.)—22
Parsons, J. L. Vibrational spectra of orthorhombic metaboric acid—1858
Patterson, Andrew, Jr. (see Ettinger, Raymond)—1597(L)
Peek, James M. and Edwin N. Lassettre. Molecular orbital treatment of hydrogen with central potentials and modified boundary conditions—1803
Pennington, K. S. and H. E. Petch. Nuclear magnetic resonance spectrum of B^{11} in inderite—329
Perls, Thomas A. and L. Bruce Wilner. Effects of pressure on dielectric relaxation in a chlorinated diphenyl—753
Person, Willis B. and Charles A. Swenson. Infrared studies of crystal benzene. IV. Absolute intensities—233
—— (see Swenson, Charles A.)—56
Petch, H. E. (see Pennington, K. S.)—329
Peterlin, Anton. Gradient dependence of intrinsic viscosity of freely flexible linear macromolecules—1799
Petersen, D. H. (see Pierce, Louis)—907
Petersen, H. L. (see Kretschmer, C. B.)—948(L)
Phillips, W. D. and R. E. Benson. Ligand spin densities and magnetic properties of some aminotroponeimine chelates of nickel—607(L)
——, **J. C. Rowell, and S. I. Weissman.** EPR studies of the tetracyanoethylene anion radical—626(L)
Phillipson, P. and R. S. Mulliken. Note on Hurley's "Improved molecular orbitals and the valence bond theory"—615(L)
Pierce, Louis and D. H. Petersen. Microwave spectrum, structure, dipole moment, and internal rotation of trimethyl silane—907
Pimentel, George C. (see Baldeschwieler, John D.)—1008
—— (see Goldfarb, Theodore D.)—105
Piotrowski, Edward A. (see Gilbert, Robert L.)—1872(L)
Piper, T. S. and R. L. Carlin. Axial crystal fields in the ionic model—1208
—— **and R. L. Carlin.** Polarized visible spectra of crystalline trisoxalatometallates: the source of intensity—608(L)
Plane, Robert A. (see Chantry, George W.)—634(L), 736
Plesner, Igor W. Diffusion in a linear lattice—652
Poland, Duncan E. (see Green, John W.)—35
Porter, Gerald B. and B. T. Connelly. Kinetics of excited molecules. II. Dissociation processes—81
Porter, Richard F. Mass spectra of vapors in the Al-AlF_3 and Al-LiF-AlF_3 systems—951(L)
—— **and Ernest E. Zeller.** Mass spectra of aluminum (III) halides and the heats of dissociation of $Al_2F_6(g)$ and $LiF \cdot AlF_3(g)$—858
—— (see Bauer, S. H.)—685
Poulet, Henri (see Zmerli, Adnan)—1177
Powell, R. S. (see Lawton, Elliott J.)—395, 405
Prager, Stephen. Diffusion in inhomogeneous media—122
Purlee, E. Lee (see Grunwald, Ernest)—556

Rabinovitch, B. S. (see Harrington, R. E.)—744, 1271(L)
Rabinowitz, Philip and George Weiss. Tables for the calculation of lattice sums—1272(L)
Radford, H. E. and F. O. Rice. Green and purple sulfur: electron-spin resonance studies—774
Randić, Milan. Out-of-plane CH vibrations in some polynuclear aromatic hydrocarbons—710
Rank, D. H., D. P. Eastman, W. B. Birtley, and T. A. Wiggins. Perturbation of molecular rotation-vibration energy levels by rare gases—323
——, **D. P. Eastman, W. B. Birtley, and T. A. Wiggins.** Shapes and breadths of some molecular rotation-vibration band lines perturbed by rare gases—327
Ransil, B. J. (see Krauss, M.)—840
Rao, B. Ramachandra (see Padmini, P. R. K. L.)—1268(L)
Rao, K. Subba (see Padmini, P. R. K. L.)—1268(L)
Rao, V. S. and Richard C. Schoonmaker. Velocity analysis of molecular beams generated from NaOH vapors—1717
Rapp, Donald and Harold S. Johnston. Nitric oxide-fluorine dilute diffusion flame—695
—— **and Irene B. Ortenburger.** Interchange of charge between gaseous molecules—1230
Rastogi, R. P. and R. C. Srivastava. Entropy production in chemical reactions—79
Rea, D. G. The effect of hydrogen bonding on the intensity of the CD Raman band of $CDCl_3$—1875(L)
Reeves, Robert R. (see Mannella, Gene G.)—636(L)
Reilly, C. A. and J. D. Swalen. Erratum: NMR spectra of some simple epoxides—617(L)
—— **and J. D. Swalen.** On the analysis of high-resolution NMR spectra by iterative methods—1257(L)
Reisfeld, M. J. (see McInteer, B. B.)—570
Reiss, H. (see Helfand, E.)—1379
Reitz, D. C., F. Dravnieks, and J. E. Wertz. Carbon-13 hyperfine splittings in semiquinones—1880(L)
—— **and S. I. Weissman.** Spin exchange in biradicals—700
Rice, F. O. (see Radford, H. E.)—774
Rice, Stuart A. Some further remarks on the coefficient of self-diffusion in simple dense fluids—1376
—— (see Allnatt, Alan R.)—573
—— (see Harris, Robert A.)—1047, 1055
Richardson, J. M. and S. R. Brinkley, Jr. Cell method in grand canonical ensemble—1467
Robben, Frank, Philip R. Monson, and John J. Allport. Correlation of experimental results for the vibrational relaxation of nitric oxide—630(L)
Robertson, W. W. Comparison of the effects of high pressure and low temperature on the absorption spectra of some condensed-ring aromatics—362
Robinson, D. W. (see Aronson, J. R.)—1004
Robinson, G. W. (see Wright, M. R.)—934(L)
Robinson, J. M. Concise method for forming two-center integrals of operators—734
Rogers, Max T. (see Narasimhan, P. T.)—727
Rogers, R. N. and G. E. Pake. Paramagnetic relaxation in solutions of VO^{++}—1107
Rogge, William H., Frederick L. Yarger, and Fred P. Dickey. Emission spectrum of the OH radical in an oxyacetylene flame in the 1.5-μ region—453
Roig, Antonio (see Krigbaum, W. R.)—921
—— (see Kurata, Michio)—151
Rosenberg, Arthur J. Activity coefficients of electrons and holes at high concentrations—665
Ross, John (see Choi, Sang-Il)—1324
Ross, Marvin (see Steele, William A.)—464
Rothe, Erhard W. (see Schumacher, Hugo)—584
Rowell, J. C. (see Phillips, W. D.)—626(L)

Rubin, Robert J. and Kurt E. Shuler. On the dissociation of polyatomic molecules—438
Rudd, De F. P. and B. Widom. Critical solution phenomenon in two-component liquid systems. The system water-ethylene glycol mono-isobutyl ether—1815
Rudolph, P. S. and S. C. Lind. Kinetics of the alpha radiolysis of carbon monoxide—705
—— (see Melton, C. E.)—1594(L)
Rupprecht, A. (see Forsén, S.)—1888(L)

Sahni, R. C. and C. D. LaBudde. Study of molecular integrals. I. Two-center exchange integrals—1015
—— (see LaBudde, C. D.)—1022
Sakamoto, Michiko (see Lin, Chun C.)—878
Salkoff, Morris (see Bauer, Ernest)—1202
Salomon, R. E. (see Graven, W. M.)—954(L)
Sanborn, Russell H. Infrared spectra and structure of the isomers of N_2F_2—1855
—— (see Gunn, Stuart R.)—955(L)
Sato, S. (see Arai, S.)—1277(L)
Satten, Robert A. and Jack. S. Margolis. Erratum: f^2 configuration in crystalline field—618(L)
——, **Donald Young, and Dieter M. Gruen.** Preliminary analysis of U^{4+} ion spectra in crystals—1140
Saturno, Antony F. and Robert G. Parr. A one-center wave function for the methane molecule—22
Scatchard, George. John Gamble Kirkwood, 1907–1959—1279
——, **B. Vonnegut, and D. W. Beaumont.** New type of freezing-point apparatus, freezing points of dilute lanthanum chloride solutions—1292
Scherer, James R., J. C. Evans, and John Overend. Infrared and Raman spectra of C_2Br_2D—314(L)
—— **and John Overend.** Transferability of Urey-Bradley force constants. V. Bromoethylenes—1680
—— (see Overend, John)—446
Scherr, Charles W. Second-order perturbation energy of the two-electron atom—317(L)
—— (see Machacek, Milos)—242
Schiff, H. I. (see Morgan, J. E.)—930(L)
Schmalzried, Hermann. Electrical conduction in magnesium oxide—940(L)
Schmidt, Paul W. (see Hight, Robert, Jr.)—1656
Schnepp, O. and K. Dressler. Absorption spectra of solid xenon, krypton, and argon in the vacuum ultraviolet—49
—— (see Dressler, K.)—270
Schoonmaker, Richard C. (see Rao, V. S.)—1717
Schug, John C., Paul E. McMahon, and H. S. Gutowsky. Electron coupling of nuclear spins. IV. Temperature dependence in substituted ethanes—843
Schuler, Robert H. (see Fessenden, Richard W.)—935(L)
Schulz, G. J. Excitation and negative ions in H_2O—1661
Schumacher, H. J. Mechanism of ozone decomposition—938(L)
Schumacher, Hugo, Richard B. Bernstein, and Erhard W. Rothe. Total collision cross sections for the interaction of molecular beams of cesium chloride with gases. Influence of the dipole-dipole force upon the scattering—584
Schurin, Bertram. Calculated band intensities for CO_2 from infrared dispersion data—1878(L)
Seager, Spencer L. (see Giddings, J. Calvin)—1579(L)
Sears, Gerald W. Growth poisoning of lithium fluoride from aqueous solutions—1068
—— Nucleation and growth of mercury crystals at low supersaturation—563
—— **and J. W. Cahn.** Interaction of condensable gases with cold surfaces—494
Sederholm, C. H. (see Crapo, L. M.)—1583(L)
Sehr, Robert (see Labes, Mortimer M.)—868
Shapiro, I. and H. Landesman. Fragmentation patterns of halogenated pentaboranes—1590(L)
—— (see Lehmann, Walter J.)—590
Shida, S. (see Arai, S.)—1277(L)
Shida, Shoji (see Kuri, Zenichiro)—1884(L)
Shuler, Kurt E. and Robert Zwanzig. Quantum-mechanical calculation of harmonic oscillator transition probabilities in a one-dimensional impulsive collision—1777
—— (see Rubin, Robert J.)—438
Shuskus, A. J., C. G. Young, O. R. Gilliam, and Paul W. Levy. Electron spin resonances in irradiated potassium azide—622(L)
Silver, M. (see Moore, W.)—1671
Silvidi, A. A. and J. W. McGrath. Proton magnetic resonance study of barium bromate monohydrate—1788
—— (see McGrath, J. W.)—644
Simha, Robert and J. L. Zakin. Compression of flexible chain molecules in solution—1790
Sinanoğlu, Oktay. Inter- and intra-atomic correlation energies and theory of core-polarization—1212
Sinclair, T. F. (see Stern, S. Alexander)—805
Singer, Sister Judith Mary and Gilbert W. Castellan. Excess free energy in dehydrogenated palladium—633(L)
Sloan, G. J. (see Chesnut, D. B.)—637(L)
Smaller, B. (see McMillan, J. A.)—609(L)
Smith, A. C. H. (see Fox, J. W.)—623(L)
Smith, G. M. and E. E. Muschlitz, Jr. Scattering of metastable helium atoms in helium, neon, and argon—1819
Smith, Richard P. Mean square length of a hindered alkane chain—876
Smith, William T., Jr. (see Holmberg, Robert W.)—541
Snyder, Lawrence C. Helium atom wave functions from Slater orbitals of nonintegral principal quantum number—1710
—— Jahn-Teller distortions in cyclobutadiene, cyclopentadienyl radical, and benzene positive and negative ions—619(L)
Snyder, Robert G., Junji Kumamoto, and James A. Ibers. Vibrational spectrum of crystalline potassium hydroxide—1171
—— (see Ibers, James A.)—1164
Soden, R. R. (see Van Uitert, L. G.)—567, 1532
Somayajulu, G. R. Dissociation energies of diatomic molecules—1541
Sommer, Armin, Patrick N. Walsh, and David White. Mass spectrometric and infrared emission investigation of the vapor species in the B-S system at elevated temperatures—296(L)
Spedding, F. H. (see Jennings, L. D.)—1849
Spence, R. D. (see Murthy, C. R. K.)—945(L)
Spindel, W. and Marvin J. Stern. Erratum: Some observations on atomic exchange in NO—942(L)
Spinner, E. Bond lengths and nuclear quadrupole coupling in vinyl halides—611(L)
Srivastava, R. C. (see Rastogi, R. P.)—79
Stafford, Fred E. (see Ackerman, Marcel)—1783
Stalinski, B., C. K. Coogan, and H. S. Gutowsky. Proton magnetic resonance studies of nonstoichiometric titanium hydride—933(L)
Stanton, H. E. (see Morrison, J. D.)—821
Stebbings, R. F., Wade L. Fite, and David G. Hummer. Charge transfer between atomic hydrogen and N^+ and O^+—1226
Steel, C. and M. Szwarc. Methyl affinities determined by photolysis of azomethane—1677
Steele, D., E. R. Lippincott, and J. Xavier. Vibrational spectra of penta-deutero-fluorobenzene—1242

Steele, William A. Physical properties of isotopically substituted classical fluids—1619
—— **and Marvin Ross.** Distribution functions of a fluid in an external potential field: application to physical adsorption—464
Stern, Marvin J. (see Spindel, W.)—942(L)
Stern, S. Alexander, P. C. Waterman, and T. F. Sinclair. Separation of gas mixtures in a supersonic jet. II. Behavior of helium-argon mixtures and evidence of shock separation—805
Sternlicht, Himan. Polycrystalline resonance line shape of π-electron radicals—1128
—— **and H. M. McConnell.** Effect of deuterium substitution on the lifetime of the phosphorescent triplet state of naphthalene—302(L)
Stevenson, D. P. and James A. Ibers. On the equilibrium C—H distance in methane—762
Stewart, John W. Compression and phase transitions of solid NH_3, SiF_4, H_2S, and CF_4—128
Stillinger, Frank H., Jr., and John G. Kirkwood. Theory of the diffuse double layer—1282
Stockmayer, Walter H. Diffusion of weak electrolytes—1291
—— (see Kurata, Michio)—151
Stogryn, Daniel E. and Joseph O. Hirschfelder. Errata: "Contributions of bound, metastable, and free molecules to the second virial coefficient and some properties of double molecules" and "Initial pressure dependence of thermal conductivity and viscosity"—942(L)
Storms, E. K. (see Kempter, C. P.)—1873(L)
Stout, J. W. Absorption spectra of $MnCl_2$ and $MnBr_2$—303(L)
Strehlow, Roger A. and Arthur Cohen. Erratum: Reflected shock technique for studying fast chemical reactions—618(L)
Sugano, Satoru. Optical rotatory dispersion of transition-metal complexes—1883(L)
Sundaram, S. Force constants for NH_4^+ and ND_4^+—708
Swalen, J. D. (see Reilly, C. A.)—617(L), 1257(L)
Swenson, Charles A. and Willis B. Person. Infrared studies of crystal benzene. II. Relative intensities—56
—— (see Person, Willis B.)—233
Szwarc, M. (see Steel, C.)—1677

Tadokoro, Hiroyuki. Normal vibrations of the polymer molecules of helical configuration—1558
Takeda, M., Y. Imamura, S. Okamura, and T. Higashimura. Dipole moment of isotactic and atactic polyvinyl isobutyl ether—631(L)
Tamor, S. Structure of transport equations—1421
—— (see Auer, P. L.)—1426
Taube, H. (see Baldwin, H. W.)—206
Thorson, Walter R. and Ichiro Nakagawa. Dynamics of the quasi-linear molecule—994
Thrush, B. A. (see Mann, D. E.)—1731
Tinoco, Ignacio, Jr. Optical and other electronic properties of polymers—1332
Tobias, Irwin, Robert J. Fallon, and Joseph T. Vanderslice. Potential energy curves for CO—1638
Tosi, M. P. (see Fumi, F. G.)—1
Truesdell, Clifford (see Coleman, Bernard D.)—28
Turrell, George C., H. Vu, and B. Vodar. Induced Q branch in the vibration-rotation spectrum of HCl pressurized with Ar—315(L)
Tuttle, T. R., Jr. (see Anderson, M. E.)—1581(L), 1591(L)
Tykodi, R. J. Thermodynamics, stationary states, and steady-rate processes. V. A collection of corollaries—40
—— (see Erikson, Ted A.)—46

Ueda, Hisashi (see Kuri, Zenichiro)—1884(L)

Valley, L. M. and Sam Legvold. Sound dispersion in ethane and 1·1-difluoroethane—627(L)
Vanderslice, Joseph T. and Edward A. Mason. Interaction energies for the H-H_2 and H_2-H_2 system—492
——, **Edward A. Mason, William G. Maisch, and Ellis R. Lippincott.** Potential curves for N_2, NO, and O_2—614(L)
—— (see Fallon, Robert J.)—944(L)
—— (see Tobias, Irwin)—1638
van Roggen, A. Satellite lines in paramagnetic resonance spectra—1589(L)
Van Uitert, L. G. and R. R. Soden. Emission spectra of erbium in the Scheelite structure—567
—— **and R. R. Soden.** Emission spectrum of trivalent holmium in the Scheelite structure—1532
Varney, Robert N. Statistical mechanics of molecular ions—1708
Varsanyi, F. and G. H. Dieke. Infrared absorption spectrum of $NdCl_3$—1616
Vaughan, Philip A. (see Muha, George M.)—194
Vodar, B. (see Turrell, George C.)—315(L)
Volk, H. and G. D. Halsey, Jr. Solubility of hydrogen and deuterium in liquid argon—1132
Volpi, G. G. (see Cimino, A.)—616(L)
Vonnegut, B. (see Scatchard, G.)—1292
Vu, H. (see Turrell, George C.)—315(L)

Wada, Yasuo (see Hisatsune, I. C.)—714
Wainwright, T. E. (see Alder, B. J.)—1439
Waite, Thomas R. Antiferromagnetic coupling and covalent bonding in almost totally ionic salts—256
Walkley, John, David N. Glew, and Joel H. Hildebrand. Relations between ultraviolet and visible absorption peaks of iodine solutions—621(L)
Walrafen, George E. Acube-root law for the activity coefficient quotient of the dissociation of HSO_4^- ion—947(L)
Walsh, Patrick N. (see Sommer, Armin)—296(L)
Waterman, P. C. (see Stern, S. Alexander)—805
Wayland, Harold. Streaming birefringence of rigid macromolecules in general two-dimensional laminar flow—769
Weatherly, T. L. (see Long, Maurice W.)—508
Webb, W. (see Nelson, R. R.)—1755
Weber, A. (see Monostori, B.)—1867(L)
Weigang, O. E., Jr. Spectral solvent shift. I. Paraffin hydrocarbon solvent interactions with polynuclear aromatic hydrocarbons—892
Weinberger, A. J. (see Livingston, Ralph)—499
Weinreb, A. (see Basile, L. J.)—1028
Weinstock, Bernard (see Claassen, Howard H.)—436
Weiss, George (see Rabinowitz, Philip)—1272(L)
Weissman, S. I. (see Phillips, W. D.)—626(L)
—— (see Reitz, D. C.)—700
Wertz, J. E. (see Reitz, D. C.)—1880(L)
Westrum, Edgar F., Jr. (see Burns, John H.)—387
Wexler, S. and G. R. Anderson. Dissociation of methyl bromide by nuclear isomeric transition of 4.4-hr Br^{80m}—850
Wharton, Lennard, L. Peter Gold, and William Klemperer. Dipole moment of lithium hydride—1255(L)
White, David (see Sommer, Armin)—296(L)
Whitmore, D. H. and J. B. Moser. Sublimation of small sodium chloride spheres into argon—917
Widom, B. (see Rudd, De F. P.)—1815
Wiggins, T. A. (see Rank, D. H.)—323, 327
Wilcox, Charles F., Jr. Ultraviolet spectrum of triptycene—1874(L)
Wildi, B. S. (see Epstein, A.)—618(L)
Williams, F. A. On the assumptions underlying droplet vaporization and combustion theories—133
Williams, Quitman (see Long, Maurice W.)—508
Wilmshurst, J. K. Orbital radii and the dependence of bond length upon ionicity, hybridization, and bond order—813

Wilner, L. Bruce (see Perls, Thomas A.)—753
Wilson, Charles O., Jr. (see Lehmann, Walter J.)—590
Wilson, E. Bright, Jr. Bond lengths and nuclear quadrupole coupling in vinyl halides—612(L)
—— (see Myers, Rollie J.)—186
Witkowski, Andrzej and William Moffitt. Electronic spectra of dimers: derivation of the fundamental vibronic equation —872
Woermann, D. (see Debye, P.)—1745
Wojtowicz, Peter J. and John G. Kirkwood. Contribution of lattice vibrations to the order-disorder transformation in alloys—1299
Wolfsberg, Max. Isotope effects on reaction rates and the reaction coordinate—21
—— Note on secondary isotope effects in reaction rates—2
—— (see Gutmann, Joel R.)—1592(L)
Wood, D. L. (see Pappalardo, R.)—1733
Wood, J. L. Diffusion theory of chemical reaction—1587(L)
Wright, M. R., R. P. Frosch, and G. W. Robinson. Phosphorescence lifetime of benzene. An intermolecular heavy-atom effect, a deuterium effect, and a temperature effect —934(L)
Wulfman, Carl E. Approximate electronic energy surfaces from cuspless wave functions—1567

Xavier, J. (see Steele, D.)—1242

Yamamoto, Tsunenobu. Quantum statistical mechanical theory of the rate of exchange chemical reactions in the gas phase—281
Yamazaki, M. (see Brion, H.)—1871(L)
Yao, Y. L. Detection of order in Ni_3Co—741
Yarger, Frederick L. (see Rogge, William H.)—453
Yaroslavsky, Samuel and Ernst D. Bergmann. Dipole moment and conformation of 2-chlorocyclohexanone—635(L)
Young, C. G. (see Shuskus, A. J.)—622(L)
Young, Donald (see Satten, Robert A.)—1140
Young, Robert A. Method for investigating the order of chemiluminescent reactions, the diffusion coefficient of the labile reactants, and the catalytic efficiency of surfaces—1044
—— Pressure dependence of some infrared and vacuum ultraviolet bands occurring in active nitrogen—1112

Zahner, J. C. and H. G. Drickamer. Pressure effects in nickel dimethylglyoxime and related chelates—1625
Zakin, J. L. (see Simha, Robert)—1790
Zandstra, P. J. (see Anderson, M. E.)—1591(L)
Zeller, Ernest E. (see Porter, Richard F.)—858
Zimm, Bruno H. Theory of "melting" of the helical form in double chains of the DNA type—1349
Zinn, John (see Chan, Sunney I.)—295(L), 1643
Zlatarich, Steven A. (see Brabbs, Theodore A.)—307(L)
Zmerli, Adnan and Henri Poulet. Polarized absorption and fluorescence spectra of 2,6-dimethylnaphthalene at different temperatures—1177
Zwanzig, Robert. Ensemble method in the theory of irreversibility—1338
—— (see Shuler, Kurt E.)—1777

Analytical Subject Index to Volume 33

(References with (L) are to Letters to the Editor)

Absorption Spectra Infrared

Electronic transitions of rare earth ions in the infrared region, G. Mandel, R. P. Bauman, and E. Banks—192

Equilibrium constant for isotope exchange in ammonia from infrared spectra, Llewellyn H. Jones—1585(L)

Erratum: Infrared and raman spectra of fluorinated ethanes. XII. 1, 1, 2, 2-tetrafluoroethane [J. Chem. Phys. **32**, 899 (1960)], Peter Klaboe and J. Rud Nielsen—617(L)

Evidence for internal rotation in the fine structure of the infrared absorption of oxygen in silicon, H. J. Hrostowski and B. J. Alder—980

Far infrared spectrum and structure of disiloxane, J. R. Aronson, R. C. Lord and D. W. Robinson—1004

Far infrared spectrum of trimethylene oxide, Alfred Danti, W. J. Lafferty, and R. C. Lord—294(L)

Induced *Q*-branch in the vibration-rotation spectrum of HCl pressurized with argon, George C. Turrell, H. Vu, and B. Vodar—315(L)

Infrared absorption spectra of alkali metal nitrates and nitrites above and below the melting point, J. Greenberg and Leander J. Hallgren—900

Infrared absorption spectrum of $NdCl_3$, F. Varsanyi and G. H. Dieke—1616

Infrared and Raman spectra of C_2Br_2D, James R. Scherer, J. C. Evans, and John Overend—314

Infrared and raman spectra of fluorinated ethanes. XIII. 1,2-difluoroethane, Peter Klaboe and J. Rud Nielsen—1765

Infrared spectra and structure of the isomers of N_2F_2, Russell H. Sanborn—1855

Infrared spectra of alkyldiboranes. III. 1,2-dimethyl- and 1,2-diethyldiboranes, Walter J. Lehmann, Charles O. Wilson, Jr., and I. Shapiro—590

Infrared spectra of complexes of NO_2F with BF_3, PF_5, and SbF_5, Denys Cook, Stephen J. Kuhn and George A. Olah—1669

Infrared spectra of crystalline CD_3Cl and CD_3Br, David A. Dows—1742

Infrared spectra of lithium halide monomers, William Klemperer, W. G. Norris, Alfred Büchler and Alfred G. Emslie—1534

Infrared spectra of some unstable isomers of N_2O_4 and N_2O_3, I. C. Hisatsune, J. P. Devlin, and Yasuo Wada—714

Infrared studies of crystal benzene. IV. Absolute intensities, Willis B. Person and Charles A. Swenson—233

Light-induced *cis-trans* isomerization of nitrous acid formed by photolysis of hydrazoic acid and oxygen in solid nitrogen, John D. Baldeschwieler and George C. Pimentel—1008

Magnetic rotation spectra of nitric oxide in the near infrared, Glen A. Mann and C. D. Hause—1117

Mass spectrometric and infrared emission investigation of the vapor species in the B-S system at elevated temperatures, Armin Sommer, Patrick N. Walsh, and David White—296(L)

Molecular collision cross sections from infrared absorption measurements, Harold Babrov, George Ameer, and William Benesch—145

Near infrared absorption spectra of ortho- and para-H_2O in solid xenon and argon, Jay A. Glasel—252

Perturbation of molecular rotation-vibration energy levels by rare gases, D. H. Rank, D. P. Eastman, W. B. Birtley and T. A. Wiggins—323

Pressure dependence of some infrared and vacuum ultraviolet bands occurring in active nitrogen, Robert A. Young—1111

Rotational isomerism involving the 2–3 carbon-carbon bond of the 1-alkenes, L. A. Harrah and D. W. Mayo—298(L)

Search for a Jahn-Teller effect in IrF_6, Howard H. Claassen and Bernard Weinstock—436

Shapes and breadths of some molecular rotation-vibration band lines perturbed by rare gases, D. H. Rank, D. P. Eastman, W. B. Birtley, and T. A. Wiggins—327

Structure of potassium hydroxide: An x-ray and infrared study, James A. Ibers, Junji Kumamoto, and Robert G. Snyder—1164

Structure of the infrared Y bands of N_2, G. H. Dieke and D. F. Heath—432

Erratum and Addendum: Substituted methanes. XXIX. Vibrational spectra, potential constants, and calculated thermodynamic properties for dibromochloro-fluoromethane and bromodichlorofluoro-methane [J. Chem. Phys. **31**, 1633 (1959)], Robert L. Gilbert, Edward A. Piotrowski, Jerome M. Dowling, and Forrest F. Cleveland—1872(L)

Vibrational spectra of penta-deutero-fluoro-benzene, D. Steele, E. R. Lippincott, and J. Xavier—1241

Vibrational spectrum of crystalline potassium hydroxide, Robert G. Snyder, Junji Kumamoto, and James A. Ibers—1171

Absorption Spectra Microwave

Change of the isobutane molecule; Change of dipole moment of isotopic substitution, David R. Lide, Jr.—1519

Dipole moment of lithium hydride, Lennard Wharton, L. Peter Gold, and William Klemperer—1255(L)

Double minimum vibration in trimethylene oxide, Sunney I. Chan, John Zinn, and William D. Gwinn—295(L)

Electron spin resonance line shape of a polycrystalline CH radical, Roland Lefebvre—1826

Erratum: Microwave spectrum of acetyl cyanide [J. Chem. Phys. **31**, 882 (1959)], Lawrence C. Krisher—304(L)

Microwave spectrum, barrier to internal rotation, and quadrupole coupling of acetyl bromide, Lawrence C. Krisher—1237

Microwave spectrum of $CFCl_3$, Maurice W. Long, Quitman Williams and T. L. Weatherly—508

Microwave spectrum of quinuclidine, Lauren G. Johnson—949(L)

Microwave spectrum, structure, and dipole moment of formyl fluoride, Oliver H. LeBlanc, Jr., Victor W. Laurie, and William D. Gwinn—598

Microwave spectrum, structure, and dipole moment of propane, David R. Lide, Jr.—1514

Microwave spectrum, structure, dipole moment, and internal rotation of trimethyl silane, Louis Pierce and D. H. Petersen—907

Temperature variation of the linewidth in nonresonant microwave absorption, J. E. Boggs, A. P. Deam and Joe M. King—1852

Trimethylene oxide I. Microwave spectrum, dipole moment, and double minimum vibration, Sunney I. Chan, John Zinn, Jose Fernandez, and William D. Gwinn—1643

Absorption Spectra
Of Crystals

Absorption lines of Cr^{3+} in ruby, W. Low—1162

Absorption spectra of $MnCl_2$ and $MnBr_2$, J. W. Stout—303(L)

Absorption spectra of solid methane, ammonia, and ice in the vacuum ultraviolet, K. Dressler and O. Schnepp—270

Absorption spectra of solid xenon, krypton, and argon in the vacuum ultraviolet, O. Schnepp and K. Dressler—49

Crystal spectra of chromium tris-acetyl acetone, Animesh Chakravorty and Sadhan Basu—1266(L)
Effect of pressure on the *M* center in alkali halide crystals, S. Minomura and H. G. Drickamer—290
Electronic absorption spectrum of diphenylene in substitutional solid solid solution, Robin M. Hochstrasser—950(L)
Electronic transitions of rare earth ions in the infrared region, G. Mandel, R. P. Bauman, and E. Banks—192
Erratum: f^2 configuration in a crystalline field [J. Chem. Phys. **32**, 573 (1960)], Robert A. Satten and Jack S. Margolis—618(L)
Evidence for internal rotation in the fine structure of the infrared absorption of oxygen in silicon, H. J. Hrostowski and B. J. Alder—980
Infrared absorption spectrum of $NdCl_3$, F. Varsanyi and G. H. Dieke—1616
Infrared spectra of crystalline CD_3Cl and CD_3Br, David A. Dows—1742
Infrared studies of crystal benzene. II. Relative intensities, Charles A. Swenson and Willis B. Person—56
Infrared studies of crystal benzene. IV. Absolute intensities, Willis B. Person and Charles A. Swenson—233
Intermolecular coupling of vibrations in molecular crystals: A vibrational exciton approach, R. M. Hexter—1833
Note on the optical absorption of $MnCl_2$ and $MnBr_2$, R. Pappalardo—613(L)
Phosphorescence lifetime of benzene. An intermolecular heavy atom effect, a deuterium effect, and a temperature effect, M. R. Wright, R. P. Frosch and G. W. Robinson—934(L)
Polarization of the first two electronic transitions of pyrene, Robin M. Hochstrasser—459
Polarized absorption and fluorescence spectra of 2,6-dimethylnaphthalene at different temperatures, Adnan Zmerli and Henri Poulet—1177
Polarized visible spectra of crystalline trisoxalatometallates: The source of intensity, T. S. Piper and R. L. Carlin—608(L)
Preliminary analysis of U^{4+} ion spectra in crystals, Robert A. Satten, Donald Young, and Dieter M. Gruen—1139
Pressure effects in nickel dimethyl-glyoxime and related chelates J. C. Zahner and H. G. Drickamer—1625
Spectrum of Yb^{3+} in yttrium gallium garnet, R. Pappalardo and D. L. Wood—1733
Structure of potassium hydroxide: An x-ray and infrared study, James A. Ibers, Junji Kumamoto, and Robert G. Snyder—1164
Vibrational spectrum of crystalline potassium hydroxide, Robert G. Snyder, Junji Kumamoto, and James A. Ibers—1171

Absorption Spectra
Visible or Ultraviolet

Absorption lines of Cr^{3+} in ruby, W. Low—1162
Absorption spectra of anodic niobium oxide films, W. M. Graven, R. E. Salomon, and G. B. Adams, Jr.—954(L)
Absorption spectra of $MnCl_2$ and $MnBr_2$, J. W. Stout—303(L)
Absorption spectra of photo-oxide of mesonaphthodianthrene, Haruo Kuroda—1586(L)
Absorption spectra of solid methane, ammonia, and ice in the vacuum ultraviolet, K. Dressler and O. Schnepp—270
Absorption spectra of solid xenon, krypton, and argon in the vacuum ultraviolet, O. Schnepp and K. Dressler—49
Absorption spectrum of chlorine in the vacuum ultraviolet, Raymond P. Iczkowski, John L. Margrave, and John W. Green—1261(L)
Comparison of the effects of high pressure and low temperature on the absorption spectra of some condensed-ring aromatics, W. W. Robertson—362
Crystal spectra of chromium tris-acetyl acetone, Animesh Chakravorty and Sadhan Basu—1266(L)
Cuprous halide films on alkali halide crystals, L. M. Kraemer—991
Electronic absorption spectrum of diphenylene in substitutional solid solid solution, Robin M. Hochstrasser—950(L)
Electronic spectra of dimers: Derivation of the fundamental vibronic equation, Andrzej Witkowski and William Moffitt—872
Flash-absorption spectroscopy of free radicals in shock waves, R. M. Ikeda—311(L)
"Forbidden" character in allowed electronic transitions, Andreas C. Albrecht—156
Identification of colloidal sodium in sodium azide, Brian S. Miller—889
Kinetic absorption spectra recorded through flash-heated grids, L. S. Nelson and N. A. Kuebler—610(L)
Lowest triplet states of ethylene, Robert S. Mulliken—1596(L)
Metastable states of acridine orange in solution, G. Blauer and H. Linschitz—937(L)
Note on the optical absorption of $MnCl_2$ and $MnBr_2$, R. Pappalardo—613(L)
On the absorption spectrum of CF_2 and its vibrational analysis, D. E. Mann and B. A. Thrush—1731
Phosphorescence lifetime of benzene. An intermolecular heavy atom effect, a deuterium effect, and a temperature effect, M. R. Wright, R. P. Frosch and G. W. Robinson—934(L)
Polarization of the first two electronic transitions of pyrene, Robin M. Hochstrasser—459
Polarized absorption and fluorescence spectra of 2,6-dimethylnaphthalene at different temperatures, Adnan Zmerli and Henri Poulet—1177
Polarized visible spectra of crystalline trisoxalatometallates: The source of intensity, T. S. Piper and R. L. Carlin—608(L)
Preliminary analysis of U^{4+} ion spectra in crystals, Robert A. Satten, Donald Young, and Dieter M. Gruen—1139
Pressure dependence of some infrared and vacuum ultraviolet bands occuring in active nitrogen, Robert A. Young—1111
Pressure effects in nickel dimethyl-glyoxime and related chelates, J. C. Zahner and H. G. Drickamer—1625
Radiative lifetime of the $B\,^2\Sigma^+$ state in N_2O^+, I. E. Dayton, F. W. Dalby, and R. G. Bennett—179
Relations between ultraviolet and visible absorption peaks of iodine solutions, John Walkley, David N. Glew, and Joel H. Hildebrand—621(L)
Solvent effects on $n\rightarrow\pi^*$ transitions in pyrazine, V. G. Krishna and Lionel Goodman—381
Spectral solvent shift I. Paraffin hydrocarbon solvent interactions with polynuclear aromatic hydrocarbons, O. E. Weigang, Jr.—892
Spectrum of ReF_6, J. C. Eisenstein—1530
Spectrum of Yb^{3+} in yttrium gallium garnet, R. Pappalardo and D. L. Wood—1733
Sum rule for transition probabilities, William L. Clinton—1603
Theory for the triplet-triplet absorption spectra of porphyrins, Martin Gouterman—1523
Ultraviolet and structural studies of polythionates, R. M. Golding—1666
Ultraviolet spectrum of triptycene, Charles F. Wilcox, Jr.—1874(L)
Vibronic calculations in benzene, Andreas C. Albrecht—169

Accommodation Coefficients

Condensation coefficient of arsenic trioxide glass, A. B. Bestul and D. H. Blackburn—1274(L)
Observation of adsorption on an atomic scale, Gert Ehrlich, and F. G. Hudda—1253(L)

Beams, Atomic and Molecular

Analysis of reactive scattering in crossed molecular beams, Dudley R. Herschbach—1870(L)
Charge transfer between atomic hydrogen and N^+ and O^+, R. F. Stebbings, Wade L. Fite, and David G. Hummer—1226
Interchange of charge between gaseous molecules, Donald Rapp and Irene B. Ortenburger—1230
Quantum mechanical (phase shift) analysis of the differential elastic scattering of molecular beams, Richard B. Bernstein—795
Total collision cross sections for the interaction of molecular beams of cesium chloride with gases. Influence of the dipole-dipole force upon the scattering, Hugo Schumacher, Richard B. Bernstein, and Erhard W. Rothe—584
Velocity analysis of molecular beams generated from NaOH vapors, V. S. Rao and Richard C. Schoonmaker—1717

Catalysis

Method for investigating the order of chemiluminescent reactions, the diffusion coefficient of the labile reactants, and the catalytic efficiency of surfaces, Robert A. Young—1044
Quantitative considerations concerning catalysis at a semiconductor surface, C. G. B. Garrett—966
Surface catalyzed excitation with N and O atoms, Gene G. Mannella, Robert R. Reeves and Paul Harteck—636(L)

Chemical Reactions (see Kinetics of Reactions)

Combustion

On the assumptions underlying droplet vaporization and combustion theories, F. A. Williams—133

Crystal Growth

Growth poisoning of lithium fluoride from aqueous solutions, Gerald W. Sears—1068
Nucleation and growth of mercury crystals at low supersaturation, G. W. Sears—563

Crystalline State

Axial crystal fields in the ionic model, T. S. Piper and R. L. Carlin—1208
Comments on Dr. Schmalzried's Letter, S. P. Mitoff—941(L)
Conduction electrons in sodium tungsten bronze, Joseph M. Keller—232
Contribution of lattice vibrations to the order-disorder transformation in alloys, Peter J. Wojtowicz and John G. Kirkwood—1298
Dissolution kinetics at dislocation etch pits in single crystals of lithium fluoride, M. B. Ives and J. P. Hirth—517
Effective ionic charge in CdS, Frederick Keffer—1267(L)
Electrical conduction in magnesium oxide, Hermann Schamlzried—940(L)
Electron spin resonance in neutron-irradiated calcite, J. C. Kemp—1269(L)
Erratum: Lattice energies of the alkali halides and the electron affinities of the halogens [J. Chem. Phys. **31**, 1646 (1959)], Daniel Cubicciotti—1579(L)
Frequency distribution and the specific heat of NaCl at low temperatures, Elizabeth M. Arase and Robert D. Hatcher—1703
Frequency spectrum for a two-dimensional lattice, Jacob Neuberger and Robert D. Hatcher—265
Hyperfine structure of F-center spin resonance in sodium azide, F. F. Carlson, G. J. King, and B. S. Miller—1266(L)
Lattice vibrations in alkali halide crystals. II. Potassium and rubidium halides; cesium fluoride, Arnold M. Karo—7
Madelung constants of the cubic perovskite structures, F. G. Fumi and M. P. Tosi—1
Molecular rotation in crystals of N_2 and CO, Barbara C. Kohin—882
On the molecular nature of the dielectric anomalies in thiourea, Crispin Calvo—1720
On the presence of NaOH in crystalline NaCl, D. A. Otterson—227
Preparation and crystal structures of RuC and OsC, Charles P. Kempter and M. R. Nadler—1580(L)
Proton magnetic resonance study of barium bromate monohydrate, A. A. Silvidi and J. W. McGrath—1788
Structure of potassium hydroxide: An x-ray and infrared study, James A. Ibers, Junji Kumamoto, and Robert G. Snyder—1164
Surface specific heat of an isotropic solid at low temperatures, Marc Dupuis, Robert Mazo and Lars Onsager—1452
Tables for the calculation of lattice sums, Philip Rabinowitz and George Weiss—1272(L)
Thermal expansion of delta and epsilon zirconium hydrides, Charles P. Kempter, Reed O. Elliott, and Karl A. Gschneidner, Jr.—837
Vibrational spectra of orthorhombic metaboric acid, J. L. Parsons—1860
Vibrational spectrum of crystalline potassium hydroxide, Robert G. Snyder, Junji Kumamoto, and James A. Ibers—1171

Crystal Structure

Comments on Carpenter's paper "Density of the bonding electrons in diamond," James A. Ibers—299(L)
Crystal structure of β-Ga_2O_3, S. Geller—676
Density of the bonding electrons in diamond, G. B. Carpenter—300(L)
Interatomic distances in FeS_2, CoS_2, and NiS_2, Norman Elliott—903
Preparation and properties of scandium dihydride, Joseph C. McGuire and Charles P. Kempter—1584(L)

Adsorption (see Surface Phenomena)

Valence structures of the higher borides, William N. Lipscomb and Doyle Britton—275

Detonation (see also Shock Waves)

Comments on hypervelocity wave phenomena in condensed explosives, R. F. Chaiken—760

Deuterium (see Isotopes)

Dielectrics

Continuum-model treatment of long-range intermolecular forces. I. Pure substances, Bruno Linder—668
Dielectric behavior and crystal structure of ethyl and vinyl stearate, Martin G. Broadhurst and Edwin R. Fitzgerald—210
Dielectric constants of imperfect gases. I. Helium, argon, nitrogen, and methane, D. R. Johnston, G. J. Oudemans, and R. H. Cole—1310
Dielectric relaxation of isoamyl bromide, Sivert H. Glarum—639
Dielectric relaxation of polar liquids, Sivert H. Glarum—1371

Dielectric study of some liquid alkyl nitrites, R. F. Grant, D. W. Davidson and Peter Gray—1712
Dipole moment and conformation of 2-chlorocyclohexanone, Samuel Yaroslavsky and Ernst D. Bergmann—635(L)
Dipole moment of isotactic and atactic poly-vinyl iso-butyl ether, M. Takeda, Y. Imamura, S. Okamura and T. Higashimura—631(L)
Dipole moments of hydrocarbons, David R. Lide, Jr.—1879(L)
Effects of pressure on dielectric relaxation in a chlorinated diphenyl, Thomas A. Perls and L. Bruce Wilner—753
Electric strength of methane and deuteromethane, J. C. Devins and R. W. Crowe—1578(L)
On the molecular nature of the dielectric anomalies in thiourea, Crispin Calvo—1720
Temperature variation of the linewidth in nonresonant microwave absorption, J. E. Boggs, A. P. Deam and Joe M. King—1852
Theoretical dielectric behavior of an ethyl stearate-heneicosane mixture, Martin G. Broadhurst—221
Trimethylene oxide I. Microwave spectrum, dipole moment, and double minimum vibration, Sunney I. Chan, John Zinn, Jose Fernandez, and William D. Gwinn—1643

Diffusion

Diffusion in a linear lattice, Igor W. Plesner—652
Diffusion in inhomogeneous media, Stephen Prager—122
Diffusion of weak electrolytes, W. H. Stockmayer—1290
Diffusion theory of chemical reaction, J. L. Wood—1587(L)
Flow equations and frames of reference for isothermal diffusion in liquids, John G. Kirkwood, Robert L. Baldwin, Peter J. Dunlop, Louis J. Gosting and Gerson Kegeles—1505
Method for investigating the order of chemiluminescent reactions, the diffusion coefficient of the labile reactants, and the catalytic efficiency of surfaces, Robert A. Young—1044
On the dynamical theory of diffusion in crystals. V. A random-walk treatment of the heat of transport, Alan R. Allnatt and Stuart A. Rice—573
Oxygen diffusion in periclase crystals, Y. Oishi and W. D. Kingery—905
Rapid determination of gaseous diffusion coefficients by means of gas chromatography apparatus, J. Calvin Giddings and Spencer L. Seager—1579(L)
Self-diffusion of oxygen in single crystal and polycrystalline aluminum oxide, Y. Oishi and W. D. Kingery—480
Some further remarks on the coefficient of self-diffusion in simple dense fluids, Stuart A. Rice—1376
Sublimation of small sodium chloride spheres into argon, D. H. Whitmore and J. B. Moser—917

Dipole Moment

Change of the isobutane molecule; Change of dipole moment of isotopic substitution, David R. Lide, Jr.—1519
Dipole moment of lithium hydride, Lennard Wharton, L. Peter Gold, and William Klemperer—1255(L)
Microwave spectrum, structure, and dipole moment of formyl fluoride, Oliver H. LeBlanc, Jr., Victor W. Laurie, and William D. Gwinn—598
Microwave spectrum, structure, and dipole moment of propane, David R. Lide, Jr.—1514

Electrical Properties

Comments on Dr. Schmalzried's Letter, S. P. Mitoff—941(L)
Conduction electrons in sodium tungsten bronze, Joseph M. Keller—232
Electrical conduction in magnesium oxide, Hermann Schmalzried—940(L)
Erratum: Electrical properties of poly-copper phthalocyanine [J. Chem. Phys. **32**, 324 (1960)], A. Epstein and B. S. Wildi—618(L)
Hole and electron drift mobilities in anthracene, Oliver H. LeBlanc, Jr.—626(L)
Organic semiconductors II. The electrical resistivity of organic molecular complexes, Mortimer M. Labes, Robert Sehr, and Monisha Bose—868
Sparking potential and molecular structure of unsaturated hydrocarbon gases, R. W. Crowe and J. C. Devins—413
Structure of glass-forming halides. II. Liquid zinc chloride, J. D. Mackenzie and W. K. Murphy—366

Electrochemistry

Cube-root law for the activity coefficient quotient of the dissociation of HSO_4^- ion, George E. Walrafen—947(L)
Diffusion of weak electrolytes, W. H. Stockmayer—1290
Excess free energy in dehydrogenated palladium, Sister Judith Mary Singer, O. P. and Gilbert W. Castellan—633(L)
Flow adaptation of the isotopic dilution method for the study of ionic hydration, H. W. Baldwin and H. Taube—206
New type of freezing point apparatus. The freezing points of dilute lanthanum chloride solutions, G. Scatchard, B. Vonnegut and D. W. Beaumont—1292
Theory of the diffuse double layer, Frank H. Stillinger, Jr. and John G. Kirkwood—1282
Transport processes in liquid alloys. II. The electrical force on an ion, Paul C. Mangelsdorf, Jr.—1151

Electron Affinity

Erratum: Lattice energies of the alkali halides and the electron affinities of the halogens [J. Chem. Phys. **31**, 1646 (1959)], Daniel Cubicciotti—1579(L)
Isoelectronic extrapolation of electron affinities, B. Edlén—98
Remarks on doubly excited states of the negative atomic hydrogen ion, E. Holøien—301(L)
Some remarks on the electron affinity of atomic lithium, E. Holøien—309(L)

Electron Diffraction

Equilibrium bond lengths in methane and deuteromethane as determined by electron diffraction and spectroscopic methods, L. S. Bartell, Kozo Kuchitsu, and R. J. deNeui—1254(L)
Molecular structure of iodine heptafluoride, Robert E. LaVilla and S. H. Bauer—182
Molecular structure of lithium chloride dimer. Thermodynamic functions of Li_2X_2 (X= Cl, Br, I)., S. H. Bauer, Tadashi Ino, and Richard F. Porter—685

Emission Spectra

Chemiluminescence of ethylene formed probably from ethylene in an inert matrix, Theodore D. Goldfarb and George C. Pimentel—105
Emission spectra of erbium in the scheelite structure, L. G. Van Uitert and R. R. Soden—567
Emission spectrum of the OH radical in an oxyacetylene flame in the 1.5-μ region, William H. Rogge, Frederick L. Yarger, and Fred P. Dickey—453
Emission spectrum of trivalent holmium in the scheelite structure, L. G. Van Uitert and R. R. Soden—1532
Spectroscopy of fluorine flames. I. Hydrogen-fluorine flame and the vibration-rotation emission spectrum of *HF*, D. E. Mann, B. A. Thrush, D. R. Lide, Jr., J. J. Ball, and N. Acquista—1731

Energy Transfer

Collisional deactivation of vibrationally excited *sec*-butyl-d_1 radicals produced by chemical activation. R. E. Harrington, B. S. Rabinovitch and M. R. Hoare—744
Correlation of experimental results for the vibrational relaxation of nitric oxide, Frank Robben, Philip R. Monson, and John J. Allport—630(L)
Efficiency of energy transfer in a solution of PPO in xylene, Isadore B. Berlman—1124
Energy transfer in liquid hydrocarbons excited by γ-rays G. R. Freeman—957(L)
Multiple vibrational relaxation in gaseous dibromomethane, Norman J. Meyer—487
Optical transparency and resistance to flash heating, W. F. Libby—1588(L)
Quantum mechanical calculation of harmonic oscillator transition probabilities in a one-dimensional impulsive collision, Kurt E. Shuler and Robert Zwanzig—1777
Quantum yield for energy transfer by resonance, Aadne Ore—31
Transfer of excitation energy in solid solutions of anthracene-polystyrene and 9,10-diphenylanthracene-polystyrene, L. J. Basile and A. Weinreb—1028
Vibrational transitions and the intermolecular potential, Robert C. Amme and Sam Legvold—91

Equation of State

Errata: Contributions of bound, metastable, and free molecules to the second virial coefficient and some properties of double molecules, and Initial pressure dependence of thermal conductivity and viscosity [J. Chem. Phys. **31**, 1531, 1545 (1959)] Daniel E. Stogryn and Joseph O. Hirschfelder—942(L)

Errata

Errata: Contributions of bound, metastable, and free molecules to the second virial coefficient and some properties of double molecules, and Initial pressure dependence of thermal conductivity and viscosity [J. Chem. Phys. **31**, 1531, 1545 (1959)] Daniel E. Stogryn and Joseph O. Hirschfelder—942(L)
Erratum: Electrical properties of poly-copper phthalocyanine [J. Chem. Phys. **32**, 324 (1960)] A, Epstein and B. S. Wildi—618(L)
Erratum: Electronic structure of nitric oxide [J. Chem. Phys. **30**, 673 (1959)], H. Brion, C. Moser and M. Yamazaki—1871 (L)
Erratum: Energy levels of a slightly asymmetric top [J. Chem. Phys. **32**, 1591 (1960)], James A. Norris and Victor W. Laurie—1256(L)
Erratum: f^2 configuration in a crystalline field [J. Chem. Phys. **32**, 573 (1960)], Robert A. Satten and Jack S. Margolis—618(L)
Erratum: Improved molecular orbitals and the valence bond theory [J. Chem. Phys. **33**, 301 (1960)], A. C. Hurley—1872(L)
Erratum: Infrared and raman spectra of fluorinated ethanes. XII. 1,1,2,2-tetrafluoroethane [J. Chem. Phys. **32**, 899 (1960)], Peter Klaboe and J. Rud Nielsen—617(L)
Erratum: Lattice energies of the alkali halides and the electron affinities of the halogens [J. Chem. Phys. **31**, 1646 (1959)], Daniel Cubicciotti—1579(L)
Erratum: Mechanics of atomic recombination reactions, Don L. Bunker [J. Chem. Phys. **32**, 1001 (1960)]—617(L)
Erratum: Microwave spectrum of acetyl cyanide [J. Chem. Phys. **31**, 882 (1959)], Lawrence C. Krisher—304(L)
Erratum: NMR spectra of some simple epoxides [J. Chem. Phys. **32**, 1378 (1960)], C. A. Reilly and J. D. Swalen—617(L)
Erratum: Reflected shock technique for studying fast chemical reactions, [J. Chem. Phys. **30**, 257 (1959)] Roger A. Strehlow and Arthur Cohen—618
Erratum: Some observations on atomic exchange in NO [J. Chem. Phys. **32**, 1579 (1960)], W. Spindel and Marvin J. Stern—942(L)
Erratum: Validity and consequences of Schreinemakers' theorem on ternary distillation lines [J. Chem. Phys. **31**, 308 (1959)], A. E. Korvezee and J. L. Meyering—304(L)
Erratum and Addendum: Substituted methanes. XXIX. Vibrational spectra, potential constants, and calculated thermodynamic properties for dibromochlorofluoromethane and bromodichlorofluoromethane [J. Chem. Phys. **31**, 1633 (1959)], Robert L. Gilbert, Edward A. Piotrowski, Jerome M. Dowling, and Forrest F. Cleveland—1872(L)

Faraday Effect

Magnetic rotation spectra of nitric oxide in the near infrared, Glen A. Mann and C. D. Hause—1117

Field Emission Microscopy

Observation of adsorption on an atomic scale, Gert Ehrlich and F. G. Hudda—1253(L)

Films (see Surface Phenomena)

Flames

Nitric oxide—fluorine dilute diffusion flame, Donald Rapp and Harold S. Johnston—695

Fluorescence

Charge transfer and fluorescence quenching, Dilip Kumar Majumdar and Sadhan Basu—1199
Efficiency of energy transfer in a solution of *PPO* in xylene, Isadore B. Berlman—1124
Transfer of excitation energy in solid solutions of anthracene-polystyrene and 9,10-diphenylanthracene-polystyrene, L. J. Basile and A. Weinreb—1028
Vibrational effect on the polarization of molecular crystal fluorescence, E. G. McRae—932(L)

Free Radicals

Behavior of the free radicals trapped in gamma-irradiated compounds which contain hydrogen bonds, Zenichiro Kuri, Yuzuru Fujiwara, Hisashi Ueda and Shoji Shida—1884(L)
Collisional deactivation of vibrationally excited *sec*-butyl-d_1 radicals produced by chemical activation, R. E. Harrington, B. S. Rabinovitch and M. R. Hoare—744
Decomposition of activated *sec*-butyl radicals from different sources and unimolecular reaction theory, R. E. Harrington, B. S. Rabinovitch and H. M. Frey—1271(L)
Electron spin resonance of electrochemically generated free radicals: The isomeric dinitrobenzene mononegative ions, August H. Maki and David H. Geske—825
EPR observation of the steady-state ethyl radical concentration in the radiolysis of liquid ethane, Richard W. Fessenden and Robert H. Schuler—935(L)
EPR studies of the tetracyanoethylene anion radical, W. D. Phillips, J. C. Rowell, and S. I. Weissman—626(L)
Flash-absorption spectroscopy of free radicals in shock waves, R. M. Ikeda—311(L)
Light-induced *cis-trans* isomerization of nitrous acid formed by photolysis of hydrazoic acid and oxygen in solid nitrogen, John D. Baldeschwieler and George C. Pimentel—1008

Method for investigating the order of chemiluminescent reactions, the diffusion coefficient of the labile reactants, and the catalytic efficiency of surfaces, Robert A. Young—1044
Methyl affinitites determined by photolysis of azomethane, C. Steel and M. Szwarc—1677
On the isomerization of *n*-butyl radicals, Alvin S. Gordon and James R. McNesby—1882(L)
Orientation dependence of magnetic hyperfine structure in free radicals, S. M. Blinder—748
Paramagnetic resonance absorption of triphenylmethyl, D. B. Chesnut and G. J. Sloan—637(L)
Paramagnetic-resonance studies of irradiated high-density polyethylene. I. Radical species and the effect of environment on their behavior, Elliott J. Lawton, J. S. Balwit, and R. S. Powell—395
Paramagnetic-resonance studies of irradiated high-density polyethylene. II. The effect of irradiation dose on the radical species trapped at room temperature, Elliott J. Lawton, J. S. Balwit, and R. S. Powell—405
Polycrystalline resonance line shape of π-electron radicals, Himan Sternlicht—1128
Quantum yield for energy transfer by resonance, Aadne Ore—31
Relation between the proton hyperfine interaction and the C^{13}-H^1 spin-spin coupling in free radicals, R. A. Bernheim and T. P. Das—1813
Spin densities in organic free radicals, Thomas H. Brown, D. H. Anderson, and H. S. Gutowsky—720

Free Rotation (see Rotation)

Gases

Dielectric constants of imperfect gases. I. Helium, argon, nitrogen, and methane, D. R. Johnston, G. J. Oudemans, and R. H. Cole—1310
Errata: Contributions of bound, metastable, and free molecules to the second virial coefficient and some properties of double molecules, and Initial pressure dependence of thermal conductivity and viscosity [J. Chem. Phys. **31**, 1531, 1545 (1959)] Daniel E. Stogryn and Joseph O. Hirschfelder—942(L)
Kinetic theory of dense gases, Henry B. Hollinger and C. F. Curtiss—1386
Potential curves for N_2, NO, and O_2, Joseph T. Vanderslice, Edward A. Mason, William G. Maisch and Ellis R. Lippincott—614(L)
Separation of gas mixtures in a supersonic jet. II. Behavior of helium-argon mixtures and evidence of shock separation, S. Alexander Stern, P. C. Waterman, and T. F. Sinclair—805
Statistical mechanics of the non-uniform gas, P. L. Auer and S. Tamor—1426

Glasses

Condensation coefficient of arsenic trioxide glass, A. B. Bestul and D. H. Blackburn—1274 (L)
Structure of glass-forming halides. II. Liquid zinc chloride, J. D. Mackenzie and W. K. Murphy—366

Heat Capacity (see Thermodynamic Properties)

Lattice heat capacity of the rare earths. The heat capacities of yttrium and lutetium from 15–350°K, L. D. Jennings, R. E. Miller and F. H. Spedding—1849

High Pressures

Comparison of the effects of high pressure and low temperature on the absorption spectra of some condensed-ring aromatics, W. W. Robertson—362
Compression and phase transitions of solid NH_3, SiF_4, H_2S, and CF_4, John W. Stewart—128
Effect of pressure on the *M* center in alkali halide crystals, S. Minomura and H. G. Drickamer—290
Effects of pressure on dielectric relaxation in a chlorinated diphenyl, Thomas A. Perls and L. Bruce Wilner—753
Effects of pressure on proton spin-lattice relaxation in several degassed organic liquids, A. W. Nolle and P. P. Mahendroo—863
First-order phase transitions of six normal paraffins at elevated pressures, R. R. Nelson, W. Webb, and J. A. Dixon—1755
Pressure effects in nickel dimethylglyoxime and related chelates, J. C. Zahner and H. G. Drickamer—1625

Hindered Rotation (see Rotation)

Energy levels of a slightly asymmetric top, John E. Beam and H. L. Davis—1255(L)
Erratum: Energy levels of a slightly asymmetric top [J. Chem. Phys. **32**, 1591 (1960)], James A. Norris and Victor W. Laurie—1256(L)

Infrared Spectra (see Absorption Spectra)

Calculated band intensities for CO_2 from infrared dispersion data, Bertram Schurin—1878(L)
Potential energy curves for OH, Robert J. Fallon, Irwin Tobias and Joseph T. Vanderslice—1638
Vibrational spectra of orthorhombic metaboric acid, J. L. Parsons—1860

Intensities of Spectra

Calculated band intensities for CO_2 from infrared dispersion data, Bertram Schurin—1878(L)
Effect of hydrogen bonding on the intensity of the CD raman band of $CDCl_3$, D. G. Rea—1875(L)
"Forbidden" character in allowed electronic transitions, Andreas C. Albrecht—156
Infrared studies of crystal benzene. II. Relative intensities, Charles A. Swenson and Willis B. Person—56
Infrared studies of crystal benzene. IV. Absolute intensities, Willis B. Person and Charles A. Swenson—233
Polarized visible spectra of crystalline trisoxalatometallates: The source of intensity. T. S. Piper and R. L. Carlin—608(L)
Radiative lifetime of the $B\,^2\Sigma^+$ state in N_2O^+, I. E. Dayton, F. W. Dalby, and R. G. Bennett—179

Isotope Effects

Calculation of equilibrium constants for several isotope exchange reactions involving N_2O_4, E. U. Monse—312(L)
Comment on the homogeneous exchange reaction between hydrogen and deuterium, A. Cimino, E. Molinari, and G. G. Volpi—616(L)
Effect of deuterium substitution on the lifetime of the phosphorescent triplet state of naphthalene, H. Sternlicht and H. M. McConnell—302(L)
Equilibrium constant for isotope exchange in ammonia from infrared spectra, Llewellyn H. Jones—1585(L)
Equilibrium in the exchange of tritium between ammonia and hydrogen and the zero-point energy difference between NH_3 and NH_2T, Joel R. Gutmann and Max Wolfsberg—1592(L)
Erratum: Some observations on atomic exchange in NO [J. Chem. Phys. **32**, 1579 (1960)], W. Spindel and Marvin J. Stern—942(L)
Flow adaptation of the isotopic dilution method for the study of ionic hydration, H. W. Baldwin and H. Taube—206

Isotope (continued)

Increasing the intensity of C^{13} NMR signals by a flowing sample method, S. Forsén and A. Rupprecht—1888(L)
Isotope effects on reaction rates and the reaction coordinate, Max Wolfsberg—21
Nonmolecular nature of the nitric-oxide-inhibited thermal decomposition of *n*-butane, Aron Kuppermann and John G. Larson—1264(L)
Note on secondary isotope effects in reaction rates, Max Wolfsberg—2
Partition function ratios for molecules containing nitrogen isotopes, G. M. Begun and W. H. Fletcher—1083
Phosphorescence lifetime of benzene. An intermolecular heavy atom effect, a deuterium effect, and a temperature effect, M. R. Wright, R. P. Frosch and G. W. Robinson—934(L)
Physical properties of isotopically substituted classical fluids, W. A. Steele—1619
Relative quenching cross sections in the reaction of $Hg(6^3P_1)$ atoms with isotopic N_2O molecules, Morton Z. Hoffman and Richard B. Bernstein—526
Separation of boron isotopes. IV. The methyl sulfide-BF_3 system, A. A. Palko and J. S. Drury—779
Single-state fractionation factor for the system: Oxygen vs cobalt di(salicylal)-ethylenediimine-oxygen, L. L. Brown and J. S. Drury—1889(L)
Size effects among isotopic molecules, Hubert W. Joy and W. F. Libby—1276(L)
Spin exchange in biradicals, D. C. Reitz and S. I. Weissman—700
Trimethylene oxide I. Microwave spectrum, dipole moment, and double minimum vibration, Sunney I. Chan, John Zinn, Jose Fernandez, and William D. Gwinn—1643
Vapor pressures and related thermodynamic properties of the isotopic nitric oxide molecules, Jacob Bigeleisen—1774

Kinetics of Reaction

Boltzmann equation and inverse collisions, J. T. O'Toole and J. S. Dahler—1487
Charge transfer between atomic hydrogen and N^+ and O^+, R. F. Stebbings, Wade L. Fite, and David G. Hummer—1226
Collisional deactivation of vibrationally excited *sec*-butyl-d_1 radicals produced by chemical activation, R. E. Harrington, B. S. Rabinovitch and M. R. Hoare—744
Comment on the homogeneous exchange reaction between hydrogen and deuterium, A. Cimino, E. Molinari, and G. G. Volpi—616(L)
Decomposition of activated *sec*-butyl radicals from different sources and unimolecular reaction theory, R. E. Harrington, B. S. Rabinovitch and H. M. Frey—1271(L)
Detection of order in Ni_3Co, Y. L. Yao—741
Diffusion theory of chemical reaction, J. L. Wood—1587(L)
Erratum: Mechanics of atomic recombination reactions, Don L. Bunker [J. Chem. Phys. **32**, 1001 (1960)]—617(L)
Erratum: Reflected shock technique for studying fast chemical reactions, [J. Chem. Phys. **30**, 257 (1959)] Roger A. Strehlow and Arthur Cohen—618(L)
Interchange of charge between gaseous molecules, Donald Rapp and Irene B. Ortenburger—1230
Isotope effects on reaction rates and the reaction coordinate, Max Wolfsberg—21
Kinetic absorption spectra recorded through flash-heated grids, L. S. Nelson and N. A. Kuebler—610(L)
Kinetics of the alpha radiolysis of carbon monoxide, P. S. Rudolph and S. C. Lind—705
Mechanism of ozone decomposition, H. J. Schumacher—938(L)
Mercury photosensitized decomposition of cylohexane at high temperatures, S. Arai, S. Sato and S. Shida—1277(L)
Metastable states of acridine orange in solution, G. Blauer and H. Linschitz—937(L)
Method for investigating the order of chemiluminescent reactions, the diffusion coefficient of the labile reactants, and the catalytic efficiency of surfaces, Robert A. Young—1044
Methyl affinities determined by photolysis of azomethane, C. Steel and M. Szwarc—1677
Nitric oxide—fluorine dilute diffusion flame, Donald Rapp and Harold S. Johnston—695
Non-molecular nature of the nitric-oxide-inhibited thermal decomposition of *n*-butane, Aron Kuppermann and John G. Larson—1264(L)
Note on secondary isotope effects in reaction rates, Max Wolfsberg—2
Nuclear spin conservation in ortho-para hydrogen conversion, Doyle Britton and Z Z. Hugus, Jr.—1830
On the dissociation of polyatomic molecules, Robert J. Rubin and Kurt E. Shuler—438
On the existence of energy chains in the ozone decomposition, Sidney W. Benson—939(L)
On the isomerization of *n*-butyl radicals, Alvin S. Gordon and James R. McNesby—1882(L)
Proton transfer studies by nuclear magnetic resonance. I. Diffusion control in the reaction of ammonium ion in aqueous acid, Merle T. Emerson, Ernest Grunwald, and Robert A. Kromhout—547
Proton transfer studies by nuclear magnetic resonance. II. Rate constants and mechanism for the reaction, $CH_3NH_3^+ + OH_2 + NH_2CH_3$, in aqueous acid, Ernest Grunwald, Photios J. Karabatsos, Robert A. Kromhout and E. Lee Purlee—556
Quantum statistical mechanical theory of the rate of exchange chemical reactions in the gas phase, Tsunenobu Yamamoto—281
Rate of the reaction of nitrogen atoms with ethylene, John T. Herron—1273(L)
Recombination kinetics of atomic oxygen at room temperature, C. B. Krestchmer and H. L. Petersen—948(L)
Recombination of oxygen atoms in the absence of O_2, J. E. Morgan, L. Elias and H. I. Schiff—930(L)
Relative quenching cross sections in the reaction of $Hg(6^3P_1)$ atoms with isotopic N_2O molecules, Morton Z. Hoffman and Richard B. Bernstein—526
Sublimation of small sodium chloride spheres into argon, D. H. Whitmore and J. B. Moser—917
Temperature dependence of the rates of addition of oxygen atoms to olefins, R. J. Cvetanović—1063
Three-body recombination of oxygen atoms, Ernest Bauer and Morris Salkoff—1202
Transient species in the radiolytic polymerization of cyanogen, C. E. Melton and P. S. Rudolph—1594(L)

Light Scattering

Critical opalescence of polystyrene in cyclohexane, P. Debye, H. Coll, and D. Woermann—1745

Liquids

Cell method in the grand canonical ensemble, J. M. Richardson and S. R. Brinkley, Jr.—1467
Classical and quantum mechanical hypervirial theorems, Joseph O. Hirschfelder—1462
Dielectric relaxation of polar liquids, Sivert H. Glarum—1371
Line shapes of electron paramagnetic resonance signals produced by powders, glasses and viscous liquids, Fritz Kurt Kneubühl—1074

Nuclear magnetic relaxation in a strongly associated liquid, C.R.K. Murthy and R. D. Spence—945(L)
On the theory of the critical point of a simple fluid, Melville S. Green—1403
Physical properties of isotopically substituted classical fluids, W. A. Steele—1619
Radial distribution functions from the Born-Green integral equation, A. A. Broyles—456
Scaled particle theory of fluids, E. Helfand, H. Reiss, H. L. Frisch and J. L. Lebowitz—1379
Some tests of the superposition approximation in the liquid phase, Frank P. Buff and R. Brout—1417
Structure of glass-forming halides, II. Liquid zinc chloride, J. D. Mackenzie and W. K. Murphy—366
X-ray scattering by a cell-model liquid, L. H. Lund—1086

Magnetic Resonance

Analysis of high-resolution NMR spectra by iterative methods, Ragnar A. Hoffman—1256(L)
"Average energy approximation" in spin-coupling calculations, Martin Karplus—941(L)
Biradical paradox, Harden M. McConnell—1868(L)
Carbon-13 hyperfine splittings in semiquinones, D. C. Reitz, F. Dravnieks, and J. E. Wertz—1880(L)
Cl^{35} NMR contact shifts in aqueous cobaltous chloride solutions, D. B. Chesnut—1234
Conduction electrons in sodium tungsten bronze, Joseph M. Keller—232
Effect of deuterium substitution on the lifetime of the phosphorescent triplet state of naphthalene, H. Sternlicht and H. M. McConnell—302(L)
Effect of thermal treatment on paramagnetic resonance spectra of rare earth impurities in calcium fluoride, E. Friedman and W. Low—1275(L)
Effects of pressure on proton spin-lattice relaxation in several degassed organic liquids, A. W. Nolle and P. P. Mahendroo—863
Electron coupling of nuclear spins. IV. Temperature dependence in substitutes ethanes, John C. Schug, Paul E. McMahon, and H. S. Gutowsky—843
Electron spin resonance in neutron-irradicated calcite, J. C. Kemp—1269(L)
Electron spin resonance line shape of a polycrystalline CH radical, Roland Lefebvre—1826
Electron spin resonance of an irradiated single crystal of N-acetylglycine, Ichiro Miyagawa, Yukio Kurita, and Walter Gordy—1599
Electron spin resonance of electrochemically generated free radicals: The isomeric dinitrobenzene mononegative ions, August H. Maki and David H. Geske—825
Electron spin resonances in irradiated potassium azide, A. J. Shuskus, C. G. Young, O. R. Gilliam, and Paul W. Levy—622(L)
EPR observation of the steady-state ethyl radical concentration in the radiolysis of liquid ethane, Richard W. Fessenden and Robert H. Schuler—935(L)
EPR studies of the tetracyanoethylene anion radical, W. D. Phillips, J. C. Rowell, and S. I. Weissman—626(L)
Erratum: NMR Spectra of some simple epoxides [J. Chem. Phys. **32**, 1378 (1960)], C. A. Reilly and J. D. Swalen—617(L)
F^{19} spectra of phosphorus (V) fluorides, W. Mahler and E. L. Muetterties—636(L)
Green and purple sulphur: Electron spin resonance studies, H. E. Radford and F. O. Rice—774
H^1-P^{31} spin coupling in phosphate esters, Gerald O. Dudek—624(L)
Identification of colloidal sodium in sodium azide, Brian S. Miller—889
Increasing the intensity of C^{13} NMR signals by a flowing sample method, S. Forsén and A. Rupprecht—1888(L)
Ligand spin densities and magnetic properties of some aminotroponeimine chelates of nickel, W. D. Phillips and R. E. Benson—607(L)
Line shapes of electron paramagnetic resonance signals produced by powders, glasses and viscous liquids, Fritz Kurt Kneubühl—1074
N^{14} pure quadrupole resonances of several nitriles, Hisao Negita and P. J. Bray—1876(L)
Nuclear magnetic relaxation in a strongly associated liquid, C.R.K. Murthy and R. D. Spence—945(L)
NMR analysis of CF_3CF_2CFICl: Example of an unexpected spin-coupling constant, L. M. Crapo and C. H. Sederholm—1583(L)
Nuclear magnetic resonance in solid adamantane, David W. McCall and Dean C. Douglas—777
Nuclear magnetic resonance spectra of systems of the A_3B_2C type: Proton magnetic resonance spectra and the absolute signs of the proton-proton spin coupling constants in ethyl acetylene and ethyl mercaptan, P. T. Narasimhan and Max T. Rogers—727
Nuclear magnetic resonance spectra of the ABX_3 type: Field dependence and the relative signs of spin-spin coupling constants, Valdemar J. Kowalewski and Dora G. de Kowalewski—1793
Nuclear magnetic resonance spectrum of B^{11} in inderite, K. S. Pennington and H. E. Petch—329
Nuclear spin-lattice relaxation in solutions, Richard W. Mitchell and Melvin Eisner—86
Observation of the overhauser effect on carbon-13 nuclear resonance signals, D. J. Parker, G. A. McLaren and J. J. Conradi—629(L)
On the analysis of high-resolution NMR spectra by iterative methods, C. A. Reilly and J. D. Swalen—1257(L)
Orientation dependence of magnetic hyperfine structure in free radicals, S. M. Blinder—748
Paramagnetic relaxation in solutions of VO^{++}, R. N. Rogers and G. E. Pake—1107
Paramagnetic-resonance absorption of ions with spin $\frac{5}{2}$; Mn^{++} in calcite, Chihiro Kikuchi and L. M. Matarrese—601
Paramagnetic resonance absorption of triphenylmethyl, D. B. Chesnut and G. J. Sloan—637(L)
Paramagnetic resonance of gamma-irradiated single crystals of ice at 77°K, J. A. McMillan, M. S. Matheson and B. Smaller—609(L)
Paramagnetic-resonance studies of irradiated high-density polyethylene. I. Radical species and the effect of environment on their behavior, Elliott J. Lawton, J. S. Balwit, and R. S. Powell—395
Paramagnetic-resonance studies of irradiated high-density polyethylene II. The effect of irradiation dose on the radical species trapped at room temperature, Elliott J. Lawton, J. S. Balwit, and R. S. Powell—405
Paramagnetic resonance study of hyperfine interactions in single crystals containing α, α-diphenyl-β-picrylhydrazyl, Robert W. Holmberg, Ralph Livingston, and William T. Smith, Jr.—541
Paramagnetic studies of radiation damage in silica gel, Harold W. Kohn—1588(L)
Polycrystalline resonance line shape of π-electron radicals, Himan Sternlicht—1128
Proton magnetic resonance studies of nonstoichiometric titanium hydride, B. Stalinski, C. K. Coogan, and H. S. Gutowsky—933(L)
Proton magnetic resonance study of barium bromate monohydrate, A. A. Silvidi and J. W. McGrath—1788

Magnetic Resonance (continued)

Proton magnetic resonance study of barium bromide monohydrate, J. W. McGrath and A. A. Silvidi—644
Proton resonance in diphenyl picryl hydrazyl, M. E. Anderson, G. E. Pake and T. R. Tuttle, Jr.—1581(L)
Proton resonance shifts in pyrene mononegative ion at 4.2°K, M. E. Anderson, P. J. Zandstra and T. R. Tuttle, Jr.—1591(L)
Proton spin coupling by pi electrons, Martin Karplus—1842
Proton transfer studies by nuclear magnetic resonance. I. Diffusion control in the reaction of ammonium ion in aqueous acid, Merle T. Emerson, Ernest Grunwald, and Robert A. Kromhout—547
Proton transfer studies by nuclear magnetic resonance. II. Rate constants and mechanism for the reaction, $CH_3NH_3^+ + OH_2 + NH_2CH_2$, in aqueous acid, Ernest Grunwald, Photios J. Karabatsos, Robert A. Kromhout and E. Lee Purlee—556
Relation between the proton hyperfine interaction and the C^{13}-H^1 spin-spin coupling in free radicals, R. A. Bernheim and T. P. Das—1813
Satellite lines in paramagnetic resonance spectra, A. van Roggen—1589(L)
Spin densities in organic free radicals, Thomas H. Brown, D. H. Anderson, and H. S. Gutowsky—720
Spin exchange in biradicals, D. C. Reitz and S. I. Weissman—700
Temperature dependence of proton relaxation times in aqueous solution of paramagnetic ions. II. $CrCl_3$, Thomas H. Brown, Robert A. Bernheim, and H. S. Gutowsky—1593(L)
Theory of ESR linewidths of free radicals, Daniel Kivelson—1094
Theory of hyperfine interactions in aromatic radicals, A. D. McLachlan, H. H. Dearman, and R. Lefebvre—65
Theory of singlet-triplet splittings in large biradicals, Harden M. McConnell—115
Variational calculation of magnetic hyperfine interaction. Nitrogen atom, T. P. Das and A. Mukherjee—1808

Magnetic Susceptibilities

Antiferromagnetic coupling and covalent bonding in almost totally ionic alts, Thomas R. Waite—256
Diamagnetism as a test of wave functions for some simple molecules, K. E. Banyard—832
Hyperfine structure of F-center spin resonance in sodium azide, F. F. Carlson, G. J. King, and B. S. Miller—1266(L)
Quantum mechanical approximations to chemical systems, R. E. Glick and D. F. Kates—308(L)

Mass Spectra

Charge transfer reactions producing intrinsic chemical change: Methyl, methylene, and hydrogen radicals produced from argon and methane reactions, C. E. Melton—647
Dissociation of methyl bromide by nuclear isomeric transition of 4.4-hr Br^{80m}, S. Wexler and G. R. Anderson—850
Excitation and negative ions in H_2O, G. J. Schulz—1661
Fragmentation patterns of halogenated pentaboranes, I. Shapiro and H. Landesman—1590(L)
Heterogeneous reactions studied by mass spectrometry. I. The reaction of B_2O_3(s) with H_2O(g), David H. Meschi, William A. Chupka, and Joseph Berkowitz—530
Heterogeneous reactions studied by mass spectrometry. II. The reaction of Li_2O(s) with H_2O(g), Joseph Berkowitz, David J. Meschi, and William A. Chupka—533
Ionization of Cu, Ag, and Au by electron impact, Normand C. Blais and Joseph B. Mann—100
Mass spectra of aluminum (III) halides and the heats of dissociation of Al_2F_6(g) and $LiF \cdot AlF_3$(g), Richard F. Porter and Ernest Zeller—858
Mass spectra of vapors in the Al-AlF_3 and Al-LiF-AlF_3 systems, Richard F. Porter—951(L)
Mass spectrometric and infrared emission investigation of the vapor species in the B-S system at elevated temperatures, Armin Sommer, Patrick N. Walsh, and David White—296(L)
Mass spectrometric determination of the dissociation energies of the molecules AgAu, AgCu and AuCu, Marcel Ackerman, Fred E. Stafford and Jean Drowart—1783
Mass spectrometric study of the heats of dimerization of the alkali chlorides, Thomas A. Milne and H. Michael Klein—1628
Mass spectrometric study of the osmium-oxygen system, R. T. Grimley, R. P. Burns, and Mark G. Inghram—308(L)
Mass spectrum and appearance potentials of tetrafluorohydrazine, John T. Herron and Vernon H. Dibeler—1595(L)
Multiple ionization in argon and krypton by electron impact, R. E. Fox—200
Quantitative relations in the mass spectra of *n*-paraffins, Norman D. Coggeshall—1247
Secondary positive ion-emission from platinum, R. C. Bradley, A. Arking and D. S. Beers—764
Secondary reactions in a gas discharge, Irene B. Ortenburger, Martin Hertzberg and Richard A. Ogg, Jr.—579
Strength of the N—N bond in tetrafluorohydrazine, Charles B. Colburn and Frederic A. Johnson—1869(L)
Threshold law for the probability of excitation of molecules by photon impact. A study of the photoionization efficiencies of Br_2, I_2, HI, and CH_3I, H. D. Morrison, H. Hurzeler, Mark G. Inghram and H. E. Stanton—821

Mechanics, Classical

Classical and quantum mechanical hypervirial theorems, Joseph O. Hirschfelder—1462

Mechanics, Quantum

Ambiguity in the determination of self-consistent bond orders, G. G. Hall—953(L)
Antiferromagnetic coupling and covalent bonding in almost totally ionic salts, Thomas R. Waite—256
Approximate electronic energy surfaces from cuspless wave functions, Carl E. Wulfman—1567
"Average energy approximations" in spin-coupling calculations, Martin Karplus—941(L)
Axial crystal fields in the ionic model, T. S. Piper and R. L. Carlin—1208
Biradical paradox, Harden M. McConnell—1868(L)
Concise method for forming two-center integrals of operators, J. M. Robinson—734
Diamagnetism as a test of wave functions for some simple molecules, K. E. Banyard—832
Dynamical Jahn-Teller effect in hydrocarbon radicals, W. D. Hobey and A. D. McLachlan—1694
Dynamics of the quasi-linear molecule, Walter H. Thorson and Ichiro Nakagawa—994
Electronic spectra of dimers: Derivation of the fundamental vibronic equation, Andrzej Witkowski and William Moffitt—872
Electronic structure and hyperfine structure constants of NO molecule, Chun C. Lin, Katsunori Hijikata, and Michiko Sakamoto—878
Energy of interaction of two helium atoms, Neal Moore—471
Erratum: Electronic structure of nitric oxide [J. Chem. Phys. **30**, 673 (1959)], H. Brion, C. Moser and M. Yamazaki—1871(L)
Erratum: f^2 configuration in a crystalline field [J. Chem. Phys. **32**, 573 (1960)], Robert A. Satten and Jack S. Margolis—618(L)

Erratum: Improved molecular orbitals and the valence bond theory [J. Chem. Phys. **33**, 301 (1960)], A. C. Hurley—1872(L)
Erratum: Potential energy curves for HF and LiH [J. Chem. Phys. **32**, 698, 1453 (1960)], Robert J. Fallon, Joseph T. Vanderslice and Edward A. Mason—944(L)
First excited $^1\Sigma_g^+$ state of H_2: A double-minimum problem, Ernest R. Davidson—1577(L)
Forces in molecules. I. Application of the virial theorem, William L. Clinton—1603
Helium atom wave function from Slater orbitals of nonintegral principal quantum number, Lawrence C. Snyder—1710
Improved molecular orbitals and the valence bond theory, A. C. Hurley—301(L)
Interaction energies for the H-H_2 and H_2-H_2 systems, Joseph T. Vanderslice and Edward A. Mason—492
Inter and intra-atomic correlation energies and theory of core-polarization, Oktay Sinanoglu—1212
Intermolecular coupling of vibrations in molecular crystals: A vibrational exciton approach, R. M. Hexter—1833
Jahn-Teller distortions in cyclobutadiene cyclopentadienyl radical, and benzene positive and negative ions, Lawrence C. Snyder—619(L)
Metal-metal bonding in dicobalt hexacarbonyl diphenylacetylene, David A. Brown—1037
Modification of Koopmans' theorem for conjugated hydrocarbons, J. R. Hoyland and Lionel Goodman—946(L)
Molecular orbital treatment of hydrogen with central potentials and modified boundary conditions, James M. Peek and Edwin N. Lassettre—1803
Note on Hurley's "Improved molecular orbitals and the valence bond theory," P. Phillipson and R. S. Mulliken—615(L)
On excited bound states of negative atomic ions, E. Holøien—310(L)
One-center wave function for the methane molecule, Anthony F. Saturno and Robert G. Parr—22
$^1\Sigma^+$ excited states of carbon monoxide, H. Lefebvre-Brion, C. M. Moser and R. K. Nesbet—931(L)
Optical rotatory dispersion of transition-metal complexes, Satoru Sugano—1885(L)
Potential curves for N_2, NO, and O_2, Joseph T. Vanderslice, Edward A. Mason, William G. Maisch and Ellis R. Lippincott—614(L)
Potential energy curves for CO, Irwin Tobias, Robert J. Fallon, and Joseph T. Vanderslice—1638
Power series expansions of vibrational potentials. I. The Heitler-London potential for H_2, Charles L. Beckel—1885(L)
Power series expansions of vibrational potentials. II. Two classical potentials for ionic molecules, Edward J. Finn and Charles L. Beckel—1887(L)
Proton spin coupling by pi electrons, Martin Karplus—1842
Quantum mechanical approximations to chemical systems, R. E. Glick and D. F. Kates—308(L)
Quantum mechanical calculation of harmonic oscillator transition probabilities in a one-dimensional impulsive collision, Kurt E. Shuler and Robert Zwanzig—1777
Quantum mechanical (phase shift) analysis of the differential elastic scattering of molecular beams, Richard B. Bernstein—795
Relation between the proton hyperfine interaction and the C^{13}-H^1 spin-spin coupling in free radicals, R. A. Bernheim and T. P. Das—1813
Second-order perturbation energy of the two-electron atom, Charles W. Scherr—317(L)
Separation theorem for degenerate eigenvalues, D. W. Davies—781
Simple configuration interaction wavefunctions. III. The three-electron atomic system. An analytic study, Milos Machacek and Charles W. Scherr—242
Some intra-atomic correlation correction studies, M. Krauss and B. J. Ransil—840
Spin densities in several odd alternant radicals, H. H. Dearman and H. M. McConnell—1877(L)
Study of molecular integrals I. The two-center exchange integrals, R. C. Sahni and C. D. LaBudde—1015
Study of molecular integrals II. The three-center one electron and two-electron integrals, C. D. LaBudde and R. C. Sahni—1022
Sum rule for transition probabilities, William L. Clinton—1603
Theorem on separability of electron pairs, Tadashi Arai—95
Theory of hyperfine interactions in aromatic radicals, A. D. McLachlan, H. H. Dearman, and R. Lefebvre—65
Theory of singlet-triplet splittings in large biradicals, Harden M. McConnell—115
Three-body recombination of oxygen atoms, Ernest Bauer and Morris Salkoff—1202
Three remarks on molecular orbital theory of complex molecules, Robert G. Parr—1183
Ultraviolet spectrum of triptycene, Charles F. Wilcox, Jr.—1874(L)
Variational calculation of magnetic hyperfine interaction. Nitrogen atom, T. P. Das and A. Mukherjee—1808

Mechanics, Statistical

Boltzmann equation and inverse collisions, J. T. O'Toole and J. S. Dahler—1487
Cell method in the grand canonical ensemble, J. M. Richardson and S. R. Brinkley, Jr.—1467
Classical and quantum mechanical hypervirial theorems, Joseph O. Hirschfelder—1462
Contribution of lattice vibrations to the order-disorder transformation in alloys, Peter J. Wojtowicz and John G. Kirkwood—1298
Density correlations, critical opalescence, and the free energy of non-uniform fluids, Marshall Fixman—1357
Distribution functions of a fluid in an external potential field; Application to physical adsorption, William S. Steele and Marvin Ross—464
Ensemble method in the theory of irreversibility, Robert Zwanzig—1338
Ensembles of maximum entropy, Joseph E. Mayer—1484
Errata: Contributions of bound, metastable, and free molecules to the second virial coefficient and some properties of double molecules, and Initial pressure dependence of thermal conductivity and viscosity [J. Chem. Phys. **31**, 1531, 1545 (1959)] Daniel E. Stogryn and Joseph O. Hirschfelder—942(L)
Excluded volume effect of linear polymer molecules, Michio Kurata, Walter H. Stockmayer, and Antonio Roig—151
Kinetic theory of dense gases, Henry B. Hollinger and C. F. Curtiss—1386
Kinetic theory of the moderately dense rigid sphere fluid. IV. The fluxes of matter, momentum and energy in a mixture, Robert A. Harris and Stuart A. Rice—1046
Kinetic theory of the moderately dense rigid-sphere fluid. V. Relaxation in momentum space, Robert A. Harris and Stuart A. Rice—1055
Mean square length of a hindered alkane chain, Richard P. Smith—876
Molecular friction in dilute gases, James T. O'Toole and John S. Dahler—1496
New solution of the Ising problem for a rectangular lattice, C. A. Hurst and H. S. Green—1059
On molecular chaos and the Kirkwood superposition hypothesis, Harold Grad—1342
On the dynamical theory of diffusion in crystals. V. A random-walk treatment of the heat of transport, Alan R. Allnatt and Stuart A. Rice—573

Mechanics, Statistical (continued)

On the theory of the critical point of a simple fluid, Melville S. Green—1403
Open first-order stochastic processes, Paul J. Gans—691
Potential curves for N_2, NO, and O_2, Joseph T. Vanderslice, Edward A. Mason, William G. Maisch and Ellis R. Lippincott—614(L)
Quantum corrections for transport coefficients, Sang-Il Choi and John Ross—1324
Quantum statistical mechanical theory of the rate of exchange chemical reactions in the gas phase, Tsunenobu Yamamoto—281
Radial distribution functions from the Born-Green integral equation, A. A. Broyles—456
Scaled particle theory of fluids, E. Helfand, H. Reiss, H. L. Frisch and J. L. Lebowitz—1379
Some further remarks on the coefficient of self-diffusion in simple dense fluids, Stuart A. Rice—1376
Some tests of the superposition approximation in the liquid phase, Frank P. Buff and R. Brout—1417
Statistical mechanical theory of the viscosity coefficients of binary liquid solutions, Richard J. Bearman and Peter F. Jones—1432
Statistical mechanics of molecular ions, Robert N. Varney—1708
Statistical mechanics of the non-uniform gas, P. L. Auer and S. Tamor—1426
Statistical mechanics of transport processes. XIV. Linear relations in multicomponent systems, John D. Kirkwood and Donald D. Fitts—1317
Structure of transport equations, S. Tamor—1421
Studies in molecular dynamics. II. Behavior of a small number of elastic spheres, B. J. Alder and T. E. Wainwright—1439
Theory of "melting" of the helical form in double chains of the DNA type, Bruno H. Zimm—1349
Theory of the diffuse double layer, Frank H. Stillinger, Jr. and John G. Kirkwood—1282
Utilization of order-disorder theory in physical adsorption. I. Fundamental equations, S. Bumble and J. M. Honig—424

Metals

Contribution of lattice vibrations to the order-disorder transformation in alloys, Peter J. Wojtowicz and John G. Kirkwood—1298
Detection of order in Ni_3Co, Y. L. Yao—741
Identification of colloidal sodium in sodium azide, Brian S. Miller—889
Number of 3*d* electrons in iron, S. K. Joshi—1261(L)
On the structure of dilute solutions of metals, E. Charles Evers—618(L)
Proton magnetic resonance studies of non-stoichiometric titanium hydride, B. Stalinski, C. K. Coogan, and H. S. Gutowsky—933(L)
Transport processes in liquid alloys. II. The electrical force on an ion, Paul C. Mangelsdorf, Jr.—1151

Microwave Spectra (see Absorption Spectra)

Molecular Beams

Dipole moment of lithium hydride, Lennard Wharton, L. Peter Gold, and William Klemperer—1255(L)

Molecular Films (see Surface Phenomena)

Molecular Spectra (see Absorption Spectra, Emission Spectra, Fluorescence and Raman Spectra

Dipole moment of lithium hydride, Lennard Wharton, L. Peter Gold, and William Klemperer—1255(L)
Ultraviolet spectrum of triptycene, Charles F. Wilcox, Jr.—1874(L)
Vibrational spectra of orthorhombic metaboric acid, J. L. Parsons—1860

Molecular Structure and Constants (see also Absorption Spectra, Fluorescence, Raman Spectra, Electron & X-ray Diffraction)

Absorption spectrum of chlorine in the vacuum ultraviolet, Raymond P. Iczkowski, John L. Margrave, and John W. Green—1261(L)
Application of symmetry principles to the rotation-internal torsion levels of molecules with two equivalent methyl groups, Rollie J. Myers, and E. Bright Wilson, Jr.—186
Biradical paradox, Harden M. McConnell—1868(L)
Bond lengths and nuclear quadrupole coupling in vinyl halides, E. Spinner—611(L)
Bond lengths and nuclear quadrupole coupling in vinyl halides, E. Bright Wilson, Jr.—612(L)
Classical and quantum mechanical hypervirial theorems, Joseph O. Hirschfelder—1462
Dielectric study of some liquid alkyl nitrites, R. F. Grant, D. W. Davidson and Peter Gray—1712
Dipole moment and conformation of 2-chlorocyclohexanone, Samuel Yaroslavsky and Ernst D. Bergmann—635(L)
Dipole moment of lithium hydride, Lennard Wharton, L. Peter Gold, and William Klemperer—1255(L)
Dipole moments of hydrocarbons, David R. Lide, Jr.—1879(L)
Dissociation energies of diatomic molecules, G. R. Somayajulu—1541
Double minimum vibration in trimethylene oxide, Sunney I. Chan, John Zinn, and William D. Gwinn—295(L)
Dynamical Jahn-Teller effect in hydrocarbon radicals, W. D. Hobey and A. D. McLachlan—1694
Dynamics of the quasi-linear molecule, Walter H. Thorson and Ichiro Nakagawa—994
Electron coupling of nuclear spins. IV. Temperature dependence in substituted ethanes, John C. Schug, Paul E. McMahon, and H. S. Gutowsky—843
Electronic structure and hyperfine structure constants of NO molecule, Chun C. Lin, Katsunori Hijikata, and Michiko Sakamoto—878
Energy levels of a slightly asymmetric top, John E. Beam and H. L. Davis—1255(L)
Equilibrium bond lengths in methane and deuteromethane as determined by electron diffraction and spectroscopic methods L. S. Bartell, Kozo Kuchitsu, and R. J. deNeui—1254(L)
Equilibrium in the exchange of tritium between ammonia and hydrogen and the zeropoint energy difference between NH_3 and NH_2T, Joel R. Gutmann and Max Wolfsberg—1592(L)
Erratum: Energy levels of a slightly asymmetric top [J. Chem. Phys. **32**, 1591 (1960)], James A. Norris and Victor W. Laurie—1256(L)
Erratum: Infrared and raman spectra of fluorinated ethanes XII. 1,1,2,2-tetrafluoroethane [J. Chem. Phys. **32**, 899 (1960)], Peter Klaboe and J. Rud Nielsen—617(L)
Erratum: Microwave spectrum of acetyl cyanide [J. Chem. Phys. **31**, 882 (1959)], Lawrence C. Krisher—304(L)
Erratum: Potential energy curves for HF and LiH [J. Chem. Phys. **32**, 698, 1453 (1960)], Robert J. Fallon, Joseph T. Vanderslice and Edward A. Mason—944(L)
Estimation of the ionization potential and dissociation energy of molecular astatine, Robert W. Kiser—1265(L)
Excitation and negative ions in H_2O, G. J. Schulz—1661

Far infrared spectrum and structure of disiloxane, J. R. Aronson, R. C. Lord and D. W. Robinson—1004
Far infrared spectrum of trimethylene oxide, Alfred Danti, W. J. Lafferty, and R. C. Lord—294(L)
First excited $^1\Sigma_g^+$ state of H_2: A double-minimum problem, Ernest R. Davidson—1577(L)
F^{19} spectra of phosphorus (V) fluorides, W. Mahler and E. L. Muetterties—636(L)
Force constants for NH_4^+ and ND_4^+, S. Sundaram—708
Forces in molecules. I. Application of the virial theorem, William L. Clinton—603
Infrared and Raman spectra of fluorinated ethanes. XIII. 1,2-difluoroethane, Peter Klaboe and J. Rud Nielsen—1765
Infrared spectra and structure of the isomers of N_2F_2, Russell H. Sanborn—1855
Infrared spectra of lithium halide monomers, William Klemperer, W. G. Norris, Alfred Büchler and Alfred G. Emslie—1534
Jahn-Teller distortions in cyclobutadiene, cyclopentadienyl radical, and benzene positive and negative ions, Lawrence C. Snyder—619(L)
Ligand spin densities and magnetic properties of some aminotroponeimine chelates of nickel, W. D. Phillips and R. E. Benson—607(L)
Microwave spectrum, barrier to internal rotation, and quadrupole coupling of acetyl bromide, Lawrence C. Krisher—1237
Microwave spectrum of $CFCl_3$, Maurice W. Long, Quitman Williams and T. L. Weatherly—508
Microwave spectrum, structure, and dipole moment of formyl fluoride, Oliver H. LeBlanc, Jr., Victor W. Laurie, and William D. Gwinn—598
Microwave spectrum, structure, and dipole moment of propane, David R. Lide, Jr.—1514
Microwave spectrum, structure, dipole moment, and internal rotation of trimethyl silane, Louis Pierce and D. H. Petersen—907
Molecular orbital treatment of hydrogen with central potentials and modified boundary conditions, James M. Peek and Edwin N. Lassettre—1803
Molecular structure correlations, Børge Bak and Lise Hansen-Nygaard—418
Molecular structure of iodine heptafluoride, Robert E. LaVilla and S. H. Bauer—182
Molecular structure of lithium chloride dimer. Thermodynamic functions of Li_2X_2 (X= Cl, Br, I)., S. H. Bauer, Tadashi Ino, and Richard F. Porter—685
Note on the internal rotation-barrier in ethanic compounds, Martin Karplus—316(L)
Nuclear magnetic resonance spectra of systems of the A_3B_2C type: Proton magnetic resonance spectra and the absolute signs of the proton-proton spin coupling constants in ethyl acetylene and ethyl mercaptan, P. T. Narasimhan and Max T. Rogers—727
On the absorption spectrum of CF_2 and its vibrational analysis, D. E. Mann and B. A. Thrush—1731
On the assignment of the lowest triplet state in benzene, Andreas C. Albrecht—937(L)
On the equilibrium C-H distance in methane, D. P. Stevenson and James A. Ibers—762
One-center wave function for the methane molecule, Anthony F. Saturno and Robert G. Parr—22
$^1\Sigma^+$ excited states of carbon monoxide, H. Lefebvre-Brion, C. M. Moser and R. K. Nesbet—931(L)
Out-of-plane CH vibrations in some polynuclear aromatic hydrocarbons, Milan Randić—710
Potential curves for N_2, NO, and O_2, Joseph T. Vanderslice, Edward A. Mason, William G. Maisch and Ellis R. Lippincott—614(L)
Potential energy curves for CO, Irwin Tobias, Robert J. Fallon, and Joseph T. Vanderslice—1638
Power series expansions of vibrational potentials. I. The Heitler-London potential for H_2, Charles L. Beckel—1885(L)
Power series expansions of vibrational potentials. II. Two classical potentials for ionic molecules, Edward J. Finn and Charles L. Beckel—1887(L)
Preparation and crystal structures of RuC and OsC, Charles P. Kempter and M. R. Nadler—1580(L)
Proton resonance shifts in pyrene mononegative ion at 4.2°K, M. E. Anderson, P. J. Zandstra and T. R. Tuttle, Jr.—1591(L)
Raman spectrum of gaseous CF_4, B. Monostori and A. Weber—1867(L)
Some intra-atomic correlation correction studies, M. Krauss and B. J. Ransil—840
Some neglected subcases of predissociation in diatomic molecules, R. S. Mulliken—247
Spectrum of ReF_6, J. C. Eisenstein—1530
Spin densities in several odd alternant radicals, H. H. Dearman and H. M. McConnell—1877(L)
Structure of the infrared Y bands of N_2, G. H. Dieke and D. F. Heath—432
Structure of the isobutane molecule; Change of dipole moment of isotopic substitution, David R. Lide, Jr.—1519
Study of molecular integrals I. The two center exchange integrals, R. C. Sahni and C. D. LaBudde—1015
Study of molecular integrals II. The three-center one electron and two-electron integrals, C. D. LaBudde and R. C. Sahni—1022
Theory of hyperfine interactions in aromatic radicals, A. D. McLachlan, H. H. Dearman, and R. Lefebvre—65
Transferability of Urey-Bradley force constants. IV. The methyl halides, John Overend and James R. Scherer—446
Transferability of Urey-Bradley force constants. V. The bromoethylenes, James R. Scherer and John Overend—1680
Trimethylene oxide I. Microwave spectrum, dipole moment, and double minimum vibration, Sunney I. Chan, John Zinn, Jose Fernandez, and William D. Gwinn—1643
Ultraviolet and structural studies of polythionates, R. M. Golding—1666
Vibrational spectra of orthorhombic metaboric acid, J. L. Parsons—1860
Vibrational spectra of penta-deutero-fluoro-benzene, D. Steele, E. R. Lippincott, and J. Xavier—1241
Vibronic calculations in benzene, Andreas C. Albrecht—169

Nuclear Quadrupole Resonance

Halogen bond character in the alkyl halides, B. P. Dailey—1641
Induction studies in several groups of halogen-containing organic compounds by their Cl^{35}, Br^{79}, or Br^{81} pure quadrupole resonance spectra, H. O. Hooper and P. J. Bray—334
N^{14} pure quadrupole resonances of several nitriles, Hisao Negita and P. J. Bray—1876(L)
Nuclear magnetic resonance spectrum of B^{11} in inderite, K. S. Pennington and H. E. Petch—329

Nuclear Resonance (see Magnetic Resonance)

Analysis of high-resolution NMR-spectra by iterative methods, Ragnar A. Hoffman—1256(L)
C^{13} chemical shifts in CO and CO_2, Raymond Ettinger, Philip Blume, Andrew Patterson, Jr., and Paul C. Lauterbur—1597(L)
On the analysis of high-resolution NMR spectra by iterative methods, C. A. Reilly and J. D. Swalen—1257(L)
Proton resonance shifts in pyrene mononegative ion at 4.2°K, M. E. Anderson, P. J. Zandstra and T. R. Tuttle, Jr.—1591(L)

Optical Activity

Optical and other electronic properties of polymers, Ignacio Tinoco, Jr.—1332
Optical rotatory dispersion of transition-metal complexes, Satoru Sugano—1883(L)

Phase Transitions

Critical solution phenomenon in two-component liquid systems. The system water-ethylene glycol mono-isobutyl ether, De F. P. Rudd and B. Widom—1815

Phosphors

Activation center in magnesium fluorogermanate phosphors, G. Kemeny and C. H. Haake—783
Phosphorescence lifetime of benzene. An intermolecular heavy atom effect, a deuterium effect, and a temperature effect, M. R. Wright, R. P. Frosch and G. W. Robinson—934(L)

Photochemistry

Chemiluminescence of ethylene formed probably from methylene in an inert matrix, Theodore D. Goldfarb and George C. Pimentel—105
Kinetics of excited molecules. II. Dissociation processes, Gerald B. Porter and B. T. Connelly—81
Light-induced *cis-trans* isomerization of nitrous acid formed by photolysis of hydrazoic acid and oxygen in solid nitrogen, John D. Baldeschwieler and George C. Pimentel—1008
Mechanism of ozone decomposition, H. J. Schumacher—938(L)
Mercury photosensitized decomposition of cyclohexane at high temperatures, S. Arai, S. Sato and S. Shida—1277(L)
Methyl affinities determined by photolysis of azomethane, C. Steel and M. Szwarc—1677
On the existence of energy chains in the ozone decomposition, Sidney W. Benson—939(L)
Photoconductivity and photolysis in cadmium iodide, Richard A. Fotland—956(L)
Photolysis of carbon dioxide, Bruce H. Mahan—959
Primary processes in the gaseous photolysis of polyatomic molecules. I. Biacetyl, Jean T. Dubois—229
Production of vibrationally excited S_2 in the isothermal flash photolysis of S_2Cl_2, W. D. McGrath—297(L)
Relative quenching cross sections in the reaction of $Hg(6^3P_1)$ atoms with isotopic N_2O molecules, Morton Z. Hoffman and Richard B. Bernstein—526
Threshold law for the probability of excitation of molecules by photon impact. A study of the photoionization effiiciencies of Br_2, I_2, HI, and CH_3I, J. D. Morrison, H. Hurzeler, Mark G. Inghram, and H. E. Stanton—821

Photoconductivity

Absorption spectra of photo-oxide of mesonaphthodianthrene, Haruo Kuroda—1586(L)
Generation of free carriers in photoconducting anthracene. I., W. Moore and M. Silver—1671
Hole and electron drift mobilities in anthracene, Oliver H. LeBlanc, Jr.—626(L)
Photoconductivity and photolysis in cadmium iodide, Richard A. Fotland—956(L)

Photoionization

Threshold law for the probability of excitation of molecules by photon impact. A study of the photoionization efficiencies of Br_2, I_2, HI, and CH_3I, J. D. Morrison, H. Hurzeler, Mark G. Inghram, and H. E. Stanton—821

Polymers

Compression of flexible chain molecules in solution, Robert Simha and J. L. Zakin—1790
Critical opalescence of polystyrene in cyclohexane, P. Debye, H. Coll, and D. Woermann—1745
Excluded volume effect of linear polymer molecules, Michio Kurata, Walter H. Stockmayer, and Antonio Roig—151
Gradient dependence of intrinsic viscosity of freely flexible linear macromolecules, Anton Peterlin—1799
Mean square length of a hindered alkane chain, Richard P. Smith—876
Molecular size distribution and gelation of irradiated copolymers, Mitio Inokuti—1607
Neighbor interactions and internal rotations in polymer molecules. IV. Solvent effect on internal rotations, Shneior Lifson and Irwin Oppenheim—109
Normal vibrations of the polymer molecules of helical configuration, Hiroyuki Tadokoro—1558
Optical and other electronic properties of polymers, Ignacio Tinoco, Jr.—1332
Osmotic pressure of moderately concentrated polymer solutions, Marhsall Fixman—370
Streaming birefrigence of rigid macromolecules in general two-dimensional laminar flow, Harold Wayland—769
Theory of dilute polymer solutions. II., W. R. Krigbaum, D. K. Carpenter, M. Kaneko and A. Roig—921
Theory of "melting" of the helical form in double chains of the DNA type, Bruno H. Zimm—1349
Transient species in the radiolytic polymerization of cyanogen, C. E. Melton and P. S. Rudolph—1594(L)

Proteins

Effect of binding of ions and other small molecules on protein structure VIII. On the isomerization of serum albumin in acidic media, John R. Cann—1410

Quadrupole Resonance (see Nuclear Quadrupole Resonance)

Quantum Mechanics (see Mechanics, Quantum)

Analysis of high-resolution NMR-spectra by iterative methods, Ragnar A. Hoffman—1256(L)
Classical and quantum mechanical hypervirial theorems, Joseph O. Hirschfelder—1462
Energy-levels of a slightly asymmetric top, John E. Beam and H. L. Davis—1255(L)
Erratum: Energy levels of a slightly asymmetric top [J. Chem. Phys. **32**, 1591 (1960)], James A. Norris and Victor W. Laurie —1256(L)
Lowest triplet states of ethylene, Robert S. Mulliken—1596(L)
Nuclear spin conservation in ortho-para hydrogen conversion, Doyle Britton and Z Z. Hugus, Jr.—1830
On the analysis of high-resolution NMR spectra by iterative methods, C. A. Reilly and J. D. Swalen—1257(L)
On the temporal evolution of isolated dynamical systems, S. Golden and H. C. Longuet-Higgins—1479
Potential curves for N_2, NO, and O_2, Joseph T. Vanderslice, Edward A. Mason, William G. Maisch and Ellis R. Lippincott—614(L)

Radiation Chemistry

Atomic and molecular hydrogen yields from irradiated acids, Ralph Livingston and A. J. Weinberger—499
Dissociation of methyl bromide by nuclear isomeric transition of 4.4-hr Br^{80m}, S. Wexler and G. R. Anderson—850

Efficiency of energy transfer in a solution of PPO in xylene, Isadore B. Berlman—1124
Energy transfer in liquid hydrocarbons excited by γ-rays, G. R. Freeman—957(L)
EPR observation of the steady-state ethyl radical concentration in the radiolysis of liquid ethane, Richard W. Fessenden and Robert H. Schuler—935(L)
Gamma radiolysis of propane, B. F. Birdwell and George W. Crawford—928
Kinetics of the alpha radiolysis of carbon monoxide, P. S. Rudolph and S. C. Lind—705
Paramagnetic-resonance of gamma-irradiated single crystals of ice at 77°K, J. A. McMillan, M. S. Matheson and B. Smaller —609(L)
Paramagnetic-resonance studies of irradiated high-density polyethylene. I. Radical species and the effect of environment on their behavior, Elliott J. Lawton, J. S. Balwit, and R. S. Powell—395
Paramagnetic-resonance studies of irradiated high-density polyethylene. II. The effect of irradiation dose on the radical species trapped at room temperature, Elliott J. Lawton, J. S. Balwit, and R. S. Powell—405
Paramagnetic studies of radiation damage in silica gel, Harold W. Kohn—1588(L)
Radiolysis of cyclohexane. I. Pure liquid cyclohexane and cyclohexane-benzene solutions, G. R. Freeman—71
Transient species in the radiolytic polymerization of cyanogen, C. E. Melton and P. S. Rudolph—1594(L)

Radiochemistry

Erratum: Some observations on atomic exchange in NO [J. Chem. Phys. **32**, 1579 (1960)], W. Spindel and Marvin J. Stern—942(L)

Raman Spectra

CN stretching bands in the raman spectra of some group I*b* and Group II*b* complex cyanides, G. W. Chantry and R. A. Plane—736
Effect of hydrogen bonding on the intensity of the CD raman band of $CDCl_3$, D. G. Rea—1875(L)
Erratum: Infrared and raman spectra of fluorinated ethanes. XII. 1,1,2,2-tetrafluoroethane [J. Chem. Phys. **32**, 899 (1960)], Peter Klaboe and J. Rud Nielsen—617(L)
Infrared and raman spectra of C_2Br_3D, James R. Scherer, J. C. Evans, and John Overend—314
Infrared and raman spectra of fluorinated ethanes. XIII. 1,2-difluoroethane, Peter Klaboe and J. Rud Nielsen—1765
Raman spectrum of gaseous CF_4, B. Monstori and A. Weber—1867(L)
Search for a Jahn-Teller effect in IrF_6, Howard H. Claassen and Bernard Weinstock—436
Erratum and Addendum: Substituted methanes. XXIX. Vibrational spectra, potential constants, and calculated thermodynamic properties for dibromochlorofluoromethane and bromodichlorofluoromethane [J. Chem. Phys. **31**, 1633 (1959)], Robert L. Gilbert, Edward A. Piotrowski, Jerome M. Dowling, and Forrest F. Cleveland—1872(L)
Vibrational spectra of penta-deutero-fluoro-benzene, D. Steele, E. R. Lippincott, and J. Xavier—1241

Reaction Rates (see Kinetics of Reaction)

Rotation

Application of symmetry principles to the rotation-internal torsion levels of molecules with two equivalent methyl groups, Rollie J. Myers, and E. Bright Wilson, Jr.—186
Erratum: Microwave spectrum of acetyl cyanide [J. Chem. Phys. **31**, 882 (1959)], Lawrence C. Krisher—304(L)
Evidence for internal rotation in the fine structure of the infrared absorption of oxygen in silicon, H. J. Hrostowski and B. J. Alder—980
Microwave spectrum, barrier to internal rotation, and quadrupole coupling of acetyl bromide, Lawrence C. Krisher—1237
Microwave spectrum, structure, dipole moment, and internal rotation of trimethyl silane, Louis Pierce and D. H. Petersen —907
Molecular rotation in crystals of N_2 and CO, Barbara C. Kohin —882
Note on the internal rotation barrier in ethanic compounds, Martin Karplus—316(L)
Note on the internal rotation problem, William L. Clinton—632(L)
Optical rotatory dispersion of transition-metal complexes, Satoru Sugano—1883(L)
Rotational isomerism involving the 2-3 carbon-carbon bond of the 1-alkenes, L. A. Harrah and D. W. Mayo—298(L)
Second-order perturbation calculation of the hindered rotator model for adsorbed hydrogen, Arthur A. Evett—789

Scattering

Quantum mechanical (phase shift) analysis of the differential elastic scattering of molecular beams, Richard B. Bernstein—795
Scattering of metastable helium atoms in helium, neon and argon, G. M. Smith and E. E. Muschlitz, Jr.—1819
Sparking potential and molecular structure of unsaturated hydrocarbon gases, R. W. Crowe and J. C. Devins—413
Total collision cross sections for the interaction of molecular beams of cesium chloride with gases. Influence of the dipole-dipole force upon the scattering, Hugo Schumacher, Richard B. Bernstein, and Erhard W. Rothe—584

Sedimentation

Comment on dynamical theory of electrosedimentation, C. J. MacCallum—1263(L)

Semiconductors

Activity coefficients of electrons and holes at high concentrations, Arthur J. Rosenberg—665
Effect of oxygen on the semiconductivities of mesonaphthodianthrene and mesonaphthodianthrone, H. Kuroda and E. A. Flood—952(L)
Organic semiconductors II. The electrical resistivity of organic molecular complexes, Mortimer M. Labes, Robert Sehr, and Monisha Bose—868
Quantitative considerations concerning catalysis at a semiconductor surface, C. G. B. Garrett—966

Shock Waves (see also Detonation)

Comments on hypervelocity wave phenomena in condensed explosives, R. F. Chaiken—760
Correlation of experimental results for the vibrational relaxation of nitric oxide, Frank Robben, Philip R. Monson, and John J. Allport—630(L)
Erratum: Reflected shock technique for studying fast chemical reactions, [J. Chem. Phys. **30**, 257 (1959)] Roger A. Strehlow and Arthur Cohen—618(L)
Flash-absorption spectroscopy of free radicals in shock waves, R. M. Ikeda—311(L)
Limitations of the reflected shock technique for studying fast chemical reactions, Theodore A. Brabbs, Steven A. Zlatarich and Frank E. Belles—307(L)
Thickness of shock fronts in argon, K. Hansen and D. F. Hornig—913

Solutions (see also Liquids)

Compression of flexible chain molecules in solution, Robert Simha and J. L. Zakin—1790
Critical solution phenomenon in two-component liquid systems. The system water-ethylene glycol mono-isobutyl ether, De F. P. Rudd and B. Widom—1815
Nuclear spin-lattice relaxation in solutions, Richard W. Mitchell and Melvin Eisner—86
On the structure of dilute solutions of metals, E. Charles Evers—618(L)
Solubility of hydrogen and deuterium in liquid argon, H. Volk and G. D. Halsey, Jr.—1132
Temperature dependence of proton relaxation times in aqueous solution of paramagnetic ions. II. $CrCl_3$, Thomas H. Brown, Robert A. Bernheim, and H. S. Gutowsky—1593(L)

Spectra (see Absorption Spectra, Emission Spectra, Fluorescence, Raman Spectra)

Electron spin resonance line shape of a polycrystalline CH radical, Roland Lefebvre—1826

Statistical Mechanics (see Mechanics, Statistical)

On the temporal evolution of isolated dynamical systems, S. Golden and H. C. Longuet-Higgins—1479

Surface Phenomena

Absorption spectra of anodic niobium oxide films, W. M. Graven, R. E. Salomon, and G. B. Adams, Jr.—954(L)
Cuprous halide films on alkali halide crystals, L. M. Kraemer—991
Distribution functions of a fluid in an external potential field; Application to physical adsorption, William A. Steele and Marvin Ross—464
Interaction of condensable gases with cold surfaces, G. W. Sears and J. W. Cahn—494
Second-order perturbation calculation of the hindered rotator model for adsorbed hydrogen, Arthur A. Evett—789
Surface catalyzed excitation with N and O atoms, Gene G. Mannella, Robert R. Reeves and Paul Harteck—636(L)
Utilization of order-disorder theory in physical adsorption. I. Fundamental equations, S. Bumble and J. M. Honig—424

Thermal Conductivity

Errata: Contributions of bound, metastable, and free molecules to the second virial coefficient and some properties of double molecules, and Initial pressure dependence of thermal conductivity and viscosity [J. Chem. Phys. **31**, 1531, 1545 (1959)] Daniel E. Stogryn and Joseph O. Hirschfelder—942(L)

Thermal Diffusion

Thermal-diffusion-column shape factors for the Lennard-Jones (12-6) potential, B. B. McInteer and M. J. Reisfeld—570

Thermodynamic Properties

Calculation of equilibrium constants for several isotope exchange reactions involving N_2O_4, E. U. Monse—312(L)
Compression and phase transitions of solid NH_3, SiF_4, H_2S, and CF_4, John W. Stewart—128
Critical solution phenomenon in two-component liquid systems. The system water-ethylene glycol mono-isobutyl ether, De F. P. Rudd and B. Widom—1815
Cube-root law for the activity coefficient quotient of the dissociation of HSO_4^- ion, George E. Walrafen—947(L)
Excess free energy in dehydrogenated palladium, Sister Judith Mary Singer, O.P. and Gilbert W. Castellan—633(L)
First-order phase transitions of six normal paraffins at elevated pressures, R. R. Nelson, W. Webb, and J. A. Dixon—1755
Frequency distribution and the specific heat of NaCl at low temperatures, Elizabeth M. Arase and Robert D. Hatcher—1703
Heat capacity of ice at low temperatures, P. Flubacher, A. J. Leadbetter and J. A. Morrison—1750
Heat capacity of uranium tetrafluoride from 1.3 to 20°K and the thermodynamic functions to 300°K. Calorimeter for the range 0.8 to 20°K, John H. Burns, Darrell W. Osborne, and Edgar F. Westrum, Jr.—387
Heats of formation of BF_2Cl and $BFCl_2$, Stuart R. Gunn and Russell H. Sanborn—955(L)
Heterogeneous reactions studied by mass spectrometry. I. The reaction of B_2O_3(s) with H_2O(g), David J. Meschi, William A. Chupka, and Joseph Berkowitz—530
Heterogeneous reactions studied by mass spectrometry. II. The reaction of Li_2O(s) with H_2O(g), Joseph Berkowitz, David J. Meschi, and William A. Chupka—533
Lattice heat capacity of the rare earths. The heat capacities of yttrium and lutetium from 15–350°K, L. D. Jennings, R. E. Miller and F. H. Spedding—1849
Lattice vibrations in alkali halide crystals. II. Potassium and rubidium halides; cesium fluoride, Arnold M. Karo—7
Mass spectra of aluminum (III) halides and the heats of dissociation of Al_2F_6(g) and $LiF \cdot AlF_3$(g), Richard F. Porter and Ernest Zeller—858
Mass spectra of vapors in the Al-AlF_3 and Al-LiF-AlF_3 systems, Richard F. Porter—951(L)
Mass spectrometric determination of the dissociation energies of the molecules AgAu, AgCu and AuCu, Marcel Ackerman, Fred E. Stafford and Jean Drowart—1783
Mass spectrometric study of the heats of dimerization of the alkali chlorides, Thomas A. Milne and H. Michael Klein—1628
Molecular structure of lithium chloride dimer. Thermodynamic functions of Li_2X_2 (X=Cl, Br, I)., S. H. Bauer, Tadashi Ino, and Richard F. Porter—685
New type of freezing point apparatus. The freezing points of dilute lanthanum chloride solutions. G. Scatchard, B. Vonnegut and D. W. Beaumont—1292
Optical transparency and resistance to flash heating, W. F. Libby—1588(L)
Osmotic pressure of moderately concentrated polymer solutions, Marshall Fixman—370
Partition function ratios for molecules containing nitrogen isotopes, G. M. Begun and W. H. Fletcher—1083
Preparation and properties of scandium dihydride, Joseph C. McGuire and Charles P. Kempter—1584(L)
Separation of boron isotopes. IV. The methyl sulfide-BF_3 system, A. A. Palko and J. S. Drury—779
Separation of gas mixtures in a supersonic jet. II. Behavior of helium-argon mixtures and evidence of shock separation, S. Alexander Stern, P. C. Waterman, and T. F. Sinclair—805
Single-stage fractionation factor for the system: Oxygen vs cobalt di(salicylal)-ethylenediimine-oxygen, L. L. Brown and J. S. Drury—1889(L)
Solubility of hydrogen and deuterium in liquid argon, H. Volk and G. D. Halsey, Jr.—1132
Some thermal data for Bi_2Te_3, G. F. Bolling—305(L)
Statistical mechanics of molecular ions, Robert N. Varney—1708
Erratum and Addendum: Substituted methanes. XXIX. Vibrational spectra, potential constants, and calculated thermodynamic properties for dibromochlorofluoromethane and bromodichlorofluoromethane [J. Chem. Phys. **31**, 1633 (1959)], Robert L. Gilbert, Edward A. Piotrowski, Jerome M. Dowling, and Forrest F. Cleveland—1872(L)

Surface specific heat of an isotropic solid at low temperatures, Marc Dupuis, Robert Mazo and Lars Onsager—1452
Thermodynamic properties of unipositive gaseous elemental ions, John W. Green, Duncan E. Poland, and John L. Margrave—35
Vapor pressures and related thermodynamic properties of the isotopic nitric oxide molecules, Jacob Bigeleisen—1774
Velocity analysis of molecular beams generated from NaOH vapors, V. S. Rao and Richard C. Schoonmaker—1717

Thermodynamics

Application of Ehrenfest equations to liquid-vapor and liquid-solid mixtures of He^4, Olli V. Lounasmaa—443
Casimir coefficients and minimum entropy production, R. E. Nettleton—237
Derivation of thermodynamic relations for three-dimensional systems, Francis S. Manning and William P. Manning—1554
Entropy production in chemical reactions, R. P. Rastogi and R. C. Srivastava—79
Erratum: Validity and consequences of Schreinemakers' theorem on ternary distillation lines [J. Chem. Phys. **31**, 308 (1959)], A. E. Korvezee and J. L. Meyering—304(L)
On inversion of the linear laws of irreversible thermodynamics, Eugene Helfand—319
On the reciprocal relations of onsager, Bernard D. Coleman and Clifford Truesdell—28
Flow equations and frames of reference for isothermal diffusion in liquids, John G. Kirkwood, Robert L. Baldwin, Peter J. Dunlop, Louis J. Gosting and Gerson Kegeles—1505
Thermodynamics, stationary states, and steady-rate processes. V. A collection of corollaries, R. J. Tykodi—40
Thermodynamics, stationary states, and steady-rate processes. VI. Forced vaporization of selected liquids, Ted A. Erikson and R. J. Tykodi—46

Transport Phenomena

Kinetic theory of the moderately dense rigid sphere fluid. IV. The fluxes of matter, momentum and energy in a mixture, Robert A. Harris and Stuart A. Rice—1046
Molecular friction in dilute gases, James T. O'Toole and John S. Dahler—1496
On the temporal evolution of isolated dynamical systems, S. Golden and H. C. Longuet-Higgins—1479
Optical transparency and resistance to flash heating, W. F. Libby—1588(L)
Potential curves for N_2, NO, and O_2, Joseph T. Vanderslice, Edward A. Mason, William G. Maisch and Ellis R. Lippincott—614(L)
Quantum corrections for transport coefficients, Sang-Il Choi and John Ross—1324
Statistical mechanics of transport processes. XIV. Linear relations in multicomponent systems, John D. Kirkwood and Donald D. Fitts—1317
Structure of transport equations, S. Tamor—1421
Transport processes in liquid alloys. II. The electrical force on an ion, Paul C. Mangelsdorf, Jr.—1151

Ultrasonics

Molar sound velocity in inorganic acids, P. R. K. L. Padmini, K. Subba Rao and B. Ramachandra Rao—1268(L)
Multiple velocity dispersion in halomethane gas mixtures, J. B. Calvert and R. C. Amme—1270(L)
Sound dispersion in ethane and 1.1-difluoroethane, L. M. Valley and Sam Legvold—627(L)
Ultrasonic attenuation in the critical region, Marshall Fixman—1363
Vibrational transitions and the intermolecular potential, Robert C. Amme and Sam Legvold—91

Valence and Chemical Bond

Ambiguity in the determination of self-consistent bond orders, G. G. Hall—953(L)
Bond lengths and nuclear quadrupole coupling in vinyl halides, E. Spinner—611(L)
Bond lengths and nuclear quadrupole coupling in vinyl halides, E. Bright Wilson, Jr.—612(L)
Bond polarizability components, George W. Chantry and Robert A. Plane—634(L)
Bond shortening by electronegative substituents, Henry A. Bent—1260(L)
Comments on Carpenter's paper "Density of the bonding electrons in diamond," James A. Ibers—299(L)
Correlation of bond shortening by electronegative substituents with orbital hybridization, Henry A. Bent—1259(L)
Density of the bonding electrons in diamond, G. B. Carpenter—300(L)
Electronegativities from a comparison of bond lengths in AH and AH^+, Henry A. Bent—1258(L)
Electronegativity effects of hybridized carbon atoms, M. G. Brown—1881(L)
Erratum: Improved molecular orbitals and the valence bond theory [J. Chem. Phys. **33**, 301 (1960)], A. C. Hurley—1872(L)
Explanation of the non-additivity of bond lengths, Henry A. Bent—304(L)
Halogen bond character in the alkyl halides, B. P. Dailey—1641
Improved molecular orbitals and the valence bond theory, A. C. Hurley—301(L)
Metal-metal bonding in dicobalt hexacarbonyl diphenylacetylene, David A. Brown—1037
Modification of Koopmans' theorem for conjugated hydrocarbons, J. R. Hoyland and Lionel Goodman—946(L)
Molecular structure correlations, Børge Bak and Lise Hansen-Nygaard—418
Note on Hurley's "Improved molecular orbitals and the valence bond theory," P. Phillipson and R. S. Mulliken—615(L)
On the existence of polyoxides of hydrogen, Sidney W. Benson—306(L)
Orbital radii and the dependence of bond length upon ionicity, hybridization and bond order, J. K. Wilmshurst—813
Strength of the N—N bond in tetrafluorohydrazine, Charles B. Colburn and Frederic A. Johnson—1869(L)
Theorem on separability of electron pairs, Tadashi Arai—95
Three remarks on molecular orbital theory of complex molecules, Robert G. Parr—1183
Valence-bond resonance structures for a triplet state, A. D. McLachlan—663
Valence structures of the higher borides, William N. Lipscomb and Doyle Britton—275

Viscosity

Errata: Contributions of bound, metastable, and free molecules to the second virial coefficient and some properties of double molecules, and Initial pressure dependence of thermal conductivity and viscosity [J. Chem. Phys. **31**, 1531, 1545 (1959)] Daniel E. Stogryn and Joseph O. Hirschfelder—942(L)
Gradient dependence of intrinsic viscosity of freely flexible linear macromolecules, Anton Peterlin—1799
Statistical mechanical theory of the viscosity coefficients of binary liquid solutions, Richard J. Bearman and Peter F. Jones—1432
Structure of glass-forming halides. II. Liquid zinc chloride, J. D. Mackenzie and W. K. Murphy—366
Viscosity of mixtures of hydrogen and water vapor at 295°K, J. W. Fox and A. C. H. Smith—623(L)

X-ray Diffraction

Crystal structure of β-Ga_2O_3, S. Geller—676
Lattice dimensions of NbC as a function of stoichiometry, C. P. Kempter, E. K. Storms, and R. J. Fries—1873(L)
Preparation and crystal structures of RuC and OsC, Charles P. Kempter and M. R. Nadler—1580(L)
Small angle x-ray scattering study of sodium montmorillonite clay suspensions, Robert Hight, Jr., William T. Higdon, and Paul W. Schmidt—1656
Structure in ionic solutions. IV., George W. Brady—1079
Structure of potassium hydroxide: An x-ray and infrared study, James A. Ibers, Junji Kumamoto, and Robert G. Snyder—1164
Structure of the complex ion in aqueous solutions of zirconyl and hafnyl oxyhalides, George M. Muha and Philip A. Vaughan—194
Thermal expansion of delta and epsilon zirconium hydrides, Charles P. Kempter, Reed O. Elliott, and Karl A. Gschneidner, Jr.—837
X-ray scattering by a cell-model liquid, L. H. Lund—1086